



ASTROPHYSICS AND
SPACE SCIENCE LIBRARY

ULTRAVIOLET RADIATION IN THE SOLAR SYSTEM

M. VÁZQUEZ
A. HANSLMEIER



Springer

ULTRAVIOLET RADIATION IN THE SOLAR SYSTEM

ASTROPHYSICS AND SPACE SCIENCE LIBRARY

VOLUME 331

EDITORIAL BOARD

Chairman

W.B. BURTON, National Radio Astronomy Observatory, Charlottesville, Virginia, U.S.A.
(bburton@nrao.edu); University of Leiden, The Netherlands (burton@strw.leidenuniv.nl)

Executive Committee

J. M. E. KUIJPERS, *University of Nijmegen, The Netherlands*

E. P. J. VAN DEN HEUVEL, *University of Amsterdam, The Netherlands*

H. VAN DER LAAN, *University of Utrecht, The Netherlands*

MEMBERS

J. N. BAHCALL, *The Institute for Advanced Study, Princeton, U.S.A.*

F. BERTOLA, *University of Padua, Italy*

J. P. CASSINELLI, *University of Wisconsin, Madison, U.S.A.*

C. J. CESARSKY, *European Southern Observatory, Garching bei München, Germany*

O. ENGVOLD, *University of Oslo, Norway*

A. HECK, *Strasbourg Astronomical Observatory, France*

R. McCRAY, *University of Colorado, Boulder, U.S.A.*

P. G. MURDIN, *Institute of Astronomy, Cambridge, U.K.*

F. PACINI, *Istituto Astronomia Arcetri, Firenze, Italy*

V. RADHAKRISHNAN, *Raman Research Institute, Bangalore, India*

K. SATO, *School of Science, The University of Tokyo, Japan*

F. H. SHU, *University of California, Berkeley, U.S.A.*

B. V. SOMOV, *Astronomical Institute, Moscow State University, Russia*

R. A. SUNYAEV, *Space Research Institute, Moscow, Russia*

Y. TANAKA, *Institute of Space & Astronautical Science, Kanagawa, Japan*

S. TREMAINE, *Princeton University, U.S.A.*

N. O. WEISS, *University of Cambridge, U.K.*

ULTRAVIOLET RADIATION IN THE SOLAR SYSTEM

by

M. VÁZQUEZ

*Instituto de Astrofísica de Canarias,
La Laguna, Spain*

and

A. HANSLMEIER

*Institut für Physik,
Graz, Austria*



A C.I.P. Catalogue record for this book is available from the Library of Congress.

ISBN-10 1-4020-3726-0 (HB)

ISBN-13 978-1-4020-3726-9 (HB)

ISBN-10 1-4020-3730-9 (e-book)

ISBN-13 978-1-4020-3730-6 (e-book)

Published by Springer,
P.O. Box 17, 3300 AA Dordrecht, The Netherlands.

www.springer.com

Printed on acid-free paper

All Rights Reserved
© 2006 Springer

No part of this work may be reproduced, stored in a retrieval system, or transmitted in any form or by any means, electronic, mechanical, photocopying, microfilming, recording or otherwise, without written permission from the Publisher, with the exception of any material supplied specifically for the purpose of being entered and executed on a computer system, for exclusive use by the purchaser of the work.

Printed in the Netherlands.

Contents

Preface	XI
1 Historical Introduction	1
1.1 The extension of visible spectra towards the red	1
1.2 Photographic plates and radiation beyond the violet	3
1.3 The Ultraviolet Catastrophe	6
1.4 Laboratory experiments	10
1.5 Composition of the Earth's atmosphere	11
1.6 Balloons	15
1.6.1 The pioneers	15
1.6.2 Observations of planets	18
1.6.3 Current projects	19
1.7 Aircrafts	20
1.7.1 The pioneers	20
1.7.2 Solar eclipses	21
1.7.3 Atmospheric measurements	21
1.8 The structure of the terrestrial atmosphere	22
1.9 Rockets	26
1.9.1 From the pioneers to the V-2	26
1.9.2 First solar UV observations	28
1.9.3 The Artificial Satellites	31
1.9.4 Sounding rockets	33
2 Solar Ultraviolet Radiation and Magnetism	35
2.1 History of Solar Observations	35
2.2 The Sun as a Star	38
2.2.1 Basic facts about the Sun	39
2.2.2 Evolution of the Sun	
2.2.3 UV Variation during solar evolution	
2.3 The Solar Irradiance	
2.3.1 First measurements	
2.3.2 The Solar UV Spectrum	45
2.4 Solar Observational Features	47
2.4.1 The Photosphere	48
2.4.2 The Chromosphere	51
2.4.3 The Transition Region	56

2.4.4	The Corona	57
2.5	Magnetic field and Radiative Losses	62
2.6	The Heating of the Outer Layers	64
2.6.1	Primary requirements	64
2.6.2	Acoustic Heating	64
2.6.3	Magnetic Heating	64
2.6.4	The Magnetic Carpet	67
3	The Solar UV Variability	69
3.1	Sources of Solar Variability	69
3.2	Short-Time Variations	71
3.2.1	Solar Flares	71
3.2.2	Coronal Mass Ejections	74
3.2.3	Activity Waves in the Corona	75
3.3	Variability of visible radiation during a solar activity cycle	76
3.3.1	Solar Activity Indices	76
3.3.2	Total Irradiance Variations	77
3.4	Solar UV Radiation and the Activity Cycle	81
3.4.1	General Trends	81
3.4.2	Instrumental stability and the Mg II Index	81
3.4.3	EUV and FUV measurements	83
3.4.4	Correlations	85
3.5	Simulation of UV variability	85
3.5.1	Empirical modelling	85
3.5.2	Synthetic modeling	87
3.6	Proxies of long-term Solar Activity	87
3.6.1	Cosmic Rays	88
3.6.2	Nitrates	88
3.6.3	Cosmogenic isotopes	88
3.6.4	Meteorites	92
3.6.5	The Moon	92
3.7	Long Term Variation of Solar Luminosity	93
3.8	Long-Term Decay of Magnetic Activity and UV emission	95
3.8.1	Observations of solar-like Stars	95
3.8.2	The Dynamo Theory	96
3.8.3	Activity–Rotation Relation	98
3.8.4	The Evolution of UV Radiation in solar-like Stars	100
4	Atmospheric Effects of Ultraviolet Radiation	103
4.1	The Extraterrestrial Solar Spectrum	103
4.1.1	The Spectral Distribution of Solar Radiation	103
4.1.2	Atmospheric extinction	104
4.1.3	Thompson and Compton Scattering	106
4.1.4	Rayleigh–Mie scattering	107
4.1.5	Absorption and Emission of Radiation by Molecules	109
4.2	Airglow	111

4.2.1	Nightglow	113
4.2.2	Dayglow	114
4.2.3	Twilightglow	115
4.3	Diffuse UV background	116
4.4	The Ionosphere	117
4.4.1	Historical development	118
4.4.2	General Structure	120
4.4.3	Effects on Communications	124
4.4.4	Variations with Solar Activity	125
4.5	Photochemical Processes	126
4.6	The Stratosphere and Ozone	127
4.6.1	Pioneering Measurements and Observing Techniques	127
4.6.2	Natural Processes of Ozone Formation and Destruction	130
4.6.3	Catalytic Loss of Ozone	133
4.6.4	Other photodissociation processes	134
4.7	Variability of Total Ozone Content	134
4.7.1	The Influence of Solar Variability on Ozone	134
4.7.2	Solar Eclipses	135
4.7.3	The Influence of Volcanoes	135
4.7.4	Photochemical Replacement Time	136
4.8	Dynamics of the Terrestrial Atmosphere	137
4.8.1	Troposphere	137
4.8.2	Planetary waves	138
4.8.3	The Stratosphere	140
4.8.4	The Quasi-Biannual Oscillation (QBO)	140
4.9	UV and Tropospheric Climate Change	142
4.9.1	Timescales and Sources of Climate Variability	142
4.9.2	The Solar Print in the Upper Atmospheric Layers	143
4.9.3	Ozone Chemistry	145
4.9.4	The Natural Patterns of Climate Variability	146
4.9.5	The Effect of Planetary Waves	149
4.10	Effects of Solar UV on the Stability of Satellite Orbits	154
5	UV Radiation, Ozone and Life	157
5.1	The Biochemistry of Life	157
5.2	Radiation and Life	159
5.2.1	Radiation Units	159
5.2.2	Wavelength-dependent Functions	160
5.2.3	Mechanism of Cell Damage	161
5.3	Long-term Evolution of Ozone and UV Radiation	162
5.3.1	Oxygen and Ozone Variation	162
5.3.2	Early UV Surface Fluxes and the Origin of Life	164
5.4	Ozone and UV Fluxes in Planets around Other Stars	169
5.5	The Ozone Hole	170
5.5.1	The Chlorofluorocarbons	171
5.5.2	The Warning and the Measurements	173

5.5.3	The Mechanism of Ozone Depletion at the South Pole	176
5.5.4	Bromine	178
5.5.5	Other anthropogenic mechanisms	181
5.5.6	Natural sources of ozone depletion	181
5.6	The Montreal Treaty	182
5.7	Time Variation of Stratospheric Ozone	183
5.7.1	Global Ozone	183
5.7.2	Polar Ozone Holes	184
5.8	The Future Evolution of the Ozone Hole	186
5.9	Health Consequences of UV Radiation	188
5.9.1	Heliotherapy	188
5.9.2	Damaging Effects of the UV Radiation	190
5.9.3	Resistance to UV Radiation	191
5.9.4	Coral Bleaching	192
5.9.5	UV Damaging Effects on Plants	192
5.9.6	Damaging Effects of UV Radiation on Humans	193
5.9.7	The Biological Consequences of the Ozone Hole	196
5.9.8	Technological Solutions to the Ozone Hole	196
5.10	Tropospheric Ozone	197
5.10.1	Sources and Relevant Reactions	197
5.10.2	Measurements	198
5.10.3	Biological Effects	199
5.11	Climatic Effects of Ozone Changes	200
5.12	Current Surface UV Fluxes	201
5.12.1	UV Index	201
5.12.2	Diurnal Variation of UV Surface Radiation	203
5.12.3	Temporal Variations	203
5.12.4	Hemispheric Differences	205
5.13	Protection against UV Radiation	205
5.13.1	Artificial UV Sources	205
5.13.2	Sunscreens	206
5.13.3	Shading	206
6	UV Fluxes on Other Bodies of the Solar System	209
6.1	Planetary Atmospheres: Basics	209
6.1.1	Photochemistry	210
6.1.2	Atmospheric Physics	211
6.1.3	The Origin of Planetary Atmospheres	215
6.2	Venus	217
6.2.1	Basic Facts	217
6.2.2	Liquid Water on Early Venus	218
6.2.3	Meteorology	219
6.2.4	Atmospheric Chemistry	220
6.2.5	Airglow	220
6.2.6	The Ionosphere of Venus	221
6.3	Mars	223

6.3.1	Basic Facts	223
6.3.2	The Atmosphere of Mars	224
6.3.3	UV Radiation Environment	225
6.3.4	The Martian Ionosphere	227
6.3.5	Airglow	228
6.3.6	Ancient Mars	228
6.3.7	Detection of Life on Mars: Viking and ALH84001	230
6.4	Mercury	234
6.5	The Giant Planets	234
6.5.1	Basic Facts	234
6.5.2	Jupiter	235
6.5.3	Atmospheres	236
6.5.4	UV Photochemistry	238
6.5.5	Aurorae	239
6.5.6	Airglow	241
6.5.7	Ionospheres	242
6.6	Comets	243
6.6.1	Basic facts	243
6.6.2	UV Photochemistry of Cometary Atmospheres	244
6.7	Meteorites	247
6.7.1	Basic facts	247
6.7.2	Surface Change on Meteorites due to UV Radiation	248
6.8	UV Radiation and Its Effect on Planetary Satellites	249
6.8.1	Jovian Satellites	249
6.8.2	Triton	251
6.9	Titan	252
6.9.1	History and Basic Facts	252
6.9.2	Atmosphere of Titan	253
6.9.3	Surface of Titan	256
6.9.4	UV Radiation and Photochemical Reactions on Titan	257
6.9.5	The Huygens Probe	262
6.10	Pluto	263
6.10.1	Basic facts	263
6.10.2	The atmosphere of Pluto	264
7	Ultraviolet Transitory Events and Life	267
7.1	Historical Introduction	267
7.2	Biological Extinctions during Earth History	268
7.2.1	The K/T extinction	269
7.3	Radiation Events in the Solar System	271
7.3.1	Solar flares	271
7.3.2	Supernova Explosions	271
7.3.3	Atmospheric effects of strong ionizing events	274
7.3.4	The Biological Effects of a Nearby Supernova	277
7.4	The Probability of Supernova Explosions	278
7.4.1	The Galactic Environment	279

7.4.2	Effects of Galaxy Collisions: The Case of Andromeda–Milky Way	280
7.4.3	Milky Way History	281
7.4.4	Activity in the galactic centre	284
7.4.5	The Local Interstellar Medium	284
7.4.6	Geomagnetic Field Reversals	287
7.5	Evidence of Nearby Supernovae	289
7.5.1	Frequency of External UV Events during the History of the Solar System	289
7.5.2	Historical Supernovae	290
7.5.3	Terrestrial Fingerprints	292
7.5.4	Future Supernova Candidates	295
7.6	Beneficial Evolutionary Effects of UV Radiation	296
7.6.1	The Role of the Mutations	296
7.6.2	Large Solar and Stellar Flares	298
7.7	UV Resistance of Living Beings and the Panspermia Theory	299
	Bibliography	303
	Index	375

Preface

In the history of science the opening up of a new observational or experimental window is always followed by an increase in knowledge of the subject concerned. This is also the case with the subject of this book, ultraviolet radiation (hereafter UV).

In principle, the ultraviolet range might be just one more of these windows, of no particular importance. However, the energy per UV photon provides the main peculiarity, its magnitude being great enough to produce important chemical reactions in the atmospheres of planets and satellites, thereby affecting the transmission of this radiation to the ground.

The Sun is the main natural source of UV radiation in the Solar System and our planet is the body where its influences can be best tested and the only one where its relation with life can be studied. However, the terrestrial atmosphere blocks most of the photons in this electromagnetic range and astronomers have had to develop various techniques (balloons, planes and rockets) to cross this barrier and access the information. These tools have been used in parallel to investigate the physical properties of the terrestrial atmosphere and the interaction of its constituents with light. This book will addresses most of these topics.

Terrestrial life is based on nucleic acids and it happen that solar UV radiation has the capacity to seriously damage the structure of these acids. The evolution of solar UV radiation at the terrestrial surface has played an important role in the origin and development of life on earth and can serve as a guideline to speculations on the conditions of habitability of other astronomical bodies. Microbes have developed DNA repair systems and have evolved successfully in intense and fluctuating UV environments. Complex beings, however, are more affected by this radiation, humans suffering particular damages such as the skin cancer and other ailments. The last decades have identified exposure to UV radiation as one of the most important problems for human health as a result our technological development. The ozone hole and its consequences will be described in chapter 5.

Hot ionized gases, called plasmas, are the most efficient sources of ultraviolet light. There are many places in the Universe where such plasmas are created. We shall limit the scope of this book to processes occurring at the Solar System. However, we do not live in an isolated system and shall therefore cover, in the last chapter, the effects of variable external UV sources on our environment, with special emphasis on those relating to life of our planet.

The study of the interactions between UV radiation and the components of

the different environments of our planetary system produces an interdisciplinary communication between different branches of science.

We are astronomers, and this book is clearly biased towards the physical and observational perspective of the problem, although we have tried also to include the basics of the important influences of UV on living beings. We have furthermore tried to give a historical description of the development of the scientific ideas in every subject because this contributes towards a better understanding of the present situation.

The book is mainly addressed to physicists with a basic background in astronomy and to scientists working in the growing field of astrobiology.

Many people have been involved, in different ways, in the preparation of this book. At the IAC, R. Castro elaborated and retouched a substantial number of the figures and the Library staff (M. Gomez, and L. Abellán) provided an excellent service in tracing old publications. J. Beckman, S. Bauer, N. Benítez, S. Chueca, O. Fernández-Capetillo, C. Muñoz Tuñón, T. Mahoney , J. Maíz Apellániz and B. Ruiz Cobo have critically read different drafts of the book and made valuable comments, advice and suggestions.

Figures, data and different suggestions have also been kindly supplied by E. Alfaro, N. Arnold, N. Benítez, P. Feldman, R. García López, F. García Pichel, J. Kasting, , D. Martínez Delgado, R. McPeters. J. J. López Moreno, K. Puschmann, I. Ribas and J. Scalo. We would also like to thank the NASA ADS service, which provides a wonderfully efficient service to the scientific community.

T. Mahoney made this book readable in English. We alone, however, bears the responsibility for its content. We thank the Kluwer/Springer staff, especially Dr. Harry Blom, for his confidence in our work.

Finally, our families showed great patience and gave us their full support during the lengthly process of writing this book, which we dedicate to our wives and children.

La Laguna and Graz, December 2004

Chapter 1

Historical Introduction

1.1 The extension of visible spectra towards the red

Radiation is the most efficient way of transporting stellar energy through the interstellar medium to planets, such as the Earth, by means of waves or particles (other forms are stellar winds and neutrinos). One practical characteristic describing it is wavelength or frequency so that we may distinguish different ranges in the electromagnetic spectrum (Figure 1.1). For centuries, the observation and measurement of a narrow interval of it, the spectrum of visible light, was the only tool available to the astronomers for observing the Universe. The study of the light is as broad as science itself. It encompasses everything from fundamental theoretical developments to advanced technology.

The human eye was for centuries the only available detector for measuring and detecting light; hence only that part of the electromagnetic spectra producing an effect on it was the object of study. The response of the eye to the radiation falls off with decreasing wavelength. Most of the radiation is absorbed in the cornea and aqueous humour. Not surprisingly the receptors of light (rods and cone cells) in the retina are quite sensitive to this radiation (Figure 1.2).

Understanding the nature of the light has occupied much time and efforts to several generations of scientists. As in other branches of science advance comes

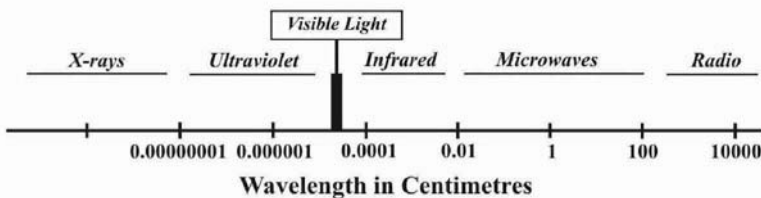


Figure 1.1: The electromagnetic spectrum.

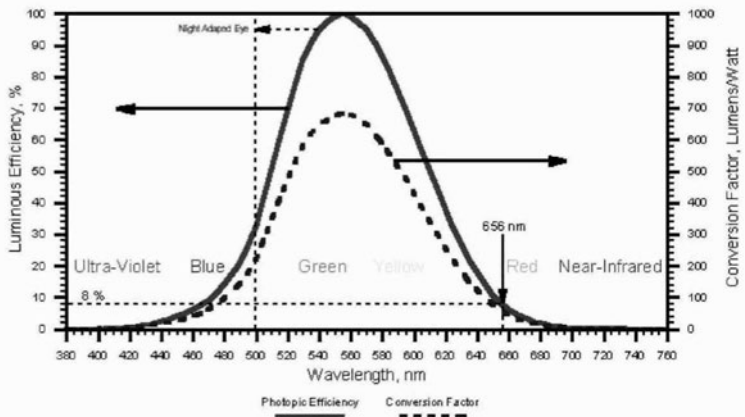


Figure 1.2: The eye’s spectral response in two different units: luminosity efficiency (solid) and conversion factor from lumens to watts (dashed).

from both the experimental (observational) and theoretical sides. The debate between the corpuscular theory of Newton and the ondulatory of Huyghens took several centuries of scientific discussions (see Park 1997) .

The rainbow is a natural proof that light is composed of different parts or colours, but Isaac Newton (1643–1727) gave the first demonstration of this phenomenon in the laboratory. Two centuries later, William Wollaston (1766–1828) and Joseph Fraunhofer (1787–1826) detected dark lines in the solar spectrum – the absorption lines – opening up the way to the determination of abundances and physical parameters in extraterrestrial bodies. Gustav Kirchhoff (1824–1887) and Robert Bunsen (1811 - 1899) built the first spectroscope (Figure 1.3) in 1859 and studied the patterns produced by elements vaporized in a flame, and established the foundation for interpreting the different types of observed spectra (continuum, absorption and emission).

The nineteenth century brought many important developments in the natural sciences, one of which was clearly the detection of radiation beyond the red. Around 1800, William Herschel (1738– 1822) began to suspect that, by observing through different filters, different amounts of heat were passed. In order to verify this, he split the sunlight in its constituent colours, using a glass prism and placed three thermometers in the visible part of the spectrum and two beyond, as a reference. To his surprise, he found that the temperature increased towards longer wavelengths, the highest values occurring beyond the red ¹. This experiment marked the discovery of the “heat or calorific rays”, known today as infrared radiation. Different experiments showed clearly that this new type of radiation behaves like the visible radiation.

¹ Obviously the solar flux peaks in the visible range. The behaviour observed by Herschel was caused by decreasing resolution in the infrared, producing a larger flux concentration in this part of the spectrum than in the visible.

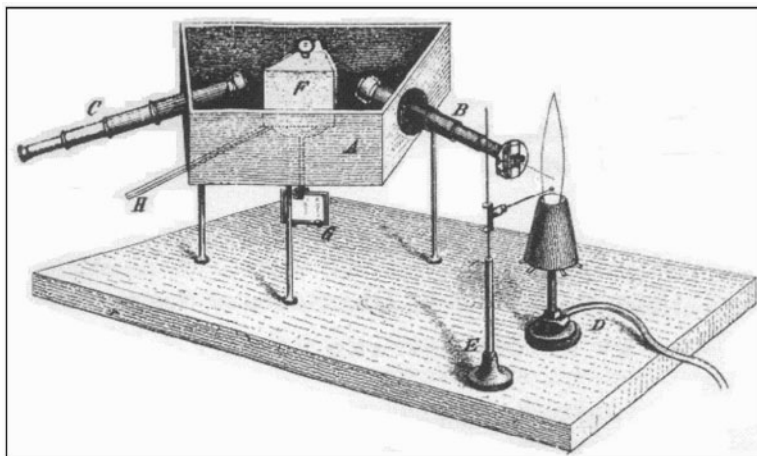


Figure 1.3: The first spectroscope. Adapted from Kirchhoff & Bunsen (1860) Annalen der Physik und Chemie 110, 161-189.

There is radiation still beyond the infrared, however. This window for observing the Universe was opened up in 1887 when Heinrich Hertz (1857–1894) produced radio waves in the laboratory. This discovery was followed by Karl Jansky’s (1906–1950) detection, in 1932, of radio waves from Sagittarius (where the galactic centre is located) and James Hey’s (1909–1990) discovery of radio emission from the Sun². On the long-wavelength side, the electromagnetic spectrum was now completed.

1.2 Photographic plates and radiation beyond the violet

In 1614 Angelo Sala (1576–1637) noticed that sunlight turned silver nitrate crystals black, which was verified, a century later, by Johann Heinrich Schulze (1687–1744), a professor of classical and oriental languages. In 1777, Karl Wilhem Scheele (1742–1786), found a similar effect on paper soaked in silver chloride solution (sodium chloride and silver nitrate), and observed that the violet part of the spectrum was more effective than the reddish one. His results were published in the book “Chemical Treaty of Air and Fire”.

In the late 1790s Thomas Wedgwood (1771–1805), uncle of Charles Darwin, combined the concept of a camera obscura with photosensitive chemicals. However, he was unsuccessful in this experiment, probably because he did not expose the images on to the photochemicals for long enough. Success came in 1802, when he and his friend Humphry Davy (1778–1829) produced “shadow images”. These were accomplished by placing objects (leaves and feathers) on paper and leather soaked

²The discovery was made serendipitously in February 1942 but its publication was postponed until the end of World War II for security reasons.

in photosensitive chemicals (e.g. silver nitrate) and exposing them to sunlight. The light turned the exposed silver nitrate to silver metal, which reappeared, and the shape of the leaves emerged as pale silhouettes, in fact a negative. Unfortunately, they were unable to fix these images, which were soon blackened when viewed in the light.

Johann Wilhem Ritter (1776–1810) was what we might truly call a natural philosopher. After learning about Herschel’s results in the infrared, he applied philosophical concepts such as dualism and polarity to look for something similar at the other side of the spectrum. In 1801 he announced his discovery in a short note (Ritter 1801): “Am 22sten Febr, habe ich auf der Seite des Violetts im Farbenspectrum, ausserhalb desselben, Sonnenstrahlen angetroffen, und zwar durch Hornfilter aufgefunden. Sie reducieren noch stärker, als das Violett Licht fehlt, und das Feld dieser Strahlen ist sehr gross. Nächstens mehr davon.”³. This was in more detail explained by Ritter (1803). For the splitting of the light into the different colours he had used a prism of crownglass instead of the usual flintglass⁴. Then, he placed silver chloride (AgCl) in different parts of the solar spectrum, in an attempt to measure the speed at which this substance is darkened by the different colours. He noticed that blue light was much more active than red light, but surprisingly the most vigorous reactions were found in the region beyond the blue, invisible to the human eye. These were known at that time as “chemical rays”. The upper wavelength limit of this new range is given by the response of the eye to radiation. Today it is called “ultraviolet”, meaning “beyond violet” (from Latin “ultra”).

The scientific method is based on offering to the colleagues proofs of one’s own observational or experimental data for verification or denial. In astrophysics, this was possible thanks to the development of the photography. The early history and development of this new technique is documented in several papers and monographs (Malin 2001 ; Hockberger 2002).

In 1815, Planché noted that chemical rays darkened many kinds of metallic salts. The heliography of Joseph Niepce (1765–1833) was the first benchmark. He coated a glass plate with a thin layer of asphaltum and then placed a drawing on top and exposed it to sunlight. After several hours of exposure, an imprint of the drawing became visible. However, the results were not satisfactory; the image remained diffuse and the practical handling of the asphaltum was difficult. This forced Niepce to collaborate with Louis Daguerre (1789 –1851), who after Niepce’s death, developed the first photographic plate, known as a daguerreotype. This consisted of a thin film of silver on a copper base. The light sensitivation was obtained by exposing the silvered side to iodine vapours, building a plate of silver iodide. After exposure the latent image became real by means of a flux of mercury vapour heated at 75 °C. The unexposed parts were washed out (we say fixed nowadays), in a bath of hyposulphite of soda (sodium thiosulphate).

The first daguerreotype of an astronomical object was of the Moon and was

³On February 22nd I found solar rays on the violet side of the colour spectrum beyond the visible solar rays, namely through a filter. They are reduced even more when the violet is not there and the field of those rays is very large. Next time I will say more about that.

⁴Flint and crown-glass differ in refractive index, which is lower for the latter.

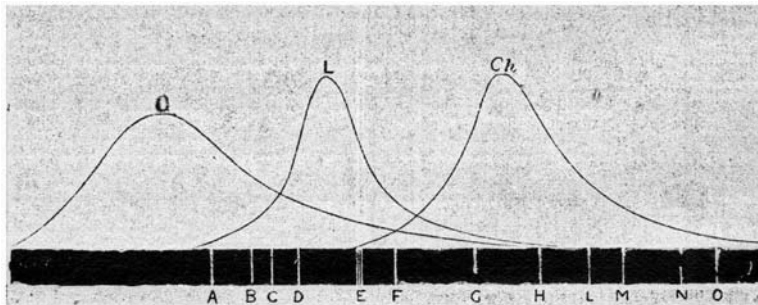


Figure 1.4: Relative intensity of chemical, visible and heat solar rays. Adapted from C. Flammarion (1881) “Astronomie Populaire”, edited by C. Marpon & E. Flammarion, p. 395

obtained by John William Draper (1837–1882) in 1840 with a 20 minutes exposure. On 2nd April 1845 Louis Fizeau (1819–1896) and Leon Foucault (1819–1868) obtained the first solar photograph, with an exposure time of 1/60 second. In 1851, Frederick Archer (1813–1857) invented the process of wet collodion, much more sensitive than the daguerrotypes, although with a more complicated procedure. The plate remained wet and it was necessary to develop it immediately. These products were especially sensitive in the blue part of the spectrum and this property would bias many applications in the decades to come.

The first steps in the development of photochemistry were taken by T.V. Grotthaus (1820) and J.W. Draper in 1843, who both recognized that for a chemical reaction to be catalyzed by “chemical rays”, these had to be absorbed by the reacting chemical substance. Draper was still more precise in remarking “For photochemistry to occur, indigo or blue light must be absorbed by the system”.

John Herschel (1792–1871) was able to photograph radiation beyond the blue, but its interpretation was biased towards the above mentioned three spectrum model. In 1839 Herschel wrote: “beyond the extreme violet rays there exist luminous rays affecting the eyes with a sensation not of violet, or of any other of the recognized prismatic hues, but of a colour which may be called lavender-grey”.

Lewis Rutherfurd (1816–1892) was interested in the application of photography for recording the solar spectrum. Being a very practical man, he also developed an apparatus for ruling diffraction gratings, finally obtaining, in 1864, a detailed atlas of the solar spectrum. The same year M.E. Mascart published one of the first studies about the near UV solar spectrum and measured the wavelength of the strongest spectral lines⁵.

Another important advance was made by Hermann Vogel (1834–1898), in 1873, with the discovery of the procedure for sensitizing plates to colours other than blue. In this way, W. Abney (1843–1920) was able to record the “complete” solar spectrum, from the violet to the infrared. Hentschel (2002) gives an excellent

⁵Mascart,M.E., 1864, *Recherches sur le spectre solaire ultra-violet et sur la détermination des longueurs d'onde*, E. Thunot, Paris.

review of the development of spectroscopy during nineteenth century.

In 1903 Robert Wood (1868–1955) invented a filter for UV transmission to exclude all visible light. He applied it mainly to photographs of the human body (Wood 1903). Two methods are now used for UV photography: a) The use of an UV light source to illuminate the object, the camera equipped with an adequate filter b) fluorescence caused by UV light (a filter absorbs UV light and allows the passage of the fluorescent light). Dyes sensitive to UV radiation have no grain structure and so considerable enlargements can be made.

It was necessary to wait until the end of the nineteenth century to gain a more complete view of the electromagnetic spectrum. Wilhelm Röntgen (1845–1923) discovered the X-rays in 1895, thus providing the lower wavelength limit to the ultraviolet range. Finally, one of the collaborators of the Curie team, Paul Villard (1860–1934), found γ -rays during experiments with radioactive substances. Some years later Rutherford demonstrated that the new rays were located at the high energy tail of the electromagnetic spectrum. This was not the case for other types of radioactive emissions also first named as rays, α rays (He nuclei) and β or cathodic rays (electrons). These new windows supplied an important increase in our knowledge of the Universe and our own environment, but at the same time posed new challenges to science and technology.

1.3 The Ultraviolet Catastrophe

In 1860 G. Kirchhoff was able to show that the ratio between emissivity, e , and absorptivity, a , must be the same for all the materials depending only on the wavelength of the radiation and the temperature of the material⁶.

$$K_\lambda(T) = e_\lambda/a_\lambda$$

The quest was to find a functional expression for $K_\lambda(T)$.

In 1896, W. Wien (1864–1928) and F. Paschen (1865–1947) had measured the intensity distribution in the infrared region and had fitted empirically the data with a exponentially decreasing function with the frequency⁷. It was not too long before H. Rubens (1865–1922) and F. Kurlbaum (1857–1927) discovered that the farther one goes in the infrared, the worse the emissivity law would be reproduced⁸. At the other end of the spectrum, John William Strutt (1842–1919), better known as Lord Rayleigh, and James Jeans (1877–1946) suggested that the energy density, E , should increase in proportion to the square to the frequency, ν .

$$E = 8\pi kT\nu^2/c^3$$

⁶Kirchhoff, G.R., 1860, Über das Verhältnis zwischen dem Emissionsvermögen und dem Absorptionsvermögen der Körper für Wärme und Licht, Annalen der Physik 109, 275–301.

⁷Wien, W., 1896, Über die Energieverteilung im Emissionsspectrum eines schwarzen Körpers, Annalen der Physik 58, 662–669

⁸Rubens, H., Kurlbaum, F., 1901, Anwendung der Methode der Reststrahlen zur Prüfung des Strahlungsgesetzes, Annalen der Physik 4, 649–666.

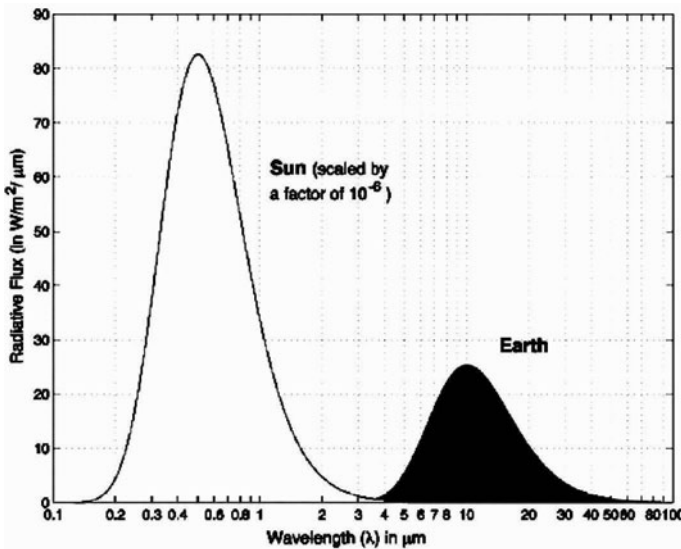


Figure 1.5: Variation with the wavelength of black–body radiation for the surface temperatures of the Earth and the Sun.

where k is a constant and c is the speed of light. However, these laws produce disproportionately high values at short wavelengths, a phenomenon called the “ultraviolet catastrophe”.

Max Planck (1858–1947) was well aware of these problems and sought a way to reproduce the entire spectrum; he proposed a revolutionary concept of radiation. On 14 December 1900, in a session of the German Physical Society in Berlin, Planck announced that light is composed of energy packets, later called photons, with energy $h\nu$, h being a constant and ν the frequency of the radiation⁹. On the basis of these assumptions, he calculated the dependence between the energy radiated by a black body, its temperature and the wavelength of the radiation. (Figure 1.5)¹⁰. According to this law, a hot body will emit most of the energy in short wavelengths (high frequencies), whereas a cooler one will emit it at longer wavelengths.

$$E = \frac{8\pi h\nu^3}{c^2} \frac{1}{\exp(h\nu/kT) - 1}$$

Table 1.1 summarizes the temperatures required to produce emission maxima in the different regions of the electromagnetic spectrum as calculated from the Wien’s displacement law: $\lambda_{\max} = 2898/T$, with λ_{\max} in microns and T in kelvins.

⁹Planck,M., 1901, Über das Gesetz der Energieverteilung in Normalspectrum, Annalen der Physik 4, 553–563

¹⁰See Kuhn,T.S., 1978, Black-body theory and the quantum discontinuity 1894-1912, Clarendon Press, Oxford.

Table 1.1: Relation between the temperature of a black body and the spectral range where most of its radiation is emitted. $1 \text{ cm} = 10^7 \text{ nm} = 10^8 \text{ Å}$.

Spectral region	Wavelength (cm)	Energy (Joules)	Temperature (K)
Radio	> 10	$10^{-30} - 10^{-23}$	< 0,03
Microwaves	10–0.01		0.03 - 30
Infrared	$0.01 - 7 \times 10^{-5}$	$10^{-23} - 10^{-19}$	30–4.100
Visible	$7 \times 10^{-5} - 4 \times 10^{-5}$	10^{-19}	4.100–7.300
Ultraviolet	$4 \times 10^{-5} - 10^{-7}$	$10^{-19} - 10^{-17}$	7.300– 3×10^6
X-rays	$10^{-7} - 10^{-9}$	$10^{-17} - 10^{-14}$	$3 \times 10^6 - 3 \times 10^8$
γ rays	< 10^{-9}	$10^{-14} - 10^{-10}$	> 3×10^8

Another paradox concerning radiation resulted from Heinrich Hertz's (1857–1894) discovery, in 1886, that ultraviolet light causes electrons to be ejected from a metal surface. Using the classical Maxwellian wave theory of light, the more intense the incident light the greater the energy at which the electrons should be ejected from the metal. That is, the average energy carried by an ejected (photoelectric) electron should increase with the intensity of the incident light. In fact, Philipp Lénard (1862–1947) had found that this was not the case¹¹. Rather, the energies of the emitted electrons were independent of the intensity of the incident radiation. Einstein (1905) solved the problem applying the quantum postulate to black body radiation. He wrote “It seems to me that the observations of black body radiation, photoluminescence, the production of cathode rays from UV light and other radiation changes in the group which could be called “light productions” are better understood if we take the point of view it leads to the prediction that light emanating from a point is not continuous but is divided into larger and larger packets in space, eventually described by an endless number of .. localized energy quanta which themselves travel, without being divided, and which can be produced or absorbed as a whole”. The maximum kinetic energy, E_{\max} , of emitted electrons should vary with the frequency, ν , of the incident radiation according to.

$$E_{\max} = h\nu - W_0 = \frac{hc}{\lambda} - W_0 \quad (1.1)$$

where c is the speed of light and W_0 is the characteristic energy associated with the metal concerned. Based on this work Johannes Stark (1874–1957) suggested that light was converted in kinetic energy by absorption that caused electronic transitions in atoms and molecules.

Looking for periodic patterns in the solar spectrum, Johann Balmer (1825–1895) found a regularity in the wavelengths of the hydrogen lines (named the Balmer series after him)¹².

¹¹Lenard, P., 1902, Über die lichtelektrische Wirkung, Annalen der Physik 8, 149-198.

¹²Balmer,J., 1885, Note on the spectral lines of hydrogen, Annalen der Physik und Chemie 25, 80-85.

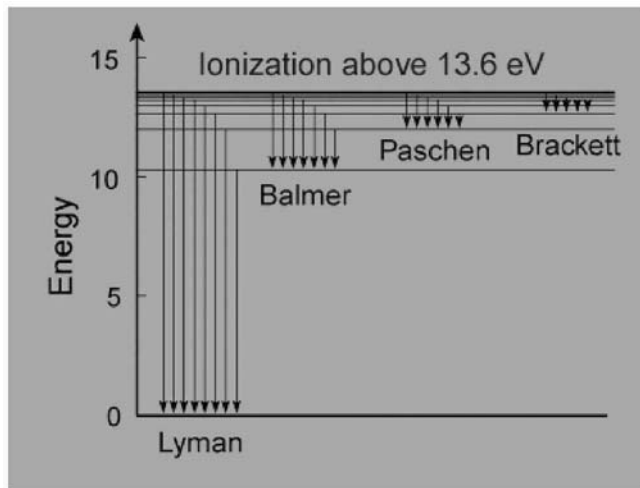


Figure 1.6: Energy levels of the hydrogen atom (0.0, 10.20, 12.09, 12.75 and 13.06 eV are the energies corresponding to the first five n levels). Transitions from different levels produce the observed periodicities (series) in the spectra. The Lyman series falls entirely in the UV range.

$$\frac{1}{\lambda} = R \left(\frac{1}{2^2} - \frac{1}{n^2} \right) \quad n = 3, 4 \quad (1.2)$$

with R , the Rydberg constant, equal to $1.097 \times 10^7 \text{ m}^{-1}$.

In UV range, the Lyman series followed a similar law

$$\frac{1}{\lambda} = R \left(\frac{1}{1^2} - \frac{1}{n^2} \right) \quad n = 2, 3$$

similar series were also identified in other spectral ranges.

The first model to explain these and other findings was presented ¹³ by Niels Bohr (1885–1962). In his theory the electrons absorbed the light energy and re-emitted it at wavelengths corresponding to the electron's energy, thereby giving rise to the observed line series (Figure 1.6). Schrödinger (1926) developed wave mechanics by considering the electrons as waves and provided a new conceptual framework. Both concepts (particles and waves) were joined in the formulation of L. de Broglie (1892–1987). In 1946 Gilbert N. Lewis (1875–1946) proposed the name *photon* for the quanta of electromagnetic energy¹⁴.

The impressive development of the atom and molecular physics in the first half of the twentieth century laid firm foundations for the interpretation of the spectra of astronomical bodies (see Aller, 1963 ; Mihalas, 1978). A crucial step was the

¹³Bohr,N., 1913, On the constitution of atoms and molecules, Philosophical Magazine 26, 1-25.

¹⁴Lewis, G. N., 1926, The conservation of photons, Nature 118, 874–875.

formula developed by Meghnad Saha (1893–1956) to compute the ionization degree of a gas as a function of pressure and temperature.

Most of the resonant spectral transitions of the most abundant elements (H, He, C, Ne) and molecular radicals (H_2 , CO) occur at wavelengths shorter than 200 nm. In this way, the UV range is an excellent diagnostic tool for discovering the physical properties of many astronomical bodies.

1.4 Laboratory experiments

Laboratory experiments were the first means of finding the characteristics of the new region beyond the violet. The development of instrumentation has always been essential to the opening up of a new spectral window for observation. An essential step was the building of suitable detectors (see Koller, 1965 ; Coulson, 1975 for summaries) together with the development of artificial sources of this radiation.

Electric arcs were the earliest source for producing UV radiation. In 1809 Humphry Davy invented the open arc lamp using charcoal electrodes attached to a large voltaic battery, but this material deteriorated rapidly. Later, in 1843, Leon Foucault tried carbon electrodes, which were more stable, but the arc produced was still very dim.

Advance in optics during the nineteenth century permitted the building of spectrographs suited to this spectral region. One of the first problems to solve was the transparency of the quartz optics. In 1852, G. G. Stokes (1819–1903) when experimenting with electric light discharged from Leyden jars¹⁵ discovered, quite by chance, that quartz optics absorbs far less light towards the violet end of the spectrum than normal glass prisms and lenses. At that time the spectral region became to be called ultraviolet (Eisenhohr, 1854). Eisenhohr explained that natural white light is nothing more than a combination of different tones (frequencies), including that beyond the violet.

V. Schumann (1841–1913) was engaged in the manufacture of machinery until he was forty years old, when he became interested first in photography and then in the spectrum analysis. Guided by previous work he got still better results by using fluorite prisms, thereby extending the available UV region down to 100 nm, through two new techniques. First, he acknowledged the limiting effect of the air, which led him to develop a vacuum spectrograph. Second, he manufactured films without gelatine, a considerable absorber of ultraviolet radiation (Schumann 1896).

T. Lyman (1874–1953) used the vacuum spectrograph to detect emission from helium at 50 nm. Carefully studying the absorption of UV radiation by different gases, he discovered the important role played by molecular oxygen (Lyman 1908). As mentioned in the previous section, a series of lines in the hydrogen spectrum

¹⁵A Leyden jar is a device that early experimenters used to help build and store electric energy. It was also referred to as a “condenser” because many people thought of electricity as fluid or matter that could be condensed. Nowadays someone familiar with electrical terminology would call it a capacitor.

(Lyman 1916) was named after him. R. A. Millikan (1868–1953) used a nickel spark lamp to measure the emission of hydrogen at 20 nm.

As in the visible range, the laboratory work of Charlotte E. Moore (1898–1990) was essential for the identification of the observed spectral lines in the ultraviolet region (Moore, 1952).

Photographic emulsion remained the main detector used in astronomy for more than 100 years. It is, now, used only for special purposes, and has been substituted by charged coupled devices (CCDs), conceived in 1970 at Bell Laboratories, the main advantages of the latter being a high linearity, a large degree of dynamic range and relatively low noise. The first front side illuminated CCDs were limited by the absorption of blue photons by the relatively thick poly-silicate gates, which decreased the quantum efficiency in this spectral range. The problem has only been partly solved by backside illuminated devices.

An important recent development is the availability of microchannel plate detectors; these have a thin disc crossed by many microscopic channels acting as individual photomultipliers. The best performance is provided by the two MAMAs (Multi-anode Microchannel Array) on board the Hubble Space Telescope (Cole *et al.* 1995).

In any case, a huge amount of information remains stored in photographic plates and films waiting to be digitized for the reference and enjoyment of future generations of astronomers. This heritage will almost certainly perish unless the astronomical community pays more attention to its preservation¹⁶.

1.5 Composition of the Earth's atmosphere

We observe the radiation from astronomical bodies through our atmosphere. The amount of radiation received at the surface depends on the physical and chemical properties of this envelope. The history of the discovery of its composition is linked to the developing of our understanding about how the UV light interacts with it.

Greek philosophers believed air to be one of the four main components of nature and this idea was maintained for several centuries. Johann Becher (1625–1682) and Georg Stahl (1660–1734) substituted this idea with the theory of phlogiston, a component able to explain all the chemical reactions happening in the presence of air. However, various laboratory experiments gradually produced evidence that air was really composed of different elements, called “gases” for the first time by Johann Baptista van Helmont (1579–1644). He gave them names such as windy gas, fat gas and smoky gas. In 1676 John Mayow (1641–1679) determined that air consisted of at least two distinct components; he named the first “fire-air”, essential for sustaining fire and life.

Joseph Black (1728–1799) discovered CO₂ (called “fixed air” by him) by heating limestone, CaCO₃, and thus demonstrated that a gas could combine with a

¹⁶Griffin, E. 1997, “Archiving observations: individual and corporate efforts” (Status Report: IAU Working Group for Spectroscopic Data Archives), in Proc. Colloq. International Cooperation in Dissemination of the Astronomical Data, ed. F. Ochsenbein & A. Hearn (Baltic Astronomy, 6,287) and Griffin, E. 2005, “Communicating lost libraries”, in Communicating Astronomy, ed. T. J. Mahoney (La Laguna: IAC), in press.

solid. Daniel Rutherford (1749–1819) was the first to publish the discovery of nitrogen in 1772 in his thesis titled “De aere fixo dicto aut mephitico (On Air said be fixed or Mephitic)”. On 1 August, 1774, Joseph Priestley (1733–1804), first prepared oxygen by directing sunlight with a large burning lens on to a sample of mercuric oxide ($\text{HgO} \longrightarrow \text{Hg} + \text{O}_2$). He described so his feelings about the experiment thus “My breast felt particularly light and easy for some time afterwards ... Who can tell, but that, in time, this pure air may become a fashionable article of luxury. Hitherto only two mice and myself have had the privilege of breathing it”¹⁷. At the same time, Carl Wilhem Scheele also obtained oxygen (“fire air”) by heating silver carbonate ($\text{AgCO}_3 \longrightarrow \text{Ag} + \text{CO}_2 + \text{O}_2$).

Henry Cavendish (1731–1810) carried out careful quantitative studies of gases¹⁸ and gave the first chemical composition of the air (79.16% nitrogen and 20.83 % oxygen) although he suggested that an important third component was also probably mixed into these estimates. He was also the first to describe the properties of hydrogen, which he called “inflammable air”. At the end of the nineteenth century, Lord Rayleigh (1842–1919) detected anomalies in the amount of nitrogen measured by two different methods, which led him and W. Ramsay (1852–1916) to announce the discovery of the argon, the first of the noble gases to be found¹⁹.

Antoine Lavoisier (1743–1794) was more or less the architect of the revolution in chemistry. He explained combustion and respiration by means of the presence of oxygen. On 12 November, 1783 he presented evidence to the French Academy that air was not an element, but can be decomposed and recombined. His “Traité élémentaire de chimie”, published in 1789, summarized the important experiments of that time and clearly influenced the demise of the idea of the phlogiston. Table 1.2 gives current data about the main constituents of the terrestrial atmosphere.

However, not only the major components of the terrestrial atmosphere were important; trace gases could also be decisive and one of them, ozone, will occupy a large part of this book. It was probably known from antiquity through its strong smell. In 1780 Martin van Marum (1750–1837) first reported the smell originating during his experiments with electric discharges, but he was not able to identify the product producing the smell, although he remarked that the gas had the property to oxidize the mercury (Hg) at low temperatures. Several decades later (March 1839) a Swiss professor of chemistry, Christian Friedrich Schönbein (1799–1868), informed the Basel Naturforschender Gessellschaft about the discovery of a new material produced in the electrolysis of water and during the slow oxidation of white phosphorus. He gave him the name ozone (from the greek ozein, to smell), owing to its characteristic smell, already known at that time from the first electric machines and from lightning storms (see also Schönbein 1845, 1850).

J.J. Berzelius (1779 - 1848) suggested to Schönbein, that the new gas might be a modification of the oxygen, a hypothesis finally proven by Jean Galissard de Marignac (1801–1873) and August de la Rive (1801–1873). In 1858 Andrei

¹⁷ However, he remained convinced of the theory of phlogiston, as is evidenced in the title of his last book: *The Doctrine of Phlogiston Established*.

¹⁸ Cavendish, H., 1785, Experiments on Air, Philosophical Transactions 75, 372.

¹⁹ Rayleigh & Ramsay, 1895, Argon, a new constituent of the atmosphere, Philosophical Transactions 186, 187.

Table 1.2: Principal constituents of the atmosphere.

Constituent		Composition by volume (%)
Nitrogen	N ₂	78.08
Oxygen	O ₂	20.95
Argon	Ar	0.93
Carbon dioxide	CO ₂	0.0375
Water vapour	H ₂ O	0.001-4
Neon	Ne	0.0018
Helium	He	0.0005
Methane	CH ₄	0.00017
Nitrous oxide	N ₂ O	0.00003
Hydrogen	H ₂	0.00005
Xenon	Xe	0.000009
Ozone	O ₃	0.000004

Houzeau found ozone in natural air.

The density of ozone is about 1.5 times that of O₂. At -112 °C it condenses to a deep blue liquid. It is a powerful oxidizing agent and, in concentrated gas or liquid forms, is highly explosive.

Schönbein developed an instrument, the ozonoscope, to measure the ozone content in the atmosphere. It consisted of a specially treated paper strip that reacted with ozone, causing its color to bleach out. The ozone in the air oxidizes the potassium iodine in the paper to produce iodine according to the following reaction



Iodine reacts with the scatch of the paper, staining it of a purple colour. The darker the paper, the more ozone is present.

Gases other than ozone influence the test paper and observers were cautioned against exposing the paper to possible sources of sulfuric acid. Moreover, the method is vulnerable to atmospheric humidity, air flow and accidental exposure to direct sunlight. Albert Levy improved the system by developing the technique of iodine-catalysed oxidation of arsenate (AsO₃³⁻) based on the reaction



Using this method, Levy started at the Paris Municipal Observatory at Park Montsouris a long series of measurements (1876–1910), still often used nowadays as a reference level of the current concentration of ozone in the lower atmosphere. Volz & Klein (1988) have compared the Schönbein and arsenite methods. Bojkow (1986) offers a review of surface ozone measurements during the second half of the nineteenth century.

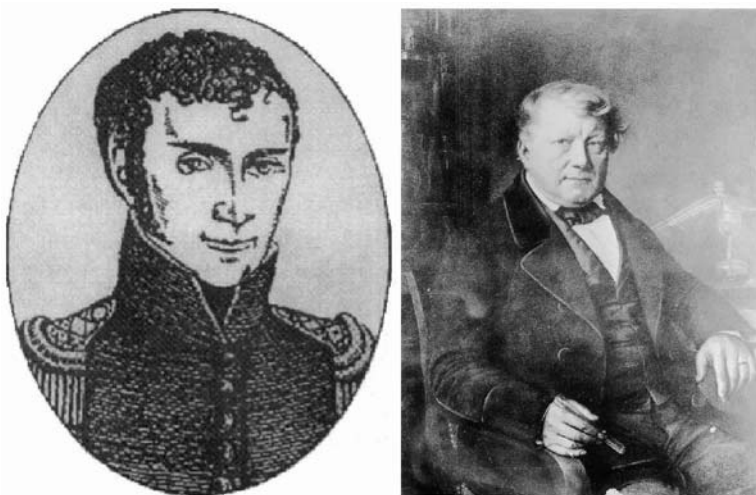


Figure 1.7: Two pioneers: J.W. Ritter discoverer of UV radiation (left) and C.F. Schönbein, the first to announce the presence of ozone in the nature (right).

In 1857, the engineer Ernst W. Von Siemens (1816–1892) was able to prepare small amounts of ozone in the laboratory. He used special tubes filled with air in which electrical discharges were produced. A year later Georg Neumayer (1826–1909) started a programme of ozone measurements at the Meteorological Observatory of Melbourne (Australia) with the sponsorship of King Maximillian of Bavaria. This support ceased abruptly in 1870 owing to financial problems. The difficulties with the practical procedure of measurement, together with the lack of a concrete application of such programmes led to a recommendation by the Meteorological Congress of Rome, in 1879, to discontinue such programmes. However, the research on ozone continued.

Alfred Cornu (1841–1902) analysed solar spectra obtained by the Austrian Oskar Simony (1852–1915) at the Mt. Teide (3710 m s.l.) on the island of Tenerife (Simony 1889, 1890). Cornu realized that it was not possible to record any radiation at wavelengths below 292.2 nm (Cornu, 1890)²⁰. Huggins (1889) used stellar observations of the star Vega to place the limit at 297.0 nm. At that time, it was known from the above mentioned laboratory experiments that the Sun should also emit at these wavelengths and therefore the conclusion was clear: a substance present in the atmosphere must also be absorbing the UV radiation.

In a short note to Chemical News, 26 November 1880, Walter N. Hartley (1846–1913) reported “the absorption band of ozone stretches from wavelength 285 to 233 millionths of m.m. with the mean wavelength of the rays intercepted by ozone at 256 millionths m.m.” (Hartley 1880) . Moreover, Hartley proposed that this ozone should be at high altitudes. The second band was measured by M.J. Chappuis in

²⁰Some years later, Kiepenheuer (1937) placed the limit at 2845 Å based on observations at the swiss observatory of Jungfraujoch (3457 m).

the visible region (450–800 nm), centered on 602 nm. Finally, the third absorption band of ozone was discovered by William Huggins (1824–1910) in the spectrum of Sirius, also in the UV region.

Some years later, in 1903, E. Meyer made careful laboratory measurements of ozone spectra and Charles Fabry (1867–1945) and Henry Buisson (1873–1944) were able from these data to calculate the amount of ozone present in the atmosphere, showing that it is regularly formed from oxygen through the action of solar radiation. Fowler & Strutt (1917) presented observational evidence that ozone is the effective agent limiting the solar spectrum in the short-wavelength range. The history of ozone was just beginning and we shall return to this topic in chapter 4.

It became clear that the air of the atmosphere was the limiting factor in accessing to the ultraviolet radiation emitted by the astronomical bodies. The only possibility of observing these spectral regions was to rise observatory equipment from the ground into the upper atmospheric layers. This enterprise has been one of the most exciting ventures of the humankind, in which purely scientific aims have been frequently mixed with show-business and finally with the curiosity of the men to cross barriers. The first scientific challenge was to find the physical properties of the terrestrial atmosphere, and this became possible lifting from the ground recording instruments and, in some cases, valiant pilots: the aeronauts, the equivalent in those times to our astronauts.

1.6 Balloons

1.6.1 The pioneers

A gas lighter than the surrounding air rises because it is buoyant, which is to say that its weight is less than that of the air it displaces. The gas lift equals the weight of the air that has been replaced minus the weight of the gas. This principle was already established by Archimedes (287–212 BC) and applied to balloons ascending from the terrestrial surface several centuries later. Pfotzer (1972); Scott (1984), Kirschener (1985), Spindler (1999) and Vázquez & Wittmann (2005) offer summaries of the history and technical characteristics of the different types of balloons.

In 1782 the brothers Montgolfier, Joseph (1740–1810) and Etienne (1745–1799), made a small bag out of silk and lighted a fire under the opening at the bottom causing it to rise. The air expanded and a sufficient amount was forced out of the interior, decreasing its total weight and making it become lighter and ascend.²¹. In June 1783 they gave different demonstrations before the public and members of the Academy of Sciences²². Jean Francois Pilatre de Rozier (1756–1785) and François Laurent (Marquis d' Arlandes) volunteered for the first manned balloon flight. On 21 November, 1783, flight commenced at the Muette garden and the

²¹Tiberio Cavallo had shown the same year in London that soap bubbles formed with hydrogen, ascend rapidly due the lower density of hydrogen.

²²The balloon passengers were a sheep, a duck, and a rooster that ascended from Versailles, in September 1783

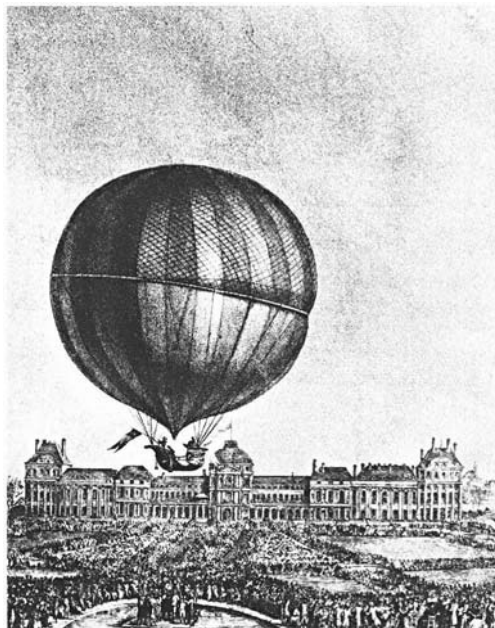


Figure 1.8: The balloon flight of 1 December, 1783. (Courtesy of National Air and Space Museum, Smithsonian Institution)

balloon travelled for 25 minutes (about eight kilometres) before landing near the road to Fontainebleau.

A different technique was used by Jacques Alexander Charles (1746–1823), also in Paris, on 27 August, 1783. The balloon was filled with a gas lighter than the air, namely hydrogen (discovered by Cavendish in 1766), obtained from the action of sulfuric acid on iron fillings. A second attempt was made in December, this time with J.A. Charles and Ainé Roberts (Figure 1.8) on board. An immense crowd watched the ascent from the Champs de Mars. The balloon stayed up for 45 minutes, finally landing in a field near Genosse, about 24 kilometres away²³. Some years later, in 1787, Charles developed one of the basic gas laws, stating that at constant pressure the volume occupied by a fixed weight of gas is directly proportional to the temperature.

The balloons were an essential tool for measuring how different physical parameters change with the altitude. One of the first facts learned about the physical structure of the atmosphere was derived from an experiment carried out by Blaise Pascal (1623–1662) in Puy de Dome, in 1647. Pascal showed that pressure decreases with height and deduced that a vacuum existed above the atmosphere. At the time of the first balloons, there already existed instruments for measuring the relevant physical parameters (temperature, pressure, rain, wind and humidity) of the terrestrial atmosphere. It was only necessary to mount them in the balloons to

²³ Benjamin Franklin witnessed this event and was so impressed he immediately wrote to scientists in the United States stressing the military importance of this new invention.

make vertical soundings of the atmosphere. The first of such soundings was performed in August 1784 by Guyton de Moreau (1737–1816) and the Abbé Bertrand, who flew to more than 3 kilometres in altitude to collect data on temperature and pressure.

Joseph Gay-Lussac (1778–1850) showed that a common thermal expansion coefficient could be applied to all gases, a basic principle for balloon flight. On 24 August, 1804, he ascended to a height of 7000 m and found that the oxygen concentration was essentially constant with height, while water vapour decreased with altitude.

In 1862, James Glaisher (1809–1903), and a professional aeronaut named Henry Coxwell (1819–1900) made a pioneering series of scientific balloon flights from Wolverhampton, England, funded by the British Association for the Advancement of Science. They took barometers, thermometers and other instruments aloft and recorded observations of atmospheric conditions at various altitudes (Glaisher 1871). They nearly perished on their last flight, which carried them above 8840 m, higher than any human had hitherto flown and survived²⁴. At the end of the nineteenth century Gustave Hermite and Georges Besançon performed unmanned launches of balloons carrying pressure and temperature sensors (Hermite, 1893). One of the main problems was to preserve the instruments from the influence of the solar radiation in order to obtain reliable measurements.

The first astronomical observations from a balloon were carried out by Henry Théodore Sivel (1834–1875) and Joseph Croce-Spinelli (1845–1875). On 22 March 1874, they flew to 7300 m in an open basket equipped with a small spectroscope. They tried to discover whether the dark spectral bands of water vapour originated in the Earth's or in the Sun's atmosphere. In April 1875 they ascended, together with Gaston Tissandier (1834–1899), in the balloon *Zenith* to test an oxygen breathing system. Although Tissandier was able to land safely, Sivel and Croce-Spinelly died during the flight.

An important set of observations of the stratosphere started in 1893 at the Königliches Meteorologisches Institut (Berlin), under the direction of Richard Assman(1845–1918), who developed a method for measuring wind velocity with balloons tracked by a theodolite. One of the most spectacular manned flights was launched on 31 July, 1901, with Reinhard Süring (1866–1950) and Arthur Berson (1859–1942) as crew. They reached a height of 10500 m, landing safely in Kottbus but after a flight full of problems (see Labitzke & van Loon 1999). Other flights followed with equipment for measuring the temperature and pressure. R. Assman and Teisserenc de Bort (1855–1913)²⁵, evidenced the increase in temperature from an altitude of 10 km, bringing the discovery of a new atmospheric layer: the stratosphere.

Around 1930 the radiosonde was invented by Vilho Väisälä (1889–1969) and Pavel A. Moltchanov (1893–1941). It consisted of a balloon equipped with a small radio transmitter, allowing the scientists to gather the data without needing to retrieve the balloon once it had landed. The balloon usually reaches an altitude of 30 km, where it bursts (at a pressure of 10 mb) and the instrument package

²⁴One fainted from lack of oxygen. The other had to open a valve with his teeth because his arms were paralyzed by the cold

²⁵He developed a similar programme of measurements in France.

returns to the ground with a parachute, to be reused.

Balloons were also used for other scientific enterprises. Victor Hess (1883–1964) ascended in a balloon in 1912 equipped with an electroscope (Hess 1912). He noticed an increase in the discharges suffered by the electroscope, as the balloon reached higher altitudes. A first interpretation suggested that this effect was produced by a new form of radiation, which therefore received the name of “cosmic rays”. Nowadays, we know that they are charged particles (mainly protons and electrons) with high energies, originating outside the Solar System in explosive events such as supernovae.

Auguste Piccard (1884–1962) and Paul Kipfer were the pilots of a hydrogen balloon, named FNRS from the Swiss sponsor Fonds National de la Recherche Scientifique, launched in 1931 from Augsburg (Germany). For the first time the cabin was pressurized with supply of oxygen. After reaching a record height of 15781 metres they landed on the Austrian Obergurl glacier. In a second attempt, on 18 August 1932, Piccard was accompanied by Max Cosyns, reaching 16 197 metres in altitude and landing again on a glacier. They gathered data on the intensity of cosmic rays (Piccard & Cosyns 1932) and recorded a wide range of stratospheric temperatures.

In 1934 Enrich Regener (1881–1955) and his son Victor (Regener & Regener, 1934) installed a UV spectrograph in a balloon, reaching an altitude of 35 km and recording the maximum UV penetration (287 nm) at an altitude of 29.3 km.

1.6.2 Observations of planets

The astronomer Audouin Dollfus should be mentioned as one of the pioneers of installing telescopes in balloons. On 30 May, 1954, together with his father Charles (1893–1981) an experienced aeronaut, he made an ascent to 7000 metres with a Cassegrain telescope (28 cm diameter). The scientific aim was to search for water vapour in the atmosphere of Mars.

The most spectacular ascent of Dollfus alone, on 22 April 1959, had as its aim the observation of Venus and the Moon. The gondola, with a 50 cm telescope, was connected with cables into a network of 100 balloons, grouped in clusters along a nylon rope of 450 m in length. He reached an altitude of 14 kilometres and estimated the water content in the atmospheres of Venus and Mars. That same year Charles B. Moore and Malcolm Ross ascended in a balloon to 24 km also to make spectroscopic studies of Venus, revealing the presence of water. This finding was verified later from data obtained with an unmanned balloon launched from New Mexico, on 21 February, 1964 (see Bottema *et al.* 1965).

At the same time, the Princeton University promoted the Stratoscope project, under the leadership of Martin Schwarzschild (1912–1997). The first prototype brought a 30 cm telescope for observations of the solar photosphere (Schwarzschild, 1959). Stratoscope II carried a 3.5 ton astronomical observatory that included a 91-centimetre telescope. In successive flights starting on 1 March, 1963, the infrared spectra of Mars and Uranus were observed.

On 3 October, 1960, Gordon Newkirk (1928–1985) used the Stratoscope gondola to carry a coronograph designed by J. Evans to an altitude of 25 kilometres

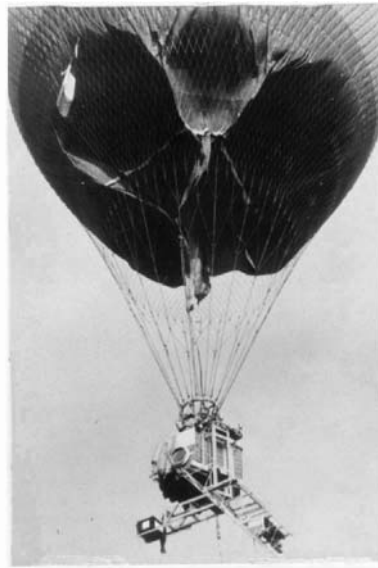


Figure 1.9: Manned stratospheric balloon. Courtesy: A. Dollfus

(Newkirk & Eddy, 1962) . The instrument recorded, at various heights in the terrestrial atmosphere, the intensity variation with wavelength for positions outside the solar disc. Later, a second flight was made (Newkirk & Bohlin, 1965) .

The first balloon-borne ultraviolet telescope was flown at the end of the sixties. Table 1.3 give a list of the main experiments up to the early nineties.

Table 1.3: A sample of balloon flights carrying equipment for UV astronomical observations during the period (1968–1990).

Project	Target	UV range	References
STRATCOM	Sun	185 - 300	Ackerman (1968, 1972)
	Zodiacal Light		Vande Noord (1970)
	Stars, Ozone		Navach <i>et al.</i> 1973
BUSS	Sun, Ozone	200 - 400	Hanser <i>et al.</i> 1978
SCAP2000	Stars Survey	220 - 340	Kondo <i>et al.</i> 1979
FOCA	Sky Survey	200	Laget 1980
			Milliard <i>et al.</i> (1991)

1.6.3 Current projects

Balloon flights are now used regularly for numerous scientific purposes, including the testing of instruments to be flown in future space missions. The interested reader can get an updated view in Crouch (1983) , De Vorkin (1989) and Nishimura

(2002) . Existing scientific balloons are now sometimes a hundred metres high and float to the edge of the atmosphere. Their reusable instrument packages are released by remote control so the package can float down to earth attached to a parachute. Following the Charles prototype, they are sealed balloons filled with gases lighter than air, such as helium or hydrogen. In summary, the field continues to hold promise for the present century (Agrawal & Tueller 2002).

Apart from free flying balloons we can also mention those fixed by a tether or mooring line to the ground (tethered balloon), being raised and lowered to an appropriate height by a winch mechanism. Stratospheric studies make use of free balloons constructed of a very light plastic that remain at a constant level for extended time intervals. Regular measurements of ozone and atmospheric parameters are made using small balloons in different observatories around the world (see chapter 4).

The NSBF (National Scientific Balloon Facility) was established in Boulder (Colorado) in 1961 and moved two years later to Palestine (Texas), where it was provided with an extensive launch area. The base was closed in the nineties due to traffic perturbations in the near Dallas-Fort Worth airport. Now, the main facilities are concentrated in Fort Sumner (New Mexico). In Antarctica, numerous balloon launches have been made from the Mc Murdo polar station, first established in 1955.

In situ measurements from balloons were essential for establishing the general structure of the terrestrial atmosphere: a mass of air, which interacts strongly with the radiation coming from the Sun and other astronomical sources.

1.7 Aircrafts

1.7.1 The pioneers

Airplanes are heavier than the air machines and fly under the action of four basic forces: lift, weight, thrust and drag. The top part of the wings is curved and the bottom is relatively flat. As the wing moves forward, the air flowing over the top travels faster than the air beneath, resulting in a lower pressure above the wing, a difference that provides the upward force called lift. For the aircraft to achieve flight the lift must be larger than the gravitational acceleration. The force of forward movement, the thrust, is produced by the engine (a propeller or jet) and must be larger than the drag.

The works of Otto Lilenthal (1848–1896) and Octave Chanute (1832–1910) prove that wings could lift a man so that he could glide in the air, and brought the attention of the brothers Wilbur (1867–1912) and Orville Wright (1871–1948) to these developments. The Wright brothers were bicycle mechanics with no special training in the subject but their model, called Flyer I, was the first machine to fly on 17 December, 1903, for 12 seconds to a distance of 80 metres at Kitty Hawk (North Carolina) with Orville as pilot. The flight was repeated three more times on the same day.

An astronomer, Samuel P. Langley (1834–1906), was deeply involved in those first attempts, and was surely better placed to be the flight pioneer. He self-

studied the principles of aerodynamic and regularly observed from a tower the flight of the birds, at the National Zoological Park of Washington. Since 1891 he had carried out several practical and theoretical studies (see his “The internal work of the wind”) generously financed by the US War Department and supported scientifically by Lord Rayleigh. In his first attempt (October 1903), the plane was placed in a boat, called “great Aerodrome” and launched using a catapult, with the pilot Charles Manley on board. Unfortunately, at the launch the boat sank and the plane finished in the waters of the Potomac river. Eight weeks later, on 8 December, they made a new attempt but with the same result. The critics of the press and the Wright’s success make Langley to abandon his dream.

The development of aeronautics was really very rapid, with important advances related with the two World Wars and finally with the increase in commercial flights. Its scientific use has been important, but mainly concentrated in the infrared range. In our context, we shall draw attention to two main applications.

1.7.2 Solar eclipses

One of the first scientific applications of aircrafts, related with our subject, was the observation of total solar eclipses. On 24 January, 1925, twenty-five aircrafts carried a team of scientists above the clouds in Connecticut to observe an eclipse. On the same day the airship “Los Angeles” flew over Rock Island with astronomers from the Naval Research Laboratory. The US Air force was once again involved in this kind of observations when Captain A.W. Stevens and the Lieutenant C.D. Mc Alister flew a DC-2 aircraft, 5 miles above Fryeburg (Maine) to observe the eclipse of 31 august, 1932.

This example was followed in other similar events. During the Tenerife total eclipse of 2 October, 1959, an F-101B of the US Air Force made polarimetric measurements of the solar corona (Felling & Witunski 1960). Some years later, and not very far from the Canaries, the supersonic aircraft Concorde followed for 74 minutes, the path of totality of the June 1973 solar eclipse over western Africa at an altitude of 16 km (Lena *et al.* 1974 ; Koutchmy 1975). The photographic work was conducted successfully, but analysis of the images showed optical aberrations caused by the external turbulent atmosphere compressed by the aircraft shock, resulting in a low image quality. More recently, total solar eclipses have been followed using aircrafts such as the C-130.

1.7.3 Atmospheric measurements

In the seventies the aircrafts were able to reach regularly stratospheric heights and directly sample the atmospheric components. Measurements of the ozone content in the stratosphere were carried out by NASA using a commercial Boeing 747 aircraft (Falconer & Holdeman 1976).

SR - 71 “Blackbird” was an aircraft used by NASA for aeronautical research (Figure 1.10). In the nineties it was proposed to use it as a platform for night-time astronomical observations in the UV region under the coordination of JPL. The first flight occurred on 9 March, 1993 from the Dryden Flight Research Center

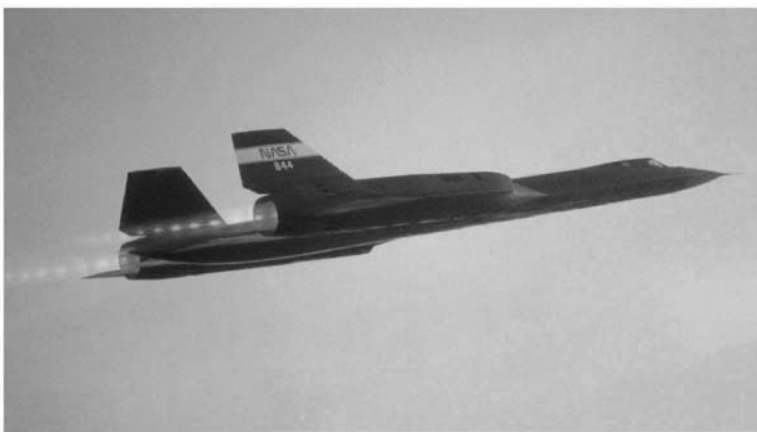


Figure 1.10: The SR-71 Aircraft (courtesy: NASA Dryden Flight Research Center, available at <http://www.dfrc.nasa.gov/gallery/photo/index.html>).

(Edwards, California) reaching an altitude of 25 km. An ultraviolet video camera was mounted in the nose of the plane to observe comets and stars. The programme was continued by the Southwest Research Institute (Texas).

Two similar ER-2 aircraft are now being used by the Airborne Science Branch of NASA for stratospheric ozone and solar irradiance measurements (Mc Elroy 1995). A DC-8 is also used to test and calibrate sensors that will fly onboard future satellites.

Other projects have been carried out with Lear Jet and CV 990 aircrafts, but mainly working in the infrared range. Similar use was made of the NASA C141 Kuiper Airborne Laboratory, equipped with a 90 cm telescope, operational from 1974 to 1995. The Kuiper will be substituted by SOFIA (Stratospheric Observatory for Infrared Astronomy) project, on board a Boeing 747.

1.8 The structure of the terrestrial atmosphere

Measurements from balloon soundings and aircraft flights, together with theoretical developments, brought a clearer understanding of the physical structure of the terrestrial atmosphere, which was divided in different layers according the different processes taking place in them. (see Figures 1.11 and 1.8).

Troposphere: Named after the Greek word for overturning. It extends from the terrestrial surface up to approximately 11 kilometres. The heat source is infrared radiation from the surface, illuminated by visible solar radiation. The heat is transferred to the troposphere by the following processes:

- The vaporation of water and release of latent heat²⁶ through the formation of clouds.

²⁶Heat absorbed during the change of state.

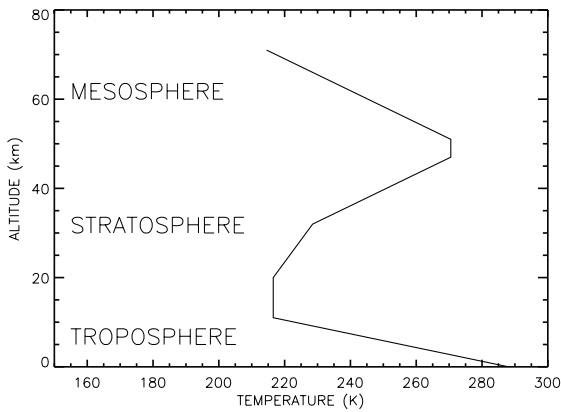


Figure 1.11: Thermal profile of the atmosphere showing the different layers. Based on the U.S Standard Atmosphere 1976.

- Infrared emission and absorption by greenhouse gases, such as water vapour, CO₂ and CH₄.
- Sensible heat flux, the heat absorbed or transmitted by a substance during a change of temperature that is not accompanied by a change of state.

Assuming hydrostatic equilibrium and the equation of state for an ideal gas ($P = n k T$), we arrive to the following expressions

$$P(z) = P_0 e^{-mgz/kT}; n(z) = n_0 e^{-z/H}$$

where

$$P = \rho g H; H = kT/mg$$

being z the geometrical altitude, P the pressure, g the gravitational acceleration, $\rho = n m$ the mass density, k the Boltzmann constant and H the scale height of the atmosphere.

Convection is the dominant mechanism for energy transport in these layers. Assuming adiabatic motion of the convective cells, the temperature gradient, dT/dz , in these layers can be derived by applying the first law of thermodynamics and the consideration of latent heat (see Houghton, 2002 for the basic concepts of planetary atmospheres)

$$dT/dz = -(g(z)/c_p)/[1 + (L/c_p)(dW/dT)] \approx 6.5^\circ\text{C}/\text{km}$$

where z is the vertical coordinate, g the gravitational acceleration, c_p the specific heat at constant pressure, W the mass of saturated air and L the latent heat of vaporization. Moisture can decrease dT/dz , by releasing latent heat. James P.

Espy (1785–1860) first derived this parameter empirically for dry and saturated conditions, some years later verified theoretically by W. Thompson (Lord Kelvin).

The temperature and water vapour content in the troposphere decrease rapidly with height. Water vapour plays a major role in regulating air temperature because it absorbs solar energy and thermal radiation from the planet's surface. The troposphere contains 99 % of the water vapour in the atmosphere.

The tropopause is highest in the tropics (~ 16 km) and lowest in the polar regions (~ 8 km), and also undergoes seasonal changes. Here, radiative processes start to dominate. Meteorological processes take place in the lower atmosphere (the tropo – and stratosphere). The upper layers are studied by aeronomy.

Stratosphere: This layer lies between 10 and 50 km and energy is transported through it by radiation. The temperature increases with altitude due to the absorption of UV radiation by ozone, a topic that will be dealt with later in some detail. The three major absorbing and emitting gases in this region are ozone, carbon dioxide and water vapour (Table 1.4) (see e.g. Taylor 2003 for a summary).

Mesosphere: This is the coldest of the atmospheric layers and is produced by the emission of radiation from carbon dioxide, CO_2 . The temperature decreases with the altitude and reaches low enough levels to freeze water vapour to produce ice clouds, also called noctilucent clouds. Because of oxidation processes and the penetration of UV radiation, which dissociates polyatomic molecules, this layer is more complex than those below.

Thermosphere: The temperature rises again because of heat released from the dissociation of molecular oxygen by UV light and photoionization by X-rays. Here, conduction is the main mode of energy transport. In this layer the absorption of solar energy is less than 1 % of that in the stratosphere but the air is so thin that a small increase in energy can cause a large increase in temperature.

Exosphere: A region, where most of the particles have enough kinetic energy to escape from the terrestrial atmosphere. The minimum velocity for escape from the Earth, the critical escape velocity, is about 11.3 km/s.

Table 1.4: Main components contributing to the absorption of radiation in the terrestrial atmosphere. Wavelengths are expressed in microns.

Absorbing agent	Absorbing window
Atomic oxygen, nitrogen	0 – 0.085 (X - rays)
Molecular oxygen, nitrogen	0.085 – 0.2 (Far UV)
Ozone (O_3)	0.2 – 0.35 (Near UV)
CO_2 , CH_4 , H_2O , NH_3	Infrared bands

The temperature above the stratosphere must be seen as a kinetic temperature measuring the kinetic energy of the particles; collisions are rare.

From another point of view, that of homogeneity, we can divide the atmosphere into two main layers:

- *Homosphere*, extending up to 90 km, where all the atmospheric components are well mixed by the action of viscosity forces. The composition is uniform

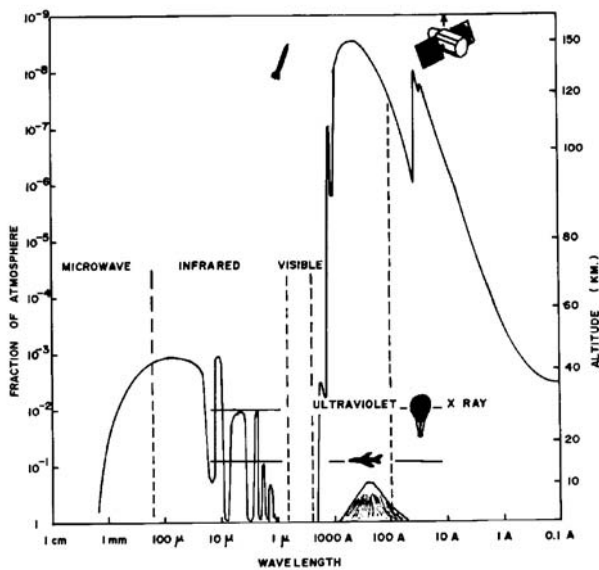


Figure 1.12: Profile of the terrestrial atmosphere showing the different layers and the instruments for observing the Sun and other astronomical bodies.

and can be expressed by a constant molecular weight.

- *Heterosphere*, situated above 90 km and where the different species separate from each other owing to the effect of gravity. According to this process, the average molecular mass decreases with altitude in this layer.

In principle, geometric distance is an adequate parameter for describing altitude, but because the atmosphere is concentrated near the surface, a small change in vertical distance means a huge change in the various physical parameters. An alternative is the atmospheric pressure (at the surface 1000 millibars, mb, or 1000 hecto-Pascals, hPa). Even better is the potential temperature²⁷, θ , the temperature a parcel of dry air would have if brought adiabatically from its initial state to the standard pressure (selected arbitrarily) of 1000 mb:

$$\theta = T \left(\frac{P_s}{P} \right)^{R/c_p}$$

where T = temperature of parcel in kelvins; P = pressure of parcel ; P_s = standard pressure (1000 mb); R = gas constant = 287 J kg⁻¹ K⁻¹ and c_p = specific heat capacity at constant pressure = 1000 J kg⁻¹ K⁻¹.

²⁷As a rule of thumb, it is possible to convert potential temperature to altitude in kilometres, just dividing by 25.

Like balloons, aircrafts need the air in the atmosphere to maintain the flight. They can reach only stratospheric heights (~ 40 km) and can therefore only access to the long wavelength tail of the UV region. To reach higher altitudes and explore fully the UV spectral window it was necessary to develop more powerful machines.

1.9 Rockets

1.9.1 From the pioneers to the V-2

The principle of action and reaction discovered by Isaac Newton²⁸ controls the motion of rockets propelled by the energy produced by the combustion of a chemical product.

The first scientific project for a rocket-propelled spacecraft was that of Hermann Ganswindt (1856–1934). In 1891 he published an article in a newspaper, in which he proposed an air machine propelled by a rocket with a motor driven by successive explosions in a steel container filled with dynamite. The thrust transmitted to the rocket would propel it, following Newton's principle. He also suggested that above a certain altitude, it would be not necessary to transmit more power to the vehicle to continue the flight. The practical possibility of using the rockets to reach the space was possible thanks to the work of separate teams of scientists and engineers, representing the independent development of the rocketry in different countries. In the following we briefly describe the work of the pioneers of the early years of rockets.

A Russian school teacher, Konstantin Tsiolkovsky (1857–1935), was making similar efforts to those of Ganswindt, but following a much more theoretical line. He mentioned the possibility of space travel for the first time in an article written in 1895. During 25 years he continued his work, remaining unknown to the rest of the world. In this period, he developed a rocket theory with liquid fuels based on kerosene, included in his book “The exploration of space by action–reaction machines”²⁹.

Robert H. Goddard (1882–1945) became interested in rockets by reading the publications of the science fiction writer H.G. Wells. In 1919 the Smithsonian Institution published his paper titled “A method of reaching extreme altitudes”, which suggested that one day a rocket could be flown to the Moon. In contrast to his predecessors he was a practical man, able to build and successfully test a liquid-fuel rocket the morning of 16 March, 1916. The experiments continued for many years, with the support of Charles Lindberg and the sponsorship of David Guggenheim. Goddard developed a gyroscope system for flight control, a payload for scientific instruments and a parachute recovery system, all essential elements in our days for the scientific research in space. The first of the rockets equipped with this system flew on 19 March, 1932. However, the success of Goddard's projects was strongly handicapped by his character; his reluctance to work with other teams cut him off from frontier research in rocketry.

²⁸For every action there is an equal and oppositely directed reaction.

²⁹He is very often remembered by the phrase: “Our planet is the birthplace of humanity, but one doesn't live one's whole life in the cradle”

Following an independent path, Theodore von Karman (1881–1963) created in 1936 the Guggenheim Aeronautical Laboratory operated by the California Institute of Technology, renamed in 1943 as the Jet Propulsion Laboratory (JPL). The first projects were related to the development of solid-fuels rockets. A good example was the WAC-Corporal (reaching 70 km on 26 September 1945) and later the Aerobee, capable of carrying a substantial load above 200 km. The name of Karman is linked to important theoretical and practical developments in aerodynamics and related technologies.

Another important developer of rocketry was Hermann Oberth (1894–1989). Born in the transylvanian city of Hermannstadt (Rumania), his interest in the space travel was motivated by reading Jules Verne “From the Earth to the Moon”. He suggested to use multiple-stage rockets, that he described the following way: “the requirements for stages developed out of these formulas. If there is a small rocket on top of a big one, and if the big one is jettisoned and the small one is ignited, then their speeds are added”. This and other ideas were included in his famous book “By rocket to interplanetary space”, written in a short version in 1923 and then expanded later in 1929. One of his main success was to popularize the idea of space travel and in 1927 the German Society for Space Travel was created³⁰.

The time was not yet ripe to reach the stars, but access to a new window for astronomical observations and unfortunately for other applications also was now possible. Germany was clearly the most advanced European country in rocketry. In spring 1930 Max Valier (1895–1930) developed a motor fuelled by gasoline and liquid oxygen attached to the frame of a racing car on railway tracks³¹. In March 1931 the first European rocket, constructed by Johannes Winkler (1887–1947), and propelled by a combination of methane and liquid oxygen, flew in Dassau (Germany).

An assistant of Oberth, Werner von Braun (1912–1977) would probably be the most decisive man in the history of rocketry. By December 1934, von Braun, had succeeded in launching an A–2 rocket powered by ethanol and liquid oxygen. On 3 October, 1942, a A–4 rocket was launched from the new base in Peenemünde, and followed a perfectly planned trajectory, finally landing 193 km away, just on target. Step by step the political situation was shifting the project from a pure research one to another with strong military implications. The change of the A–4 rocket to V–2, was a symbolic proof of this shift in emphasis³². In September 1944, the first V–2 was launched against London. The V–2 was already a very complex machine, 14 metres in length and with a weight of 13 tons at launch. The fuel was liquid oxygen mixed with ordinary alcohol and water (Figure 1.13).

For an extended description of rocket history, see von Braun *et al.* (1985), Neufeld (1994), Piszkiewicz (1995) and Blecker *et al.* (2002).

³⁰However, the only rocket builded by Oberth was the model used in the Fritz Lang film “A woman in the Moon”, in which the popular procedure of the countdown was used for the first time.

³¹Unfortunately the engine exploded and a metal splinter cut the aorta of Valier, who died in a few minutes

³²In fact, “A” comes from Aggregate (prototype) and “V” from Vergeltung (Vengeance).

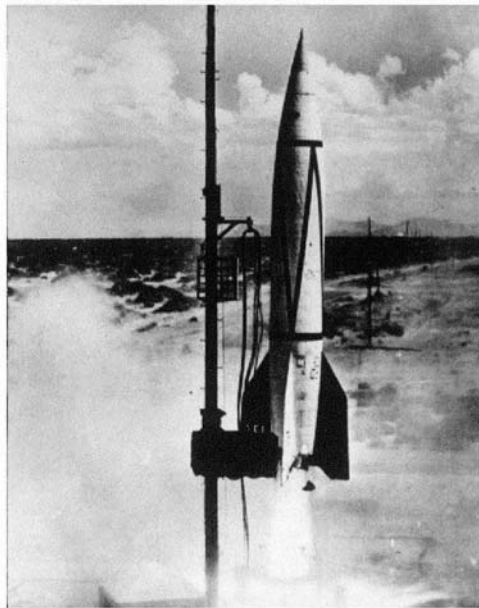


Figure 1.13: The launch of a V–2 at Peenemünde.

1.9.2 First solar UV observations

Observations during the brief moments of a total solar eclipse showed that there was material outside the solar disc seen in visible light. The inner part was called chromosphere and the outer layers, spanning several solar radii, received the name of corona. In 1930 Bernard Lyot (1897–1952) designed a system, the coronograph, that allowed these layers to be observed even when there was no eclipse.

In 1870 Charles Young (1834–1908) observed some spectral lines in the corona during a total solar eclipse in southern Spain and a debate started about their identification. Different analogies were sought, from terrestrial volcanoes to distant nebulae, but finally W. Grotrian (1890–1954) and later B. Edlen (1906–1993) successfully identified them with Fe X (637.4 nm) and Fe XIV (530.3 nm)³³. The implied temperatures, more than one million degrees, evidenced that the plasma of the outer solar layers should emit most of its radiation in ultraviolet and X-rays. However, these rays do not reach the terrestrial surface, so to study them it is necessary to go into space.

At the beginning of the World War Two the German astronomers Johann Pendl (1900–1991) and K.O. Kiepenheuer (1910–1975), convinced the Luftwaffe to build a set of observatories to monitor solar activity. The connection of solar activity with the ionosphere (see chapter 4) and its influence on communication systems was the main argument presented before the Wehrmacht authorities to create a set of observatories with the mission of patrolling solar activity. As a consequence of

³³Grotrian (1939), Edlen (1943, 1945).

this programme the observatories of Zugspitze, Wendelstein and Schauinsland, on German territory, Kanzelhöhe in Austria and Syracuse in Italy, were built³⁴.

Moreover, Kiepenheuer was always interested in studying the solar UV (Lyman- α) region and his contacts allowed the approval of a scientific programme using the V-2 developed by the team of Werner von Braun in Peenemünde. In fact, he designed a spectrograph for the ultraviolet and made observations with it at the Jungfraujoch Observatory (3600 m s.l.) and with stratospheric balloons. A new design, based on LiF optics (to observe at $\lambda < 200$ nm) was to have flown from Peenemünde in the summer of 1945, but the end of the war changed the programme.

Under the name Operation Overcast, an US army unit led by Colonel Holger T. Toftoy (1903–1967) rounded up von Braun's team, 118 persons, and captured an important quantity of material (~ 1000 rockets). The rockets were transported to the USA, where a new programme was initiated, financed by the US Navy, under the coordination of James G. Bain. White Sands (New Mexico) was established as the principal site for development and launching facilities. The situation looked very promising for the scientific research as expressed in a letter of Leo Goldberg (1913–1987) to Donald Menzel (1901–1976)³⁵: *If anyone asked you what technological development could, at one stroke, make obsolete all our textbooks written in astronomy, I am sure your answer and mine would be the same, namely the spectroscopy of the Sun outside the Earth's atmosphere ... I would like nothing more than to be involved in such a project, even if it meant shaving my head and working in a cell for the next ten or fifteen years.*

Richard Tousey (1908–1997) at the Naval Research Laboratory (NRL), designed a small spectrograph, 60 cm height, to be installed in the nose-cone of a V-2 rocket, and constructed by Baird Associates (Cambridge, Massachusetts). It consisted of a Rowland grating, two entrance apertures made of lithium fluoride and two sets of folding mirrors. After a number of failed attempts³⁶, on 10 October 1946, the rocket reached an altitude of 173 kilometres. By recovering the capsule, from the nosecone of the rocket it was possible to observe the first UV spectrum of the Sun in the range between 210–300 nm (Tousey *et al.* 1947). The spectral resolution was only 0.3 nm, but it was high enough to detect clearly the Mg II doublet at 280 nm (Figure 1.14). Alltogether, NRL spectrographs were flown on ten V-2 rockets during 1946–1948, of which four flights were successful. De Vorkin (1992) describes scientific research with V-2 rockets.

In a letter to Leo Goldberg, Henry Norris Russell (1877–1955) expressed his excitement after seeing the photographs: *these rocket spectra are certainly fascinating. My first look at one gives me a sense that I was seeing something that no astronomer could expect to see unless he was good and went to heaven!*

On V-2 flights between 1948 and 1950 the team headed by Tousey succeeded in proving the existence of solar Lyman α emission by means of a device that during

³⁴By including in the network observatories in occupied countries (for example Meudon, Pic du Midi and Ondřejov) Kiepenheuer was able to provide these institutions with some protection against military interference.

³⁵Cited in Hufbauer (1991), pg. 136.

³⁶A first attempt was made on 28 June, 1946, but the camera was never retrieved from the crater made by the V-2 impact on the desert floor

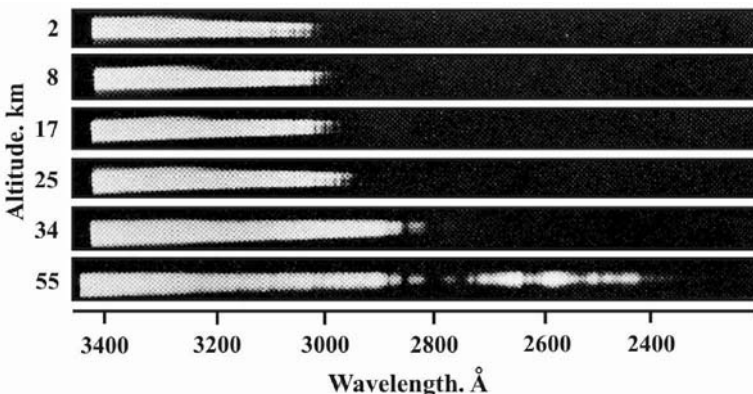


Figure 1.14: Solar spectra in the ultraviolet region obtained during the ascent of a V-2 rocket. A sequence of exposures shows how more and more ultraviolet radiation of the Sun is recorded as the rocket rises in altitude from 2 to 55 km above sea level (US Navy Photograph. NASM SI 87-8423).

flight exposed a thermoluminescent phosphor behind lithium fluoride and calcium fluoride windows. The lithium fluoride was transparent to Lyman α , whereas the calcium fluoride was not. The intensity of Lyman α inferred from that experiment was later confirmed by data obtained from spectra (Purcell & Tousey 1960) .

From this moment on, we have a continuous development in rocketry, clearly driven by the “Cold War” and the “space race”. At the same time, new UV spectrographs were developed with better resolution and with diminished effects of stray-light, allowing an increasing knowledge of the solar UV spectrum (Johnson *et al.* 1955; Behring *et al.* 1958). In July 1950 the first rocket was launched from Cape Cañaveral. It was the Bumper-2, a two-stage rocket combining a V-2 with a WAC Corporal, which successfully performed a temperature sounding of the upper atmosphere. On 13 March 1959, an Aerobee rocket, with instruments from the Naval Research Laboratory, obtained an image of the Sun in the Lyman - α line (121.6 nm) in which was possible to distinguish some faculae and which a larger contrast than in other spectral regions, in a similar way to Ca II K (Purcell *et al.* 1959 a,b) .

In the 1950s, NRL used a balloon-rocket combination (“Rockoon”) to investigate solar radiation and cosmic rays. A plastic balloon lifted a Deacon rocket to 21 km where a rocket was fired. By this technique the rockets carried a 22 kg payload to an altitude of more than 130 km. In recent times, a plane–rocket combination, in which a Pegasus rocket is launched from an L-1011 aircraft is often used.

The first ozone measurements were obtained by a team of the NRL using a V-2 rocket. They use the occultation method consisting in observing the Sun setting or rising behind the limb of Earth. The absorption spectrum of the upper atmosphere can thus be observed as a function of altitude to yield the vertical distribution of the different elements (Johnson *et al.* 1952).

The first evidence³⁷ of solar X rays, was obtained on 12 October, 1958, during a total solar eclipse in the South Pacific. From the platform of the portahelicopter USS Point Defiance four Nike-Asp rockets lifted a capsule equipped with suitable detectors to an altitude of 240 km. The first of these recorded a solar image just before the totality. Fortunately, there were two active regions close to the solar limb and their enhanced brightness allowed the detection of the radiation. Approximately 15% of the normal X-rays flux remained during the occultation of the solar photosphere (Chubb *et al.* 1961). Later on 19 April, 1960 the team led by H. Friedmann (1916–2000) at the Naval Research Laboratory, obtained from a rocket flight, what is considered the first solar image in X-rays, with a spatial resolution of approximately one arc minute (Blake *et al.* 1963). The last remaining doubts concerning the existence of a hot envelope encircling the solar surface were eliminated.

Progressive advances in detector technology and pointing systems continued to be made; however, the main goal was to reach the uppermost layers of the atmosphere to allow longer observations.

1.9.3 The Artificial Satellites

A major step forward in space research was marked by the launch of artificial satellites into orbits, that permitted the observation of astronomical bodies in spectral windows blocked by the Earth's atmosphere. In 1952, the International Council of Scientific Unions decided to establish the International Geophysical Year (IGY), a time interval in which the solar activity was expected to be very high. Two years later, the council adopted a resolution calling on all nations to launch artificial satellites during the IGY. In fact, the US government approved a plan for a satellite, whose construction was finally allocated to the NRL project, known by the name of Vanguard.

The Soviets stunned the world when, on 4 October, 1957, they announced the launch of Sputnik I, the first artificial satellite of the Earth. It was followed one month later by the Sputnik II, what apart from its greater weight (508 kg), carried the first living being into space: the little dog Laika.

Sergei Korolev (1906–1966) led the project. In 1931 he had developed the RP-318, the first Soviet rocket propelled aircraft. A victim of Stalin purges, he was imprisoned until the end of the World War Two. He was later appointed as the chief of a long-range ballistic missile, the R-7, launched on 1 April 1953. An improved version of the R-7 lifted the Sputniks to the skies. The third Soviet spaceship, launched in 1959, was already equipped with a spectrometer for UV solar observations. Work continued with the Cosmos 166 satellite, which recorded the solar spectrum in the region 80–95 nm (Bruns *et al.* 1970).

The British have the honour of launching the first satellite designed purely for astronomical research. Launched on 26 April, 1962, Ariel I measured solar UV and X-radiation, also obtaining a cosmic rays spectrum (LaFond 1962). The first

³⁷A instrument to measure solar X-rays flew on Sputnik II, in 1958, Un, a project led by S. Mandelshtam. However, there were electronic problems and the data were useless.

UV astronomical observations were obtained with free-spinning rockets, which did not permit pointing to a source.

After the first shock produced by Sputnik, the US tried to respond and after several failures of the Navy project Vanguard, on 31 January 1958, the Army used a rocket Jupiter-C to insert the Explorer I into orbit; a small ball weighting 13.1 kilograms. However, one of the most important consequences of the soviet successes was the creation of a US civil body responsible for space research. In July 1958, the US Congress passed the National Aeronautics and Space Act, which created the National Aeronautics and Space Administration (NASA) as of 1 October, 1958 (see Bilstein, 1990).

One of the first successful NASA programmes was related with the study of solar UV radiation. The Orbiting Solar Observatories series of satellites (Behring, 1970 ; Goldberg, 1967 , 1974) were equipped with a pointing system developed at the Ball Brothers Research Corporation (Colorado, USA). For the first time the UV spectrographs on board delivered spectra in different parts of this range, allowing models to be developed of the variation of physical parameters in the outer solar layers (e.g. Vernazza, Avrett & Loeser, 1973) .

The OSO project was complemented by SOLRAD, a series of eight satellites, developed at the NRL, to monitor solar high-energy radiation (Landini *et al.* 1972) . SOLRAD I was launched in June 1960, and the last was flown in 1976. Observations during the solar eclipse of 1966 showed that solar X-ray emission was concentrated spatially in small regions.

The astrophysical counterpart of OSO was constituted by the Orbiting Astronomical Observatories (OAO), equipped with UV cameras from the Smithsonian Institute and a spectrograph from the GSFC (Code *et al.* 1970) . After the failure of the first attempt, the OAO-2 was successfully launched on 7 December, 1968, and carried eleven UV telescopes. It was the first to detect UV radiation from the centre of the Andromeda Galaxy (Hills 1971). OAO-2 was followed by the OAO-3, better known as Copernicus, with a 80 cm UV telescope and a grating spectrometer equipped with four UV-sensitive phototubes covering the short (95–145 nm) and the long (165–300 nm) wavelength range. The scientific programme of Copernicus was mainly devoted to the interstellar medium.

Several western European countries also started joint astrophysical space projects. ESRO (European Space Research Organization), the predecessor of ESA (European Space Agency) was created in 1962. In March 1972 the ESRO TD-1 satellite was launched from the US base in Vandenberg with a Delta rocket and remained operational until May 1974. Its scientific mission was to carry out a survey in the UV and high energy spectral regions, collecting, in the UV range, data from approx. 58000 cosmic sources, in four different spectral bands, centred on 155, 195, 235 and 275 nm (Boksenberg *et al.* 1973) . Its UV Spectrophotometric Catalogue still constitutes a valuable reference for research (Jamar *et al.*, 1976 ; Thompson *et al.* 1978).

These projects led to the most successful astronomical satellite to date: The International Ultraviolet Explorer (IUE), a joint ESA, NASA and United Kingdom project (Bogess *et al.* 1978) . The 45 cm telescope and its auxiliary instrumentation were operational from 1978 to September 1996, obtaining about 104000

spectra of approximately 9600 objects, practically covering all the astrophysical research, with the sole exception of the Sun. Various conferences offer an adequate summary of the scientific highlights of the mission (Willis 1979; Rolfe & Heck 1982; Rolfe 1986; Kondo 1987 ; Wamsteker & González Riestra 1998).

Nowadays, the INES archive permits easy access to the huge amount of information supplied by the IUE, an unique archive for monitoring UV long-term variability of various astronomical bodies (Ponz *et al.* 1993; Barylak *et al.* 1995; Barylak & Ponz 1998; Talavera *et al.* 2001).

Various reviews (Tousey 1961, Wilson & Boksenberg 1969; Brosch 1999) and monographs (Browyer & Malina 1995) offer an extended overview of frontier astrophysical research at UV wavelengths.

1.9.4 Sounding rockets

Sounding rockets are sub-orbital vehicles carrying a payload above the Earth's atmosphere for periods of several minutes. The data are collected and returned to the ground station by telemetry. These rockets have mainly been used to investigate the physical properties of the mesosphere not directly accessible to balloons and satellites. Both relatively small launching sites and large installations are being used for this purpose.

The ESRO Sounding Rocket Programme was one of the pioneers, starting in 1964 in a military range in Sardinia and ending in 1972, with its activities mainly concentrated at the scandinavian Kiruna site.

NASA has currently fifteen sounding rockets, from the small Super Arcas (3 metres high) to the four-stage Black Braut X (20 meters high) capable of reaching altitudes of more than 1000 km.

The combination of satellites and sounding rockets is, in principle, an ideal tool for making vertical scans of the whole terrestrial atmosphere. However, the high costs implied have led to the gradual substitution of rockets by ground-based instruments such as Lidars and radars.

Chapter 2

Solar Ultraviolet Radiation and Magnetism

In this chapter we shall briefly review some basic facts concerning the main source of UV radiation in the Solar System, the Sun. The temperature of the solar atmosphere rises as one goes from the surface (the photosphere) to higher layers (the chromosphere and corona). The high temperature in these layers causes UV radiation to be emitted. Solar magnetism plays a key role in the heating of the outer solar atmosphere. We shall show how complex phenomena on the Sun are generated and influenced by magnetic fields and how the solar output varies with time on both short and long scales. This, of course, has influences on the Earth and other planets that will be discussed in the following chapters¹.

2.1 History of Solar Observations

The Sun was already identified as the source of life by ancient civilizations. Any variations, especially eclipses, were observed with fear. Possibly the oldest eclipse record is found on a clay tablet uncovered in the ancient city of Ugarit (in what is now Syria) for which two plausible dates are usually cited: 3 May 1375 BC or 5 March 1223 BC. The latter date is favoured by most authors. By the eighth century BC, the Babylonians were keeping a systematic record of solar eclipses and may even have been able to predict them fairly accurately based on simple numerical rules.

A very well known phenomenon of solar activity are sunspots, which are strong concentrations of magnetic fields. Most are too small to be visible to the naked eye. When the sun is partially obscured by clouds or thick mist then extraordinarily large spots (with a diameter of more than 40000 km) can be seen with the naked

¹For textbooks see e.g. Zirin, H., 1988, *Astrophysics of the Sun* (Cambridge University Press); Lang, K.R., 2001, *The Cambridge Encyclopedia of the Sun*, (Cambridge Univ. Press); K.H. Phillips, 1995, *A Guide to the Sun* (Cambridge Univ. Press); M. Stix, 2002, *The Sun*, (Springer Verlag)

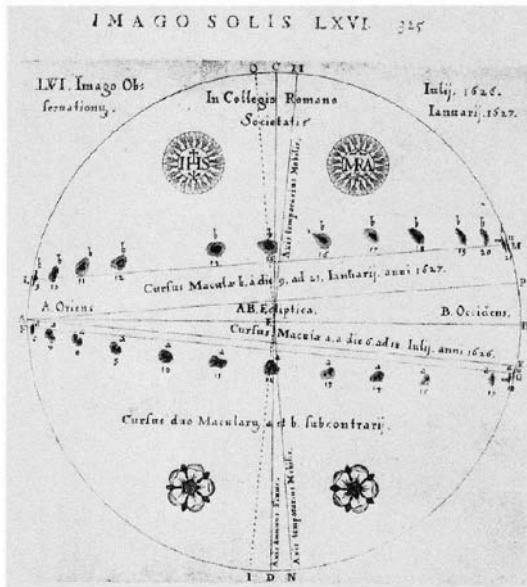


Figure 2.1: Sunspot drawing of Scheiner (1630) in “Rosa Ursina”, reproduced from *The history of the discovery of the solar spots*, in Popular Astronomy, 24, W.M. Mitchell, 1916. This drawing illustrates the apparent paths of sunspots across the solar disc, for two sets of observations taken six months apart. Based on such observations, Scheiner correctly concluded that the Sun’s equatorial plane is inclined by 7° with respect to the ecliptic.

eye. Around of 800 BC there are records from Chinese astronomers concerning sunspots. Aristarchus of Samos (310–230 BC) made a first attempt to measure the distance Earth-Moon and Earth-Sun. The measuring principle can be found in many basic textbooks on astronomy. The first sunspot drawing was made in 1128 found in the “Chronicles” of John of Worcester. Copernicus placed the Sun in the center of the known universe (1543) with all the planets, including the Earth, moving around it.

The development of science made it possible to consider the Sun as an object with the same kind of physical properties known on Earth, such as mass and temperature. The mass of the Sun was calculated by Isaac Newton (1642–1727). Making use of his law of universal gravitation the calculation was presented in “Principia Mathematica”. Newton also initiated the scientific analysis of sunlight by demonstrating that sunlight can be separated into different colours using a glass prism.

At the beginning of the seventeenth century four astronomers made the first telescopic solar observations: Johann Goldsmid (1587–1616, known as Fabricius) in Holland, Thomas Harriot (1560–1621) in England, Galileo Galilei (1564–1642) in Italy, and Christoph Scheiner (1575–1650) in Germany. The oldest recorded telescopic sunspot observation belongs to Thomas Harriot and was made on 8

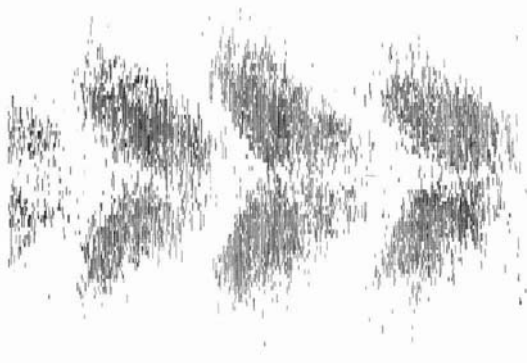


Figure 2.2: The first butterfly diagram plotted by E. Maunder

December, 1610. The sunspots were first considered by Scheiner as intra-Mercurial planets. It was Galilei who supposed them to be features on the solar surface (see also Figure 2.1). William Herschel (1738–1822), suggested that sunspots are much cooler than the rest of the solar surface.

Step by step, the observations became more systematic. S.H. Schwabe (1789–1875) found an 11 year periodicity of the number of sunspots, the solar activity cycle and the first clear signal of solar variability². R. Wolf (1816–1893), who was professor at the ETH Zürich, defined the sunspot relative number, measuring the activity independently of the quality of the observations. Gustav Spörer (1822–1895) and R.C. Carrington (1826–1875) found that the Sun does not rotate as a rigid body but differentially and that the sunspots drift gradually to the equator in the course of the sunspot cycle, now known as Spörer's law (Spörer 1885; Carrington 1858). In 1904 Maunder plotted the first sunspot “butterfly diagram”, showing the migration of sunspot groups from higher latitudes at the beginning of a sunspot cycle to lower latitudes at the end (Figure 2.2)³.

Spörer also found that during the second half of the seventeenth century there were exceptionally few sunspots. This finding was later published by E.W. Maunder (1894) and verified many years later by Eddy (1976). This period is known as the Maunder Minimum of solar activity (see Soon & Yaskell 2003).

The discovery of the spectrograph allowed the determination of the physical properties and chemical composition of the solar atmosphere. In 1868 Pierre-Jules-Cesar Janssen (1824–1907) and Norman Lockyer (1836–1920) discovered an unidentified yellow line in solar prominence spectra and suggested that it originates from a new element which they named “helium”.

G.E. Hale (1868–1938) and Henri Deslandres (1853–1948) simultaneously and independently, invented the spectroheliograph. With this instrument it was possi-

²Schwabe, S.H., 1844, Sonnen- Beobachtungen im Jahre 1843, Astronomische Nachrichten 21, 233.

³Maunder, E.W., 1904, Note on the distribution of sunspots in heliographic latitude, 1874 to 1902, Monthly Notices Royal Astronomical Society 64, 747–761.

Table 2.1: Basic characteristics of the Sun.

Quantity	Value
Solar radius, R_{\odot}	6.96×10^5 km
Solar mass, M_{\odot}	1.989×10^{30} kg
Temperature, surface	5800 K
Temperature, center	1.5×10^7 K
Density (centre)	151 g cm^{-3}
Density (mean)	1.4 g cm^{-3}
Age	4.55×10^9 yr
Chemical composition	H 92.1% (number of atoms) He 7.8% (number of atoms)
distance from Earth	150×10^6 km = 1 Astronomical unit (AU)
Energy output	3.86×10^{33} erg s $^{-1}$

ble to observe the Sun in a narrow spectral range. From the broadening of spectral lines due to the Zeeman effect it was concluded that sunspots must be sources of very intense magnetic fields (Hale 1908)⁴. In 1931 Bernard Lyot (1897–1952) designed the coronograph, a telescope equipped with an occulting disc, sized in such a way as to block out the solar disc and to observe the outer layers of the Sun.

Of course, for us it is very important to study the relationships between the Sun and the Earth. The discovery of the variability of the solar output in different channels (UV, X-rays, solar wind) was important and will be described in detail in the next chapter. For now, let us introduce the topic by speaking about the most spectacular manifestation of this variability: flares. While observing a prominent group of sunspots on 1 September, 1859, R.C. Carrington wrote “two patches of intensely bright and white light broke out” (Carrington, 1859). The patches brightened rapidly and then decayed again and, by chance, the observation was confirmed by another English astronomer. Carrington had seen a flare, of the rare variety that is visible in white light (only about 50 are known)⁵.

2.2 The Sun as a Star

From the astrophysical point of view, our Sun is an ordinary star. There are stars that are much larger than the Sun and there are others that are smaller. Some basic physical parameters for the Sun are given in Table 2.1.

However, the study of the Sun as a star is of great astrophysical relevance. The Sun is the only star for which we can directly observe details on its surface, since all other stars are too distant to see surface details, even with large telescopes.

⁴For a historical review see Del Toro Iniesta (1996) and Harvey (1999).

⁵For textbooks about the history of solar physics see Meadows (1970) and Hufbauer (1993).

Table 2.2: Basic characteristics of the main zones of the solar interior. $\rho_{\text{atm,SL}}^1$ is the density of Earth's atmosphere at sea level

Name	Extension in R_\odot	Temperature	Density [g/cm ³]
Core	0–0.25	1.5×10^7 – 7×10^6	150–20
Radiative zone	0.25–0.70	7×10^6 – 2×10^6	20–0.2
Tachocline	thin		
Convective zone	0.70–1.0	2×10^6 – 7×10^3	0.2 – $1/10000\rho_{\text{atm,SL}}^1$

2.2.1 Basic facts about the Sun

Basically, we can make a distinction between the interior of the Sun and its atmosphere. The Sun's interior can be further divided into the following layers starting from the centre (see Table 2.2):

- Core: this is the region where nuclear fusion takes place. Hydrogen is converted into helium and since the Sun is mainly composed of H and He, its nuclear fuel lasts for 10^{10} years in total. The temperature is about 1.5×10^7 K.
- Radiative zone: here the energy is transported outwards by radiation.
- Tachocline: in this thin zone shearing motions occur between the fluid motions of the upper lying convection zone and the stable radiative zone; this generates magnetic flux.
- Convection zone: because of the lower temperature, atoms become only partially ionized, which increases the opacity giving rise to convective motions.

We now briefly discuss the solar atmosphere, from which the radiation originates.

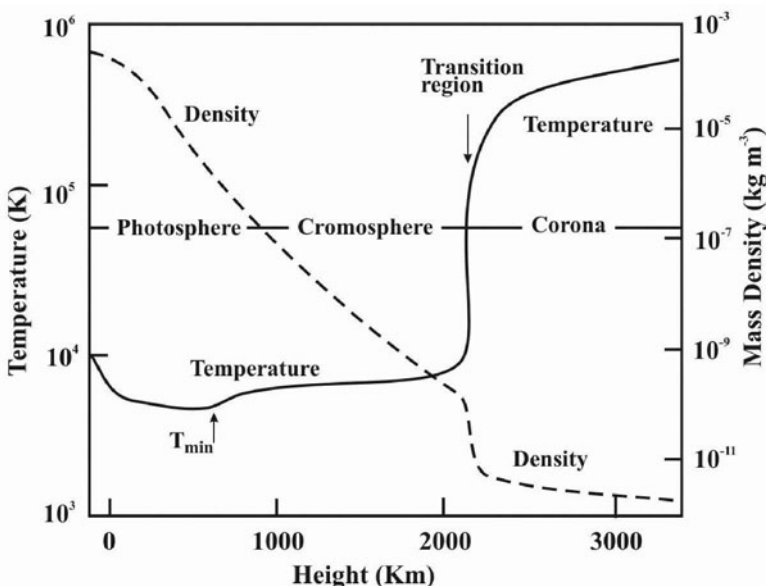
The photosphere is a layer that is only about 400 km thick and where more than 90% of the solar radiation is emitted (especially in the visible). This layer is often referred to as the solar surface.

Above the photosphere the temperature rises from a minimum of about 4500 K to several 10^4 K in the chromosphere. In the subsequent transition zone the temperature increases very sharply to several 10^5 K and the outermost layer of the solar atmosphere is called the corona. The chromosphere and the corona cannot be observed under normal conditions because these layers are very faint in comparison with the solar surface. First observations of the corona were made during total solar eclipses. The temperature there is several 10^6 K. In Table 2.3 and Figure 2.3 we give the basic parameters of these layers.

The solar material is a plasma, a highly ionized medium with a characteristic behaviour: the plasma motions generate magnetic fields. In the Sun there exist two extremes which describe the interaction of magnetic fields and plasma motions. In some cases the magnetic fields drift in response to the plasma motions and in other cases the magnetic fields force these motions to follow the field lines. To

Table 2.3: Basic characteristics of the solar atmosphere.

Name	Extension in R_{\odot}	Temperature	Density [g cm^{-3}]
Photosphere	400 km	7000–4500	$\sim 10^{-7}$
Chromosphere	$\sim 10^4 \text{ km}$	$\times 10^4 \dots \times 10^5$	10^{-12}
Transition region	thin		
Corona	R_{\odot}	10^6	10^{-17}

Figure 2.3: Variation of temperature and density in the solar atmosphere. Adapted from Athay (1976) *The Solar Chromosphere and Corona: Quiet Sun*, D. Reidel, Figure I-1.

understand this, let us introduce the so-called plasma β which is the ratio of gas pressure, p over the magnetic pressure $B^2/8\pi$:

$$\beta = 8\pi p/B^2$$

In the corona, the ratio between the plasma pressure and the magnetic pressure is much less than unity. The magnetic field therefore determines the motion of plasma in the corona as it can be seen by X-ray and EUV observations of loops. In the photosphere, however, the gas pressure is greater than the magnetic pressure owing to enhanced density. That means that here the plasma motions dominate the magnetic structure⁶.

⁶We say that the magnetic field is “frozen in”.

2.2.2 Evolution of the Sun

The Sun is a variable star. During the lifetime of an observer the global changes of the Sun are practically negligible. Information about its evolution can be deduced, however, by comparing it with other stars. There are solar-like stars⁷ at similar ages to that of the Sun, but there are also much older and younger ones.

We can follow the evolution of the Sun by comparing it with these stars. For the study of UV radiation the evolution of the Sun is of fundamental importance since its UV output changed significantly from the formation of the planets about 4.5 billion years ago to now.

The evolution of the Sun can be mainly divided into the three following phases.

The Birth of the Sun

The vast space between the stars is filled with the so-called interstellar medium, which has an extremely low density (about one atom per 10 cm^3 ; for comparison the air that we breathe contains 3×10^{19} molecules per cm^3) consisting mainly of gas (mostly hydrogen $\sim 90\%$) with some dust. The dust particles are extremely small – their size being about the wavelength of blue light – and consist of silicates, carbon, ice, and/or iron compounds. On average, the density of the dust particles is about one particle per 10^6 m^3 .

Interstellar gas can be observed as optical absorption lines (e.g. Ca II) or as H II regions (ionized H) or H I regions. H II regions fluoresce stellar radiation: UV radiation from the hot stars embedded within them is converted to lower energy photons. Also molecular lines are observed. Typical molecular clouds have masses up to 1000 solar.

Such molecular clouds start to collapse as soon as gravity becomes dominant (the Jeans criterion). Typical conditions found in the interstellar medium are: $T = 50\text{ K}$ and density $\rho = 10^{-20}\text{ kg m}^{-3}$. For these values one can easily estimate that a spherically symmetric collapse would take about $\sim 3 \times 10^7\text{ yr}$. Because of the conservation of angular momentum such contracting objects would start to spin faster and faster and the magnetic field to act as a lever arm for the torque required to remove angular momentum. Therefore, during the first phase of collapse magnetic braking takes place. When the density has become sufficiently large, neutral particles can form via recombination, and the cloud is no longer coupled to the magnetic field.

The cloud fragments into $\sim 10^3$ stars (typical for a galactic cluster) and subsystems are formed. The Sun and the planets were formed out of such a typical subsystem. One such a fragment, known as the pre solar nebula, had a density between 10^{-17} and $10^{-15}\text{ kg m}^{-3}$. Within about 10^6 years the protosun was formed - the core heated up to a few million degrees and thermonuclear reactions commenced. The subsequent increase in temperature causes the pressure to grow to such a point that the gravitational collapse stopped: the Sun was born. The star became stable, no further contraction that releases gravitational energy occurs.

⁷Stars are classified as solar-like when their mass, temperature, composition and radius are similar to those of the Sun. See chapter 3 for more details.

Table 2.4: Future evolution of the Sun.

Time (Ga)	Luminosity (L_{\odot})	Radius (R_{\odot})
5.5	1.08	1.04
6.6	1.19	1.08
7.7	1.32	1.14
8.8	1.50	1.22
9.8	1.76	1.36

Hydrostatic equilibrium was reached. At this stage the Sun is a zero age main sequence star.

Main sequence Sun

Stars are on the main sequence for most of their evolution; they are stable and in hydrostatic equilibrium. Energy is provided by thermonuclear reactions, mostly by the conversion of hydrogen into helium ($4^1\text{H} \rightarrow ^4\text{He}$).

The mass of the resulting He nucleus is smaller than its constituents and 0.7% of the total mass is converted to energy ($\sim 26.5 \text{ MeV}$)⁸. At this point we stress that how long a star stays on the main sequence depends on its mass.

Post main sequence evolution

The main sequence lifetime of the Sun is about 9 billion years. Owing to thermonuclear fusion, the core becomes enriched with He. When there is no H left in the core, energy generation occurs in a shell around the core, and the Sun expands into a red giant. At this stage its size will exceed that of the orbit of the Earth. The outer layers of the Sun are unstable and are expelled. The core evolves into a white dwarf, which is an extremely compact Earth-sized object (see Table 2.4).

2.2.3 UV Variation during solar evolution

As has been shown, the thermonuclear fusion process leads to a gradual increase in the molecular weight μ in the core. At the present time about 50% of its central H content has been already transformed into He. The thermal pressure is given by $P \sim \rho RT/\mu$, where R is the gas constant. A lower mean molecular weight during the early phases of solar evolution implies a lower temperature (or density) in order to balance the gravitational force.

We therefore see that the temperature must have increased during the Sun's evolution until the present and will continue to increase. As nuclear reaction rates depend strongly on temperature, the luminosity of the Sun was affected by the gradual increase in the temperature of its core. For the initial He content, Y_0 , one

⁸The Sun transforms 4 million tons per second into energy and has lost about 1% of its original mass during its 4.5 billion years of evolution

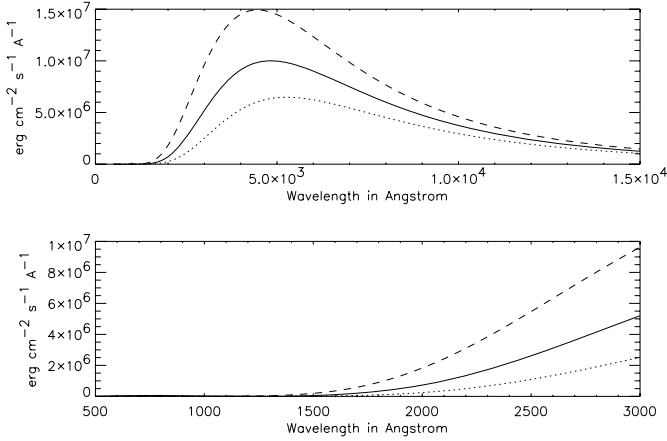


Figure 2.4: Variation of solar energy output for the early Sun (dots), present Sun (full line) and late Sun (dashed). For the early Sun a reduction of 10% in effective temperature compared its present value is assumed, for the late Sun an enhancement of 10%. The lower panel shows the variation in UV emission. From the early to the late Sun the variation is about a factor of 10!

could take the amount of He that was created during the Big Bang⁹. However, the age of the solar system is only about one third of that of the universe, hence different values are taken for the He content, Y , in order to match the current luminosity.

Let us make a simple estimate for the energy output of the Sun, especially for the UV radiation as it evolves along the main sequence. In Figure 2.4 we give the plot for a variation of the Planck function for a young Sun (with a temperature reduction of 10%), the present Sun and the Sun near the end of its main sequence lifetime (where we assume an 10% enhancement of temperature). The upper panel shows the variation from the whole UV and visible range to the IR. It is seen that in the IR the variation is very low. In the UV from 150 to 300 nm the variation is up by a factor of 10 during the evolution of the Sun on the main sequence (total time about 9 Ga) (see lower panel of Figure 2.4).

The UV radiation of the Sun is a very important factor in the history of the evolution of life on Earth and it is therefore extremely important to know about it in detail. It also plays a key role in developing photochemical models of the prebiotic and Archean atmosphere of the Earth (see chapter 5). Please note that these considerations only describe the conditions of a quiet Sun with no activity at all.

⁹This is also called the primordial value.

2.3 The Solar Irradiance

2.3.1 First measurements

The amount of solar radiation that is received on Earth is a fundamental quantity called solar irradiance S . Since it is the basic input parameter for the weather system and climate it is highly desirable to know this quantity with high precision and to estimate whether it is constant or not. Because of the influence of the Earth's atmosphere it is extremely difficult to determine this value with great precision.

Claude Pouillet (1790–1868) and John Herschel (1792–1871) first attempted to measure the energy input from the Sun with an apparatus in which a known amount of water is exposed to sunlight for a fixed period of time and the rise in temperature is recorded. It later became clear that the Earth's atmosphere absorbs a significant portion of the incident radiation and S. Langley (1834–1906) verified this by determining the solar constant during an expedition to Mt. Whitney in California (1881).

Charles Abbot (1872–1973) developed a programme of measurements of the so-called solar constant in an attempt to verify first its possible variations (Abbot *et al.* 1913 ; Hoyt, 1979a,b) and then its possible connection with terrestrial climate changes (Clayton, 1930) . A group of high mountain observatories around the world was dedicated to this topic in order to minimize the disturbing effects of the Earth's atmosphere. Collaborating with the Weather Bureau and Signal Corps and Anders Knut Angström (1857 - 1910)¹⁰, Abbot installed a new type of robotic pyrheliometers fully automatic and self-recording on several balloons. His assistant, B. Aldrich, launched these balloons which reached heights of up to 25 km from the Californian coast during several campaigns in 1913 and 1914. At least one of them returned clear evidence for thermometric and barometric variations that confirmed Abbot's corrections for atmospheric extinction and allowed him to determine the value of the solar constant at the top of the Earth's atmosphere.

High altitude (30–36 km) measurements with balloons were also performed by Kondratyev & Nikolsky (1970). The NASA B-57B research aircraft measured solar irradiance, supplemented later with the X-15 (Laue & Drummond 1968) and Convair CV-990 (Thekaekara *et al.* 1969). The Mariner VI and VII spacecrafts were the first to measure the solar constant entirely outside the atmosphere.

Figure 2.5 gives an overview of the different historical measurements of solar irradiance carried out on different platforms (balloons, rockets, aircrafts). Finally, radiometers on board satellites have provided an adequate standard for measurements, although problems remain with the absolute calibration and the long-term stability (for recent reviews see Pap 2003 and Krivova & Solanki 2003).

The solar constant, S , is defined as the integrated solar spectral irradiance over all wavelengths. It is given in Wm^{-2} and corrected to 1 AU¹¹. The derived value from daily averages from six satellites over 1978–1998 is $S = 1355.1 \text{ Wm}^{-2}$.

¹⁰Son of Anders Jonas Angström (1814–1874), the proposer of the wavelength unit, the Angström (\AA).

¹¹1 AU = 1 Astronomical unit = mean Sun–Earth distance = 149 598 500 km

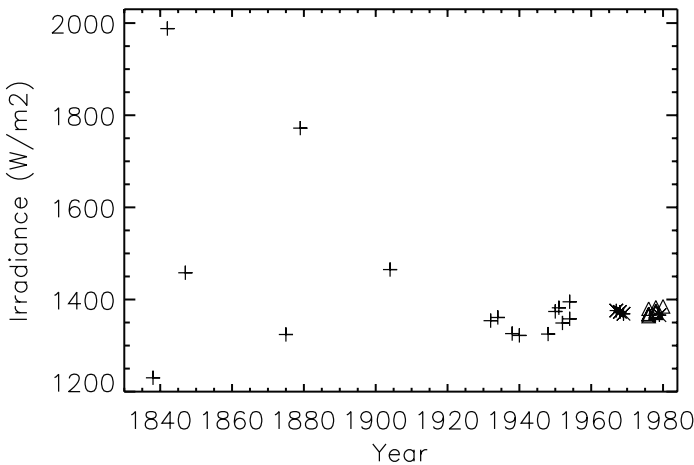


Figure 2.5: Variation of the measured values of solar irradiance over the period (1840–1980). (+) ground observations; (Δ) rockets and (*) balloons.

The total solar irradiance (TSI) varies by 0.1–0.2% over a solar cycle. This small fluctuation reflects stability of the solar photosphere as seen in the visible spectrum which extends from the blue at 400 nm to 800 nm. The shorter the wavelengths however, the larger the fluctuations.

2.3.2 The Solar UV Spectrum

Global Description

In the previous chapter we described the first attempts to measure the solar UV radiation using rockets. We shall now describe the characteristics of this part of the electromagnetic spectrum in more detail.

The solar spectrum from 1 to 10^6 nm is given in Figure 2.6. It is seen that in the EUV the intensity is a 10^{-4} that at maximum. The solar UV spectrum approximates a black-body spectrum in the range 300–400 nm, but the Sun emits less radiation than this theoretical curve shortward of 300 nm, because of absorption in the upper photosphere and lower chromosphere. The solar ultraviolet (UV) irradiance, defined here as the wavelength region between 150 and 400 nm, represents less than 8% of the total solar output. The UV irradiance in the spectral region $\lambda < 300$ nm accounts for less than 1% of the TSI.

A very well known phenomenon on the Sun visible with even small instruments is limb darkening. The Sun appears brighter near the centre of its disc than near the limb. The explanation of this is that, when we look at the Sun in the visible range, near the centre we look into deeper and hence hotter regions (the temperature increases with depth) than we look towards to the limb, where an

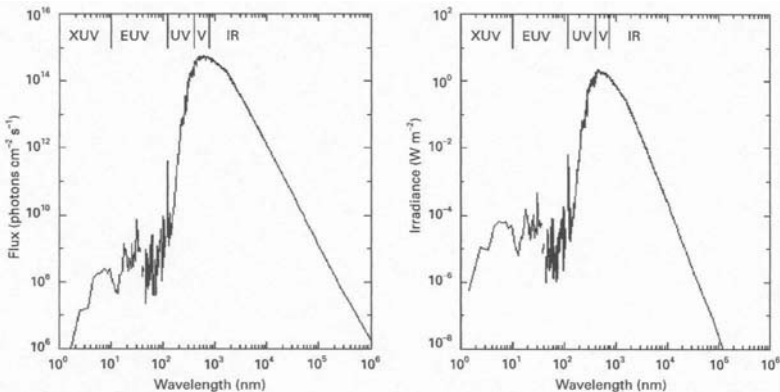


Figure 2.6: Solar irradiance from the X-rays region to the infrared. Adapted from Tobiska *et al.* (2000) Journal of Atmospheric and Solar Terrestrial Physics 62, 1233-1250. Courtesy of Elsevier.

optical depth of unity is reached at higher and hence cooler levels. This is valid for the visible part of the solar spectrum. However, when we proceed to the ultraviolet part of the spectrum, the absorption coefficient, which determines how deep we see into the solar atmosphere, increases rapidly. This means that we see higher parts of the solar atmosphere. At observations below $\lambda = 150.0$ nm limb darkening changes to limb brightening. This phenomenon can be interpreted as follows. At wavelengths shorter than 150 nm, we look into areas above the temperature minimum of the Sun which occurs at a height of about 500 km above solar surface level¹².

For $\lambda > 400$ nm the empirically derived absorption coefficient very well coincides with the theoretical absorption coefficient of the negative hydrogen ion H⁻. In the UV range the contribution of metals to the absorption becomes much more efficient than H⁻.

In Table 2.5 we give an overview over the different designations of solar radiation in the UV domain.

The longer wavelength of the UV range ($\lambda > 200$ nm) is dominated by the photospheric continuum, which is overlapped by an absorption line spectrum and is very similar to the continuum in the visible spectrum. There is a continuum absorption edge associated with each of the hydrogen series (Balmer at 365 nm and Lyman at 912 nm). For a given ion, such as the hydrogen atom, one will see series of emission lines with progressively shorter wavelengths up to a boundary defined by the ionization energy (Figure 2.7).

The appearance of emission below 200 nm indicates that the source function is increasing in the lines relative to the continuum towards higher solar atmospheric layers. As a rule of thumb the state of ionization increases towards the shorter

¹²The surface level is defined as $\tau_{500} = 1$ where the subscript refers to the wavelength at which τ is given (500 nm).

Table 2.5: UV radiation and its division into different ranges

Name	Range
UV	$100 \text{ nm} < \lambda < 400 \text{ nm}$
Vacuum UV	$10 \text{ nm} < \lambda < 200 \text{ nm}$
Extreme UV, EUV	$10 \text{ nm} < \lambda < 100 \text{ nm}$
Far UV, FUV	$100 \text{ nm} < \lambda < 200 \text{ nm}$
Middle UV, MUV	$200 \text{ nm} < \lambda < 300 \text{ nm}$
Near UV	$300 \text{ nm} < \lambda < 400 \text{ nm}$
UV-C	$100 \text{ nm} < \lambda < 280 \text{ nm}$
UV-B	$280 \text{ nm} < \lambda < 315 \text{ nm}$
UV-A	$315 \text{ nm} < \lambda < 400 \text{ nm}$

wavelengths (Table 2.6). This correlation is simply explained. Most of the observed lines are resonance lines and the wavelength of the resonance of a particular ion is roughly correlated with the ionization potential of that ion.

Table 2.6: Averaged ionization potential in the solar atmosphere for different wavelength intervals. Adapted from Pottasch (1970) *IAU Symp. 36: Ultraviolet Stellar Spectra and Related Ground-Based Observations, pages 241-249.*

Wavelength interval [nm]	Averaged ionization potential [eV]
100–200	30
60–100	60
30–60	150
4–30	300
1.5–6	600

At wavelengths shorter than 170 nm only emission lines are seen. The Lyman α of hydrogen at 121.6 nm is as strong as all the other UV lines put together. The line of HeII at 30.4 nm is as strong as all the UV lines below 50.0 nm.

Figure 2.8 show a plot of a range of the EUV solar spectrum compared with that of α Centauri and table 2.7 lists selected observations obtained in the EUV range. Wilhelm *et al.* (2004) and Harrison (2005) have recently reviewed solar observations in the UV spectral range.

In the next section we discuss how the solar structures are related to the different types of emission.

2.4 Solar Observational Features

In this section we will give a summary of the various phenomena seen on the Sun. Some are always present others vary with the solar activity cycle. As it will turn out, all processes that occur in the higher layers of the solar atmosphere are related

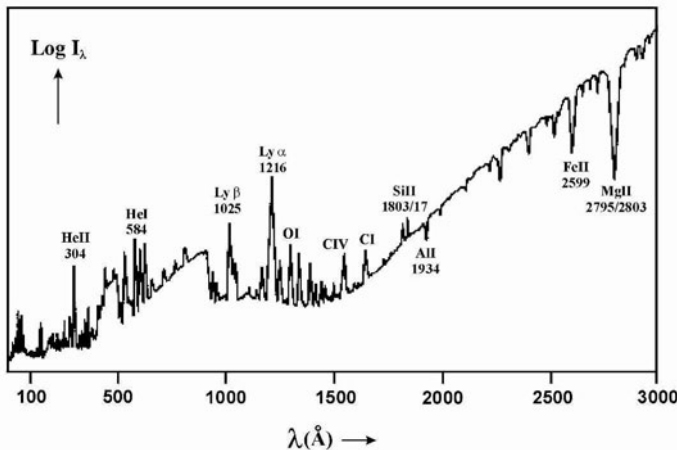


Figure 2.7: The solar ultraviolet spectrum. Adapted from Scheffler & Elsässer, 1974, *Physik der Sterne und der Sonne*, Bibliographisches Institut, Figure I.6 .

to the taking place on the solar surface. The solar cycle itself will be discussed in the next chapter.

2.4.1 The Photosphere

The photosphere is the deepest visible layer. The temperature at the surface of the Sun is about 5700 K. However, the photosphere is far from homogeneous in appearance and reveals several phenomena.

Solar Granulation

Under excellent observing conditions, the photosphere exhibits a cellular pattern, called granulation, the cells being about 1000 km in diameter and a lifetime of 5-10 minutes. This structure was already detected by William Herschel (1738-1822) in 1801. Solar granulation is the visible manifestation of the convection zone that lies below the photosphere. Hot matter rises in the bright granules, cools and then descends in the intergranular lanes. Whereas the upflow is relatively smooth, the downflow is more turbulent and in the downflowing areas turbulent motions occur that can induce shock waves that penetrate into the overlying chromosphere and contribute to a heating there. A recent review of solar granulation is given by Muller (1999).

The supergranulation was first detected as a pattern in the velocity field and the typical cell size is about 30 000 km. In the centre the upflow is about 50 m s^{-1} , the downflow is about 100 ms^{-1} ; the lifetime of the supergranular cells is in the order of a day.

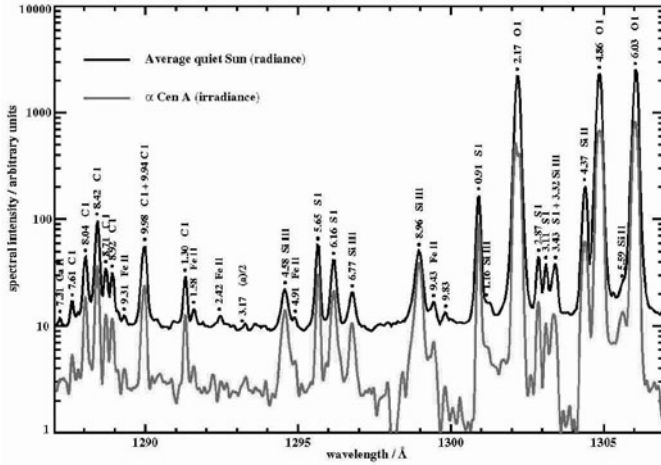


Figure 2.8: A close-up of a tiny part of the spectral atlas released from the SUMER instrument, compared with the irradiance spectrum of Alpha Cen A from HST-STIS. Courtesy; SOHO/SUMER (ESA & NASA), HST-STIS (NASA & ESA), W. Curdt.

Sunspots

Sunspots are the oldest known direct manifestations of solar activity. Most consist of a central dark region, known as the umbra (temperature about 4000 K) and a surrounding less dark filamentary region, known as penumbra (temperature about 5000 K). Since sunspots are darker than their surroundings they emit less energy per unit area.

The Zeeman splitting of magnetically sensitive lines and the polarization of the split components in the spectra of sunspots imply that sunspots are related to strong intense magnetic fields¹³.

Biermann (1941) showed that the strong sunspot magnetic field would impede convective currents carrying energy in the convective zone. In strong fields, matter can move only along the field lines. In normal convection there must always be some horizontal circulation associated with vertical convection. When an element of gas becomes convectively unstable, it can only rise if the surrounding gas flows in horizontally, otherwise there would be a pressure imbalance.

Consider a sunspot as a vertical tube. The values for magnetic field and pressure inside the tube are subscripted by a zero (P_0, B_0) and outside by e . There must be an equilibrium between the pressure outside the tube and inside, owing to the pressure generated by the magnetic field ($P_m = B^2/8\pi$)

$$P_e = P_0 + \frac{B_0^2}{8\pi}$$

¹³For some atoms, spectral lines split in three under a magnetic field. This is known as the normal Zeeman effect. For other atoms, the spectrum displays a more complex pattern of splittings, known as the anomalous Zeeman effect.

Table 2.7: Sources of Relevant UV spectra. ATM (Apollo Telescope Mount). For rockets we understand suborbital short flights.

Satellite	Range (nm)	Reference
OSO-III	26–130	Hinteregger & Hall (1969)
OSO-IV	30–140	Reeves & Parkinson (1970)
Skylab ATM/NRL	97–394	Bartoe <i>et al.</i> (1977)
Skylab ATM/HCO	28–134	Reeves <i>et al.</i> (1977)
SMM	115–360	Woodgate <i>et al.</i> (1980)
HRTS	119–173	Brekke <i>et al.</i> (1991)
SUMER/SOHO	47–161	Curdt <i>et al.</i> (2001)
CDS/SOHO	30.7–38.0; 51.5–63.2	Brekke <i>et al.</i> (2000)
Rockets		
LPSP/TRC	Ly- α	Bonnet <i>et al.</i> (1980)
SERTS	17–45	Brosius <i>et al.</i> (1998)
Atlas-1	200–350	Thuillier <i>et al.</i> (1997)
VAULT	Ly- α	Korendyke <i>et al.</i> (2001)

Since the pressure is given by $P = nkT$ we immediately see that $T_0 < T_e$.

Recent reviews on sunspots were given by Sobotka (1999) and Thomas & Weiss (2004).

Faculae

Sunspots are usually accompanied by bright structures called faculae (see Figure 2.9). They often precedes and considerably outlast the sunspots. The brightening in white light near the disc centre is barely detectable but increases towards the limb. Like sunspots faculae are associated with strong magnetic fields.

The method of observing faculae near the disc centre is to use narrow-band filters centred on temperature-sensitive lines such as the CN-band at 384 nm (Sheeley 1969) and the G-band at 430.8 nm (Figure 2.10). It was found that these bright structures correspond to small-scale concentrations of the magnetic field (Stenflo 1966 , Livingston & Harvey 1969).

The increased magnetic pressure in spots and faculae causes a decrease in their internal gas pressure and opacity relative to layers of equal geometric depth in the photosphere. We observe at greater geometrical depth in these magnetic concentrations than in the surrounding photosphere (see Figure 2.11).

Table 2.8 show the relevant parameters of the various magnetic structures observed in the solar photosphere.

A critical point is to understand how brightness is related to magnetic flux, going from bright faculae to dark sunspots. This phenomenon has been simulated numerically by Spruit & Zwaan (1981), who calculated the balance between the inhibition of convective energy transport (strong in large magnetic concentrations and in deep layers) and lateral radiative heating from the non-magnetic surroundings, which is substantial in small structures and in their upper layers because of

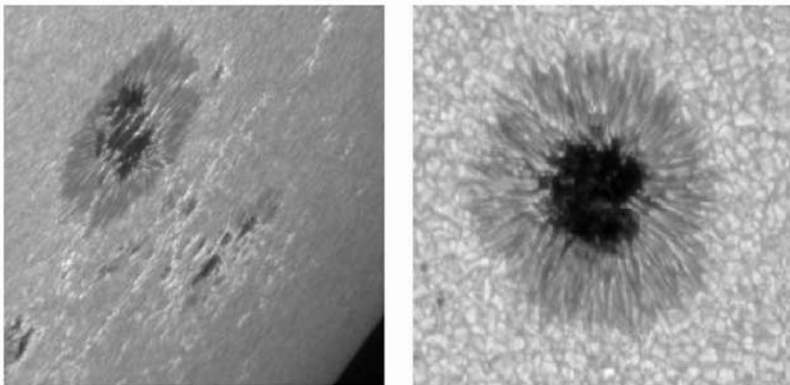


Figure 2.9: Sunspots near the limb, where also faculae are seen (left) and near the disc centre where the surrounding granulation can be seen. (Sobotka, Vazquez, Bonet, Hanslmeier, 0.5 m Swedish Vacuum Solar Telescope, La Palma, Observatorio Roque de los Muchachos).

Table 2.8: Hierarchy of magnetic concentrations in the solar photosphere. Adapted from Schrijver & Zwaan (2000)

	Sunspots	Pores	Faculae
Flux (10^{18} Mx)	3×10^4 –500	250–25	≤ 20
Radius (Mm)	28–4	1.8–0.7	~ 0.1
\vec{B} (Gauss)	2900–2400	2200	1500
Cohesion	Compact		In clusters
Occurrence	Active Regions		QR and AR

the increase in the photon mean free path with decreasing density. They found that the transition between bright and dark structures occurs at sizes around 1 arcsec. In the meantime, a intermediate family has been found, dark faculae, which are dark in the centre and brighter at the limb (see Figure 2.12).

2.4.2 The Chromosphere

The chromosphere is an irregular layer above the photosphere and can be observed during a total solar eclipse or in the light of special lines formed there. The temperature rises in the chromosphere from the temperature minimum to up to 20 000 K and the layer is approximately 2000 km thick. It is highly structured in three dimensions and very dynamic.

Most of the solar UV comes from the chromosphere, which is therefore of special interest here. A review of the chromosphere and line formation and radiative transport has been given by Kneer & von Uexküll (1999). Table 2.9 lists a set of

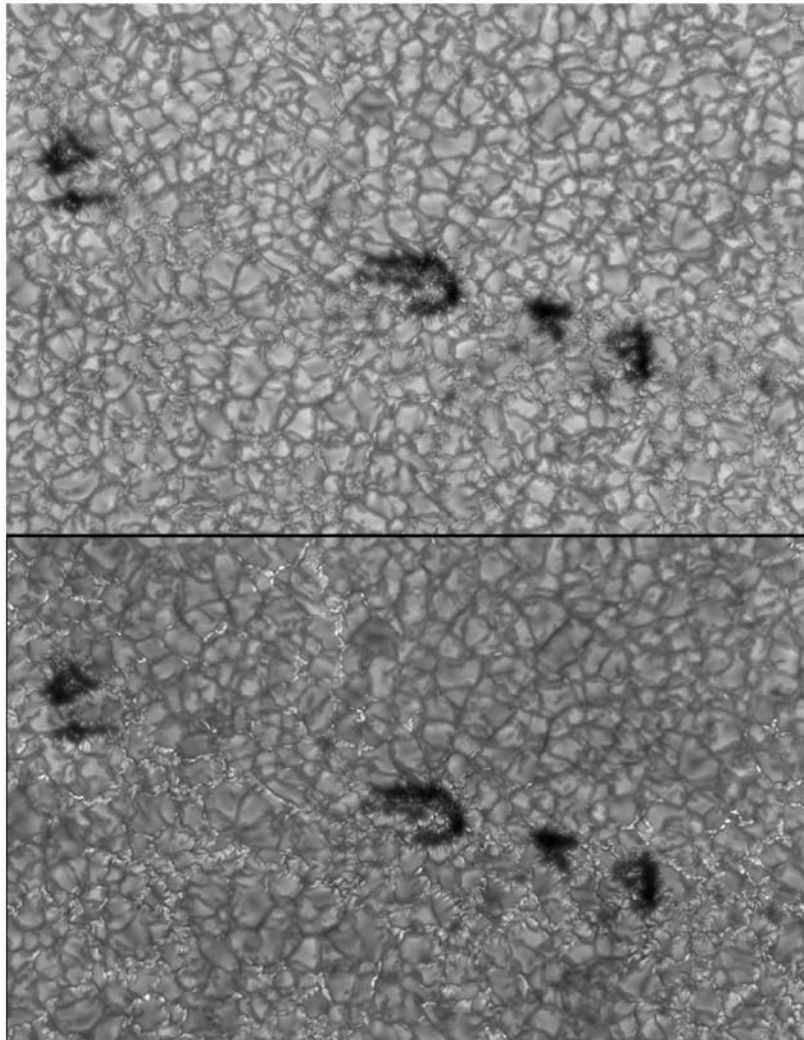


Figure 2.10: Speckle reconstruction by K.G. Puschmann (University Observatory Göttingen) of active region AR 0635 showing pores and bright points at 450.75 nm (blue continuum, upper panel) and 430.86 nm (G-band lower panel). Observations taken by K. G. Puschmann, M. Sobotka and C. Moestl on 21 June, 2004, at the 1 m Swedish Solar Telescope (Roque de los Muchachos Observatory, La Palma). Image size $60'' \times 40''$.

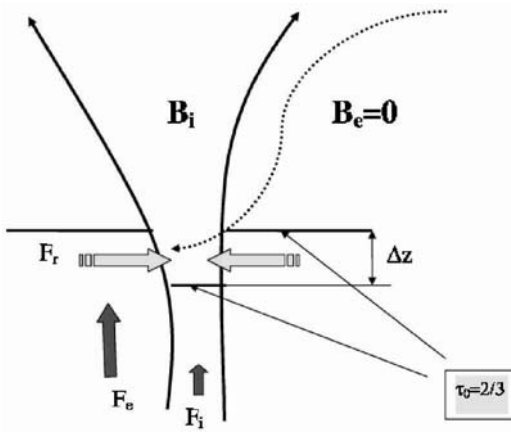


Figure 2.11: Magnetohydrostatic flux tube model. Inside the fluxtube we see at greater optical depths, the difference for $\tau = 2/3$ being given by Δz .

spectral lines formed in the chromosphere.

The most prominent of these lines are:

H_α : the core appears at a wavelength of 656.2797 nm and is formed between 1200 and 1700 km above the solar surface (which is usually defined as the layer where the optical depth at a wavelength of 500 nm becomes unity). The wings are produced between 100 and 300 km (Vernazza *et al.* 1981). Socas-Navarro & Uitenbroek (2004) have recently studied the diagnostic potential of this line for chromospheric magnetism.

Ca II doublet (H and K): These are absorption features centred at 396.8 nm (H1) and 393.46 nm (K1), which originate in the photosphere (see Figure 2.13). The so-called plages are hotter than the surrounding areas, and their number and area increase with the level of solar activity. This increase causes the enhancements of the emission cores (H2, K2), where a self-reversal is produced (H3, K3). The formation heights according to Vernazza *et al.* 1981 are 450–650 km (at 0.15 nm from the core, K1), 700–1450 km (K2), 1800–2000 km (core, K3). This emission is seen in other solar-type stars, thus providing important information about their chromospheres and activity cycles. Figure 2.14 show full disc images in the two lines mentioned.

Mg II doublet (h and k): This doublet is very similar to that of Ca II, although the photospheric background is smaller. The positions of the absorption features are 280.35 nm (h) and 279.63 nm (k). Table 2.10 list some of the most relevant solar observations of this spectral feature.

We next describe the most important observable structures in the chromosphere.

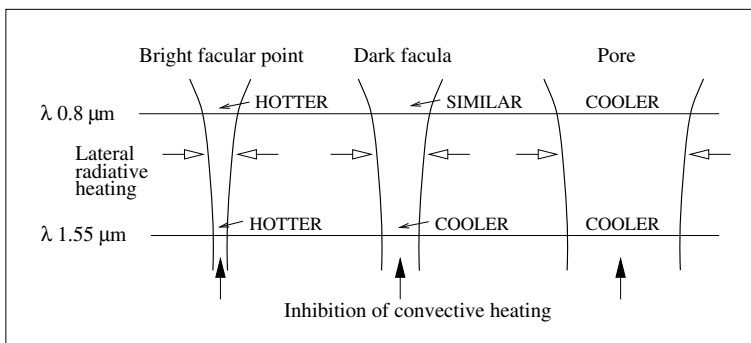


Figure 2.12: Schematic view of temperature conditions in magnetic features of different sizes. Adapted from Sobotka *et al.* (2000) *Astrophysical Journal* 544, 1155-1168. At 1.55 and $0.8 \mu\text{m}$ are located the minimum (deep layers) and the maximum (upper layers) of the absorption continuum coefficient of the solar atmosphere, respectively.

Plages and the Chromospheric Network

Plages are hotter, denser regions than the normal chromosphere. They can be observed in the monochromatic light of spectral lines formed in the chromosphere, the H _{α} and Ca II being used most often for their study. Their typical lifetime is up to 40 days. It is known that they are related to magnetic fields of up to several 10^3 gauss. Their size is about 50000 km.

The chromospheric network is a cellular web-like pattern most easily seen in H _{α} and Ca II K emission. Simon & Leighton (1964) found that there exists a chromospheric emission network that coincides with the borders of supergranules and the photospheric network. The magnetic flux tends to be concentrated in the downdrafts, and chromospheric heating occurs predominantly in regions of enhanced magnetic field strength.

We have seen that the gas pressure inside flux tubes is lower than in the surrounding photosphere. Now as the gas pressure decreases with altitude the field lines will expand and the magnetic field strength will decrease. As the magnetic flux ($\Phi = BA$) must remain constant, the cross section of the tube must increase, thereby explaining the larger extension of chromospheric active regions (Figure 2.15).

Prominences

During a total solar eclipse one observes bright features that may reach high into the corona; these are called prominences. In H _{α} they are observed in emission near the limb and in absorption (as dark filaments; therefore, they must be cooler than the surroundings) across the solar disc.

Eruptive prominences rise rapidly from the solar surface, and quiescent prominences have a much longer lifetime, typically several solar rotation periods, hanging suspended by magnetic fields in loop-like structures. The length of prominence

Table 2.9: List of chromospheric indicators

Spectral Line	Wavelength (nm)	Temperature
Continuum	160.00	4.2×10^3
Continuum	$200 \mu\text{m}$ –1 mm	$0.8\text{--}1.5 \times 10^3$
Ca II (H,K)	393.300 ; 396.800	6.0×10^3
Ca II IR	848.200 ; 856.200 ; 866.200	6.0×10^3
H _α	656.300	
He I	1083.000	
He I	587.600	
Mg II (h,k)	279.553 ; 280.270	7.0×10^3
Si II	180.801	6.2×10^3
O I	130.200 ; 130.500	8.0×10^3
C II	133.453 ; 133.566	2.0×10^4
H I (Ly _α)	121.567	1.5×10^4
Si III	130.100	3.5×10^4
C III	117.5	7.0×10^4
Si IV	139.375 ; 140.277	7.3×10^4
He II	164.000	8.0×10^4

Table 2.10: Sources of high spectral resolution observations of the solar Mg II doublet

Platform	Reference
Rocket	Durand <i>et al.</i> (1949)
Balloon	Lemaire & Blamont (1967)
Rocket	Kohl & Parkinson (1976)
Skylab	Doscheck & Feldman (1977)
Balloon	Staath & Lemaire (1995)

arch is several 10^5 km. However, as the magnetic loops that support them change slowly, filaments and prominences can erupt and rise from the Sun’s surface over the course of a few minutes or hours. Active prominences are associated with sunspots and flares.

Spicules

Discovered in 1877 by A. Secchi (1818–1878), spicules are small, jet-like eruptions seen throughout the chromospheric network. They last for a few minutes and eject material into the corona at 30 km s^{-1} to a height of about 7000 km. They tend to occur above supergranular lanes.

Recently, de Pontieu *et al.* (2004) have shown that the origin of spicules is linked to the oscillatory waves, p-modes, of the photosphere. In inclined magnetic fields, p-modes leak sufficient energy to power shocks that drive flows upward to form spicules.

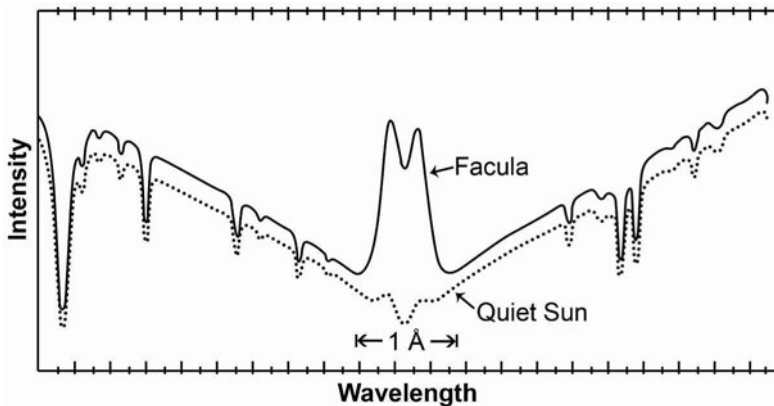


Figure 2.13: Average profiles of Ca II K for an active region and a nearby quiet region. Adapted from an original figure of White & Livingston (1981) *Astrophysical Journal* 249, 798-816.

Table 2.11: Indicators of the transition region.

Spectral Line	Wavelength (nm)	Temperature
C IV	154.818; 155.077	1.1×10^5
O IV	140.100; 140.500; 140.700	1.2×10^5
N V	123.882; 124.280	1.8×10^5
O VI	103.191; 103.761	3.2×10^5
Mg V	132.400	2.5×10^5

2.4.3 The Transition Region

The transition region is a thin and very irregular layer of the Sun's atmosphere that separates the hot corona from the much cooler chromosphere¹⁴. The temperature increases from about 20 000 K to more than 10^6 K in this thin region. The light emitted by the transition region is dominated by such ions as C IV, O IV, and Si IV rather than by ionized hydrogen. These ions emit light in the ultraviolet region of the solar spectrum which is accessible only from space (Table 2.11).

TRACE (Transition Region and Coronal Explorer) is a NASA Small Explorer (SMEX) mission (launched in 1998) to image the solar corona and transition region at high angular and temporal resolution. Observations of active regions show peculiar extreme ultraviolet (EUV) emission over certain plage areas called "moss" (Berger *et al.* 1999). The location of EUV emission in this moss does not correlate well with the locations of underlying magnetic elements in the chromosphere and photosphere, implying a complex magnetic topology for coronal loop

¹⁴See the monograph by Mariska, J.T., 1992, *The Transition Region*, Cambridge University Press.

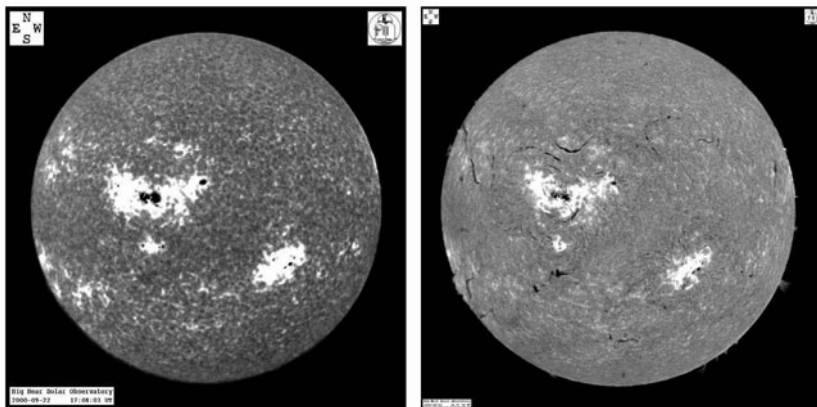


Figure 2.14: The chromosphere seen in two spectral lines: Ca II K and H _{α} . Courtesy: Big Bear Solar Observatory.

footpoint regions.

2.4.4 The Corona

The corona is the outermost layer of the solar atmosphere. It is visible during total eclipses of the Sun as a pearly white “crown” surrounding the Sun and its shape is strongly dependent on the phase of the solar activity cycle. At solar maximum, the corona appears more symmetric around the occulted solar disc, during activity minimum it is more elongated about the solar equator.

The identification of the puzzling coronal spectrum in the visible gave rise to the discovery of a new element apparently unknown on Earth, at first named coronium. It was realized later that the spectrum could be explained by forbidden lines of high degree of ionization of the elements such as Fe XIV and Ca XVI implying temperatures of several 10^6 K (Grotrian 1939; Edlen 1943). The density of the corona is extremely low and collisions occur infrequently thus allowing the observation of forbidden transitions¹⁵.

The corona can be studied in the UV and X-ray region of the spectrum. Several lines can also be observed between 330 nm and 1000 nm, such as Ca XII, Ca XV, Fe XI and Fe XV (Table 2.12)¹⁶. The higher the degree of ionization, the higher the coronal layer where the line is formed and the higher the temperature. Observing the chromosphere in the continuum about 124 nm corresponds to a layer at a temperature of about 10^4 K.

Figure 2.16 show a full disc X-rays image, in which we can distinguish two structures: a) *Bright regions* corresponding to active regions with a closed topology of the magnetic field and b) *Dark regions* characterized by magnetic lines open

¹⁵The ion can spend an unusual long time in an excited state.

¹⁶The roman numeral is one more than the degree of ionization (the number of electrons removed from the atom)

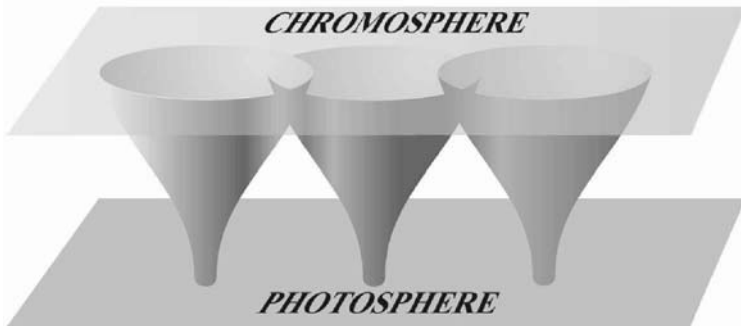


Figure 2.15: Expansion of magnetic field lines from the photosphere to the chromosphere. The photosphere is covered with flux tubes of intrinsically strong magnetic field, forming a magnetic canopy at chromospheric heights.

Table 2.12: Coronal Lines

Spectral Line	Wavelength (nm)	Temperature
Continuum	~ 124	10^4
Si VIII	144.049	8.0×10^5
Mg X	62.49	1.1×10^6
S X	119.600 ; 121.300	1.2×10^6
Fe XIV	530.286	
Ca XVI		
Fe X	637.451	
Fe XIII	1074.680 ; 1079.795	
Ni XIV	186.675 ; 186.700	2.1×10^6
Fe X	158.260 ; 158.350	1.1×10^6
Fe XXI	135.400	1.1×10^7

towards the interplanetary medium. We now describe the typical parameters of coronal structures (see Table 2.13):

Bright Closed Structures

Coronal loops are found around sunspots and in active regions and are associated with the closed magnetic field lines that connect magnetic regions on the solar surface¹⁷. Loops can last for days or weeks but most change quite rapidly. Some loops, however, are associated with solar flares and are visible for much shorter periods. These loops contain denser material than their surroundings. A scaling law can be derived for coronal loops relating their length L (given in cm) and the density ρ to the observed T_{\max} (see Kano & Tsuneta 1995):

¹⁷ see Bray, R.J., Cram, L., Durrant, C.J., Loughhead, R.E., 1991, Plasma Loops in the Solar Corona, Cambridge University Press

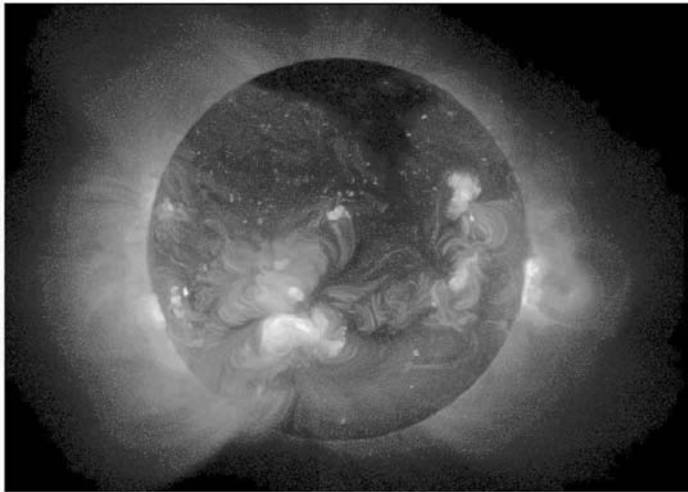


Figure 2.16: Full disc X-ray image obtained by Yohkoh. A polar coronal hole is clearly seen. Courtesy: T. Shimizu. The Institute of Space and Astronautical Science, Japan.

Table 2.13: Physical parameters of the principal coronal structures. N_e is the electron density. Source: Lang (2001) *The Cambridge Encyclopedia of the Sun*, Cambridge University Press.

Structures	Extension (Mm)	T (10^6 K)	N_e (cm^{-3})
Coronal Holes	700–900	1.0–1.5	4.0×10^{14}
Hot Loops	10	2.0–4.0	$1.0\text{--}7.0 \times 10^{15}$
Bright Points	5–20	2.5	1.4×10^6

$$T_{\max} = 3.8 \times 10^4 (\rho L)^{1/(5.1 \pm 0.5)}$$

Figure 2.17 illustrates the transition of the topology of magnetic field from the photosphere to the corona.

One important observational fact is the existence of two types of coronal loops that are not spatially coincident. Soft X-ray Yohkoh images show hot diffuse loops with temperatures higher than 2 MK. TRACE observes thin cool loops ($T \sim 1$ MK) (Figure 2.18) in EUV. The roots of both types are located in the photosphere and it has been observed that their magnetic filling factors¹⁸ are very different. The high mobility of magnetic elements in the low filling factor region gives rise to highly interlaced magnetic field lines.

Data from the YOHKOH (soft X-rays) and SOHO (EUV) can be used to study coronal *X-ray bright points* and their coincidence with EUV bright points.

¹⁸The fraction of area occupied by magnetic fields.

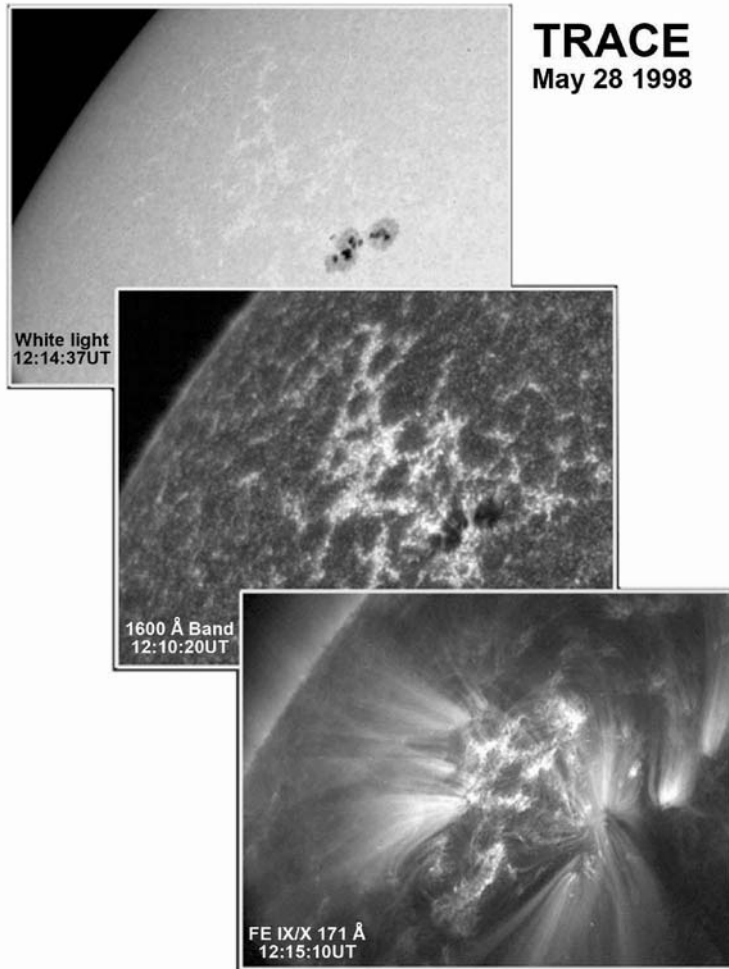


Figure 2.17: Composite images (TRACE) showing the Sun in white light (photosphere), the UV continuum (160 nm), where the chromospheric network is clearly seen, and in the X-rays region (17.1 nm) where the loop structure dominates. Courtesy of C. Schrijver.

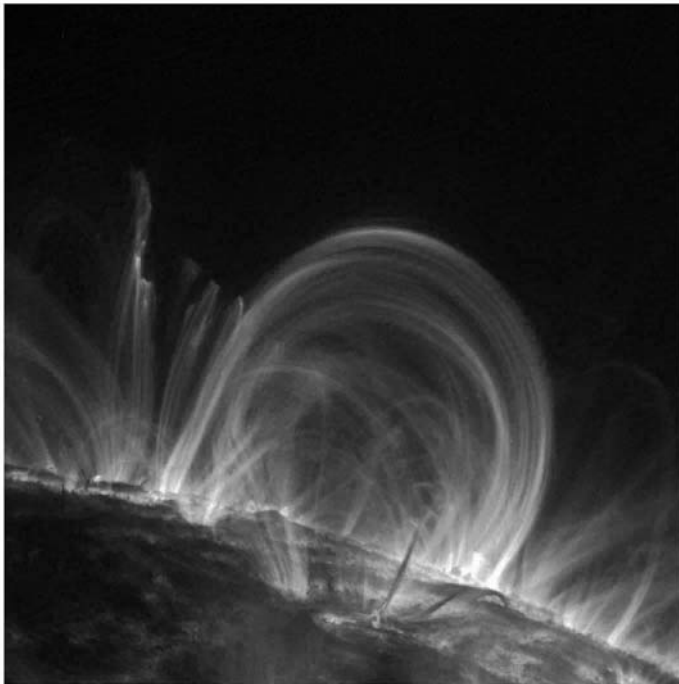


Figure 2.18: This image of coronal loops over the eastern limb of the Sun was taken in the TRACE 17.1 nm pass band, characteristic of plasma at 10^6 K, on 6 November, 1999, at 02:30 UT. Courtesy: TRACE

There is a high level of coincidence between the X-ray bright points and EUV bright points; both exhibit a cellular structure similar to that of Ca II. These cells have characteristic sizes larger than those typical for the supergranulation network (Hojaev 2003).

Brković *et al.* (2002) studied the quiet Sun variability with the SUMER (Solar Ultraviolet measurements of Emitted Radiation) spectrometer and the CDS (Coronal Diagnostic Spectrometer) on board SOHO. The instruments scanned a $1'' \times \sim 100''$ region in several UV lines and compared the results with He I (58.43 nm) and O V (62.97 nm). The UV emission lines sampled the temperature of the chromosphere, transition region and corona. They found a high correlation of variability in different lines.

Helmet streamers are large cap-like coronal structures with long pointed peaks that usually overlie sunspots and active regions. At the base of helmet streamers there is a prominence or a filament (in most cases). Helmet streamers are formed by a network of magnetic loops connecting the sunspots in active regions and help suspend the prominence material above the solar surface. The magnetic field lines are closed and electrically charged particles are trapped to form these dense structures.

Dark Open Structures

If the corona is observed in X-rays it is clearly seen that it does not appear to be uniform but there are regions of lower temperature called *coronal holes*. These holes are particularly prominent during activity minima and near the solar poles (see Figure 2.16). The high-speed solar wind is known to originate in coronal holes.

Coronal holes were discovered by M. Waldmeier (1912–2000), in 1957, who was observing visible coronal lines, as missing coronal material¹⁹. Their existence was confirmed years later by X-ray instruments on board Skylab.

Polar plumes (see Figure 2.19) are long thin streamers that project outward from the Sun’s north and south poles. These structures are associated with the open magnetic field lines at the Sun’s poles in contrast to helmet streamers that are associated with loops. Again, the plumes are formed by the action of the solar wind.

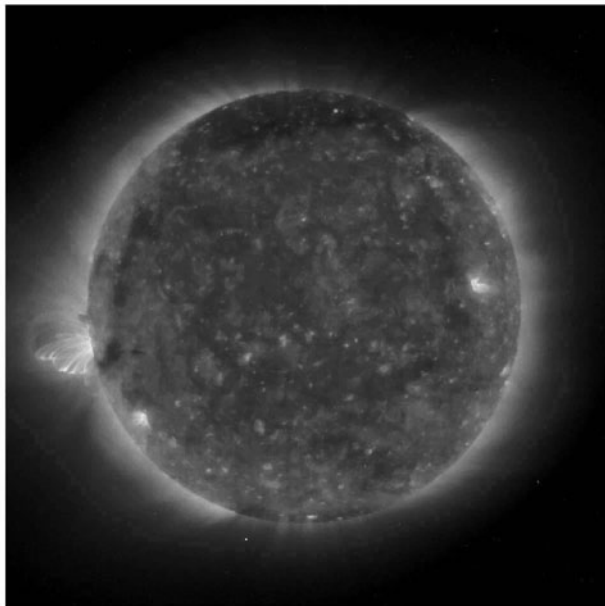


Figure 2.19: Polar plumes as seen by the SOHO EIT instrument in the far UV.

2.5 Magnetic field and Radiative Losses

Before entering into a discussion of the heating mechanisms of the solar outer layers, it is worth dedicating some space to the empirical relationships between

¹⁹Waldmeier, M., 1957, Die Sonnenkorona II, Verlag Birkhauser, Basel.

radiative losses at different altitudes in the atmosphere and the strength of the photospheric magnetic field.

At around 160 nm the height of the formation of the continuum is very close to the temperature minimum in the photosphere (also coincident with the Ca II K₁ features). At this wavelength a quiet photosphere can be seen with a network pattern of supergranular cells with bright patches. These coincide with magnetic elements in the network. Inside the cells transient brightenings are observed that are related to acoustic phenomena. Cook & Ewing (1990) found a relation between magnetic flux densities, $|\phi|$, and brightness temperature T_b :

$$T_b = 6|\phi| + 4380 \text{ K}$$

The relation between enhanced chromospheric emission and photospheric flux can be studied by using for example, the Ca II K line. This has been done by Skumanich *et al.* (1975) and Schrijver *et al.* (1989).

The excess ΔF_{CaII} is calculated by subtracting from the measured values of Ca brightness a basal contribution, probably acoustic in origin:

$$\Delta F_{\text{CaII}} = 6.5 \times 10^4 |\phi|^{0.6 \pm 0.1}$$

Full disc magnetograms and Ca II K images were analysed by Harvey & White (1999), which isolated the contributions of active regions, the enhanced network, the quiet network and the quiet atmosphere. The $|B|$ vs. $\Delta F_{\text{CaII}K}$ relationships were calculated for the four structures. The log-log curves are linear with a slope of 0.5, which suggests that the Ca II K residual intensity is proportional to the half-power of the magnetic flux density.

Excess intensities in a line i are related to other excess intensities through power laws (see Schrijver & Zwaan 2000):

$$\Delta I_j = a_{ij} (\Delta I_i)^{b_{ij}}$$

Schrijver (1992) found that the relationships between line intensities originating at different temperatures in the solar atmosphere are quantified presupposing a two-component model, comprising 1) a background basal emission and 2) a magnetically controlled emission showing power-law relationships between emissions in different spectral lines. The deviation from linearity increases owing to the increasing difference in the temperature formation of the lines.

These relations can be extended to the transition region where one of the most prominent spectra diagnostics is the C IV doublet (154.8 nm and 155.1 nm). The formation temperature is approximately 10^5 K. Schrijver (1990), using Solar Maximum Mission data, showed the relationship

$$F_{\text{CIV}} = 80|\phi| + 900|\phi|^{0.6} = \frac{F_X}{40} + \frac{\Delta F_{\text{CaII}}}{70} (\text{erg cm}^{-2} \text{s}^{-1})$$

The basal flux at the transition region is probably negligible and the non-linear relationship may reflect both local heating and heat conduction downwards from the corona.

2.6 The Heating of the Outer Layers

2.6.1 Primary requirements

As has already been stated, the temperature increases from about 6000 K to several 10^6 K as one moves away from the solar surface to the chromosphere and the corona. This has to be explained by some heating mechanism. First of all, we must evaluate the radiative losses that must be compensated for a certain mechanism of energy production. Estimates made by Withbroe & Noyes (1977) give values of 5×10^6 , 10^5 and 10^4 erg cm $^{-2}$ s $^{-1}$ for an active region, a quiet region and a coronal hole, respectively.

Of all the possible sources of heating, mechanical heating is the most important²⁰ by which we understand all processes that convert non-radiative, non-conductive, hydrodynamic or magnetic energy propagating through a gas element into heat. Moreover, the outer layers can only be maintained if mechanical heating is applied without interruption. A mechanical heating mechanism consist of three processes: the *generation* of the energy carrier, the *transport* of this energy and its *dissipation*. Clearly, all possible heating sources are generated in the solar convection zone.

2.6.2 Acoustic Heating

Heating of the upper layers by waves seemed to be an attractive hypothesis since, unlike radiation, moving material can flow from cold to hot regions. Coronal heating by sound waves was first suggested by Biermann (1946, 1948) and Schwarzschild (1948). Turbulent motions within the convection zone can generate sound waves. These accelerate and strengthen into supersonic shocks as they propagate outward through the increasingly rarefied gas in the chromosphere and corona. Thus their energy²¹ is dissipated to those layers.

However, because of the steep density gradient in the photosphere, most sound waves are reflected back. Observations from the Orbiting Solar Observatory (OSO 8) showed that the sound waves do not transport significant amounts of energy beyond the chromosphere and probably do not have sufficient energy to heat the chromosphere beyond a temperature of only 10 000 K. Thus the mechanism by sound waves can explain part of the UV radiation from the chromosphere but not beyond.

2.6.3 Magnetic Heating

Several mechanisms have been proposed, all of them related to the magnetic field, with the heating source rooted in the mechanical energy of photospheric fluid motion. These mechanisms are usually divided in fast or wave mechanisms called *ac* (alternate current), more important in the chromosphere, and slow mechanisms called *dc* (direct current), dominating in the corona.

²⁰We can also consider Joule dissipation, thermal conduction and viscous dissipation.

²¹The energy flux of plane acoustic waves is given by $F_w = 1/2\rho V^2 C_s$, where C_s is the sound speed.

Wave mechanisms: The coronal magnetic field is rooted in the turbulent photosphere (see Figure 2.20). This leads to the generation of waves, which are driven by magnetoconvection, with phase mixing due to gradients and absorption on small scales. We may distinguish the following types: a) magnetoacoustic slow-mode MHD waves, b) longitudinal tube waves and c) torsional Alfvèn waves. The latter two types are difficult to dissipate in the chromosphere.

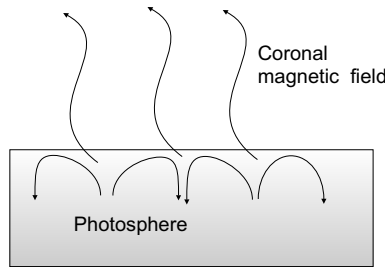


Figure 2.20: Coronal magnetic fields are anchored in the turbulent photosphere, where MHD waves are generated by turbulent motions.

Alfvèn waves are like waves traveling along a stretched string. The magnetic field line tension B^2/μ_0 is analogous to string tension, and when the magnetic field is “plucked” by a perturbation, the disturbance propagates along the field line. The Alfvèn velocity, v_A , is the ratio $\sqrt{\text{Tension}/\text{density}}$.

If the induction equation and the equation of motion are combined, perturbations in density, waves, are found which propagate with a velocity v :

$$v = \sqrt{C_s^2 + v_A^2}$$

where $v_A = \sqrt{B^2/\mu_0\rho}$ and c_s is the velocity of sound. These are called fast magneto-acoustic waves since they are faster than sound and Alfvèn waves. They act as compressions and rarefactions of the gas and the field. When $c_s \ll v_A$ we speak of compressional Alfvén waves, which propagate in a direction perpendicular to the magnetic field with the particles oscillating in the direction of propagation.

The width of coronal lines can be used to detect Alfvèn waves. However, their existence is still not definitively proven. Moreover, there are problems in turning these waves into heat.

Current sheet mechanism: The electric conductivity of hot coronal plasma is so high, and hence the resulting Ohmic dissipation rate so small, that the conventional conversion of magnetic energy into heat becomes completely irrelevant. For magnetic heating to be effective, fine-scale structures, known as currents sheets, must develop within the coronal magnetic field in response to its photospheric deformation. Their continuous motions of field lines at a boundary leads to the creation of current sheets (Parker 1972). Solanki *et al.* (2003) have detected a tangential discontinuity in the magnetic field direction, the observational signature of an electrical current sheet.

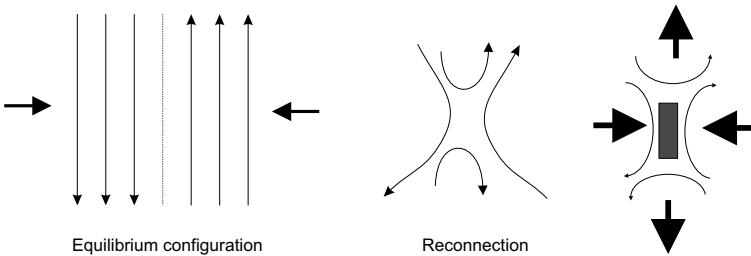


Figure 2.21: Left and centre: Magnetic reconnection from two antiparallel fields that are disturbed as indicated by the arrows. Right: the Sweet–Parker model. The plasma flows into the shaded diffusion region where reconnection occurs and the plasma is expelled through the ends.

The Poynting flux, P , is a good descriptor of a magnetic heating mechanism²². Parker (1983) and Van Ballegooijen (1986), using different approaches, obtained the following expression

$$P = QL = \frac{B^2}{8\pi} V \tan \phi$$

where Q is the heating per unit of volume, L the loop length, V the speed and ϕ the inclination of the magnetic field lines.

Three-dimensional numerical simulations by Galsgaard & Nordlund (1996) reached a simpler solution of the heating term:

$$Q \propto \frac{B^2 V}{8\pi} \frac{1}{L^2}$$

where l is the typical length of the random motions at the photospheric level. Large values of Q lead to rapid dissipation in a hierarchy of current sheets.

It is probable that current sheets are ubiquitous in the corona, making the process of coronal magnetic heating highly fragmented, both in space and in time. Gudiksen & Nordlund (2002) found that the heating is intermittent in both space and time – at any one height and time it spans several orders of magnitude. They conclude that loop formation and bulk heating is caused by the braiding of the magnetic field by photospheric motions. This leads us to a related mechanism,

Heating by micro-, nano- and pico flares: Magnetic reconnection refers to the breaking and reconnecting of oppositely directed magnetic field lines in a plasma. In the process, magnetic field energy is converted into plasma kinetic and thermal energy. Many high energy phenomena that occur on the Sun are caused by this effect. For example, solar flares which occur near sunspots, are believed to be powered by magnetic reconnection.

According to Parker's conception of ubiquitous magnetic reconnection (Parker 1988), the corona is modelled as an externally driven dissipative dynamical system.

²²The Poynting flux is the energy flux of a propagating electromagnetic wave.

Larger catastrophes are driven by a chain reaction of smaller ones. His nanoflare concept predicts a power law of flare frequency, f , against energy E :

$$f(E) = f_0 E^{-\alpha}$$

The spectral index $\alpha < -2$ is valid for nanoflare dominated heating. Krucker & Benz (1998) found α to be in the range $[-2.3, -2.6]$ for $8 \times 10^{24} < E < 160 \times 10^{24}$ erg cm $^{-2}$ s $^{-1}$. If $f(E)$ extends down to 0.3×10^{24} erg cm $^{-2}$ s $^{-1}$ the nanoflares will dominate the energy input in the quiet solar corona²³.

This approach allows us to predict various X-ray signatures of coronal loops and scaling laws representing the dependence of physical parameters on the length of loop and the strength of the coronal magnetic field (Vekstein & Katsukawa 2000).

TRACE has observed EUV nanoflares with energies in the range of $10^{24} - 10^{26}$ erg. They often represent miniature versions of larger flares that are observed in soft and hard X-rays. The temperatures are $T_e \sim 2$ MK, the densities $n_e \leq 10^9$ g cm $^{-3}$ and the spatial scales are smaller. The frequency matches soft X-ray microflares (Aschwanden *et al.* 2000).

2.6.4 The Magnetic Carpet

Observations with the MDI (Michelson Doppler Imager) on board SOHO has provided long-duration highly detailed movies of the magnetic fields on the surface of the Sun. It was found that there tens of thousands of small magnetic dipoles, which are constantly popping up at the solar surface, forming the magnetic carpet. These are the footpoints of magnetic loops extending into the solar corona. As new loops emerge, they collide with pre-existing ones. Reconnection releases the stored magnetic energy.

These small magnetic regions emerge, fragment, drift and disappear over periods of only 40 hours or so. Figure 2.22 compares theoretical predictions for the structure and heating of the magnetic field above the solar surface with observations of the EIT on board SOHO.

In summary, the corona is extremely dynamic and full of flows and wave phenomena in which loops evolve. Coronal heating can turn on and off on short time scales of less than minutes along field-line bundles. The cross sections of these bundles are below the resolution of TRACE instruments (700 km). The heating occurs predominantly inside the first 10 to 20 Mm from the loop footpoints. The inner parts of active-region coronae therefore have a higher average temperature than the outer domains (Schrijver *et al.* 1999). Combined observations by the instruments CDS and EIT on board SOHO show small-scale brightenings, known as blinkers, of which several thousands may be occurring on the solar disc at any moment (Harrison *et al.*, 1999 2003). They are probably connected with vigorous heating at the feet of coronal loops, thereby verifying that the heating process takes place at these sites by small-scale reconnection.

²³This will require 28000 nanoflares to go off per second over the entire Sun. Katsukawa & Tsuneta (2001) increase this value to 10^6 per second.

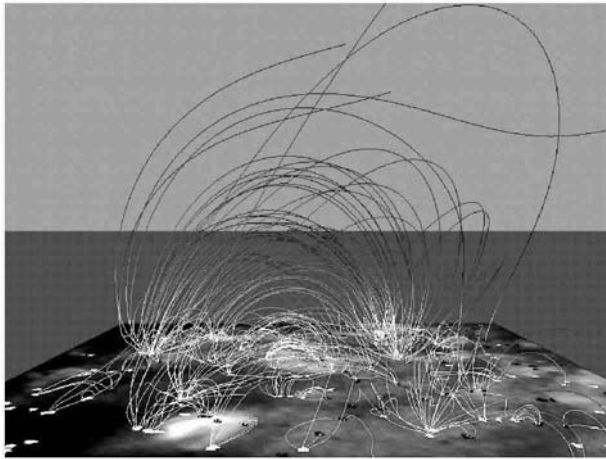


Figure 2.22: The magnetic carpet. Current theories predict that length and curvature of these arches determine the degree to which they are heated. The image underlying the arches is the heating observed at the same time by EIT in the iron line at 19.5 nm, with bright green corresponding to relatively hot regions and dark green corresponding to cool ones. Credit: SOHO Consortium, ESA, NASA.

Another variant for the contribution to the heating of the corona was introduced by Priest *et al.* (2002). This model is called flux-tube tectonics. Observations show that most of the magnetic flux in the quiet Sun emerges as ephemeral regions. These regions quickly move towards the supergranule boundaries and the original concentrations fragment, merge and cancel over a relatively short time period between 10 and 40 hr. There are millions of coronal separatrix surfaces caused by the highly fragmented photospheric magnetic configuration, and it is suggested that the formation and dissipation of current sheets along these separatrices are an important contribution to coronal heating. The dissipation of energy along sharp boundaries is called the tectonics model of coronal heating.

Parnell (2002) explains the observed distribution of magnetic fluxes as being made up of the following three processes: a) the emergence of new flux over all the scales, b) the fragmentation and partial cancellation producing smaller and smaller fluxes thus creating excess small fluxes and c) excess large fluxes created by coalescence and an additional injection of flux from remnants of active regions. An essential point in estimating the importance of reconnection processes for the heating of the outer layers is a knowledge of the frequency of these events. Close *et al.* (2004) have found that, outside active regions, the timescale for magnetic flux to be remapped in the quiet-Sun corona is only 1.4 hours. The inclusion of intranetwork magnetic concentrations would reduce this timescale still more.

Chapter 3

The Solar UV Variability

In the preceding chapter we described the various aspects of solar phenomena. In this chapter we concentrate on solar variability, which is mainly represented by a quasi-cyclic behaviour, the solar activity cycle. Emphasis will be given to solar UV variability. Indices for quantifying these variations and their correlation will be discussed and will be useful for describing and comparing solar activity with stellar activity. We must exploit proxy data in order to reconstruct solar activity in the past. From the variation of solar activity in the past we can infer on the regularity of the cycle itself and make predictions about the future.

Overviews of the solar UV irradiance and its variation and relevance to the Earth are given by Floyd *et al.* (2002) and Lean (1997).

3.1 Sources of Solar Variability

The variability of the Sun is linked to the dissipation of the available energies (De Jager 1972). Different sources are characterized by distinct time-scales. Since in the previous chapter we established the connection between solar UV emission and the magnetic field, we shall be interested in the variability of the magnetic energy, with only a brief excursion into nuclear energy, because of its relationship with the early times of the Earth and the origin of life.

The total magnetic flux emerging at the solar surface has two main components, differing in the topology of the magnetic field (Figure 3.1):

a) The magnetic flux of the active regions (hereafter closed magnetic fields, CMF), characterized by magnetic configurations with closed field lines dominating the variations of the total irradiance and the emission in the high energy range of the solar spectrum (ultraviolet and X-rays). Most of the radiative losses from the outer layers occur in these regions.

b) Large-scale magnetic regions have field lines open toward the interplanetary medium. They are the main source of a continuous outward flow of charged particles (protons, electrons and He nuclei) known as the solar wind. The solar magnetic field of the open regions (OMF) is frozen into this wind, configuring the interplanetary magnetic field (IMF), which produces a huge magnetic region, the

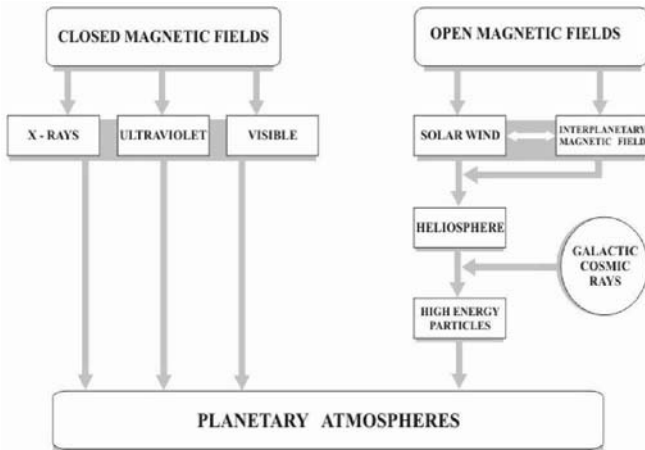


Figure 3.1: Sources of solar variability.

heliosphere, that practically fills the whole Solar System. Galactic cosmic rays (hereafter GCRs) are high-energy particles (mainly protons with energies in the range 1–20 GeV), originating outside our planetary system and striking the Earth from all directions. Both the flux and energy spectrum of GCRs are modulated by the strength of the heliosphere, being stronger when the IMF is weaker. Lockwood *et al.* (1999) and Lockwood (2003) have derived the intensity of the interplanetary magnetic field from the *aa* geomagnetic index, a record that extends back to 1868. They found that the average strength of the solar magnetic field has doubled in the last 100 years. Usoskin *et al.* (2002) have simulated variations of the OMF with a model based on the emergence and decay rates of active regions (Solanki *et al.* 2002) that fits reasonably well with other proxies of solar activity, such as the ^{10}Be records in ice cores.

The variability of both the CMF and OMF is dominated by the 11 year period, but longer periods exist, as is evidenced by the presence of several deep minima of solar activity; for example, the Maunder Minimum in the second half of the seventeenth century. Figure 3.2 shows the variation of these two parameters over the last 300 years.

We shall proceed now from short to longer time-scales, describing both the variability in the radiation (visible and UV) and in the flux of particles. Where direct or indirect records of UV flux are lacking, we shall use this latter information as a proxy for the UV radiation, especially on longer time scales.

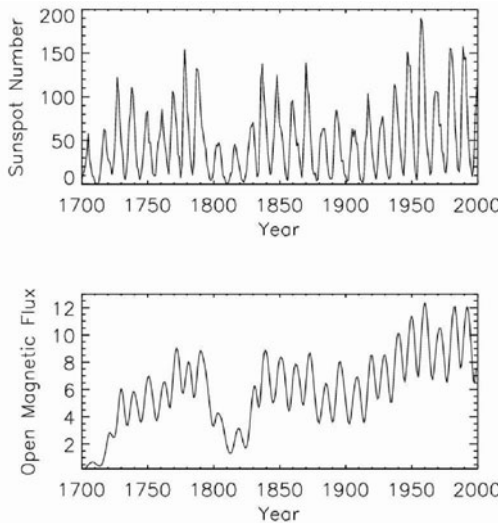


Figure 3.2: Variation of the closed magnetic field (CMF), indicated by the sunspot number (top) and open magnetic flux (bottom), calculated by Usoskin *et al.*, 2002 (data courtesy of M. Schüssler, MPIfA, Germany).

3.2 Short-Time Variations

3.2.1 Solar Flares

A flare¹ is defined as a sudden, rapid, and intense variation in brightness. A solar flare occurs when magnetic energy that has built up in the solar atmosphere is suddenly released. The basic process involved is magnetic reconnection.

Energy Release in Flares

Flares are among the most intense phenomena in the solar system. The energy released during a flare is typically of the order of 10^{27} ergs per second. Large flares can emit up to 10^{32} ergs of energy².

There are typically three stages:

- Precursor stage: The release of magnetic energy is triggered. Soft x-ray emission is detected.

¹For textbooks see for example: B. V. Somov, Physical Processes of solar flares, Kluwer, 1992; E. Tandberg-Hanssen and A. G. Emslie, The Physics of Solar Flares, 1988, Cambridge Univ. Press and M.J. Aschwanden, Particle Acceleration and Kinematics in Solar Flares: A Synthesis of Recent Observations and Theoretical Concepts, Kluwer, 2002.

²The amount of energy released is the equivalent of millions of 100-megaton hydrogen bombs exploding at the same time!

- Impulsive stage: protons and electrons are accelerated to energies of more than 1 MeV³. Radio waves, hard X-rays and gamma rays are observed.
- Decay stage: gradual build up and decay of soft x-rays.

The duration of these stages can be from a few seconds to an hour. Figure 3.3 shows the time evolution of a typical flare in different ranges of the electromagnetic spectrum.

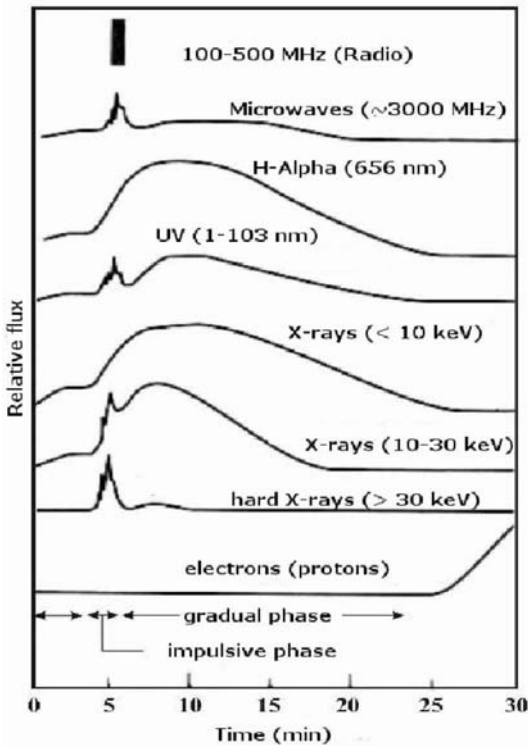


Figure 3.3: Gradual and impulsive phases of solar flares and their energy output.

Location of flares

Classically, flares have been observed in the chromosphere in $H - \alpha$ but very intense flares, called white light flares, can also be observed in the photosphere. As a general rule, flares occur above locations in the photosphere where the electric current has a maximum (the highest $\nabla \times B$). Preferred are those regions in sunspots or groups of sunspots where new and oppositely directed magnetic flux emerges from below. Large gradual flares often occur above the neutral lines in the

³1 eV = 1.6×10^{-12} erg.

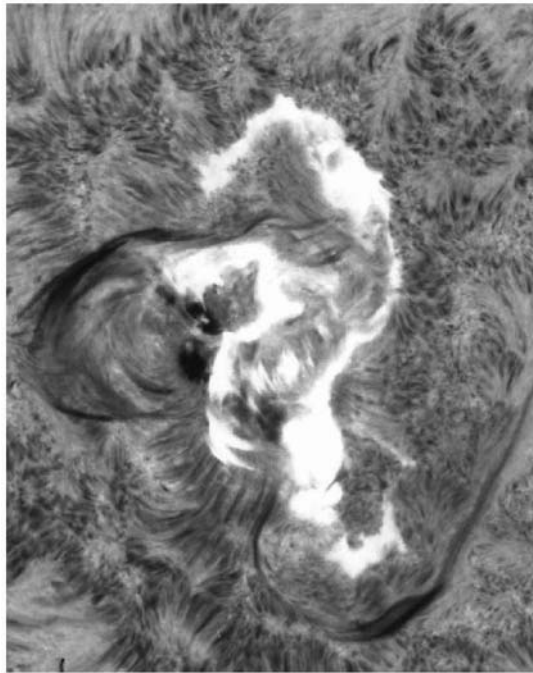


Figure 3.4: The great ‘Seahorse Flare’ of 7 August, 1972. This image in the blue wing of the spectral line H- α shows the two-ribbon structure late in the event, with bright loops connecting the ribbons. Courtesy: Big Bear Solar Observatory.

photosphere, which separates regions of opposite magnetic polarity. Neutral lines are bridged by arcades of loops and in H- α one sees two bright ribbons formed by the footpoints on each side of the neutral line (Figure 3.4). Flares then occur above the part of the neutral line that has experienced most shear due to different surface motions on both sides. In quiet regions, the most powerful microflares occur at the boundary of supergranular cells. The frozen-in magnetic field lines are swept to the down-draft region near the supergranular boundary forming the magnetic network. On time-scales of a few tens of minutes these magnetic elements can be observed to appear and disappear.

The access to space data has allowed observations of flares in the upper layers of the solar atmosphere (UV and X-rays).

Classification

The different classification schemes for solar flares are given in Tables 3.1 and 3.2.

Gradual flares occur near the poles, and electrons, protons and ions are accelerated. Impulsive flares occur mainly near the equator and mostly electrons are accelerated; they last from minutes to hours.

The letter *S* stands for subflares. Since 1970 flares have also be classified on

Table 3.1: Optical classification scheme for solar flares

Importance class	Area A at disc 10^{-6} sol. hemisphere
S	$A < 100$
1	$100 \leq A < 250$
2	$250 \leq A < 600$
3	$600 \leq A < 1200$
4	$A \geq 1200$

Table 3.2: Soft x-ray classification scheme of solar flares

Soft X-ray class	Peak in powers of 10 in the 0.1–0.8 nm flux W m^{-2}
A	−8
B	−7
C	−6
M	−5
X	−4

the basis of soft X-ray observations of the Sun in the 0.1–0.8 nm band by Earth-orbiting satellites.

According to Table 3.2, a B5 flare has a peak flux of $5 \times 10^{-7} \text{ W m}^{-2}$. Flares smaller than C1 can only be detected during a solar minimum phase when the general X-ray background is low. Occasionally, flares exceed class X9 in intensity and are referred simply to as X10, X11, etc. On 4 November 2003, the largest ever recorded flare was observed and was classified as X28 (Figure 3.5).⁴

3.2.2 Coronal Mass Ejections

Coronal mass ejections (CMEs) were first detected in observations made with a coronograph on board the OSO 7 observatory (1971–1973). During a solar eclipse the corona is visible only for a few minutes and no change in the coronal structure can be observed. CMEs are huge bubbles of gas that are ejected from the Sun over the course of several hours. They disrupt the flow of the solar wind.

Images of the CMEs in different spectral lines in the UV with the SOHO Ultraviolet Coronograph show how the morphology depends on the temperature, density, and outflow speed of the ejected plasma. H I Ly- α is the line that best resembles the white-light data (Chiaravella *et al.* 1993). Linker *et al.* (2003) have reviewed CME models. EUV waves and coronal dimming were observed by different instruments, mainly in the EUV (SOHO, TRACE and YOHKOH)

⁴The TIMED and SORCE spacecrafts detected an increase in X-ray levels by a factor of 60 and a increase in EUV by a factor 1.5

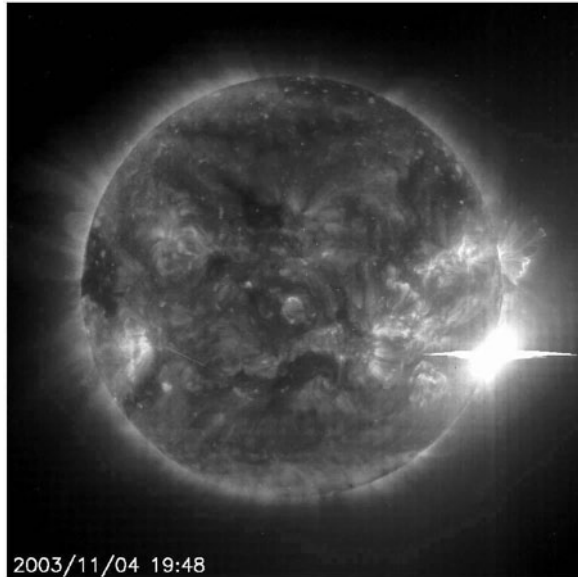


Figure 3.5: The X28 flare observed by the EIT (19.5 nm) on board SOHO. The flare erupted just beyond the edge of the visible hemisphere. Courtesy: ESA and NASA.

(Harrison 2003). These dimmings were found to coincide with CMEs and mass-loss can be deduced from the data (Harrison *et al.* 2003).

A review of CMEs associated with the major geomagnetic storms when hitting the Earth's magnetic field can be found, for example, in Hundhausen (1996), Webb (1998) and Gopalswamy (2003).

3.2.3 Activity Waves in the Corona

Alfvén or acoustic waves propagating through the solar corona and heating the ambient plasma could be detected through the measurement of ultraviolet line widths. This was predicted by McClements *et al.* (1991).

An investigation of EUV coronal structures during 1996–2000 using SOHO EIT data in the 171, 195, 284, and 304 Å lines was performed by Benevolenskaya *et al.* (2001). During this period, poleward- and equatorward-migrating waves of solar activity have been found in axisymmetrical distributions of EUV intensity in all four lines. In the axisymmetrical distribution of the ratio of 195 Å to 171 Å intensities, which is a proxy of coronal temperature from 1×10^6 to 2×10^6 K, the polar branches are less prominent. The high-latitude activity waves are caused by giant coronal magnetic loops connecting the polar magnetic field (formed during the preceding solar cycle) with the magnetic field of the “following” parts of active regions that emerged during the rising phase of the current cycle.

3.3 Variability of visible radiation during a solar activity cycle

In Table 3.3 we give a summary of the variation of the above- discussed phenomena during an 11 year solar activity cycle. In the following, we shall describe some activity indices and the variability of the solar output on the magnetic cycle scale.

Table 3.3: Variation of solar phenomena during activity cycle.

Name	Variation between activity minimum and maximum
Spots, R	0 – > 150
Flares, gradual	0 – 100/yr
Flares, impulsive	0 – 1000/yr
Faculae	contribution during maximum \gg spot
CMEs	0.5–2.5 per day

3.3.1 Solar Activity Indices

The sunspot relative index (also called the Wolf number) is defined as

$$R = k(10g + f)$$

here g is the number of spot groups, f the number of individual spots and k a correction factor taking into account the observing site, the telescope, atmospheric conditions and the enthusiasm of the observer. Although the sunspot number contains many uncertainties, it is the oldest known parameter to determining the solar activity directly. The official sunspot number is given by the Sunspot Index Data Center (SIDC), which was founded in 1981 to continue the work of the Zürich Observatory. The sunspot area, A , and the Zürich number are related by $A \sim 16.7R$, where A is given in millionths of the disc area.

Hoyt *et al.* (1994) proposed using the number of groups, a parameter less sensitive to calibration uncertainties, especially for earlier epochs. Table 3.4 summarizes other indices of solar activity based on magnetic and chromospheric ground-based observations.

The magnetic plage strength index (MPSI) is determined at Mount Wilson Observatory. The absolute values of the magnetic field strengths for all pixels where the absolute value of the magnetic field strength is between 10 and 100 gauss is divided by the total of number of pixels (regardless of magnetic field strength) in the magnetogram. The MWSI values are determined in much the same manner as the MPSI, although summation is done only for pixels where the absolute value of the magnetic field strength is greater than 100 gauss. The Ca K emission index is defined as the equivalent width of a 0.1 nm band centred on the K line core.

Table 3.4: Global indices of solar activity: MPSI is the magnetic plage strength index and MWSI is the Mount Wilson sunspot index.

Observatory	Period	Index
Big Bear	1991–	K-index
Kitt Peak	1974–	He I 10830 equivalent width
Kitt Peak	1974–	Ca K 1 Å index
Sac Peak	1976–	Ca K index
Kitt Peak	1977–	Average magnetic field
Mount Wilson	1970–	MPSI (non-spot magnetic fields < 100 gauss)
Mount Wilson	1970–	MWSI (spot magnetic fields > 100 gauss)
Ottawa	1947–	Radio Flux 10.7 cm (F10.7)

3.3.2 Total Irradiance Variations

The time-scales of solar variability are the dissipation rates of the available solar energies. Here we shall concentrate on the magnetic time-scales.

During the past two decades, satellite observations have revealed that the total solar irradiance, S_{\odot} , changes both the short-time scale, dips of 0.1% to 0.25% lasting for several days during the passage of large sunspot groups (Willson *et al.* 1981) and the time-scale of the solar cycle (Willson *et al.* 1986).

The measurements suffer from the relative inaccuracy of the absolute values needing to overlap data from different satellites in order to get a composite view of the variations during the last two solar cycles. Fröhlich & Lean (1998) did not find a clear change between the two solar minima (Figure 3.7). A different result was obtained by Willson & Mordvinov (2003), who proposed a + 0.047 % decade trend between the two solar minima, with implications for the long-term variation of the solar irradiance.

Simulations of the measured solar irradiance are necessary, first to understand the cause and second to be able to extrapolate current records to the past. The irradiance fluctuations can be expressed as the sum of various components, which probably change with different time scales

$$\frac{\Delta S_{\odot}}{S_{\odot}} = \frac{\Delta S_S}{S_{\odot}} + \frac{\Delta S_F}{S_{\odot}} + \frac{\Delta S_N}{S_{\odot}}$$

where ΔS_S , ΔS_F and ΔS_N , are the contributions to the irradiance fluctuations due to sunspots, faculae and the network, respectively.

The calculation of the sunspot component is based on the PSI index (Hudson *et al.* 1982),

$$\Psi = \frac{\Delta S_S}{\Delta S_{\odot}} = \sum \alpha \mu A_s \frac{3\mu + 2}{2}, \quad (3.1)$$

where α is the bolometric sunspot contrast, A_s the sunspot area and μ the cosine of the heliocentric angle, θ .

For faculae, Chapman & Meyer (1986) define the facular irradiance excess as

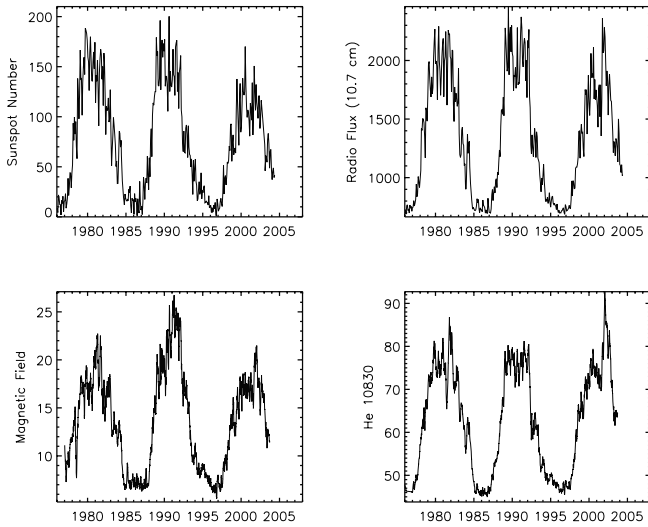


Figure 3.6: Time variability of different activity indices of solar activity at the level of the photosphere. Source: National Geophysical Data Center.

$$\Phi = \frac{\Delta S_F}{\Delta S_\odot} = \sum C_P A_p \mu f(\mu) L_F(\mu), \quad (3.2)$$

where C_P is a calibration coefficient, A_p the area of the chromospheric plage, $f(\mu)$ the limb darkening law of the quiet Sun and $L_F(\mu)$ the centre-to-limb variation (CLV) of the facular contrast.

Owing to the difficulties in measuring the facular excess directly at the photospheric level, the chromospheric emission of plages has been used instead. C_P is the calibration factor (see eq. 3.2), which has been considered constant at 0.019 ± 0.002 (Chapman and Meyer 1986) and as intensity dependent. Vršnak *et al.* (1991) established a relation between C_P and I_{SGD} (the Ca K brightness as published in the Solar Geophysical Data), complemented by Steinegger *et al.* (1996) with an empirical relation between I_{SGD} and the mean intensity, \bar{I} , of the Ca K spectroheliograms.

The calibration factor, C_P , accounts for the differences in area and brightness of faculae between the chromospheric and photospheric levels. C_P increases with plage area, because larger plages are also brighter, and we have assumed a dependence of C_P on plage brightness. The observed power-law trend could be explained in terms of the variation of the merging height with the magnetic filling factor (Solanki & Steiner 1990) and therefore with the plage brightness. C_P , after its definition, should be proportional to A_F/A_p .

The first proxies used to study the magnetic variability were provided by ground-based observations in selected chromospheric lines. Figure 3.8 clearly

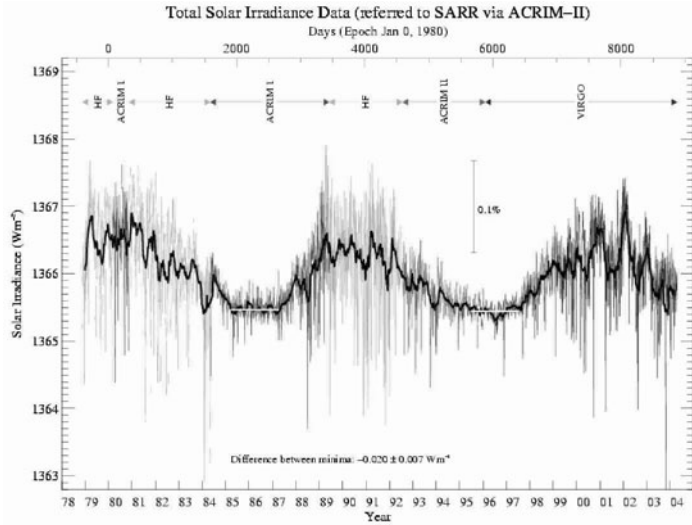


Figure 3.7: Composite Total Solar Irradiance (based on Frölich & Lean, 1998). Short-time variations due to sunspots are overlapped with a solar cycle change produced by photospheric bright structures.

shows the variation in the number and area of plage regions during the solar activity cycle.

Models of the variation of the total solar irradiance, S , can be obtained if the two competing factors of the spots and faculae are known⁵:

$$S = S_0 + A \times \Psi + B \times \Phi$$

where S_0 represents the solar irradiance in the absence of solar activity. The sunspot deficit is correlated with short term variations of S , the total variation in the facular regions is correlated with long term variations of S (Walton *et al.* 2003).

Such models could be used as proxies for the calculation of S before accurate satellite measurements became available by following different approaches (Hoyt & Schatten 1993; Fligge & Solanki 2000).

The following archives (Table 3.5) are essential sources of data for estimating the facular contribution, both at the chromospheric and photospheric levels.

In analogy to the faculae, we define for the quiet network

$$\frac{\Delta S_N}{S_\odot} = \sum C_N A_N \mu f(\mu) L_N(\mu).$$

The contribution of the quiet network to the irradiance fluctuations has been a matter of much debate, because of its possible influence on the long-term variabil-

⁵San Fernando Observatory, Northridge (Calif.), determines the values of Ψ and Φ on a daily basis.

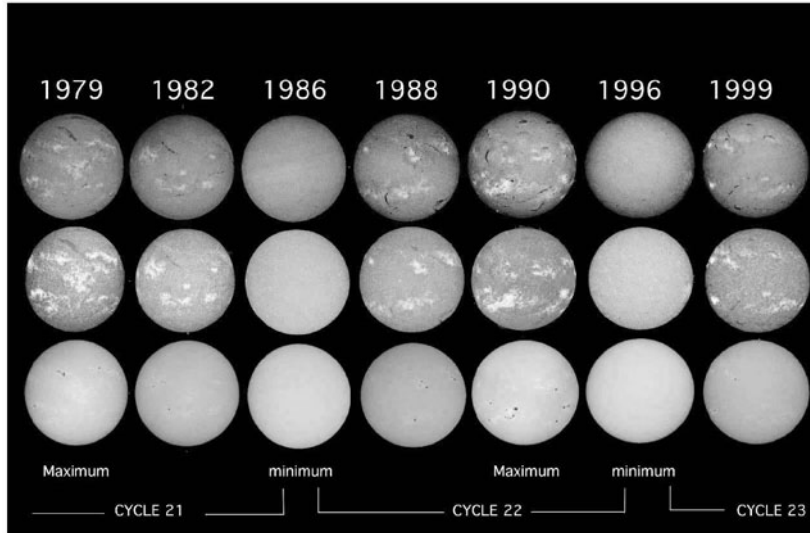


Figure 3.8: Time variability of full disc images obtained at two chromospheric lines ($H-\alpha$ and $Ca\ II\ K$) and in the visible. Courtesy: Meudon Observatory.

Table 3.5: Indices of solar activity. Available at National Geophysical Data Center.

Sunspot areas	A_s	1874 –	
Mt Wilson Ca II plage areas	A_p	1915–1984	Foukal (1996)
Mac Math/Hale plage areas	A_p	1942–1987	
White light facular areas	A_f	1874–1976	Foukal (1993)
Sacramento Peak calcium index		1976–2002	Keil & Worden (1984)
San Fernando calcium index		1988–1998	Chapman <i>et al.</i> (1996)
Big Bear calcium index		1991–	Johannesson <i>et al.</i> (1998)

ity. Foukal & Milano (2001) discounted the absence of the quiet chromospheric network as an explanation of the Maunder Minimum.

The problem of the timescale at which the energy is blocked by sunspots and re-radiated by photospheric faculae on scales comparable to the lifetime of active regions (see Chapman *et al.* (1986) or even stored in the convection zone for months and longer (Foukal *et al.* 1993) is still open. These works showed that the heat blocked in proportion to a spot's area and contrast is stored very efficiently in the slightly increased thermal and potential energy of the solar convection zone. The radiative flux blocked during high sunspot activity periods is only radiated away over many subsequent 11-year cycles. Such efficient storage could imply a contribution to the variation of the solar luminosity and irradiance over the 11-year cycle at an amplitude that can be computed from the known variation of sunspot areas.

Other possible mechanisms of irradiance variations are related to changes within the convection zone (see Li & Sofia 2001). Using an updated stellar evolution model, which includes magnetic fields, they find that the observations can be explained by fields with peak values ranging from 120 to 2.3 kG, located in the convection zone between 0.959 and 0.997 R_{solar} , respectively. The corresponding maximum radius changes are 17 km when the magnetic field is located at 0.959 R_{solar} and 3 km when it is located at 0.997 R_{solar} .

The inclusion of a UV index in sunspot and facular photometric measurements slightly improves the fits to S_{\odot} . Lean (1989) and Mitchell *et al.* (1991) estimated the contribution of the 300–400 nm variation to the measured S_{\odot} changes at 13 and 36%, respectively.

3.4 Solar UV Radiation and the Activity Cycle

Systematic measurements of irradiance in different parts of the UV spectrum are made from space. They share some common trends and problems with the measurements of TSI.

3.4.1 General Trends

The first aspect to comment on is that the amplitude of the variations during the solar cycle is wavelength dependent, with remarkable enhancements in some spectral lines. The amplitudes of the variation due to the solar cycle are given by Floyd *et al.* (2003) and are summarized in Table 3.6 and Figure 3.9.

Spectral solar UV irradiance data for cycle 21 are discussed in Deland & Cebula (2001), whose estimated long-term irradiance changes from the Nimbus 7 SBUV data during solar cycle 21 are 8.3 ($\pm 2.6\%$) at 205 nm, and 4.9 ($\pm 1.8\%$) at 240 nm.

3.4.2 Instrumental stability and the Mg II Index

Instruments measuring the UV irradiance suffer from degradation. Responsivity changes must therefore be carefully corrected. This can be done by on board cali-

Table 3.6: The solar UV irradiance variation amplitude due to the activity cycle (data are given from the maximum of cycle 22 to the maximum of cycle 23).

Wavelength	Amplitude (Max-Min)
~50%	O I, C II, and Si IV below 145nm
~8-18%	between the Al edge and 145 nm
~4%	between the Al edge and 263 nm
> 300nm	~ 0.1%

ibration sources, redundant optics, stellar observations and vicarious measurements that use duplicates of similar instruments flown separately. The solar ultraviolet spectral irradiance monitor (SUSIM, Brückner *et al.* 1993) consists of two identical double-dispersion scanning spectrometers, seven detectors and a deuterium calibration lamp. The spectrometers and detectors are sealed in a canister filled with 1.1 atm of argon gas. One spectrometer is used more-or-less continuously; the second is used infrequently to track the stability of the first. The deuterium lamp serves as a secondary standard for in-flight calibration.

For this reason an index of solar UV activity that is less sensitive to instrument behaviour was defined. The Mg II index core-to-wing ratio was first developed from Nimbus-7 SBUV spectral scan irradiance data by Heath & Schlesinger (1986) and is calculated by taking the ratio of the irradiance at the core of the Mg II absorption feature at 280 nm to the average irradiance in the wings of the Mg II feature at approximately 276 and 283 nm. The reason for such a definition is as follows. The Mg II k and h emission lines at 279.55 and 280.27 nm are generated in the upper chromosphere. The nearby wings are generated in the upper photosphere. Thus, by calculating the ratio of core/wing emission one has a measure for the chromospheric activity that is practically insensitive to temporal and spectral changes in instrument response.

Mg II index data sets have been produced by many instruments over the last two decades (Table 3.7). The Solar Ultraviolet Spectral Irradiance Monitor (SUSIM) is a dual dispersion spectrometer that measures the absolute irradiance of the sun in the ultraviolet (UV) wavelength range of 115 nm to 410 nm for near-Earth orbit. SUSIM UARS is one experiment on board the Upper Atmosphere Research Satellite (UARS). SUSIM UARS makes daily measurements over its 115-410 nm wavelength range at 1 and 5 nm resolutions and weekly measurements at 0.15 nm resolution. The SOLar STellar Irradiance Comparison Experiment (SOLSTICE) is a NASA project that provides the scientific community with accurate long-term, measurements of solar ultraviolet (UV) and far ultraviolet (FUV) radiation. SOLSTICE is operated from the Laboratory for Atmospheric and Space Physics (LASP) at the University of Colorado in Boulder.

A composite Mg II Index has been constructed after these measurements (Figure 3.10). Two frequencies dominate the time series, one with an 11 year period and a second superposed on the higher frequencies and a period of ~ 27 days (rotational modulation). These two phenomena are different manifestations of the appearance and disappearance of bright active regions on the solar disc.

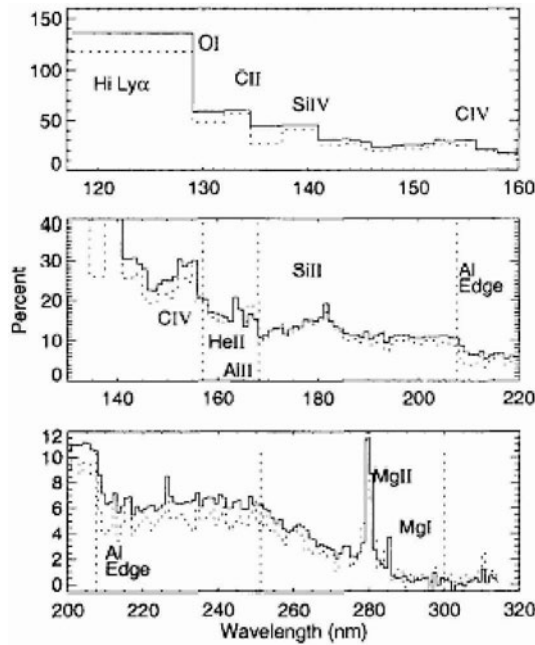


Figure 3.9: Solar UV spectral irradiance peak-to-peak variation (SUSIM data). Adapted from Floyd *et al.* 2002.

While Mg II index data sets from different instruments typically differ in absolute value owing to differences in resolution, wavelength selection and method of derivation, there is excellent agreement in the response to solar variations.

3.4.3 EUV and FUV measurements

Images illustrate clearly the variability of the EUV/FUV radiation. The instrument EIT on board SOHO is the main source of information for images in this spectral range (see Figure 3.11).

The Ly- α line falls in the EUV range and approximately 50% of the variation of the flux in this range is attributable to this line. The records in Ly- α span now more than 25 years. Table 3.8 lists the instruments supplying data in the EUV and FUV for variability studies.

The Ly- α emission from the Sun can also be used for indirectly monitoring the far side of the Sun by satellite as it was done by SOHO's SWAN (Solar Wind Anisotropies) experiment. A huge cloud of interstellar hydrogen surrounds the Sun (this is valid for most stars). This gas lights up when hit by photons in the UV. Active regions are brighter in the UV; therefore, the sky is brighter in the region facing them.

Table 3.7: Sources of Mg II measurements for temporal variations

Spacecraft	Instrument	Interval	Reference
Nimbus 7	SBUV	1978–1987	Heath & Schlesinger (1986)
NOAA 9		1985–1990	
NOAA 11	SBUV2	1989–1993	Viereck & Puga (1999)
UARS	SOLSTICE	1991–	Rottman <i>et al.</i> (1993)
UARS	SUSIM	1991–	Brückner <i>et al.</i> (1993)
GOME		1995–	Weber <i>et al.</i> (1998)

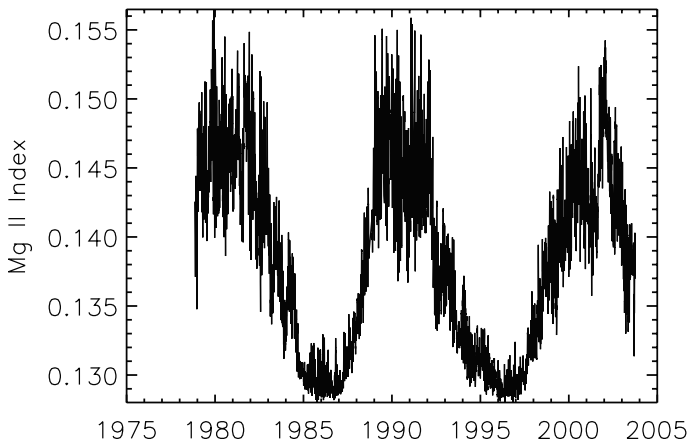


Figure 3.10: A composite Mg II Index based on measurements by NOAA, SUSIM and GOME.

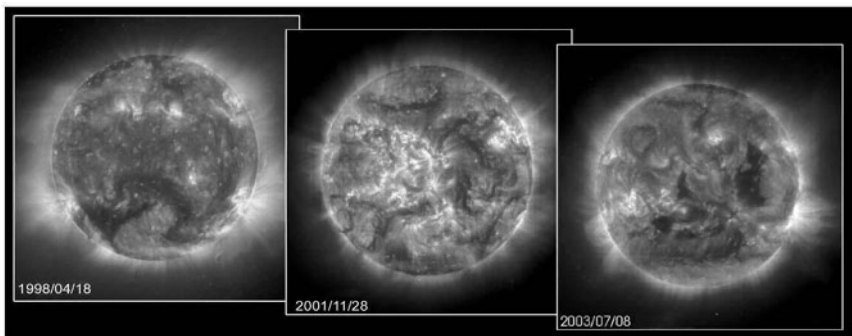


Figure 3.11: Extreme ultraviolet images in three different phases of the solar cycle (1998, 2001 and 2003). Courtesy of SOHO/EIT consortium. SOHO is a project of international cooperation between ESA and NASA.

Table 3.8: Sources of EUV/FUV measurements

Spacecraft	Instrument	Interval	Reference
AE-C		1974–1976	Hinteregger (1977)
AE-E		1976–1979	Hinteregger <i>et al.</i> (1981)
Pioneer Venus		1979–1992	Pryor <i>et al.</i> (1998)
TIMED	GUVI SEE	2002–	Christensen <i>et al.</i> (2003)
UARS	SOLSTICE SUSIM	1991– 1991–	Rottman <i>et al.</i> (1993)
SORCE	SOLSTICE	2003–	Rottman (2003)

3.4.4 Correlations

Correlations between different activity indices can be extremely useful for estimating the behaviour of solar activity in the past, where no direct observations of the indices (UV, for example) were possible.

Heath & Schlesinger (1986) derived scale factors for the 170–400 nm region to relate them to variations in the Mg II index,

$$\Delta F(\lambda, t) = A(\lambda) \times \Delta \text{MgII}(t)$$

where ΔF and ΔMgII are given as percentages. DeLand & Cebula (1998) verified the correctness of this approach during the maximum and decline of Cycle 22.

The existence of a relationship between the $F_{10.7\text{cm}}$ and the EUV flux is an extremely important correlation in deducing the solar EUV variation in the past⁶. This parameter lags the variation of radio flux (10.7cm) and Mg II by ~ 54 days (Woods *et al.* 2000) because such emission, originating in the transition region, is more sensitive to the active network than are chromospheric or coronal emissions. This lag is well known for other activity indicators and produces a loop of elliptical shape in the scatter plots, also known as hysteresis (Bachmann & White 1994).

Floyd *et al.* (1997) and Woods *et al.* (2000) proposed a three-component model to establish a correlation between both parameters of the form

$$F_{\text{Ly}\alpha} = A + B \times \text{MgII}_{\text{sm}}(t) + C \times (\text{MgII}(t) - \text{MgII}_{\text{sm}}(t))$$

where MgII_{sm} represents the Mg II index smoothed over multiple solar rotations.

3.5 Simulation of UV variability

3.5.1 Empirical modelling

What are the solar features that emit UV? In principle there are three primary components: a) the quiet Sun b) the active network, and c) plages.

⁶The $F_{10.7\text{cm}}$ flux is given in $10^{-22}\text{WHz}^{-1}\text{m}^{-2}$. The Φ_{EUV} flux is given in units of 10^{10} photons $\text{cm}^{-2}\text{s}^{-1}$ characterizing the total flux between 30.0 and 130.0 nm

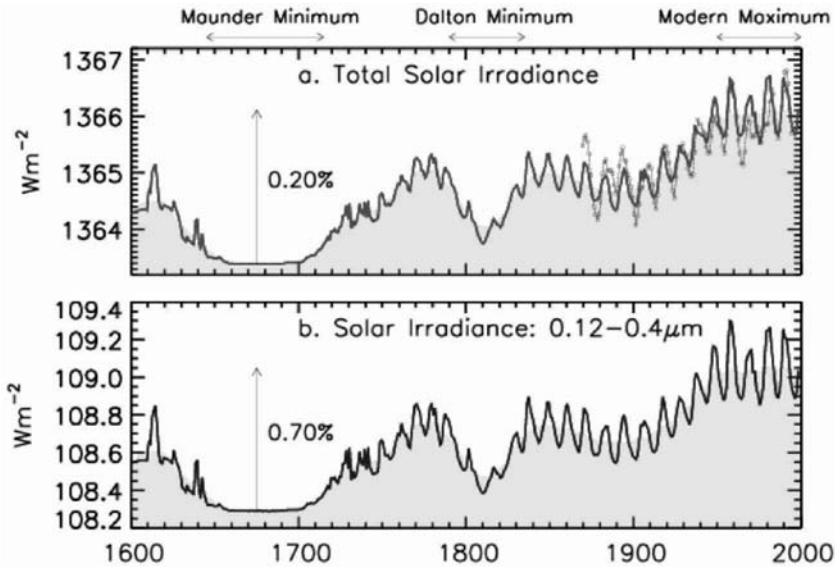


Figure 3.12: Simulation of the solar irradiance in different spectral ranges: a) Total Solar Irradiance; b) UV range. Courtesy of J. Lean, Naval Research Laboratory.

Cook *et al.* (1980) used a two-component model to reproduce the UV flux in the spectral range 117.5–210 nm.

$$F(\lambda) = F_0(\lambda) + F_0(\lambda)f(I_p(\lambda) - 1)$$

where $F_0(\lambda)$ is the quiet Sun irradiance, f the fraction of solar disc covered by active regions and I_p the plage contrast relative to the quiet Sun.

The UV irradiance can also be parameterized in three-component models by adding the contribution of the active network. The first models were based on ground-based measurements of Ca II K spectroheliograms (Lean *et al.*, (1984); Skumanich *et al.*, 1984 ; Worden *et al.* 1998). Lean *et al.* (2001) have constructed a composite of the chromospheric irradiance by combining different parameters as daily plage index, 100-day smoothed radio flux ($F_{10.7cm}$) and sunspot numbers.

Lean *et al.* (1995) and Lean (2000) estimate the reduction of solar output between the Maunder Minimum and 1986, in the range 120–300 nm.

$$F_{\text{Maunder}}(\lambda) = F_q[A(\lambda) + B(\lambda) \times P_{\text{Maunder}}]/[A(\lambda + B(\lambda) \times P_q]$$

where $A(\lambda)$ and $B(\lambda)$ are linear regression coefficients derived from rotational modulation correlations and P_q is the quiet Sun index during the solar minimum in 1986. For the calculation of P_{Maunder} it was assumed that the Ca II emission during the Maunder Minimum was quantified by the levels of non-cycling stars (see Figure 3.12).

Foukal (2002) has compared the solar total and UV irradiance variations. He found a different behaviour attributed to the non-dependence of the UV on the presence of sunspots.

Observations with the SUMER spectrograph on SOHO showed that the quiet-Sun UV radiance depends on the solar cycle (Pauluhn & Solanki 2003). They tested the hypothesis that the He I 58.4 nm line variations are due to changes in the magnetic network.

The centre to limb variations in the UV were investigated by Donnelly & Puga (1990), Worden *et al.* (2001) and Crane *et al.* (2004), who analysed time series of solar ultraviolet irradiance measured by the Solar Ultraviolet Spectral Irradiance Monitor on the UARS to describe the centre-to-limb behaviour of the excess surface brightness of solar active regions over the wavelength range 142–265 nm.

Models of solar EUV irradiance models are given by Tobiska (1993), Warren *et al.* (2001) and Lean *et al.* (2003).

Tobiska *et al.* (2000) have modelled the EUV variation in the past from the radio flux (10.7 cm) and other proxies⁷. Thuillier *et al.* (2004) have constructed two composite solar irradiance spectra for two distinct periods, characterised by different levels of magnetic activity, during cycle 22.

3.5.2 Synthetic modeling

The basic idea behind of the synthetical modelling is to associate models of the different structures contributing to the UV irradiance by computing the spectral intensity of each component. The emergent intensity is then calculated as a sum over all contributing structures of the individual intensities of features of their radiance, I (Fligge *et al.* 2000; White *et al.* 2000).

$$I(\lambda, \mu) = \sum_{\text{structures}} \sum_{\mu} I_{\text{structure}}(\lambda, \mu)$$

being

$$I_{\text{structure}}(\lambda, \mu) = \int S_{\lambda}(\tau) \exp(-\tau/\mu) d\tau / \mu$$

where S_{λ} is the source function, τ the optical depth, λ the wavelength and μ the heliocentric viewing angle.

In the next section we discuss how the Sun's activity has varied in the past, before telescopic observations, and how it is possible to reconstruct this variation.

3.6 Proxies of long-term Solar Activity

To make predictions about future solar activity cycles it is a necessary requirement to know long series of activity cycles in the past. However, the longest indicator of UV radiation variability, the number of sunspots, is available only for about 400 years. Therefore, to reconstruct the solar UV emission in the past on intermediate

⁷These data are available at Space Environment Technologies <http://spacewx.com>

time-scales we must find suitable proxies. The best way is to look for fingerprints of particle flux in the Solar System. However, we must keep in mind that secular variations in these proxies do not necessarily imply equivalent secular trends in the solar UV irradiance (see Lean 2000).

3.6.1 Cosmic Rays

The subatomic charged particles that bombard the Earth isotropically from beyond its atmosphere are known as cosmic rays. They consist of 90% protons, $\sim 10\%$ alpha particles and $\sim 1\%$ heavier elements.

Cosmic rays include: a) Galactic cosmic rays (GCRs): which originate from outside the solar system b) anomalous cosmic rays, which originate from the interstellar space at the boundary of the heliopause, and c) solar energetic particles (SEPs), associated with solar flares. SEPs move away from the Sun driven by plasma heating, acceleration and numerous other forces. Flares frequently inject large amounts of energetic nuclei into space whose composition varies from flare to flare.

The GCR flux incident on the Earth's atmosphere is modulated by three processes: a) variations in the solar wind within the heliosphere, b) variations in the Earth's magnetic field and c) variations in the interstellar flux of GCRs. We are now primarily interested in the first factor.

The heliosphere is a huge magnetic shield that protects the Solar System from penetrating charged particles and is responsible for the modulation of GCRs. Cosmic ray particles can therefore be used as a proxy for solar activity. At high activity levels, the magnetic field of the heliosphere reduces the number of cosmic ray particles entering the Solar System, so that an anticorrelation between the flux of cosmic ray particles and solar activity (e.g. sunspot number) is observed (see Figure 3.13) over the past 50 years, a period of high solar activity. However, the sunspot number is a poor proxy for the parameters that control the long-term (> 22 years) modulation of cosmic rays.

3.6.2 Nitrates

Nitrates are generated in the Earth's atmosphere in a chain of reactions with NO, produced by solar cosmic rays. The nitrates are captured by aerosols, fall with precipitation and get mixed finally in polar ices. There is thus a strong correlation between NO sources with solar activity (Kocharov *et al.* 1999). Short term pulses of nitrate abundance are related to strong solar proton events and these events have a tendency to occur mainly during periods of increase or decrease in solar activity (Shea & Smart 1995).

3.6.3 Cosmogenic isotopes

Cosmic Rays interacting with N, O and Ar produce a wide variety of secondary particles (protons, neutrons, mesons) and radioisotopes. The two longlived radioisotopes with the highest mean global production rates are:

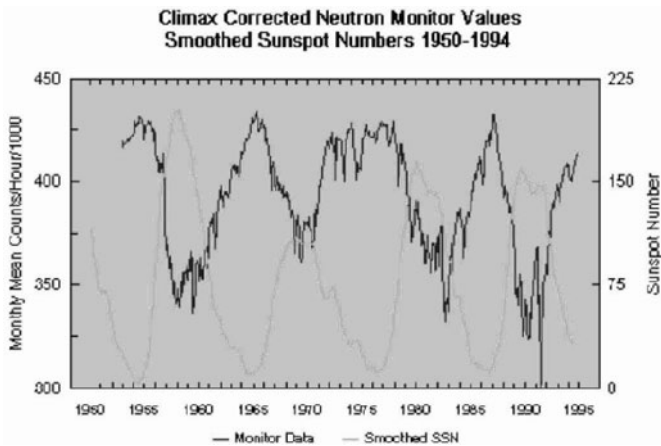


Figure 3.13: Data from the Climax, Colorado, neutron monitor operated by the University of Chicago. Cosmic rays show an inverse relationship to the sunspot cycle because Sun's magnetic field is stronger during sunspot maximum and shields the Earth from cosmic rays.

1. ^{14}C : half-life = 5730 yr, production rate $\sim 2.5 \text{ atoms cm}^{-2} \text{ s}^{-1}$,
2. ^{10}Be : half-life = 1.5 Ma, production rate $\sim 3 \times 10^{-2} \text{ atoms cm}^{-2} \text{ s}^{-1}$.

We recall that low energy ($< 5 \text{ GeV}$) galactic cosmic rays are modulated by the solar activity cycle. These cosmic rays in turn influence the isotope production in the Earth's atmosphere and in meteorites. The rate of production varies inversely with solar activity.

^{10}Be

The production of the ^{10}Be isotope depends on altitude and latitude. In the highest 16 to 20 km of the atmosphere the production rate increases because of the effects of secondary particles, but going deeper into the atmosphere more and more particles are stopped. The latitude dependence can be explained by the geomagnetic dipole field, which prevents particles below a certain magnetic rigidity (defined as momentum per charge) from penetrating into the atmosphere. This shielding effect is greatest at the equator and decreases towards the poles. Because 2/3 of the ^{10}Be is produced in the stratosphere ($h > 10 \text{ km}$) we must bear in mind that it takes 1–2 yr to settle from the stratospheric aerosols onto the surface of the Earth (this is known from studies of the radioactive fallout of nuclear bomb tests: the mean residence time in the troposphere is of the order of days to weeks).

Changes in the atmospheric circulation pattern during spring at mid-latitudes cause a mixing of stratospheric air into the troposphere, where the radioisotopes are removed by precipitation; therefore, the ^{10}Be fallout is proportional to and influenced by precipitation. There may, however, be short term variations during, for example, supernova explosions, variations of solar activity (this influences the low energy spectrum of cosmic rays because of a better shielding due to stronger heliospheric field) and secular changes of the geomagnetic dipole field (this sets a lower limit on the momentum of the cosmic ray particles that are able to penetrate into the Earth's atmosphere; for an almost zero dipole field, such as may occur during a magnetic reversal, the mean production rate is enhanced by a factor of ~ 2.5 (O'Brien (1979).

What are the best archives of ^{10}Be ?

- Deep sea sediments: the sedimentation rates are between 0.1 and 10 cm per 1000 yr. These provide the longest records (1–100 Ma). Of course the drawback is the time resolution, which is affected in this case by the oceanic residence time (depending on chemistry and biological parameters, typically between 400 and 4000 yr) and bioturbation (small organisms penetrating into the top 5–10 cm of the sediments and mixing this layer). The time resolution is limited to $\sim 10\,000$ yr.
- Lacrustine sediments: Lakes are distributed quite homogeneously, the recovery of lacrustine sediments is rather simple. In favorable cases the time resolution is about 1 yr. Problems are caused by the drainage area that may vary and input additional ^{10}Be .
- Polar Ice: These are the best archives. Mixing processes owing to snowdrifts are small. The accumulation rates are high $2\text{--}50\text{ g water cm}^{-2}\text{ yr}^{-1}$. Young ice ($< 10^3$ yr) from high accumulation rates can be also dated by measuring the seasonal variations of $\Delta^{18}\text{O}$ (the ratio of two oxygen isotopes, ^{18}O and ^{16}O , is a good indicator of past temperatures), ΔD (The ratio of deuterium to hydrogen, D/H, is also used as a indicator of past temperatures) and H_2O_2 . Drawbacks are that ice is not stable and starts to flow from inland to the coast.

So we can state that for the studies of solar activity variability the best archive is polar ice. A study was made on a 300 m ice core from station Dye 3, in Greenland (Beer *et al.* 1990). Absolute time marks were detected (e.g. the maximum of nuclear fallout in 1963, the Tambora eruption 1815 and the Laki eruption of 1783). A correlation with the 11 yr sunspot cycle was found with a lag of about 2 yr (this agrees with the atmospheric residence time). The ^{10}Be concentration reflects the 11 yr cycle but also the long term trend of the amplitude of sunspot numbers.

The Maunder Minimum of solar activity (1645–1715) is also seen in the data. Other grand minima of solar activity are: the Spörer Minimum (1420–1540) and Wolf Minimum (1280–1350). These are also found in the ^{14}C records (see Eddy 1976, Beer *et al.* 1994 and Figure 3.14).

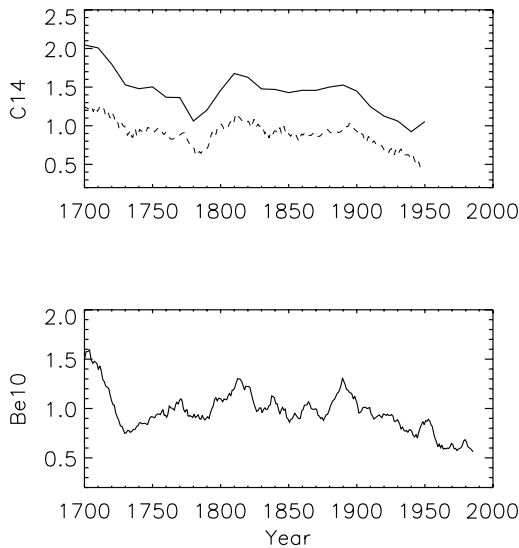
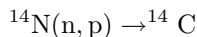


Figure 3.14: Variation of cosmogenic isotopes: (Top) ^{14}C . The first record (solid) is based on the ^{14}C calibration data (Stuiver & Reimer, 1998, Radiocarbon 40, 1041–1083) and the second record (dashed) is based on annual ^{14}C data covering the period 1500–1945 (Stuiver & Braziunas 1993, The Holocene 3, 289–305). (Bottom) ^{10}Be isotope (Beer *et al.* 1994). Data: Courtesy of J. Beer.

^{14}C

The nuclear reactions involved in the production of ^{14}C are



and ^{14}C decays by



where $\bar{\nu}$ is the antineutrino and β^- the electron. The half-life is 5730 yr. Causes of radiocarbon fluctuations are:

- Variations in the global rate of radiocarbon production such as modulation of the cosmic ray flux through solar activity and changes in the geomagnetic field.
- Variations in the rate of exchange between geochemical reservoirs and the CO₂ reservoir inventory. Involved in these processes are problems such as the control of CO₂ solubility, dissolution and residence time through temperature variations, sea level variations, ocean circulation, the assimilation of CO₂ by the biosphere, etc.

- Variations in the total CO₂ in the atmosphere, biosphere and hydrosphere. Changes in the input rate of carbon dioxide (e.g. by volcanism), the combustion of fossil fuels, etc.

How does this method work? When plants and animals die they stop taking in ¹⁴C and, the ¹⁴C they have absorbed begins to decay radioactively. After 5730 years only half of it will be left. This decreases to 25% after 11460 years, 12.5% after 17190 years, 6.25% after 22290 years, and so on. Eventually, in about 70 000 years, it will all be gone. Given this known rate of decay, it is possible to calculate the age of organic material by measuring the amount of radiocarbon remaining in a sample.

De Vries (1958) correlated the atmospheric ¹⁴C fluctuations from the sixteenth to the eighteenth century with climate change in the Little Ice Age. Later Stuiver (1961) demonstrated a relationship between the findings of de Vries and solar activity. In Figure 3.14 is shown the ¹⁴C time variation for the last millennium. During the Maunder Minimum of solar activity we clearly see a peak in the ¹⁴C concentration. The anticorrelation with solar activity is clearly demonstrated. During the Medieval Warm the concentration was lower, indicating higher solar activity (about the year 1200).

Solanki *et al.*(2004) reconstructed the sunspot number covering the past 11 400 years, based on ¹⁴C concentrations. They find that the level of solar activity during the past 70 years is exceptional and that the Sun spent only 10% of this long period at a similar high level of activity.

3.6.4 Meteorites

Cosmic rays also leave their imprints on isotope production in meteorites. In these objects their rate production again varies inversely with solar activity; at times of high activity their production rates are lowered because of better shielding from high energetic galactic cosmic rays.

For meteorites the time resolution is between 10 and 10⁹ years. Sodium-22 measurements in meteorites clearly confirm the 11 year cycle and ⁴⁴Ti measurements an 88 year cycle of activity (the Gleissberg cycle). Meteorite measurements eliminate the terrestrial processes on isotope records on Earth, because they are outside the geomagnetic field. This topic will be dealt with again in chapter 6.

3.6.5 The Moon

The moon provides us with information on solar corpuscular radiation in ancient times because it has no atmosphere and no magnetosphere that acted as a shield. The formation of the moon is still uncertain but the most preferred idea is that it was originated from a large asteroid impact on the early Earth. Its dynamics is strongly coupled to that of the Earth. The rotation of the Earth decelerates (because of tidal forces from the Moon) and because of conservation of angular momentum the Earth–Moon distance increases with time. This has two important effects:

- The Earth rotated faster in early times, and therefore the terrestrial magnetic field was stronger.
- The Moon was closer to the Earth, and contamination of the Moon by ions from the Earth's atmosphere was more intense.
- During this early phase the free solar wind could not reach the Moon.

In the early history of the Moon there was a global melting - the formation of the anorthositic crust. At that time, however, the Sun was already a main sequence star. The mare basaltic extrusion ended some 3 Ga ago. So it is important to note that the solar record on the Moon is restricted to the main sequence Sun.

In lunar samples volatile elements are rare and many noble gas isotopes of solar origin found in the samples can be easily identified.

What are the signatures of solar wind irradiation left in lunar surface material?

- Atoms from the solar wind trapped in the lattices of lunar grains
- Solid state alterations

One finds, for example, an amorphous layer of a few tens of nm around silicate crystals, these can be explained by an enormous energy dosage and exposition by the ions in the solar wind. The thickness of the layer is proportional to the speed of the solar wind.

Our knowledge on the solar-wind activity during the last several 10^9 years (1 Ga) has come mainly from the study of the lunar regolith. Variations of the isotopic compositions of trapped He, Ne, Ar, and N in the surface layer of lunar soil grains were attributed to long term changes in the isotopic composition of solar irradiation, or in the ratio of solar particles to lunar atmospheric species (Clayton & Thiemens 1980; Kerridge 1993). The study of such variations requires a knowledge of the age of a particular sample; that is, the time when a sample was exposed to solar and lunar atmospheric particles. A practical and sensitive age indicator is the ratio $^{40}\text{Ar}/^{36}\text{Ar}$ of trapped Ar.

Since a substantial fraction of the older soil is greatly altered, a great portion of its gas content must have been lost so the discrepancy must be even higher.

Measurements of the cosmic ray flux from meteorites and Moon show that it was constant ($\pm 30\%$) within the last 1 Ma (Reedy *et al.* 1983).

The conclusion of these studies is simple: The average solar wind flux must have been significantly higher than the contemporary flux. This can be explained by enhanced solar activity leading to enhanced solar wind intensity. As has been shown already, enhanced solar activity means enhanced UV radiation. The UV radiation about 3 billion years ago was thus certainly much higher than it is today. We must look to the Early Earth and to the stars to verify this hypothesis.

3.7 Long-Term Variation of Solar Luminosity

Geological evidence indicates that oceans of liquid water have existed on the earth at least since 4.3 Ga ago (Wilde *et al.* 2001), approximately coinciding with the

end of the late bombardment period. Moreover, temperatures at the early times were probably much higher than in our time.

However, the theory of stellar evolution clearly predicts an increase in solar luminosity during its time on the main sequence (Gough, 1981). As a consequence, the Sun was a 30% dimmer than at the present. Let us quantify this effect.

The theory of stellar evolution tells us that stellar luminosity depends on mass, M , the mean molecular weight, μ , and the radius, r , according to the expression

$$L \propto M^{5.5} R^{-0.5} \mu^{7.5} \quad (3.3)$$

The process of energy generation in the Sun during its stay on the main sequence is the nuclear transformation of hydrogen to helium. This produces an increase in the mean molecular weight and, according eq.3.3, an increase in solar luminosity:

$$L(t) = [1 + 0.4(1 - t/t_0)]^{-1}$$

This luminosity increase is the main factor limiting the duration of the habitability of earth-like planets (see Franck 2001 and Ward & Brownlee 2002).

Climate modelling indicates that the mean temperature of the Early Earth should be below zero, a status called snowball Earth, from which it would be impossible to escape (Newman & Rood 1977)⁸. This apparent contradiction, called *The faint Sun paradox* has been explained classically in terms of an enhanced greenhouse effect produced by larger abundances of CO₂ in the primitive terrestrial atmosphere. The amounts of iron carbonates present in lithified remains of soils (paleosols) give an upper limit to the amount of CO₂ 2.5 Ga ago of about 100 times the present value, just sufficient to keep the oceans above freezing (see chapter 5 for more details).

Microorganisms have clearly influenced the evolution of the atmosphere, and this was probably true since the early times through the production of an important amount of methane, another greenhouse gas, contributing to the necessary warming to keep the oceans liquid (Kasting & Siefert 2002; Kasting & Catling 2003). In fact, methanogenic bacteria are evolutionarily very ancient.

Additionally, the possible existence of liquid water on Mars at that time put an additional constraint to the models of the Early Sun (see Sonett *et al.* 1991).

Another possibility of solving the paradox arises from the equation 3.3 namely the existence of an early phase of significant mass loss. Wood *et al.* (2002) obtained high-resolution Ly α spectra and found that the mass loss per unit surface is correlated with the level of magnetic activity. They derived a time dependence of the mass loss of the form

$$dM/dt = t^{-2.00 \pm 0.52}$$

which suggests that the wind of the active young Sun may have been around 1000 times stronger than of the present. Sackmann & Boothroyd (2003) also proposed

⁸Our planet has suffered, at least two of such periods (2.45–2.2 and 0.7 Ga ago), emerging from this situation through an enhanced volcanic activity. The first one was surely caused by the decrease in methane due to the increasing levels of atmospheric oxygen.

also the existence of a more massive and larger Early Sun, with the planets being closer with respect to their present positions. A phase of rapid mass loss would lead to the present situation within a period of 1 Ga.

In the context of our book, it is pertinent to ask now how the UV flux of the Sun in that early times affected the primitive Earth and the other planets. Observations of pre-main sequence stars indicate that before the Sun reached the main sequence, it may have emitted as much as ten thousand times the amount of ultraviolet radiation as it does today. To know this we need to understand how magnetic activity evolves with time on very long time-scales.

3.8 Long-Term Decay of Magnetic Activity and UV emission

The Sun is the only star that can be observed in detail; however, by observing other stars we can cover the full parameter space, and the past history of the Sun can be inferred as well as its distant future.

In our context this will lead us to a somewhat more precise estimate of the UV radiation history of the early Sun. A recent review of this strongly evolving topic has been given by Pallavicini (2003).

3.8.1 Observations of solar-like Stars

The solar and stellar scientific communities use different methods for observing their targets. Whereas the Sun can be observed in high resolution mode (with details down to about 300 km) stars can only be observed in integrated light⁹. In the previous chapter we have indicated the spectral lines used to get information about the different layers of the solar and solar-like atmospheres.

In principle, all stars have chromospheres and coronae. Mass loss and stellar winds also occur, sometimes at much higher intensity than on the Sun. There are stars with huge flares and sunspots that cover considerable amounts of their surface. Stars show activity cycles sometimes similar to that of the Sun, sometimes much more chaotic.

The Ca II monitoring programme is carried out at Mt. Wilson Observatory and stars have been investigated for activity cycles for more than 30 years. Baliunas *et al.* (1985) found that: 1) about one third of solar-type stars have cycles between 7 and 15 years, 2) one third have rather chaotic cycles, and 3) one third have no cycle or signs of activity at all; maybe these stars are in a Maunder Minimum like phase.

In addition to the Ca II H and K lines the chromospheric Mg II line in the UV can be used as diagnostic tool; however, it can only be observed from space. The advantage is that its cosmic abundance is 14 times larger than that of Ca. The optical depth reached is about an order of magnitude larger at a given geometric depth. This greater line strength makes Mg II lines more sensitive to weak atmospheres.

⁹Using techniques such as speckle interferometry one can deduce some surface details.

The Ly α line is formed over a broad range of temperatures, several nm away from the centre the wings are formed in the low chromosphere and the centre is formed in the transition region. The use of the H α line is complicated: a) because it is formed over a wide range, from the photosphere in the line wing to the middle and high chromosphere in the core and b) owing to its ambiguous response to magnetic activity (absorption and emission indicate a heated atmosphere).

Convection can be measured as a blueshift of spectral lines, especially weak lines formed in the deeper stellar atmosphere. Such blueshifts have recently been measured by Allende-Prieto *et al.* (2002) where further references can be found on that topic. The Ca II excess flux density, ΔF_{HK} , is correlated with the Rossby number R_0 ¹⁰ (Montesinos *et al.*, 1993).

Rapidly rotating stars are covered with spots (up to several 10%, the spot coverage of the solar disc is only $\sim 1\%$).

We can detect stellar coronae from X-ray observations. It was believed that only F- and G-type stars possess X-ray emitting coronae (because of their heating mechanism). There seem to be two different types of heating mechanisms for stars:

- Early-type stars: there exist massive radiatively driven winds. Shocks in these winds cause the heating.
- Late-type stars (including the Sun): magnetic heating of coronal loops.

We know much less about surface phenomena on stars and, in any case, these phenomena must be inferred indirectly from spatially unresolved observations. Stellar flares in the optical have been known for quite a long time, while the presence of cool dark spots has been inferred from rotational modulation of photometric observations and, more recently, from the detailed analysis of line profiles by Doppler imaging. Additional information, particularly on stellar flares, have been provided by X-ray and UV observations as well as by radio. It is now well established that solar-type activity phenomena are a common feature of active late-type stars, often on a much larger scale than on the Sun.

3.8.2 The Dynamo Theory

To explain the generation of the solar and stellar magnetic fields, dynamo theory is used in considering the coupling of the magnetic field with the subphotospheric velocity field.

Let us treat the solar plasma as an electrically conducting field of conductivity σ and magnetic diffusivity $\eta = 1/(\mu_0\sigma)$, where μ_0 is the permeability of free space. The induction equation (see any standard textbook), gives the time dependence of the magnetic field, \vec{B} :

$$\frac{\partial \vec{B}}{\partial t} = \nabla \times (\vec{v} \times \vec{B}) + \eta \nabla^2 \vec{B}$$

¹⁰This is the dimensionless ratio of inertial to coriolis force; it describes the importance of rotation (in astrophysics the Rossby number is often defined by the stellar rotation period divided by the subphotospheric convection turnover time).

For the dynamo theories¹¹ one must discern between small scale and large scale dynamos. Stars are rotating objects and the Rossby radius, R_1 , measures the scale at which both rotation and gravity becomes important.

For scales larger than R_1 : the motions are rotationally constrained. There is differential rotation, helical motions, large scale dynamo action, $\alpha - \omega$ dynamos, activity cycles. For scales smaller than R_1 : non-helical flows, small scale dynamo action.

In general there is a close connection between rotation rates and stellar activity. The chromospheric emission of stars, which can be used as a measure of their magnetic activity, increases with rotation rate. There also seems to exist a kind of basal flux that is commonly believed to be acoustic.

For the Sun $R_1 \sim 50000$ km and granulation is unaffected and supergranulation only weakly.

Non-helical turbulent convection is likely to be a (small-scale) dynamo. This dynamo field is extremely intermittent and evolves on the same timescale as the turbulence.

In order to explain the solar activity cycle we use the so called $\alpha - \omega$ dynamo. As we have shown above, magnetic fields follow the plasma motions on the solar surface because they are frozen in. Therefore, magnetic fields within the Sun are stretched out and wound around the Sun by differential rotation. This is called the omega-effect after the Greek letter used to represent rotation. The Sun's differential rotation with latitude can take a north-south orientated magnetic field line and wrap it once around the Sun in about 8 months.

Twisting of the magnetic field lines is caused by the effects of the Sun's rotation. This is called the alpha-effect after the Greek letter that looks like a twisted loop. Early models of the Sun's dynamo assumed that the twisting is produced by the effects of the Sun's rotation on very large convective flows that carry heat to the Sun's surface. One problem with this assumption is that the expected twisting is far too great and that it produces magnetic cycles that are only a couple years long. More recent dynamo models assume that the twisting is caused the effect of the Sun's rotation on the rising "tubes" of magnetic field from deep within the Sun. The twist produced by the alpha effect creates sunspot groups that obey Joy's law¹² and also makes the magnetic field reverse from one sunspot cycle to the next (Hale's law).

Early models of the Sun's magnetic dynamo worked on the idea that dynamo activity occurs throughout the entire convection zone. It was soon realized, however, that magnetic fields within the convection zone would rapidly rise to the surface and would not have enough time to experience either the alpha or the omega effect. Since a magnetic field exerts a pressure on its surroundings, regions with a magnetic field should push the surrounding gas aside and create a bubble that would continue to rise all the way to the surface. This buoyancy is not produced in the stable layer below the convection zone. Within the radiative zone the magnetic bubble would rise only a short distance before it found itself just as

¹¹See also: Lectures on Solar and Planetary Dynamos, M.R.E. Proctor, A.D. Gilbert, 1994, Cambridge University Press

¹²The tilt of sunspot groups depends on the heliographic latitude.

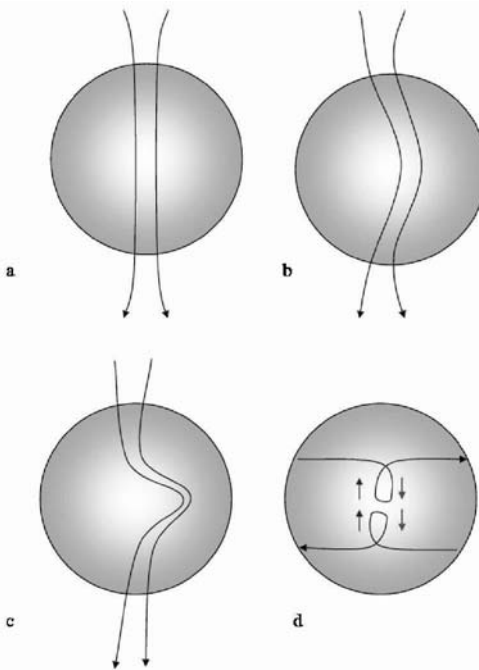


Figure 3.15: Four phases of the solar dynamo: a) poloidal field, b) differential rotation, warping the magnetic field lines, c) concentration of field lines near equator and d) reversal of field because of the α effect.

dense as its surroundings. This led to the idea that the Sun's magnetic field is produced in the interface layer between the radiative and the convection zones. This interface layer is also where we find rapid changes in rotation rate as we look inward or outward across it.

3.8.3 Activity–Rotation Relation

There seems to be a relation between the strength of stellar coronae and their rotation rates. The higher the rotation rate, the more intense the corona. Young rapidly rotating stars have coronae orders of magnitude stronger than that of the Sun, whereas old slowly rotating stars have only very weak coronae.

As outlined in the previous chapter, there are reasons to believe that dynamo action occurs at the base of the convection zone, and in particular at the interface between the base of the convective zone and the radiative interior.

Active, young and rapidly rotating stars have stronger chromospheric emission than the Sun. The non-radiative heating of the chromospheres occurs mainly by acoustic and magneto-acoustic waves.

The first measurements already indicated that the stellar rotation is decaying with the stellar age (Kraft 1967). The mechanism of magnetic braking (Schatzman

1962) was able to explain this observational fact (Figure 3.16).

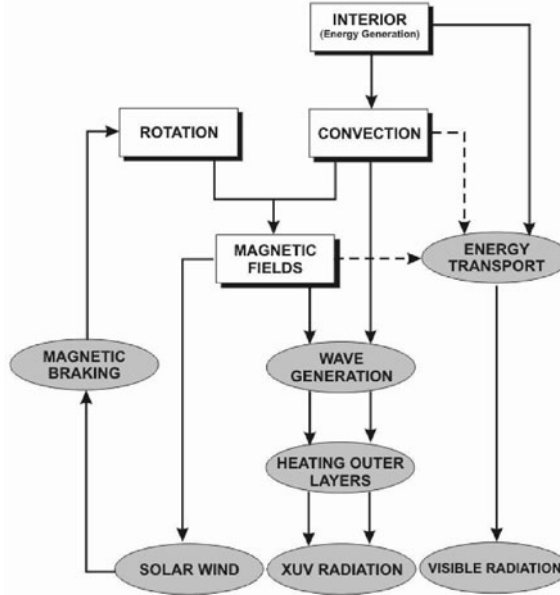


Figure 3.16: The connection between solar/stellar rotation and solar/solar-like magnetic activity.

Skumanich (1972) first proposed a $t^{-1/2}$ law describing the decay of chromospheric emission, lithium abundance (an age indicator) and rotational braking. Messina & Guinan (2002) studied young solar-like stars. As is seen in Table 3.9 these stars have ages below 1 Ga and rotate rapidly. There exists a relation between the frequency of the magnetic cycle, ω_{cyc} , the rotational frequency, Ω , and other stellar parameters (Saar & Brandenburg 1999).

UV spectra of α Cen A and the Sun in the range 114–161 nm were compared by Linsky *et al.* (2003). Using the HST Imaging Spectrograph these authors found many similarities. The differences between the two stars can be explained by slight differences in gravity, age and chemical composition.

The star 18 Scorpis (HD 146233, HR 6060) is currently regarded as the nearest solar twin. The observations of Hall *et al.* (2000) suggest that the activity cycle of 18 Sco may be of greater amplitude than the Sun's and that its overall chromospheric activity level is noticeably greater than the Sun's. The rotation period is 25.8 d, the age 4.8 ± 0.8 Ga and the mass $1.0 \pm 0.03 M_\odot$. The magnetic activity and related coronal X-ray and chromospheric emission vary as function of the star's rotation period, and thus age. Therefore a stellar flux can be estimated from the rotation period, P_{rot} , by using activity–rotation relations (see Wood *et al.* 2004).

$$F(\text{Ly}\alpha) \propto P_{\text{rot}}^{-1.09 \pm 0.08}$$

Table 3.9: Young solar-like stars (adapted from Messina & Guinan (2002) *Astronomy and Astrophysics* 393, 225-237.

Star HD	Name	Rotation period	Spectral type	Age (Ma)	Cycle length (yr)
1835	BE Cet	7.75d	G2 V	600	66.7 ± 0.7
20630	k^1 Cet	9.21 d	G5 V	750	5.9 ± 0.2
72905	π^1 UMa	4.9 d	G 1.5 V	300	13.1 ± 0.9
129333	EK Dra	2.49 d	G0 V	130	9.2 ± 0.4
206860	HN Peg	4.64 d	G0 V	300	5.5 ± 0.3
82443	DX Leo	5.42 d	K0 V	130	3.2 ± 0.05

It is important to know whether the decay in rotation rates and the associated ionizing and UV radiation emission can suffer discontinuities. Vaughan & Preston (1980) found a gap in the plot representing the relation between the chromospheric emission and stellar spectral type. This was interpreted in terms of an abrupt transition in the mode of operation of the stellar dynamo, producing a change from strong irregularities in the ionizing radiation emission to the smooth variation that characterises the present solar cycles (Durney *et al.* 1981 ; Brandenburg *et al.* 1998).

Observations in stars of different open clusters have gradually revealed that there are two types of evolutionary paths for stellar rotation, depending on the interaction star–planetary disc, the fast and the slow, both converging at ≈ 1 Ga towards a common Skumanich decay. A possible explanation has been suggested based on the existence, in the majority of solar-like stars, of a magnetic field connecting the convective envelope to the stellar radiative interior and the exterior where winds drain off angular momentum, breaking the stellar rotation after the Skumanich law (Barnes 2003).

3.8.4 The Evolution of UV Radiation in solar-like Stars

An intense UV radiation field has important consequences for the formation of stars in clusters. Stars are formed in discs, which are gradually destroyed via photoevaporation as the UV photons heat the gas in the outer layers of the disc to thermal escape velocities. Only the central collapsing objects remain. An early intense UV irradiation favours the formation of low mass cluster members (Richling & Yorke 2003). The problem of star formation under intense UV irradiation field has also been discussed by Omukai (2001) and Richling & Yorke (2000).

Solar-type dwarf stars (stars of about 1 solar mass) arrive on the Zero-Age Main Sequence (ZAMS) with large angular momentum from their T-Tauri phase. The equatorial velocities expected are between 20 and 50 km s⁻¹, which is high in comparison to that of the present Sun (2 km s⁻¹). These stars are extremely active. There exists a strong dependence of surface magnetic activity on stellar spin. Stars in the young Pleiades cluster (age about $50-70 \times 10^6$ yr)(Terndrup *et*

al. 2001) have rotation rates of $v_* \leq 50 \text{ km s}^{-1}$, in the α Persei cluster (age $600 \times 10^6 \text{ yr}$) the slowest rotators have $v_* \sim 10 \text{ km/s}$, indicating an age similar to that of the stars in the Hyades cluster. For studies of our Solar System we have to take into account, that there was the great bombardment phase during the first 0.5–0.8 Ga. During that phase the planetary surfaces were reformed and the Solar System “lost memory”.

For the evolution of planets, and especially their atmosphere, it is crucial to consider the evolution of photoionization rates. The main result of an investigation by Ayres (1997) was to predict an enhancement in four photoionization frequencies for H, O, O₂ and N₂, from present-day values backward in time revealing an enhancement in the rates over the present day value of more than 100 at a solar ZAMS age of 0.05 Ga. It must also be stressed that, currently the ionization rates R (see next chapter for its definition), differ from solar maximum to minimum by a factor of 100.

For solar-like stars, the level of magnetic activity depends mainly on two parameters; namely, the thickness of the convection zone and the rotation. As the UV flux is related with the level of solar activity, this is particularly relevant for the temporal changes in UV solar flux throughout the history of our planet.

Zahnle & Walker (1982) suggested that the young Sun was a much more powerful source of energetic particles and radiation than it is today, and while on the main sequence, its activity has declined according an inverse power law of age. They refer to observations of pre-main sequence stars, which indicate that before the Sun reached the main sequence, it may have emitted as much as ten thousand times the amount of ultraviolet radiation as it does today.

Ayres (1997) describes how, with declining overall stellar activity, different emissions fade: shorter wavelength emission fade more rapidly. Coronal X-rays ($T \sim 10^6 - 10^7 \text{ K}$) are the first to decline, followed by the EUV ($T \sim 10^5 - 10^6 \text{ K}$) and then the UV in the chromosphere ($T \sim 10^4 \text{ K}$). This was shown by Simon *et al.* (1985). Such a relation might be expressed for rotational velocities as a power law:

$$P_{\text{rot}} \propto t^{-0.6 \pm 0.1}$$

We have then, a similar expression for the radiative emissions

$$F(t) = t^{-\alpha}$$

with α values increasing from the chromosphere to the corona. Walter & Barry (1991) prefer a functional fit of the form

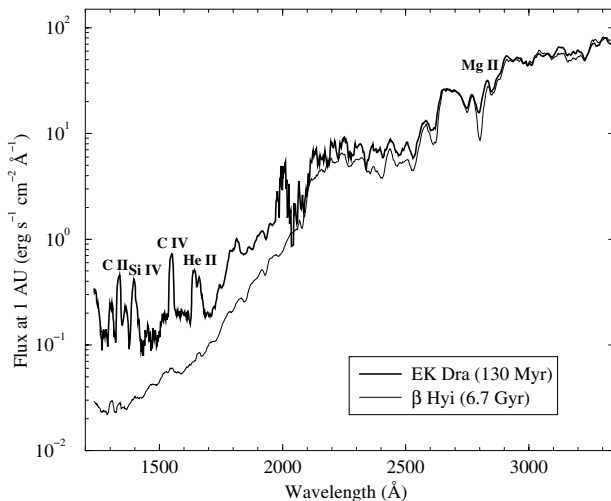
$$F(t) \propto \exp(A \times t^{0.5})$$

where Table 3.10 gives values of A for different spectral indicators of the outer layers.

“The Sun in Time” project studies the long-term evolution of a G-type star by selecting solar analogues of different ages (Guinan *et al.* 2002, 2003; Lammer *et al.* 2003). Well calibrated UV spectra of solar-like stars have been calculated

Table 3.10: Different values of A fitting the activity -age relationship

Lower chromosphere	Ca II	-0.54 ± 0.02
	Mg II	-0.60 ± 0.18
	C I	-0.58 ± 0.35
	O I	-0.64 ± 0.37
	Si II	-0.63 ± 0.19
Transition region	C IV	-0.98 ± 0.24
	Si IV	-0.93 ± 0.23
Corona	X-rays	-2.20 ± 0.22

Figure 3.17: Comparison of the UV flux of a young star, EK Dra, and a old one, β Hyd. Courtesy of I. Ribas (University of Barcelona).

that show a clear dependence on the age (Figure 3.17). The resulting EUV fluxes have been recently updated by Ribas *et al.* (2005)

$$F(0.1 - 120 \text{ nm}) = 29.7 [t(\text{Gyr})]^{-1.23} \text{ erg cm}^{-2} \text{ s}^{-1}$$

$$F(\text{Ly}\alpha) = 19.2 [t(\text{Gyr})]^{-0.72} \text{ erg cm}^{-2} \text{ s}^{-1}$$

Chapter 4

Atmospheric Effects of Ultraviolet Radiation

A photon arriving at the top of the terrestrial atmosphere interacts with the matter there through two main processes: scattering and absorption. The preponderance of one or the other process depends on the wavelength of the radiation and the size and internal structure of the impacted particle of matter. Both are globally integrated in the concept of extinction¹.

Solar UV photons have enough energy to configure the structure and variability of the upper and middle layers of the Earth's atmosphere. We shall describe the different photochemical processes, starting with the most evident influences and finishing with the description of the possible connection with the climate of the troposphere. Ozone will play the major role in this chapter.

4.1 The Extraterrestrial Solar Spectrum

4.1.1 The Spectral Distribution of Solar Radiation

The measurement of the spectral distribution of solar irradiance was one of the primary objectives of the solar astronomers during the last decades of nineteenth century and beginning of the twentieth. Following the pioneering work of the Smithsonian scientists, high mountains were selected for this purpose such as the Jungfraujoch (Labs & Neckel 1962), Tenerife (Muller 1912) and Mauna Loa (Stair & Ellis 1968).

High altitude aircrafts were also used to measure the solar spectral output. Aversen *et al.* (1969) measured the solar irradiance during eleven flights on board a NASA CV-990 aircraft at altitudes between 11.6 and 12.5 km.

¹For a deeper study in this topic see Banks & Kockarts (1973); Iqbal (1983); Houghton (1985); Jacob (1999); Finlayson-Pitts & Pitts (2000) and Ghost (2002).

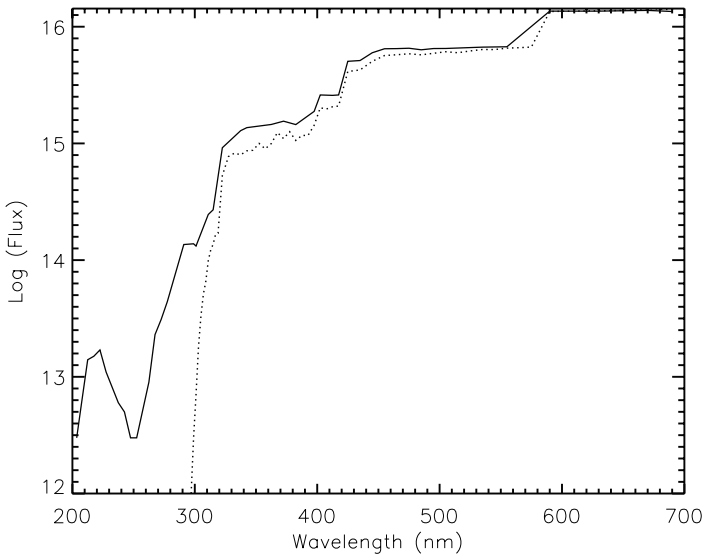


Figure 4.1: The solar spectrum at an altitude of 40 km (solid line) compared with that recorded at the surface (dotted line). Adapted from values given in Tables 3.11 and 3.17 of Finlayson-Pitts & Pitts (2000) *Chemistry of the upper and lower atmosphere*, Academic Press. Units are photons per square centimeter per second

As an example, Figure 4.1 compares the solar spectrum at the top of the atmosphere (~ 40 km) with that recorded at the ground.

4.1.2 Atmospheric extinction

To derive, from ground-based observations, the amount of energy incident at the top of the terrestrial atmosphere, we need to estimate the light that is eliminated from the solar beam during its travel through the atmosphere.

Johann Lambert (1728–1777), August Beer (1825–1863) and Pierre Bouger (1698–1758) studied the amount of light “lost” from a beam, after passing through a physical medium. Assuming a monochromatic light beam of wavelength λ and intensity I_0 passing through a sample of length l (in cm) and concentration c (in moles per liter), the intensity of the emerged light, I , will be reduced according to

$$\ln(I/I_0) = -\epsilon lc$$

where ϵ is the molar absorption ($\text{mol}^{-1} \text{cm}^{-1}$) characterizing the extinction properties of the physical media contained in the sample. Experimental measurements are made in terms of the transmittance $T = I/I_0$ or the absorption $A = \log T$.

In atmospheric gas chemistry, the following expression is used

$$\ln(I_0/I) = \sigma N l$$

where σ is the absorption cross section, l the path of the light through the medium N the concentration expressed in molecules per cm³.

In astronomical applications, for a homogeneous atmosphere of height H , the observed intensity, I , at a particular wavelength and zenith distance ($z = \cos \theta$)², is given by

$$I(z, \lambda) = I_0(H, \theta, \lambda) e^{-m\tau(z)} \quad (4.1)$$

where I_0 is the incident solar flux at the top of the atmosphere, m the air mass given by $m = \rho H \sec z$ and $\tau(z)$ is the vertical optical depth expressed by

$$\tau(z) = \sum_{i=1}^n \int_0^H N(i, z)(\kappa_i + \sigma_i)(i, z) \sec z dh$$

where $N(i, z)$ is the number density (particles per cubic metre) and κ and σ are the absorption and scattering effective cross-section, respectively.

The logarithmic expression of eq. 4.1 is

$$\ln I(\lambda) = \ln I_0 \lambda - \tau_\lambda m$$

If the atmospheric properties do not change during the observations ($\tau_\lambda = \text{const.}$), a plot of $\ln I$ vs m results in a straight line which may be extrapolated to give $I_0(\lambda)$ at $m = 0$. The integration of the monochromatic intensity over λ yields the total flux, F (Figure 4.2).

Different units are used for these coefficients. The scattering (absorption) coefficient per particle, σ , has the units of a cross-section (cm⁻²), per unit of volume, σ_{vol} , is (cm⁻¹) and per unit of mass (cm²/g). The main relations between them are

$$\sigma_{\text{vol}} = \sigma N = \sigma_{\text{mass}} \rho = \sigma_{\text{mass}} N_H \bar{\mu} m_H$$

where N is the number density of particles, ρ the mass density and $\bar{\mu}$ the mean molecular weight.

The ratio between the absorption and scattering coefficients at a particular wavelength is called the scattering albedo:

$$\bar{\omega} = \frac{\sigma}{\sigma + \kappa}$$

Combining the extinction and Kirchhoff laws, we obtain the Schwarzschild equation

$$\frac{dI_\lambda}{ds} = -(\sigma_\lambda + \kappa_\lambda)I_\lambda + \epsilon_\lambda B_\lambda(T)$$

²At $z > 60^\circ$ the curvature of the Earth and atmospheric refraction must be taken into account.

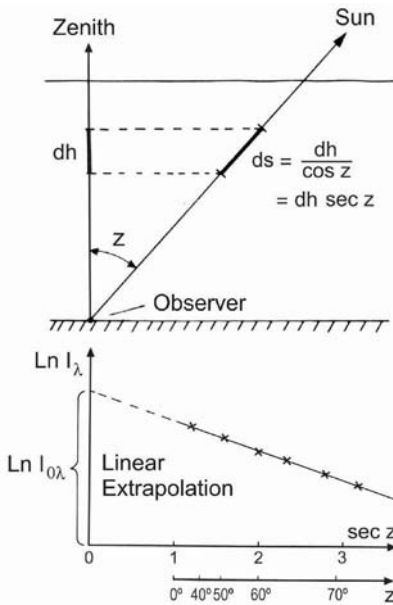


Figure 4.2: Estimation of light extinction in the atmosphere.

where the first term indicates the change in the radiative flux, due to the balance between the absorption (plus scattering) and emission of radiation.

Let us start by describing first the scattering of light by particles. Generally, this causes a deviation of light from the incident direction without changing the frequency (see van de Hulst 1957 for the basic theory). Scattering is a consequence of different processes depending on the size of the particles, whose contribution has an additive character, including also phenomena of atmospheric optics such as reflection, refraction and diffraction caused by raindrops and ice crystals.

The scattering cross-section for a classical oscillator can be written as

$$\sigma(\nu) = \frac{8\pi e^4}{3m_e^2 c^4} \left[\frac{\nu^4}{(\nu^2 - \nu_0^2)^2 + (\gamma/2\pi)^2 \omega^2} \right]$$

where γ is the damping constant and ν_0 the frequency of a classical oscillator

4.1.3 Thompson and Compton Scattering

Thompson scattering is produced by free electrons ($\gamma = 0$ and $\nu_0 = 0$). The corresponding cross-section σ , is small, because the electron makes a poor target for an incident photon:

$$\sigma_T = \frac{8\pi e^4}{3m_e^2 c^4} r_e^2 \longrightarrow \sigma_T = 6.65 \times 10^{-25}$$

where r_e is the electron radius.

Thompson scattering is important in atmospheres of hot stars and in the outer layers (the corona) of the Sun and solar-like stars, but negligible in the terrestrial atmosphere.

Scattering by electrons can also produce a wavelength shift in the radiation, when the electron has high energies. This was shown by A.H. Compton (1892 - 1962) in 1923, who found that the scattered light has a wavelength different from that of the incident light. Compton analyzed this problem by considering light as a photon with energy $E = h\nu$, and a momentum $p = h/\lambda$. Using the energy and momentum conservation for such a collision, he found the following relation between the wavelengths of incident and scattered photons:

$$\lambda - \lambda_0 = 2\lambda_c \sin^2 \frac{\theta}{2}$$

with the Compton scattering cross-section given by (Harwitt 1973)

$$\sigma_C = 2\pi r_e^2 \left[\frac{1+\alpha}{\alpha^2} \left[\frac{2(1+\alpha)}{1+2\alpha} - \frac{1}{\alpha} \ln(1+2\alpha) \right] + \frac{1}{2\alpha} \ln(1+2\alpha) - \frac{1+3\alpha}{(1+2\alpha)^2} \right]$$

where θ is the angle between the incident and scattered photon, α the ratio of photon to electron energy ($h\nu/m_e c^2$), c the speed of light and m_e the mass of the electron. Relativistic energy and momentum are conserved in this process and the scattered photon has less energy and therefore a longer wavelength than the incident photon.

Such a small difference in wavelengths between the incident and scattered light is very hard to detect using visible light (~ 0.005 nm in 500 nm). However, it is a comparatively large effect for X-rays, which have wavelengths of the order of 0.1 nm. In chapter 7 we shall study the relevance of this process for the transformation of impinging γ and X-rays at the top of the terrestrial atmosphere for UV radiation at the surface.

4.1.4 Rayleigh–Mie scattering

Lord Rayleigh studied the scattering of light by molecules of air and obtained the following expression (Strutt 1871) by assuming an isotropic scattering:

$$\sigma_R = \frac{8}{3} \frac{\pi^3 N}{N_0^2 \lambda^4} (n_0 - 1)$$

where n_0 is the bulk index of refraction of the air, N_0 the number of molecules per unit volume (2.547×10^{19}), both at normal pressure and temperature (15°C) and N the number of particles per volume unit at a given pressure and temperature.

Later, the expression was extended to non-spherical symmetry:

$$\sigma_R = \frac{8}{3} \frac{\pi^3 N}{N_0^2 \lambda^4} (n_0 - 1) \frac{6 + 3\rho_n}{6 - 7\rho_n}$$

where ρ_n is the depolarization factor (0.014 for air). In a simplified form, we have

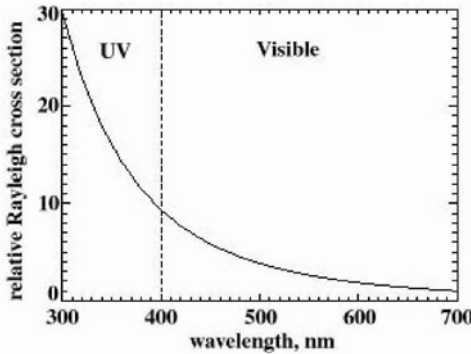


Figure 4.3: Variation of Rayleigh scattering with wavelength.

$$\sigma_R = 8.79 \times 10^{-3} \lambda^{-4.09} \propto \lambda^{-4}$$

The scattering-cross section is about nine times as great at the blue-violet end of the visible spectrum than at the red end. Over the UV region, the scattering cross-section increases by a further factor of about 3 (Figure 4.3).

The pressure dependence is given by

$$\sigma_R(\lambda) = 0.008569 \lambda^{-4} (1 + 0.00113 \lambda^{-2} + 0.00013 \lambda^{-4}) p/p_0$$

where p is the pressure (mbar) at altitude z , and $p_0 = 1013.25$ mbar is the sea-level pressure ³.

Gustav Mie (1868 - 1957) was the first to study the interaction of radiation with larger particles of a given radius r (Mie 1908). The corresponding parameter is

$$\sigma_M = \beta \lambda^{-\alpha}$$

with α depending on r . We will have $\alpha = 0$ for $r \gg \lambda$ and $\alpha = 4$ for molecules ($r \ll \lambda$).

Rayleigh scattering is symmetric about a plane normal to the incident radiation. As we enter the Mie regime more radiation is scattered into the forward than into the backward hemisphere.

This process is especially important in the terrestrial atmosphere, where the higher scattering of blue photons produces the colour of our daytime skies ⁴ The

³Twersky (1964) gives an excellent historical review of the work of J. W. Strutt on the process of scattering.

⁴Leonardo da Vinci (1452– 1519) first suggested that the colour of the sky is caused by the scattering of sunlight from small particles suspended in the atmosphere and proposed an experiment to prove it.

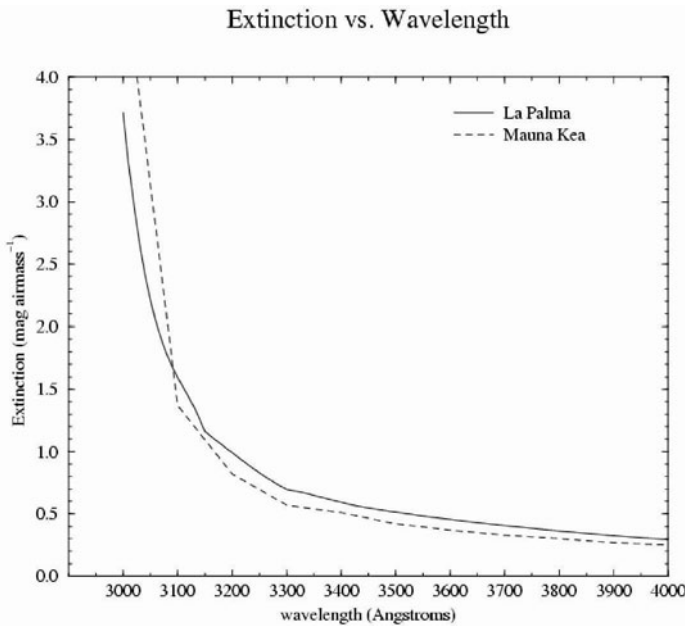


Figure 4.4: Extinction curves obtained at the observatories of Roque de los Muchachos (La Palma, Spain) and Hawaii. Courtesy: R. García López (IAC)

almost white scattering in the direction of the sun can be attributed to larger particles, resulting in a process which is weakly dependent on wavelength.

Figure 4.4 compares extinction curves obtained at two well known astronomical observatories, where we can easily see the wavelength dependence of the scattering.

4.1.5 Absorption and Emission of Radiation by Molecules

In isolated atoms, absorption of photon energy is related with the transition between energy levels of the electrons. Molecules may also acquire energy in other ways (see the classic book of Herzberg, 1950).

- Rotational changes: The molecule may rotate about an axis perpendicular to the line joining the atoms. This occurs only in molecules that have a dipole moment, and for this reason N₂ and O₂ have no rotational bands. The most important are those corresponding to H₂O, CO₂ and O₃, which are triatomic. Because of the small energies involved, the lines are concentrated in the far infrared and radio ($\lambda > 20\mu$).

- Vibrational changes: The atoms may vibrate back and forth along the line joining them. The spectral lines are mainly in the near IR (0.7 - 20 μ). The vibrational energy levels are quantified and have energies given by

$$E_\nu = h\nu_{\text{vib}}(\nu + 1/2)$$

where ν_{vib} is a constant characteristic of the molecule.

As in atoms, the molecule may be excited to definite electron energy states. The lines are mainly located in the UV range with only a few in the visible.

The spectrum of a molecular gas occurs in bands that consist in a rather large number of closely spaced lines. In intermolecular processes, the excited molecule reacts with a different molecule. In intramolecular processes one part of the excited molecule attracts another part of the same molecule.

The absorption of radiation is followed by the emission of radiation, produced by the de excitation of the excited electrons to lower energy levels. *Resonance fluorescence* occurs when the emitted radiation is of the same wavelength as that absorbed. This is observed only in the gas phase at low pressures (where collisional processes are negligible) and only with atoms or simple molecules. For higher pressures collisional processes dominates and the de-excitation takes places stepwise, leading to different wavelengths in the emission spectra.

Finally, emission followed excitation by chemical reactions (of neutral or charged particles) is called *Chemoluminescence*.

These mechanisms are essential to understanding the different processes taking place in the Earth's atmosphere induced by solar radiation.

The absorption optical depths for different atmospheric gases define the length a given wavelength can penetrate (Figure 4.5) and can be expressed as the product of the mean cross-section, σ , and the column abundance X:

$$X = \int_0^\infty N(z)dz = \frac{A_0}{\mu_a g} \int_0^P r(p')dp'$$

where A_0 is the Avogadro number, μ_a the molecular weight of the air (≈ 29 kg kmol $^{-1}$), g the gravitational acceleration, and p the pressure. Table 4.1 gives X values for the most important atmospheric molecules.

Table 4.1: Column abundances of atmospheric gases

Gas	X (cm $^{-2}$)
O ₂	4.47×10^{24}
O ₃	7.97×10^{18}
H ₂ O	8.12×10^{22}
CO ₂	7.04×10^{21}
N ₂ O	6.36×10^{18}
NO ₂	1.27×10^{16}

Finally, the column integrated optical depth is given by

$$\tau(\lambda) = \sigma(\lambda)X$$

Particularly relevant in our context are the absorption properties of gases in the ultraviolet range. Ozone and to a much lesser extent molecular oxygen are responsible for most of the absorption of the solar radiation in the UV, especially between 180 and 290 nm; thanks to these processes

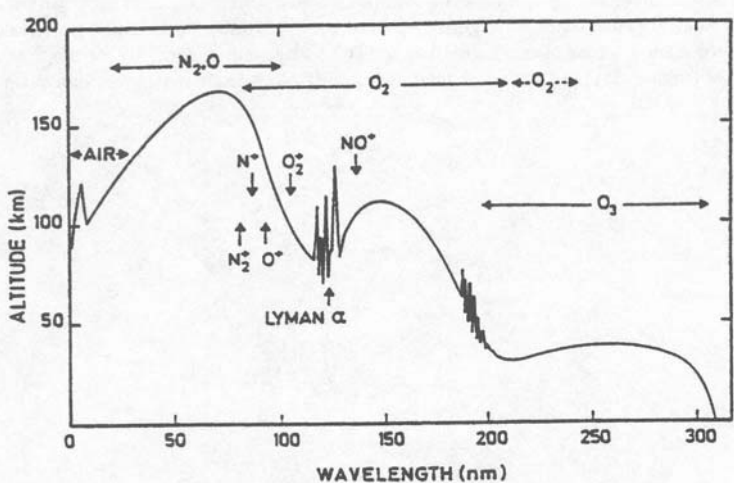
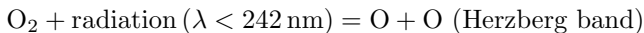
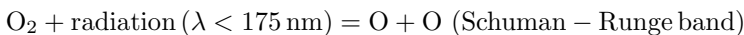
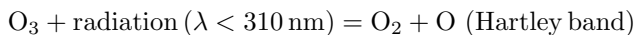


Figure 4.5: Depth of penetration of solar radiation as a function of wavelength. Altitudes correspond to an attenuation of $1/e$. The principal absorbers and ionization limits are indicated: Schumann–Runge continuum and bands of O_2 and Hartley band of ozone.



The bottom of Figure 4.6 shows the flux of different wavelengths reaching three different altitudes: the top of the atmosphere, 30 km, and the surface. The amount of very energetic UV ($< 242 \text{ nm}$) radiation falls off sharply. A molecule of ozone is much more efficient at absorbing light than a molecule of oxygen. However, there is much more oxygen than ozone (by a factor of about 10^5).

At 30 km, from 200 to 225 nm, about as much radiation is absorbed by oxygen as by ozone. However, at the surface, the UV radiation has been completely absorbed, and mostly by ozone as the radiation passes through the ozone layer.

4.2 Airglow

The thermal emission of the Earth takes place in the infrared range. However, observed from the space our planet also glows as a result of other mechanisms described in the previous section. Together with high energy particles, solar UV radiation is one of the most important agents for the excitation of the atomic and molecular energy levels, giving rise to the subsequent emission of light in several spectral lines.

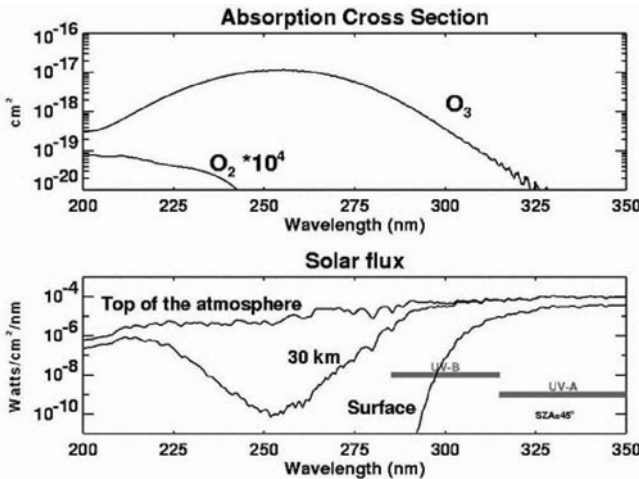


Figure 4.6: Efficiencies of molecular oxygen and ozone in absorbing photons. (Top): Absorption cross-section for ozone and oxygen. (Bottom): UV spectral irradiance at different altitudes in the terrestrial atmosphere. Note that the O_2 curve has been multiplied by 10^4 to put it on the scale of the graph. From the “Ozone Electronic Book” funded, developed, written and edited by members of NASA’s Goddard Space Flight Center, Atmospheric Chemistry and Dynamics Branch. (http://www.ccpo.odu.edu/SEES/ozone/oz_class.htm).

The most spectacular manifestation of these processes are the aurorae, which originate during periods of enhanced solar activity. Outside these transitory events a glow of light is also observed encircling our planet.

Anders Angstrom (1814–1874) discovered green airglow light in 1868. At Groningen in 1909 L. Yntema presented his PhD thesis “On the brightness of the sky and the total amount of starlight”, where he drew attention the long time variability of the phenomenon and showed that starlight scattered by atmospheric molecules was insufficient to explain the night-sky glow. Robert John Strutt (1875–1947), son of the third Lord Rayleigh, showed in 1922 that the geographical distribution of the strength of this line differed from that of aurorae. He gave the name of the units normally studied for these type of studies, the rayleighs⁵.

McLennan & Shrum (1925) identified the green line as due to atomic oxygen. It was in 1931 when S. Chapman suggested that airglow should result from chemical recombination. Chamberlain (1955) identified the UV airglow lines (340–380 nm) as due to oxygen Herzberg bands.

The interpretation of the airglow measurements requires: a) excitation fluxes (EUV/UV; particles) b) mechanisms of interaction of the radiation with the at-

⁵The Rayleigh is the unit commonly used to quantify the intensity of night-sky emission lines. It is defined as $1 R = 1.583 \times 10^{-5} / (\lambda)$ erg s⁻¹ cm⁻² sr⁻¹, where λ is expressed in Å.

mospheric components, and c) radiative transfer.

Chamberlain (1961, 1995); Mc Cormack (1971); Roach & Gordon (1973); Brasseur & Solomon 1994 and Slanger & Wolven (2002) provide the necessary background on this subject.

Depending of the time of the observation, we can distinguish different components in the airglow, that we will describe in the following subsection. The main source is solar radiation, the immediate emission is called *dayglow* and the subsequent delayed emission *nightglow*.

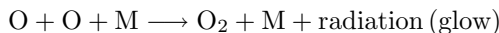
4.2.1 Nightglow

Observing the night side of our planet from space, we can distinguish several sources of UV light. Man-made sources consist of city lights and lights from ships and aircrafts and are easily identified. Transient sources are mainly aurorae, at high latitudes, and lightning. Here, we are interested in the “constant” glow produced as a consequence of the interaction between the radiation and the atmospheric components.

The term “geocorona” refers to the solar far-ultraviolet light (the Lyman α line) that is scattered off the cloud of neutral hydrogen atoms that surrounds the Earth (see figure 4.7) and by neutral interstellar hydrogen entering the heliosphere. Solar far-ultraviolet photons scattered by exospheric hydrogen have been observed out to a distance of approximately 100 000 km (~ 15.5 Earth radii) from Earth.

The present rate of escape of hydrogen atoms equals a layer of 1 millimeter depth every million years due to the evaporation of water from the oceans and the corresponding dissociation of water vapour molecules by UV radiation. This rate will grow in the future due to the increase in terrestrial temperatures following the increase of solar luminosity (see previous chapter). However, most of the glow spectrum is produced by the principal components of the atmosphere (nitrogen and oxygen).

Nightglow is produced by chemoluminescence, the emission of radiation resulting from chemical reactions mainly between oxygen and nitrogen atoms and molecules and hydroxyl molecules at a height of between 100 and 300 km. In the UV spectral region the major contribution is from the O₂ Herzberg I band with weaker contributions from the Herzberg II and Chamberlain bands (Chamberlain 1955):



where M is usually nitrogen.

Figure 4.8 shows a global view of UV nightglow. The NUV is brighter than the MUV, but fainter than the FUV. Rocket measurements by Greer *et al.* (1986) confirmed that the bulk of the UV nightglow comes from a region between 90 and 110 km.

Koomen *et al.* (1956) and Heppner & Meredith (1958) first measured altitude profiles of oxygen and sodium emission in Earth night airglow using data from sounding rockets. Bedinger *et al.* (1957) used sodium released by a rocket to quantify twilight and night airglow emission and measured mesospheric winds.

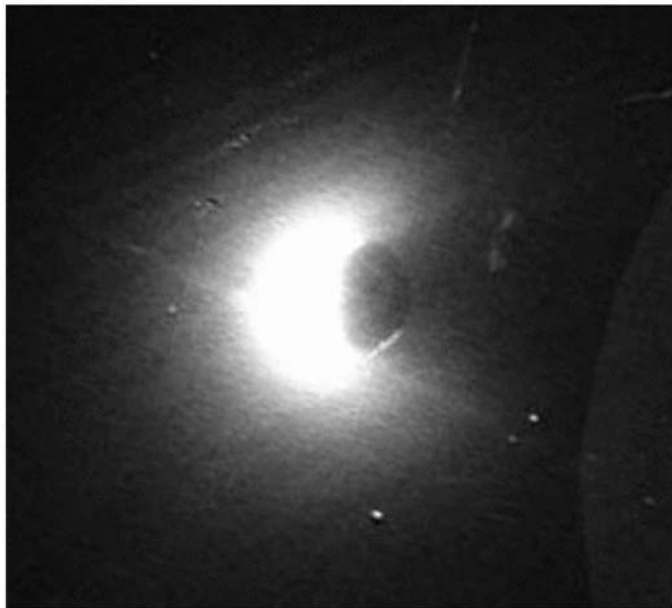


Figure 4.7: The Earth’s geocorona as viewed from the surface of Moon. Image acquired during the Apollo 16 mission (April 1972) with the Naval Research Laboratory’s far-ultraviolet camera/spectrograph. The Sun is to the left and the Earth’s North Pole is towards the upper left. Source: Carruthers *et al.* (1976) Journal of Geophysical Research 81, 1664-1672.

López-Moreno *et al.* (1998), by observing the EUV night airglow, were able to identify the complete Lyman series up to Lyman ϵ .

Inversion techniques are being applied to UV airglow observations with the ARGOS (Advanced Research and Global Observation Satellite) spacecraft to derive neutral density profiles. Table 4.2 gives the typical brightness of the most important UV spectral lines.

An instrument called NIGHTGLOW has been built to monitor the nightglow in the near ultraviolet. It has been designed to be flown from a high-altitude balloon (Barbier *et al.* 2005).

4.2.2 Dayglow

Dayglow is produced when the atmosphere is illuminated by the Sun. The responsible processes are resonance and fluorescence . Although it is intrinsically bright dayglow is overwhelmed by direct and scattered sunlight. The UV spectrum is dominated by single ionized and neutral lines of oxygen and nitrogen, produced by UV photons and photoelectron impacts. Some lines are also present in the solar spectrum (He I 58.4 nm; O II triplet 83.4; Lyman α and β).

Various space experiments have measured the dayglow in the FUV range

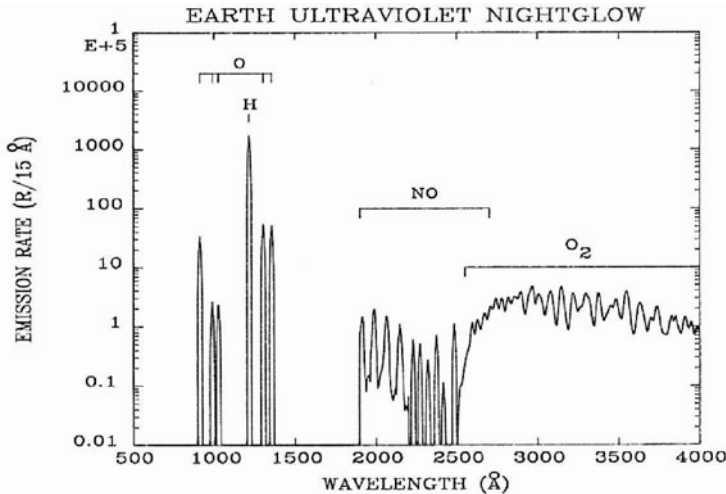


Figure 4.8: The different UV regimes of UV nightglow. (source: R.R. Meier Space Science Reviews 58, 19, available from <http://nightglow.gsfc.nasa.gov>).

Table 4.2: UV Nightglow Spectral Lines. R stands for Rayleigh.

Source	Wavelength (nm)	Height of emitting layer	Intensity
Lyman β	102.6	geocorona	10 R
Ly α	121.6	geocorona	3 kR (night)–34 kR (day)
O I	130.4	250–300 km	40 R (tropical airglow)
O I	135.6	250–300 km	30 R (tropical airglow)
O ₂	300–400	90 km	0.8 R/ Å

(Chakrabarti *et al.* 1983; Link *et al.* 1988 and Feldman *et al.* 2001). Craven *et al.* (1994), Meier *et al.* (2002) and Strickland *et al.* (2004) have respectively studied the dayglow response to an intense period of auroral activity, to a large solar flare and to short-term solar EUV variations.

4.2.3 Twilightglow

A phenomenon known as twilightglow may be observed at the transition between the dark and fully illuminated atmosphere as the shadow height moves vertically over the full range of emissive layers. Like airglow, it results from direct excitation by solar UV photons. Most of ultraviolet astronomical observations are taken from above the atmosphere by rockets or satellites. The viewing line of the spacecraft on the night side of the atmosphere may cross the terminator and continue through the sunlit parts of the atmosphere. Under these twilight conditions, dayglow features

become important.

The EURD experiment on board Minisat (Giménez & Sabau-Graziatti 1996) has obtained high resolution spectra corresponding to nightglow and twilight conditions (see López-Moreno *et al.* (1998) and Figure 4.9).

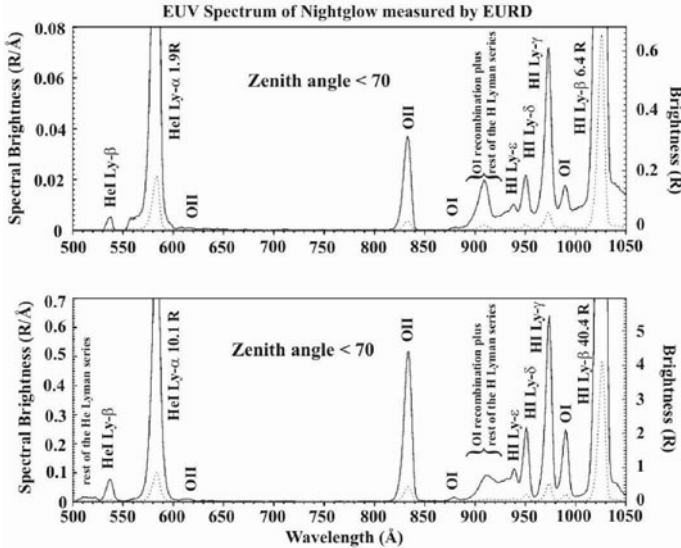


Figure 4.9: Airglow spectrum in the Extreme Ultraviolet, taken by the EURD observing in the antisolar direction at two zenithal distances. Note the difference of scales. Dotted line: emission divided by 10. Courtesy of J.J. López Moreno (IAA, Granada).

4.3 Diffuse UV background

All the mentioned sources contribute to the sky brightness over which we should measure the brightness of astrophysical point targets, becoming a main limitation for the detection of faint sources (see Paresce & Jakobsen 1980; O'Connell 1987; Bowyer 1991 ; Henry 1991).

Moreover we should also consider (Leinert *et al.* 1998): a) Zodiacal light, both as scattered sunlight and thermal emission of interplanetary particles, b) Integrated starlight not individually accounted for c) Diffuse galactic light and d) Extragalactic background light.

Zodiacal light is a faint cone-shaped glow in the night sky stretching along the ecliptic ⁶. It is caused by sunlight scattered by interplanetary dust particles in the plane of the ecliptic. The λ dependence of the zodiacal light follows the solar

⁶Given a dark sky and the absence of moonlight, it is visible at all times from the tropics.

Table 4.3: UV observations of Zodiacal Light. “P” stands for photometry and “S” for spectroscopy.

Platform	λ range (nm)	Reference
Rocket	120-320 S	Feldman (1977)
Balloon	P (215,295)	Frey <i>et al.</i> (1977)
Rocket	P(180,220,260)	Pitz <i>et al.</i> (1979)
Satellite	P(169,220,310)	Maucherat <i>et al.</i> (1979)
Rocket	170–315 S	Cebula & Feldman (1982)
Space Shuttle	165–310	Murthy <i>et al.</i> (1990)

spectrum from 0.2 to 2.0 μm . Some of the UV observations⁷ are summarized in the Table 4.3.

In the UV range it is possible to carry out deep surveys at reduced levels of sky background. At 200 nm we have a sky background that is four magnitudes darker than at any visible wavelength from the ground (see Figure 4.10, where the background at UV and optical wavelengths are compared).

Aurorae produce extremely bright UV emission, but it is confined to polar regions. However, this light will be scattered off the atmosphere and could contribute to a general increase in the background level. Lightning is a source of UV light and its contribution is much larger over the tropical regions. Night observations at 121.6 nm (Lyman- α) are also severely impeded by different sources in the Solar System.

Recently, Brown *et al.* (2000) have measured the diffuse background in the FUV (145 - 190 nm) by using the Hubble Space Telescope.

Some of the UV contamination can be reduced going to remote regions of the Solar System, as was done with the Voyager far-UV spectrometers (Sandel *et al.* 1979).

As expected, the long-term variations of the sky brightness are correlated with the solar activity cycle (Mattila *et al.* 1996).

Table 4.4 lists the various components contributing to the UV night brightness (Cox 2000).

4.4 The Ionosphere

The troposphere and stratosphere are electrically neutral. However, in the upper atmospheric layers (approximately from 70 to 1000 km) the neutral components coexist with ionized particles produced by the Sun and cosmic rays. This layer, called the ionosphere, contains only a small fraction of the Earth’s atmosphere (less than 1% of the mass above 100 km).

⁷In the UV, the maps of zodiacal light brightness are less complete than in the visible, and calibration is more difficult. At $\lambda < 200$ nm the brightness levels are very low.

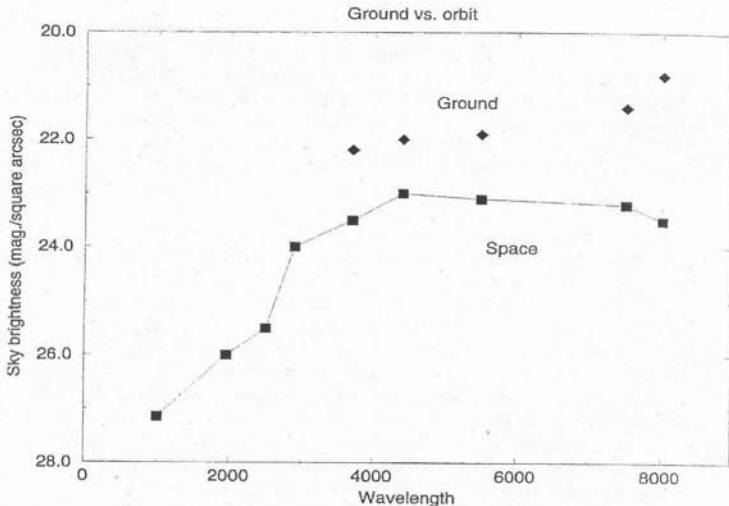


Figure 4.10: UV and optical sky background for space and ground observatories. Adapted from Figure 10 of Brosch (1999) Experimental Astronomy 9, 119-187.

4.4.1 Historical development

The first ideas about an electric conducting layer in the terrestrial atmosphere were advanced by C. F. Gauss (1777–1855), in 1839, who proposed that small daily variations in the geomagnetic field could be explained by electric currents flowing in such a layer. Belfour Stewart (1828–1887) pictured such currents, around 1886 , as arising from electromotive forces generated by periodic motions of the electric layer across the terrestrial magnetic field.

In 1901 G. Marconi (1874–1937) was able to establish a transatlantic radio-communication ⁸. In 1902, Oliver Heaviside (1850–1925) and Arthur E. Kennelly (1861–1939), independently, explained this in terms of a reflection of the radiowaves by free charges in the high atmosphere. J. A. Fleming ⁹ proposed that solar UV radiation generates such free charges.

The first observational evidence of a new layer in the atmosphere, the ionosphere ¹⁰, came from Edward Appleton(1892–1965) and M. A. F. Barnett in 1925. Later, this finding was later verified by Gregory Breit (1899–1981) and Merle Anthony Tuve (1901–1982) by using pulsed radio waves (Breit & Tuve 1926)¹¹.

On 29 June 1927, an eclipse provided an opportunity to study the effect of the

⁸On 12 December 1901, he transmitted a Morse code signal from Cornwall (England) to Newfoundland (Canada), a distance of 2900 km, a big surprise for the scientists that could not explain how the waves propagating as straight lines could curve over the 160 km of the bulge of the Earth.

⁹Fleming, J.A. 1906, On the electric radiation from bent antennae, Proceedings Physical Society London, 20, 409–426.

¹⁰This term was first used in 1926, by Robert Watson-Watt (1892–1973), the father of radar.

¹¹See “Physik des Erdnahen Weltraums”, G. W. Prölss, Springer Verlag (2004).

Table 4.4: Components of the night sky brightness. m is the magnitude and the “nit” is the power per area per solid angle expressed in $\text{W}/\text{m}^2\text{-sr}$.

Source		Photographic 10th mag stars	Visual deg^{-2}	Photometry 10^{-5} nit
Airglow (near zenith)				
Atomic lines		40	3	
Bands and continuum	30	50	4	
Zodiacal light (away from zodiac)	60	100	6	
Faint stars, $m > 6$ (galactic pole)	16	30	2	
(mean sky)	48	95	7	
(gal. equator)	140	320	23	
Diffuse galactic light	10	20	1	
Total brightness (zenith, mean sky)	145	290	21	
(15° latitude, mean sky)	190	380	28	

Sun on the ionosphere. Appleton verified that as soon as the rays of light were cut off, the height of the reflecting layer increased.

Independently, Appleton and Tuve developed the ionosonde, an instrument that measures the time radio signals take to travel up to the ionosphere and back again, thus allowing a determination of the height of reflection. The frequency of the broadcast radio signal is generally increased from 1 up to 30 MHz. Each frequency resonates with a different altitude of the ionosphere depending on the density of electrons at that height. The higher the layer, the longer the radio signal takes to return to the radio receiver. Finally, a plot of the travel time of the radio signal versus resonant frequency, an ionogram, is produced to determine the vertical electron density profile at the location of the ionosonde. Nowadays, sounding rockets release chemical products that emit visible light, which allows winds in the ionosphere to be tracked by ground-based cameras.

In 1928, E. O. Hulbert proposed that the ultraviolet radiation shortwards of 123 nm might be the source of the ionosphere . Soundings with V-1 and V-2 rockets, after the World War II, showed that these radiations shaped the bottom of the ionosphere.

The components of the atmosphere may be ionized by capturing photons whose energy exceeds the corresponding ionization potential (see Table 4.5). Thus, only radiation with $\lambda < \lambda_{\max}$ produces ionization; we therefore concentrate only on the X-ray and EUV regions of the spectrum.

At the highest levels of the Earth’s outer atmosphere, the density is low and therefore the ionization is also low. As the altitude decreases, more gas atoms are present so the ionization process increases. At the same time, however, an opposing process called recombination begins to take place in which a free electron is “captured” by a positive ion if it moves close enough to it. As the gas density increases at lower altitudes, the recombination process accelerates since the gas

Table 4.5: Ionization potential of components of the terrestrial atmosphere. From Hargreaves (1979) *The upper atmosphere and solar-terrestrial relations*, Van Nostrand Reinhold.

	I (ev)	λ_{\max} (nm)		I (ev)	λ_{\max}
NO	9.25	134	CO ₂	13.79	89.9
O ₂	12.08	102.7	N	14.54	85.3
H ₂ O	12.60	98.5	H ₂	15.41	80.4
O ₃	12.80	97.0	N ₂	15.58	79.6
H	13.59	91.2	Ne	21.56	57.5
O	13.61	91.1	He	24.58	50.4

molecules and ions are closer together. The point of balance between these two processes determines the degree of “ionization” present at any given time and location.

Apart from high energy radiation, cosmic rays and solar particles also play an important role in these processes. A number of monographs give deeper insight into the subject (Rishbeth & Garriot (1969); Bauer (1973); Kelley (1989); Hargreaves 1979 and Hunsucker & Hargreaves (2002)).

4.4.2 General Structure

In equilibrium, the process of ionization is balanced by the reversed of recombination (see Table 4.6 for a summary).

Table 4.6: Ionization and recombination processes: X^{+m} denotes the element X stripped of m electrons. Adapted from Harrison (2005).

IONIZATION	
Collisional	$X^{+m} + e^- \longrightarrow X^{+m+1} + e^- + e^-$
Autoionization	$(X^{+m})^{**} \longrightarrow X^{+m+1} + e^-$
Charge transfer	$X^{+m} + X^{+m+1} \longrightarrow X^{+m+1} + X^{+m}$
Photoionization	$X^{+m} + \text{radiation} \longrightarrow X^{+m+1} + e^-$
RECOMBINATION	
Radiative	$X^{+m+1} + e^- \longrightarrow X^{+m} + \text{radiation}$
Dielectronic	$X^{+m+1} + e^- \longrightarrow (X^{+m})^{**} + \text{radiation}$
Charge transfer	As above

The rate of change of electron density, N_e , is given by the continuity equation (see Hargreaves 1979):

$$\frac{\partial N_e}{\partial t} = q - L - \text{div}(N_e V)$$

where q is the rate of production, L the recombination rate and $\text{div}(N_e V)$ the loss of electrons by movements with speed V .

The rate of produced ions, q , can be expressed by

$$q = n F \sigma \eta$$

where n is the number density of particles, F is the flux of the ionizing radiation ($\text{J m}^{-2} \text{ s}^{-1}$), σ is the absorption cross section and η is the ionization efficiency (the number of electrons produced per absorbed photon). As F increases and n decreases with the altitude in the atmosphere, we expect there to be at a particular height a maximum q and hence a maximum in the electronic density.

Assuming a plane stratified atmosphere and monochromatic radiation, we can derive the altitude variation of this production rate:

$$q(z, \chi) = q_0 \exp \left(1 + \frac{h - z}{H} - \frac{1}{\cos \chi} e^{(h-z)} \right)$$

where z is the vertical altitude, h the height of maximum ionization, H the scale height¹² and χ the angle between the line of sight and the vertical. Figure 4.11 shows the distribution of the ionization normalized to the maximum density.

There are two main ways of producing loss of electrons. Occasionally, the electrons recombine directly with positive ions¹³ following the relation $L = \alpha N_e^2$ where α is the recombination coefficient. Another option is that electrons are removed by becoming attached to neutral molecules, $Z (e^- + Z \rightarrow Z^-)$, a process expressed by $L = \beta N_e$, β being an altitude dependent attachment coefficient.

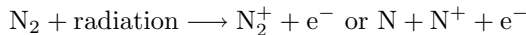
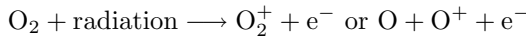
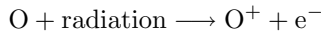
Figure 4.11 gives the variation with the altitude of the ion production rate from various sources (Richmond 1987).

The total electron content of the ionosphere is

$$N_T \equiv \int_0^\alpha N_e dz$$

where z is the altitude. Typically, N_T is about 10^{17} m^{-2} .

The major ionization sources are:



with the inverse process, recombination, returning the original constituents; for example: $\text{O}_2^+ + \text{e}^- \rightarrow 2\text{O}$.

The combination of the amount of incident radiation and the density of the atmospheric particles configures the extension of this layer (Figure 4.12), which is subdivided into different regions, also called Chapman layers.

¹²A e-folding distance, commonly used to describe the fall off in atmospheric pressure or other related quantities.

¹³We have two options: radiative recombination ($e^- + X^+ \rightarrow X + \text{radiation}$) and dissociative recombination ($e^- + XY^+ \rightarrow X + Y$).

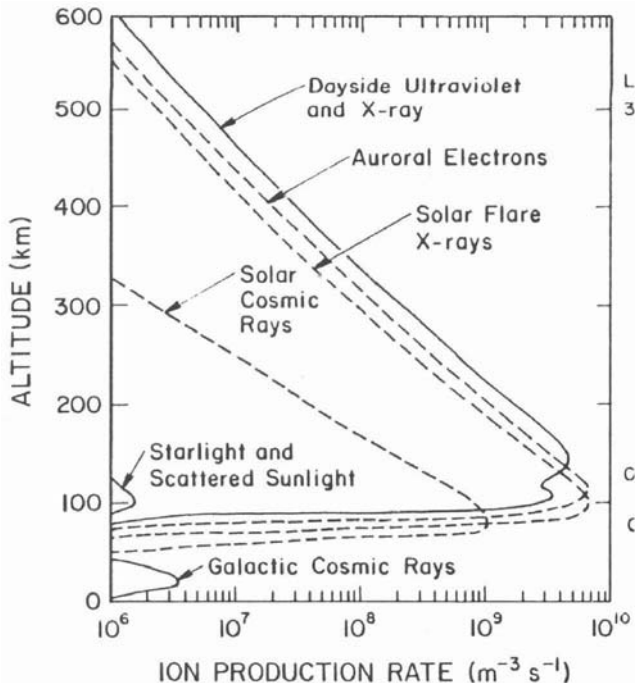
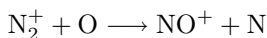
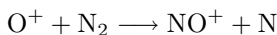


Figure 4.11: Various sources of ionization in the upper atmosphere. The solid lines show regular sources. During the day, EUV light is the main ionization source. At night, EUV scattered from the geocorona as well as from stars, helps to maintain the E ionosphere.

- D layer: The lowest, at altitudes between 50 and 80 km. It disappears during night, when solar radiation is blocked by the Earth. The main sources of ionization are Lyman- α (121.5 nm) on NO; EUV (102–111 nm) on oxygen and hard X-rays and cosmic rays on all atmospheric constituents.
- E layer: Found between 100 and 125 km. Also practically disappears at night. Ions in this region are mainly O_2^+ and NO^+ , produced through the following reactions:



- F layer: The ionization production is smaller than in lower layers, but the much longer electron lifetime permits large values of electron density to be reached. Its strength varies according the time of the day, the season and

the level of solar activity. During daytime it is split into two sub-layers, with the F1 placed around 180 km, where NO^+ and O_2^+ ions dominates, and the F2 at 400 km or more, with O^+ as the main contributor.

At low latitudes the largest N_e values are found in peaks on either side of the magnetic equator, called the equatorial anomaly. One would expect the largest concentration to occur at the equator because of the maximum of the solar ionizing radiation. This peculiarity can be explained by the special geometry of the magnetic field and the presence of electric currents.

The International Reference Ionosphere (IRI) is an empirical reference model of the physical parameters of this layer. It is updated biannually and distributed by the National Space Science Data Center and World Data Center A for Rockets and Satellites. Figure 4.12 illustrates the change of N_e between day and night and two phases of solar activity.

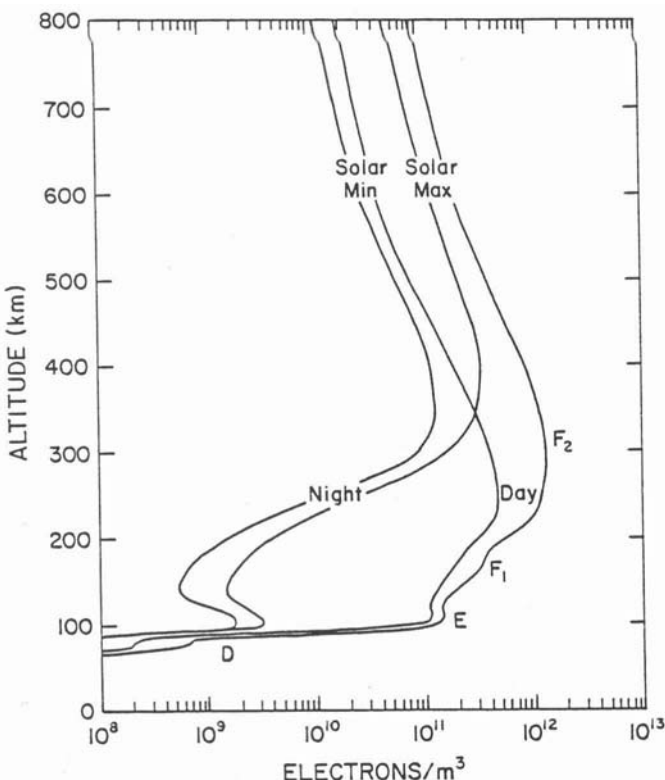


Figure 4.12: Variation in the electronic density with the altitude during day and night for two different phases of solar activity.

4.4.3 Effects on Communications

High-Frequency communication depends on radiowaves reflected from the ionosphere enabling communications from one part of the globe to another, as well as from spacecrafts to the ground and between spacecrafts.

H. A. Lorentz (1853–1928) investigated the propagation of a radiowave in a plasma with refractive index n . When n^2 is less than unity, the incoming waves are bent away from the normal to the layer and radiowaves are consequently reflected. This behaviour is expressed as the Appleton–Hartree formula, obtained after observations made during the solar eclipse of 29 June 1927:

$$n^2 = 1 - \left(\frac{\omega_p}{\omega} \right)^2$$

with the plasma frequency, ω_p , given by

$$\omega_p = \sqrt{\frac{N_e e^2}{m_e \epsilon_0}} \quad (4.2)$$

where N_e and m_e are the electron density and mass, respectively, e the electron charge, ϵ_0 the dielectric constant of free space, and ω the angular frequency of the transmitted signal.

As the wave penetrates into the ionosphere, the refractive index becomes smaller. If $\omega_p > \omega$, the wave cannot propagate because the refractive index is imaginary. The energy carried by the radiowave is therefore reflected back to the ground.

The limiting frequency, ω_0 , above which a radiowave is no longer reflected by an ionized layer depends on the square root of the electronic density, N_e . This parameter can therefore be routinely measured by ionosondes, in which a transmitter and a receiver are slowly swept in frequency.

The radio transmission is characterized by the Maximum Usable Frequency (MUF) and the Lowest Usable Frequency (LUF). MUF values change progressively in the D- (16 MHz), E- (28 MHz) and F- layers (16 MHz).

Neither the MUF nor the LUF is a practical operating frequency. While radio waves at the LUF can be refracted back to Earth at the desired location, the signal-to-noise ratio is still much lower than at the higher frequencies, and the probability of multipath propagation is much greater. Operating at or near the MUF can result in frequent signal fading and dropouts when ionospheric variations alter the length of the transmission path. The Optimum Usable Frequency (OUF) is roughly about 85 percent of the MUF, but the actual percentage varies and may be either considerably more or less than this value.

The MUF depends on the maximum of N_e in the F region and the angle of incidence of the emitted radiowave. The LUF is controlled by the amount of absorption of the radiowave in the lower D and E layers.

The maximum distance over the Earth's surface that can be reached by a single ionosphere reflection ¹⁴ is

¹⁴This distance is not sufficient for transatlantic communications, for which at least two reflections are required

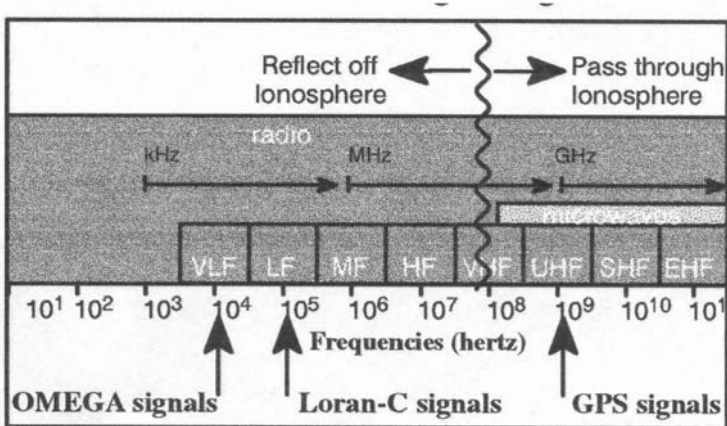


Figure 4.13: Working range of various communication systems.

$$2R \arccos\left(\frac{R}{R + h_i}\right)$$

where R is terrestrial radius and h_i the altitude of the different ionospheric layers involved in the transmission.

Variations in the total electronic density of the ionosphere are of great importance for the precision of satellite-based positioning systems as the Global Positioning System (GPS), Very Long Baseline Interferometry (VLBI) and Satellite Laser Ranging (SLR), as illustrated in Figure 4.13. In the near future these will be followed by the European system Galileo.

4.4.4 Variations with Solar Activity

The ionosphere shows transient perturbations that have been attributed to solar activity in the form of variable emission of particles. We can reasonably expect the variable effects of solar activity reflected in the EUV radiation (see the previous chapters) to cause variable levels of electronic density, with their concomitant effects on the properties of the ionosphere. In 1935 J. H. Dillinger (1886–1962) summarized observations of ionospheric disturbances over a period of six months stressing the connection between radio fadeouts and the solar activity. Kiepenheuer (1946) was one of the first to study the relation of the solar UV flux and the ionosphere.

Davis *et al.* (2001) have used the ionospheric response to EUV changes during solar eclipses to derive a long-term increase of this radiation since 1932. The electronic density increases by factors of five from low to high levels of solar activity. Transient events, such as solar flares, produce sudden ionospheric disturbances (SIDs).

The following empirical laws expressed the relation of the limiting ionospheric frequencies with the sunspot number, R (see Hargreaves, 1979, pp. 98–100).

$$\omega_0(E) = 3.3[(1 + 0.008R) \cos \chi]^{1/4} \text{ MHz}$$

$$\omega_0(F_1) = 4.25[(1 + 0.015R) \cos \chi]^{1/4} \text{ MHz}$$

$$\omega_0(F_2) \propto (1 + 0.02R)^{1/2} \text{ MHz}$$

where χ is the zenith distance and E, F1 and F2 are the layers of the ionosphere.

A total solar eclipse constitutes an opportunity to test the influence of reduced UV flux on the ionosphere, as done recently by Baran *et al.* (2003) and Farges *et al.* (2003).

4.5 Photochemical Processes

In contrast to the previous described photophysical processes of interaction between UV radiation and the components of the terrestrial atmosphere, photochemistry produces new chemical species. Molecules taking part in a photo-induced chemical reaction may break apart (photodissociate), rearrange, isomerize¹⁵, dimerize¹⁶, eliminate or add small molecules, or even transfer their energy to other molecules.

Photodissociation is the most important of the photochemical processes and consists in breaking a molecule into two or more (smaller) atomic or molecular components through the absorption of radiant energy. Only photons with wavelength in the visible and UV ranges are involved in this process. Below, the most important parameters are defined and briefly explained.

The dissociation rate, R_l , is the number of molecules n of the species l that are dissociated by radiation in an unit volume of air each second. It is expressed as

$$R_l = J_l n_l$$

where the photodissociation coefficient, J_l , depends on the wavelength of the solar radiation and the absorption properties of the molecule. It has the unit of inverse time (s^{-1}). If the coefficient is large ($\geq 10^{-6} s^{-1}$) the molecule is considered photochemically unstable.

The quantum yield, Φ , describes the number of molecules of reactant consumed per photon of light absorbed. Values range from 10^{-6} to more than 10^6 . If $\Phi > 1$ there are secondary reactions in the process.

The photolysis frequency, J , at a given point is given by

$$J = \int_{\lambda_1}^{\lambda_2} I(\lambda) \sigma(\lambda) \Phi(\lambda) d\lambda$$

¹⁵The changing a substance to another with different arrangement of atoms but with the same molecular weight (isomers).

¹⁶A polymer is transformed to two or more components (monomers).

where $I(\lambda)$ is the solar photon flux depending on the amount of ozone located above the point, the albedo of the surface and the solar zenith angle; $\sigma(\lambda)$ is the absorption cross spectrum and $\Phi(\lambda)$ the quantum yield¹⁷. We may therefore expect variations of J with altitude and season.

Emil Warburg (1846–1931) pioneered the application of photochemistry to biological studies, making the first experimental measurements of the quantum yield, Φ , by showing that for every photon absorbed by HBr, one molecule of H_2 and one molecule of Br_2 are formed. Wildt (1934, 1937) first discussed the role of photochemical processes in the structure of planetary atmospheres, dealing in particularly with the effects on methane, ammonia and carbon dioxide.

4.6 The Stratosphere and Ozone

In chapter 1 we described the discovery of ozone and its properties as an absorber of ultraviolet radiation. Its concentration characterizes the main properties of the stratosphere.

4.6.1 Pioneering Measurements and Observing Techniques

In 1921, F. A. Lindemann (later Lord Cherwell) suggested that it should be possible to obtain information about the vertical variation in temperature and density of the air from observations of meteor trails. The records were interpreted by G. Dobson (1889–1976) as evidence of a warmer and denser stratosphere produced by the absorption of UV radiation by ozone (see Lindemann & Dobson 1922). This was soon confirmed by Whipple (1932), studying the propagation of sound waves through the upper atmosphere, and marked the start of a growing knowledge of the physical structure of our atmosphere.

In 1926 Dobson designed an instrument to measure the atmospheric vertical column of ozone from the ground (see Dobson 1968). It was based on the previous design by Fabry and Buisson, but was cheaper and more suitable for working in the free air. The Dobson spectrophotometer measures ultraviolet light from the Sun in two to six different wavelengths from 305 to 345 nm. the amount of ozone can be calculated by measuring UV light at two different wavelengths. One of the wavelengths used is absorbed strongly by ozone (305 nm), whereas the other wavelength (325 nm) is not. The ratio between the two light intensities is therefore a measure of the amount of ozone in the light path from the sun to the spectrophotometer.

Beer's law is used to calculate the amount of light transmitted, T , through the ozone:

$$T = \frac{F}{F^\infty} = \exp[-n \sigma(\lambda)]$$

where n is ozone column density, F^∞ is the solar intensity above the ozone layer, F the solar flux reaching the ground and $\sigma(\lambda)$ the absorption cross-section at the wavelength λ .

¹⁷It is the fraction of photons absorbed that leads to the fragmentation of a molecule.

Dobson built seven identical spectrophotometers and installed them in Oxford (UK), Valentia (Eire), Lerwick (Scotland), Lindberg and Arosa (Switzerland). As of 1993, there were 71 Dobson stations worldwide. The instruments are routinely calibrated by operating side by side with a secondary instrument itself recalibrated against the International Standard Instrument located at Mauna Loa, Hawaii.

The LIDAR method relies on the absorption of laser light by ozone. A telescope is used to collect UV light scattered by two laser beams, one absorbed by ozone (308 nm), and the other (351 nm) not. (see for example Leblanc & McDermid 2000). Other methods use microwave radiometers (de la Noë 1998) and spectrographs.

Airborne measurements, have provided a direct measurement of ozone. Balloons can measure ozone concentrations to a height of 40 km and rockets increase this altitude limit to 75 km. However, both are limited by their short life and narrow geographic range.

The space age has enabled global records to be kept. The first observations started in 1970 on board Nimbus 4 operating in nadir geometry (Backscatter Ultraviolet); i.e. they measured solar light reflected from the ground or scattered from the atmosphere. However, the measurements suffered from instrumental instabilities. An important breakthrough took place in 1979 with the launch of TOMS (Total Ozone Mapping Spectrometer) on Nimbus 7. The main advantages were a better coverage of the UV range and better stability. The GOME (Global Ozone Monitoring Experiment) was launched on the European satellite ER-2, covering a large spectral range (240–790 nm) making it possible to retrieve a wide variety of atmospheric trace gases. The basic process of analysis consist of a simultaneous numerical fit of synthetic profiles of different trace gases to a measured atmospheric spectrum. On 15 July 2004, NASA launched the AURA satellite. The instruments on board will enable daily global observations of Earth's ozone layer.

For a homogeneous atmosphere the concentration of a gas in the atmosphere can be described by the number density, X, expressed in molecules per cm³. This parameter is a function of pressure, P, and temperature

$$X = 7.25 \times 10^{18} P/T$$

In order to avoid this dependence we can use the volume mixing ratio (VMR), which is the fraction of the molecules of the element X in a given volume¹⁸.

The ozone content is measured in Dobson units (Figure 4.14). The Dobson unit (DU) is defined to be a thickness of 0.01 mm at standard atmospheric pressure and temperature.

The column ozone ($\Delta\Omega$) between two pressure surfaces P_{low} and P_{high} can be derived by integrating O₃ volume mixing ratio (X) over pressure:

$$\Delta\Omega = A \int_{P_{\text{low}}}^{P_{\text{high}}} dp.X$$

¹⁸Because the VMR is typically small, it is multiplied by 10⁶ or 10⁹ to obtain parts per million in volume (p.p.m.v) or parts per billion in volume (p.p.b.v), respectively.

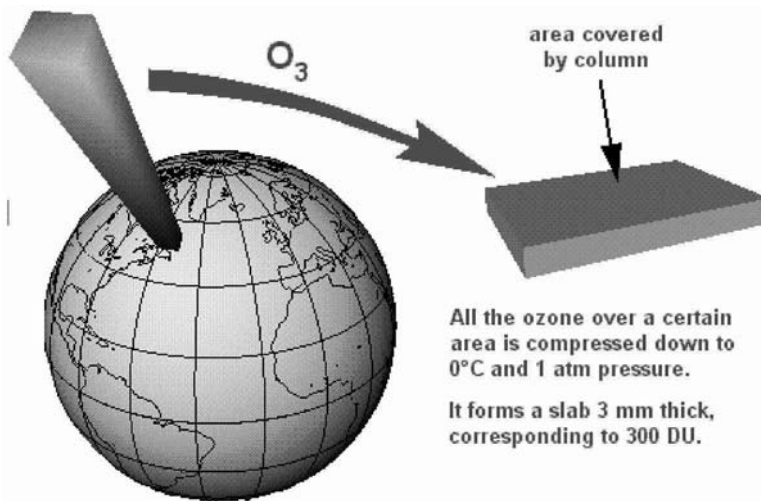


Figure 4.14: The Dobson unit. © “The Ozone Hole Tour”, Cambridge University.

where A is a constant ensuring DUs in the integration ($A = 0.79 \text{ hPa}^{-1} \text{ ppmv}^{-1}$, provided that the units for X and P are ppmv and hPa respectively). The average amount of ozone is 300 DU, which corresponds to 800×10^{16} molecules lying above each square centimetre of the Earth’s surface. The surface area of our planet is $\approx 5 \times 10^{18} \text{ cm}^2$. Therefore the total number of ozone molecules is 4×10^{37} . As the total number of air molecules is 1×10^{44} , the mixing ratio is $0.4 \times 10^{-6} = 0.4$ parts per million in volume (ppmv).

A measure of the sensitivity of photolytic processes to total column ozone is provided by the sensitivity factor S , which is defined as the percentage change, ΔJ , in a photodissociation rate, J , for a percentage change in total column ozone, Ω :

$$\frac{\Delta J}{J} = S \frac{\Delta \Omega}{\Omega}$$

The sensitivity factor, S , depends on the total column ozone, as well as on the altitude of the ozone perturbation and on the solar zenith angle. The photodissociation of ozone is most sensitive to changes in total column ozone: a 1% decrease in total column ozone resulting in a 1.4 to 2.3% increase in the photodissociation rate in the troposphere, depending on location, time, and spatial and temporal averaging.

The first Ozone Conference was organized in Paris in 1929 under the auspices of the Commission on Solar Radiation and following the initiative of Charles Fabry. S. Chapman presented evidence of the existence of large amounts of ozone at stratospheric heights. At the Lisbon assembly of the International Association for Meteorology (IAMAS) in 1933, the Committee on Ozone was established *in recognition to the importance of ozone research for better understanding of the*

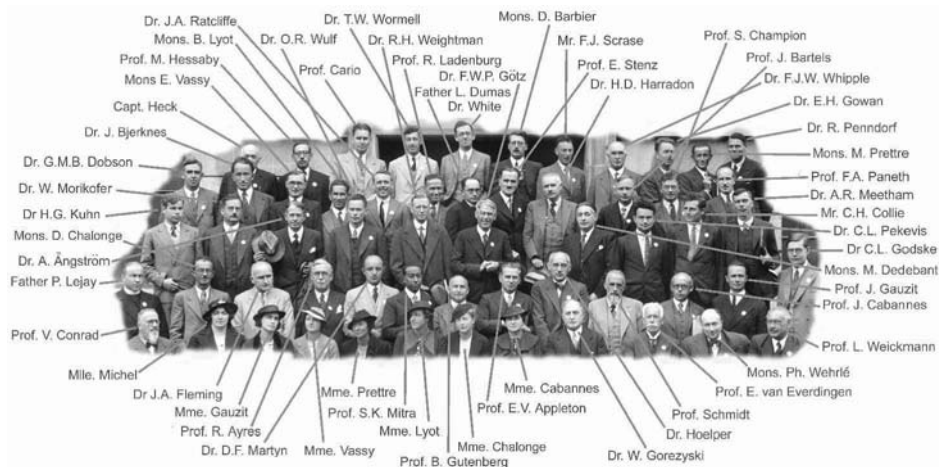


Figure 4.15: Participants of the II Ozone Conference in 1937. Courtesy: Clarendon Laboratory, Oxford University.

stratosphere. In 1937 Oxford University hosted the second Ozone Conference, where scientists from sixteen countries met (Figure 4.15).

The International Ozone Commission was set up in 1948 during a meeting of the IAMAS in Oslo, with Dobson as its first president. Ozone measurements were included among the tasks of the International Geophysical Year (IGY), which was planned for a maximum of solar activity. Analysis of these data was carried out in collaboration with the World Meteorological Organization (see Dobson, 1968). Further meetings took place in Brussels (1951), Oxford (1952), Rome (1954), Ravensburg (1956), Oxford (1959) and Arosa (1961), the most recent being in L'Aquila (1996) and Sapporo (2000).

4.6.2 Natural Processes of Ozone Formation and Destruction

Stratospheric ozone is created and destroyed primarily by ultraviolet radiation. When high energy photons strike molecules of oxygen (O_2), they split the molecule into two single oxygen atoms. The free oxygen atoms can then combine with oxygen molecules (O_2) to form ozone (O_3) molecules (Chapman 1930), as shown in Figure 4.16. The main equations have already been given at the end of Section 4.1, and Figure 4.6 shows the variation of the absorption coefficient with the wavelength for molecular oxygen and ozone.

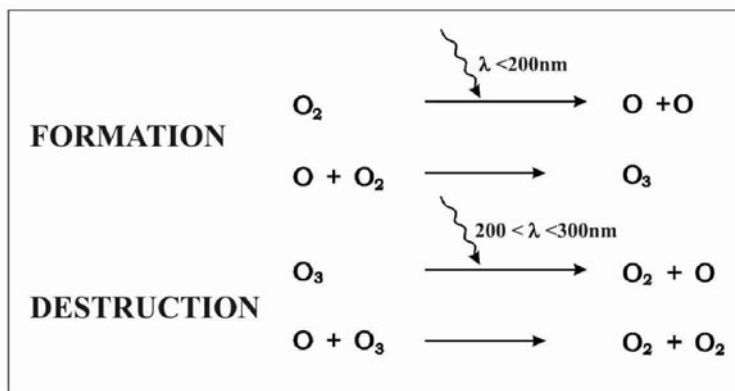


Figure 4.16: Formation and destruction of ozone, according to the Chapman cycle.

Ozone Formation

Ozone production is a photolysis process driven by UV radiation. It occurs in the tropical stratosphere at heights between 20 and 50 km:



Absorption in the Schumann–Runge continuum ($130 < \lambda < 175 \text{ nm}$) has a maximum cross-section of $1.5 \times 10^{-17} \text{ cm}^2$ at 142.5 nm and results in the production of two O atoms, one in the ground state and the other in the first excited state. Absorption in the weak Herzberg continuum ($195 \text{ nm} < \lambda < 200 \text{ nm}$) has a $\sigma_{\max} \simeq 10^{-23} \text{ cm}^2$ and produces two ground state atoms, giving rise to feeble absorption.

Subsequent recombination of the oxygen atoms may occur either directly,



or via the intermediate formation of ozone (the dominant process in the stratosphere),



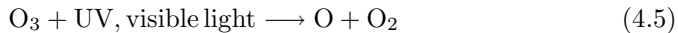
where M represents any other molecule (most probably N_2 or O_2) that absorbs the surplus energy but is not changed in the process.

The lifetime of oxygen atoms increases almost linearly with the altitude, being very brief in the stratosphere, typically less than 1 second. Hence, oxygen atoms almost immediately form ozone after they are dissociated.

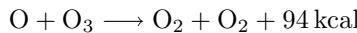
The absorption of UV radiation heats the stratosphere and is therefore largely responsible for the formation of the stratosphere and the mesosphere.

Ozone Destruction

The same characteristic of ozone that makes it so valuable, its ability to absorb a range of ultraviolet radiation, also causes its destruction. When an ozone molecule is exposed to ultraviolet or visible photons ($\lambda < 1200$ nm) it may break back into O_2 and O :



The free oxygen atom may then combine with an oxygen molecule to create another ozone molecule, or it may take an oxygen atom from an existing ozone molecule to create two ordinary oxygen molecules:



The Continuity Equation

The net amount of a substance, X , in the atmosphere is given by a continuity equation similar to that used for the ionosphere, but neglecting the transport term (e.g. Dessler 2000):

$$\frac{d[X]}{dt} = P - L[X]$$

where $[X]$ denotes the number density (molecules per volume), P is the photochemical production term (the amount of X produced per unit volume), usually assumed variable with time ($P = P_0[1 + \sin(\omega t)]$). Therefore, for a steady state solution we can assume

$$X(t) = P_0/L$$

Under these assumption we can apply these concepts to the ozone:

$$\frac{d[O_3]}{dt} = k_{O+O_2}[O_2][O][M] - J_{O_3}[O_3] - k_{O+O_3}[O][O_3] \quad (4.6)$$

$$\frac{d[O]}{dt} = -k_{O+O_2}[O][O_2][M] - k_{O+O_3}[O][O_3] + J_{O_3}[O_3] + 2J_{O_2}[O_2]$$

Now, assuming photochemical equilibrium in odd O , means $[O] + [O_3]$, we can add the two former equations getting

$$2k_{O+O_3}[O][O_3] + 2J_{O_2}[O_2] = 0 \longrightarrow$$

$$[O] = \frac{J_{O_2}}{k_{O+O_3}[O_3]} \quad (4.7)$$

Coming back to eq. 4.6 and considering that the term $k_{O+O_3}[O][O_3]$ is much smaller than the others

$$\frac{d[O_3]}{dt} = k_{O+O_2}[O_2][O] - J_{O_3}[O_3]$$

Assuming ozone photochemical equilibrium ($d [O_3]/dt = 0$) again,

$$[O_3] = k_{O+O_2}[O][O_2][M]/J_{O_3}$$

Now, substituting the value of $[O]$ obtained in expression 4.7

$$[O_3] = [O_2] \left([M] \frac{J_{O_2} k_{O+O_2}}{J_{O_3} k_{O+O_3}} \right)^{1/2}$$

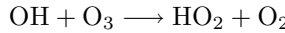
4.6.3 Catalytic Loss of Ozone

The Chapman cycle is inconsistent with observed levels of ozone in the stratosphere and produces too much ozone (Bates & Hays 1967; Kinnison *et al.* 1988). Ozone is a highly unstable molecule that readily donates its extra oxygen molecule to free radical species naturally occurring in the stratosphere. We clearly need other ozone loss reactions. We now consider some examples

Reactive Hydrogen Species

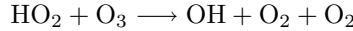
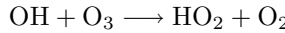
These are known as HO_x , which consist of the hydroxyl radical, OH, and the hydroperoxyl radical, HO_2 . They are produced mainly through reactions of water with oxygen atoms ($\text{H}_2\text{O} + \text{O} \longrightarrow 2\text{O}_2$).

In the upper and middle stratosphere we have



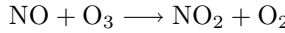
with the net effect ($\text{O}_3 + \text{O} \longrightarrow 2\text{O}_2$).

The lack of oxygen atoms in the lower stratosphere favours the following alternative cycle with the same net effect of ozone destruction



Nitrogen

This mechanism was first proposed by Crutzen (1970). The starting point is the nitrous oxide, N_2O , also known as the “laughing gas”, produced by biological processes. The relevant reactions are

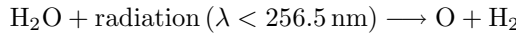
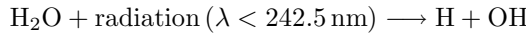


also with the net effect $\text{O}_3 + \text{O} \longrightarrow 2\text{O}_2$

4.6.4 Other photodissociation processes

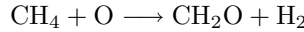
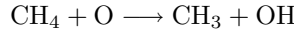
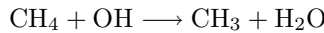
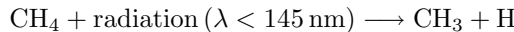
Solar ultraviolet also plays a role in the photolysis of other atmospheric components and we briefly include below the main reactions involved.

The photodissociation of water vapour appears when radiation of $\lambda > 175$ nm penetrates into the mesosphere:



However, the importance of this process in the upper layers is small because of the predominant role of the absorption by molecular oxygen. The same happens with the photodissociation of nitrogen, a very slow process, at least 10^6 times slower than the parallel process of molecular oxygen.

Methane is also dissociated by UV sunlight and by reactions with the hydroxyl radical (OH) and excited atomic oxygen:



Similar reactions configure the direct photolysis of substances such as NH_3 and H_2S .

4.7 Variability of Total Ozone Content

4.7.1 The Influence of Solar Variability on Ozone

The amount of UV radiation produced by the Sun is not constant but varies by several percent in a roughly 11-year cycle (see previous chapters). As the ozone content is controlled by UV radiation, we can expect a variation in its concentration during the cycle, as was first suggested by Moffat (1875).

Ground-based records indicate the existence of a variation in column ozone in phase with the solar activity cycle (Angell 1989 ; Zerefos *et al.* 1997), confirmed by satellite measurements (Hood & Mc Cormack 1992 ; Chandra & McPeters 1994) and numerical modeling (Fleming *et al.* 1995; Lee & Smith 2002). These correlations are weaker near the equator, where the ozone is produced, and in polar regions, towards which the ozone is transported.

Williams *et al.* (2001) have simulated the impact of the 27-day solar rotation period on stratospheric ozone and temperatures.

We have seen in previous chapters how solar activity dropped to very low levels during the Maunder Minimum (MM) in the seventeenth century. We may assume that this episode was also characterized by low solar UV emissions, resulting in a decrease in stratospheric ozone. Models (Lean & Rind, 1998) and climatic evidence (Fagan 2000) indicate an average tropospheric cooling of ~ 1 °C with respect to present values.

Wuebbles *et al.* (1998) simulated the MM ozone abundance, showing that a cooler atmosphere produces a decrease in total ozone column. We shall return to this topic later in the chapter.

4.7.2 Solar Eclipses

During solar eclipses the spectral composition of solar radiation undergoes changes caused either by solar factors or by changes in total ozone content. Mikhalev *et al.* (1999) observed an abrupt change in relative transparency in the ground ozone spectral region (310–330 nm) that could correspond to an increase in total ozone content, as verified also by Chakrabarty *et al.* 2001. Gil *et al.* (2000) studied the behaviour of NO₂ and O₃ concentrations.

The total solar eclipse of 11 August 1999 was followed by numerous teams, also with the purpose to measure UV and ozone changes (see Zerefos *et al.* 2000).

4.7.3 The Influence of Volcanoes

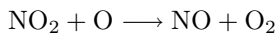
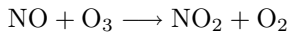
Gas emission from volcanoes usually contains SO₂, which combined with water vapour, quickly form H₂SO₄ molecules, that readily nucleate into sulfate aerosol particles. During volcanic explosions a significant amount of aerosols are injected into the atmosphere. Depending on the strength of the event and the latitude of the site, the aerosols can reach the stratosphere. Aerosols reflect solar light and therefore produce a cooling of the troposphere lasting for up to three years, the estimated residence time of the particles in these layers.

Table 4.7 lists the most important eruptions in the last two centuries.

Atmospheric aerosols can scatter and absorb the UV radiation. This combined with molecular scattering, affects ozone measurements from space.

Marshall (1928) was the first to speculate on the reduction of UV radiation caused by the atmospheric injection of volcanic dust. As a result, various illnesses could be produced by the weakening of biological species.

The mechanism for the depletion of ozone is triggered by the excitation of atmospheric nitrogen atoms, denoted by N*, followed by combination with the also abundant oxygen:



Measurements of ozone levels before and after the eruption of Mt. Pinatubo show that there were significant decreases in lower stratospheric ozone (Grant *et al.*

Table 4.7: Recent major volcanic eruptions

Year	Month	Location	References
1783		Laki (Iceland)	Stothers (1996) Thordarson <i>et al.</i> (2003)
1815	April	Tambora (Indonesia)	Chenoweth (2001) Stothers (1984)
1883	August	Krakatau	Self & Rampino(1981)
1902	May	Mt Pelee (Martinique)	
1902	October	Sta. Maria (Guatemala)	
1903	February	Colima (Mexico)	
1912	June	Katmai (Alaska)	Volz (1975)
1963	February	Agung (Indonesia)	Angell (1997)
1980	May	St. Helens (USA)	Evans & Kerr (1983)
1982	March	El Chichón (Mexico)	Krüger (1983)
1991	June	Pinatubo (Philippines)	Ramachandran <i>et al.</i> (2000)

1994), with consequent larger surface levels of UV–B radiation (Vogelmann *et al.* 1992), although no correlation was found between ozone depletion and increased mortality. The amount of ozone in the 16–28 km region was reduced by 33% compared to pre-eruption levels. However, already in 1994, the impacts of Mt. Pinatubo were negligible.

An important mechanism is the decreased photolysis of O₂ due to the absorption of solar UV by SO₂ contained in the volcanic plume. Volcanic eruptions also lead to anomalously strong and cold polar vortices that favour ozone depletion. The contrast with solar influences is detected only in the troposphere with reversed effects.

Volcanoes also emit a substantial amount of chlorine compounds. This mechanism will be discussed in the next chapter in the context of the ozone hole.

4.7.4 Photochemical Replacement Time

The short-time variation of tropospheric ozone is dominated by the passage of weather systems. When a high pressure region is generated the air moves downward in the opposite direction at the stratospheric level. Rising air has less ozone, because originates in the troposphere. The effect of a low pressure region is obviously the opposite. However, these changes are mainly a redistribution of ozone with no net gain or loss. To look for these global variations we need to investigate the average patterns.

The Photochemical Replacement Time (PRT) is the time it would take to generate the observed ozone concentration at a specific location at the existing production rate with no loss processes. The PRT is a convenient way to measure whether photochemistry or transport is the controlling factor in determining the ozone concentration at a particular location. In seconds it is expressed by

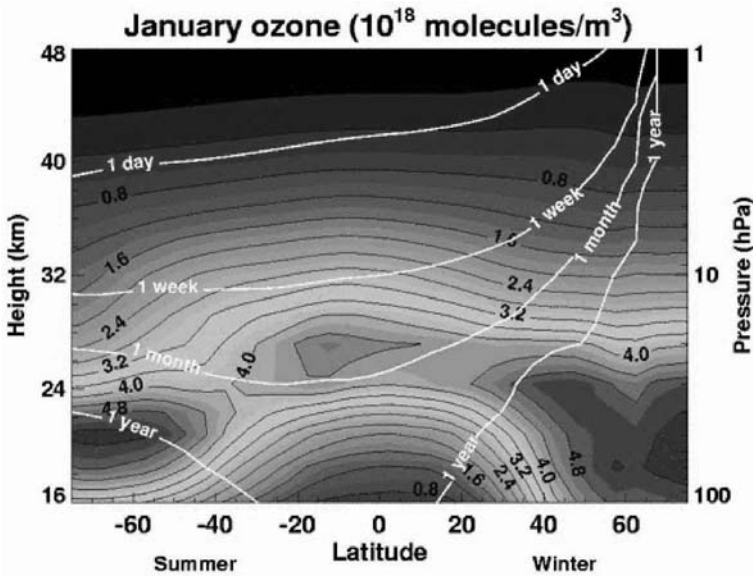


Figure 4.17: Variation of total ozone with the latitude and altitude. Superimposed are the contours of the calculated PRT for ozone. From “Ozone Electronic Book”.

$$\text{PRT} = \frac{n(\text{O}_3)}{P(\text{O}_3)}$$

where $n(\text{O}_3)$ is the density of ozone in molecules per cm^3 and $P(\text{O}_3)$ is the production rate in molecules per cm^3 per second.

Because of the higher insolation, we may expect a high concentration of ozone in the tropics. However, the observed values of total ozone at mid-latitudes are almost doubled (Figure 4.17). There are two main reasons for this remarkable discrepancy; first, the abovementioned catalytic processes of ozone loss and, second, the dynamical aspects of the terrestrial atmosphere. In the lower stratosphere values of PRT are high and the concentration of ozone is dominated by transport of air.

4.8 Dynamics of the Terrestrial Atmosphere

4.8.1 Troposphere

The main characteristics of the average circulation in the terrestrial troposphere are driven by rotation (and hence Coriolis forces) and pole-equator differences. Figure 4.18 gives a polar view of the main patterns observed.

Gravity inhibits upward flow in the atmosphere, but there is no obvious analogy in the horizontal direction. Air in the troposphere flows polewards in response to

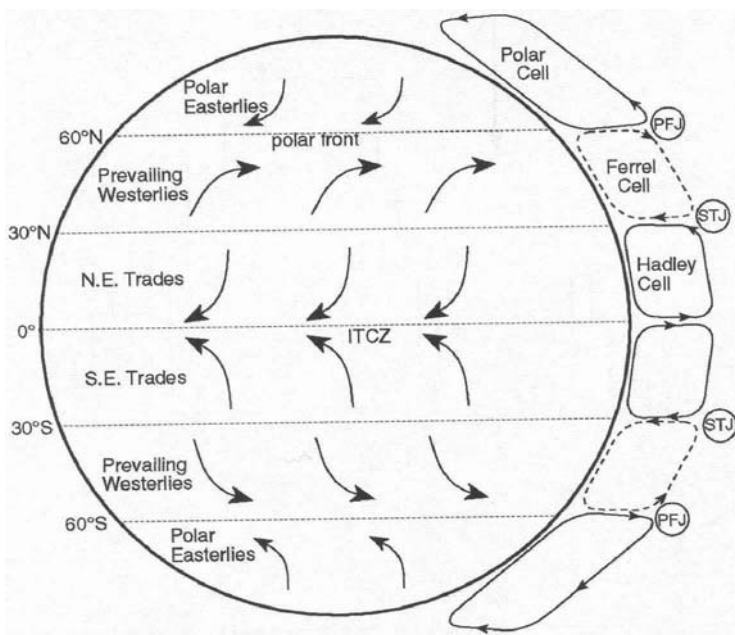


Figure 4.18: Global atmospheric patterns in the troposphere.

a horizontal gradient in pressure. However, the Coriolis forces¹⁹ prevent these horizontal pressure gradients from producing infinitely large flows. The resulting undulating flow is designated as geostrophic flow or geostrophic wind.

An example of this effect is the formation of jets. At 30°N the Earth's rotation halts the poleward flow of air and a large horizontal current develops: the sub-tropical jet. A second jet is generally found between 50 and 60° N in summer and 35–45° in winter (the mid-latitude jet-stream or polar front), which is essential for the formation in winter of a spinning vortex over the poles²⁰.

4.8.2 Planetary waves

The terrestrial atmosphere supports wave motions at many temporal and spatial scales, excited when air is disturbed far from equilibrium. They are only possible in presence of a positive restoring force. Carl Gustav Rossby (1898– 1957) was the first to investigate those where the restoring force is produced by the variation with latitude of the Coriolis force, which links them directly to the Earth's rotation. Planetary waves (hereafter PWs) are large-scale distortions of the mean flow with periods in the range 3–30 days. They are formed in the troposphere by oro-

¹⁹The Coriolis effect has a magnitude given by $f = 2 V \omega \sin \phi$, where V is the speed of the parcel of air, ϕ the latitude and ω is the angular speed of the Earth.

²⁰The horizontal area covered by the polar vortex is greater at the top than at the bottom.

graphic obstacles (the Tibetan plateau, the Rocky Mountains, etc.) and land-sea contrasts (see Volland 1988) and are clearly stronger in the northern hemisphere during winter²¹. The air masses are forced to ascend (by the changing surface level), then allowed to descend (under gravitational influence), and the resultant “squashing” and “stretching” respectively of the air columns lead to alterations in the rates of spin of air flow (vorticity). These variations must be balanced for a rotating earth. In the northern hemisphere the ascending air tends to turn to the left, and the descending one to the right, inducing a ridge/trough pattern in the westerlies.

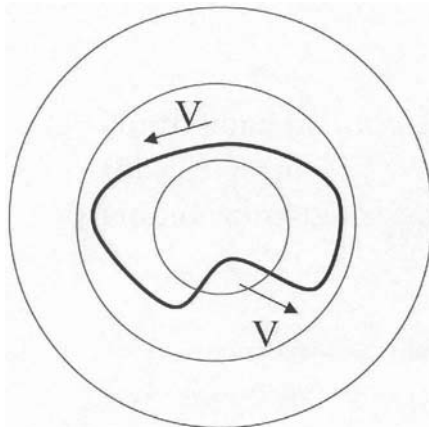


Figure 4.19: Simplified scheme of planetary waves. Looking down on the North Pole, the flow (thick line) meanders across latitudes circles.

Planetary waves have a vertical component and when propagating upward they grow in response to the decreasing background density. In the middle atmosphere the wave motions become large and unstable, and so the waves break down into turbulence, causing strong compressional warming. In winter conditions a temperature gradient is formed, generating a vortex through which the planetary waves cannot penetrate. The amount of PW drag within the stratosphere is related to the vertical component in the lower stratosphere and to the ozone concentrations, at least in the period 1979–2000 (Fusco & Salby 1999; Randel *et al.* 2002).

At any given time, there are between three and seven such waves in the stratosphere. Rossby derived the following expression for the speed of the horizontal motion, C:

$$C = U - \frac{2\omega \cos \phi}{4\pi R_E} L^2$$

²¹These waves are associated with the frontal systems in the troposphere that regularly bring bad weather to the west coast of Europe from the Atlantic. PW are evident in time-mean circulation maps, in which unsteady weather systems are filtered out.

where U is the mean zonal (west to east) wind aloft; ω the angular velocity of the Earth, ϕ the latitude, R_E the mean terrestrial radius and L the wavelength. For a particular latitude band, there is a combination of U and L giving $C = 0$ (stationary wave).

The stratospheric winds are westerly in winter and easterly in summer owing to pole-equator temperature and pressure differences. Stratospheric westerlies can be considered as a medium “transparent” to PWs, whereas with easterlies PWs they cannot propagate (Geller 1981).

Soukharev & Labitzke (2000) have found that the PW amplitudes are much larger at high than at low solar activity, an effect that is most pronounced in the latitude band 40–60 °N.

4.8.3 The Stratosphere

In the stratosphere, we have a slow circulation driving the ozone to the poles, known as Brewer–Dobson circulation, named after Brewer (1949) and Dobson (1956). First, there is a rising tropical motion from the troposphere into the stratosphere, followed by poleward transport in the stratosphere. Finally, the air descends in both the stratospheric middle and polar latitudes, though there are important differences. At mid latitudes descending air is transported back into the troposphere, while at polar latitudes the descending air is transported into the polar lower stratosphere, where it accumulates (Figure 4.20). This effect is stronger during the northern hemisphere winter. The ozone is primarily produced in the tropics but the abovementioned atmospheric motions transport ozone polewards to lower stratospheric regions where its concentration rises because of the increase in atmospheric pressure.

The variability of the stratosphere is characterized by a “see-saw” of temperature and mass between the polar region and mid-latitudes: anomalously weak wave forcing leads to a strong polar vortex and a weak Brewer–Dobson circulation with a cold polar region and warmer mid-latitudes (see Newman *et al.* 2001).

In the upper stratosphere and mesosphere (30–90 km) during the solstices, the circulation is dominated by a single circulation cell with rising motion in the summer hemisphere and sinking in the winter hemisphere. As a result, the summer polar mesosphere is much colder than its radiative equilibrium, and the winter mesosphere much warmer. Gravity waves are produced by the restoring force of buoyancy. They can propagate both vertically and horizontally up to the mesosphere with a typical spatial scale of 10 km. Their flux at the mesosphere is much lower at solar maximum than at solar minimum. Stronger winds are produced in the upper atmosphere and planetary wave propagation into high altitudes will be affected.

4.8.4 The Quasi-Biannual Oscillation (QBO)

Circumpolar flow in the tropics is mainly zonal, but it is also modified by an interannual variation. During the Krakatoa eruption, on 27 August 1883, meteorologists noticed that the cloud of ash and dust produced drifted to the west at

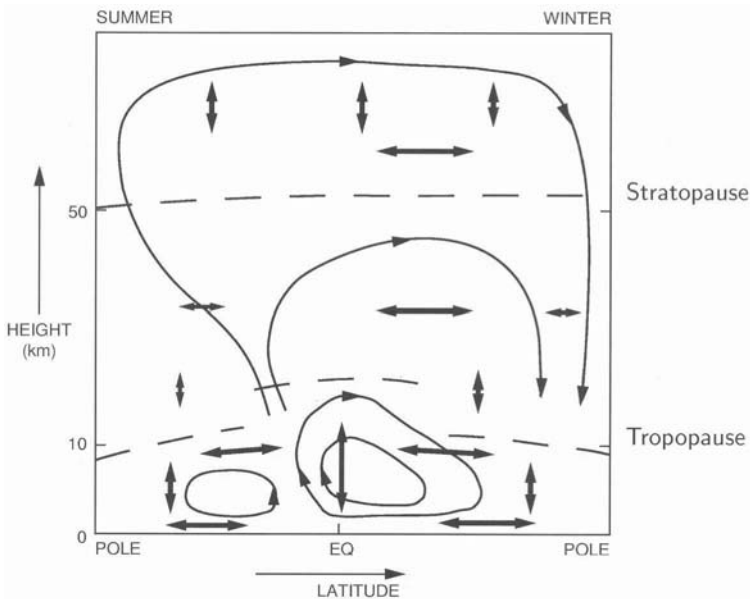


Figure 4.20: Scheme of the meridional circulation in the atmosphere. Adapted from WMO Report (1985).

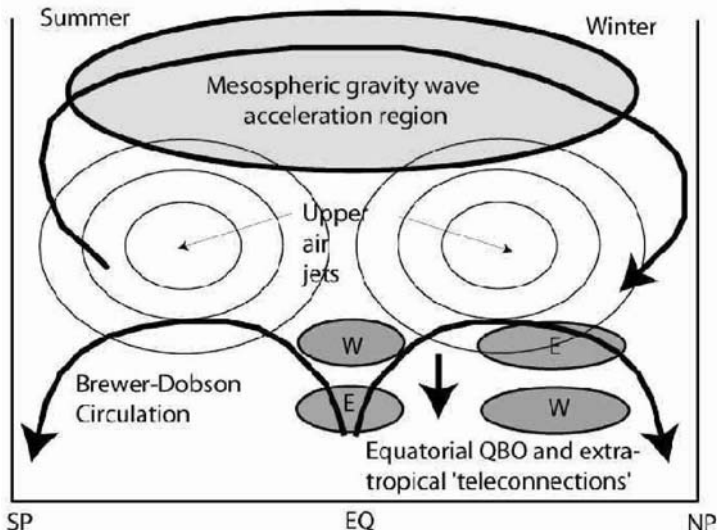


Figure 4.21: Global-scale circulation in the middle atmosphere at solstice. Courtesy: Neil Arnold (University of Leicester).

stratospheric heights. Some years later, in 1908, measurements by Benson with a balloon at 15 km altitude (120 mb), in the proximities of the Lake Victoria, indicated a predominantly eastward stratospheric wind.

Reed *et al.* (1961) discovered that in the equatorial regions the stratospheric winds change with an average cycle of 28.5 months; this is known as the Quasi-Biannual Oscillation (QBO). The winds drift to lower layers (≈ 1 km/month) with the progress of the oscillation (see Baldwin *et al.* 2001 for a review).

At solar maximum the QBO has a relatively short period, whereas at minimum the oscillation appears to halt for months before starting again (Salby & Callaghan 2000).

The ozone profile in the tropics changes in shape accompanying the descent of the westerly shear zone in the altitude range 10–45 hPa (Logan *et al.* 2003). The Berlin Observatory has calculated mean zonal wind components for different altitudes (70–10 hPa) from 1953 to the present (see Naujokat 1986).

4.9 UV and Tropospheric Climate Change

In the previous section, we have described mechanisms influencing the ozone concentration in the stratosphere in this way modulating the UV flux arriving at the Earth's surface. We are now ready to study how these processes can link solar UV variability with the global climate.

4.9.1 Timescales and Sources of Climate Variability

Throughout its history the Earth has suffered changes in climate on all timescales, lasting from eons to few decades (Mitchell 1973; Rudiman 2001). These changes have been produced by the dissipation of external energies listed in Table 4.8 together with an unknown amount of intrinsic variability.

Table 4.8: Temporal variation of energy sources producing changes in terrestrial climate

	Timescales (yr)	Effects
PLANETS		
Gravitational	10^3 – 10^4	Earth's orbit and inclination
	10^8	Impacts (> 1 km)
SOLAR		
Gravitational	10^7	Solar luminosity
Nuclear	10^9	Solar luminosity
Rotation	10^9	Magnetic energy
Magnetic	10^3 – 10^1	?
TERRESTRIAL		
Tectonic Activity	10^8 – 10^9	Atmospheric composition
Volcanic eruptions	10^1	Aerosol emission
Life evolution		Atmospheric composition

We are interested here in climate fluctuations during the last millennium, characterized in its latter part by a rapid growth of temperatures known as global warming (Houghton 1997; Houghton *et al.* 2001). The main potential factors are summarized in Figure 4.22. As far as the solar contribution is concerned it is the magnetic energy the mechanism that needs to be investigated (see Lean 1997; Hoyt & Schatten 1998; Vázquez 1999 and Benestad 2002).

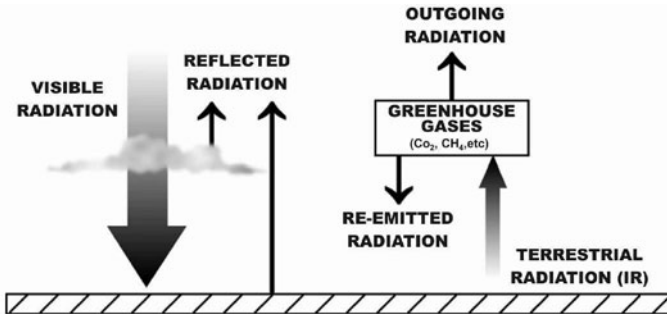


Figure 4.22: The various factors related to changes in the Earth's surface temperatures.

Satellite measurements have clearly indicated that the solar irradiance is changing in phase with the 11 year solar cycle (Pap *et al.* 2002; Willson & Mordvinov 2003). Even though a purely thermal response of the terrestrial climate to this output should be too small, different empirical correlations between solar and terrestrial parameters show that this interaction is significant. There are two possibilities to explain this apparent paradox. One is to look for the solar–terrestrial connection over longer timescales and the second is to investigate the potential role of other channels of solar output (see Table 4.9) for example solar UV radiation, in order to study how the observed response of the middle atmosphere is transmitted to the troposphere.

Various monographs and reviews supply an extended view of the possible specific link between the solar UV and the terrestrial climate (e.g. Reid 2000, Thuillier 2000, Arnold 2002; Bochníček & Hejda 2002).

4.9.2 The Solar Print in the Upper Atmospheric Layers

The solar UV produces considerable heating of the upper layers of the atmosphere, which therefore expand. Temperatures in the thermosphere change significantly from solar minimum to solar maximum (Roble & Emergy 1983). Figure 4.23 show how the temperature change with the altitude between two periods with different levels of solar activity (Schmidtke 2000).

Radiosonde observations by R. Scherhag (1907–1970) in Berlin provided the first information about midwinter warmings in the stratosphere, connected with the solar activity. Since the International Geophysical Year in 1957, the Berlin data set have supplied continuous monitoring of geopotential heights (GH)²² at

²²Geopotential is a measure of the energy required to lift a mass of air from the surface to a

Table 4.9: Energy densities in the three main channels for the Sun–Earth connection. From National Research Council Report “Solar Influences on Global Change”, National Academy Press, 1994.

Source	Energy (W/m ²)	Solar cycle change	Terrestrial deposition (km)
SOLAR RADIATION			
Total irradiance	1366	0.002	Surf. and Trop.
UV (200–300 nm)	15.4	1.3	0–50
UV (0–200 nm)	0.1	0–16	50–500
PARTICLES			
Solar protons	0.002		30–90
G. Cosmic rays	0.000007		0–90
Solar wind	0.0003		> 500

different pressures in the lower stratosphere since 1957. The NCEP/NCAR (US NAtional Center for Environmental Prediction/National Center for Atmospheric Research) has kept world-wide records since 1968.

During northern winters, the solar UV signal is more clearly identified in GH measurements if the latter are grouped according the phase of the QBO (Labitzke 1987; Labitzke & Van Loon 2000; Van Loon & Labitzke 2000; Labitzke 2001)). See Figure 4.24 for an update.

During the QBO–West over the Arctic major stratospheric warmings tend to take place during solar maximum; they are connected with cooling outside the high latitudes over the rest of the hemisphere, acting against the usual warming (produced by the enhanced UV) and therefore decreasing the correlation between GH values and solar activity (Labitzke 2001; Labitzke *et al.* (2002)). Naujokat *et al.* (2002) have described three exceptional warming periods in recent years, that evidence a strong troposphere–stratosphere coupling.

Labitzke (2003) found that the influence of the QBO on solar–terrestrial relations must also be extended to the northern summers (Figure 4.25). The data hint at a connection between Hadley circulation in the troposphere and stratospheric Brewer–Dobson circulation. In the QBO–East we have a weakening of Brewer–Dobson during solar maxima. In the QBO–West Hadley circulation is intensified during the maxima of solar activity.

Tinsley (1988) grouped the data on winter storm tracks above the North Atlantic with respect to QBO changes and studied the latitudinal dependence with the level of solar activity. He found that around the solar maximum the storms track equatorwards and at the solar minimum polewards.

The change in atmospheric response with QBO phase clearly indicates a con-

given altitude, working against gravity. Geopotential height (GH) is the geopotential divided by g_0 , the globally averaged value of terrestrial gravity. Usually, it is considered as the GH at which atmospheric pressure has a particular value; for example 70 mb at 18.5 km. If the temperature in the column below increases, the level of 70 mb will be found to be higher.

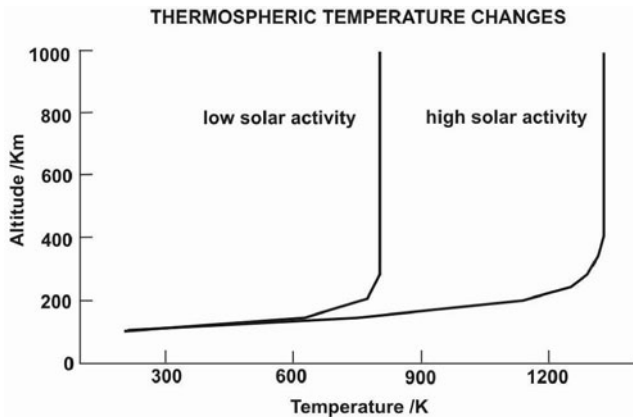


Figure 4.23: XUV-induced temperature changes in the thermosphere for two levels of solar activity.

nexion between equatorial and polar regions. The emerging idea behind this is that the solar radiation simply redistributes the energy contained in the terrestrial atmosphere.

4.9.3 Ozone Chemistry

The interaction of UV radiation with stratospheric ozone via the processes of formation and decay seems to be a promising mechanism for explaining the correlation between solar activity and tropospheric climate. As solar UV radiation increases so does O_3 production in the upper stratosphere. The extra amount is transported polewards and downwards, resulting in more ozone for absorption. As mentioned above, the net effect over the solar cycle is an increase of a few per cent in ozone abundance.

The thermal consequence of enhanced ozone absorption is stratospheric heating in sunlit areas, which is balanced by subsequent infrared cooling, producing a small radiative forcing in the summer hemisphere (Haigh 1996, 1999; Larkin *et al.* 2000). However, the structure of the ozone change does affect the detailed temperature response and the spectral composition of the radiation entering the troposphere, and thus the location of the absorption. These authors modelled together the ozone photochemistry and the spectral distribution of solar irradiance, finding changes in zonal wind during the solar maximum, which are associated with modifications to the mean meridional circulation such that the winter Hadley cell weakens and broadens and the summer hemisphere cells are moved polewards. Previous studies had assumed a constant change in the distribution of solar irradiance or a constant ozone content (e.g. Rind & Balachandran 1995).

However, the positions of the maximum correlations between the solar activity and ozone concentrations, and with stratospheric temperatures, are not coincident, which seems to exclude a direct link between insolation and ozone values.

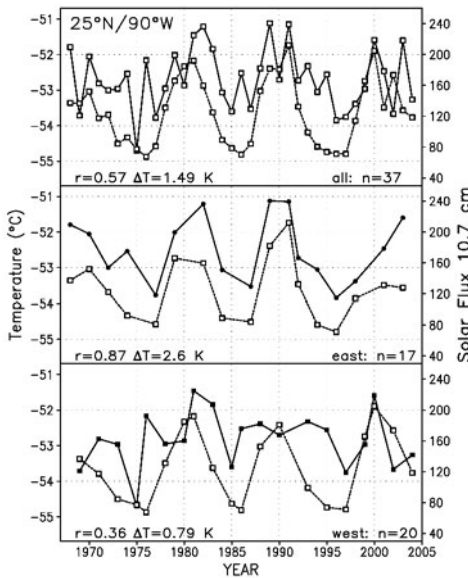


Figure 4.24: Time series of the solar activity (10.7 cm radio wave, so-called solar flux [1 s.f.u. = 10^{-22} Wm $^{-2}$ Hz $^{-1}$], dashed with squares, right hand scale); time series of the detrended 30-hPa temperatures ($^{\circ}$ C) in July at 25°N/90°W, full lines, left hand scale. Upper panel: all data; middle panel: only years in the east phase of the QBO (at about 45 hPa); lower panel: only years in the west phase of the QBO. r = correlation coefficients; ΔT = temperature difference between solar max and solar min; n = number of years. (NCEP/NCAR re-analysis, 1968-2004, Kalnay *et al.* 1996). Courtesy: K. Labitzke (Frei Universität, Berlin).

Figure 4.26 shows the altitude profile of the ozone concentration together with the corresponding temperature response.

Shindell *et al.* (1999) reproduce the record of geopotential height variations and show that, at least partially, they are driven by solar variability. Two main regional patterns are found: 1) an increase in pressure over north-eastern Pacific bringing warmer air up from lower latitudes over Canada, and 2) a similar effect occurring over the North Atlantic and Northern Eurasia, bringing warming air up over the Arctic Ocean in the eastern hemisphere.

In any case, it is remain the dynamical channel that transfers the perturbation to lower layers and so to the terrestrial climate. In the following subsection we explain how this mechanism might work. We should keep in mind that the amplitude of any disturbance propagating downwards in the atmosphere is reduced by a factor of ten over a couple of scale heights owing to the exponential rise in pressure. Only non-linear processes can be responsible for this interaction.

4.9.4 The Natural Patterns of Climate Variability

Apart from the various external forcings the terrestrial climate has an intrinsic variability. This is reflected by certain patterns, classically measured by the pressure difference between two geographical locations. In the Pacific we have El Niño/La

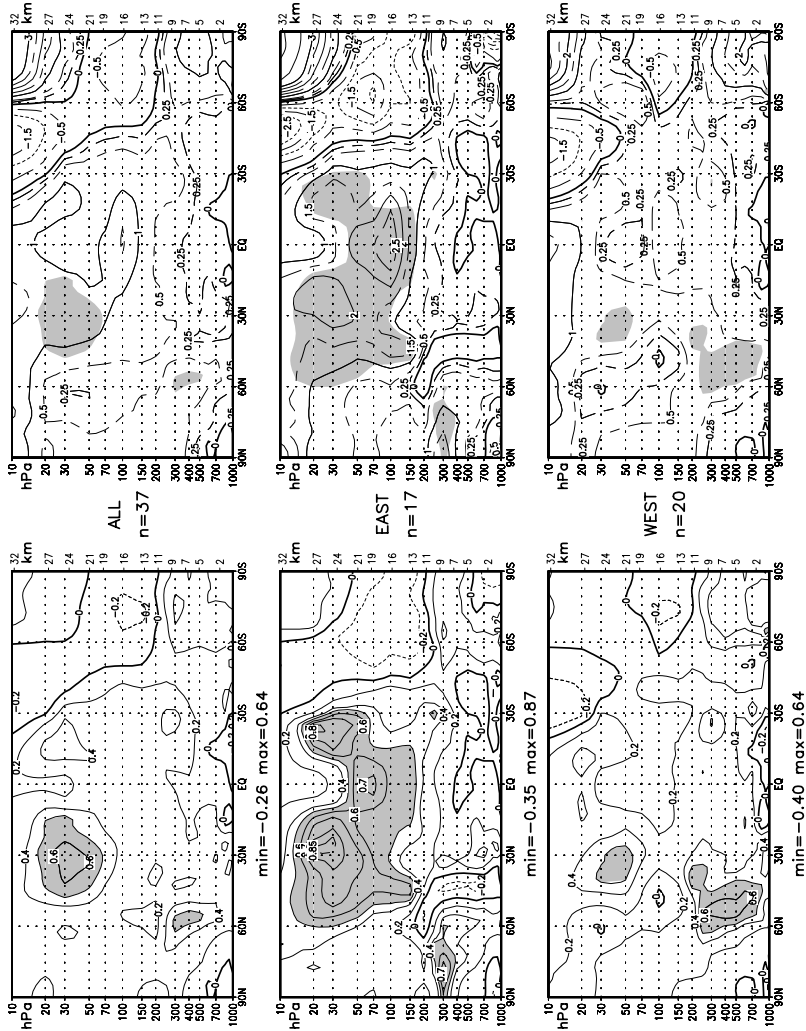


Figure 4.25: Left: Vertical meridional sections of the correlations between the 10.7cm solar flux and the detrended zonal mean temperatures in July; shaded for emphasis where correlations are above 0.5. Right: The respective temperature differences (K) between solar maxima and minima, shaded where the corresponding correlations on the left hand side are above 0.5. Upper panels: all years; middle panels: only years in the east phase of the QBO; lower panels: only years in the west phase of the QBO. (NCEP/NCAR re-analyses, 1968-2004). Courtesy: K. Labitzke.

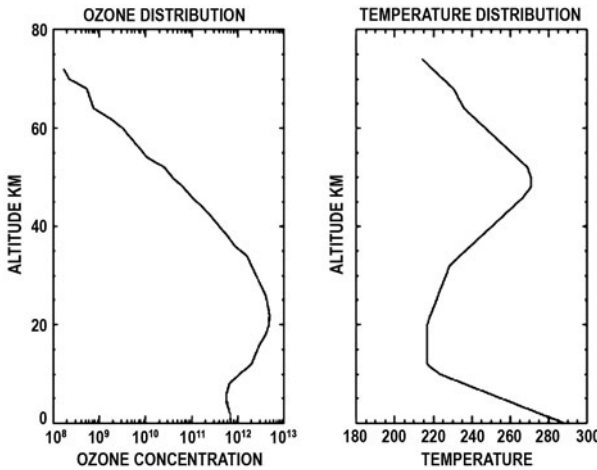


Figure 4.26: Impact of ozone on stratospheric temperatures. Adapted from “The Stratospheric Ozone Electronic Textbook” funded, developed, written, and edited by members of NASA’s Goddard Space Flight Center, Atmospheric Chemistry and Dynamics Branch.

Niña, also known as the Southern Oscillation, the Pacific Decennial Oscillation (PDO) and in south-east Asia the monsoons.

Similarly, in the Atlantic we have the North Atlantic Oscillation (NAO), that fluctuates between two phases (Figure 4.27). In its positive phase, there is a pronounced low-pressure region over Iceland, and high pressure over the subtropical Atlantic (around the Azores and the coast of Portugal). In the negative phase, the Icelandic low and the subtropical high are much weaker. These two phases switch every year or so, bringing changes in weather and temperatures over Europe and Scandinavia.

An extension of this pattern to the stratosphere constitutes the Arctic Oscillation (Thompson & Wallace 1998). In the *positive phase* a ring of strong westerly winds circulating counterclockwise around the North Pole (north of 55° N), acts to isolate cold Arctic air within the polar regions. Warm high pressure conditions prevail between 35° N and 45° N and cold anomalies occur in the tropics, accompanied by a strengthening of the trade winds. Moreover, low ozone values are observed at high latitudes. In the *negative phase*, the ring is distorted, which makes it easier for chilly Arctic air masses to escape to lower latitudes. The link between the AO phases and the strength of the stratospheric polar vortex has been studied by Black (2002).

The strengthening or weakening of the circulation around the pole tends to begin in the stratosphere and work its way down through lower levels of the atmosphere (Baldwin & Dunkerton 1999).

The difference between the NAO and AO terms consists in whether that variability is interpreted as a regional pattern controlled by Atlantic sector processes (NAO) or as an annular mode (AO) whose strongest teleconnections lie in the

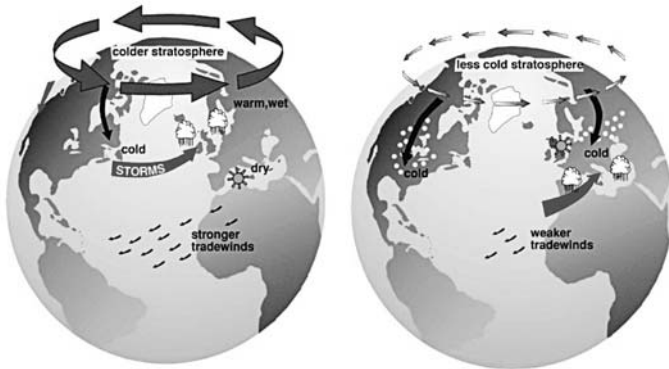


Figure 4.27: The troposphere and stratosphere during the two main phases of the pattern AO/NAO.

Atlantic sector (Wallace 2000).

4.9.5 The Effect of Planetary Waves

We have described previously the general characteristics of planetary waves. We now study in more detail their role in climate changes connecting the troposphere and the stratosphere. Solar activity modifies the index of refraction of PWs by changing the propagation of these waves in the atmosphere.

Figure 4.28 illustrates the influence of PW strength in stratospheric temperature and therefore on ozone depletion. Total column ozone measurements are used to derive a daily Dynamics Activity Index (DAI), which represents an estimate of PW amplitudes²³. The DAI allows the identification of peculiar situations such as stratospheric warming. It is systematically higher during local winter than during local summer, because vertical propagation of planetary waves from tropospheric altitudes into stratospheric regions depends on the direction of the zonal mean flow.

High solar activity was shown to promote strong PW activity and these waves could therefore be the agent connecting solar-induced stratospheric changes with the troposphere (Arnold & Robinson 1998, 2000 a,b). These authors (Arnold & Robinson 2003) have recently extended their simulation to the mesosphere by studying the supplementary influence of gravity waves, whose flux also changes with solar activity. The whole wave field between the ground and the thermosphere adjusts to the changes caused at the upper boundary by UV radiation. Large-amplitude stratospheric anomalies propagate downwards through the troposphere and tend to precede tropospheric anomalies.

After Kodera (1995) and Kodera *et al.* (1999), the scheme proposed for the interaction UV –climate consists of the following main steps: a) reduction in polar

²³The DAI-n is defined as the hemispheric mean of the zonal amplitude of the planetary wave number n , where $n = 1,2$.

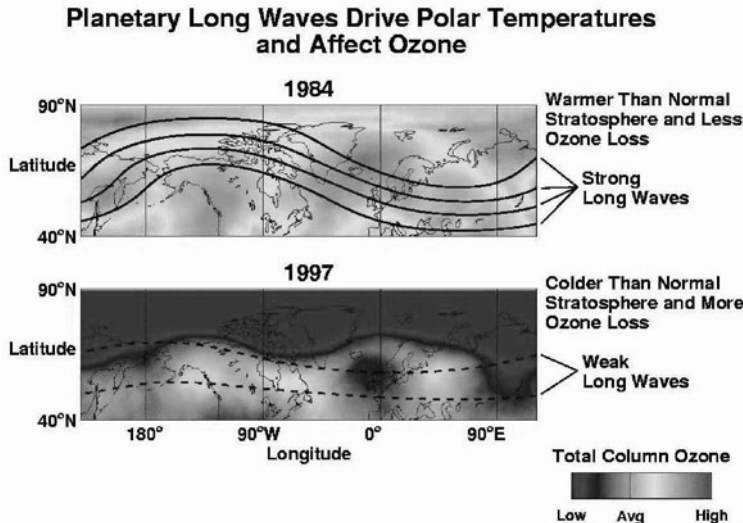


Figure 4.28: Strength and shape of planetary waves in both 1984 and 1997 in the northern mid-latitudes. Source: Goddard Space Flight Center.

night jet speed, b) change in the refractive index of planetary waves, originated by weaker zonal mean wind at high latitudes and stronger zonal mean wind at low latitudes, and c) poleward propagation of mid-latitude planetary waves.

Rind & Balachandran (1995) and Balachandran *et al.* (1999) proposed that an increase in solar UV directly alters the vertical temperature and zonal wind profiles of the atmosphere. The degree of stratospheric temperature changes depends on the relationship between UV forcing and the transfer of energy from lower latitudes. During the eastern phase of the QBO, the tropical east winds lead to greater poleward propagation of PW energy in the lower stratosphere, thus producing warming at midlatitudes. The increased UV also produces warming at low and mid-latitudes, and increases westerlies at high levels in the extratropics. The vertical shear of the winds is associated with larger upward PW energy propagation, taking energy out of the polar lower stratosphere, which thus cools. Perturbations in the stratospheric vortex provides the necessary link between the stratosphere and tropospheric climate (see Hartley *et al.* 1998).

The key features of NAO/AO changes due to enhanced solar activity can be explained in terms of wave refraction. At mid-latitudes, upwardly propagating PWs (stronger at solar maximum) are refracted more or less strongly towards the tropics, depending on the strength of the lower stratospheric polar vortex. In the negative phase of the AO, the polar vortex is weak, so more waves are refracted into it. When these waves break they decelerate the vortex even more (see Figure 4.29).

Table 4.10 shows the response of the polar vortex to the two phases of the QBO.

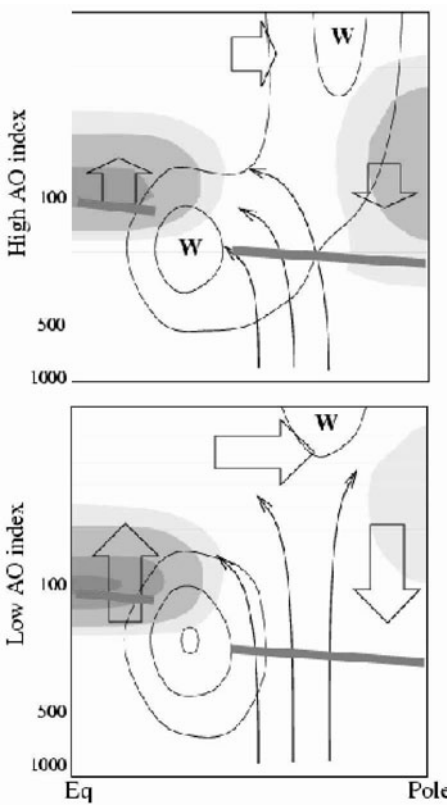


Figure 4.29: Phases of the Arctic Oscillation. Sketch of temperature (shading); zonal wind (contours); meridional circulation, also known as the Brewer-Dobson circulation (thick arrows); flux of planetary waves (thin arrows). Courtesy: J. M. Wallace.

If one considers only the winters in the QBO-West phase, then the correlation between stratospheric temperatures and the solar activity is positive, whereas the opposite happens during the QBO-East (cf. Labitzke & van Loon 2000)

Castanheira & Graf (2003) have recently found an anticorrelation between pressure in the North Atlantic and the North Pacific, but only under “strong polar vortex” conditions.

Figure 4.30 show schematically the solar influences on the winter stratosphere during the eastern QBO phase, but now extended to the upper atmospheric layers. The thermosphere is heated and the gravity flux is reduced with an associated weakening of the global circulation. Transport of ozone and heat into the polar regions is reduced as the strengthened polar vortex diminishes planetary wave penetration.

Summarizing, various models have shown that energy propagating via PWs

Table 4.10: Response of the polar vortex to the phases of the QBO for different levels of solar activity. After Labitzke & van Loon, 1988

	Solar minimum	Solar maximum
QBO East	Weak and warm	Strong and cold
QBO West	Strong and cold	Weak and warm

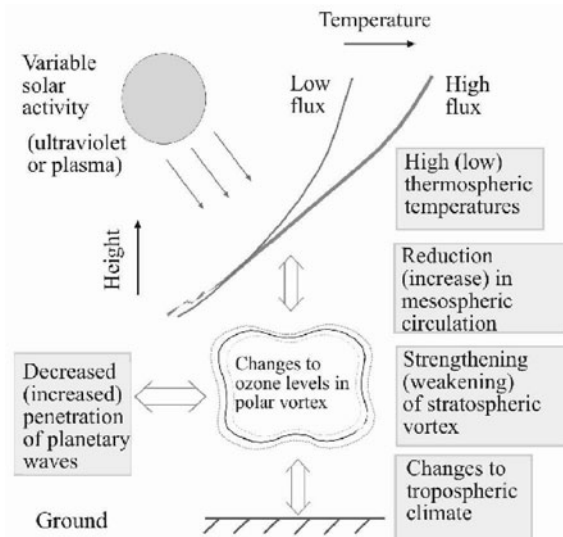


Figure 4.30: Schematic of the influences of enhanced solar UV on the (eastern-phase) winter stratosphere. Courtesy: N. Arnold (University of Leicester)

in the lower stratosphere towards the pole is far greater during the QBO–East phase than during the QBO–West ²⁴. In polar regions, the direction of energy propagation changes to vertical. If the stratospheric westerlies are sufficiently strong, the upward energy flux is intensive and the lower stratosphere cools as a consequence of a decrease in energy. In other words, in the NW circulation there are two different regimes characterized by the penetration, or otherwise, of tropospheric vertically propagating planetary waves in the stratosphere. The hopping between these states depends mainly on the strength of the polar vortex.

Simulation of the response to a 0.25% reduction in solar irradiance, results in a 0.47 °C average cooling but shows a non-homogeneous spatial response (Rind & Overpeck 1993). On the basis of the code developed by Shindell *et al.* (1999), Shindell *et al.*, (2001) and Rind *et al.* (2004) have studied the atmospheric response

²⁴Paradoxically, the influence of solar forcing is strongest at solar maximum in the western phase.

to conditions of reduced solar activity (the Maunder Minimum), keeping the sea surface constant. They found that the global ΔT is small ($0.3\text{--}0.4^\circ\text{C}$), but that the regional ΔT values are quite large. They interpret this behaviour as a shift towards the low index state of the NAO/AO, leading in winter to strong cooling ($1\text{--}2^\circ\text{C}$) in central Europe, in clear agreement with the historical and proxy data for surface temperatures (Luterbacher *et al.* 1999).

Shindell *et al.* (2001a) found that the reduced UV during the Maunder Minimum caused the ozone to increase in the upper stratosphere compared with the year 1750, a period of higher solar activity. The simulations of Rind *et al.* (2004) give a 2.7% reduction in ozone in the upper stratosphere and of 1.4% in the total ozone, but with little effect in the troposphere.

Stenchikov *et al.* (2002) have suggested that the climate effect of the 1991 eruption of the Mount Pinatubo was linked to a strengthening of the Arctic Oscillation. For two years following the volcanic eruption, the AO caused winter warming over land areas in high and mid-latitudes of the northern hemisphere, despite a cooling effect from volcanic particles that blocked the passage of sunlight to the surface. Shindell *et al.* (2004) have examined the distinct climatic response to volcanic events and solar UV irradiance changes. They find that in the solar case the radiative and dynamical effects reinforce each other²⁵, whereas for volcanic aerosols both effects are compensated.

The present global warming seem to excite the positive phase of NAO more. Orsolini & Limpasuvan (2001) have suggested that during this phase mini-ozone depletions can be produced by the additional stratospheric cooling.

Shindell *et al.* (2001b) have numerically simulated the impacts of increasing greenhouse gases, polar ozone depletion, volcanic eruptions and solar-cycle variability on climate. They show that, while ozone depletion has a significant effect, greenhouse gas forcing is the only factor capable of causing the large, sustained increase in the AO over recent decades²⁶.

The terrestrial atmosphere seem to possess two or more stable states that are separated by an energy barrier that could undergo “hopping” between these two states in harmony with small changes in an external forcing as the solar UV irradiance. Different models support this kind of interaction between an external forcing and the terrestrial climate (Tobias & Weiss 2000).

We now have the influential elements in such transitions; namely, planetary waves, ozone chemistry, polar vortex strength, QBO phase, and the time and location of the event winter in the northern hemisphere.

Summarizing, during the QBO-East, the observed differences between maxima and minima of the solar cycle are interpreted as an intensification of the polar vortex and a weakening of the Brewer–Dobson circulation during solar maximum. As a result, distinct anomalies in the zones ($90^\circ\text{S}\text{--}60^\circ\text{N}$) and ($60^\circ\text{--}90^\circ\text{N}$) are produced.

²⁵Reduced (increased) solar activity produces tropospheric cooling (warming), with the same trends observed in the stratosphere.

²⁶Since the high frequency variability of AO/NAO is much higher than its decadal variability, it is more appropriate to speak of a preference for the positive phase rather than a steady increase over time.

We now understand why many Sun–climate relations were found to be contradictory (see Hoyt & Schatten 1997 for a historical review). At a given stage, the atmosphere can occupy a number of states, especially during the winter, and the energy difference between them is small. Over time, the situation will change because of external forcing; for example, enhanced UV flux at the upper layers. The challenge for the future is to separate in the records the solar contribution from other influences.

4.10 Effects of Solar UV on the Stability of Satellite Orbits

An important consequence of the thermal heating of the thermosphere is the change of altitude of satellites in low orbits (see Hanslmeier 2002 for more details).

In the upper atmosphere the drag force on a satellite is

$$f_D = \rho V^2 C_D \frac{A}{2} \quad (4.8)$$

where M_E is the mass of the Earth (5.9737×10^{24} kg), ρ is the air density, A the cross-sectional area of the satellite, V the velocity of the satellite relative to the ambient atmosphere and C_D a coefficient depending on the shape of the satellite. For altitudes between 200 and 1000 km $C_D = 2.0\text{--}2.2$ and below 200 km $C_D \ll 2$.

The orbital period, P , of a satellite (assuming a circular orbit of radius a) is given by the expression

$$P^2 GM_E = 4\pi^2 a^3$$

The drag forces causes a change in the period of the satellite given by

$$\frac{dP}{dt} = 3rC_D\rho \frac{A}{m} \quad (4.9)$$

where m is the satellite mass and r the radial distance from the Earth's centre.

Atmospheric drag has important consequences for the stability and lifetime of satellites placed in low-altitude orbits; therefore, an important amount of information on atmospheric density and composition is obtained from the orbital periods of artificial satellites. Increased satellite drag also magnifies the risk of collisions with orbiting debris.

The lifetime of a satellite is strongly dependent on its altitude. At an altitude of 300 km it may last for 20–50 days (depending on the Sun's activity level) before it re-enters the atmosphere and burns up. However, at 180 km this lifetime reduces to mere hours. Two well-known spacecrafts affected are the Hubble Space Telescope (HST) and the International Space Station (ISS), which require periodic reboosting with the Space Shuttle Orbiter. For the case of no further reboost it is predicted that HST will re-enter the atmosphere in late 2013²⁷.

²⁷Space Environment Technologies (<http://www.spacewx.com>) provides solar EUV input for models of the thermosphere that be used in satellite drag analysis.

In June 1999, astronauts on the Space Shuttle deployed a 40 kg. beach-ball sized satellite designed to study the effect of solar activity on the Earth's atmosphere. The satellite, named STARSHINE, is a hollow aluminum sphere covered with 2.5 cm-square mirrors. They were followed by other similar satellites. The project is a consortium of volunteers, led by the US Naval Research Laboratory and the Space Grant Program. Picone *et al.* (2003) have derived time series of thermospheric density from data obtained with this project. They have quantified the thermospheric response to solar forcing in the EUV range.

Chapter 5

UV Radiation, Ozone and Life

In the first part of this chapter we describe how UV radiation can play a role in the origin of life. This will be followed by a description of the various effects of UV radiation on living beings, some of these effects being produced by the action of one living species, *Homo Sapiens*.

5.1 The Biochemistry of Life

The work of George Mendel (1822–1884) with peas, led him to hypothesize that phenotypic traits (physical characteristics) are the result of the interaction of discrete particles and that both parents provide particles which make up the characteristics of their offspring (Mendel 1866). His research remained unknown for several decades until, in the early years of the twentieth century, scientists noticed similarities in the theoretical behaviour of Mendel’s particles and that of the newly discovered chromosomes. These last structures had been discovered by microscopic observations as tiny rod-like features inside the cells. Step by step, most scientists were convinced that chromosomes and the hereditary material responsible for giving living things their characteristic traits must be one in the same. Experiments by Thomas Morgan (1866–1945) with the fruit fly “*Drosophila melanogaster*” showed that still smaller structures existed inside the chromosomes: the genes. The main results appeared in his book “Mechanism of Mendelian Heredity” published in 1915.

Nucleic acids were discovered inside cells by Friedrich Miecher (1844–1895) around 1869 and in 1920 Phoebus Levene (1869–1940) showed that there existed two different types: deoxyribonucleic acid (DNA) and the ribonucleic acid (RNA). DNA contains the master archive and building plan of the organism and RNA stores the blueprints for the individual construction process (Hershey & Chasse 1952). These acids were synthesized in the 1950s by Arthur Kornberg and Severo Ochoa (1905–1993), respectively.

Watson & Crick (1953) demonstrated that the DNA looks like a long ladder twisted into a helix. The sides of the ladder are formed by a backbone of sugar and phosphate molecules. The rungs consisted of nucleotide bases joined weakly by hydrogen bonds. DNA is composed of four nucleic acids, adenine and guanine (purine derivatives) and thymine and cytosine (pyrimidine derivatives). In the RNA uracil substitutes the thymine. The DNA molecule becomes so long that adopts the form of a spiral in order to fill in the cell (see Figure 5.1).

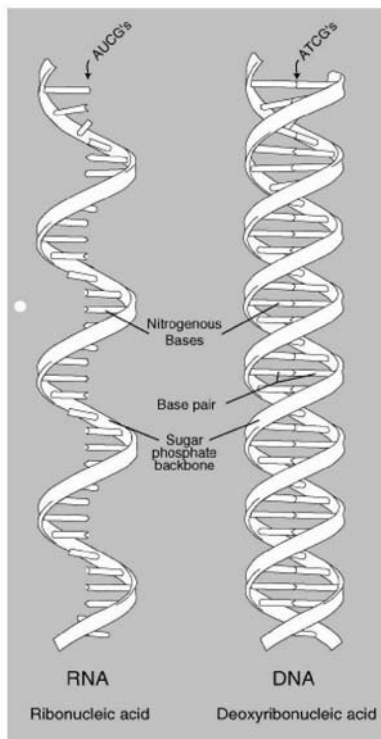


Figure 5.1: DNA and RNA structure.

The genes are contained in strands of DNA, the chromosomes, which are situated inside the cell's nucleus. Chemical analysis of genes showed them to be composed of both protein and DNA (Avery *et al.* 1944). Each gene is the blueprint for a particular protein. The building blocks are a particular set of molecules called "aminoacids".

DNA is passed from a cell to its daughter cells by a conservative process called mitosis. In sexual organisms, a scrambled chromosomal content is present in germ cells, which are generated by a reductional division called meiosis. The existence of both processes was proposed in the late nineteenth century by A. Weissmann (1834–1914)¹. The genome of an organism is its set of chromosomes, containing

¹The experimental proof of mitosis was made by W. Flemming (1843–1905). In 1902 W. S.

all its genes and associated DNA. The sequence of nucleotides in each gene serves as a chemical code instructing the manufacture of a protein at one of the many minute factories called ribosomes scattered through a cell.

5.2 Radiation and Life

Ionizing radiation² has the power to produce damaging effects on living beings. Several parameters and functions are used to describe this effect in a quantitative way.

5.2.1 Radiation Units

Specific units are used to describe the action of radiation on living beings. They are based in similar parameters used in the physical sciences, some of them defined in the previous chapter.

- *Absorbed dose*: $D = \Phi E (\mu/\rho)$, where Φ is the number of photons per unit time, E is the energy per photon and (μ/ρ) the mass energy absorbing coefficient, describing the absorbing properties of biological tissue following the definition of such parameter in previous chapters. First, the absorbed dose was expressed in *Rads* ($1 \text{ rad} = 10^{-2} \text{ J kg}^{-1}$); this unit was replaced by the *Gray* equivalent to one joule per kilogram.

- *Equivalent dose*: This includes a weighting factor, ω_R , to take into account the distinct efficiencies of the various particles implicated in the ionizing radiation. It is expressed as $H = D \times \omega_R$. The corresponding units are the *rem* and the *sievert*.

- *Effective dose*: This includes a weighting factor, ω_T , to take in consideration the part of the body interacting with the radiation. It is expressed as $H_{ef} = H \times \omega_T$. Table 5.1 gives some values of these weighting factors

Table 5.1: Values of the weighting factors ω_R and ω_T .

ω_R		ω_T	
Photons	1	Gonads	0.20
Electrons/muons	1	Lungs	0.12
Protons	5	Thyroid	0.05
Neutrons	5–20	Liver	0.05
Alpha particles	20	Stomach	0.12
Heavy nuclei	20	Skin	0.01

A direct and clear relationship between radiation exposure and its consequences is found only for some effects, almost always at high levels of absorbed dose. These effects also have a threshold dose below which they do not occur. Effects of this

Sutton (1877–1916) and T. Boveri (1862–1915) demonstrated the process of meiosis.

²For historical reasons described in the first chapter, high-energy particles such as the cosmic rays are also included under the name of ionizing radiation.

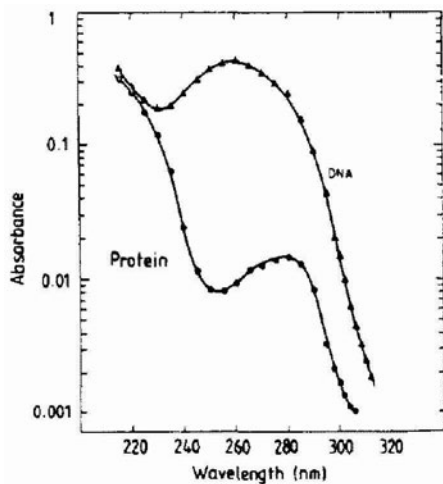


Figure 5.2: Absorption spectra of DNA and a protein at equal concentrations.

type are called *deterministic*, and the severity of the response depends on the dose. For skin reddening, for example, the higher the dose the more severe the effect on the skin.

With regard to the effects of irradiation for which there is no evidence of a threshold dose, such as the induction of cancer, it is known that if a group of people are exposed to radiation then a certain fraction will show the effect, that is, develop cancer. But the severity of the cancer does not depend on the dose. Also, there is no way at present of predicting which individuals will be affected. For any individual, therefore, exposure to radiation may be thought of as increasing the probability that the effect will occur. For example, the likelihood of developing cancer increases with increased exposure to ionizing radiation. These effects are called *stochastic* and it is assumed for protection purposes that the risk of stochastic effects from exposure to radiation depends directly on the absorbed dose.

5.2.2 Wavelength-dependent Functions

An *absorption spectrum* is a measure of the amount of energy that has passed through a given substance. A common feature of nucleic acids is an absorption maximum in the range 260–265 nm with a rapid reduction at longer wavelengths. The proteins also absorb strongly in the UV-C region with a maximum around 280 nm, although the absorption is lower than that of the nucleic acids (Figure 5.2).

The *action spectrum* describes the relative effectiveness of energy at different wavelengths in producing a particular biological response (Figure 5.3)³. “Bio-

³Data from Setlow (1974). The parameterization used is that suggested by G. Bernhard &

logical response" may refer to effects at a molecular level, such as DNA damage, or at whole organism level, such as plant growth. Action spectra may be derived *in vivo*, *in vitro* or *in situ* and the light source can be either monochromatic or polychromatic.

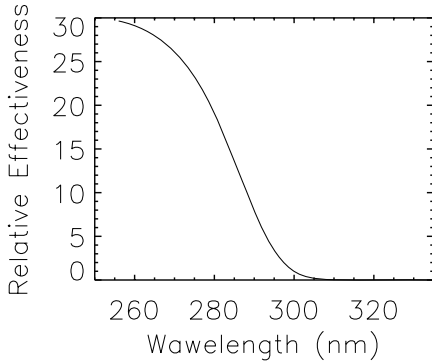


Figure 5.3: Action spectrum of DNA. The resulting action spectrum is 1 at 300 nm.

Note, however, that a direct comparison of dose amounts for any induced effect cannot be made on the basis of action spectrum alone; these spectra only give an indication as to the relative effectiveness of particular wavelengths, not the actual dose amount required to produce a biological response. For these purposes the *biologically weighted irradiance*, B , is used as a function of the incident solar spectrum, F , and the action spectrum S :

$$B(\lambda) = \int_{200 \text{ nm}}^{400 \text{ nm}} S(\lambda)F(\lambda)d\lambda.$$

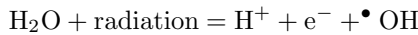
5.2.3 Mechanism of Cell Damage

The duplication of the cell implicates also duplicating the DNA; in the copying procedure, although normally followed with a high degree of accuracy, there damage sometimes appears. A mutation is any change in the normal sequence of nucleotides in a gene. Human chromosomes are made up of 30 000 genes and about three billion nucleotides; there are therefore plenty of opportunities for mutation to arise. There are two major ways to produce injuries in the DNA by the action of ionizing radiation (Sinha *et al.* 2002) :

- 1) Direct collision with DNA molecules, ionizing them, breaking its bonds and damaging it directly:



2) Absorption of UV-A radiation by the water in the body causing it to become ionized. Highly reactive molecules (free radicals) are formed through this process, that subsequently damage the DNA molecules. This second action of radiation on water, produces the splitting of the molecule:



where $\cdot\text{OH}$ is a free radical that is highly reactive. When $\cdot\text{OH}$ radical reacts with a protein or DNA molecule it snatches an electron to itself. If radiation strips a second electron from water, the next intermediary in the process is hydrogen peroxide (H_2O_2), whose oxidizing properties can kill microorganisms.

Ultraviolet radiation is not energetic enough to remove electrons from atoms and molecules directly. Rather, UV photons cause two adjacent thymine residues in the DNA to dimerize, connecting themselves with a cyclobutane ring. Dimmers preclude the normal transcription of genes and produce mutations and biological damage. The UV radiation leaves one of the DNA chains intact, making repair work easier. Ionizing radiation, however, is able to produce all kinds of breaks in the DNA; hence its effects are much more severe.

The biological effects are directly related with the frequency of the radiation ($\nu(\text{UV-C}) > \nu(\text{UV-B}) > \nu(\text{UV-A})$). If the damage is not extensive, cancerous or pre-cancerous cells are created from healthy cells. If the damage is widespread, the cell will die.

It is now pertinent to study the physical conditions in the Sun at the time of the emergence of life on the Earth. A previous overview has already been given in chapter 3.

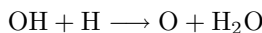
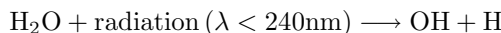
5.3 Long-term Evolution of Ozone and UV Radiation

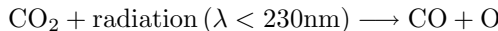
In the context of this book it is highly pertinent to consider the UV flux of the Sun and how this affected the primitive Earth and other planets.

5.3.1 Oxygen and Ozone Variation

Throughout its history the composition of the terrestrial atmosphere has undergone important changes mainly involving the abundance of the principal greenhouse gases. This has clearly influenced the amount of UV-B and UV-C arriving at the surface, whereas the UV-A range has experienced the general increase described in the previous section.

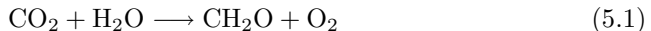
In a primordial atmosphere dominated by carbon dioxide and water vapour, free oxygen atoms can be produced by the following reactions





The free oxygen will produce molecular oxygen and ozone through Chapman reactions (see chapter 4). On the basis of UV measurements of T Tauri stars, Canuto *et al.* (1982) indicated that the O₂ surface mixing ratio was a factor 10 000–1 000 000 times greater than the standard value of 10⁻¹⁵. Canuto *et al.* (1983) extended their calculations to other atmospheric components such as OH, H, HCO and formaldehyde (H₂CO).

At the beginning of the Proterozoic era the cyanobacteria – photosynthetic prokaryotes also known as blue-green algae – brought about one of the greatest changes this planet has ever known: a massive increase in the concentration of atmospheric oxygen through the reaction ⁴:



The amount of ozone required to shield the Earth from biologically lethal UV radiation, at wavelengths from 200 to 300 nanometers (nm), is believed to have been in existence ~600 million years ago. At this time, the oxygen level was approximately 10% of its present atmospheric concentration. Prior to that period, life was restricted to the ocean. The presence of ozone enabled multicellular organisms to develop and live on land, playing a significant role in the evolution of life on Earth and allowing life as we presently know it to exist. Rye & Holland (2000) have raised the suggestion that land-dwelling microbes existed at least as early as 2.7 Ga ago. If this is true, something is wrong with our estimate of the abundance of ozone in the stratosphere at that time, unless such microorganisms developed strong defense mechanisms against UV action.

The evolution of the concentration of oxygen in the atmosphere is not very well known, especially at early times (Figure 5.4). Oxygen photosynthesis arose long before O₂ became abundant in the atmosphere. Sulphates and the oxidation of organic matter indicate that oxygen was present locally at early times. An upper limit on oxygen abundances is given by the abundances of uranite (UO₂), whereas a lower limit is given by the amount of oxygen needed to produce *Banded Iron Formations* (BIFs)⁵.

An apparent paradox arose because, whereas the terrestrial crust contains 1.1 × 10²¹ moles⁶ of reduced carbon (freed from its oxygen after reaction 5.1), the total amount of organic carbon to account for all the atmospheric oxygen is only 0.038 × 10²¹ moles. In other words, the atmosphere contains too little oxygen. Clearly, the missing oxygen is trapped in oxidized reservoirs such as sulphates and ferric iron.

During the Phanerozoic the oxygen content underwent an important increase during the Carboniferous period reaching values around 35%, accompanied by a decrease in CO₂ with its subsequent biological implications (Graham *et al.* 1995).

⁴Here CH₂O is a shorthand for more complex forms of organic matter.

⁵Banded iron formations are very large bodies of sedimentary rock laid down some 2.5 billion years ago. More precisely, BIFs are laterally extensive, marine-derived sedimentary deposits consisting of alternating iron-rich (dominated by magnetite, siderite, and hematite) and iron-poor layers (dominantly silica dioxide).

⁶One mole of an element is equal to 6.02 × 10²³ atoms of that substance.

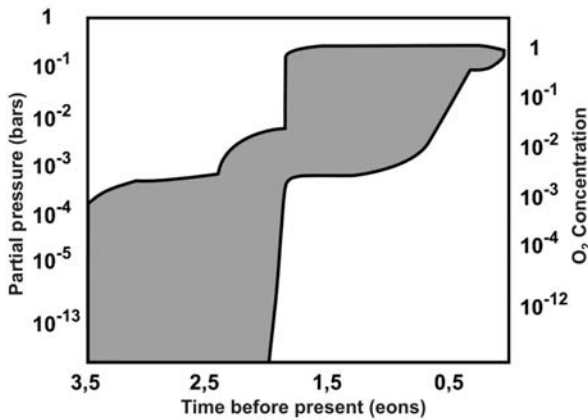


Figure 5.4: Time evolution of atmospheric oxygen.

The pattern and timing of the rise in complex multicellular life in response to the oxygen increases has not been established. Hedges *et al.*(2004) suggest that mitochondria and organisms with more than 2-3 cells types appeared soon after the initial increase in oxygen levels at 2300 Ma. The addition of plastids at 1500 Ma, allowing eukaryotes to produce oxygen preceded the major rise in complexity.

5.3.2 Early UV Surface Fluxes and the Origin of Life

It is relevant to ask how strong the UV surface fluxes were at these early times and what their influence was on the early stages of the evolution of life.

García Pichel (1998) considers three main phases in the evolution of UV radiation at the Earth's surface (Figure 5.5).

- a) High environmental fluxes of UV-C and UV-B restricting protocyanobacteria to refuges, coinciding with the period of heavy bombardment from interplanetary debris.
- b) The appearance of true oxygen cyanobacteria, producing a compound called scytonemin, which screens out the UV radiation but allows through the visible radiation, essential for the photosynthesis, and
- c) Gradual oxygenation and the formation of the ozone shield.

Louis Pasteur (1822–1893) clearly showed that the spontaneous generation of life is not possible in our days, but such a process necessarily took place in the early history of the Earth. In a letter to the botanist Joseph Hooker, Charles Darwin (1809–1882) first expressed some thoughts about this problem: *It is often said that all the conditions for the first production of a living organism are now present, which could ever have been present. But if (and oh! what a big if!) we could conceive in some warm little pond, with all sorts of ammonia and phosphoric salts, light, heat, electricity etc. present, that a protein compound was chemically formed ready to undergo still more complex changes, at the present day such matter*

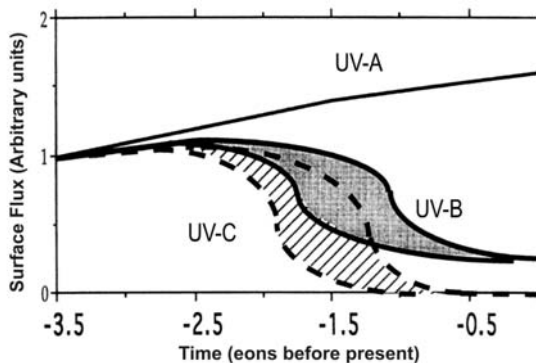


Figure 5.5: Time variation of the UV radiation reaching the terrestrial surface. The scale is in relative arbitrary units of energy normalized to 1 at 3500 Ma before present. Courtesy: F. García Pichel, Dept. of Microbiology, Arizona State University

should be instantly devoured or absorbed, which would not have been the case before living structures were formed.

A. Oparin (1884–1980) first suggested that the organic molecules needed for primitive life were formed in an atmosphere dominated by methane. J.B.S. Haldane (1892–1962) independently proposed the existence of a prebiotic soup in the oceans (Haldane 1954) and suggested that subjecting a mixture of water, carbon dioxide and ammonia to UV light should produce a variety of organic substances. Garrison *et al.* (1951) first attempted to synthesize prebiotic substances by applying high-energy particles supposed to mimic cosmic rays or radioactivity. However, the yields obtained were very small. The first successful laboratory experiments of prebiotic synthesis were carried by Miller (1953), who exposed a mixture of methane, ammonia, hydrogen and water to electric discharges. After a week he identified four natural aminoacids (glycine, alanine, aspartic acid and glutamic acid) together with some other organic molecules. Further simulations showed that it is possible to form purines and pyrimidines with a yield of 30–50% in evaporating lagoons or pools near beaches (Robertson & Miller 1995).

Dauvillier (1947) was one of the first in suggesting UV radiation as an energy source for the synthesis of organic matter. Ponamperuma *et al.* (1963) attempted the synthesis of nucleoside phosphates⁷ by irradiation with UV light dilute solutions of organic compounds. Their results indicated that adenosine triphosphate (ATP) and other nucleoside phosphates can be formed under primitive Earth conditions⁸. In the words of Sagan & Khare (1971), “the

⁷A sugar-base compound that is a nucleotide precursor. Nucleotides are nucleoside phosphates.

⁸ATP is an energy-carrying molecule found in the cells of all living things. ATP captures chemical energy obtained from the breakdown of food molecules and releases it to fuel other cellular processes. This molecule is composed of three components. At the centre is a sugar molecule, ribose (the same sugar that forms the basis of DNA). Attached to one side of this is a base (a group consisting of linked rings of carbon and nitrogen atoms); in this case the base is

availability of the ultraviolet solar radiation was some 100 times greater than of all the others". Garzón & Garzón (2001) have studied the contribution of radioactivity to prebiotic synthesis, finding that at a depth of 30 km the total energy is equivalent to the solar EUV. Table 5.2 compares the various energy sources available in the primitive Earth (GV82 (Gaustad & Vogel 1982); CS95 (Chyba & Sagan 1997)).

Table 5.2: Energy sources (joules per year) in the primitive Earth and in contemporary times. GV82 (Gaustad & Vogel 1982); CS95 (Chyba & Sagan 1997)

Energy source	GV82	CS97	Contemporary GV82
Total solar radiation	2.80×10^{24}		5.64×10^{24}
Solar UV	$10^{21}\text{--}10^{23}$	1.0×10^{22}	2.98×10^{19}
Radioactivity	10^{21}		3.20×10^{20}
Volcanic	$> 0.32 \times 10^{19}$		0.32×10^{19}
Electric discharges	8.50×10^{19}	1.0×10^{18}	8.50×10^{19}
Impacts		1.0×10^{17}	

Table 5.3 summarizes the different efficiencies in producing organic matter, both for a reducing atmosphere (rich in CH₄) and for a more neutral one (rich in CO₂), using different energy sources (Chyba & Sagan 1992,1997).

Given a period of 300 million years for the prebiotic processes, UV radiation could produce 9.0×10^{16} kg of organic matter (for a CO₂ atmosphere). Assuming that a third of the radiation could have been absorbed in the atmosphere, that could leave 3.0×10^{16} kg. Given a total oceanic volume similar to that of the present (1.4×10^{24} cm³), this would give a concentration of 2.1×10^{-5} grammes per cubic centimetre. Whether this was enough for the origin of life or whether an external supply of organic matter (e.g. by comets) was needed is still an open question. This information is complemented by the calculations of Ehrenfreud *et al.* (2002) concerning the major sources of prebiotic organic compounds on the early Earth (Table 5.4).

Sekine *et al.* (2003) have considered a process of organic synthesis induced by asteroid impacts delivering $10^{12}\text{--}10^{13}$ kg of methane and $10^{10}\text{--}10^{12}$ kg of HCN. This is $10^3\text{--}10^4$ times the inventory of HCN maintained by UV radiation and

adenine. The other side of the sugar is attached to a string of phosphate groups.

Table 5.3: Efficiency in the production of organic matter.R(reducing atmosphere); N(neutral atmosphere).

Source	Efficiency		Production	
	(kg/J) R	(kg/J) N	(kg/year) R	(kg/year) N
Electric discharges	3.0×10^{-9}	3.0×10^{-11}	3.0×10^9	3.0×10^7
UV Radiation	2.0×10^{-11}	5.0×10^{-14}	2.0×10^{11}	3.0×10^8
Impacts			2.0×10^8	2.0×10^8

Table 5.4: Major sources (Kg yr^{-1}) of prebiotic organic compounds on the Early Earth. IDP:Interplanetary dust particles. Source: Ehrenfreud *et al.* (2002)

Terrestrial sources	
UV Radiation	3×10^8
Electric discharges	3×10^7
Shocks from impacts	4×10^2
Hydrothermal vents	1×10^8
Extraterrestrial sources	
IDP	2×10^8
Comets	3×10^{11}

electric discharges in a mildly reducing (CO , CO_2) atmosphere.

Tables 5.5 and 5.6 compare the levels of UV flux density and biological DNA irradiance on the early and present Earth (Cockell 1998).

Table 5.5: Integrated levels (in W m^{-2}) in the three UV ranges. From Cockell (1998).

UV range	Present Earth	Early Earth
UVC (200–280 nm)	0	3.1
UVB (280–315 nm)	3.7	11.7
UVA (315–400 nm)	71.3	56.3

Table 5.6: Percentage of biologically effective irradiance received by DNA

UV range	Present Earth (%)	Early Earth (%)
UVC (200–280 nm)	0	66.7
UVB (280 - 315 nm)	97.1	33.2
UVA (315–400 nm)	2.8	0.1

In principle it is a paradox how the molecule responsible for the replication of information has such a large absorption in the damaging UV spectral range. Sagan & Chyba (1997) proposed the existence of strong absorption by organics present in the primitive atmosphere. Calculations by Cockell (2001) seem to confirm this possibility if the concentration of organics reaches critical levels (see Table 5.7). Another factor to consider is the length of the day. At 3–2.5 Ga ago, it may have been 14 hours. Therefore, although the instantaneous DNA-weighted irradiance would have been over three orders of magnitude higher than today, the daily weighted flux would have been only 500 times greater (Cockell 1999).

Table 5.7: Weighted irradiances for various atmospheric scenarios. From Cockell (2001)

Atmosphere	DNA-weighted irradiance	Photosystem inhibition
Present value	0.071	17.5
1 bar CO ₂ , 0.8 bar N ₂ (~ 3.5 Ga ago)	54.1	16.3
40 mb CO ₂ , 0.8 bar N ₂	101	26.3
Organic haze ($\tau = 7$)	0.034	0.013

Apart from external protections, we may think also of an internal mechanism. Sagan (1973) suggested the existence of a protecting layer of purines and pyrimidines surrounding the primitive organisms. Cockell & Airo (2002) investigated the existence of a UV transparent biochemistry to compensate for damaging effects, with tryptophan as the best candidate because of its absorption properties (see Figure 5.6).

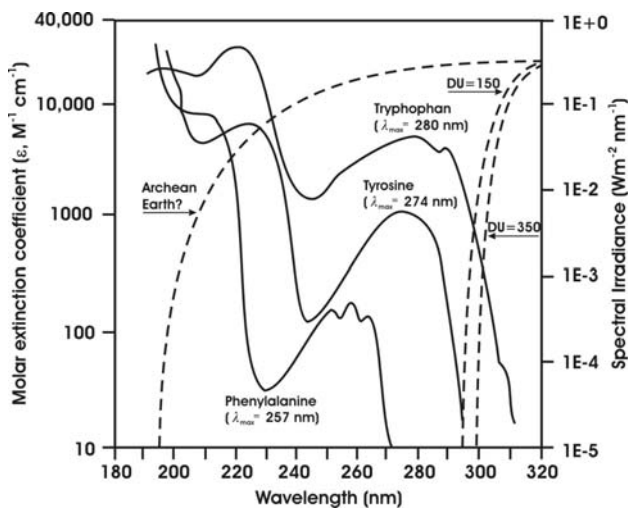


Figure 5.6: Absorption spectra of three aromatic acids. Also shown are the spectral irradiances for three atmospheric irradiances. Adapted from Cockell & Airo (2002).

García Pichel (1998) distinguish three different types of cyanobacteria habitats at early times with respect to UV exposure: a) terrestrial (rock, soil) offering new refuges to UV and where diffuse UV radiation might play a significant role; b) planktonic, where exposure is determined by the interplay of the optical (absorption) and hydrodynamical (mixing) properties of water masses, and where refuges are found in deep layers; and c) sedimentary⁹, where multiple light scattering might produce UV light trapping.

Mulkidjanian *et al.* (2003) have recently suggested that a key event in the

⁹Here the cyanobacteria were immersed in a matrix of solid particles.

origin of life, the formation of RNA self-replicating molecules, was brought about by the absorption of UV radiation by the nitrogenous bases of the RNA, in this way protecting the pentose–phosphate backbones of the nucleic acids.

The decrease in UV surface fluxes was essential for the access of living beings to the land and the subsequent evolution of complex life forms. Livio (1999) proposed the existence of a relation between the time necessary to deploy a protective ozone layer, τ_{bio} and the stellar lifetime in the main sequence, τ_* :

$$\tau_{\text{bio}}/\tau_* \approx \tau_*/\tau_s^{1.7}$$

where τ_s is the evolutionary time for the Sun (10^9 years).

5.4 Ozone and UV Fluxes in Planets around Other Stars

Apart from other criteria, we can take into account how the luminosity of a parent star in the UV range might affect the continuous habitability of a planet, an additional constraint to that already mentioned of the existence of liquid water (e.g Kasting *et al.* 1993).

Kasting *et al.* (1997) and Segura *et al.* (2004) have investigated the implications of the UV emitted by stars of different spectral types. Because of the process of ozone production (see chapter 4) F-stars develop stronger ozone layers, partially shielding the planetary surface from the also stronger UV radiation. At the another end of the H–R diagram, K-stars have thinner ozone layers (see Figure 5.7) but also receive less UV radiation. In the middle the G spectral type range, where the Sun is located, are the least suited, at least from this point of view (Figure 5.8). High-O₂ planets orbiting K- and F-stars are both better protected from surface UV radiation than is the modern Earth.

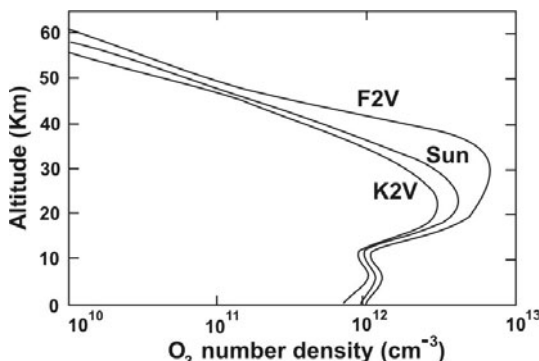


Figure 5.7: Variation with altitude of ozone number densities for a planet with a 1-PAL O₂ atmosphere circling different types of stars: Adapted from Segura *et al.* 2004. Courtesy: J.Kasting, Penn University. Reprinted with permission of Mary Ann Liebert Inc. Publishers.

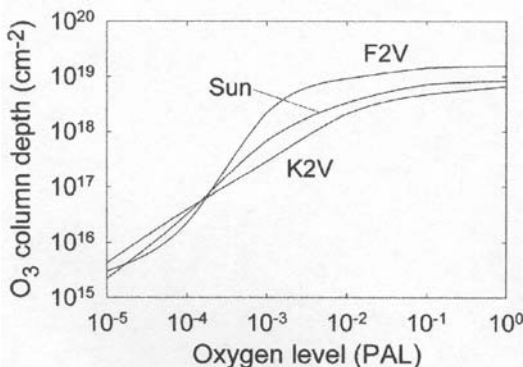


Figure 5.8: Ozone column depth as a function of atmospheric O_2 level for planets circling different types of stars. Adapted from Segura *et al.* 2004. Courtesy: J. Kasting. Reprinted with permission of Mary Ann Liebert Inc. Publishers.

Segura *et al.* 2004 have calculated action spectra for erythema and DNA damage (see Table 5.8). They show the results normalized to a dose rate of unity for Earth at 1 PAL O_2 . For high O_2 levels the atmospheres of K2 V and F2 V planets provide better protection to UV damage. At low O_2 levels, the F2 V planets are the most UV dangerous.

Table 5.8: Normalized surface UV dose rates relative to the present Earth for erythema and DNA damage for planets with different O_2 levels and around different stars. From Segura *et al.* (2004).

Star type	1	10^{-1}	10^{-2}	10^{-3}	10^{-4}	10^{-5}
Erythema						
G2 V (Sun)	1.00	1.32	4.43	23.57	55.11	60.07
K2 V	0.44	0.75	2.27	9.58	13.99	15.33
F2 V	0.68	0.82	1.87	18.88	148.87	164.99
DNA						
G2 V (Sun)	1.00	1.54	10.44	214.13	3688.03	5459.83
K2 V	0.50	1.19	8.39	173.29	813.07	1236.71
F2 V	0.38	0.51	1.85	63.72	16316.62	22651.23

5.5 The Ozone Hole

We have seen how the living beings were not a passive agent in the history of the Earth influencing the composition of our atmosphere. We now change the time-scale dramatically to study how the technological development of Homo Sapiens

can also affect the atmospheric composition, namely the concentration of ozone and the stratosphere, with the subsequent increase of UV fluxes at the Earth's surface. We shall study the physics of the process keeping in mind the primary reactions for ozone production and destruction given in the previous chapter.

As with life processes, industry produces residuals, most of them are emitted into the atmosphere. The history of chlorofluorocarbons (hereafter CFCs) and the Ozone Hole is a good example of how technological development made with the intention of improving the quality of life, can actually become a serious threat for mankind.

Different monographs provide a suitable background to the environmental effects of human activity (Carson 1962; Somerville 1996; Turco 1997 ; McNeill 2000). The problems related with the ozone depletion are explicitly handled in Abbatt & Molina (1993), Benedick (1998); Christie (2000); Middlebrook & Tolbert (2000); Dessler (2000) and particularly in different reports published by International Organizations (WMO 1995; Greenpeace 1997; Harris *et al.* 1998 ; WMO 1999 ; WMO 2002).

5.5.1 The Chlorofluorocarbons

Thomas Midgley (1889–1944) was a brilliant scientist who, at the request of the General Motors Frigidair Division, was involved in problems of refrigeration (see Midgley & Henne 1930). Aided by Charles Kettering (1876–1958) he invented, in 1928, a class of chemicals called CFCs, composed of chlorine, fluorine and carbon.

CFCs are a family of chemical compounds developed as safe, non-toxic, non-flammable alternative to dangerous substances like ammonia for purposes of refrigeration, propellants in aerosol spraycans and as blowing agents for producing polyurethane foams. They are chemically very stable, non-flammable, non-carcinogenic, can be readily converted from a liquid to a gas and viceversa, and are almost insoluble in water. In 1930, the companies General Motors and DuPont formed the Kinetic Chemical Company to produce such products, under the commercial name of Freons. Their usage grew enormously over the years, especially after World War II ¹⁰.

The five main CFCs include CFC-11 (trichlorofluoromethane - CFCl_3), CFC-12 (dichloro-difluoromethane - CF_2Cl_2), CFC-113 (trichloro-trifluoroethane - $\text{C}_2\text{F}_3\text{Cl}_3$), CFC-114 (dichloro-tetrafluoroethane - $\text{C}_2\text{F}_4\text{Cl}_2$) and CFC-115 (chloropentafluoroethane - $\text{C}_2\text{F}_5\text{Cl}$); see also Table 5.9 (Turco 1997).

James Lovelock, the inventor of the most sensitive analytical detector for CFCs—the electron capture detector—sailed into the South Pacific Ocean (1971-72), on the RRS Shackleton, far away from the majority of CFC polluting sources in the northern hemisphere (mainly the United States and Western Europe). In his travels through the marine troposphere he detected CFCs all along the route using his new detector, thereby proving that CFCs that had been released in the

¹⁰The same year that Midgley invented the CFCs, the Nobel Prize winner Robert Millikan (1868–1953) said that there was no risk that humanity could do any real harm to anything so gigantic as the Earth.

Table 5.9: Characteristic parameters of the main chlorofluorocarbons. The atmospheric lifetime (AL) corresponds to the time over which about two-thirds of the matter will be removed from the atmosphere. From Turco (1997).

	Trade name	Emission (10^3 ton/yr)	Atmos. conc. (pptv)	AL (years)
CFC-11 (CFCl_3)	F-11	260	270	76
CFC-12 (CF_2Cl_2)	F-12	450	460	139
CFC-113 ($\text{CFCl}_2\text{CF}_2\text{Cl}$)	F-113	150	65	92

northern hemisphere had evaporated and diffused throughout the well-mixed troposphere (Lovelock 1971; Lovelock & Maggs 1973).

CFCs have a lifetime in the atmosphere of about 20 to 100 years; consequently, one free chlorine atom from a CFC molecule can do a lot of damage, destroying ozone molecules for a long time. They cannot be photolysed in the troposphere, are insoluble in rain and do not react with hydroxyl radicals, cancelling the most important routes which can remove gaseous molecules from the atmosphere.

The atmospheric concentrations of many of those gases that are both ozone-depleting and greenhouse gases are either decreasing (CFC-11, CFC-113, CH_3CCl_3 and CCl_4) or increasing more slowly (CFC-12) in response to reduced emissions under the regulations of the Montreal Protocol and its Amendments. The combined tropospheric abundance of ozone-depleting gases peaked in 1994 and is slowly declining.

The abundances of the hydrochlorofluorocarbons (HCFCs) and hydrofluorocarbons (HFCs), substitutes for CFCs, are increasing as a result of a continuation of earlier uses. For example, the concentration of HFC-23 increased by more than a factor of three between 1978 and 1995.

The perfluorocarbons (PFCs; e.g. CF_4 and C_2F_6) and sulphur hexafluoride (SF_6) are of anthropogenic origin, have extremely long atmospheric residence times, and are strong absorbers of infrared radiation. These compounds, even with relatively small emissions, therefore have the potential to influence climate far into the future. Perfluoromethane (CF_4) is produced as a byproduct of the manufacture of the aluminium and resides in the atmosphere for at least 50 000 years. It has a natural background; however, current anthropogenic emissions exceed natural ones by a factor of 1 000 or more and are responsible for the observed increase. Sulphur hexafluoride (SF_6) is 22 200 times more effective as a greenhouse gas than CO_2 on a per-kg basis. The current atmospheric concentrations are very small (4.2 ppt), but have a significant growth rate of 0.24 ppt/yr (Houghton *et al.* 2001).

Table 5.10 summarizes the different sources of chlorine and shows the dominant anthropogenic origin.

The amount of ozone that is expected to be destroyed by the emissions of a quantity of a gas x over the gas's entire atmospheric lifetime is defined relative to

Table 5.10: Primary sources of chlorine (in percentages) entering the stratosphere in the early 1990s. From World Meteorological Organization (WMO), 1998

Man-made		Natural sources	
CFC-11	23	CH ₃ Cl	15
CFC-12	28	HCl	3
CFC-113	6		
HCFc-22	3		
C Cl ₄	12		
CH ₃ C Cl ₃	10		

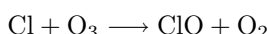
the ozone destruction due to CFC-11 (Solomon & Albritton 1992):

$$\text{ODP}_X = \frac{\text{Time} - \text{integrated global O}_3 \text{ loss due to the gas X}}{\text{Time} - \text{integrated global O}_3 \text{ loss due to CFC} - 11}$$

5.5.2 The Warning and the Measurements

Stolarski & Cicerone (1974) made a study for NASA of the influence on the ozone layer of chlorine releases in the form of hydrochloric acid (H Cl) in the stratosphere by the emission from the rockets of ammonium perchlorate (NH₄ClO₄). However, the amount of material involved in the process was too small to produce measurable depletions.

Some months later¹¹, Molina & Rowland (1974) first warned that some chlorine products released by the human activities would lead to a depletion of the stratospheric ozone layer. The main argument was a set of reactions applied here to the chlorofluorocarbon CFCl₃. Under illumination by the UV solar radiation, at altitudes between 20 and 30 km, the CFCs are decomposed into chlorine atoms (Cl) and chlorine monoxide (ClO).



The ClO can go on to react with the atomic oxygen, O, to release Cl again, closing a catalytic cycle:



The last reaction can also proceed as



In summary, the net reaction is 2O₃ + UV radiation → 3O₂. Because the concentration of oxygen atoms increases with altitude, this cycle is important primarily in the upper and middle stratosphere (García & Solomon 1994).

¹¹In a note added in proof Stolarski & Cicerone mention the paper of Molina & Rowland as recently submitted to the journal Nature

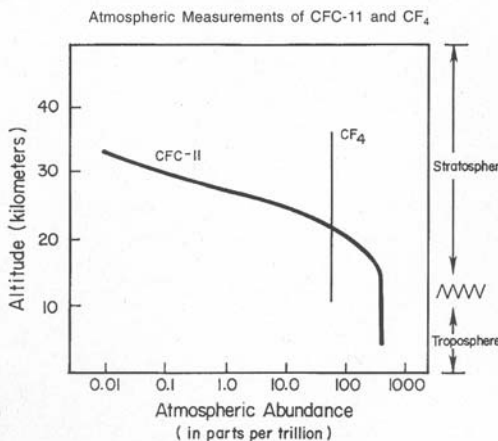
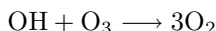
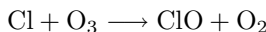


Figure 5.9: Concentration of CFCs vs altitude in the atmosphere.

For lower altitudes other reactions are relevant for the ozone balance; for example,



producing the same net reaction $2\text{O}_3 + \text{Radiation} \longrightarrow 3\text{O}_2$.

Reactions with other atmospheric components prevent all the chlorine remaining in the stratosphere in active form (Cl and ClO). Otherwise, the concentration of these products would be roughly 100 times larger and also the amount of ozone depletion. The empirical proof of these reactions was made by Anderson *et al.* (1989), who analysed ER-2 latitude scans to show a clear anticorrelation between ClO and O₃ concentrations.

CFC molecules are several times heavier than the air. Nevertheless, measurements indicate that they are present in the stratosphere (Figure 5.9). This is because different air motions mix the atmosphere by convection and gravity waves to altitudes above the top of the stratosphere much faster than molecules can settle according to their weight (molecular diffusion).

CFCs are an excellent way of introducing chlorine into the ozone layer. The ultraviolet radiation at this altitude breaks down CFCs, freeing the chlorine. Under the proper conditions, this chlorine has the potential to destroy large amounts of ozone. This has indeed been observed, especially over Antarctica. As a consequence, levels of genetically harmful ultraviolet radiation have increased.

The Antarctic Treaty was negotiated in 1959 by twelve founder nations for the purpose of promoting international peace and scientific cooperation in the

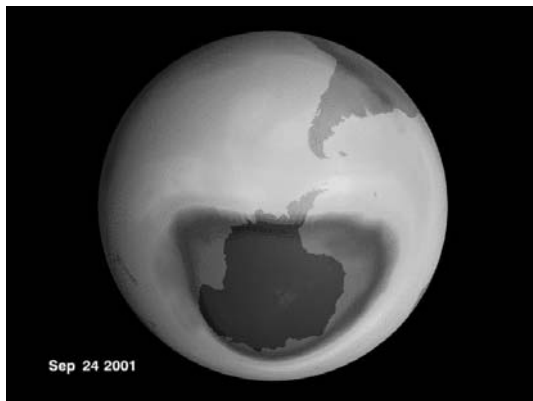


Figure 5.10: The Ozone hole. Courtesy: NASA

region. The Treaty provides the primary legal framework for all decision-making in the area south of 60 degrees latitude. It applies to the land and ice-shelves but does not cover the high seas. There are now 38 member countries of the Treaty. In 1992, a new Environmental Protocol added to the Antarctic Treaty banned the exploitation of minerals in Antarctica for many years. This continent therefore constituted a wonderful laboratory for numerous scientific experiments taking advantage of the location and special physical conditions of the site.

After a first Italian attempt to set up an instrument in the Antarctic, the British Station at Halley Bay (76° S latitude) started the measurements. They soon noticed a different pattern than in the North Pole and accordingly called it “the southern anomaly” (Farman *et al.* 1985). One year earlier Sigern Chubachi presented a poster in a meeting celebrated at Thesaloniki (Greece), announcing anomalous low values at the Syowa station, but without indicating the presence of a new phenomenon (Chubachi 1984).

Nimbus 7 regularly measured the ozone content at this time. However, the checking software rejected low values as erroneous. After the announcement of Farmer’s team, an inspection of the raw data confirmed the existence of values lower than 180 DU. Modern instruments on board satellites now map the evolution of the Antarctic “ozone hole” (Figure 5.10).

Vertical ozone profiles observed with ozonesondes at the South Pole station provide a clear picture of the evolution of the ozone hole as the sun rises over Antarctica during the August–September period (Hofman *et al.* 1986). Figure 5.11 shows a sequence of profiles acquired at the South Pole station in 1994 in which we can see two key features of the ozone hole: 1) the ozone hole is largely confined to the 14–22 km region over Antarctica, and 2) virtually 100% of the ozone is destroyed in this region between early August and late September.

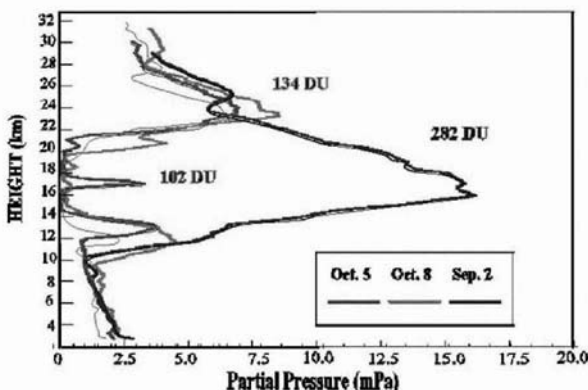


Figure 5.11: Ozone partial pressure (mPa) profiles at the South Pole, measured from balloons. The profile of 2 September 1994, before the yearly depletion, is compared with profiles for 5 and 8 October 1994, during the minimum ozone period. Courtesy: NOAA/CMDL (<http://www.cmdl.noaa.gov>).

5.5.3 The Mechanism of Ozone Depletion at the South Pole

The CFCs are mainly released in the northern hemisphere and spread around the globe, becoming well mixed throughout the troposphere in one year. They enter the stratosphere through the tropical upper troposphere region, drifting to the poles because of Brewer–Dobson circulation. This mechanism, together with some specific chemistry, explains why the largest ozone depletion is found above Antarctica.

Formation of the Stratospheric Polar Vortex

In the previous chapter we described the formation of the Arctic Polar Vortex and its connection with a possible link between solar activity and terrestrial climate. We shall now speak about the situation in the South Pole and some of its peculiarities.

During winter the polar regions experience 24 hours of darkness. There is, therefore no heating by absorption of UV light, but IR thermal emission continues. As consequence, there is a cooling of the low stratosphere. The contrast with the relatively warm mid-latitudes produces a strong pressure gradient, which, associated with the Coriolis forces, creates a zonal E–W wind. The jet stream that sets up at the limiting latitude between dark and illuminated regions is called the polar night jet. The region poleward of the southern polar night jet is known as the Antarctic polar vortex (Figure 5.12), a region of air isolated from the rest of the stratosphere where the long polar night allows extremely cold temperatures to develop (cf. Schoeberl *et al.* 1992).

The degree of isolation is quite different between the Arctic and Antarctic. The cold temperatures and cloud formation are favoured by a stable air-mass formed

over the Antarctica on winter. Moreover, the warming action of the planetary waves is absent in this case.

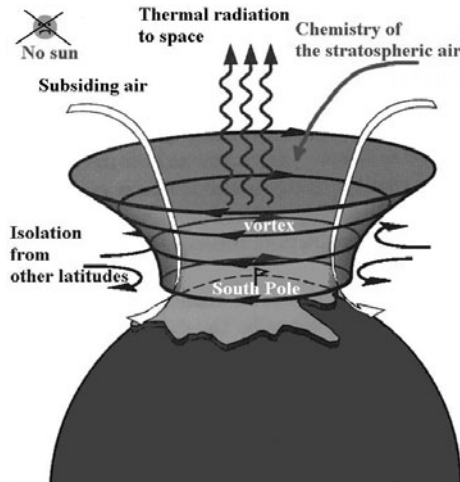


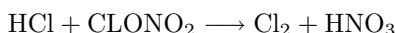
Figure 5.12: The southern polar vortex

Polar Stratospheric Clouds

The cold temperatures of the antarctic winter (< 200 K) produce condensation of water vapour and nitric acid on nuclei which form the polar stratospheric clouds (PSC)¹², first described in scientific terms by Störmer (1929). They are of two types: 1) Type I form at $T \leq 193$ K, about $1\text{ }\mu\text{m}$ in diameter and composed of HNO_3 and H_2O ; and 2) Type II, formed at ≤ 187 K, about $10\text{ }\mu\text{m}$ in diameter and composed mainly by water ice (Hamill *et al.* 1986). These particles are essential for the production of new chemical reactions.

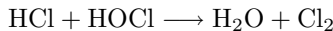
Heterogeneous Chemistry

Polar stratospheric clouds provide solid surfaces on which certain reactions, called heterogeneous¹³, proceed much faster than in the gas phase. The inert chlorine reservoir species HCl and ClONO_2 stick to and react on the PSC ice surfaces (Type I) and are converted into active chlorine gases, Cl and ClO (Solomon *et al.* 1986):

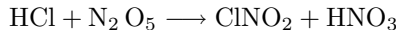


¹²These are related to the nacreous, or mother-of-pearl, clouds

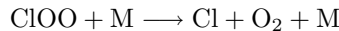
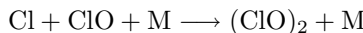
¹³Heterogeneous chemistry occurs on or in condensed particles that are in contact with gaseous molecules.



Moreover, removal of nitrogen oxides occurs in the PSC via the following reactions. The nitric acid formed in these reactions remains in the particles that make up the PSC, thereby increasing the effect:



Other reactions are also particularly strong in Antarctic conditions; for example, the formation and photolysis of ClO are responsible for the 75% of the destruction of ozone in the 13–19 km region (Anderson *et al.* 1991).



Reactions in the PSCs favour the release of Cl and HOCl from the HCl and ClONO₂, whose concentration builds up during the Antarctic winter. In late October (the Antarctica spring) the returning sunlight causes the photolysis of Cl₂ and HOCl:



The rapid release of radicals produces the rapid destruction of the ozone. Later, as the temperatures increase, the above mentioned species (HCl and ClONO₂) again becomes stable, and the ozone starts to recover. The air-masses with poor O₃ concentration tend to move northwards when the polar vortex breaks up. Figure 5.13 summarizes the main processes implicated in ozone depletion.

5.5.4 Bromine

Bromine is less abundant than chlorine in the terrestrial atmosphere (by two orders of magnitude) but is much more ozone destructive (~ 50 times). The natural source of bromine is dominated by methyl bromine (CH₃Br), a by-product of biological activity in the oceans (Khalil *et al.* 1993), and volcanoes (Bobrowski *et al.* 2003). About two-thirds of the bromine (in the form of the halons CBrClF₂ and ClBrF₃) in the stratosphere is anthropogenic in origin (Schauffler *et al.* 1998). The use of these compounds has been phased out since 1996, but their atmospheric concentration is still rising because of their long atmospheric lifetimes.

As with chlorine we can distinguish two different types of reactions.

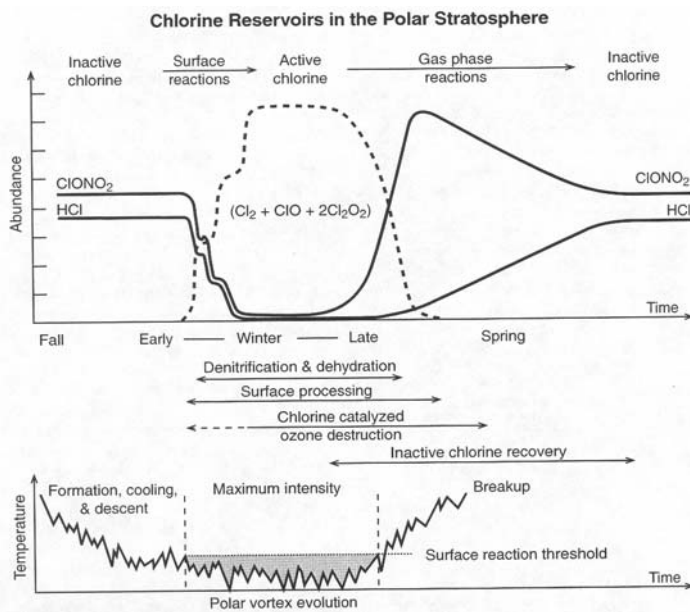


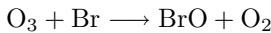
Figure 5.13: Schematic diagram of the chemistry producing the ozone hole. Adapted from WMO Report, 1994

Gas phase

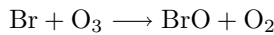
The first step is the photolysis of the organic bromine, liberating atomic bromine,



followed by ozone depletion

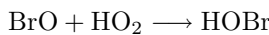


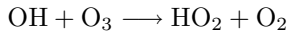
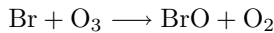
Another important pathway also involves the chlorine cycle



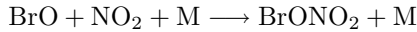
both paths with the net effect $2\text{O}_3 \longrightarrow 3\text{O}_2$

The HOx radicals also interact with the bromine oxides:





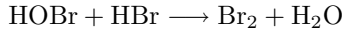
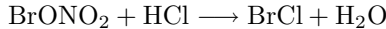
Other reactions contribute to the elimination of the active bromine:



For more details see Wofsy *et al.* (1975); Mc Elroy *et al.* (1986) and Lary (1996).

Heterogeneous chemistry

Laboratory studies show that there exists an analogous cycle for bromine (Lary *et al.* 1996). The main effect of this chemistry is to amplify the chlorine destruction of ozone through the conversion of HCl species into Cl active forms.



Measurements

Wamsley *et al.* (1998) used ground-based trends and stratospheric observations of brominated compounds to describe the bromine loading of the stratosphere. Many of the stratospheric observations were made from the Airborne Chromatograph for Atmospheric Trace Species instrument (ACATS-IV) operated on the NASA ER-2 high-altitude aircraft.

In principle, iodine could play a role similar to that of Cl and Br, but at the moment it is not known whether there is enough of this element in the stratosphere to produce a measurable contribution to the overall ozone balance.

5.5.5 Other anthropogenic mechanisms

Stratospheric flights

Johnston (1992) and Brasseur *et al.* (1996) have studied the contribution of stratospheric aircrafts (SST) to the emissions of NO_x, especially at high altitudes in northern mid-latitudes with the subsequent damaging effects to the ozone layer. The cancellation of most of these projects (e.g. the Tupolev-1444), limited during the last few decades only to a few Concorde planes, has considerably reduced this potential danger (see the IPCC 2001 Report). In any case, British Airways and Air France have recently definitively cancelled these flights. However, new versions of high-speed civil transports are being considered, and their designs should take these effects into account.

Spacecrafts

Each launch of the Space Shuttle produces about 68 tons of HCl, most of which is released in the troposphere. Ten launches per year would amount to less than 0.06% of the yearly chlorofluorocarbons released, which was 1.2 million tons per year in the 1980s (Prather *et al.* 1990).

5.5.6 Natural sources of ozone depletion

The natural cycle of stratospheric ozone has already been described in the previous chapter. Here, we shall study the additional contribution of the chlorine cycle. First, we should remark that very little chlorine exists naturally in the atmosphere. Biological processes releases it mainly in the form of methyl chloride (CH₃Cl).

Volcanic emissions contribute to the depletion of stratospheric ozone by injecting hydrogen chloride (HCl) into the stratosphere. As the eruption cloud of El Chichon was spreading, the amount of HCl in the cloud increased by 40% (Mankin & Coffey 1984). This increase represents about 10% of the global inventory of HCl in the stratosphere. Other large eruptions (Tambora, Krakatoa and Agung) may have released almost ten-times more HCl into the stratosphere than the amount of chlorine commonly present in the stratosphere (Pinto *et al.* 1989). At least two factors reduce the impact of HCl: a) chlorine appears to be preferentially released during low-levels of volcanic activity and may thus be limited to the troposphere, where it can be washed out by rain and b) hydrogen chloride may also condense in the rising volcanic plume, again to be washed out by rain or ice. Lack of HCl in ice cores with high amounts of H₂SO₄ (from large eruptions) may indicate that ambient stratospheric conditions are extremely efficient at removing HCl. A considerable amount of HCl thus never has the opportunity to react with ozone. No increase in stratospheric chlorine was observed during the 1991 eruption of Mt. Pinatubo, although measurements of ozone amounts before and after the eruption show that there were significant decreases in lower stratospheric ozone (Grant *et al.* 1994).

An Antarctic volcano, Mount Erebus, suffered several eruptions from 1976 through 1983, but its impact on stratospheric chlorine levels was minimal (Zreda-

Gostynska 1993). This was surely because the air descends from the stratosphere to the troposphere over Antarctica; also, because the event was not energetic enough.

In total, natural sources contribute 25% of the present amount of chlorine in the stratosphere.

During the late 1950s and early 1960s extensive atmospheric testing of nuclear bombs was carried out. The temperature within the fireball is sufficient to convert N₂ and O₂ into nitrogen oxides, which can reach the stratosphere and participate in the reactions of ozone destruction. However, the available ozone data of this period is too small to verify the significance of this process.

We should also mention the potential influence of the chlorine released in particles from sea spray, some of which leads to gaseous chlorine in the form of HCl. However, its lifetime in the troposphere is very short, since it returns rapidly to the surface by gravitation and precipitation.

5.6 The Montreal Treaty

In 1977, the Coordinating Committee on the Ozone Layer was established by the United Nations Environment Program (UNEP), and UNEP's Governing Council adopted the World Plan of Action on the Ozone Layer. In the late 1970s and early 1980s, action against CFCs was taken by some national governments.

The Vienna Convention for the Protection of the Ozone Layer (March 1985), attended by representatives of 43 nations, outlined the responsibilities of states in protecting human health and the environment against the adverse effects of ozone depletion. They did not, however, impose any obligations upon the signatory nations.

The Montreal Protocol on Substances that Deplete the Ozone Layer was a landmark international agreement designed to protect the stratospheric ozone layer. The treaty was originally signed on 16 September 1987 by 24 nations at the Headquarters of the International Civil Aviation Organization. The Montreal Protocol stipulates that the production and consumption of compounds that deplete ozone in the stratosphere—chlorofluorocarbons (CFCs), halons, carbon tetrachloride and methyl chloroform—are to be phased out by 2000 (2005 for methyl chloroform). For developing countries, the phaseout was set for 2010.

This agreement was made possible not only by the strength of the scientific arguments but also owing to adequate information supplied to society through the media. The World Meteorological Organization (WMO), NASA, NOAA, the United Nations Environment Programme (UNEP) and the European Commission all played decisive roles.

Three years later (June 1990) in London the Montreal Protocol was strengthened in a number of ways, through the agreement of 80 countries. The Amendment called for a ban on damaging products by the year 2000.

Between 23 and 25 November 1992, representatives from more than 100 states gathered in Copenhagen for the Fourth Meeting of the Parties to the Montreal Protocol on Substances that Deplete the Ozone Layer. The Copenhagen gathering

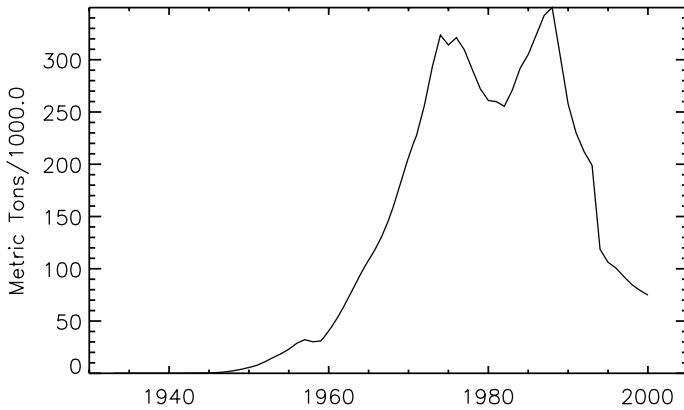


Figure 5.14: Global mean CFC-11 (CFC13) abundances in thousands of metric tonnes. Source of data: McCulloch *et al.* 2001.

was significant not only because the international community had to respond to the continuing deterioration of the Earth's protective layer of stratospheric ozone but also because it was one of the first major international environmental conferences to be held after the June 1992 UN Conference on Environment and Development (UNCED) in Rio de Janeiro. One of the main decisions was to anticipate the ban on damaging ozone products to 1996. The meetings in Cairo (1998) and Beijing (1999) tried to introduce consistently the Montreal Treaty and the Kyoto Protocol (1997) on climate change, due to the greenhouse properties of HFCs and perfluorocarbons, substitutes of the CFCs. The list of states that have ratified the Protocol has now grown to 163. Rowlands (1993), Parson & Greene (1995) Benedick (1998) and the UNEP reports give the background of the political issues related to these meetings.

Today the Treaty has been ratified by more than 160 nations, and the original list of eight controlled substances has been increased to more than 90. Figure 5.14 shows the substantial decline in one of most abundant CFCs as consequence of these treaties (McCulloch *et al.* 2001).

5.7 Time Variation of Stratospheric Ozone

5.7.1 Global Ozone

The stratospheric ozone trends in mid-latitude regions (25° – 60°) show that ozone abundance over recent years was $\approx 4\%$ below its 1979 values. The winter/spring and summer/autumn losses were of the order of 5.5% and 2.8%, respectively (Godin 2001).

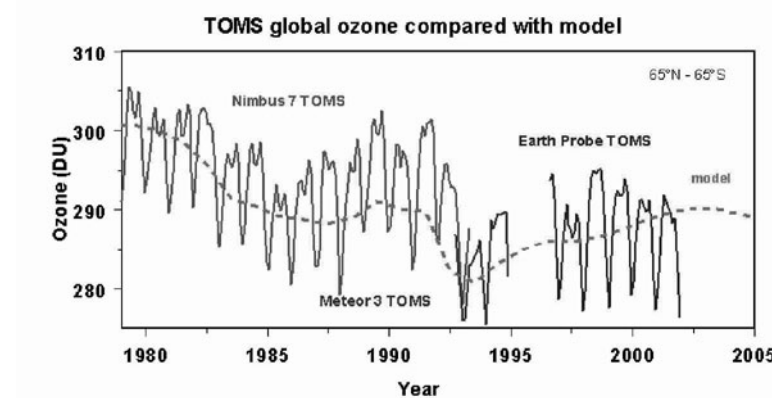


Figure 5.15: TOMS-Derived Global ozone in the latitude range (65°N - 65°S). Data Courtesy of Richard D. Mc Peters, NASA Goddard Space Flight Center.

Figure 5.15 illustrates the time variation of global ozone in the latitude range (65°N - 65°S) and shows a clear decline over that period. However, no significant long-term trend has been observed in the tropics.

Ground-based measurements provide longer coverage of ozone temporal trends. Figure 5.16 shows the results obtained in the Swiss Observatory of Arosa (Staehelin *et al.* 1998).

Using historical observations and model simulations, Shindell & Faluvegi (2002) have estimated a trend in the stratospheric ozone of -7.2 ± 2.3 DU in the interval 1957–1975, mainly attributed to an increase in water vapour at these altitudes driven by the enhancement of greenhouse gases and solar activity. Extrapolation based on proxies give a trend in column ozone of -9 ± 4 DU for the period 1850–1975, confirming that most of the ozone depletion prior to the CFCs action was produced by greenhouse gases.

5.7.2 Polar Ozone Holes

Wuebbles *et al.* (1998) have simulated the preindustrial atmosphere and found that there was over 200% more ozone in the Antarctic in 1880 than observed in 1990.

The area enclosed by the 220 DU contours is a measure of the severity of the ozone hole. Figures 5.17 and 5.18 show the seasonal and temporal evolution respectively of the area occupied by Antarctic ozone hole. Ozone concentrations clearly drop in the southern spring (September to October), recovering their normal values in November, although this recovery has been progressively delayed

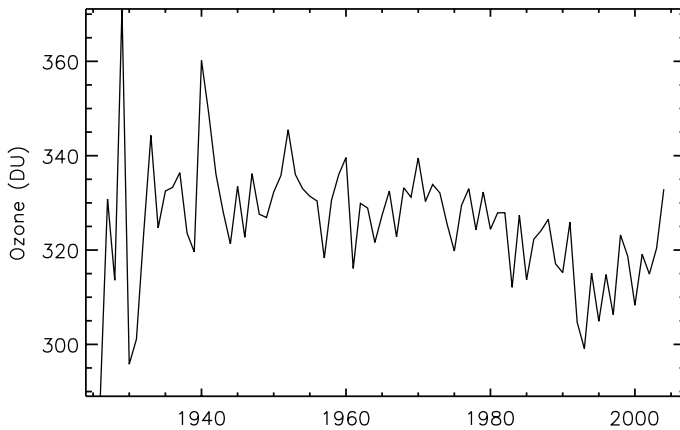


Figure 5.16: Column Ozone measurements in the Arosa Observatory showing a clear decrease in the last part of the past century. Courtesy: Johannes Staehlin.

in recent times. It is not yet possible to say whether the area has reached its maximum extension.

The 2000 ozone hole reached its greatest extent in early September, and the edge of the ozone hole passed over the southern tip of South America for several weeks. In 2002 the Antarctic Hole was split into two sections. The warmer temperatures during those years around the edge of the polar vortex slowed down the CFCs ability to dissociate ozone, and so the ozone molecules that were created have been able to survive. Warmer temperatures also sparked more intense weather patterns that were strong enough to split the one giant hole into two smaller ones.

Manney *et al.* (2003) analysed Microwave Limb Sounder observations during seven Arctic winters. Ozone depletion was observed in the Arctic vortex each year except for 1998, when temperatures were too high. The energy of the planetary waves, only present in the northern hemisphere, warms the stratosphere and suppresses the formation of PSC. Therefore ozone loss in the Arctic is greater when the planetary waves are unusually weak. Ozone loss was more rapid near the vortex edge, the biggest loss occurring in 1993 and 1996 February and March being the most affected months.

Mini–ozone holes are sometimes observed at lower latitudes. Low values (< 220 D.U) were measured over Europe towards end of November 1999. The depleted region was observed on 29 November around Greenland and drifted in two days to the Mediterranean, where on 2 December the ozone layer in this area was rebuilt (Allen & Nakamura, 2002). The role of the phase of the North Atlantic Oscillation in these events should be considered (Orsolini & Limpasuvan 2001).

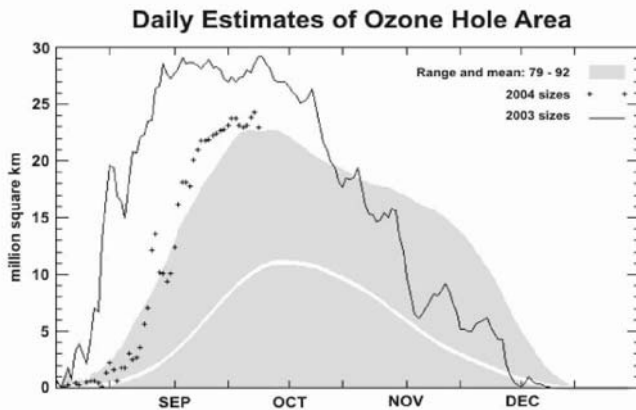


Figure 5.17: Seasonal and daily variation. TOMS-Derived Ozone Hole Areal Size for 2003 and 2004 with 1979–1992 data as Background Average. Courtesy: Ozone Processing Team, NASA/GSFC.

5.8 The Future Evolution of the Ozone Hole

Measurements of hydrogen chloride (HCl) and chlorine nitrate (ClONO_2) total column abundances by Rinsland (2003) show a broad plateau after 1996, and a model based on these records predicts a slow chlorine decline, reaching 12–14% relative to the peak by 2010, thereby confirming the effectiveness of the Montreal Protocol and its Amendments and Adjustments. Figure 5.19 shows the future evolution of ozone-depleting substances according to the different decisions taken at international conferences.

In the absence of other changes, stratospheric ozone abundances should rise in the future as the halogen loading falls in response to regulation. As a first consequence, the ozone layer should be recovered by the middle of the present century. However, future behaviour depends on methane, nitrous oxide (N_2O), water vapour, sulphate aerosol and global warming. Following the international treaties, chemical companies have tried to find suitable replacements for CFCs. The HCCs (Hydro-chloro-fluorocarbons) break up in the troposphere and are therefore not able to inject chlorine into the stratosphere. However, their power as a greenhouse gas is much more important. A recent analysis of the last 20 years of space-based ozone measurements seem to indicate a clear slowing down in the decline of ozone depletion (Newchurch *et al.* 2003).

However, not all the news are optimistic. Levels of methyl chloroform (CH_3CCl_3), originating from buried waste, are still present in the atmosphere over Europe (Krol *et al.* 2003). This substance is scheduled to be phased out by the year 2005.

Another worrying aspect is related to current climate change. The terrestrial troposphere is undergoing a rapid warming, due mainly to the combustion of fossil

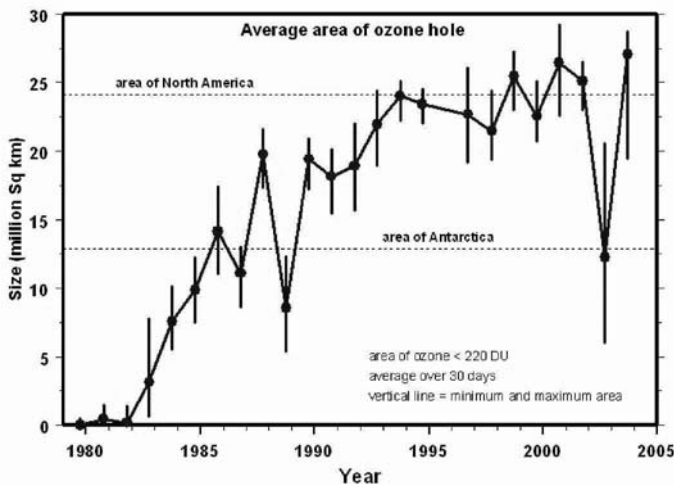


Figure 5.18: Growth in the average area of the ozone hole from 1979 to 2003. The ozone hole was defined as the area for which ozone concentration is less than 220 DU. Courtesy: TOMS/NASA.

fuels, which give rise to the emission of greenhouse gases. This has two important consequences in relation to ozone depletion. The first is stratospheric cooling that could increase ozone depletion through the above described chlorine process. Radiosonde and satellite observations have confirmed this and Langematz *et al.* (2003) estimates the rate of cooling in 2.5 K/decade.

Results from a model by Gillet & Thompson (2003) suggest that as consequence of ozone depletion at the South Pole, the circumpolar westerly winds have increased in strength, according to the observations, and enhanced the isolation of the Antarctic stratospheric flows (the polar vortex).

The situation in the Arctic is, in principle, different from that at the South Pole because of the distinct distribution of land masses and oceans. Arctic ozone depletion is highly variable, but a future Arctic ozone hole similar to that over Antarctica seems unlikely (WMO/UNEP Report, 2002). Shindell *et al.* (1998) suggest that the unusually cold and stable Arctic vortices during early March are caused by a decrease in the poleward propagation of planetary waves, a process driven by the enhanced concentration of greenhouse gases. Rex *et al.* (2004) have recently analysed 2000 balloon measurements over the Arctic during the last 12 years. Based on the relation between ozone loss and PSC, they found that every kelvin of cooling results in an additional ozone destruction of 5%, a sensitivity factor three times larger than that predicted by models.

The present tropospheric warming (stratospheric cooling) may additionally

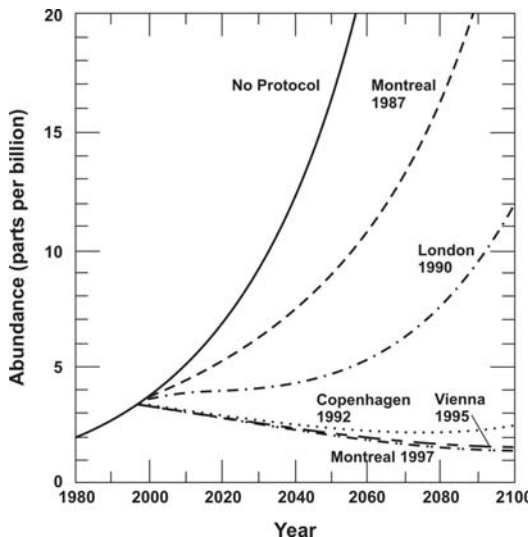


Figure 5.19: Estimated abundance of ozone depleting substances for controls contained in the different international protocols.

influence ozone depletion in the polar regions through changes in the water vapour cycle (Kirk-Davidoff *et al.* 1999; Shindell 2001).

A second important issue is related to a technological solution of the problem. The use of fuel cells that produce energy just by burning hydrogen has been suggested (Ogden 1999). Tromp *et al.* (2003) have recently warned about a possible new danger for the ozone layer. The amount of hydrogen liberated in the process would rise rapidly, reaching the stratosphere, where would react with oxygen to form water. A wetter stratosphere would cool the ambient air, thus introducing a new mechanism for ozone depletion just at the time (≈ 2050), when the action of CFCs would not be longer a problem.

We now study how the UV radiation can affect living beings, especially humans, in our days. Let us start with a little history.

5.9 Health Consequences of UV Radiation

5.9.1 Heliotherapy

As with many other products of nature, including poisons, nothing is absolutely benign or malign for living beings, the benign or lethal effects of a substance depending essentially of the dose. Belief in the healing power of solar light is rooted in early civilization ¹⁴. In fact, after the discovery of UV radiation in the

¹⁴The first report about heliotherapy probably dates from about 1400 B.C. (see Fitzpatrick & Pathak, 1959, J. Invest. Dermatology 31, 229–231). The Greeks coined the term “heliotherapy” in recognition of the Sun’s importance to life.

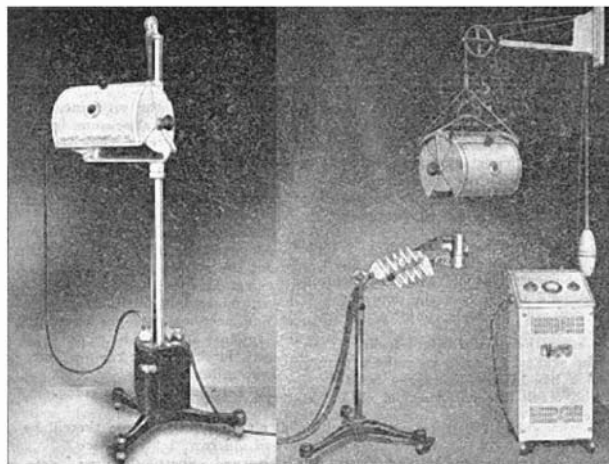


Figure 5.20: Equipment used for UV heliotherapy around the year 1925.

nineteenth century therapeutic effects were attributed to what at the time were called chemical rays, especially for diseases related with the skin.

Niels R. Finsen (1860–1904) pioneered this field. Affected by a degenerative illness he spent a great part of his life almost as an invalid. Probably for this reason he was interested in medicine and especially in the health benefits he could receive from the Sun. From laboratory experiments he found that if irradiation with chemical rays is too strong tissue damage is produced, and that this could be prevented by the pigmentation of the skin. However, by applying the rays concentrated, in a particular area of the skin he obtained benefits in the treatment of lupus vulgaris and other skin diseases. Finsen used two methods: the first consisted in passing sunlight through a large biconvex lens filled with a copper sulphate solution to absorb the “heat rays” while allowing the transmission of the UV light; a second procedure was based on his own design of a carbon–arc apparatus, but this was very large and expensive and was later replaced by a lamp of mercury vapour, small and relatively cheap¹⁵.

Following Finsen’s suggestion, UV treatment was applied for the tuberculosis and several centres were built in places with high levels of “chemical rays”, as the Swiss Alps. Finsen received the 1903 Nobel Prize in Physiology and Medicine for his method of treating skin disease, especially lupus tuberculosis, with ultraviolet light. The Nobel award coincided with others related to the physical properties of high-energy radiation (Röntgen, 1901; Pierre and Marie Curie, 1903).

Another exponent of sunbathing was Auguste Rollier (1874–1954), who in 1903 opened the Institute of Heliotherapy at Leysin, Switzerland. For a period of time just after World War I, 1 746 of the 2 167 tubercular patients under Rollier’s care completely recovered their health. His experience is described in the book “La

¹⁵Finsen, N.R., 1899, Über die Bedeutung der chemischen Strahlen des Lichtes für Medicin und Biologie, Vogel, Leipzig.

Cure de Soleil” .

Finsen’s experiments were followed by those of Axel Reyn (1872–1935) and Ove Strandberg, who extended the light treatment to the whole human body by shortening the water– cooled telescope that focused the light, thereby rendering it suitable for individual use. During the first decades of the twentieth century, therapeutic sunbathing was a widely prescribed treatment for many diseases (see Albert & Ostheimer 2002; Roelandts 2002). The discovery of penicillin in 1938 decreased interest in the healing effects of the Sun.

In fact, for many vertebrates, exposure of the skin to the UV–B radiation results in the synthesis of vitamin D₃, required for calcium deposition in bones (cf. Webb & Holick 1988). Illness due to a deficit in this vitamin, rickets¹⁶, was already described by Daniel Whistler and Francis Glisson (1597–1677) in the seventeenth century. In 1921, Edward Mellanby (1884–1965) was experimenting with dogs living exclusively indoors and noticed the need to add a trace component to the diet, the product became known after that as vitamin D (Mellanby & Cantag 1919). Several experiments followed (Hess 1922; Goldblatt & Soames 1923) that clearly established that “ultraviolet light equals vitamin D”. The adult form of rickets, osteomalacia, has been strongly reduced in recent times due to the amount of vitamins contained in food.

Skin production of vitamin D by the action of UV light decreases with age, the decline beginning in the third decade (Holick *et al.* 1989) . Moreover, the amount of naturally synthesized vitamin varies with degree of skin pigmentation, season, latitude, time of day, atmospheric conditions and duration of exposure. It is also interesting to note that the chronic use of sunscreen can reduce vitamin D levels (Matsuoka *et al.* 1988) . Bodiwala *et al.* (2003, 2004) presented statistical evidence that exposure to UV radiation is associated with a reduced risk of prostate cancer.

5.9.2 Damaging Effects of the UV Radiation

Downes & Blunt (1877) first showed that bacteria were killed by sunlight, but the lethal effect was attributed to heat, although it was mentioned that the actinic rays could play a role. In 1910, P. Becquerel (1879–1955), a plant physiologist, exposed a dried sample of fungi, bacteria and other microbes to UV light, and verified their extinction in a short period of time. Gates (1928) showed that the bactericidal action of UV on *Staphylococcus* cells closely matched the absorption spectra of nucleotide bases. These discoveries marked the beginning of the bactericidal application of the UV radiation, nowadays widely used for sanitary purposes. This effectiveness is wavelength-dependent, with a maximum at 260 nm, resembling the absorption curve for nucleic acids. For this reason low-pressure mercury lamps, which have maximum efficiency in this spectral range, are mainly used for these purposes.

Before the availability of drugs to cure tubercular infections, a popular treatment for non-pulmonary tuberculosis (glands, bones, etc) was sunbathing. This was based on the killing action on the Tubercular Bacillus, apart from the above

¹⁶The name rickets is from the Old English wricken, to twist. The medical term for this illness is rachitis.

mentioned effect on vitamin D. Other medical applications of UV light include sterilization of human blood (photoluminescence) and treatment of psoriasis and infant jaundice. At the times, there was no reason to suspect any particular danger to the humans from unseen rays. Thomas Alva Edison (1847–1931) was one of the first to warn of their potential threat to health. Most of the precautions involved the placement of some kind of material between the radiating sources and the humans. Particularly damaging was the application of X-rays in medicine after the development of the X-ray tube by W.D. Coodridge (1873–1975). A generation of doctors suffered serious injuries.

However, the damaging effects are much more important and gradually became known when the biological research progressed and cell biochemical principles were investigated. In the first section of this chapter we have described the basic process of the action of ionizing radiation on DNA. It is generally considered that cyclobutane pyrimidine dimers and pyrimidone photoproducts are the most important premutational DNA lesions induced by UV radiation (Wood *et al.* 1984).

5.9.3 Resistance to UV Radiation

When bacteria are exposed to a lethal agent, such as UV radiation, the survival¹⁷ ratio is expressed by

$$S = N/N_0 = e^{-kIt}$$

where N_0 is the number of bacteria initially present, N the number surviving at time t (the exposure time expressed in hours), I the intensity of the lethal agent (in W/m^2) and k a constant characteristic of the process.

Fluence, or radiation dose, is the product of the solar intensity (I) and exposure time ($F = I t$). Summarizing, as percentage we have

$$S = 100e^{-kF}$$

Microorganisms have developed different systems to repair DNA damage, such as photoreactivation, excision, and repair. We have already commented on how primitive organisms could develop mechanisms to survive under strong UV exposure. In our times, the most spectacular example is the bacterium *Deinococcus radiodurans*, discovered in the 1950s by Arthur Anderson at Oregon Agricultural Experimental Station. The bacteria are able to survive 3 000 times the lethal dose of radiation for humans. Its genetic code repeats itself many times so that damage can be recognized and quickly repaired. It is believed to be 2 billion years old, dating from a time when the radiation environment was much more intense than at present. In 1999 however a team headed by Owen White published the complete genomic sequence of *Deinococcus radiodurans*, which turned out to be very close to the DNA of the thermophilic *Thermus Themophilus*, suggesting a recent modification from resistance to heat to resistance to radiation (White *et*

¹⁷The test of whether a bacteria has been killed is its ability to reproduce itself and form colonies, when placed in a suitable medium.

al. 1999; Makarova *et al.* 1999). It has been also suggested that UV resistance is a result of desiccation selection pressure (Mattimore & Battista 1996). In fact, cellular damage caused by dehydration and radiation are very similar¹⁸.

5.9.4 Coral Bleaching

Coral bleaching is the whitening of coral colonies caused by the loss of symbiotic zoonxanthellae from the tissues of polyps, which exposes the white calcium carbonate skeletons of the colony (see Mac Munn (2003)). Experiments have shown that an increase in UV light causes coral bleaching (Gleason & Wellington 1993, with increasing temperature acting as a second factor (Lesser *et al.* 1990; Lyons *et al.* 1998; Hoegh-Guldberg 1999). However, some bleaching may actually be an infectious disease spread by microbes, called Vibrio shiloi, which are more virulent at higher temperatures (Kushmaro *et al.* 1996; Rosenberg & Falkovitz 2004).

5.9.5 UV Damaging Effects on Plants

The leaves of plants must be directly exposed to the sunlight for their photosynthetic activities to occur and are therefore subjected to its damaging effects. Photosynthetically Active Radiation (PAR) is related to the absorbed UV-B (Rozema *et al.* 2002). Engelsen *et al.* (2004) reconstructed UV and PAR doses at a north Norwegian station in spring on the basis of total ozone and cloud cover data. Action spectra for plants are given in Green *et al.* (1974) and Coohill (1989).

Exposed to UV radiation aquatic organisms suffer reduced growth, their motility and orientation being affected. Marine plankton populating the top two meters of ocean water is deeply affected by increasing levels of UV-B. A possible defense is to sink deeper into the water, but this reduces the amount of visible light needed for photosynthesis. Many algae living in surface waters are also sensitive to UV radiation and change in their population can affect the food supplies for fish.

Ries *et al.* (2000) have reported that UV damage on plants seems to affect future generations. If true, this would produce a temporal extension of the damage produced by the ozone hole beyond its own lifetime.

An interesting secondary effect on climate of UV damage to aquatic plankton is related to the production of dimethylsulphide (DMS) aerosols¹⁹ (see Charlson *et al.* 1987). In principle, the UV increase resulting from ozone depletion, should produce less aerosols, in this way contributing to the enhancement of the present global warming of the planet (Kniveton *et al.* 2003). However, the anthropogenic emission of aerosols is clearly dominant at the present time.

¹⁸Experiments have also shown a strong resistance of Halobacterium to normally lethal doses of UV radiation. These microorganisms are found in water saturated with salt, and its genome contains a wide variety of DNA-repair mechanisms.

¹⁹These aerosols contribute to the cooling of the atmosphere by reflecting sunlight back into space.

5.9.6 Damaging Effects of UV Radiation on Humans

Evidence that ultraviolet radiation could be harmful to health came from scientists working with arc lamps (Foucault & Foucault 1843; Burge 1916). Various effects began to be reported (see Diffey 1991 and Hockberger 2002 for a complete review). The dermatologist Paul G. Unna (1850–1929) was the first to associate UV exposure and precancerous skin changes seen in sailors (Unna 1894); this work was further verified by subsequent epidemiological studies (Hyde 1906). The set of papers by Albert & Ostheimer (2002, 2003 a,b) provide an excellent summary of the evolution of medical and popular attitudes towards UV light exposure.

Jan van der Leun began, in 1956, to irradiate human skin with different light sources. He found that the clearest effect was a reddening after a couple of hours (erythema, more commonly called “sunburn”). The light triggers the production of substances that diffuse in the dermis below, dilating the blood vessels.

Figure 5.21 shows the action spectra for bacteria and mammals in the UV range (Coohill 1996). The close agreement with the absorption spectra for DNA is remarkable. The CIE (1987) erythemal action spectrum for humans has been employed for assessing the UV effect on human skin²⁰. The IRPA (1989) actinic action spectrum has been employed for assessing the UV effects on both human skin and eye²¹.

A second consequence of UV exposure is skin tanning caused by the migration of melanin, a dark biological pigment found in the skin and formed as an end-product during the metabolism of the amino acid tyrosine. Tanning of the skin is mediated by a combination of intermediate pigment darkening (IPD) caused by UV-A, and delayed pigment darkening (DPD), produced with either UV-A and UV-B.

Overly damaged cells will normally self-destruct through a process called apoptosis, and if this does not work, the immune system should get rid of any resulting aberrant cells.

The effect depends on the different skin types²² as summarized in Table 5.11. Non-melanoma skin cancer (also called basal-cell carcinomas or squamous cell cancers²³) are clearly related to the UV exposures and are found primarily in unexposed areas such as the head and neck²⁴. The second group of skin cancers comprises the melanoma cancers, which start in the melanocytes, cells that produce melanin. Melanoma tumors appear as brown or black spots. They are less

²⁰CIE (International Commission on Illumination), Research Note 1987, “A reference action spectrum for ultraviolet induced erythema in human skin”, CIE Journal 6, 17-22 (CIE Pub. 106/4). In short, the values are: 1.0 in the wavelength range [250–298]; $10^{0.094(298-\lambda)}$ for [298–328] and $10^{0.015(139-\lambda)}$ for values in the interval [328–400], where the wavelength, λ , is expressed in nanometres.

²¹IRPA (International Radiation Protection Association, 1989, “Proposed change to the IRPA 1985 guidelines on limits of exposure to ultraviolet radiation”, Health Physics 56, 971-972.

²²Skin colour is owed primarily to the presence of a pigment called melanin. Both light and dark complexioned people have this pigment. However, two forms are produced—pheomelanin, which is red to yellow in color, and eumelanin, which is dark brown to black.

²³Basal cells, small round cells found in the lower part of the epidermis, the outer layer of the human skin.

²⁴These forms are rarely lethal but surgical treatment is painful and often disfiguring.

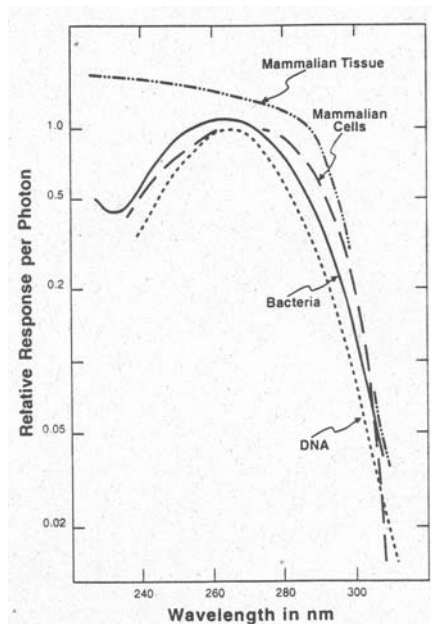


Figure 5.21: Action spectra for bacterial and mammalian cell killing, and mammalian tissue necrosis. For comparison purposes the DNA absorption spectrum is included. Adapted from Coohill (1996).

common than non-melanoma cancers, but much more serious and are likely to spread, or metastasize, to other parts of the body. In contrary to the first type, melanoma incidence seems not to follow a pattern of increased risk with cumulative UV radiation.

UNEP (United Nations Environment Programme) has estimated that more than two million non-melanoma skin cancers and 200 000 malignant melanomas occur globally each year. Skin cancer is clearly a function of latitude, in other words available sunshine. People born in Europe and who migrate to sunnier countries (such as Australia or New Zealand) after childhood have an increased risk of developing melanoma than people of European descent born in these countries (Lee 1989). Two out of three Australians develop some form of skin cancer in their lifetime (Giles *et al.* 1988). However, arrival during childhood results in a comparable risk (Holman *et al.* 1986)²⁵. UV carcinogenesis seem to be amplified by increasing temperatures, a feature of current global warming (Van der Leun & De Gruyl 2002).

Table 5.12 indicates the doses required to produce biological effects for different types of skin (Guy *et al.* 2003).

²⁵Norman Paul commented on 1918: "The common occurrence of these cancerous and precancerous diseases of the skin in Australia is one of the penalties to be paid for inhabiting a country normally destined [in geographical location] to be occupied by a colored race".

Table 5.11: Sun-reactive skin types. IPD stands for Immediate Pigment Darkening.

Skin type	Skin reaction	Examples
I	Always burns easily and severely, tans little and peels	Fair skin, blue eyes, freckles
II	Usually burns easily and severely, tans slightly, peels	Fair skin, red or blond hair blue or even brown eyes
III	Burns moderately and tans about average	Normal average Caucasian Unexposed skin is white
IV	Burns minimally, tans easily and above average IPD reaction	White or light brown skin dark or dark/brown eyes
V	Rarely burns, tans easily IPD reaction	Brown skin
VI	Never burns and tans profusely IPD reaction	Black skin

Table 5.12: Dose (J/m^2) required to induce minimal, marked and painful erythema for different types of skin. From Guy et al. (2003).

Skin Type	Minimal	Marked	Painful
I	150	450	750
II	200	600	1000
III	300	900	1500
IV	400	1200	2000

UV-A photons penetrate deeper into the skin than UV-B, but cellular changes occur slowly although they accumulate with time. UV-A radiation induces the formation of free radicals, which in turn attack the lipids in the skin. The resulting damage gives rise to visible signs of aging such as wrinkles and thickened skin. The natural defenses of the skin against these free radicals are ascorbic acid (vitamin C) and alpha-tocopherol (vitamin E).

Acute effects of UV on the eye, were detected early on producing the development of photokeratitis and photoconjunctivitis²⁶ (Van der Hoeve 1920). However, these problems are reversible and preventable, which is not the case with other chronic effects, such as the development of pterygium²⁷, squamous cell cancer of the conjunctiva and cataracts. A 1% sustained decrease in stratospheric ozone would result in an increase of 0.5% in the number of cataracts. UV also affects the eyes of rabbits, mice, beavers and other animals.

Photoaging of the skin is manifested by dryness, deep wrinkles, loss of elasticity

²⁶Acute inflammation of the cornea and conjunctiva as in “welders flash”.

²⁷Pathology of the cornea. It is a tissue growth that can block vision.

and mottled pigmentation and is produced both by UV-B and UV-A.

UV-B, and possibly UV-A, suppresses the immune responses and contributes to the development of skin tumors (De Favo & Noonan, 1983; Ichihashi *et al.* 2003). These authors also discuss the role of antioxidants (e.g. polyphenols and vitamins C and E) to prevent UV-induced skin cancer.

According to the WHO (World Health Organization), a number of studies indicate that UV exposure at environmental levels suppresses immune responses in both rodents and humans. In rodents, this immune suppression results in enhanced susceptibility to certain infectious skin-related diseases, and some systemic infections. Mechanisms associated with UV-induced immunosuppression and host defense mechanisms that provide for protection against infectious agents are similar in rodents and humans. It is therefore reasonable to assume that exposure to UV may enhance the risk of infection in humans, but additional research is necessary to substantiate this (see Garssen & Van Loveren 2001).

Supplementary information about UV influences can be obtained in the monographs by Harm (1980), Urbach & Gauge (1986) and Urbach (1992).

5.9.7 The Biological Consequences of the Ozone Hole

The weakening of the ozone layer is worrying because of its effect on living beings. From the existence of the ozone hole we may expect an increase in UV radiation over Antarctica (see Figure 5.22). However, no significant damage has been reported in areas outside the polar vortex region, such as Punta Arenas (Chile) or Argentina (Micheletti & Piacentini 2002), although the effects probably have a long-term component (see also Schein *et al.* 1995).

The existence of differences in the UV surface flux between Europe and New Zealand are obscured owing to differences in the position of the perihelion, which influences the summer sunshine, concentration of aerosols and the amount of tropospheric pollution (Mc Kenzie *et al.* 2003).

Changes in the duration and area of the ozone hole are more important for surface UV levels than the annual ozone minimum (WMO/UNEP 2002).

A survey of Antarctic phytoplankton has been carried out by Smith *et al.* (1992), who found a 6–12 % drop in productivity in the area of the spring-time ozone hole. This clearly affects the food-chain formed by krills, seals, penguins and whales.

The microbes react to increased levels of UV radiation in Antarctica. The cyanobacterias produce a suite of colourless compounds, that absorb UV radiation, called mycosporine-like aminoacids (MAASs), although little is known about how these substances have evolved. For more details see Tevini (1993).

5.9.8 Technological Solutions to the Ozone Hole

Improvements in the reduction of damaging substances would be intensified yet further. Moreover, we have the possibility of planning of planetary engineering. One obvious solution is to fill the hole with ozone, but this is completely impractical on a mass basis.

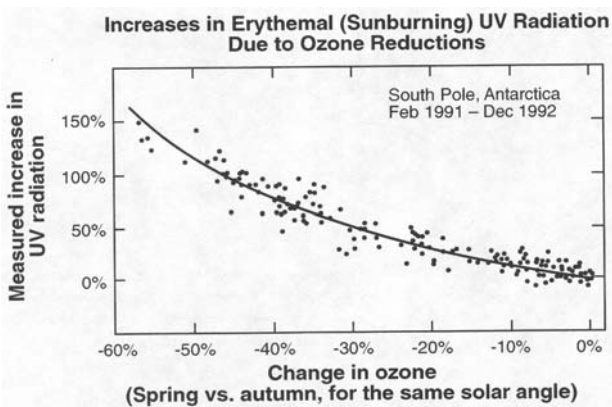
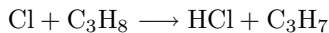
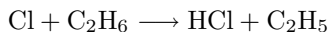


Figure 5.22: Measured increase in erythema (sunburning) UV radiation at the South Pole as a function of ozone change. Source: WMO 1994 Report No.37

Cicerone *et al.* (1991) proposed injecting ethane (C_2H_6) and propane (C_3H_8) to destroy the stratospheric chlorine with the following reactions:



Turco (1997) summarizes other approaches to reduce the present Antarctic ozone hole by attacking the implicated molecules.

Technological solutions have also been proposed for reducing the level of greenhouse gases, mainly CO_2 . We agree with Turco that the application of technological schemes to fix environmental problems is generally a mistake, the most logical solution being to eliminate the source of the problem.

5.10 Tropospheric Ozone

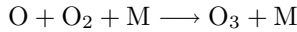
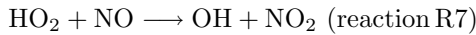
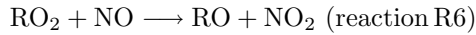
5.10.1 Sources and Relevant Reactions

Around 90% of the atmospheric ozone is located in the stratosphere. The rest is in the troposphere, and its presence has attracted growing interest in the last years because of its relation to city pollution and associated health effects. Tropospheric ozone has two major sources. One is intrusion from the stratosphere, with the ozone sometimes flowing into the troposphere through the upper layer and cutting low activities. Part of the ozone may subside in the troposphere directly by the Hadley circulation or Brewer-Dobson circulation. The exchange is greater at the mid- and high latitudes in the northern hemispheric winter.

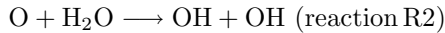
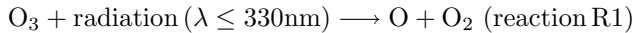
Unlike most other air pollutants, ozone is not directly emitted from any one source. Tropospheric ozone is formed by the interaction of sunlight, particularly ultraviolet light, with hydrocarbons and nitrogen oxides, emitted by cars, petrol

vapours, fossil fuel power plants, refineries and certain other industries. A major role is played by the reactive hydrocarbons, R, released mainly by motor driven vehicles (Haagen-Smit & Fox 1954).

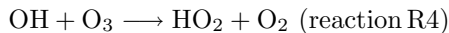
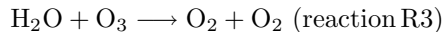
The production of tropospheric ozone occurs through the reactions



The loss of tropospheric ozone is controlled by the following reactions:



Most of the O atoms undergo relaxation to ground state via collisions with O₂ or N₂. Additional loss occurs through reaction of OH radicals with ozone:



The loss processes can be summarized by the expression

$$L_{\text{O}_3} = [\text{O}_3] \{ F \text{J}_{\text{O}_3} + k_4[\text{HO}_2] + k_5[\text{OH}] \}$$

where F is the fraction of O(¹D) that reacts with water vapour (usually a few percent)

Summarizing,

$$P_{\text{O}_3} = [\text{NO}] \{ k_6[\text{RO}_2] + k_7[\text{HO}_2] \}$$

The chemical budget of ozone in a given region is therefore governed by P_{O₃} - L_{O₃}.

5.10.2 Measurements

Comparison of ozone surface values in the nineteenth century with present records indicates a growth by a factor two (see Bojkov 1986). Measurements of tropospheric ozone were sporadic until the celebration of the International Geophysical Year in 1957, after which the number of stations began to grow to their present number, which now sums thousands of stations. Over the next 50 years tropospheric ozone levels will increase by 1%. A typical diurnal variation shows maximum values in mid- or late afternoon at any time of the year. The concentrations are higher in summer, owing to the available sunshine.

Table 5.13 shows the variation in the different sources of tropospheric ozone. We can see the constant levels of natural processes, the clear increase of anthropogenic sources and the lowering of stratospheric origin, probably caused by the existence of ozone holes (Lelieveld & Deutener 2000).

Table 5.13: Variations in the sources of tropospheric ozone. Eq (Equator); MidL (Mid Latitudes (40-50°); NH (Northern Hemisphere). Adapted from Lelieveld & Deutener (2000).

Sources	1860		1993		
	Eq	MidL	Eq	MidL (NH)	MidL (SH)
Stratosphere	20	45	10	25	40
Lightning	55	15	35	5	20
Soils	10	10	10	5	10
Biomass Burning	15	30	25	10	15
Industry	—	—	20	55	15

In the late 1940s a remarkable phenomenon of air pollution was observed in Los Angeles and later extended to other large cities. It consisted in the production of ozone from the reaction of organic products (Volatile Organic Compounds, VOCs) with NO and NO₂.

Experiments have shown that some trees grow larger in cities such as New York compared to rural sites. This is probably caused by the higher ozone exposures in the countryside (Gregg *et al.* 2003).

Chandra *et al.* (1999) witnessed a decadal solar-cycle signal in tropospheric ozone that is out of phase with stratospheric ozone. This phase-shift reduces the 11-year solar signal in measurements of total column ozone by approximately 50%.

Artificial sources of ozone include also dry-process photocopying machines (Wolkoff 1999) and laser printers. Ozone decomposes on surfaces; therefore, indoor values are usually lower than those outdoors.

5.10.3 Biological Effects

Ozone damages plants in two main ways: 1) acute effects involving elicitation of plant defense responses and hypersensitive responses or necrosis, resulting in patches of brown or white colour; 2) chronic effects, including reduction in growth and fitness with pigmentation change. In practice, yield reductions of up to 30% are observed in common crops such as potato, beans and wheat when exposed to ambient ozone concentrations (see Heagle 1989 for a review.). High concentrations of ozone cause plants to close their stomata²⁸. This slows down photosynthesis and plant growth. Ozone may also enter plants through the stomata and directly damage internal cells.

In humans, ozone can irritate the respiratory system, also reducing the working of the lung aggravating diseases such as asthma. Table 5.14 summarizes these effects.

The best way to protect health is to become informed about the current levels of ozone concentration, information that is starting to be delivered together with

²⁸The cells on the underside of the plant that allow carbon dioxide and water to diffuse through the plant tissue.

Table 5.14: Human responses to ozone exposure. From Turco (1997).

Ozone (ppmv)	Response
0.02	Odor Threshold
0.1	Nose and throat irritation in sensitive people
0.3	General nose and throat irritation
1.0	Airway resistance, headaches Aging of lung tissue

meteorological data. The US Environmental Protection Agency (EPA) has developed the Air Quality Index for reporting the levels of ozone and other pollutants (see Table 5.15).

Table 5.15: Air Quality Index

Ozone concentration (ppm) (8-hours average)	Air Quality Index	Air Quality Descriptor
0.0–0.064	0– 50	Good
0.065–0.084	51–100	Moderate
0.085–0.104	101–150	Unhealthy
0.105 -0.124	151–200	Unhealthy
> 0.125	201–300	Very unhealthy

5.11 Climatic Effects of Ozone Changes

In the last chapter we have commented the possible link between the cycles of ozone production and depletion and the terrestrial climate. Therefore it is worth now to consider the climatic effects of current ozone depletion.

The ozone is a greenhouse gas; therefore, its depletion will contribute to a decrease in present global warming. On the other hand, the growth of tropospheric ozone reveals an opposite behaviour. The recent IPPC report (Houghton *et al.* (2001) gives a summary of the radiative forcing of different factors related to present global warming (Figure 5.23). We can see how the ozone has a different climatic effect, depending on the atmospheric layer where is located.

Shindell & Schmidt (2004) have modelled the temperature response to ozone depletion and greenhouse gases in the Antarctic from 1945 to 2055. They found that the southern regions are expected to warm in the near future with the subsequent danger of the breaking up of ice sheets and increased sea levels.

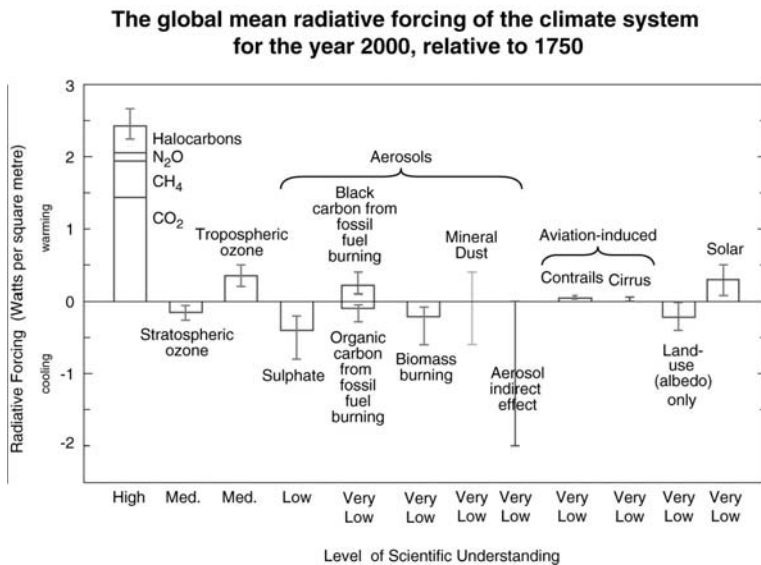


Figure 5.23: Global mean radiative forcing of the climate system for the year 2000, relative to 1750. Adapted from Houghton et al. (2001). Courtesy of M. Noguer (IPCC).

5.12 Current Surface UV Fluxes

5.12.1 UV Index

The global Solar UV Index (UVI) was developed by the World Health Organization to make accessible to the public information about the UV surface fluxes and warn of their possible danger. The UVI provides an estimate of the maximum solar UV exposure at the Earth's surface. The values range from zero upwards; the higher the Index, the greater the likelihood of skin and eye damaging exposure to UV, and the less time it takes for damage to occur (see Table 5.16).

The UVI²⁹ is a unitless quantity defined by the formula

$$\text{UVI} = K_{\text{er}} \int_{250\text{nm}}^{400\text{nm}} I(\lambda) \omega_{\text{er}}(\lambda) d\lambda$$

where λ is the wavelength in nm, K_{er} a normalization constant equal to $40 \text{ m}^2/\text{W}$, $I(\lambda)$ the irradiance in $\text{W m}^{-2} \text{ nm}^{-1}$ and $\omega_{\text{er}}(\lambda)$ the erythemal weighting function (i.e. sun-reddening or sunburning), defined of the form

$$\omega_{\text{er}}(\lambda) = 1.0 \text{ for } 250 < \lambda \leq 298 \text{ nm}$$

$$\omega_{\text{er}}(\lambda) = 10^{0.094(298-\lambda)} \text{ for } 298 < \lambda \leq 328 \text{ nm}$$

²⁹UVI can be determined through two different approaches: the first is to use a spectroradiometer and to calculate the UVI using the above formula; the second is to use a broadband detector calibrated and programmed to give the UVI directly.

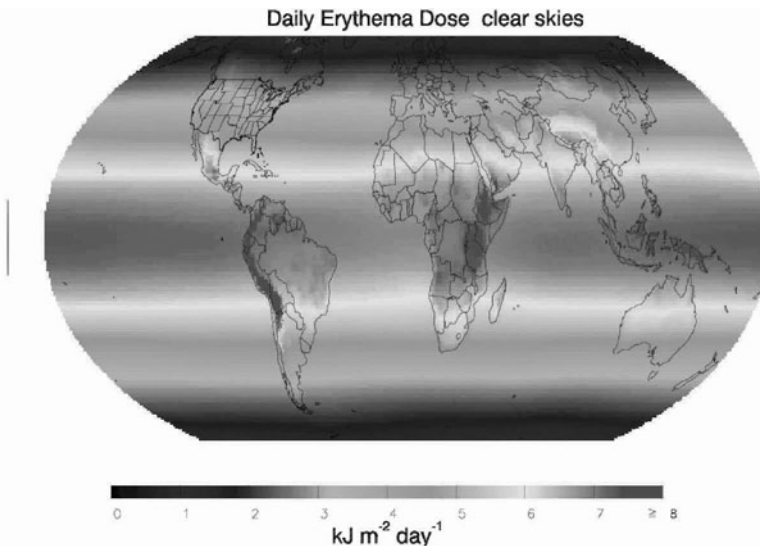


Figure 5.24: Climatological erythema dose averaged over 14 years, without clouds, from 1979 to 1992, (Available at <http://www.acd.ucar.edu/TUV/>).

$$\omega_{\text{er}}(\lambda) = 10^{0.015(139-\lambda)} \text{ for } 328 < \lambda \leq 400 \text{ nm}$$

$$\omega_{\text{er}}(\lambda) = 0 \text{ for } \lambda > 400 \text{ nm}$$

Table 5.16: The Ultraviolet Index

Exposure category	UVI Range
Low	< 2
Moderate	3–5
High	6–7
Very high	8–10
Extreme	> 10

The daily integrated erythema dose is found by estimating the instantaneous dose values every half-hour during the day and summing these values over the course of the day using a simple trapezoidal numerical integration scheme. When summed over time, the instantaneous values calculated in watts per square centimetre are then given in kilojoules per square metre, the total amount of radiant energy received over a 1 square metre area during the daytime.

Figure 5.24 shows the spatial distribution of the UV erythema dose averaged over 14 years.

5.12.2 Diurnal Variation of UV Surface Radiation

Like visible radiation on a cloudless day, the amount of UV radiation follows a variation related with the altitude of the Sun above the horizon. There are two main components: direct beam and diffuse sky, the latter being produced by the described scattering processes in the terrestrial atmosphere.

Grant *et al.* (1997) have derived the laws describing the variation of the diffuse component for the UV-A and UV-B ranges:

$$N_{\text{UV}A} = 0.151 + 0.058z^2 + 2.4e^{-7.6\Psi} + 0.106 \cos^2 \Psi$$

$$N_{\text{UV}B} = 0.201 + 0.020z^2 + 1.48e^{-7.8\Psi} + 0.148 \cos^2 \Psi$$

where Ψ is the scattering angle between the Sun and the location on the sky, defined by

$$\cos \Psi = \cos z \cos z^* + \sin z \sin z^* \cos \Phi$$

z being the solar zenithal distance and z^* the difference between the solar azimuth and the sky position.

Table 5.17 summarizes the percentage of daily UV radiation received in the two relevant spectral ranges at different times of day (Diffey 1991).

Table 5.17: Percentage of daily UV-B and UV-A received during different periods on a clear summer's day. From Diffey (1991).

Latitude	UV-B		UV-A	
	11 am–1 pm	9 am–3 pm	11 am–1 pm	9 am–3 pm
20	30	78	27	73
40	28	75	25	68
60	26	69	21	60

5.12.3 Temporal Variations

Apart from the daily change with solar elevation, the amount of UV-B reaching the earth is mainly determined by three factors

Relation with the Ozone:

$$UV_{\text{bio}} \sim (\text{Ozone})^{\text{RAF}}$$

where the factor RAF must be calculated with models of propagation of spectral UV radiation through the atmosphere, combined with the appropriate action spectrum, or from spectral UV measurements made at the Earth's surface (see Table 5.18 UNEP 1994, 1998 Reports).

Latitude and elevation of the location: At the high-latitude polar regions the sun is always low in the sky; because the sunlight passes through more atmosphere

Table 5.18: Radiation Amplification Factors (RAFs) for different processes, derived at 30 °N. Source: UNEP 1994, 1998 Reports.

Effect	January (290 DU)	July (305 DU)
Erythema	1.6	1.5
Skin edema	1.6	1.5
DNA damage	2.2	2.1
Cornea damage	1.2	1.1
Cataracts	0.8	0.7
Immune suppression	1–0.4	0.8–0.4

so more of the UV-B is absorbed. For this reason average UV-B exposure at the poles is over a thousand times lower than at the equator.

As a rule of thumb, the UV-B dose people receive as they go higher in the mountains increases by about 4% in terms of sunburning power with every 300 metres in altitude.

Cloud cover; the reduction in UV-B exposure depends the cover's thickness (Schafer *et al.* 1996; Bodeker *et al.* 1996). We can compare Figure 5.25 with the previous one. TOMS satellite data over Europe have confirmed that UV increases due to ozone depletion are partly masked by the increases cloudiness in some regions.

In case of an ozone recovery, clouds will appear as the most important modulator of the UV radiation, both over long- and short-time scales, during the coming decades (Krzyscin *et al.* 2004).

Surface Albedo: The presence of snow in the surrounding area of the observing site can increase the UV irradiance appreciably.

Proximity to an industrial area: Produced because of the protection offered by photochemical smog. Industrial processes produce ozone, one of the more irritating components of smog, which absorbs UV-B. This is thought to be one of the main reasons that significant ozone losses in the southern hemisphere have not been mirrored in the northern hemisphere.

Under the auspices of the WMO the Global Atmosphere Watch was created in 1989 to coordinate the measurements of parameters related to the atmospheric chemistry. The data on ozone and UV radiation are stored in the World Ozone and Ultraviolet Radiation Data Centre (<http://www.woudc.org>). The ozone data archive contains the following data categories: Lidar vertical profiles, ozonesonde vertical profiles, total column ozone (daily and monthly values), surface ozone (daily summaries), and Umkehr N-value and C-Umkehr vertical profiles. The UV data archive contains the following data categories: broad-band, multi-band and spectral.

Within the Tropospheric Emission Monitoring Internet Service (TEMIS) project a near-real time service has been set-up for total ozone and UV surface data (<http://www.temis.nl/UVradiation>). The satellite data are mainly from GOME (aboard the ERS-2 satellite) and SCIAMACHY (aboard the Envisat). Parameters such as aerosols, ozone, reflectivity, erythemal UV and UV irradiance are given by the TOMS instrument aboard different satellites (<http://toms.gsfc.nasa.gov>).

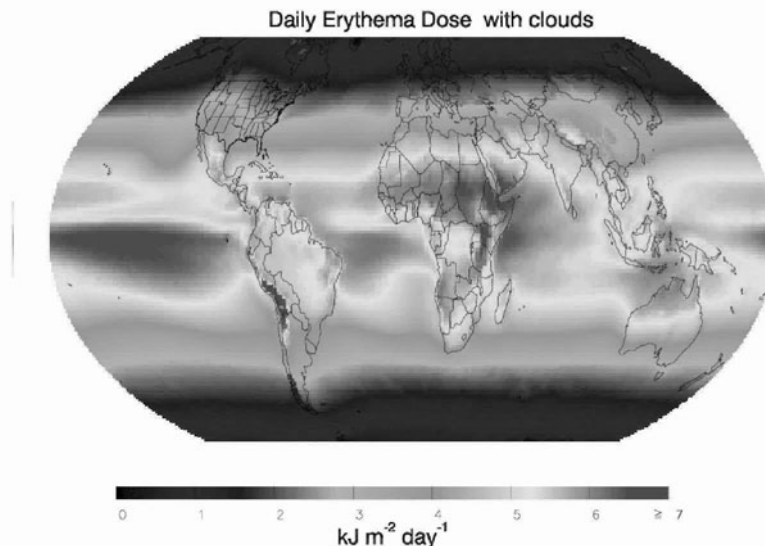


Figure 5.25: Climatological erythema dose averaged over 14 years, with clouds, from 1979 to 1992. (Available at <http://www.acd.ucar.edu/TUV/>).

5.12.4 Hemispheric Differences

Locations in the southern hemisphere should receive approximately 15% more UV than locations at similar latitudes north of the Equator. This is caused by differences in ozone between both hemispheres, and also because the Earth is slightly closer to the Sun during the southern hemisphere summer (McKenzie and Elwood 1990).

Measurements show still larger differences in the UV biologically-damaging component, mainly by the larger amount of tropospheric pollution (tropospheric ozone and aerosols) in the north (Seckmeyer & McKenzie 1992), which absorbs part of the UV solar flux.

5.13 Protection against UV Radiation

We have already described the different effects of the UV radiation on living beings. Let us to finish this chapter by commenting briefly on some new artificial sources of UV and how we can protect ourselves from the damaging effects of the sunbathing.

5.13.1 Artificial UV Sources

UV rays can be made artificially by passing an electric current through a gas or vapour. Lamps emitting ultraviolet radiation are used primarily for recreational (sunless) tanning and phototherapy of skin diseases (e.g. psoriasis). They can

emit in the three UV ranges, although those used for tanning emit only UV-A. However, the problem is the delivered dose and the correct calibration of the lamp. The American Cancer Society warns about the high levels of UV released by tanning beds, which can cause premature aging of the skin, increase risk of skin cancer, skin and eyes burning, and damage to the immune system.

Electric welding arcs are strong sources of ultraviolet radiation; they can produce acute overexposure to UV within a radius of several meters in just a few seconds. Eye and skin protection are necessary for welders and people working nearby. Germicidal lamps, commonly used for sterilization in hospitals, are strong emitters of UV-B and UV-C radiation. Normally, they are placed so that people are not directly exposed, but they are capable of producing serious exposure to UV at close range. Ultraviolet lasers can be quite intense and hazardous and their exposure may be unexpected owing to the invisibility of the beam.

5.13.2 Sunscreens

Most types of textiles, both natural and man-made, provide good protection against UV-B. It is the density of the weave, not the type of fibre or colour, that determines whether the material offers a good protection (Welsh & Diffey 1981). Typical window glasses transmit less than 10% of UV light.

A sunscreen stops the UV photons before they can reach the skin and damage it. They contain organic molecules that absorb UV and inorganic pigments that absorb, scatter and reflect ultraviolet radiation. The most common measure of the efficacy of a sunscreen is the Sun Protection Factor (SPF), which gives an indication of screen effectiveness in blocking UV. For example, an SPF of 15 means that it should take 15 times as long before skin damage occurs (i.e. the creams should block about 93% of the radiation that causes skin damage).

$$\text{SPF} = \frac{\int S(\lambda)E(\lambda)d\lambda}{\int S(\lambda).E(\lambda)T(\lambda)d\lambda}$$

where $S(\lambda)$ is the solar spectrum, $T(\lambda)$ is the transmittance of the sunscreen and $E(\lambda)$ the “Commission Internationale de l’ Eclairage” erythemal spectrum. $T(\lambda) = I_\lambda / I_0(\lambda)$, where I is the intensity of the radiation after the transmission through sunscreen and I_0 is the unscreened intensity.

Smith *et al.* (2002) compare different sunscreens and stress the importance of also filtering the UV-A component as well as the classical UV-B.

The best protection is to avoid the central hours of the day, when the UV concentration can reach up to 60% of its total amount. An anti-cancer campaign in Victoria (Australia) recommends: “Between eleven and three, sleep under a tree. The best suncreams of all is absolutely free”.

5.13.3 Shading

In principle, to be in shade is a good protection. However, in such conditions we get also a significant UV diffuse component. Turnbull *et al.* (2003) have evaluated the UV protection of different covers (see Tables 5.19 and 5.20).

Table 5.19: Summary of Ultraviolet Protection factors. Source: Turnbull *et al.* (2003)

	Autumn		Winter	
	Noon	Afternoon	Noon	Afternoon
Shade umbrella	1.7	1.7	3.3	1.4
Covered verandah	10.0	6.7	6.7	5.0
Covered sand pit	10.0	5.0	5.0	3.3
Covered path	10.0	2.0	2.5	2.5

Table 5.20: Average exposure times (in minutes) to be spend beneath each shade structure, before receiving mild erythema. Source: Turnbull *et al.* (2003).

	Autumn		Winter	
	Noon	Afternoon	Noon	Afternoon
Shade umbrella	35	35	60	60
Covered verandah	170	175	230	277
Covered sand pit	155	222	90	166
Covered path	105	101	125	81

Chapter 6

UV Fluxes on Other Bodies of the Solar System

In this chapter we describe the effect of UV radiation on different bodies in the Solar System. Emphasis will be given to the effect of planetary atmospheres and their chemistry as well as on the surface properties of the bodies considered. The effects on the Earth's atmosphere, described in chapter 4, will serve as a guideline¹.

Most of the observations undertaken by planetary astronomers are of targets that do not emit their own radiation but are observable principally because they reflect the sunlight that falls on them or emit energy as a result of different physical processes. Measuring reflected light at UV wavelengths poses certain problems. First, instrumental spectral responses become weaker with decreasing wavelength and so does the solar output. Second, the contribution of the observed solar spectrum to the planetary spectrum observed must be removed. Finally, Solar System objects change position against the background of an individual observation (see Nelson & Domingue 1999).

6.1 Planetary Atmospheres: Basics

Sunlight entering a planetary atmosphere can undergo a variety of processes: a) scattering of photons by aerosols (haze and dust), b) absorption of UV light by atmospheric species, c) stimulation of an atmospheric gas by incident sunlight and subsequent emission by fluorescence, d) excitation of gas by precipitation of magnetospheric particles and e) photoionization and photodissociation processes that produce a chemical reaction.

¹A general textbook on planetary science: I. de Pater and J. Lissauer, *Planetary Sciences*, Cambridge University Press, 2001. Eleven planetary atmospheres are studied in *Photochemistry of Planetary Atmospheres*, Y. L. Yung, W.B. Demore, DeMore Yung, 1998, Oxford Univ. Press

6.1.1 Photochemistry

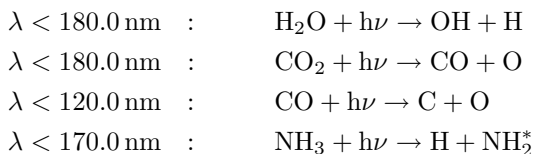
UV radiation from the Sun affects planetary atmospheres (i.e. those of Venus, Earth, Mars, Jupiter, Saturn, Uranus and Neptune) and those of planetary satellites; namely Titan (a satellite of Saturn), Io (a satellite of Jupiter) and Triton (a satellite of Neptune). For planets with no atmosphere, the solar radiation will fully penetrate to the ground and cause erosion (Mercury, Moon) or other specific chemical reactions. Moreover, those having magnetospheres will produce intrinsic UV radiation (airglow) by the action of high energy particles.

The distance of a planet to the Sun of course determines the amount of radiation received. Let us first consider the total solar irradiance received by the planet. These values and the values for the semi major axes of the planetary orbits can be found in Table 6.1.

Table 6.1: Solar irradiance (W/m^2) and semi-major axes of planets

Planet	Solar irradiance (W/m^2)	Solar irradiance (Earth = 1.00)	Semi-major axis (10^6 km)
Mercury	9126.6	6.673	57.91
Venus	2613.9	1.911	108.21
Earth	1367.6	1.000	149.6
Mars	589.2	0.431	227.92
Jupiter	50.50	0.037	778.57
Saturn	14.90	0.011	1433.53
Uranus	3.71	0.0027	2872.46
Neptune	1.51	0.0011	4495.06
Pluto	0.89	0.0007	5869.66

Because of its relatively high energy, solar UV radiation strongly regulates the photochemistry of planetary atmospheres. This had already been studied by Wildt (1937), who described some basic reactions:



Here, $h\nu$ denotes the energy of a UV photon. Such processes are called photolytic. As can be seen from these basic reactions, photons with $\lambda < 180.0 \text{ nm}$ are capable for example, of splitting H_2O molecules into OH and H.

For a better understanding of the relevant processes let us first give a brief overview of the physics of planetary atmospheres².

²Monographs on the photochemistry of the atmospheres: V.A. Kransnopol'sky, 1986, Photochemistry of the atmospheres of Venus and Mars, Springer; Yuk L. Yung and WilliamB. DeMore, 1998, Photochemistry of Planetary Atmospheres, Oxford Univ. Press.

6.1.2 Atmospheric Physics

Let us consider an atmosphere that is characterized by its pressure and density stratification. From hydrostatic equilibrium, the pressure differences are related to the temperature gradients ³.

$$dp = -g\rho dz$$

The equation of state of an ideal gas is $P = nkT$. Assuming that T , g and m are constant, we arrive at the well known equations

$$p(z) = p_0 e^{-mgz/kT} \quad n(z) = n_0 e^{-z/H}$$

$$p = \rho g H \quad H = \frac{kT}{mg}$$

where p denotes pressure, g gravitational acceleration, $\rho = nm$ the mass density, k the Boltzmann constant and H the atmospheric scale height. The atmospheric scale height denotes the height, h , at which the pressure drops by a factor of e^{-1} .

The number of particles through a cross-section of an atmosphere with constant scale height is given by:

$$N = \int_0^\infty n dz = n_0 H = \frac{p_0}{mg}$$

From this equation we can estimate the mass of a planetary atmosphere:

$$M_A = \left(\frac{p_0}{g} \right) 4\pi R_0^2$$

This implies that two thirds of the total mass of an atmosphere is concentrated within the scale height.

The distribution of particles in the atmosphere may be assumed to follow a Maxwell-Boltzmann distribution:

$$f(z, v) = \frac{n(z)}{(2\pi kT/m)^{3/2}} e^{-mv^2/2kT}$$

Dynamic processes in the atmosphere can be divided into vertical transport, which leads to a vertical distribution of density, and into horizontal motions. The vertical diffusive flux depends on the molecular diffusion coefficient $D_j \sim T^{1/2} n^{-1}$ and the Eddy-diffusion coefficient, $K_D \sim n^{-1/2}$, as well as on the temperature gradient, dT/dz , the number of particle gradient, dn/dz , and the thermal diffusion coefficient α . A characteristic time for the turbulent mixing (Eddy-diffusion) τ_{KD} and the molecular diffusion τ_D can be given:

³Basic equations and tables used in this subsection to describe the physics of planetary atmospheres are from: Bauer,S. 2001, "Erde und Planeten", W.D. Gruyter, Lehrbuch der Experimental Physik, Bd.7, pp. 605.

Table 6.2: Comparison of the temperatures of Venus, Earth and Mars.

	Venus	Earth	Mars
T_{eff}/K	232	255	217
T_{B}/K	750	288	225
$\Delta T/\text{K}$	518	33	8

$$\tau_D = \frac{H^2}{D} \quad \tau_{kD} = H^2/K_D$$

The height at which both times are equal corresponds to the homopause⁴. For the horizontal motions, which are influenced by pressure gradients, the Coriolis force and a friction force, \vec{K} we have:

$$\frac{d\vec{V}_n}{dt} = -\frac{1}{\rho} \nabla p_n + 2(\vec{V}_n \times \vec{\Omega}) - \vec{K}$$

where \vec{V}_n denotes the horizontal velocity of a neutral gas and $\vec{\Omega}$ is the planetary angular velocity.

Thus a characteristic property of a planetary atmosphere is the pressure at the planet's surface, which is given by the mass of the atmosphere. The temperature at the surface depends on insolation. The effective temperature, T_{eff} , is derived from the equilibrium between insolation and reflection:

$$S(1 - A) \frac{\pi R_0^2}{D^2} = a \pi R_0^2 \sigma T_{\text{eff}}^4$$

where S is the solar constant, A the albedo (measure for the reflectivity, influenced by the surface and clouds), σ the Stefan–Boltzmann constant, R_0 the radius of the planet, D its distance from the Sun (measured in AU) and a depends on the rotation rate ($a = 4$ for a slowly rotating planet such as Venus and $a = 2$ for a fast rotating planet like the Earth).

In the presence of gases that absorb in the infrared (e.g. CO₂, H₂O and CH₄) there is a greenhouse effect and the surface temperature, T_B , is higher than the effective temperature:

$$T_B = T_{\text{eff}}(1 + \tau_{\text{IR}})^{1/4} = T_{\text{eff}} + \Delta T$$

Here, τ_{IR} is the optical depth in the infrared. Table 6.2 gives a comparison for the temperatures of the terrestrial planets.

⁴Homopause is the critical level below which an atmosphere is well-mixed. Below the homopause, each species adopts the same scale height, which is given by the average mass of an atmospheric particle. Above the homopause, each species assumes its own scale height based on its mass. This can lead to a depletion of heavy isotopes.

The greenhouse effect in the atmosphere of Venus is caused 90% by CO₂; in the case of Earth it is produced 60% by H₂O, 30% by CO₂ and 10% by CH₄; in the case of Mars it is caused 100% by CO₂.

Radiative processes control the temperature gradient above the troposphere (the tropopause is at a level of 100 hPa for Earth, Jupiter and Saturn). In the Earth's atmosphere UV radiation between 200 and 300 nm produces the ozone layer. Molecular and atomic oxygen are needed for the ozone production in the Earth's atmosphere (produced in the mesosphere by radiation with $\lambda < 167$ nm). Near the surface of Mars ozone is produced also by the dissociation of CO₂.

Above the mesopause, absorption of EUV radiation ($\lambda < 170$ nm) leads to an increase in temperature. Therefore, $dT/dz > 0$, and this layer is also denoted as thermosphere. The intensity of solar EUV radiation decreases with depth because of the optical depth,

$$\tau(z) = \int_z^{\infty} \sigma_a n_1(z) dz$$

Therefore,

$$I = I_{\infty} e^{-\tau(z)}$$

where I_{∞} is the intensity above the absorbing atmosphere.

Thus the distinction of different layers of planetary atmospheres according to temperature shows us that solar UV radiation mainly influences the stratosphere (ozone and carbon-hydrogen compound aerosols) and the thermosphere. The higher the energy of solar UV radiation (higher energy means shorter wavelengths since $E \sim 1/\lambda$) the higher the layer in the planetary atmosphere where it is absorbed.

For terrestrial planets the temperature of the exosphere, T_{∞} , depends solely⁵ on XUV solar flux

$$T_{\infty} \sim \left[\frac{\epsilon \alpha I_{\text{XUV}} \kappa \sigma_c}{\kappa_0 m_i g \sigma_a} \right] + T_0$$

where σ_c and σ_a are the collision and absorption cross-sections, respectively, I_{XUV} the intensity at the planet orbital distance, ϵ the heating efficiency, κ_0 the thermal conductivity coefficient, α_a a factor depending on the rotation of the planet (<1), m_i the mass of the atmospheric constituents and T_0 the temperature at the base of the thermosphere (see Bauer & Hantsch 1989 and Lammer *et al.* 2003).

As an application of this relationship let us compare the exospheres of Venus, Earth and Mars.

Venus receives almost twice the solar flux, S , but its exosphere temperature, T_{∞} , is between 100 and 300 K because the main component is the heavy CO₂ with $m = 44$ whereas the thermosphere of the Earth has a mean temperature of about 1000 K and its main component is O ($m = 16$). On the other hand, I_{∞} on

⁵For giant planets, other sources such as accelerated particles and atmospheric gravity waves can become important.

Mars is only a quarter that at Venus but, because of the lower surface gravity its T_∞ is similar to that of Venus, although the variation between day and night is lower. It is also important to recall here (see chapter 4), that the temperature of the exosphere, T_∞ , depends on the solar activity; varying between high and low solar activity by a factor of two.

EUV radiation from the Sun is not only absorbed in the thermosphere but also contributes to the dissociation and ionization of the atmospheric constituents:



Here, χ denotes the ionization potential given in eV. For typical constituents of an atmosphere this is between 24.6 eV ($\lambda = 50$ nm) and 12 eV ($\lambda = 102.6$ nm, Lyman β). The electrons in the above reaction receive the energy that is in excess of χ . Therefore, the temperature of the electrons, T_e , is higher than those of the ions, T_i , and of the neutral gases, T_n . Because of Coulomb interactions, the temperature of the ions may be higher than that of the neutral particles; therefore,

$$T_e > T > T_n$$

In the case of a non-magnetic planet like Venus, the upper limit of the ionosphere is given by the ionopause, and on the dayside this layer forms where there is a balance between the pressure of the solar wind, p_{sw} , and the ionospheric plasma pressure, p_{ion} :

$$p_{sw} = (\rho v^2)_{sw} = p_{ion} = Nk(T_e + T_i)$$

If we consider a planet with a magnetic field things become complicated. The planet has a magnetosphere, and the distribution of ions is controlled by the magnetosphere. The expansion of the ionosphere is therefore given by the corotation of the magnetic field with the planet and the field by the interaction between the solar wind and the magnetosphere.

In the exosphere, collisions between particles becomes very rare. Here, particles with velocity components similar to the escape velocity are very likely to escape, the escape velocity being given by

$$v_\infty = \sqrt{\frac{2GM}{R}}$$

Here, R denotes the radius of the planet and M its mass. Given a Maxwell-Boltzmann distribution, the most probable velocity is given by

$$v_0 = \sqrt{\frac{2kT}{m}}$$

The escape of particles because of their thermal motions is called thermal, or Jeans escape,

$$X = \left(\frac{v_\infty}{v_0}\right)^2$$

Table 6.3: Comparison of the atmospheres of Venus, Earth, Mars and the Saturian satellite Titan.

	$V_\infty / \text{km s}^{-1}$	T_∞ / K	T_c / K
Venus	10.4	~ 300	~ 4000
Earth	11	1000	5000
Mars	5.3	250	1000
Titan	2.4	190	200

and by substituting previous results ($H = kT/mg$ and $g = GM/R^2$):

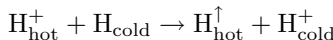
$$X = \frac{R}{H}$$

Let us consider different values of X :

- Very large X : the escape of particles can be neglected
- $X \leq 10$; escape must be included
- $X \sim 1.5$, here the thermal energy is equal to the escape energy of a particle, $3/2kT = mv_\infty^2/2$, leading to so-called hydrodynamic escape (blow off) which is very efficient.

For present day planetary atmospheres blow-off is not significant but it could have led to the mass loss of early H₂O dominated atmospheres as in the case of Venus. It could also be an important mechanism for the existence of the hydrogen torus around Saturn caused by particles from Titan's atmosphere.

At present thermal escape is negligible in planetary atmospheres but, because of charge exchange, for example, particles can escape easily. Energetic (hot) protons trapped in the magnetic field can react with cold H-atoms:



Another process leading to escape is dissociative recombination. This is important for Mars, where the main constituent of the ionosphere is O⁺; dissociative recombination leads to the formation of a hot oxygen corona, a part of which gains enough energy to escape. For Titan, the N₂ atmosphere can obtain particles with high enough energy. Collisional ionization and dissociation by energetic electrons and sputtering by ions in the Saturnian magnetosphere can lead to nitrogen particles acquiring escape energy.

6.1.3 The Origin of Planetary Atmospheres

When considering planetary atmospheres, we need to remember the distinction between terrestrial and giant planets. The origin of their atmospheres may be summarized as follows:

Table 6.4: Comparison of the atmospheres of Venus, Earth and Mars.

	Venus	Earth	Mars
Relative mass	0.8	1.0	0.1
Relative distance from Sun	0.7	1.0	1.5
Relative atmospheric mass	100	1.0	0.01
Bulk atmospheric composition	CO ₂	N ₂ , O ₂	CO ₂
Relative water vapour	0.0001	1.0 (1%)	0.03
Surface temperature	460 °C	20 °C	-60°C

Giant planets (Jupiter, Saturn, Uranus, Neptune): the composition of their atmospheres is nearly identical to that of the Sun; it is believed that these atmospheres were formed together with the planet from the nebula from which the Sun was also formed.

Terrestrial planets: these now possess the so-called secondary atmospheres. The famous experiment of S. Miller (see previous chapter) demonstrated that a mixture of CH₄ and NH₃ exposed to electric discharges leads to the formation of amino acids. Thus primary atmospheres consisting of these components were favoured. It was later shown that a mixture of CO₂, CO, H₂, N₂ and H₂O could also lead to the formation of amino acids when there is no free oxygen. There is geologic evidence that in the early terrestrial atmosphere there could only have been little NH₃ because otherwise the pH-value of the oceans must have been higher. Also, the properties of sedimentary rocks clearly favour a non-reducing early terrestrial atmosphere, similar to what we find today on Mars and Venus (CO₂ and N₂).

Another proof for the secondary nature of the atmospheres on Earth and the terrestrial planets is the deficit of certain isotopes of primary noble gases: ³⁶Ar by a factor of 10⁶, ²⁰Ne by 6 × 10⁷ with respect to the cosmic abundance. Rubey (1974) considered the present outgas products of terrestrial volcanoes (80% H₂O, 17% CO₂, 1.7% HCl, Cl₂) as a basis for the origination of the atmospheres of Venus, Earth and Mars. Such a scenario is also reviewed by Bauer (2002). Two scenarios are discussed for the outgassing itself: a) sudden catastrophic outgassing and b) continuous outgassing over a period of ∼ 10⁹ years.

A comparison of the atmospheres of Venus, Earth and Mars is given in Table 6.4.

6.2 Venus

6.2.1 Basic Facts

Venus⁶ is the Earth's nearest planet with a distance from the Sun of 0.723 AU⁷. Venus is very similar to Earth in size and average density. However it rotates very slowly and therefore has no magnetic field. Its orbit round the Sun is highly circular with a very small eccentricity. The sidereal year of Venus is 224.7 days but the length of a venusian day, which was determined in the 1960s, is 243.08 days and its rotation is retrograde (clockwise as seen from above the North Pole). The planet shows no seasonal effects because the inclination of the equator of Venus to its orbit plane is only 2.6 degrees.

Because of its slow rotation, a point on the surface would have almost 60 Earth days of Sun and the same for night. The surface is not visible from space because of its dense atmosphere. Seen in UV light, Venus is not featureless. Already in 1927, NUV images by F. E. Ross, at Mt. Wilson Observatory showed dark, high-contrast structures interpreted as clouds (Ross 1928).

Venus has been explored by several spacecrafts. In 1967 Venera 4 passed through the clouds and in 1975 Venera 7 reached the surface. This spacecraft was able to broadcast information back for 23 minutes before succumbing to the 740 K surface temperature. In 1982, the landers Venera 13 and 14 photographed the surface (1983–1984). The Pioneer Venus mission in 1978 performed a radar mapping. Later (1990–1994) better resolved radar images of the surface were obtained by Magellan (resolution < 1 km). The temperature of the cloud tops, which are highly reflecting, is 240 K. The great temperatures at the surface can be explained by the greenhouse effect of CO₂. This gas is opaque to IR and prevents heat from escaping.

In 1985 two spacecrafts, VEGA 1 and VEGA 2, dropped two descent probes into the night-side of Venus. They used a UV light source that was absorbed by the constituents of the Venus atmosphere to measure these constituents from an altitude of 62 km to the ground level (Bertaux *et al.* 1996).

The pressure at the surface may be compared with that on Earth: 10 ms of water on Earth result in 1 bar of pressure; 90 bars would be the pressure exerted on a submarine at a depth of 900 m. The Venusian atmosphere contains clouds with H₂SO₄ droplets and these clouds occur at about 50 km. They are produced by the reaction of SO₂, the main constituent responsible for cloud absorption, with water vapour⁸. Data recorded by Venera 13 showed that chlorine is also one of the most common elements in the clouds. UV reacts with the Cl compounds following a similar process to the CFCs on Earth (see the previous chapter).

There are two large continents on Venus, Aphrodite and Ishtar, but five-sixths of the surface are volcanic plains (on Earth the proportion is two-fifths). The density of craters is considerably lower than on Mercury, the Moon or Mars. Thus the surface of Venus cannot be more than 500 million years old. Venus has no

⁶Recent general textbooks on Venus are: D.H.Grinspoon: Venus Revealed, 1998, Basic Books or the book of P. Moore, Venus, 2002, Sterling.

⁷Astronomical unit (the mean Sun-Earth distance). 1 AU = 1.5×10^6 km.

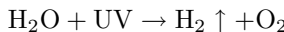
⁸There would be a constant sulphuric rainfall, something similar to the terrestrial acid rain.

magnetic field. It must be assumed that the interior is hot and melted (there are signs of young volcanism) because its size is comparable to the Earth and enough energy is produced by radioactive decay. However, Venus rotates very slowly and therefore has no magnetic field.

6.2.2 Liquid Water on Early Venus

At present the atmosphere of Venus⁹ is very different from the Earth's. The atmosphere of Earth is dominated by N₂ and O₂ whereas on Venus CO₂ dominates. But if all the CO₂ that is locked in rocks on Earth were released, this would result in a more similar composition. Thus one of the differences is caused by life on Earth, which converts CO₂ into O₂. Another striking difference is the absence of H₂O on Venus. How can this be explained? Venus of course could have simply formed without water, or it could have started with a similar amount of H₂O and later it lost it.

Let us do a thought experiment in which we put Earth in Venus' position. Here, the more intense UV radiation from the Sun comes into play. The UV breaks up the H₂O molecules:



In this formula it is indicated that the lighter H would escape to outer space. The remaining oxygen reacts with surface rocks and the atmosphere becomes dry, dominated by CO₂. This is called runaway greenhouse effect and is an explanation of why Venus has no water (Kasting 1988). This had already happened in the early history of Venus because of its closer distance to the Sun. On Earth, CO₂ is washed out of the atmosphere by liquid H₂O and is deposited (through chemical reactions involving silicate rocks) in limestone on the seabed. Volcanic outgassing and recycling of the crust returns the CO₂ to the atmosphere. This process has tied up massive amounts of CO₂ in the Earth's surface rocks (about 100 times the current mass of atmosphere).

This hypothesis can be verified. If oceans of water had escaped from Venus, than the H on Venus would be enriched with the heavier deuterium and this was tested by the Pioneer Venus probe which confirmed the hypothesis. Because deuterium is a heavier isotope of hydrogen (having 1 neutron in the nucleus in addition to just the proton) it rises more slowly in the atmosphere. Thus, the lighter isotope of hydrogen largely escaped but the heavier isotope remained. This provides evidence that there was more water on Venus and a a surface covering ocean would have been about 25 metres deep.

On Earth, the ratio of ordinary hydrogen to deuterium (H/D) is 1000 to 1, while on Venus the H/D ratio is 100 to 1. The H/D ratios on Venus and Earth are assumed to have been originally the same, UV dissociation of water causing the light hydrogen isotope to reduce drastically (see Fig. 6.1).

⁹see also: Venus II: Geology, Geophysics, Atmosphere, and Solar Wind Environment, S. W. Bougher, D. M. Hunten, R. J. Phillips, H. U. Bougher (Eds.), 1997, Univ. Ariz. Press

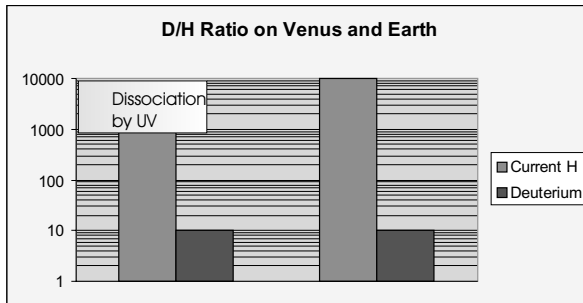


Figure 6.1: Comparison of D/H ratios on Venus and Earth. Note that the y axis is in logarithmic scale.

This process configurated the UV history of Venus. In a relatively short space of time, Venus went from a planet exposed to harsh UV radiation to one on which the surface UV is absolutely clement (see Cockell 1999).

6.2.3 Meteorology

The complex circulation system of the atmosphere of Venus becomes apparent when studying the clouds in UV (Figure 6.2). Violet images show the clouds near the top of the cloud deck, at 60 km altitude, where they are moving west at about 100 m/s; near-IR images look deeper into the clouds to the lower part of the cloud deck, at 50 km altitude, where the motion is westward at about 67 m/s.

The most prominent feature is Y-shaped near the equator and was observed also by satellite missions (Mariner 10, Pioneer Venus and Galileo). It indicates atmospheric waves (like the high and low pressure cells on Earth) and bright clouds toward the poles follow latitude lines. A haze of small particles overlying the main clouds cause the bright polar regions, whereas dark regions indicate enhanced SO₂ near the cloud tops. It is known that there is a 4 day periodic east to west movement in the atmosphere of Venus¹⁰. This superrotation leads to wind speeds near the equator of 110 m/s.

Bright clouds toward Venus' poles appear to follow latitude lines. The polar regions are bright, possibly showing a haze of small particles overlying the main clouds. The dark regions show the location of enhanced sulphur dioxide near the cloud tops. From previous missions, astronomers know that such features travel east to west along with Venus' prevailing winds, making a complete circuit around the planet in four days.

¹⁰A comprehensive study on the atmospheres of Earth, Venus and Mars was done in G. G. Shepherd, W. R. Skinner, E. Thrane, D. K. Chakrabarty, F. J. Lubken, T. Blix, D.K. Chakrabarty, A. Shepherd (Editor), 1995, Pergamon Press

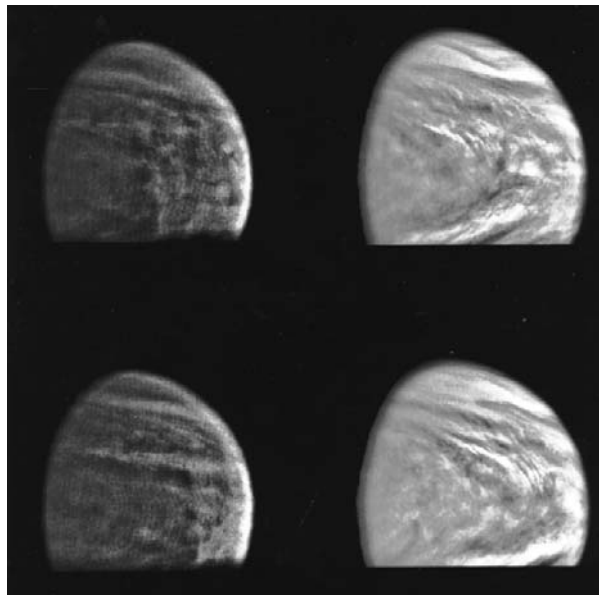
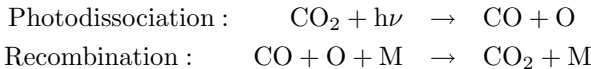


Figure 6.2: Galileo images of Venus. Left: IR images showing deeper clouds. Right: UV images showing higher clouds. The UV dark structures are due to absorption by SO_2 .

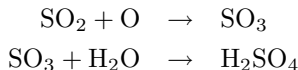
6.2.4 Atmospheric Chemistry

Since the primary constituent on Venus, as well Mars, atmosphere is CO_2 , the following reactions become important:



The photodissociation requires UV photons at $\lambda < 169 \text{ nm}$. The recombination rate is very low and thus CO accumulates. In order to reduce CO catalytic reactions from chlorine and sulphuric components help to recombine the CO.

As it was already stated, Venus' clouds consist of sulphuric acid formed by the following reactions:



The sulphuric acid condenses out in the upper troposphere producing sulphuric acid droplets.

6.2.5 Airglow

The airglow of Venus was first treated by Newkirk (1959). Kumar & Broadfoot (1975) investigated Mariner 10 UV spectrometric data to study the He 58.4 nm

emission caused by the resonance scattering of solar radiation and from the altitude variation of the brightness emission, derived the helium distribution in the atmosphere. Lawrence *et al.* (1977) interpreted bands between 300 and 800 nm as originating from molecular oxygen.

Spatially and temporally variable intensities of the oxygen 130.4 and 135.6 nm lines have been observed on the nightside of Venus and have been labeled “auroral”; that is, ascribed to electron precipitation.

Steward & Barth (1979) discuss the global character of Venus UV night airglow. Their dataset consisted of narrow band 198 nm images of NO and they found an increase of radiation at the antisolar point, where N and O recombine. Thus, N and O must be transported from their formation on the dayside to the nightside. The airglow is brightest at equatorial latitudes and at longitudes on the morning side of the antisolar meridian.

Durrance *et al.* (1980) reported on observations of the Venus dayglow spectrum at 125–143 nm. Hord *et al.* (1991) discusses a spectrum of Venus atmospheric emission in the 55.0– to 125.0 nm wavelength region. Emission of helium (58.4 nm), ionized atomic oxygen (83.4 nm), and atomic hydrogen (121.6 nm), as well as a blended spectral feature of atomic hydrogen (Lyman- β) and atomic oxygen (102.5 nm) were obtained with the Galileo Extreme Ultraviolet Spectrometer.

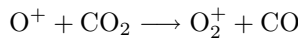
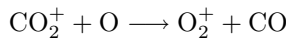
Bouger *et al.* (1990) used data from the Pioneer Venus Orbiter UV spectrometer and combined the data with a thermospheric general circulation model of Venus to determine the nitric oxide airglow.

Feldman *et al.* (2000) obtained FUV spectra of Venus in the range 82–184 nm with the Hopkins Ultraviolet Telescope (HUT) as a part of the Astro-2 experiment onboard the space shuttle Endeavour (Figure 6.3).

The complex structure of the Venusian atmosphere can be traced by oxygen airglow. Oxygen is formed by UV photolysis of CO₂ in the atmosphere of Venus. Above 100 km there is an east-west superrotation and below 70 km a solar-locked circulation. On the dayside of the planet material rises, flows around the nightside and descends at the antisolar point. The oxygen atoms are formed in the sunlit side, transported to the nightside and during their descent they recombine to molecular O producing the airglow (see Allen *et al.* 1992). Observations in 1.27 μm are reported by Crisp *et al.* (1996). Slanger *et al.* (2001) report on observations of the oxygen green line 557.7 nm in the night airglow of Venus using Keck observations.

6.2.6 The Ionosphere of Venus

The ionosphere of Venus is mainly formed by the photoionization of the major neutral components CO₂ and O



The Pioneer Venus orbiter measured over 14 years the properties of the ionosphere of Venus. The solar EUV radiation varies with solar activity. At solar

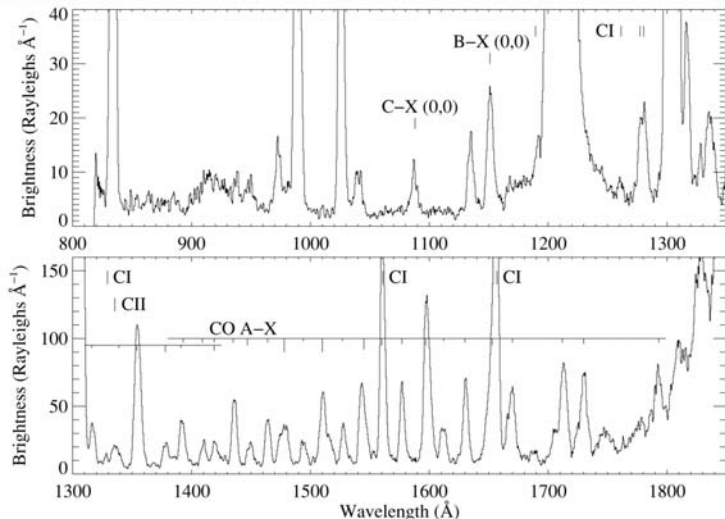


Figure 6.3: HUT spectrum of Venus obtained on 1995 March 13. Emission of carbon and CO are indicated. The positions of the strongest solar Ly α and O I 130.4 nm CO bands are also indicated separately. The spectrum also contains emission from the daytime terrestrial atmosphere. Courtesy: P. Feldman. Reprinted with permission of the American Astronomical Society

maximum the Venus ionosphere extends to its highest altitudes and nightward ion transport was the main source of the nightside ionosphere. Studying the upper and lower ionosphere, Ho *et al.* (1993) found that nightward ion transport was reduced during solar minimum, when electron precipitation appears to be the main source.

- Upper ionosphere ($h > 1800$ km): solar EUV flux effects are significant. The electron density decreases by about an order of magnitude from high to low EUV flux, while the electron temperature at least doubles.
- Lower ionosphere (200 - 600 km): lower EUV fluxes are associated with slightly reduced density and higher temperature.

During high solar activity the Venusian ionosphere has three distinct regions: the photochemical, the diffusion-dominated (ionospheric topside) and the ionopause. During low solar activity the diffusion region is nearly extinct (Mahajan & Dwivedi 2004).

The direct interaction of the solar wind with the ionosphere of Venus also leads to a loss of e.g. O_2^+ in the oxygen corona. This process is called ion pick-up.

6.3 Mars

Since antiquity, Mars has attracted the interest of the astronomers, first for its apparently erratic orbit and then for the possibility of being Earth-like and habitable¹¹.

In the 1960s, observations from Earth and flyby spacecraft changed this picture completely . The Mariners 4, 6, and 7 returned images of a Moon-like, heavily cratered surface. The atmosphere was found to be almost pure carbon dioxide (CO_2), only a hundredth the density of Earth's, and the polar caps proved to be almost entirely frozen CO_2 . The first global views of Mars, returned by the Mariner 9 orbiter in 1972, revealed that the planet was far more complex than the earlier flyby missions had shown, with huge volcanoes, an enormous canyon system, and evidence of running water at some point in the past. The possibility of organisms on the surface could not yet be ruled out.

6.3.1 Basic Facts

Mars is the fourth planet from the Sun and the seventh largest, its diameter being 6 794 km. Because there are no oceans on Mars, its surface area is about the same as the land surface on Earth even though the planet is only half the size of the Earth. The semi-major axis of its orbit around the Sun has 227×10^6 km (1.52 AU). Mariner 4 was the first spacecraft to visit the planet in 1965. In 1976 two spacecraft set down landers (Vikings 1 and 2) that photographed the surface and measured meteorological conditions at the surface. In 1997 Mars Pathfinder landed successfully with a small vehicle carrying different probes to analyse Martian surface. In January 2004 two landers (Spirit and Opportunity) again equipped with mobile vehicles, successfully analysed the surface¹². Few days before the European Mars Express arrived to the Martian orbit, starting a search for subsurface water and a detailed mineralogy mapping.

Because of the highly elliptical orbit of Mars there is a large temperature variation of about 30°C at the subsolar point between aphelion (when Mars reaches its greatest distance from the Sun) and perihelion (when Mars reaches its closest distance to the Sun). The average temperature on Mars is about 218 K (-55°C), but the surface temperatures range from 140 K (-133°C) (in winter near the poles) to almost 300 K (27°C) during summer near the equator. The temperature variations are so large because the atmosphere is very thin (only 1% that of the Earth).

The interior of Mars consists of a dense core about 1700 km in radius, a molten rocky surface mantle which is denser than the Earth's, and a thin crust. Data from the Mars Global Surveyor mission indicate that this crust is about 80 km thick in the southern hemisphere and only 35 km in the northern. Also, the

¹¹For textbooks and reviews on Mars see: Spohn et al., 1998, *Mars*, The Astronomy and Astrophysics Review 8, 181-236; *The Smithsonian Book of Mars*, J. M. Boyce, 2003, Smith. Inst. Press.

¹²The data supplied by the landers strongly support a wetter and warmer Early Mars. See the special issues of the journal *Science* (June and December 3) and the book of S. Squyres (2005) *Roving Mars: Spirit, Opportunity, and the Exploration of the Red Planet, Hyperion*.

surface appears quite asymmetric. The northern hemisphere consists of plains that are much younger and lower in elevation (the number of craters in an area gives an indication of when this area was formed). The southern hemisphere is predominantly ancient, there are many craters and it resembles the lunar surface. The relatively low density of Mars compared to the other terrestrial planets may be explained by a large fraction of sulphur in addition to the iron in its core.

Olympus Mons is the largest mountain in the Solar System, rising 24 km above the surrounding plain. The base has a diameter of about 500 km. The Tharsis region is a huge bulge about 10 km high and 4000 km across. Valles Marineris is a system of canyons, 4000 km long and 2–7 km deep.

Mars has an extremely weak magnetic field because it is about half the diameter of the Earth and has about 1/10 the Earth's mass, so its internal heat should have dissipated long ago. So even though Mars rotates quickly (once every 24.6 hours), its metallic core is may be solid and thus no dynamo action for the creation of magnetic fields is possible (such a dynamo requires freely moving charged particles in a molten core).

6.3.2 The Atmosphere of Mars

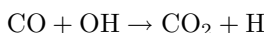
As has already been pointed out, the atmosphere of Mars is very thin. It is composed mostly of CO₂ (95.3%) and N (2.7%), Ar (1.6%), and traces of oxygen (0.15%) and water (0.03%). The average pressure on the surface is only 7 mbar (less than 1% of Earth's). But strong winds and dust storms occur that can engulf the entire planet for months. The greenhouse effect produced by the thin atmosphere rises the temperature by 5 K, which is much less than on Venus or Earth.

At both poles there are permanent ice caps composed of water ice and solid carbon dioxide. In the northern summer the CO₂ completely sublimes leaving a residual layer of water ice. There are also clouds of water ice in the vicinity of large mountains. There is also evidence of large amounts of water below the surface. With the the neutron spectrometer of the Mars Odyssey orbiter it was possible to measure huge quantities of water ice at a depth of 1–2 m.

The first papers on the determination of Martian temperatures were given by Menzel *et al.* (1926) and Petit & Nicholson (1924) . The presence of water in the Martian atmosphere was first suggested by V. M. Slipher (1875–1969) and later verified by Spinard *et al.* (1963).

There are indications for drastic climate changes on Mars in which H₂O and CO₂ freeze out in a runaway condensation from a dense atmosphere (e.g. Nakamura 2004). Over the last 80% of the history of Mars permafrost and the cryosphere have dominated the surface.

The UV radiation influenced photochemistry of Mars is quite similar to that of Venus: the photodissociation of CO₂ and a slow recombination of CO. In the case of Mars a rapid downward transport of CO, O and O₂ is expected. Here, the recombination of CO and O is catalysed in the presence of OH which is produced by



This has been pointed out, for example, by Jakosky & Lindner (1984).

Bougher *et al.* (2000) have shown that there is a large variability in exospheric temperature (~ 60 K) from perihelion to aphelion during high solar activity, and that there is a large variability between minimum and maximum (200–380 K).

6.3.3 UV Radiation Environment

Since Mars is one of the primary targets in astrobiology the study of the UV and ionizing radiation incident on its surface is of great interest.

In order to understand the evolution of UV radiation on Mars we have to take into account the following considerations:

- Mars does not have an appreciable intrinsic magnetic field at present.
- Mars has a comparatively small gravitational acceleration.
- Atmospheric loss processes may be active and several important constituents escape into space. The escape rates of atmospheric constituents, including water, from Mars indicate that the red planet could have lost an atmosphere of at least 1 bar to space during the past 3.5 Ga (see Molina-Cuberos *et al.* 2001).

On Earth, protection against UV radiation is provided by ozone (O_3), and solar UV radiation at $\lambda \leq 300$ nm does not reach the surface. Mars has an atmosphere that is rich in CO_2 and this atmosphere prevents UV radiation at $\lambda \leq 200$ nm from reaching the surface. The CO_2 absorption cross-section for different temperatures (adapted from Lewis & Carver 1983) is shown in Figure 6.4. CO_2 on Mars provides significant absorption at $\lambda < 200$ nm. Above this wavelength limit, the CO_2 extinction cross-section is equivalent to the Rayleigh scattering cross section and thus negligible.

UV radiation on Mars surface has higher energy and is an important agent for weathering. Laboratory experiments on putative Martian surface materials were therefore performed and it was found that this weathering process could be important on long time scales (> 100 yr) (Morris 1981). Aspects of the past and present ultraviolet radiation environment of Earth and Mars are discussed by Cockell *et al.* (2000) and Cockell (2002).

For high latitude regions in winter the O_3 absorption becomes significant. Today, the total integrated UV flux between 200 and 400 nm is comparable to the Earth's; however, on Mars the shorter wavelengths contribute much more.

O_3 was first detected in the Martian atmosphere using Mariner 7 data and the concentration is seasonally and spatially variable. The Earth's ozone layer corresponds to 300 Dobson Units (DU). For Mars levels at high latitudes towards northern winter are typically 5.7 DU. Clancy *et al.* (1996) using the HST Faint Object Spectrograph, measured the presence of small amounts of O_3 at low latitudes (0.3 DU) towards aphelion.

The biological response of organisms is highly wavelength-dependent. DNA, for example, has a peak absorption near 260 nm that decreases by a factor of six towards 290 nm. We therefore discuss the variation of ozone in more detail.

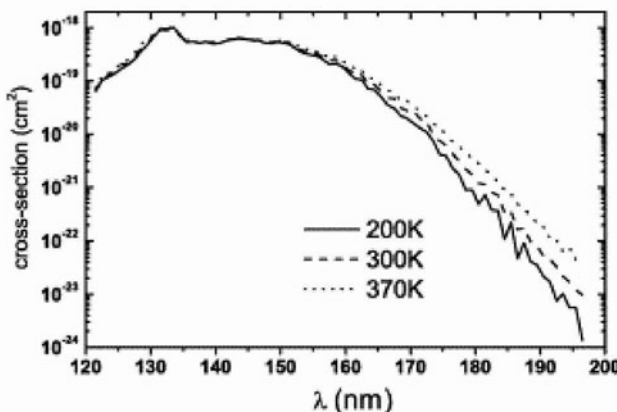


Figure 6.4: UV absorption cross-section of the carbon dioxide for various temperatures. The CO₂ absorption shows a characteristic cut-off between 190 and 200 nm.

The presence and disappearance of O₃ can be explained through photochemical interactions with H₂O, with which it is anti-correlated in abundance. During northern winter, the formation of the northern water–ice polar cap removes water vapour from the atmosphere, allowing the formation of O₃ through the photolysis of CO₂ and the reaction of atomic oxygen and O₂. Thus O₃ abundance reaches a maximum towards northern winter and begins to fall during spring as the northern polar cap begins to recede, releasing trapped water vapour which in turn begins the photolytic destruction of O₃.

A still unresolved issue is the properties of Martian dust with regard to UV absorption. The periods of low dust levels in the Martian atmosphere tend to occur near aphelion (northern summer), with high activity and possible global dust storms occurring towards perihelion (southern summer). Incident UV flux is significantly higher at perihelion than at aphelion ($\sim 4\%$), but this is counteracted by the higher dust activity, which increases the lower limiting dust optical depth to 0.5. This causes a corresponding decrease in flux that brings the surface irradiance almost to the aphelion levels. The problem of dust absorption of UV was stressed by Firsoff (1978) who commented on the remarkably bright Martian sky near the horizon. Cordoba-Jabonero *et al.* (2003) have shown that volcanic ash and SO₂ (10^{14} – 10^{15} g) considerably reduces the levels of UV radiation, leading to a biological dose comparable to that existing on present day Earth.

Patel *et al.* (2003, 2004) have developed a model to study the UV surface irradiance at any time and place during the Martian year. A solar UV “hotspot” has been revealed towards perihelion in the southern hemisphere ¹³. Calculations were performed for two dust scenarios. The average dust scenario, as expected, creates the highest UV dose levels as less dust in the atmosphere allows greater

¹³A UV sensor was incorporated in the Beagle 2 mission (Patel *et al.* 2002) with the aim of measuring for first time UV fluxes at the Martian surface. Unfortunately, the spacecraft failed to land safely.

penetration of UV to the surface. In the high dust scenario the UV hotspot is spread out in the equatorial region over a substantial part of the Martian year. The polar regions clearly suffer the lowest UV irradiation and therefore afford the best biological protection. Studies in Antarctica using a 254 nm source (UV-C) showed that at an ice depth of 1 cm the UV-C is reduced by 40% and at a depth of 5 cm about 90% of the UV-C radiation is attenuated (Cockell 2002).

Table 6.5: Instantaneous UV flux (zenith angle = 0°) and daily fluences (vernal equinox for Earth and Mars, 2-week light period for Moon) for UV-A, UV-B and UV-C. IF stands for “Instantaneous flux” (W/m^2), DF for “Daily fluence” (kJ/m^2) and DNA for “DNA-Weighted irradiance” (relative to present day Earth). Note that for DNA daily fluences the values are divided by 1000. Source: Cockell (2001) pg. 203

	Earth		Moon		Mars	
	IF	DF	IF	DF	IF	DF
UV-C	~ 0	~ 0	8.3	10,039	3.4	120
UV-B	2.0	39	18.5	22 377	7.9	286
UV-A	56.8	1 320	74.2	89 752	31.1	1 126
DNA	1	21	2 358	2.8×10^6	950	19 950

Cockell (2001) has compared the UV Flux on the Earth, the Moon and Mars (see Table 6.5). The UV-B and UV-C fluxes are higher on Mars, but because the length of the day and the obliquity on Mars are almost identical to the Earth, the UV flux at any given latitude can be made similar to Earth’s by simply changing the spectral quality of the instantaneous flux using UV-screening materials. However, UV-A fluxes are lower on Mars than on our planet. The potential biological consequences of this are still unclear.

Recently Cockell & Raven (2004) have studied possible habitats for phototrophic life¹⁴. They calculated the “Martian Earth-Like Photosynthetic Zone (MEPZ)” for different materials available on the martian surface (rocks, polar snow, ferric iron and gneiss) and found that under the worst assumptions of UV radiation (no ozone layer, only UV absorption by CO_2) photosynthesis could have been sustained in micro-habitats of Archaean Mars. The lack of an ozone shield does not seem to be a limitation for the colonization of land by photosynthetic organisms.

6.3.4 The Martian Ionosphere

The first indication of a Martian ionosphere was obtained by the Mariner IV (Fjelbo *et al.* 1966). Subsequent results have been obtained by the Viking landers (Chen *et al.* 1978 and different radio occultation experiments).

Observations from US and USSR Mars missions were analysed to derive neutral gas temperatures inferred from topside plasma scale heights on electron density distributions (Bauer & Hantsch 1989). They show a higher dependence on solar

¹⁴These microorganisms use visible light, otherwise known as Photosynthetically Active Radiation (PAR), as a source of energy. On Earth they manage to synthesize UV-screening compounds or have good DNA-repair mechanisms.

activity than found on Venus and the discrepancy with the observed solar cycle dependence of ionospheric peak plasma densities could be explained by the fact that topside scale heights are derived from a greater altitude and may be affected by transport and other processes.

All dayside profiles have nearly constant constant slopes above the peak regardless of the phase of the solar cycle and the solar zenith angle (Ness *et al.* 2000). Molina-Cuberos *et al.* (2001) show the complexity of ionospheres in a CO₂-rich atmosphere.

The maximum density of the Martian ionosphere occurs at a height of about 135 km, where O₂⁺, CO₂ and O⁺ are found and can be explained by the theory of Chapman. There is thus a corona mainly of oxygen that is lost by dissociative recombination processes in addition to the loss of hydrogen by thermal escape. Also, the solar wind directly influences the oxygen.

6.3.5 Airglow

The interaction of solar UV radiation with CO₂, the main constituent in the Martian atmosphere, produces the airglow observed, for example, by Mariner 9 ultraviolet spectrometer observations¹⁵ (Barth *et al.* 1972). Atomic H and O also produce airglow emission. Such observations also permit investigation of the escape rate of atomic H, and it can be shown that if the current escape rate has been operating for 4.5 billion years and if water vapour is the ultimate source, an amount of O has been generated that is far in excess of that presently observed.

A more detailed description on the martian airglow can be found in Conway (1981). The brightest feature that originate between 88 and 180 km are the carbon monoxide Cameron bands in the wavelength region 180.0-260.0 nm.

Figure 6.5 shows a UV spectrum of Mars obtained by Feldman *et al.* (2000) with the Hopkins Ultraviolet Telescope (HUT).

6.3.6 Ancient Mars

There is evidence that during the early history there was tectonic activity on Mars but at present there is none. This also means that hotspots remain stable and can explain the Tharsis bulge and the enormous volcanoes.

From surface features it can be deduced that large floods and river systems with some liquid must have caused erosion¹⁶. There may have been even large lakes or oceans as inferred from images of layered terrain. The age of the erosion channels is about 4 billion years.

The young Mars was much more like Earth. But plate tectonics played an important role on Earth, where almost all of the CO₂ was used up to form carbonate rocks. Mars was unable to recycle any of its CO₂ back into its atmosphere because there were no plate tectonics and thus no significant greenhouse effect.

¹⁵Mariner 9 UV spectrometer measurements are based on Lyman- α emission.

¹⁶The history of water on Mars was described in the book by M. H. Carr, Water on Mars, 1996, Oxford University Press

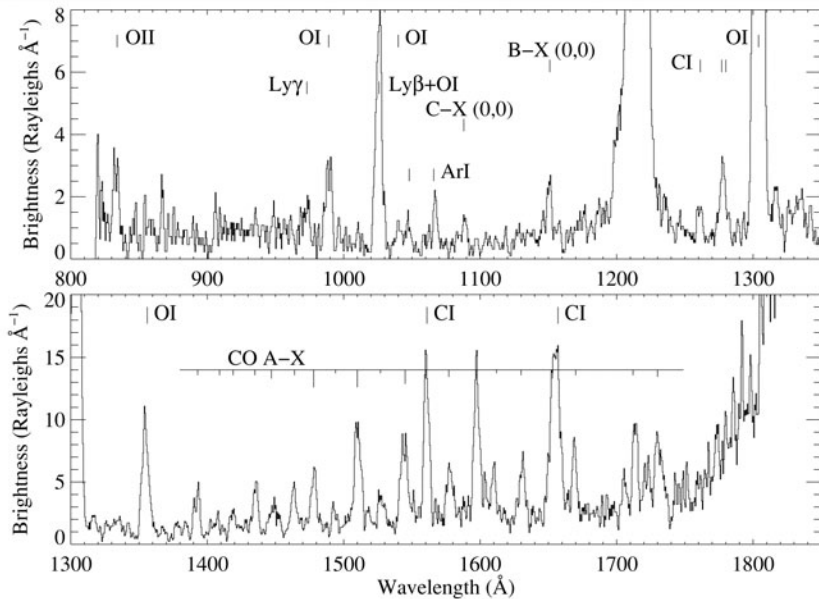


Figure 6.5: HUT spectrum of Mars. It was obtained during orbit night and does not show the strong terrestrial emissions (with the exception of H I) seen in the Venus spectra. Courtesy: P. Feldman. Reprinted with permission of the American Astronomical Society.

The surface of Mars therefore got much colder than the Earth's would be at the same distance.

Let us come back to the question of the Early Sun problem. As it was shown in the previous chapter, the Sun was much more active in the post-Hyades phase; only this phase is relevant for planetary formation because it starts at a zero age main sequence of the Sun of 600 Ma. As was shown in Ayres (1997), the photoionization rate of important atmospheric components such as H, O, O₂ and N₂ scales backwards in time as $\sim t^{-1}$. A primordial Martian atmosphere that formed at a solar age of 0.5×10^9 yr would have been subjected to approximately twice the photoionization rate as the same atmosphere forming at 1 Ga. At the later age photoionization rates were five times the present values at solar maximum. This has played thus a key role in the loss of volatiles in the primitive Martian atmosphere. The evolution of the solar wind have played also an important role. The young Sun and the photochemistry of Mars was investigated by Nair *et al.* (1993). Because there are many hints at surface structures that must have been formed by liquid water, it was suggested that a dense CO₂ atmosphere is required to initiate a large greenhouse effect allowing liquid water. The problem with that scenario, however, is that CO₂ would freeze out (Kasting 1991). Since the young Sun emitted considerably more strongly at the UV wavelength, the CO₂ would have been rapidly dissociated by $\lambda < 200$ nm photons. The calculations led to the conclusion that by this intense UV radiation of the early Sun : a) CO₂ is split in

to CO and O, b) O transforms to O₂ and c) because of the intense UV radiation O₂ transforms into ozone, O₃.

A similar scenario is assumed for the early Earth. Another solution to explain the fluvial networks detected on Mars that were formed during the first 1 Ga requires greenhouse gases such as NH₃ and CH₄. The first, however, would also have been photolyzed by the intense UV radiation of the early Sun. Methane, which is very rare in volcanoes on Earth, could have been produced by methanogenic bacteria (Kasting 1993). Methane was also photolysed by the strong early solar UV radiation; hence, it must have been replenished. An atmosphere of a few bars of CO₂ and a few per cent of CH₄ would have been sufficient to keep temperatures on Mars above freezing. Of course, another alternative to explain the fluvial channels on Mars is climate changes driven by orbital variations.

Another important parameter in the primitive Martian atmosphere is, or could have been, water. Oxygen, produced by photodissociation of water vapour in an earlier stage of terrestrial planet evolution may be lost by hydrodynamic escape (Chassefiere 1996).

Various scenarios are possible. If a continuous supply of water by comets is assumed during the heavy bombardment phase (about one 1 Ga), about 0.3 terrestrial ocean accreted. A primitive ocean corresponding to 0.45 and 0.2 of the present terrestrial oceanic volume could have been lost because of the high solar EUV flux on Venus and Mars and 30 and 50% of the O contained in the ocean could have been released by hydrodynamic escape. No significant escape of oxygen is found for Earth, whatever the model parameters chosen: when comparing the three terrestrial planets, the Earth is the least favorable for escape, since Venus receives more solar energy and Mars, although more distant from the Sun, has a weaker gravitational field.

A gradualist view of the UV history of Mars might be different if the planet had suffered atmospheric collapse producing a reduction in the atmospheric CO₂ reservoir from ~1 bar to ~6 mbar increasing the DNA-weighted biological irradiance by a factor five and giving rise to an “ultraviolet spring” (Cockell 2001). In the opposite direction, episodic CO₂ releases of up to 2 bar resulting from catastrophic floods may have occurred, producing a decrease in the UV surface radiation (Gulick *et al.* 1997).

Ronto *et al.* (2003) suggest that the UV irradiance on Mars 3.5 Ga ago may have been comparable to that of present-day Earth. Table 6.6 compares the biological effects for T7 bacteria and uracil at various UV irradiance levels.

Cockell *et al.* (2000) used a radiative transfer model to quantify the past and present Martian UV environment. Table 6.7 summarizes the main results, where, together with UV fluxes, the biologically weighted irradiance is also calculated.

6.3.7 Detection of Life on Mars: Viking and ALH84001

The Viking landers were the first instruments to measure any changes on the martian surface that might be explained by microorganisms. The results were negative or unclear. For a general review on the topic the reader is referred to a

Table 6.6: Dose rates of biological effects at various solar UV irradiance levels on the Martian surface. Different values of τ (optical depth) represent distinct concentrations of dust. Minimal erythema dose (MED). From Ronto *et. al.* (2003).

	H^{T7}/hour	H^U	MED/hour
PRESENT MARS			
Without O_3			
$\tau = 0.1$	1806.92	18.73	16.53
$\tau = 3.0$	280.42	2.90	2.37
With O_3			
$\tau = 0.1$	22.79	0.28	0.79
$\tau = 3.0$	9.73	0.10	0.14
ANCIENT MARS			
Pure CO_2	121	0.012	0.093
CO_2, O_3, O_2, NO_2	7.2×10^{-3}	8.7×10^{-6}	0.027

number of textbooks¹⁷.

The Viking biology experiment weighed 15.5 kg and consisted of three subsystems (Klein 1978,1998):

- Pyrolytic Release experiment (PR): A 0.25 cm^3 soil sample was incubated in a simulated martian atmosphere of CO_2 and CO labelled with C^{14} . A xenon arc lamp provided simulated sunlight. After 5 days, the atmosphere was flushed and the sample heated to 625°C to break down, or pyrolyze, any organic material, and the resulting gases were passed through a C^{14} detector to see if any organisms had ingested the labelled atmosphere.
- Labelled Release Experiment (LR): A 0.5 cm^3 sample of soil was moistened with 1 cm^3 of a nutrient consisting of distilled water and organic compounds. The organic compounds had been labelled with C^{14} . The sample was allowed to incubate for at least 10 days in the hope that microorganisms would consume the nutrient and give off gases containing the C^{14} which would then be detected¹⁸. After the injection of the first nutrients, the level of ^{14}C climbed over several days before levelling off.
- Gas Exchange Experiment (GEX): A 1 cm^3 sample of soil was partially submerged in a complex mixture of compounds and after an incubation time of > 10 days in a simulated Martian atmosphere of CO_2 , with helium and krypton added, gases that might be emitted from organisms consuming the nutrient would then be detected by a gas chromatograph – this instrument could detect CO_2, O_2, CH_4, H_2 and N_2 . Oxygen levels were not inconsistent with biological activity. However other abiotic explanations were favoured, such as the oxidation of organics present in the nutrient by gamma Fe_2O_3

¹⁷Horowitz,N., 1986, To Utopia and back: the search for Life in the Solar System, W. H. Freeman;The Search for Life on Mars, M. Walter, M. Walters, P. Davies, 2000, Pers. Publ.

¹⁸Terrestrial organisms would give off CO_2 , carbon monoxide (CO), or methane (CH_4).

Table 6.7: UV Fluxes, Fluences, and Biologically Weighted Irradiances (DNA) at the Equator (for Vernal Equinox) of Mars and Earth, 3.5 Ga Ago and Present Day. Values at zenith angle = 0° are given in W/m²; values of daily fluences and doses are given in kJ/m². From Cockell et al. (2000) Table I.

	UV-C and UV-B (200 - 315 nm)	UVA (315-400 nm)	DNA
Early Mars (1 bar CO ₂)			
Daily fluence	119	542	838
Zenith angle 0°	4.8	22.3	33.8
Early Earth			
Daily fluence	78	519	615
Zenith angle 0°	5.2	34.1	41.0
Present day Mars			
Daily fluence	361	1126	3183
Zenith angle 0°	13.2	41.5	116.4
Present day Earth			
Daily fluence	39	1320	2.10
Zenith angle 0°	1.86	52.81	0.10

in the surface samples (Oyama & Berdahl 1977) and the reaction of residual humidity with peroxides and superoxides produced by solar UV.

In addition, independent of the biology experiments, Viking carried a Gas Chromatograph/Mass Spectrometer (GCMS) that could measure the composition and abundance of organic compounds in the Martian soil. Surprisingly, it found no trace of any organic compound on the surface of Mars. Organic compounds are known to be present in space (for example, in meteorites).

Two main options were debated: a) the existence of Martian microorganisms and b) chemical reactions caused by the presence of strong oxidants on the martian surface. Solar UV was thought to activate soil particles, producing the emission of gases.

Koscheev *et al.* (1994) discussed the problem of the stability of martian salts under the enhanced UV radiation and low energy particle impact on a simulated Martian surface. They analysed MgSO₄ and CaCO₃ during UV -irradiation and particle impact. A release of CO₂ and SO₂ caused by UV irradiation was observed. The Martian surface is altered by UV radiation. Laboratory experiments show that electrons can be mobilized in mineral samples and in the presence of O, electrons are captured on grain surfaces to form superoxide radicals. This explains the reactive nature of the soil and the absence of organic molecules (Yen *et al.* 2000). UV degrades the organic material coming from meteoritic impacts (Bullock *et al.* 1989).

In the atmosphere of Mars oxidants such as H₂O₂ may exist. The stability of organic macromolecules against these oxidants is critical and can be tested in the laboratory. The results show that throughout the entire history of Mars some

organic macromolecules may be stable against oxidation on the martian surface, at least in the polar regions and thus serve as biomarkers (Mc Donald *et al.* 1998). The apparent biological results could be explained in terms of a non-biological process: H₂O₂ is formed chemically in the upper Martian atmosphere and descends to the soil where it causes chemical reactions (Hunten 1979). A sensitive search for H₂O₂, H₂CO, HCl and CH₄ and the detection of HDO was made by Krasnopolksky *et al.* (1997). These results show an enrichment in the D/H ratio by a factor of 5.5 ± 2 relative to Earth. The given uncertainty is mainly caused by possible variations in Mars' atmospheric water abundance. Levin (2002) argued that there is no highly oxidizing material on the surface of Mars that could have destroyed all the organic matter and therefore explain the negative results of the Viking experiment. Recent measurements of H₂O₂ by Encrenaz *et al.* (2004) give a mean column density of $6 \times 10^{15} \text{ cm}^{-2}$, but with spatial and possibly seasonal variations.

Series of GCMSs and LR tests were made on Antarctic soil samples (Levin & Straatt 1981). In some of the samples the LR showed identical results to those on Mars whilst the GCMSs could not detect any organic molecules. Moreover, we can mention that H₂O₂ was detected in ancient permafrost on Earth, and clearly did not eliminate the life. The debate continues.

Meteorites found on Earth could originate on other large bodies in the Solar System (the Moon, asteroids and planets) from which are ejected from. The so-called SNC meteorites¹⁹ have a very similar composition to the material on the martian surface. ALH84001 (ALH stands for Alan Hills) is by far the oldest Martian meteorite, with a crystallization age of 4.5 Ga and is therefore a sample of the early Martian crust. The cosmic ray exposure age of 16 million years dates the ejection from Mars by impact, while the termination of that exposure gives a terrestrial age of 13 000 years. A small amount of carbonate in ALH84001 ranging up to 200 microns in size appears to have formed in fractures inside this igneous rock in the presence of liquid water or another fluid. There is considerable debate about the origin of these carbonates. McKay *et al.* (1996) suggested that these grains are the sites of the three types of evidence that represent fossil life on Mars: PAHs²⁰, very stable organic molecules; oxide and sulphide biominerals; and nanofossil-like structures. However, alternative abiotic explanations have been proposed. We shall surely need *in situ* investigation, including underground drilling, to solve the problem.

Bianciardi *et al.* (2001) have suggested that if the present microorganisms of Mars are nannobacteria²¹, similar to those in ALH84001, GCMS's sensitivity should be unable to detect a million of nannobacterias per gram of Martian soil, a quantity sufficient to produce the positive results of the LCR experiment.

An interesting question is whether the planet might have been contaminated by terrestrial microbes via inadequately sterilized spacecraft landers, rovers, or the impact of orbiters. Mancinelli & Klovstad (2000) used spores of *Bacillus*

¹⁹The SNC meteorites, so named for the shergottite, nakhelite, and chassigny classes which comprise this group of petrologically similar specimens, consist of 12 meteorites that share a set of similar properties that are highly anomalous compared to other meteoritic samples.

²⁰PAH = Polycyclic Aromatic Hydrocarbons

²¹Nanobacteria (sometimes Nannobacteria) are claimed to be cell-walled microorganisms with a diameter well below the generally accepted lower limit (about 0.2 micrometres) for bacteria.

subtilis that were dried and then covered by thin layers of simulated Martian soil. The probe was then exposed to UV radiation from a deuterium lamp and the samples were collected periodically to determine survival. As a control and reference the samples were prepared in triplicate. The main results were that an unprotected monolayer would be killed within minutes when exposed to the UV radiation expected on the Martian surface. However, if they are covered either by an additional layer of spores or a few microns of dust, they will survive for long periods of time. Thus the main result of this study is that spore-forming microbes on spacecraft could be protected by a thin layer of Martian dust and potentially contaminate the planet.

Finally, we should mention the recent detection of methane in the Martian atmosphere, opening a new window in the search of life (Formisano *et al.* 2004; Krasnopolsky *et al.* 2004).

6.4 Mercury

Mercury has an unstable atmosphere. Some elements were detected by Mariner 10 (Broadfoot *et al.* 1976). Two possible sources are considered: solar photon sputtering and solar wind sputtering (Morgan & Killen 1997)²².

Mercury's core is large compared to other terrestrial planets. It has been suggested that strong solar wind and high XUV fluxes of the Young Sun (during the first 0.5-1 Gyr of its life) swept away its early atmosphere and much of its outer mantle (see Ribas *et al.* 2004 and references therein)²³.

The Mariner measurements show that Mercury has a magnetosphere, probably produced through a dynamo process. The weak magnetic moment of Mercury, about 4×10^{-4} of that of the Earth's, combined with a solar wind pressure about seven times higher than that on the Earth, results in a very small planetary magnetosphere. The presence also of an ionosphere implies the existence of some of the processes that we have described for other terrestrial planets.

In principle, singly ionized species emitting in EUV can be good tracers for imaging the ionosphere/magnetosphere of Mercury. An ultraviolet imaging spectrometer is being developed for the BepiColombo mission (Yoshikawa *et al.* 2004). The Messenger spacecraft, on its way to Mercury, has no UV instruments on board.

6.5 The Giant Planets

6.5.1 Basic Facts

Jupiter is the fifth planet from the Sun and the largest in the Solar System²⁴. It possesses 28 known satellites, four of which - Io, Europa, Ganymede and Callisto -

²²Sputtering is a physical process in which atoms in a solid target material are ejected into the gas phase through bombardment of the material by energetic ions or photons.

²³An alternative hypothesis is a front impact of an asteroid or a comet.

²⁴A textbook on the Jupiter system: Jupiter : The Planet, Satellites and Magnetosphere, F. Bagenal, T. E. Dowling, W. B. McKinnon (Editors), 2004, Cambridge Univ. Press.

were observed as long ago as 1610 by Galileo Galilei (1564–1642). Another twelve satellites have been recently discovered. A ring system was discovered in 1979 by Voyager 1 spacecraft, but it is very faint and is totally invisible from the Earth.

The atmosphere of Saturn is primarily composed of hydrogen with small amounts of helium and methane. Saturn’s ring system makes this planet one of the most beautiful of the Solar System. Most of our knowledge derives from the visit of the Voyager, and will now clearly increase with the observations of Cassini. Figure 6.6 shows a recent view of the rings observed in UV radiation.

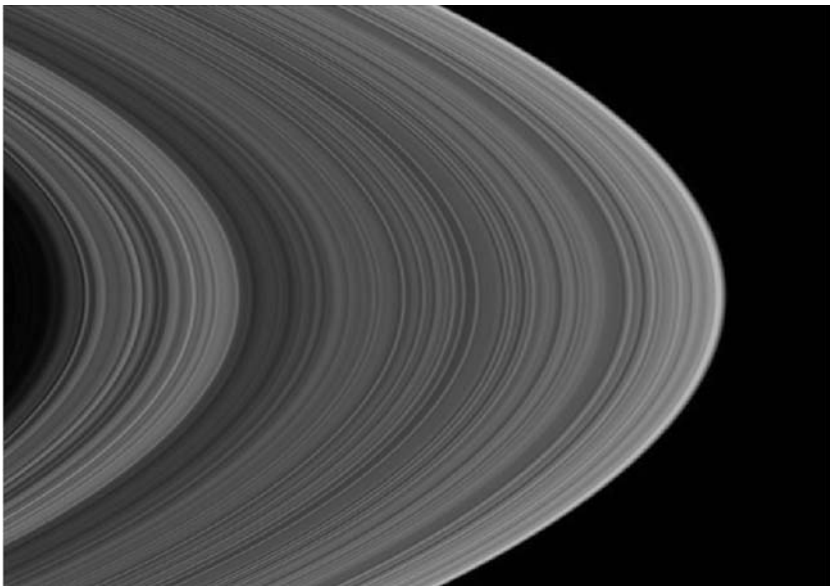


Figure 6.6: Ring system of Saturn observed with the UVIS spectrograph onboard Cassini. The Cassini–Huygens mission is a cooperative project of NASA, ESA and the Italian Space Agency. Image Credit: NASA/JPL/University of Colorado.

Uranus is the seventh planet from the Sun and the third largest in the solar system. It was discovered by William Herschel in 1781.

Neptune was discovered on 1846 September 23 by Johann Gottfried Galle (1812–1910) of the Berlin Observatory and Louis d’Arrest (1822–1875), an astronomy student, through mathematical predictions made by Urbain Jean Joseph Le Verrier (1811–1877).

6.5.2 Jupiter

Jupiter is the largest planet in the Solar System. Since many properties of the other giant planets (Saturn, Uranus and Neptune) are comparable to those of Jupiter, we shall discuss only Jupiter in detail.

The atmosphere of Jupiter is composed of hydrogen and helium, with methane, ammonia, H_2S and water as condensable aerosols. These gases interact in complex

Table 6.8: Comparison of the atmospheres of the giant planets.

	Jupiter	Saturn	Uranus	Neptune
Surface pressure	> 1000	$\gg 1000$	$\gg 1000$	$\gg 1000$
Temperature at 1 bar	165 K	134	76	72
Temperature at 0.1 bar	112 K	84	53	55
Density at 1 bar	0.16 kg/m ³	0.19	0.42	0.45
Wind speeds	150 m/s ($\phi < 30^\circ$)	~ 400	0–200	0–200
Scale height	27 km	59.5	27.7	20
Mean molecular weight	2.22 g/mol	2.07	2.64	2.53–2.69

ways to produce rotating horizontal bands and spinning cyclones (such as the Great Red Spot).

In order of decreasing condensation height (as well as saturation vapour pressure), the condensable gases are CH₄, NH₃, NH₄SH (NH₃H₂S) and H₂O. Below Jupiter's 150 km thick gaseous atmosphere, layers of liquid hydrogen and liquid metallic hydrogen are thought to be present, followed by a rocky core. Jupiter has a magnetic field ten times stronger than the Earth and a small ringlet discovered by Voyager 1. Jupiter also emits 1.7 times as much radiation as it receives from the Sun. In addition, it emits sporadic bursts of non-thermal radio noise at 22.2 MHz (decametric waves), in addition to a constant non-thermal emission at 300–3000 MHz (decimetric waves).

The Great Red Spot has a dimension of 11000 km \times 20000 km and is an anticyclonic storm that rotates counterclockwise with a period of 6 days. The red colour could be caused by photochemical products of sulphur and phosphorus compounds. However, no enrichment of phosphine is seen in the GRS, making phosphorus compounds unlikely chromophores. Jupiter's South Equatorial Belt vanished in early 1989, but reappeared when Jupiter emerged from behind the Sun in 1990. Jupiter is at its brightest as seen from earth every 23 years (the last peak was in 1987).

6.5.3 Atmospheres

A comparison of the chemical composition of the atmospheres of giant planets is given in Table 6.9 and temperature profiles in Figure 6.7. The main components of aerosols are ammonia ice and water ice, as well as ammonia hydrosulphide ice²⁵.

The atmospheres of Jupiter and Saturn are similar but there are also differences. First, Saturn's outer atmosphere of molecular hydrogen appears to be much deeper than Jupiter's. This is evidenced by Saturn's more oblate shape. Another important difference between Jupiter and Saturn's atmospheres is the difference in their helium content. Jupiter's helium content (relative to hydrogen) is very similar to the Sun's. Saturn's helium content is significantly lower. The reason for

²⁵The hydrosulphide NH₄HS can be obtained in the laboratory as a white solid by mixing well-cooled ammonia with a slight excess of sulphuretted hydrogen.

Table 6.9: Comparison of the chemical composition of the atmospheres of the giant planets. Values are given in percentages or ppm, uncertainties are given in ().

	Jupiter	Saturn	Uranus	Neptune
H ₂	89.9% (2%)	96.3 (2.4)	82.5 (3.3)	80.0 (3.2)
He	10.2 % (2%)	3.25 (2.4)	15.2 (3.3)	19.0 (3.2)
CH ₄	3000 (1000)	4500 (2000)	2.3%	1.5%
NH ₃	260 (40)	125 (75)		
Hydrogen deuteride (HD)	28 (10)	110 (58)	148	192
Ethane	5.8 (1.5)	7 (1.5)		
H ₂ O	~ 4			1.5

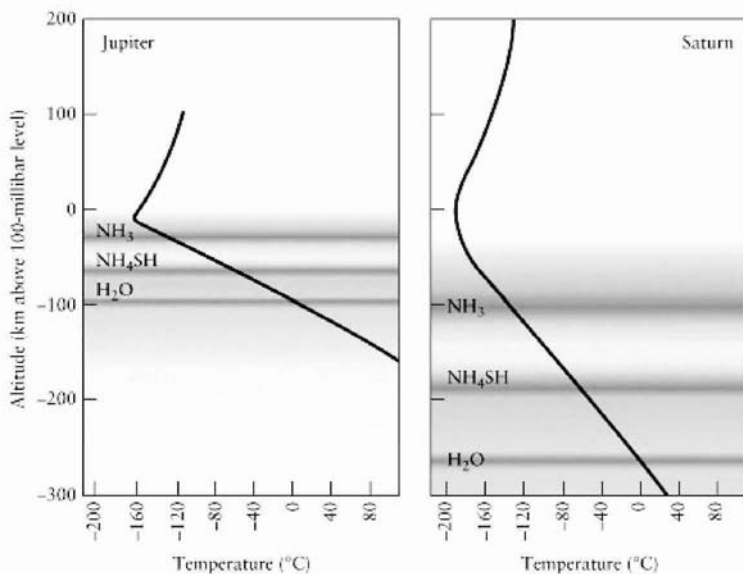


Figure 6.7: The atmospheres of Jupiter and Saturn.

Table 6.10: UV radiation photochemistry on giant planets

Photolyzed molecule	Wavelength
Ammonia, NH ₃	$\lambda < 230$ nm
Methane, CH ₄	$\lambda < 160$ nm
H ₂ S	$\lambda < 371$ nm
Phosphine, PH ₃	$160 < \lambda < 235$ nm

this is unknown, but one theory is that Saturn's helium condensed in the form of rain and sank to lower regions of the atmosphere. This raining process may have also contributed to Saturn's unexpectedly large internal heat output.

In the infrared Saturn emits 2.5–3 times as much energy as it receives from the Sun (Jupiter only 1.7–2 times as much). The viscous friction of the sinking He drops in Saturn causes the additional warming and explains the lower He content.

6.5.4 UV Photochemistry

On Jupiter, Saturn, Uranus and Neptune, temperatures are so low that most equilibrium constituents condense deep in the atmosphere and only the most volatile molecules survive to reach altitudes where they can interact with solar ultraviolet radiation. For instance, metals, rock-forming elements, and even H₂O molecules are tied up in condensed phases so deep in giant-planet atmospheres that they seldom or never interact with ultraviolet photons. The interesting photochemistry on the outer planets is therefore centered around small amounts of volatile molecules that contain elements such as carbon, nitrogen, phosphorus and sulphur.

The troposphere, where convection is prevalent, is generally defined as the atmospheric region located below the temperature minimum in planetary atmospheres. Thermodynamic equilibrium controls the chemical abundances within the tropospheres of the giant planets, but photochemical processes can also be significant. The thermodynamically stable form of nitrogen on the giant planets is ammonia (NH₃). Although ammonia is tied up in condensed phases in the tropospheres (e.g. as NH₄SH, NH₃ ice and/or a water solution cloud), its vapour pressure at the cloud tops of Jupiter and Saturn is sufficient enough for NH₃ photochemistry to be important. In the upper troposphere where ammonia is photolysed by photons with wavelengths in the ~190 to 220 nm range, phosphine (PH₃) is also present, and ammonia and phosphine photochemistry are linked as was described, for example, in Kaye & Strobel (1984). The major photochemical products are expected to be hydrazine (N₂H₄), molecular nitrogen (N₂), diphosphine (P₂H₄), aminophosphine (NH₂PH₂), and elemental phosphorus (e.g. P₄), although direct evidence for any of these species is lacking. Deeper in the troposphere, hydrogen sulphide (H₂S) may also be present, longer wavelength UV radiation (~260 nm) may penetrate deep enough. A review of that processes can be found in Lewis & Prinn (1984).

In the stratosphere radiative processes dominate the transport of energy. Methane (CH₄) is the most abundant equilibrium constituent and its photolysis therefore

dominates stratospheric photochemistry on Jupiter and the other outer planets. Strobel (1969) recognized that long-lived disequilibrium hydrocarbons are synthesized by methane photolysis in the upper atmosphere. They slowly diffuse downward to deeper, hotter, and denser atmospheric regions where they thermally decompose and react with H₂ to re-form methane. This recycling prevents the permanent conversion of methane into more complex hydrocarbons.

The observed NH₃ abundance in Jupiter and Saturn near and above the tropopause is well below saturation levels. On Uranus and Neptune the tropopause temperatures are so low that NH₃ is completely frozen out and no evidence of that molecule can be observed. The detection of NH₃ in Jupiter's stratosphere after the impact of comet Shoemaker-Levy presented a test of its abundance²⁶.

When UV photons break up H₂S molecules, the subsequent reactions lead to elemental sulphur, S₈ (yellow), ammonium polysulfide, (NH₄)_xS_y (orange) and hydrogen polysulphide H_xS_y (brown). This explains the colour bands on Jupiter and Saturn. The photolysis of phosphine leads to phosphorus P₈ which is red and may cause the colour of the Great Red Spot on Jupiter.

Studies of the atmospheric chemistry of Jupiter show that the photolysis of methane and ammonia initiate the formation of complex organics there (Moses 2000). UV radiation shortwards of 150 nm converts methane to acetylene, ethylene and other unsaturated hydrocarbons. The longer wavelength UV light reaching the ammonia clouds dissociates ammonia into radicals that initiate the further reaction of the acetylene and ethylene formed by methane photolysis. The coupled ammonia-acetylene photochemistry yields a series of C, H and N-containing compounds which are derived from products of hydrazine and acetylene. These molecules combine to make clouds of complex molecules, such as clouds of water and smog²⁷.

Far-ultraviolet images and spectra show a combination of reflected sunlight from Jupiter's upper atmosphere (tens of miles above the visible cloud tops) and the northern and southern lights (aurorae) produced by the impact of high energy charged particles trapped in Jupiter's magnetic field. Jupiter's polar regions normally appear dark in the far-UV because of absorbing aerosols apparently associated with the auroral process, and the northern lights appear clearly in the otherwise dark polar regions. Earlier baseline far-UV observations of Jupiter indicate the morphology and brightness of "normal" Jovian aurorae, which have been seen to vary on time scales of 5–10 minutes before the cometary fragment impacts began.

6.5.5 Aurorae

Aurorae result from a precipitation of charged particles from planetary magnetospheres. Earth-orbiting satellites have measured auroral emission for the outer planets. In the IR and UV these emissions are produced by atmospheric particles

²⁶See, for example, the textbook: The Collision of Comet Shoemaker-Levy 9 and Jupiter, K. S. Noll, H. A. Weaver, P. D. Feldman (Editors), 1996, Cambridge Univ. Press

²⁷The photochemical growth of complex organics in planetary atmospheres is studied by Raulin *et al.* (1996).

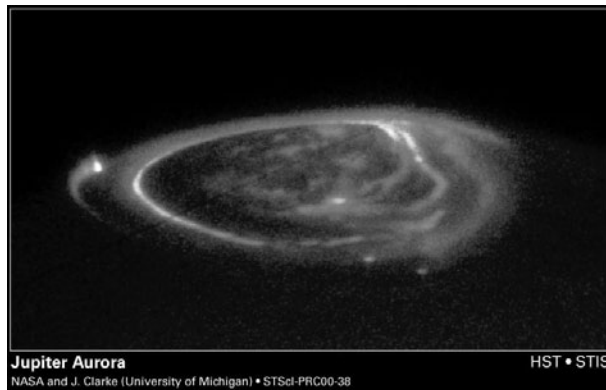


Figure 6.8: Hubble Space Telescope ultraviolet view of a blue aurora glowing half a billion miles from Jupiter.

excited by the incoming charged particles. Radio and X-rays are beam emissions of the incoming particles themselves.

Radio emissions from Jupiter provided the first evidence that this giant planet has a strong magnetic field and a large magnetosphere so large that, seen from the Earth, it has an angular size over four times that of our Moon. Jupiter also has polar aurorae, which are similar in many respects to Earth’s aurorae.

Figure 6.8 show a UV image of a blue aurora obtained by the Hubble Space Telescope (HST). We can see the main oval of the aurora, centred on the magnetic north pole, plus unique emission from the magnetic “footprints” of three of Jupiter’s largest moons. (These points are reached by following Jupiter’s magnetic field from each satellite down to the planet). Particles ejected from Io by volcanic eruptions flow along Jupiter’s magnetic field lines which thread through Io to the planet’s north and south magnetic poles.

Observations of aurorae in UV were made also from Saturn with the HST. Let us briefly describe the main difference between the aurora mechanism of the Earth, Jupiter and Saturn:

- Earth: Aurorae controlled by the interaction of the Earth’s magnetic field with the solar wind.
- Jupiter: Dominated by internal dynamics and plasmas; particles from Io.
- Saturn: Intermediate case.

In the December 2000 Cassini flyby of the Jupiter system, the Cassini Ultraviolet Imaging Spectrograph (UVIS) monitored Jupiter’s auroral emissions from day 275 of 2000 to day 81 of 2001. Several brightenings were seen in Jupiter’s aurorae in which the global auroral output increased by a factor of 2–4. These events persisted over a number of hours and were tied to large solar coronal mass ejection events. The auroral UV emissions from these bursts also correspond to hectometric radio emission increases reported by the Galileo and Cassini Radio and Plasma

Wave experiments (Pryor *et al.* 2001). Gurnett *et al.* (2002) report on simultaneous Cassini and Galileo observations of hectometric radio emission and extreme ultraviolet auroral emission from Jupiter. Their results show that both types of emission are triggered by interplanetary shocks propagating outwards from the Sun. Such a shock arriving at Jupiter causes a major compression and reconfiguration of the magnetosphere, which in turn produces strong electric fields and therefore electron acceleration along the auroral field lines similar to the processes occurring during geomagnetic storms on Earth.

A comparison of the aurorae seen on the outer planets was given by Bhardwaj & Gladstone, 2000. A introductory description of Saturn's aurorae can be found in Szuromi (1995). Ben Jaffel *et al.* (1995) claim that auroral activity of Saturn is also related to the formation of aerosols, because in UV images of the HST near 220 nm a dark oval ring was found encircling the magnetic north pole of Saturn, and this structure correlates very well to the aurorae detected by the Voyager UV spectrometer.

6.5.6 Airglow

Carlson & Judge (1971) made calculations of both resonant scattering and fluorescence of the incident solar flux in the wavelength region 30–130 nm for the upper atmosphere of Jupiter.

During the occultation of the star Regulus by Jupiter, as seen from the Voyager 2 spacecraft on 1979 July 9, two absorbing regions were detected between 91.1 and 120 nm that provided the height profiles of molecular hydrogen, methane, ethane and acetylene, as well as the thermal profile in Jupiter's upper atmosphere (Festou *et al.* 1981).

In situ measurements and comparisons of variations of the Jovian atmosphere can be made by using Pioneer and Voyager data. Measurements of Jupiter's He 58.4 nm airglow showed variations with longitude that are out of phase with Ly- α . Properties of the atmosphere (temperature, eddy diffusion coefficient) and excitation play a role (McConnell *et al.* 1981).

The question (with regard to dayglow emission) is whether the anomalously bright UV emission seen in the upper atmospheres of the outer planets is from solar fluorescence or electron excitation. Mc Grath *et al.* (1989) examined IUE spectra of Jupiter and found no conclusive evidence for the dominance of either process producing the Jovian dayglow emission. Feldman *et al.* (1993) obtained UV spectra of the Jovian equatorial dayglow in the spectral range 83–185 nm (Fig. 6.9). The observed spectrum is dominated by electron impact excitation of the H₂ Lyman and Werner band systems and, on the basis of model calculations, photoelectron excitation does not appear able to account for the amount of observed electron-excited H₂ emission, but only a weak airglow emission. This was also examined by Liu & Dalgarno (1996) : the UV spectra of HD and H₂ can be explained by solar fluorescence and photoelectron excitation, and the emission can be characterized by an atmospheric temperature of 530 K and an H₂ column density of 10²⁰ cm⁻².

Herbert & Sandel (1999) report on FUV and EUV observations of Uranus and

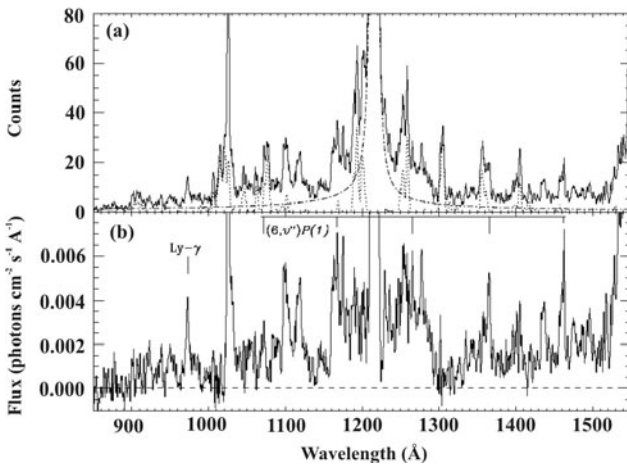


Figure 6.9: Composite HUT spectrum of the equatorial region of Jupiter. The spectrum also includes contributions from the terrestrial geocorona, grating-scattered Lyman- α (dot-dashed line) and the Io plasma torus (dashed line). The latter two are subtracted to give the spectrum in (b). Courtesy: P. Feldman. Reprinted with permission of the American Astronomical Society.

Neptune by the Ultraviolet Spectrometer on Voyager 2. The temperature, energy deposition and major-constituent compositional profiles of these atmospheres above the 0.1–1 mbar level could be derived, as well as observations of airglow, the light emitted by these atmospheres.

Results from the occultation of the Sun by Neptune imply a temperature of 750 ± 150 K in the upper levels of the atmosphere (composed mostly of atomic and molecular hydrogen) and define the distributions of methane, acetylene and ethane at lower levels. The ultraviolet spectrum of the sunlit atmosphere of Neptune resembles the spectra of the atmospheres of Jupiter, Saturn, and Uranus in that it is dominated by the emissions of H I Ly- α (340 ± 20 rayleighs) and molecular hydrogen. Weak auroral emission has been tentatively identified on the night side of Neptune (Broadfoot *et al.* 1989).

6.5.7 Ionospheres

As the magnetosphere rotates with Jupiter, it sweeps past Io and strips away about 1 000 kg of material per second. The material forms a torus, a doughnut-shaped cloud of ions that glow in the ultraviolet. Heavy ions in the torus migrate outwards, and their pressure inflates the more energetic Jovian sulphur and oxygen ions, which fall along the magnetic field into the planet's atmosphere, resulting in aurorae. Io acts as an electrical generator as it moves through Jupiter's magnetic field, developing 400 000 volts across its diameter and generating an electric current of 3 million amperes that flows along the magnetic field to the planet's

ionosphere. The Voyagers observed ionospheric temperatures that changed with altitude, reaching about 1 100 K (830°C). That was also not observed by Pioneers 10 and 11, and Voyager scientists believe they are witnessing large temporal or spatial changes in the ionosphere of Jupiter.

The electron-density profiles of the ionosphere of Jupiter and Saturn were modeled by Majeed & McConnell (1991), using Voyager data. Six radio occultation experiments were conducted with the Galileo orbiter in 1997, yielding detailed measurements of the distribution and motion of plasma surrounding Io (Hinson *et al.* 1998). A model for an explanation of far ultraviolet emission observed from the Io flux tube footprints in the Jovian ionosphere has been presented by Shaposhnikov *et al.* (2001).

6.6 Comets

6.6.1 Basic facts

Comets belong to the minor bodies of the Solar System but because of their spectacular appearance they have been known since antiquity. There are Chinese records of the periodic comet Halley from 240 BC and the famous Bayeux Tapestry, which commemorates the Norman conquest of England in 1066, also shows an apparition of Halley. About 1000 comets are catalogued, and from these some 200 are periodic with orbital periods of less than 200 years²⁸.

To describe the physical structure of a comet Whipple's term "dirty snowball" is appropriate²⁹. They are a mixture of ices (water and frozen gases) and dust. As soon as they are near the Sun (that means inside the orbit of Mars approximately), they become active and begin their typical appearance with a large coma and a long tail.

The following parts can be distinguished:

- Nucleus: relatively solid, stable; large amounts of ice and gas and other solids; diameter only several tens of km.
- Coma: a dense cloud of water, carbon dioxide and other neutral gases sublimed from the nucleus.
- Hydrogen cloud: millions of km in diameter; consists of neutral H.
- Dust tail: up to 10^7 km long. It is yellowish in appearance as a consequence of reflected sunlight and forms when solar photons strike micron-sized dust particles that dislodge from the sublimating nucleus (radiation pressure).
- Ion tail: may reach lengths of up to 100 million km and is usually narrow and linear in appearance, and display much fine structure. Ionized atoms are swept directly from the Sun by the solar wind to form this tail. The ion

²⁸For a recent monograph see: Introduction to Comets, J.C. Brandt & R. D. Chapman, 2004, Cambridge University Press.

²⁹Whipple, F., 1950, A comet model. The acceleration of Comet Encke, *Astrophysical Journal* 111, 375–394.

tail is generally blue in colour due to fluorescing ions of carbon monoxide (CO^+).

During their passes close to the Sun comets lose a fraction of their mass. After about 500 passes most of the ice and gas is lost and the object looks like an asteroid. Perhaps half of the near-Earth asteroids may be such dead comets. A comet whose orbit reaches the inner Solar System is also likely to impact one of the planets (this happened recently in 1994, when comet Shoemaker-Levy 9 broke into several parts that impacted on Jupiter) or on the Sun (Sun grazer's comets³⁰).

Observations of the nucleus of comet Halley's by spacecraft in 1986 showed that its nucleus was potato-shaped, reflecting only about 4% of the light falling onto it (darker than coal). The principal constituents of the nucleus are H_2O^+ , OH , OH^+ and H_3O . Ice (in the general sense) makes up to 50% of comets and is the dominant constituent.

Space weathering is defined as any process that erodes and alters surfaces, here confined to small bodies in the Solar System. Mechanisms that possibly alter asteroids and cometary surfaces include solar wind bombardment, UV radiation, cosmic ray bombardment and micrometeorite bombardment. These processes are likely to contribute to surface processes in different ways. For example, solar wind bombardment would be more important on a body closer to the Sun compared to a comet where cosmic ray bombardment might be a more significant weathering mechanism.

6.6.2 UV Photochemistry of Cometary Atmospheres

Comets occupy a unique position in our Solar System since they are the least processed material remaining from its origin, four and a half billion years ago. It is known that hydroxyl radicals are formed in the coma by UV radiation that splits up water molecules. Thus OH is the most abundant constituent in cometary comas³¹.

When water molecules are exposed to UV sunlight the following photodissociation reactions start:



Of these, reaction 6.1 is the most common because it occurs in response to photons with energies that commonly occur in the solar flux. The other reactions require higher energy photons and at even higher energies there can be additional reactions due to photoionization. Other common molecules are HCN, CH_3CN and $(\text{H}_2\text{CO})_n$.

³⁰Sungrazers get to within about 50 000 km of the solar surface, just passing through the corona and possibly evaporating there. SOHO instruments have detected more than 800 new comets of this type.

³¹All the comets observed by IUE have shown the 308.5 nm hydroxyl line, which is consistent with water as being a major part of cometary composition.

The dark colour of cometary nuclei is mostly due to carbon-rich compounds and dust that remain as the comet's ice sublimates.

Table 6.11 summarizes the main observations of comets in the UV range.

Table 6.11: Ultraviolet observations of comets, IAA stands for IRAS-ARAKI-ALCOCK.

COMET	Satellite	UV range (nm)	Obs. Year	Reference
KOHOUTEK	Skylab	110–150	1973–74	Carruthers <i>et al.</i> (1974)
	Rocket	120–320	1974	Feldman <i>et al.</i> (1974)
BENNETT	OGO-5	Ly- α	1970	Bertaux <i>et al.</i> (1973)
ENCKE	OGO-5	Ly- α	1970	Bertaux <i>et al.</i> (1973)
	IUE		1980	Feldman <i>et al.</i> (1984a)
	SOHO	Ly- α	2000	Raymond <i>et al.</i> (2002)
WEST	Rocket	Ly- α	1975	Opal & Carruthers (1977)
BRADFIELD	IUE		1980	Feldman <i>et al.</i> (1980)
IAA 1983d	IUE		1983	Feldman <i>et al.</i> (1984b)
HALLEY	SUISEI	Ly- α	1985–86	Kaneda <i>et al.</i> (1986)
	Rocket	FUV	1986	Woods <i>et al.</i> (1986)
	Rocket	FUV	1986	Mc Coy <i>et al.</i> (1986)
	IUE		1985–86	Feldman <i>et al.</i> (1987)
	Vega 2	275–710	1986	Clairemedi <i>et al.</i> (2004)
LEVY	HUT	41 - 185	1990	Feldman <i>et al.</i> (1991)
HYAKUTAKE	HST	Ly- α	1996	Combi <i>et al.</i> (1998)
	SOHO	Ly- α	1996	Bertaux <i>et al.</i> (1998)
	IUE		1996	Laffont <i>et al.</i> (1998)
WIRTANEN	HST	MUV	1996–97	Stern <i>et al.</i> (1998)
HALE-BOPP	Rocket	128–188	1997	Mc Phate <i>et al.</i> (1999)
	POLAR	Ly- α	1997	Brittnacher <i>et al.</i> (2001)
	SOHO	Ly- α	1996	Combi <i>et al.</i> (2000)
LINEAR	FUSE	90–118	2001	Feldman <i>et al.</i> (2002)

Comet Hyakutake (C/1996 B2) provided a target of opportunity for performing a systematic study of water photodissociation products in which data were obtained from three instruments on the Hubble Space Telescope. Hydrogen is the most abundant gas in the entire coma of the comet. They are thus produced when solar ultraviolet light divides molecules of water, the major constituent of the nucleus of the comet. Using Hubble's High Resolution Spectrograph, Combi *et al.* (1998) were able to determine that comet Hyakutake was churning out between 7 and 8 tons of water per second.

Lyman- α observations in the ultraviolet (120.6 nm) indicate that some comets are surrounded by a vast (10^7 km) halo of hydrogen atoms. Calculations have shown that the production rate of hydrogen required to explain the atomic density of the cloud is too great by an order of magnitude or so to be explained by sublimation of the nucleus. This hydrogen is probably a consequence of dissociation of hydroxyl (OH) by sunlight.

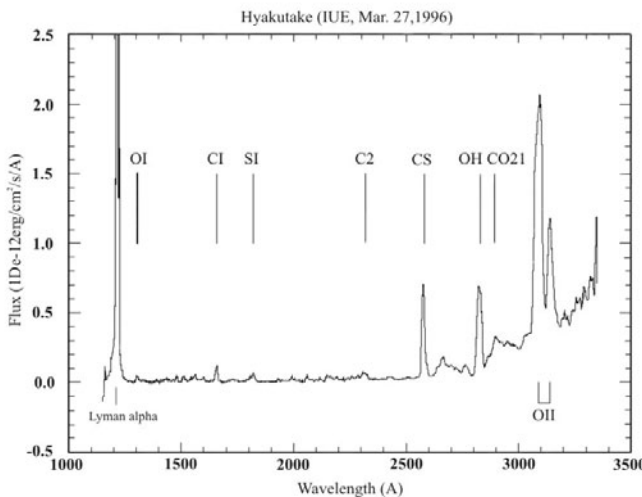


Figure 6.10: Spectrum of Comet Hyakutake by IUE (Courtesy: Daniel Ponz, ESA).

McDonald *et al.* (1996) produced organic heteropolymers by plasma discharge irradiation of water/clathrate hydrates³² by exposure of a probe simulating cometary chemistry.

SWAN/SOHO observations of Comet Hale–Bopp in Lyman– α were performed in 1997 as the comet slowly approached the Sun. Figure 6.11 shows the huge hydrogen cloud, 100 million kilometres across, produced by photo–dissociation of water vapour molecules evaporated from the solid nucleus, 40 km in diameter. The analysis of the data showed that about 600 tons of ice are vaporized and ejected into space each second during the closest approach to the Sun (Combi *et al.* 2000).

Finally, we should mention the UV observations of the dramatic impact of the comet Shoemaker–Levy 9 on Jupiter (Table 6.12).

ROSETTA is now on its way to the comet Churyumov–Gerasimenko. The ALICE ultraviolet imaging spectrometer onboard will analyse gases in the coma and tail, mapping also its surface.

³²Clathrate hydrates are a class of solids in which gas molecules occupy “cages” made up of hydrogen-bonded water molecules. These “cages” are unstable when empty, collapsing into conventional ice crystal structure, but they are stabilized by the inclusion of the gas molecule within them.

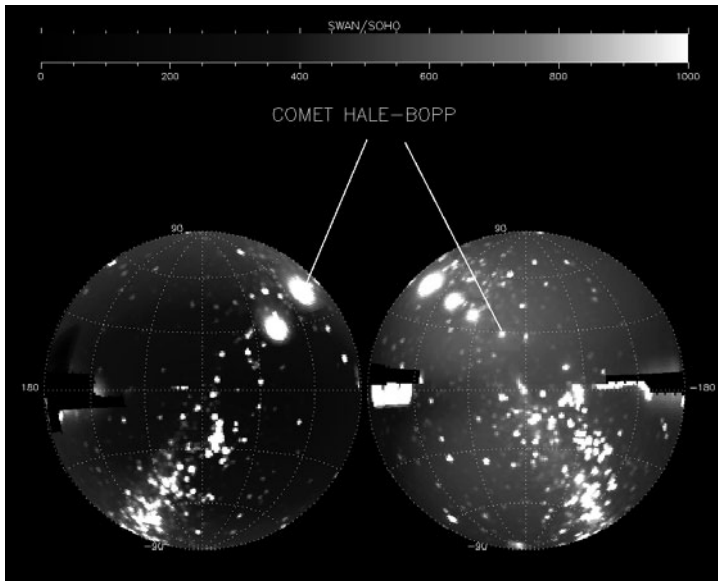


Figure 6.11: Ultraviolet Image (110–180 nm) of the comet Hale-Bopp (Courtesy: SWAN/SOHO team).

Table 6.12: UV observations of the SL-9 impact on Jupiter.

Instrument	UV range (nm)	Reference
GALILEO/UVS		Hord <i>et al.</i> 1995
HST		Clarke <i>et al.</i> (1995)
		Noll <i>et al.</i> (1995)
IUE	FUV	Ballester <i>et al.</i> (1995)
EUVE	He I 58.4	Gladstone <i>et al.</i> (1995)

6.7 Meteorites

6.7.1 Basic facts

Let us give some definitions first. A meteorite is a piece of rock from outer space that strikes the surface of the Earth and can be found there whereas a meteoroid is a meteorite before it hits the surface of the Earth. Meteors are small glowing fragments of cometary matter from outside the Earth's atmosphere that burn and glow upon entering the Earth's atmosphere and are known as shooting stars in popular literature. The larger ones reach the surface, the smaller evaporate in the atmosphere ³³.

³³See also O. R. Norton, The Cambridge Encyclopedia of Meteorites, 2002, Cambridge University Press.

Meteorites are fragments of larger bodies such as: a) objects in the asteroid belt (between Mars and Jupiter). IUE observations (Roettger & Buratti 1994) indicated low albedos in the UV range (230–325 nm), b) Comets; for example, the collision of a cometary fragment is thought to have occurred in the Tunguska region of Siberia in 1908. The blast was about the size of a 15 megaton nuclear bomb the size of the object was between 20 and 60 m.

Meteorites can be classified into three types (valid also for UV observations):

1. Stony; composed mainly of olivine and pyroxene.
 - (a) Chondrites: contain small round glassy chondrules; radiometric age ~ 4 billion years.
 - (b) Achondrites: do not contain chondrules.
2. Irons: contain iron and nickel. When cut and polished they show the Widmanstätten pattern which results from slow cooling of once hot solid material.
3. Stony irons: mixture of silicates and irons.

6.7.2 Surface Change on Meteorites due to UV Radiation

UV radiation changes the surface of meteorites. Under certain conditions complex molecules such as amino acids can be formed.

The delivery of extraterrestrial organic molecules is a possible alternative or complement to their generation on early prebiotic Earth. Some meteoritic amino acids may be the result of interstellar ice photochemistry (UV photolysis of interstellar ice grains; see Sanford *et al.* 2002).

Indigenous amino acids have been found in several meteorites (over 70 in the Murchinson meteorite); the usual explanation for their presence is that they formed in liquid water reactions on parent bodies such as comets or asteroids. A review of amino acids in meteorites can be found in Cronin & Pizzarello (1983) and Botta *et al.* (2002).

An experimental and theoretical study (Woon 2002) reported that glycine and other amino acids were formed when cryogenic H₂O ice containing small amounts of CH₃OH, NH₃ and HCN were subjected to ultraviolet irradiation.

The most abundant and widespread class of organic compounds in the universe are polycyclic aromatic hydrocarbons. Stars that are embedded in dense clouds show absorption bands in their spectra due to PAHs. The UV processing of PAHs in H₂O ice in meteorites was investigated by Bernstein *et al.* (2002). The UV irradiation of naphthalene ices was performed in a vacuum chamber. The resulting products play an essential role in biochemistry (the methyl group with long isoprene chain, known as K vitamins).

Meteorite isotopic anomalies can also be produced by ultraviolet light as was discussed by Thiemens (1986).

Remote sensing of planetary surfaces is still important. Information about the albedo in the UV gives valuable information for the classification of their

surfaces. According to Dollfus *et al.* (1980), reflectance spectrometry extended to the UV of asteroids, meteorites and some of the planets compared with laboratory spectra permits a classification into several types: lunar, carbonaceous chondrites, ordinary chondrites, achondrites, basaltic rocks and irons. For lunar-type surfaces, a simple albedo measurement at 650.0 nm can be converted into quantitative abundance determinations of silicate, aluminium oxide and iron; a large amount of telescopic lunar photometry data is available for mapping these abundances. Extension of the photometry to 230.0 nm permits quantitative measurement of TiO_2 abundances. For asteroids and non-icy satellites, rock-type classification and constraints on the chemical abundances of Si, Al, Fe and Ti can be derived from photometry at 230.0 and 650.0 nm.

6.8 UV Radiation and Its Effect on Planetary Satellites

Our Solar System contains four large planets, Jupiter, Saturn, Uranus and Neptune, all of which have satellites. Some of these satellites are captured asteroids and are only tens of km across³⁴. They often move in a retrograde sense about the planet (in the opposite sense of the rotation of the planet). The large satellites like the four large Galilean satellites of Jupiter and Titan, the largest satellite of Saturn, must have originated in the disc-like nebula that surrounded the giant planets in the early stages of their evolution. Of course, in the Solar System the temperature declines with increasing distance from the Sun. Therefore, planets relatively near to the Sun are composed of dense rock and metal (like Mercury), whereas the outer planets accumulated atmospheres of light, volatile gases. When Jupiter and Saturn condensed they were hot and sources of heat. Closest to Jupiter is Io, which is made of rock and sulphur. Next is Europa, consisting of an icy crust and most of its interior being rock. There may exist a subsurface ocean below the ice crust - the energy supply being tidal forces exerted by the giant Jupiter (which cause Io's volcanism). Ganymede and Callisto, the two other Galilean satellites of Jupiter, have more ice and perhaps also a subsurface water layer. The conditions were slightly different however for the formation of Titan.

The icy planets and satellites of the Solar System are exposed almost unprotected to UV radiation from the Sun. This radiation drives photochemistry on the icy surfaces of planets like Pluto, Jupiter's moon Europa, and Saturn's moon Tethys.

6.8.1 Jovian Satellites

Europa is a key target in the search for life beyond the Earth because of consistent evidence that below the icy surface there is liquid water. Each of the Galilean satellites of Jupiter has a tenuous atmosphere by terrestrial standards. Io has an SO_2 atmosphere with column densities $\sim 10^{16} \text{ cm}^{-2}$ in the equatorial regions

³⁴See also D. A. Rothery, *Satellites of the Outer Planets: Worlds in Their Own Right*, 1999, Cambridge Univ. Press

Table 6.13: UV geometric albedos (%) of the Jovian Satellites. Band 1 (240 - 270 nm), Band 2 (280 - 300 nm), Band 3 (300 - 320 nm). L = Leading side ($45^\circ < 0^\circ < 135^\circ$); T = Trailing side ($235^\circ < 0^\circ < 315^\circ$). Source: Nelson & Domingue.

Satellite	Band 1	Band 2	Band 3
Io (L)	1.5 ± 0.1	1.7 ± 0.1	4.2 ± 0.1
Io (T)	2.8 ± 0.2	3.0 ± 0.5	3.8 ± 0.3
Europa (L)	18.0 ± 0.4	26.0 ± 1.0	37.0 ± 2.0
Europa (T)	9.6 ± 0.2	12.9 ± 0.4	17.1 ± 0.6
Ganymede (L)	12.8 ± 0.7	16.8 ± 0.9	20.0 ± 0.1
Ganymede (T)	7.0 ± 0.3	7.5 ± 0.04	10.5 ± 0.8
Callisto (L)	4.0 ± 0.8	4.9 ± 0.1	6.6 ± 0.02
Callisto (T)	5.6 ± 0.2	6.4 ± 0.02	10.5 ± 0.8

and densities at least an order of magnitude smaller in the polar regions. Europa and Ganymede have O₂ atmospheres with column densities in the range of $(1-10) \times 10^{14} \text{ cm}^{-2}$, whereas Callisto has a CO₂ atmosphere of comparable column density (Strobel 2003).

Table 6.13 summarizes the UV geometric albedos³⁵ of the Jovian satellites, obtained by the IUE in three different spectral bands (Nelson & Domingue 1999). Changes are apparent on all four bodies, and these contrasts are more pronounced when two opposite hemispheres are compared for a given object. These albedo differences imply that differences in chemical composition exist across the surface of each satellite. Hendrix *et al.* (2005) have analyzed UV phase curves of these icy satellites.

The atmosphere of Io is produced by a combination of surface material vaporized and sputtered by charged particles and material liberated from active volcanoes. Io's atmosphere is the major source of heavy ions for Jupiter's immense magnetosphere, through interaction with the plasma torus encompassing its orbit.

The first detection of oxygen on Europa was reported by Hall *et al.* (1995). Recent HST UV observations indicate that Europa has a substantial quantity of O₂, and near Europa's orbit a large neutral cloud comparable to Io's neutral cloud was detected (Mauk *et al.* 2003). Because of the high water-ice coverage of Europa's surface, low surface temperature (temperature below about 120 K), but large high energy particle flux, it seems reasonable that the sputtering of water-ice by energetic ions is the main source of the atmosphere composed by H₂O, OH, O, H, O₂, and H₂.

The Galilean satellites are bombarded by energetic particles that profoundly affect the surface composition. Examples are reactive sulphur from Io's plasma torus and new chemical species produced by radiolysis. The depth of the radiolytic influence is about 1 mm. Europa's radiolytic products include hydrogen peroxide and molecular oxygen, as well as a hydrated material that exhibits a strong trailing side enhancement. Ganymede contains O₂ in its surface and atmosphere,

³⁵The ratio of the brightness of a Solar System object to the brightness of a perfectly diffusing disc at the same distance from the Sun.

probably produced from the radiolysis of H₂O. Further information on radiolysis and chemical weathering can be found in Carlson (2002).

HST observations of atomic oxygen UV emission lines on Ganymede have been reported by Hall *et al.* (1998) and Feldman *et al.* (2000). Eviatar *et al.* (2001) proposed that the tenuous nature of the atmosphere precludes the excitation of the auroral emission and requires a local acceleration mechanism.

UV absorption features at 280 nm have been observed in Europa (Lane *et al.* 1981) and Callisto (Lane & Domingue, 1997; Noll *et al.*, 1997) arising from the presence of SO₂, although the source could be different in both satellites.

Europa shows an unusual water spectrum, whose features are interpreted as sulphuric acid hydrate and hydronium, H₃O. The non-icy spectrum is mainly interpreted as hydronium, created by ionization effects from particle bombardment (magnetospheric particles, implantation of protons in the ice surface). Spectra of Ganymede and Callisto show similar but less pronounced features. Europa's "non-icy" spectra might comprise > 99% ordinary ice that has been disrupted by the particle bombardment, or an acid-hydrogen peroxide mixture composed of about 2/3 water. Liquid acid-hydrogen peroxide mixtures readily attack organic molecules, metals and other compounds. This could cause great problems for a lander, because an acid-hydrogen peroxide mixture is a hostile environment for life.

There is mounting evidence for a deep (~ 100 km) ocean beneath Europa's icy outer shell. Why is there fluid H₂O? This ocean results from tidal interactions between the massive Jupiter and Europa, which causes heating, and if the global tidal heat flux of $\sim 8.7 \times 10^{12}$ W enters the base of the ocean through its rocky crust an average thermal gradient of approximately 150 °C/km is expected (Lowell *et al.* 2003).

Borucki *et al.* (2002) report on colored regions on Europa and other icy bodies in the outer Solar System. These regions may be contaminated by organic macromolecular solid material produced when surface ices are exposed to electrical energy. Hypervelocity meteorite impacts and fractures may release tidal and tectonic stresses in icy crusts in the form of electrical discharges, that provide the energy for *in situ* synthesis of the organic solids.

In the absence of contaminants, O₂ is a relatively stable, photoresistant product that forms more efficiently with increasing temperature. O₂ can accumulate in voids in which O₃ is then formed by photolysis.

6.8.2 Triton

Triton is the seventh and by far the largest of Neptune's satellites. Its distance from Neptune is 354 760 km and its diameter is 2700 km. The satellite was detected by W. Lassell (1799–1880) in 1846. Triton was visited only by Voyager 2 on 1989 Aug 25. Almost everything we know about it comes from this encounter. The orbit of Triton is retrograde and it is the only large moon that orbits its planet "backwards". Therefore, it is supposed that Triton must have been formed elsewhere, far away from Neptune and that it was later captured. This retrograde motion causes strong tidal interactions with Neptune and the satellite's distance

to Neptune is decreasing.

Triton's density, $\rho = 2.0 \text{ gcm}^{-3}$, is slightly greater than that of Saturn's icy moons (e.g. Rhea). Triton is probably only about 25% water ice, the remainder being rocky material.

Voyager found that Triton has a very tenuous atmosphere with pressure $p = 0.01 \text{ mbar}$, composed mostly of nitrogen with a small amount of methane. A thin haze extends up 5–10 km. The temperature at the surface of Triton is 34.5 K, which makes it as cold as Pluto. This is due in part to its high albedo (0.7–0.8). At this temperature methane, nitrogen and carbon dioxide all freeze solid. Airglow and occultation observations of Triton's atmosphere with the ultraviolet spectrometer onboard Voyager showed that it is composed mainly of molecular nitrogen, with a trace of methane near the surface. The temperature of Triton's upper atmosphere is $95 \pm 5 \text{ K}$, and the surface pressure is roughly 14 microbars (Broadfoot *et al.* 1989).

The surface of Triton must be relatively young since only few craters are visible and almost the entire southern hemisphere is covered with an “ice cap” of frozen nitrogen and methane. On Triton there exist ice volcanoes, the eruptive material is liquid N₂, dust or CH₄ compounds; these eruptions are driven by seasonal heating from the Sun.

Using IUE data, typical UV albedos are found on Triton that agree with Voyager photopolarimetric results (Stern *et al.* 1991).

A model of Summers & Strobel (1989) for photochemical reactions in the atmosphere of Uranus was modified and used for quantitative calculations of the methane content in the atmosphere of Triton. It is shown the rate of methane photolysis calculated is sufficient to generate a smog of condensed C₂H₂, C₂H₄, C₂H₆ and C₄H₂ particles in the lowest 30 km of Triton's atmosphere (Strobel *et al.* 1990).

6.9 Titan

The largest satellite of Saturn and second largest satellite in the Solar System is of special interest for astrobiology and planetary atmosphere research. Therefore, we treat this satellite separately³⁶.

6.9.1 History and Basic Facts

In 1610 G. Galilei recorded observations of Saturn but he did not discover any satellites. The discovery of Titan, the largest satellite of Saturn, was made by C. Huygens in 1655 as well as the famous ring of Saturn. The orbit of Titan ranges between $1.11 \times 10^6 \text{ km}$ and $1.26 \times 10^6 \text{ km}$. There is a 3:4 resonance with the orbit of the satellite Hyperion: this means that when Titan has completed three revolutions about Saturn, Hyperion has completed four. This allowed the determination of

³⁶see also R. Lorenz, J. Mitton, Lifting Titan's Veil : Exploring the Giant Moon of Saturn, 2002, Cambridge University Press

Titan's mass in the 1880s by G. W. Hill (1838–1914), who obtained a value of 1/4714 that of Saturn (the modern value is 1/4262).

In this context we mention the observation of Titan made by the Spanish Astronomer Josep Comas Solà (1868–1937) on 1907 August 13 at the Fabra Observatory in Barcelona³⁷. He wrote: *...with a clear image and using a magnification of 750, I observed Titan with very darkened edges (somewhat similar to those one observes on the disk of Neptune), while on the central part, much brighter, one sees two round, whiter patches, which give the appearance of a blurred Titan.*

In 1925 J. Jeans (1877–1946) claimed that if Titan has an atmosphere, which would be consistent with the observations made by Comas Solà, its atmosphere should consist mainly of heavier molecules such as methane and atoms such as Ar, Ne and N. Jeans showed that a planet or satellite could have an atmosphere if it is massive enough (i.e. with a strong gravity), if the gas molecules are themselves relatively heavy and, ideally, if it is cold so that the molecules have insufficient kinetic energy (which is proportional to the temperature) to escape. In 1943 G. Kuiper (1905–1973) recognized that Titan's spectrum contained absorption bands that he could easily identify as methane (CH_4).

In November 1980 Voyager 1 reached Saturn after a journey of 13 years. At that time it was thought that Titan's atmosphere contained clouds and haze but it was also hoped that the satellite was not completely covered by clouds, and that it would be possible to glimpse to the surface. However, Voyager's camera, which was sensitive only to visible light, returned images of Titan that showed only a global blanket of orange. We shall see in the next sections that solar UV radiation plays an important rôle in producing these layers.

In Table 6.14 the basic facts about Titan are given. The Bond albedo is defined as the ratio of total reflected light to total incident light. V_0 is the magnitude in visible light when Saturn is in opposition to the Sun (when it is closest to Earth). The inclination of the orbit is given relative to Saturn's equatorial plane. This inclination is very low. Therefore, the Saturnian rings would be seen edge-on on Titan's surface. The obliquity gives the inclination of the equator to the orbital plane.

6.9.2 Atmosphere of Titan

Basic information about Titan's atmosphere come from simple observations:

- Occultations of stars by Titan: because of refraction in Titan's atmosphere starlight shows a series of spikes before complete occultation (observations by the amateur astronomer T. Platt, 1989).
- Disk meter: this device, invented by B. Lyot, consists of an adjustable disc that is seen in the same field of view as Titan.
- Lunar occultations: The Moon has no atmosphere; as it moves in front of Titan the light is progressively cut until it disappears.

³⁷This description appeared in *Astronomische Nachrichten* (1908) 179, 289

Table 6.14: Basic dynamical and physical data for Titan. Source: Lorentz & Mitton (2002), pg. 249

Parameter	Value
Radius (surface)	2575 km
Mass	1.346×10^{23} kg = 0.022 mass of Earth
Mean density	1880 kg/m ³
Surface temperature	94 K
Surface pressure	1.44 bar
Surface gravity	1.35 m/s ²
Escape velocity	2.65 km/s
Albedo (Bond)	0.29
Magnitude V_0	8.3
Mean distance from Saturn	1.223×10^6 km = 20 Saturn radii
Mean distance from Sun	9.539 AU = 1427×10^6 km
Orbital period around Saturn	15.945 days
Mean orbital velocity	5.58 km/s
Obliquity	26.7°
Inclination of orbit	0.33°
Rotation period	15.945 days
Orbital period around Sun	29.458 yr

- Voyager 1 radio occultation experiment: as the spacecraft passed behind Titan, its microwave radio signals were monitored on Earth. Because of refraction in Titan's atmosphere it was possible to reconstruct the pressure and temperature profile in it.

It turned out that some parts of the atmosphere of Titan are warm while others are not. This could be explained in terms of the absorption of sunlight similar to the absorption in the Earth's ozone layer, or in terms of convective motions. With the Very Large Array (VLA) ultra-short radio waves from Titan were measured. It was possible to define a temperature of 87 K. The main characteristics of Titan's atmosphere are:

- Thermosphere: the temperature decreases from over 180 K to about 155 K at the lower boundary where the pressure is about 5×10^{-4} K.
- Mesosphere: here the temperature increases again to about 175 K at its lower limit where the pressure is about 0.5 bar.
- Stratosphere: the temperature falls from 155 K to 62 K. At the lower boundary (tropopause) the pressure is about 100 mbar.
- Troposphere: in the lowest layer the temperature increases to about 90 K at the surface.

Table 6.15: Major components of Titan's atmosphere. Adapted from Titan, The Earth like Moon, A. Coustenis and F. Taylor, World Scientific (1999).

Component	Mole fraction (at level h)	Band position
Molecular N ₂	0.98–0.85	radio occultation; UV
Argon Ar ³⁶	< 6 × 10 ⁻² at 3900 km < 7 × 10 ⁻² near surface	104.8 nm
Methane CH ₄	4.5 – 8.5 × 10 ⁻² surface 1.7 – 3.0 × 10 ⁻² strat. (8 ± 3) × 10 ⁻² at 3700 km	

Table 6.16: Minor components of Titan's atmosphere (adapted from Coustenis & Taylor, 1999).

Composition	Mole fraction (at height)	Band position of detection
N	?	113.4 nm
H	< 10% at 3900 km	121.6 nm
H ₂	-0.0011	360, 600 cm ⁻¹
Ne	< 10 ⁻²	736 cm ⁻¹
Ethane (C ₂ H ₆)	1.3 × 10 ⁻⁵ at 130 km	822 cm ⁻¹
Propane (C ₃ H ₈)	5 × 10 ⁻⁷ at 110 km	748 cm ⁻¹
Water (H ₂ O)	8 × 10 ⁻⁹ at 400 km	237, 243 cm ⁻¹
CO	5 × 10 ⁻⁶ – 5 × 10 ⁻⁵ strat. 1 – 6 × 10 ⁻⁵ trop.	mm, sub mm IR
CO ₂	1.4 × 10 ⁻⁸ 110 km	667 cm ⁻¹

The pressure at Titan's surface is 1.5 bar (50% greater than on Earth). These conditions are very close to the triple point of methane. At its triple point a substance can exist simultaneously in solid, liquid and gaseous state.

The atmosphere consists generally between 85 and 95% nitrogen (N₂) and there is about 2% methane in the stratosphere; near the surface the methane content could be between 6 and 8%. If methane is exposed to UV radiation it undergoes a chemical process known as photochemistry.

The profile of the temperature variation throughout Titan's atmosphere is shown in Fig. 6.12 and in Table 6.15 the gaseous composition is given. The minor gaseous components are given in Table 6.16. The origin of oxygenated molecules, such as H₂O and CO is thought to be from cometary impacts.

Nagy *et al.* (2001) studied the interaction of Titan's ionosphere with Saturn's magnetosphere and found an outward escape flux of the major ionospheric species (i.e. the heavy ion species) from the tail of approximately $6.5 \times 10^{24} \text{ s}^{-1}$.

Stevens (2001) discusses the EUV airglow of Titan. Strobel *et al.* 1991 quantified the individual contributions of direct solar excitation, photoelectron excitation, and magnetospheric electron excitation of Triton and Titan airglow observed

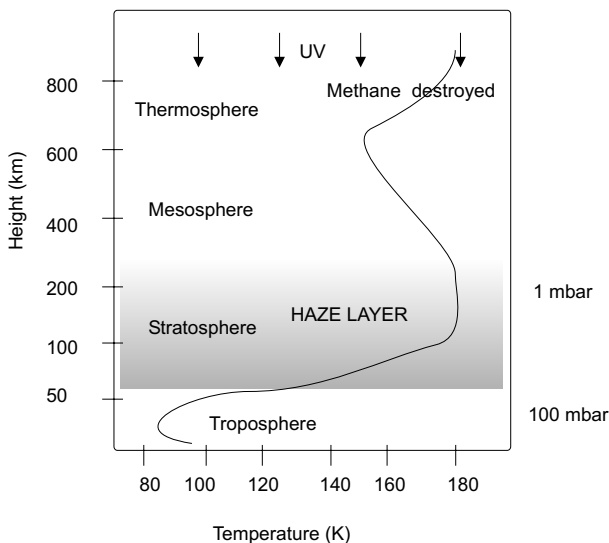


Figure 6.12: Temperature variation with height in Titan’s atmosphere.

by the Voyager Ultraviolet Spectrometer (UVS).

6.9.3 Surface of Titan

The 1.88 g cm^{-3} mean density of Titan can be explained only if the main constituent of the satellite has a density much lower than rock. Thus, it is suggested that Titan has a rocky core covered by a thick mantle of ice (H_2O , CO_2 , NH_3). The surface would therefore be solid ice to a great depth (many satellites of the outer planets have an ice crust). As was pointed out in previous chapters a rain of methane, CO_2 snow and oily droplets is expected in these conditions. The water crust therefore could be completely or partially covered with material and also liquid areas, but this requires the atmosphere to be replenished with material from space (comets, etc) and/or cryovolcanism.

The surface of Titan is formed by the photolysis of methane in the stratosphere—the products precipitate out of the atmosphere, and the CH_4 vapour pressure is reduced. The predominant photochemical product ethane is liquid at 94 K and has a vapour pressure much lower than methane, allowing the two to mix in a solution, thus creating an ethane–methane ocean that acts as source and sink for the photolysis cycle. Models suggest that the depths of such an ocean could range from 500 m to 10 km. Sophisticated imaging processing techniques applied to the Voyager and HST images reveal permanent structure. A sketch showing the basic mechanisms of the methane cycle is given in Figure 6.13.

Observations using adaptive optics (Combes *et al.* 1997) of Titan with the ESO 3.6-m telescope in La Silla were made between 1994 and 1995. In the near-infrared range from 1 to $2.5 \mu\text{m}$ the methane atmospheric windows at 1.3, 1.6

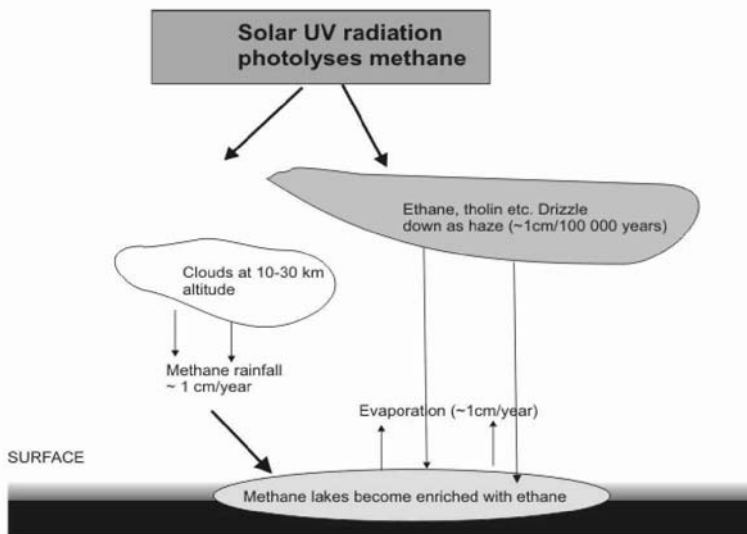


Figure 6.13: CH_4 cycle in Titan's atmosphere. The photolysis of methane through UV radiation is a crucial feature of the cycle.

and $2.0 \mu\text{m}$ could be used with narrow-band filters and diffraction-limited images were obtained (0.14 arcsec at $2 \mu\text{m}$). HST observations (Smith *et al.* 1996) also rule out the presence of global oceans but favour small lakes because permanent features were seen. VLT adaptive optics observations were made by Gendron *et al.* (2004).

Another technique for studying the surface of a planet or satellite is to use radar mapping (Muhslemann *et al.* 1990). The statistically significant echoes obtained (which take 2.5 hours to come back from Titan) indicate that Titan is not covered with a deep global ocean of ethane. A global ocean as shallow as about 200 m. would exhibit reflectivities an order of magnitude smaller, which would be below the experiment's detection limit. Campbell *et al.* (2003) suggested the existence of surface areas areas of liquid hydrocarbons from Arecibo radar observations of Titan at 13-centimetres. Ten per cent of the Titan's surface might be impact craters large enough to create transient but prolonged liquid water layers (Thompson & Sagan 1992).

An important step forward in the knowledge of Titan has been given with the successful arrival of the Cassini-Huygens to Saturn. Figure 6.14 shows a recent image of Titan obtained by the Cassini spacecraft in orbit around Saturn.

6.9.4 UV Radiation and Photochemical Reactions on Titan

There are several similarities between the atmosphere of Titan today and the early Earth. Both atmospheres are dense and composed mainly of nitrogen and rich in organic compounds. As pointed out by Raulin & Owen (2002) several conditions

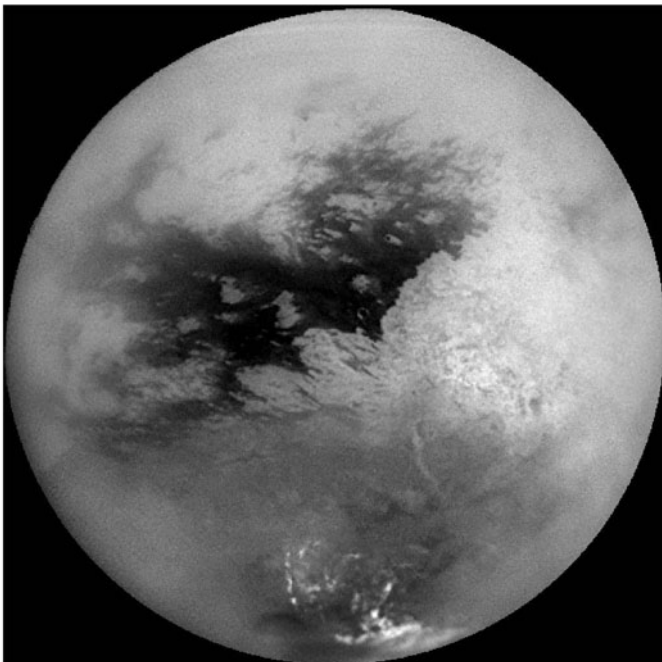


Figure 6.14: A mosaic of nine processed images recently acquired during Cassini's first very close flyby of Saturn's moon Titan on October 26, 2004. Surface features are best seen near the center of the disc, where the spacecraft is looking directly downwards; the contrast becomes progressively lower and surface features become fuzzier towards the outside, where the spacecraft is peering through haze, a circumstance that washes out surface features. The brighter region on the right side and equatorial region is named Xanadu Regio. Credit: NASA/JPL/Space Science Institute.

prevail on Titan for the evolution of complex organic systems such as a dense mildly reducing atmosphere and the presence of energetic sources necessary to transform the main atmospheric constituents into more complex forms. These energy sources are UV radiation and energetic electrons from Saturn's magnetosphere. Furthermore, a low temperature tropopause containing submicron particles (haze) allows the condensation of organics. Finally, the presence of liquid hydrocarbons (ethane and propane; see Strobel 1982) allow the partial or total dissolving of atmospheric organics. Such a medium provides at the same time a protection against destruction.

Voyager 1 Ultraviolet Spectrometer (UVS) observations are the only direct measurements we have of Titan's upper atmosphere (Smith *et al.* 1982). For recent reanalysis of these data see Shindo *et al.* (2003) and Vervack *et al.* (2004).

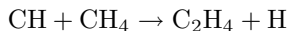
Solar radiation (mainly in the UV domain) is absorbed and molecules are consequently dissociated. However, models before the Voyager results were restricted

to hydrocarbons that were detected from Earth-based observations. The Voyager encounters revealed that N₂ is predominant, so that photochemical models had to be extended to take into consideration the formation of nitriles.

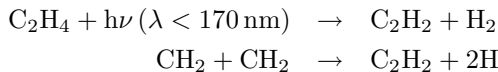
Today, the picture of photochemical reactions occurring in Titan's atmosphere is quite complex: there are reactions between carbon, nitrogen, hydrogen and oxygen. We now describe some basic reactions;

Hydrocarbons

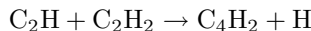
Methane (CH₄) is decomposed by UV radiation to CH₂ and CH. These products undergo further reaction that produces ethylene C₂H₄:



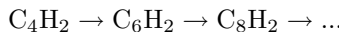
The photolysis of ethylene leads to acetylene³⁸:



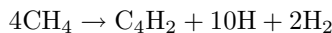
The acetylene (C₂H₂) diffuses down to the stratosphere and photolyses to C₂H, which is converted to diacetylene (C₄H₂):



Diacetylene can further react with C₂H and other polyacetylenes are produced, i.e.



Another process to form diacetylene is



From a photolysis of CH₄ the methyl radical CH₃ is produced and ethane can be formed in the mesosphere and lower thermosphere (below 800 m). Another way to produce ethane is by a catalytic process



again this occurs in the UV at $\lambda > 145 \text{ nm}$. For shorter wavelengths in the UV ($\lambda < 145 \text{ nm}$) C₂H₂ is produced. The ethane can be transported to the tropopause where it condenses followed by a rain-out. CH₄ is recycled mainly by reaction of CH₃ with H.

³⁸The International Union of Pure and Applied Chemistry designates this molecule as "ethyne".

Nitriles

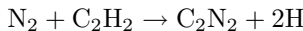
N_2 is highly inert and does not react directly with the hydrocarbons. However, it reacts readily with methane. The dissociation of N_2 may occur by different processes:

1. solar radiation $\lambda < 100 \text{ nm}$, process dominant above 700 km;
2. magnetospheric electrons (most effective mechanism);
3. galactic cosmic rays

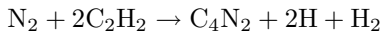
Let us consider some examples for the production of nitriles. Hydrogen cyanide is produced by:



Cyanogen is produced by



Dicyanogen is produced by



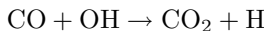
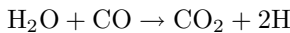
Also complex molecules like



are formed.

Oxygen compounds

Carbon monoxide (CO) is produced in reactions between OH , CH_3 and CH_2 . Carbon dioxide is formed by



A discussion about the complex photochemistry in Titan's atmosphere can be found in Yung *et al.* (1984) and Toublanc *et al.* (1995). Vertical profiles for Titan's atmospheric components are given by Lara *et al.* (1996).

Aerosols

The aerosols dominate the visual appearance of Titan. Laboratory experiments have been widely used to investigate their nature. An energy source is applied to a vessel containing a gas mixture approximating Titan's atmosphere. After a period of hours to days a brownish residue, called tholins, is observed coating the walls of the vessel (see Coll *et al.* 1998 for a review of techniques). These organic

polymers are created, in Titan, by UV sunlight and electrons streaming out from Saturn's magnetic field.

Pioneering experiments were carried out by Kahre *et al.* (1986) and Sagan *et al.* (1992)) obtaining tholins with optical properties matching the spectrum of Titan. The tholins were found to contain over 75 different constituents, mainly hydrocarbons, nitriles and PAH.

With the start of the Cassini-Huygens mission, interest in the properties of Titan's tholins has experienced resurgence. Tran *et al.* (2003) simulated haze formation in Titan's atmosphere, irradiating a gaseous mixture (N_2 , CH_4 , H_2 , C_2H_2 , C_2H_4 and HC_3N) in a photochemical flow reactor using a lamp emitting 185 and 254 nm light, generating a solid (a Titan haze analogue) and over 180 volatile reaction products.

As has been shown above, the chemistry of Titan's atmosphere is quite complex. The temperatures are low and the formation of aerosols is therefore a logical consequence. The haze on Titan is often described as a photochemically produced smog extending high in the atmosphere. By the photodissociation of nitrogen and methane, complex molecules build up and condensation in the stratosphere occurs. At least some of these products will consist of refractory materials forming oily or solid substances. Once they are formed these will not evaporate again. They move down to the troposphere and may drizzle down to Titan's surface. However it must be stressed here that these considerations are still based on models.

Observations by Voyager have shown that particles are observed as high as 500 km above the surface, and that a detached haze layer exists from 300 to 350 km. The base of the haze layer is probably at an altitude between 100 and 200 km, where coalescence and condensation form larger and more numerous particles that might be similar to clouds. At that time Titan was a disappointment because it appeared only as an orange-brown sphere. In the images a difference between north and south was detected, the south showed a higher albedo. These variations seem to be seasonal as was also proven by Hubble Space Telescope observations. Which hemisphere is brighter depends on wavelength; visible and near IR data show opposite effects. At wavelengths $> 1\mu\text{m}$ the haze becomes increasingly more transparent. The composition is organic material, the C/N ratio is between 2 and 4, and the C/H ratio between 0.5 and 1. A recent image obtained by the UVIS instrument³⁹ onboard Cassini shows a surprising double haze around Titan, showing the existence of different aerosol layers.

Note that there is a distinction between haze and clouds. Haze certainly exists in Titan's atmosphere; clouds may or may not exist⁴⁰. In this context haze means a more extensive, generally horizontal layer of similar aerosols. The haze has a banded appearance, which suggests rapid zonal motions caused by winds parallel to the equator. This is also confirmed by IR temperature maps which indicate small contrasts in the longitudinal directions but a difference of 20 K from equator to pole. This difference seems to vanish in the deep atmosphere (perhaps only 2–3

³⁹UVIS (Ultraviolet Imaging Spectograph) will provide information on the atmospheric composition and photochemistry of Saturn and Titan, and the nature of Saturn's rings. It has two channels: EUV (55.8–118 nm) and FUV (110–190 nm).

⁴⁰Cassini has observed a field of clouds near Titan's south pole, probably composed of methane.

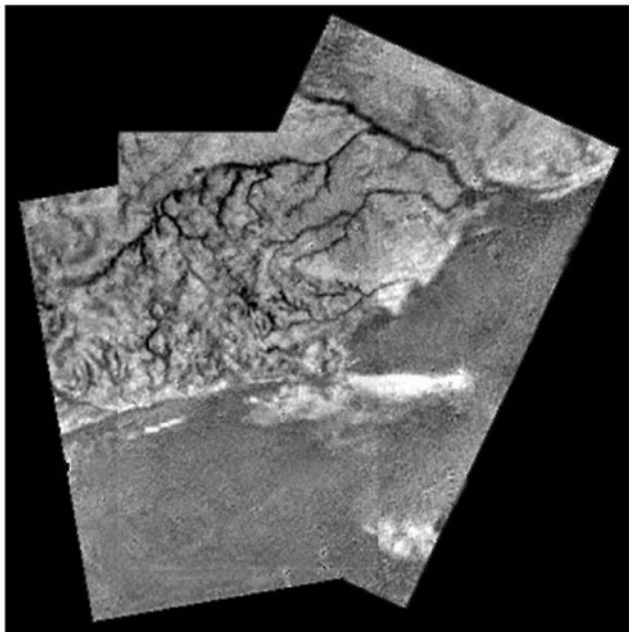


Figure 6.15: Mosaic of river channel and ridge area on Titan obtained by the Descent Imager of Huygens. Credit: ESA.

K), which requires meridional motions; heat is transported polewards by advection.

6.9.5 The Huygens Probe

On 25 December 2004, the Cassini spacecraft successfully released the European Huygens probe, starting the descent towards Titan. Some days later (14 January 2005) the probe made a successful descent and landing on Titan. After the haze cleared the images taken during the final phase of the descent (Figure 6.15) show the boundary between the lighter-coloured uplifted terrain, marked with what appear to be drainage channels, and darker lower areas.

Images at the surface show small rocks or ice blocks with evidence of fluvial erosion at its base. The texture of the surface resembles wet sand or clay with a thin solid crust, and it is probably composed of a mixture of dirty water ice and hydrocarbon ice.

Detailed analysis of these images and the data recorded by the different instruments onboard Huygens during the descent will provide an outstanding increase in our knowledge about Titan.

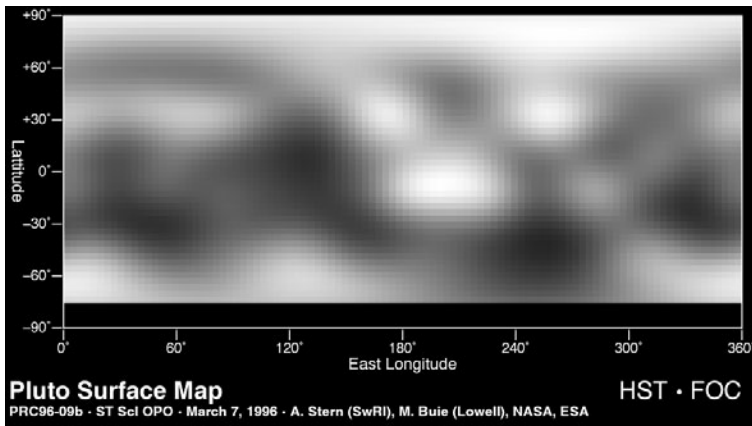


Figure 6.16: Map of the surface of Pluto, which covers 85% of the total surface area. Pluto has a dark equatorial zone, as can be noticed in this picture. The picture was taken in blue light when Pluto was at a distance of 3 billion miles from Earth. Courtesy: NASA/HST

6.10 Pluto

6.10.1 Basic facts

The outermost planet of our Solar System was discovered by Clyde Tombaugh (1906–1997) in 1930⁴¹. Because of its great distance (1200 times that of distance Earth-Moon) it took until the advent of the Hubble Space Telescope to detect structure on its surface (Fig. 6.16). Pluto is two-thirds the size of the Moon. Its rotation period is 6.4 days and its orbit is the most anomalous of the Solar System, with its 17 degrees inclination to the plane of the ecliptic and the most eccentric (with an eccentricity of 0.246). The distance between Pluto and the Sun at the aphelion is 7 900 million km; the mean distance is 5 913 million km. Pluto completes its orbit in 248.54 years. Its orbit is so eccentric that it intersects that of Neptune, so that for a time (as occurred in the period 1979–1999) Neptune is the farthest planet from the Sun.

Pluto itself probably shows even more contrast and perhaps sharper boundaries between light and dark areas than is shown here, but Hubble’s resolution (just like early telescopic views of Mars) tends to blur edges and blend together small features sitting inside larger ones.

Some of the variations across Pluto’s surface may be caused by topographic features such as basins, or fresh impact craters. However, most of the surface features unveiled by Hubble, including the prominent northern polar cap, are probably produced by the complex distribution of frosts that migrate across Pluto’s

⁴¹See A. Stern & D. J. Tholen Edrington (Eds.), *Pluto and Charon*, 1997, University of Arizona Press; A. Stern & J. Mitton (1998) *Pluto and Charon: Ice worlds in the ragged edge of the Solar System*, John Wiley & Sons.

surface with its orbital and seasonal cycles and chemical byproducts deposited out of Pluto's nitrogen–methane atmosphere.

6.10.2 The atmosphere of Pluto

The basic characteristics of Pluto's atmosphere are:

1. Surface pressure: ~ 3 microbar
2. Average temperature: ~ 50 K (-223 °C)
3. Scale height: ~ 60 km
4. Mean molecular weight: $\sim 16\text{--}25$ g/mole
5. Atmospheric composition: methane (CH_4), nitrogen (N_2)

Observations of the UV spectrum of the Pluto–Charon system obtained between 1987 and 1988 using the large aperture of the IUE long-wavelength prime spectrograph were discussed by Stern *et al.* (1989).

The variation of UV photometric properties of Pluto and Charon with rotational phase were studied with IUE data. The visible–UV colour differentiation was found to increase as Pluto reaches its maximum bolometric brightness, suggesting that this could be caused by a UV surface absorption feature on Pluto or Charon (Stern *et al.* 1991).

The atmosphere of Pluto and its variation with solar UV flux has been described by Krasnopolsky *et al.* (1999). These authors modeled the photochemistry for 44 neutral and 23 ionic species. Because of the high methane mixing ratio, Pluto's photochemistry is more similar to that of Titan than that of Triton. Charge exchange between N and CH_4 significantly reduces the production of atomic nitrogen. The most abundant photochemical products are C_2H_2 (3×10^{17}), C_4H_2 (10^{17}), HCN (6×10^{16}), H_2 (4×10^{16}), C_2H_4 (4×10^{16}), HC_3N (3.4×10^{16}), C_2H_6 (2×10^{16}), C_3H_2 (9×10^{15}), and C_3H_4 (8×10^{15}). All units are given in cm^{-2} . Concerning to UV absorption we may distinguish two processes:

- Parent molecules, N_2 , CH_4 and CO: these absorb photons < 145 nm.
- The above mentioned products absorb almost completely photons with < 185 nm; thereby significantly increasing the number of dissociation events.

Let us consider losses due to photochemical processes and due to escape. It seems that the photochemical losses of the parent molecules are much smaller than their escape.

The precipitation rate given in $1/10^9$ yr is highest for C_2H_2 with 65 g cm^{-2} . The seasonal variation is estimated to be a factor 3 times that value. Escape of photochemical products is highest for H_2 ($2 \times 10^{26} \text{ s}^{-1}$). The electron density reaches a maximum of 800 cm^{-3} at 2250 km. The most abundant ions are HCNH^+ and C_3H . Some of the photochemical products might be detected using the technique of UV solar occultation spectroscopy from a spacecraft flyby.

Lara *et al.* (1997) described Pluto's atmosphere as follows. The major species is supposed to be N₂ and CH₄. As a result of photolytic reactions, a number of hydrocarbons and nitriles are produced mainly in the 50–300 km region. Condensation of light hydrocarbons and nitriles occur between 3 and 5 km, depending on the compound and the surface temperature. Scaling the downward flux of these compounds to the amount of ice that would be deposited on the surface, we have deduced that the most abundant surface ices would be C₂H₆, C₂H₂, HCN and C₂H₄, in that order.

Krasnopolksy (2001) examined Pluto's spectrum in the range 200 to 250 nm from the Hubble Space Telescope (HST) archive observations acquired during 24 orbits. Variable quantities of haze, clouds, and rime may explain the higher variations at 2200–230 nm. A search for gaseous absorption resulted in upper limits to C₄H₂, C₆H₂, HC₃N and C₄N₂.

Beyond Pluto is the Kuiper Belt, a reservoir of short-period comets. Planetary bodies similar to Pluto have been discovered in this region⁴². Ultraviolet observations of these objects, so far as we know, are still lacking.

⁴²These are called Edgeworth-Kuiper ice bodies. For example, Quaoart and Sedna both have a diameter more than half that of Pluto and are located at 42 and 90 AU from the Sun, respectively.

Chapter 7

Ultraviolet Transitory Events and Life

7.1 Historical Introduction

The order that characterizes all the structures, including the living beings, existing in the Universe is at cost of being an open thermodynamical system. This is also the case of our Solar System. There is a continuous exchange with the media surrounding it, in form of radiation of all the energy ranges and flux of material particles of different sizes and energies. In this chapter we will study how this interaction has affected, in a direct or indirect way, the solar UV radiation arriving at the surface or atmospheres of the different bodies, with a logical larger emphasis to our planet, due to the larger amount of available information and to the presence of life.

Two main theories have been put forward concerning the interaction between life and environment. The idea about an old but almost static and uniform Earth, with only slight gradual changes was defended by James Hutton (1726–1797) in his “Theory of the Earth” and Charles Lyell (1797–1875) with the reputed “Principles of Geology”¹. The principle that “the present is the key to understand the past” is a logical consequence of these views. In this context, Charles Darwin (1809–1882) proposed the evolution of living beings by natural selection. In any case, his theory was based in gradual changes, without abrupt jumps: “nature non facit saltum”.

These principles were challenged by the catastrophist theory, mainly developed by G. Cuvier (1769–1832) in his “Discours sur les Révolutions du la surface du Globe”. Based on geological observations of sediments, Cuvier assumed that biological evolution was driven by sudden events producing the disappearance of some species and the emergence of new ones. Excluding astronomical causes, he favoured sudden changes in the positions of continents and oceans (see Rudwick

¹Four types of uniformities were the base of the theory: laws, processes (actualism), rates (gradualism) and state.

1997 for a translation of Cuviers works with excellent commentary on the source texts). According to this idea, processes operating in the past are not necessarily taking place today.

It soon becomes evident that the different biological species have rapidly evolved throughout time, some becoming extinct and others rapidly emerging. Alfred Wallace (1823–1913) expressed this with the words “We live in a zoologically impoverished world, from which all the hugest and fiercest, and strangest forms have recently disappeared”. In short, the discussion was about the main driving agent in the biological evolution: chance (contingency) or necessity (natural selection), recalling Jacques Monod (1917–1976) classic book “Chance and Necessity”²

The division of the history of the Earth in different periods (Table 7.1) has been marked, at least in the Phanerozoic era, by transitions coinciding with important changes in the biological diversity.

Table 7.1: Geologic periods. The time in brackets are Ma.

Precambrian	Hadean (4500 - 3800)
	Archaean (3800 - 2500)
	Proterozoic (2500 - 550)
Phanerozoic	Paleozoic
	Cambrian (550 - 490)
	Ordovician (490 - 443)
	Silurian (443 - 417)
	Devonian (417 - 354)
	Carboniferous (354 - 290)
	Permian (290 - 248)
	Mesozoic
	Triassic (248 - 206)
	Jurassic (206 - 144)
	Cretaceous (144 - 65)
	Cenozoic
	Tertiary (65 - 1.8)
	Quaternary (1.8 - Today)

The living beings have a hierachic classification: kingdoms, phyla, classes, orders, families, genera and species.

Now our task is to look for external influences that could have influenced the evolution of living beings on our planet with special emphasis on extraterrestrial UV sources.

7.2 Biological Extinctions during Earth History

The record of the number of biological species reveals five important crisis over the last 500 Ma, although many others are also evident (cf. Benton 1995; Hallan

²In this context, it should mentioned the theory of “punctuated equilibrium”, supporting the effect of chaotic events as a major force driving diversity bursts. Evolutionary change occurs relatively rapidly in comparatively brief periods of environmental stress, separated by longer periods of evolutionary stability. This theory has been popularized in various books by S.J. Gould (1940–2002).

& Wignall 1997).

The extinction occurring at the end of the Ordovician period (443 Ma ago) was probably caused by a glaciation produced by the position of the supercontinent Gondwana, close to the South Pole (Sheehan 2001). Two pulses have been recorded with the level of oceanic circulation playing a major role.

The end of the Devonian period was marked by an important decline in many biological species, being specially affected the brachiopods and the foraminifera (Wang *et al.* 1991 ; McGhee, 1996). An impact at this time cannot be ruled out (Name 2003).

At the boundary between the Triassic and Jurassic periods, about 200 million years ago, a mass extinction, occurring in a very short interval of time, destroyed at least half of the species on Earth (Ward *et al.* 2001). In the late Triassic the thecodontians and many mammal-like reptiles were extincted and this is the widely accepted view of how the dinosaurs attained dominance, as there were fewer predators to compete with them (Benton 1993). Olsen *et al.* (2002) claim to have found enhanced level of iridium at this stage. The Manicougan crater impact (210 ± 4 Ma), located in Quebec (Canada), has been proposed as a possible scenario of the asteroidal impact.

The end of the Permian period occurred 250 Ma before present and was characterized by the extinction of 80% of all ocean-dwelling creatures and 70% of those on land (cf. Ervin 1994; Berner 2002; Benton 2003). Enhanced UV radiation, following the disruption of stratospheric ozone by the impact, could account for a worldwide increase in land plant mutation (Visscher *et al.* 2004). Becker *et al.* (2001) discovered fullerenes³ containing helium and argon with isotopic compositions like those in meteorites called carbonaceous chondrites. Becker *et al.* (2004) have recently found evidences of an impact at the end of the Permian period, in the crater Bedout (Australia).

However, the best studied event has been that which occurred at the end of the Cretaceous, probably because it is related with the extinction of the dinosaurs.

7.2.1 The K/T extinction

The Cretaceous extinction, hereafter called the K/T event⁴, is the one that has been most intensively studied. The palaeontologist M. W. de Laubenfels had already suggested in 1956 that the extinction of the dinosaurs might have been caused by heat associated with the impact of a large meteorite (De Laubenfels 1956). Urey (1973) and Hoyle & Wickramasinghe (1978) suggested that ecocatastrophes such as the K/T extinction were probably caused by the collision or close passage of a giant comet, respectively.

There was a surge of interest in the scientific and press media with the publication of the paper of Alvarez *et al.* (1980), which provided a degree of empirical association between massive biological extinction and the impact of a large (> 10

³Large carbon compounds consisting of 60 or more carbon atoms, arranged as regular hexagons in a hollow shell. They are often called buckyballs, after Richard Buckminster Fuller (1895–1983), inventor of the geodesic dome, which their natural structure resembles.

⁴K stands for Cretaceous (from German) and T for the Tertiary Era – the Age of Mammals

km) extraterrestrial body, a comet or asteroid being the logical candidates (see Shoemaker 1983; Gehrels *et al.* 1994). Evidence of enhanced concentrations of iridium in the sediments corresponding to this period in the Italian site of Gubbio was verified by similar findings at other sites around the world (Orth *et al.* 1981). The publication of the paper immediately provoked different reactions supplying proofs for and against this hypothesis.

After several failed attempts, the crater produced by the Cretaceous event was finally identified, the so-called “smoking gun” being the Chicxulub crater on the Yucatan coast (Hildebrand *et al.* 1991). Recently Kyte (1998) has tentatively identified materials that might have come from the impacting object.

These five large extinctions were not the only ones, and their magnitude is probably due to a combination of two or more external influences. The Earth mantle periodically undergoes instabilities producing the eruption of material to the surface in form of giant volcanic events, called hotspots or superplumes depending of their intensity and duration (Courtillot 1999 ; Condé 2001). The Permian (Siberian Traps) and Cretaceous (Deccan Traps) periods are associated with these manifestations, which lasted millions of years. Rampino (2002) considered these supereruptions to be a limiting factor for the survival of extraterrestrial civilizations in Earth-like planets.

It has recently been proposed (Abbott & Isley 2002) that large meteoric impacts could also trigger important volcanic eruptions. These authors proposed that the dating of the 38 known impact craters coincides with mantle eruptions. In principle, this could join the two main theories explaining the K/T mass extinction; however, the timing of mantle events on the one hand is not accurate enough and on the other they are characterized by quite different temporal extensions (see Palmer 1997). Purely biological explanations of mass extinctions should also be considered (see Raup 1992).

In this book, we shall concentrate on the effects of the impacts on the ozone layer and subsequently on the amount of UV-B radiation at the surface. The mechanism would be very similar to present volcanic emissions rich in SO₂ (see Chapter 5).

Excitation of the nitrogen atoms in the terrestrial atmosphere could happen through a radiative process as the absorption of X or UV radiation or through a collision with particles of high energy (cosmic rays or material particles injected by the impact). A similar process, but now of anthropogenic origin, would be the massive explosion of nuclear weapons, producing a considerable emission of aerosols and given rise to a form of climate cooling, known as the nuclear winter (Turco *et al.* 1983; Toon *et al.* 1997).

The clearing of atmospheric dust following an impact, could result in an enhancement of UV radiation at the surface, an “ultraviolet spring”. Cockell & Blaustein (2000) have suggested that the K/T impact was a special case since the impact occurred in an anhydride (CaSO₄) rock. They calculated that the sulphate haze produced only a small increase of UV-B (25%) over a period of 2–3 months.

Cockell (1998, 1999) give excellent reviews of the possible role of UV radiation as a mechanism of biological extinction, a process not only limited to the five events mentioned. In the following we summarize the possible sources of the enhanced

ionizing and UV flux arriving at the Solar System and the consequences on the UV flux at the terrestrial surface.

7.3 Radiation Events in the Solar System

7.3.1 Solar flares

Concerning radiation effects on the Solar System, changes of the solar output are obviously the first source to be considered. As was shown in chapter 3, we may consider two different events, solar flares and coronal mass ejections.

Solar flares are manifested by a rapid enhancement in UV and X-ray radiation. Their effects on the photochemistry processes in the Earth's atmosphere have been studied previously. The intensity and frequency of flares was probably greater in the past and in order to identify such events on the surfaces of the different bodies of the Solar System we are interested in knowing whether the current large flares have left some kind of fingerprint in the terrestrial records.

The famous flares of August 1972 clearly contributed to ozone depletion (Haeth *et al.* 1977; Shumilov *et al.* 1991). More recently, the solar storm of 2000 July 14 (Jackman *et al.* 2001) and October 2003 (Degenstein *et al.* 2005) produced an important reduction in the ozone levels. Once the protons associated with the flare reached the upper atmosphere, they broke up nitrogen gas molecules, creating nitrogen oxides that can last for weeks to months and destroy up to nine per cent of the ozone in the upper stratosphere, between 15 and 50 kilometres in altitude. The relevant reactions have already been stated.

Solar protons also break down the atmosphere's water vapour molecules into hydrogen oxides, which can destroy up to 70 percent of the ozone in the middle mesosphere, located at height between 50 and 90 kilometres⁵. However, the hydrogen oxides last only for the duration of the solar proton event.

It is worth considering whether our Sun is exceptional or normal according the strength of these events. Recently giant flares have been detected in solar-like stars (Schaefer *et al.* 2000). Table 7.2 compares the observed released energies with those corresponding to large solar flares. Although the sample is not very large, the Sun seem to have an anomalous behaviour, at least in this aspect.

It has been suggested (Rubenstein & Schaefer 2000) that the enhancement in flare strength could be caused by the presence of giant planets close to the star. In such conditions a reconnection of the magnetic field lines of the stellar corona with those of the planetary magnetosphere could be produced, giving rise to an important release of energy.

7.3.2 Supernova Explosions

Supernovae constitute one of the most spectacular phenomena in the Universe and represent the catastrophic end of the lives of massive stars. Approximately 12000 supernova events have been discovered, most of them in external galaxies,

⁵Only a small percentage of the ozone is located in the mesosphere and upper stratosphere.

Table 7.2: Energies of flares observed in solar-like stars. From Schaefer *et al.* (2000).

Star	Duration (min)	Released Energy (ergs)
Grombridge 1830	19	1.0×10^{35}
κ Ceti	40	2.0×10^{34}
MT Tauri	10	1.0×10^{35}
π Ursae Majoris	35	2.0×10^{33}
S Fornacis	17–367	2.8×10^{38}
BD + 10 2783	49	3.0×10^{34}
Omicron Aquilae	5–15 days	9.0×10^{37}
5 Serpentis	3–25 days	7.0×10^{37}
UU CrB	57 min	7.0×10^{35}
Sun	150 min	1.0×10^{32}

although this number is growing rapidly owing to new systematic surveys. In this section we shall study how and when the explosion of a nearby SN could affect life on the Earth.

The first classification system of supernovae was proposed by W. Baade and F. Zwicky in 1934. Nowadays, we have mainly two types according to the observed spectrum and the progenitor. a) *Type Ia supernova* are found among old star systems (e.g. globular clusters and elliptic galaxies), the trigger mechanism being the mass transfer in a binary system containing a white dwarf⁶. The spectrum shows lines of many heavy elements but no hydrogen lines (Hillebrandt & Niemeyer 2000; Leibundgut, 2000). Recently, Maund *et al.* (2004) have identified the massive binary companion of SN1993J. b) *Type II supernova* are produced by the collapse of a massive star and are therefore found among young stellar systems, where the processes of star formation take place (e.g. open clusters, spiral arms). The explosion leaves a neutron star and produces an injection of all kinds of elements into the interstellar medium, forming a supernova remnant (McCray & Wang 1996 ; Wheeler 2000; Aschenbach 2001). Types Ib and Ic are unusual supernovae with most of the properties of type II, but without hydrogen lines. Tables 7.3 and 7.4 summarize the main characteristics of the different types.

Table 7.3: Absolute magnitudes of the different types of supernovae and the critical distance at which they would have the same visual magnitude as the Sun

Object	Peak M(V)	Critical distance
Sun	+4.8	1 A.U
Type Ia	-19.0	58.000 A.U = 0.3 pc
Type II	- 18.5	46.000 A.U = 0.2 pc

⁶We could also consider a possible collision of two white dwarfs.

Table 7.4: Energy distribution of the different types of supernovae

Type	Energy (J)	Neutrinos (%)	Kinetic (%)	Radiative (%)
Type I	10^{44}	0	99	1
Type II	10^{46}	99	1	0.01

The optical output of SNe rises over a period of several weeks, peaks for a few days (types Ia, Ib) or a few months (type II) and then slowly decays. The absolute values at the peak are -19 (type Ia) and -18.5 (type II). This means that they would have the same apparent magnitude as the Sun placed at a distance of 0.3 pc and 0.2 pc, respectively.

The core collapse of a type II SN produces high-energy radiation through two distinct processes: a) a first UV-flash overlapping in time with the blast wave breakout (Enzman & Buurrows 1992; Matzner & Mc Kee 1999); b) a long-lasting gamma and X-rays powered by the decay of the radioisotopes ^{56}Ni , ^{56}Co and ^{57}Co (Table 7.5). There is a simultaneous emission of cosmic rays energized by the SN shock waves.

Table 7.5: Radioactive decay time scales in supernovae. From Cox (2000).

Element	Half-life	e-fold	Per magnitude
^{56}Ni	6.10 d	8.80 d	8.11 d
^{56}Co	77.12 d	111.3 d	102.3 d
^{57}Co	271.8 d	392.1 d	361.2 d
^{44}Ti	54.2 yr	78.2 yr	72.0 yr

The typical luminosity of a SN in the soft X-ray domain ($0.2\text{--}0.5$ kev) is $4\text{--}8 \times 10^{45}$ erg/s with a duration of $3\text{--}7 \times 10^4$ seconds. This corresponds to a peak flux during the UV flash of $(4\text{--}8) \times 10^3$ erg cm $^{-2}$ s $^{-1}$ (Chevalier & Klein 1979).

Figures 7.1 and 7.2 show light-curves for SN 1987A in different spectral ranges (Pun *et al.* 1995). Note how the UV in the first moments dominates the output, but rapidly drops owing to the combined effects of cooling in the SN atmosphere and the associated increase in opacity.

The observed γ -ray spectrum for SN 1987A was (Gehrels *et al.* 2003)

$$\frac{dN}{dE} = 1.7 \times 10^{-3} \left(\frac{E}{1 \text{ Mev}} \right)^{-1.2} \text{ cm}^{-2} \text{ s}^{-1} \text{ Mev}^{-1}$$

lasting 500 days with a total energy output of 9.0×10^{46} erg.

Gamma Ray Bursts

Strong bursts of γ -rays (Gamma Ray Bursts, hereafter GRBs) were discovered in 1967 by the U.S *Vela* satellites, monitoring possible violations of the Nuclear Test Ban Treaty (Klebesadel *et al.* 1973). They consisted in a short pulse of γ -rays from <20 keV up to tens of GeV). If GRBs are at cosmological distances

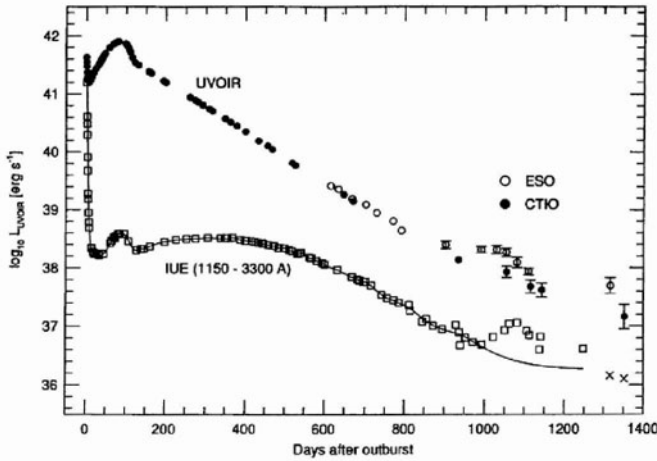


Figure 7.1: Bolometric light-curve (UVOIR) for SN 1987A and the UV lightcurve (IUE) are shown separately in this figure. Courtesy: W. Wamsteker (ESA)

and emit radiation isotropically, these facts would imply an incredible release of energy ($\approx 10^{53}$ erg) for the most energetic events (Kulkarni *et al.* 1998; Preece *et al.* 2000).

The photon number distribution is given by (Band *et al.* 1993)

$$\frac{dN}{dE} = k \left(\frac{E}{100 \text{ kev}} \right)^\alpha \exp(-E/E_0)$$

where $E_0 = 250$ kev is the turnover energy.

It is generally accepted nowadays that GRBs are associated with processes of active star formation and therefore with SN explosions (Meszaros 2003; Hjorth *et al.* 2003). They are probably produced by a special SN type “hypernova”⁷, in which the matter is blowing out in two opposing directions.

7.3.3 Atmospheric effects of strong ionizing events

A nearby supernova would produce a considerable enhancement in the incidence of high-energy radiation (UV and X-rays) on the terrestrial environment. However, these events are intrinsically short-lived and we may reasonably ask, whether they have left some imprints in the geological history of our planet or in that Solar System in general. Krasovskii & Shklovskii have suggested that the K/T extinction was produced by the explosion of a nearby supernova⁸.

⁷A massive star (~ 30 solar masses) exhausts its nuclear fuel supply and collapses, forming a black hole surrounded by an accretion disc.

⁸Cited in Sagan & Shklovskii (1966).

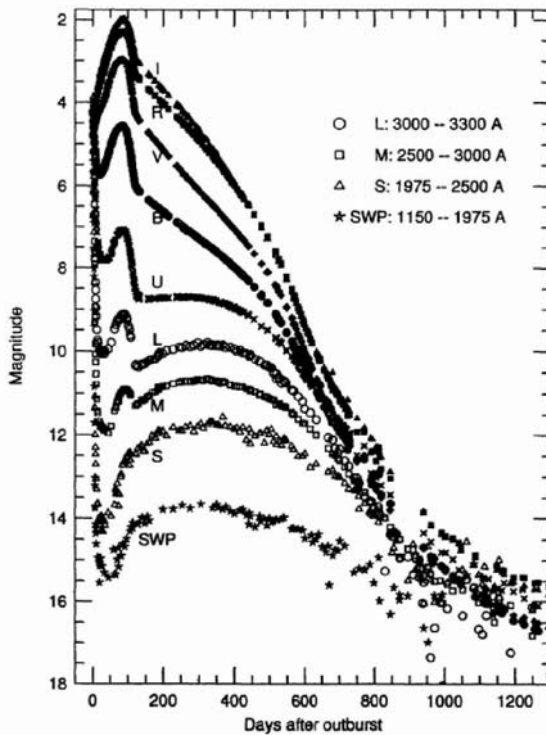


Figure 7.2: This figure shows the lightcurves of SN 1987A in various photometric bands from 150 to 900 nm. The lightcurves have been shifted vertically for clarity of display. Courtesy: W. Wamsteker (ESA)

The main action of the enhanced ionizing (γ - X- and cosmic rays) and UV radiation would be on the main components of the atmosphere producing a destruction of ozone through reactions similar to those recently put forward for solar flares.

Ruderman (1974) was the first to propose the nitrogen mechanism for ozone depletion by SNe. He found that a nearby (< 17 pc) SN would cause an ozone reduction of $\sim 80\%$ for more than two years originating from γ -radiation and 40%–90% from cosmic rays. The topic has been revisited by other authors (Whitten *et al.* 1976), who have obtained similar results. Aikin *et al.* (1980) studied the effect of an SN on the structure of the terrestrial atmosphere, finding that the arrival of UV photons produces a momentary increase in ozone, followed by an important depletion with the delayed arrival of cosmic rays.

Ellis & Schramm (1995) concluded that SN explosions can produce massive extinctions as a result of ozone depletions as high as 95%. Different values were obtained by Crutzen & Bruhl (1996) ranging from at most 60% at high latitudes to below 20% at the equator.

Dar *et al.* (1998) have studied the effects of cosmic ray jets associated with an SN explosion. These jets originated mainly when some ejecta fall back on to the remaining central object, developing an accretion disc and triggering the collapse towards a neutron star or a black hole (Accretion Induced Collapse). A jet with energy of about 1 TeV per nucleon at a distance of 1 kpc will produce a flux of atmospheric muons of 10^{12} per cm^2 at sea level. The consequences would be: a) pollution of the environment by radioactive nuclei and b) depletion of the ozone layer by the above mentioned process via nitrogen oxides.

The rate of production of NO (in mol/cm^2) by a γ -ray burst is (Horvath 2003)

$$\epsilon = 10^{17} \phi_7 \left[\frac{13}{10 + y} \right]$$

where $\phi_7 = (\phi/10^7 \text{ erg cm}^{-2})$ is, by definition, the incident γ flux scaled to a reference value, and the factor in brackets is the ratio of efficiencies of the steady production to the GRB flash in the stratosphere. The same author estimates the ratio, X, of produced [NO] to the present ambient $[\text{NO}]_0$ to be $16 \phi_7^{1/2}$. Consequently, the ozone depletion is given by

$$\frac{[\text{O}_3]}{[\text{O}_3]_0} = \frac{(16 + 9X^2)^{1/2} - 3X}{2}$$

Fluences (time-averaged fluxes), ϕ , larger than $0.7 \times 10^7 \text{ erg cm}^{-2}$ would produce a catastrophic destruction of 90% of the ozone. Melott *et al.* (2004) have proposed that a burst of γ -rays devastated the Earth 443 Ma ago, producing the Ordovician extinction. Planktonic organisms and those animals living in shallow water seem to have been particularly hard hit during the loss of the ozone layer.

More optimistic are the results obtained by Gehrels *et al.* (2003), who found that for a supernova to deplete the terrestrial ozone significantly ($\approx 35\%$) should this occur within 26 light years of our planet ($\phi = 1068 \text{ erg cm}^{-2}$). They considered two main components, a brief gamma-ray blast (300 days) and a longer-lived cosmic ray component (20 years), with total energies of $\sim 2 \times 10^{47} \text{ erg}$ and $4 \times 10^{49} \text{ erg}$, respectively. They estimated this to happen only every 1.5 billion years, making the threat from these events not particularly relevant for the biological evolution. Thomas *et al.* (2005) have calculated the effects of a γ -ray burst from within 2 kpc. A ten second burst delivering 100 kJ m^{-2} to the Earth, would result in a globally averaged ozone depletion of 35%.

We should also consider the transmission properties of a planetary atmosphere. Smith, Scalo & Wheeler (2004a,b) have simulated the irradiation by high-energy radiation of planetary atmospheres for a wide range of column densities (see Figure 7.3 for a schematic overview). These authors follow the path of individual photons as they scatter off the electrons formed in molecules and gradually lose energy until they are absorbed by atoms, obtaining spectra as a function of depth in the atmosphere and underlying oceans for various incident energy spectra, angles of incidence, and atmospheric column densities. Independent of composition, the fraction of photons reaching the ground and their spectra are partly controlled by Compton scattering to energies $\sim 50 \text{ keV}$, below which the atmosphere becomes

optically thick because of strong absorption. Moreover, secondary electrons from these processes are capable of exciting UV spectral lines whose yield can be a significant fraction of the incident ionizing radiation.

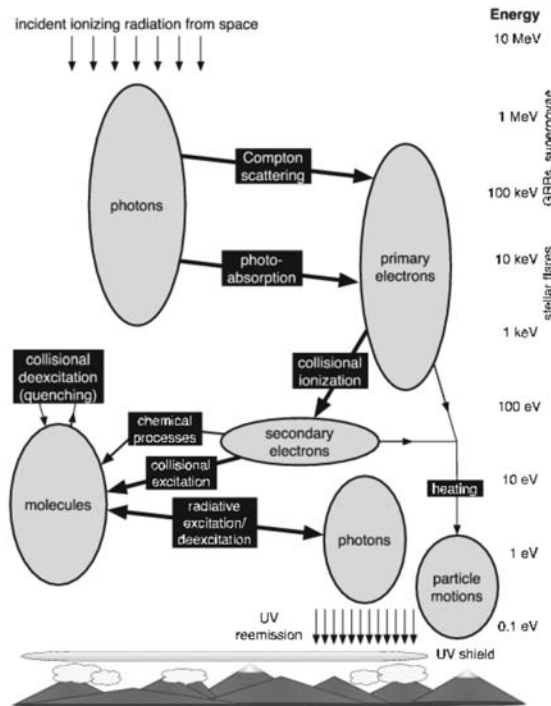


Figure 7.3: Physical processes mediating the redistribution of incident γ - and X-rays (arrows at top left) to UV reemission. Courtesy: J. Scalo, University of Texas, Austin.

Thin atmospheres with a column density less than about 100 g cm^{-2} transmit a substantial portion of any incident γ -ray flux but X-rays are blocked. For thick atmospheres, both γ - and X-rays would be blocked and a substantial fraction would arrive as UV radiation in the absence of UV-blocking agents. For the Earth, between 2×10^{-3} and 4×10^{-2} of the incident flux reaches the ground in the biologically effective range 200–320 nm, depending on O_2/O_3 shielding (see chapter 4).

7.3.4 The Biological Effects of a Nearby Supernova

In chapter 5 we described the main biological effects of ultraviolet radiation. This consideration also applies in case of the explosion of a nearby supernova.

As a further example we may try to calculate the amount of ionizing radiation

capable of providing a lethal dose for a human of 5 rem/year. We approximate the cross-section of a human by a rectangle 1.5 meters high and 0.4 meters wide, giving an effective cross-section of 0.6 m^2 . We now estimate at roughly 50 kg the typical body mass of an astronaut flying in a spaceship on a voyage to Mars.

Assuming that a supernova explodes at a distance D from the Solar System, with an intrinsic luminosity L (erg/s), the astronaut would suffer a dose⁹.

$$\begin{aligned}\text{dose} &= \text{flux} \times \text{area}/\text{mass} \times \omega_R = L/(4\pi D^2) \times (A/M) \times \omega_R = \\ &1.0 \times 10^{-39}(L/D^2) \times \omega_R \text{ (rem/s)}\end{aligned}$$

keeping in mind the relation between rem and ergs (see chapter 5).

If we further assume $L = 10^{42}$ erg/s and $\omega_R = 1$.

$$\text{dose} = 1000/D^2 \text{ (rem/sec)}$$

So we calculate the time it takes (Table 7.6) the astronaut to accumulate a lethal dose of radiation (300 rem)¹⁰.

Table 7.6: Time necessary to accumulate a lethal dose of ionizing radiation. (1 pc = 3.1×10^{18} cm)

Distance to SN	Time for lethal dose
1 pc	> 1 s
10 pc	30 s
100 pc	3.000 s
1.000 pc	300.000 s = 3.5 days
10.000 pc	30.000.000 s = 1 year

Any SN exploding within a kiloparsec presents an immediate threat to unshielded humans. However, more distant events are not very dangerous because their high L would drop after a few days.

7.4 The Probability of Supernova Explosions

The Milky Way produces on average one SN event every 40 ± 10 years, consistent with the observation that the very largest late-type spirals produce approximately 10 SNe per century (see Tammann *et al.* 1994). In the vicinity of the Solar System this frequency could change depending on how much and how often our environment of massive stars changes. We may explore this point at different spatial scales.

⁹Source: M. Richmond “Will a nearby supernova endanger life on Earth?” Available at <http://stupendous.rit.edu/richmond/answers/snrisks.txt>

¹⁰In order to be lethal this dose has to be applied in a very short period of time. The explanation for this is that most DNA breaks are repaired within 30 minutes of being generated.

7.4.1 The Galactic Environment

Our Galaxy, like other spiral galaxies is rotating, completing one revolution in about 230 million years. The stars move in orbits around the galactic centre. Such motions have a random component – they do not orbit in exact circles. The solar motion can be described by the Sun's speed in three different directions: $U = 10 \text{ km/s}$ (radially inward), $V = 5 \text{ km/s}$ (in the direction of the Galactic plane) and $W = 7 \text{ km/s}$ (northwards out of the Galactic plane¹¹).

A possible 28 Ma periodicity in the impact of large cosmic objects on the Earth (Raup & Sepkoski 1984) has raised considerable debate. One suggested explanation was based on the vertical motion of the Sun with respect to the plane of the Galaxy (Rampino & Stothers 1984; Schwartz & James 1984). This velocity component has an amplitude of ~ 230 light years and takes ~ 60 Ma; therefore a crossing takes places approximately every 30 Ma, a value not too far from the supposed periodicity of mass extinctions. On the one hand, the value of the motion is highly uncertain, depending on the amount of matter in the Galactic disc (Stothers 1998); on the other hand, no clear explanation has been given of the biological effects related to these crossings.

Another important aspect to consider is the motion of the Sun with respect to the spiral arms of our Galaxy. The density of gases and interstellar matter in these arms leads to the formation of massive stars and therefore to an enhancement of nearby supernova explosions when our Solar System crosses them. Marochnik (1983) studied the position of our Sun close to the corotation line, showing that this placement is exceptional in the sense that it minimizes the frequencies of passage through large molecular clouds contained in the spiral arms.

To describe the motions of the stars inside the Milky Way two main systems of reference are used: a) The Fundamental Standard of Reference (FSR) refers the motions to the Centre of the Galaxy; b) The Local Standard of Reference (LSR), where the reference is a circular orbit at the distance of the Sun.

V_{LSR} depends on the orbital eccentricity of the star, e , and on the maximum distance to the Galactic plane, z_{max} . The Sun is very close to the corotation distance, at which the galaxy rotation equals to the spiral arms. A star with $e = 0$ will never cross the spiral arms. The time, Δt between crossings is given by

$$\Delta t = \frac{2\pi}{m|\Omega_{\odot} - \Omega_p|}$$

where m is the number of crossings, Ω_{\odot} and Ω_p are the rotation rates of the Sun and the spiral pattern, respectively. Taking $|\Omega_{\odot} - \Omega_p| = 11.1 \pm 1 \text{ km s}^{-1} \text{ kpc}^{-1}$, we get a crossing period of 134 ± 25 Ma on average (Shaviv 2003), taking about 10 Ma to pass through the spiral arm. Figure 7.4 shows the position of the Sun with respect to the spiral arms, during the different geological periods of the Phanerozoic (Leitch & Vasishth 1998).

An additional source of potential cosmic catastrophes in the Solar System could be stellar collisions. Most stars spend most of their lifetimes in relative isolation, but stars in dense star clusters or in galactic nuclei do sometimes collide with each

¹¹See Mihalas & Binney (1981), Galactic Astronomy: Structure and Kinematics, W. H. Freeman

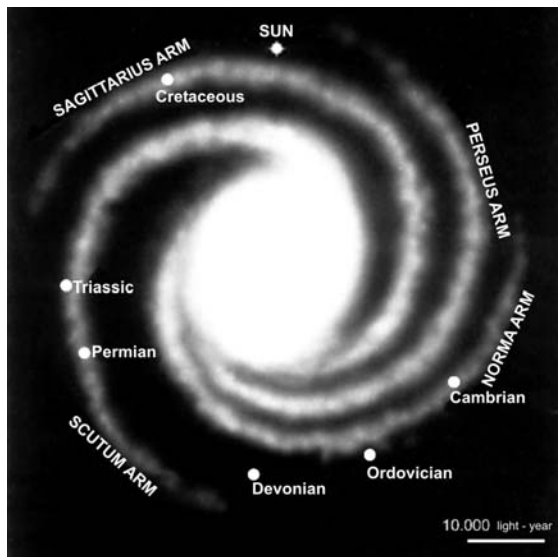


Figure 7.4: Position of the Sun with respect to the spiral arms of the Galaxy. Based on the model of Leitch & Vasisht (1998).

other. Such collisions may build up massive stars (Bonnell 2002) and in some cases form exotic stellar systems (blue stragglers, see Saffer *et al.* 2002). Based on Hipparcos data, García Sánchez *et al.* (2001) have estimated the frequency of stars passing within 1 parsec from our Solar System and have obtained a value of 11.7 (~ 1.3 encounters per Ma). Quillen *et al.* (2004) have suggested that a star of 0.2 solar masses entering the Solar System could scatter one third of the bodies of the Kuiper belt into moderately inclined eccentric orbits, explaining the dichotomy of objects observed in this region. A recent workshop (Shara 2002) summarizes the current state of knowledge in this field.

7.4.2 Effects of Galaxy Collisions: The Case of Andromeda–Milky Way

Like other structures in the Universe, galaxies are not static, but undergo gravitational interactions that could lead to collisions. These events are one of the main drivers of galaxy evolution and involve large amounts of energy. For example, if two objects with masses of the order of 10^{12} solar masses meet with relative velocities of 300 km/s, the kinetic energy is of the order 10^{53} J, equivalent to 10^8 supernovae. Galaxy collisions have typical time-scales of 3×10^8 years, with an energy dissipation rate $L = E/t = 10^{37}$ watts (see Parker 1990 ; Struck 1999).

Our Local Group contains three large galaxies: the Milky Way, the Andromeda Galaxy (M31) and the Triangulum Galaxy (M33). The system also has many dwarf galaxies and satellites. The Local Group is clearly the best place to study

the possible implications of galactic collisions for our environment.

Several models indicate that the Milky Way and M31 will collide in the future to form a giant elliptical. The estimate of this time and the study of its consequences for the habitability of planets in both galaxies will provide a further constraint on the limitations on life in the Universe.

In principle, we may assume that the Local Group is collapsing towards a centre of gravity located somewhere between the Milky Way and M31. We may therefore reasonably expect a value of the transversal velocity considerably smaller than the measured radial velocity (-121 km/s).

The fusion time, T_f , is dependent on the transversal velocity, V_t . We get a value of 5 Ga if $V_t < 40 \text{ km/s}$. T_f increases rapidly for large values, the relationship depending strongly on the mass and dimensions of the haloes of the two galaxies.

Assuming a conservative value for V_t of 60 km/s, the time for the first pericentre at $R_p \approx 100 \text{ kpc}$ will be in 3.5 Ga from now, producing several important effects on our Galaxy, leading to a rearrangement of its internal structure. The stars will change their orbits but are unlikely to collide because of the vast distances separating them.

In our context, more relevant are the effects on the spiral arms structure, whose molecular clouds will be compressed, giving rise to a higher rate of star formation (Genzel *et al.* 1998 ; Arribas & Colina 2002), producing a larger background flux of high-energy radiation with important biological effects. Ultra-luminous infrared galaxies reveal a surprising amount of complexity and structure because they glow fiercely in infrared light. The bright infrared glow is caused by a firestorm of star birth triggered by the multiple-galaxy pileups¹².

The Star Formation Rate (SFR) is the number of stars formed per unit time and the Star Formation Efficiency (SFE) is the number of stars per unit time and mass, M , of gas. The time variation is given by

$$\frac{d \text{SFR}}{dt} = \frac{d \text{SFE}}{dt} + \frac{d M}{dt}$$

For larger regions $d(\text{SFE})/dt$ dominates.

A minor effect will be produced by the gravitational tides. A mass of 10^{12} solar masses at 100 kpc, representing M31, would produce a tide on Pluto's orbit of approximately 4×10^{-15} times the force of the Sun on Pluto. This simple calculation indicates that the perturbation of the orbits will be negligible.

7.4.3 Milky Way History

The Milky Way has probably already had some encounters in the past with some of its satellites. Ibata *et al.* (1994) found traces of a dwarf galaxy, Sagittarius, whose remains now orbit our Galaxy (Figure 7.5) as part of the Sagittarius Tidal Stream, a loose trail of stars and possibly dark matter (Martínez-Delgado *et al.* 2001) . It has been suggested that the primitive Sagittarius galaxy was once pulled through the Milky way disc very close to our Sun's current location and that stars

¹²Launched on 28 April 2003 the Galaxy Evolution Explorer (GALLEX) will map, in UV light, the story of star formation in the Universe.

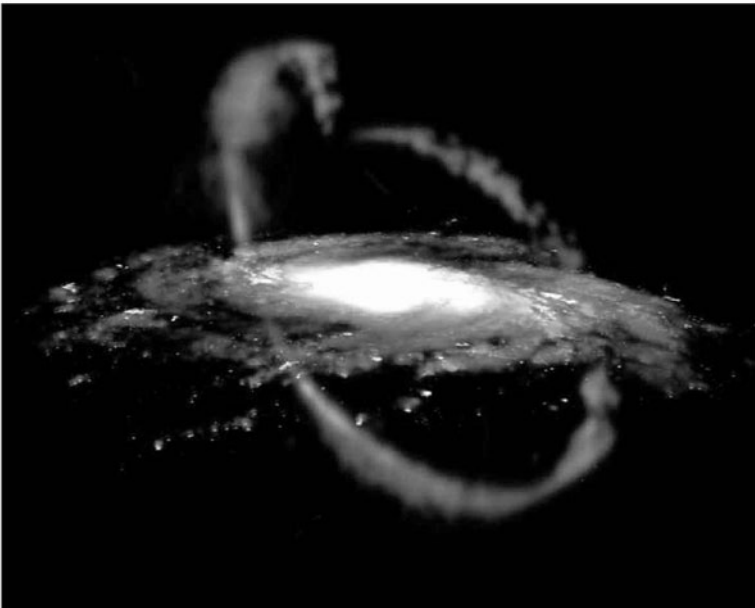


Figure 7.5: The Sagittarius dwarf Tidal Stream. Courtesy: David Martínez Delgado (MPIA, Heidelberg) and G. Pérez (IAC).

once belonging to it can now be found in the solar neighborhood. The event took place approximately 10 Ga ago. Edelshon & Elmegreen (1997) have modelled this interaction, suggesting that the dwarf galaxy passed through the disc 1.7×10^8 years ago and will cross it again in 3.5×10^7 year's time.

Another event is probably associated with the Monoceros tidal stream, which orbits the Galaxy around the galactic disk. A suggested candidate of the original galaxy is the Canis Majoris dwarf (Newberg *et al.* 2002; Yanny *et al.* 2003), although the main core has been already destroyed.

A variable star formation rate in the Milky Way and could be related with variable tidal interactions produced by the Large Magellanic Cloud (LMC), a mechanism first proposed by Scalo (1987). Figure 7.6 plots a history of the SFR after Shaviv (2003), showing a clear minimum between 1 and 2 Ga BP and two prominent peaks around 0.3 and 2.2 Ga. The author proposes that the maximum could be related to the closest approaches of the LMC. The modelling is based on open cluster data and assumes that all the SFRs consist in the formation of stars in clusters¹³.

A more direct method of estimating the SFR history of the Milky Way is to determine the ages of individual stars. This was done by Rocha-Pinto *et al.* (2000), based on the relation between stellar age and chromospheric activity (corrected for

¹³However, the cluster distribution does not necessarily take into account all the stellar formation, and this fraction is also not necessarily constant.

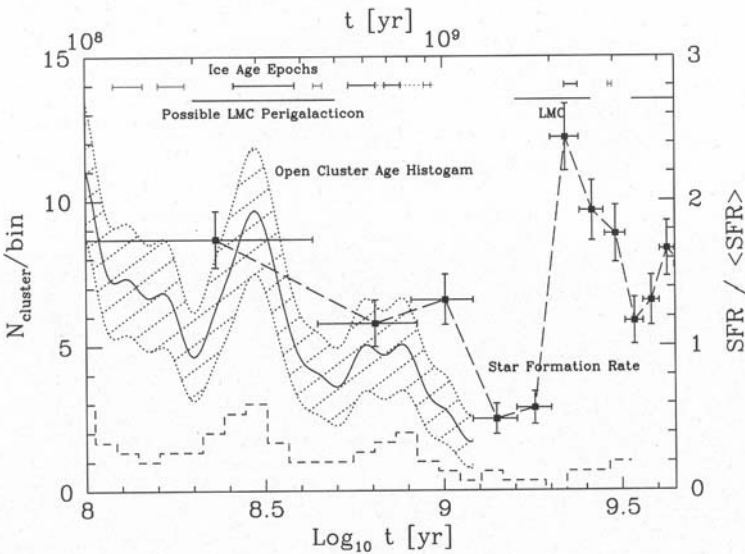


Figure 7.6: The story of the Star Formation Rate in our Galaxy. From Shaviv (2003). Reprinted with the permission of Elsevier.

the metallicity dependence). They find enhanced SF episodes at 0–1 Ga, 2–5 Ga, and 7–9 Ga. A comparison with the close encounters with the LMC show some agreement within the uncertainty in both determinations (see Figures 7.6 and 18 of Rocha Pinto *et al.* 2000).

De la Fuente Marcos & de la Fuente Marcos (2004) have recently derived the SFR history of the Milky Way over the last 2 Ga from the age distribution diagram of a large sample of open clusters. Although the uncertainty is large, the authors suggest that SF bursts are related with close encounters of the Milky Way with the LMC and the Sagittarius dwarf galaxy. However, detected cyclic behaviour of 0.4 Ga period could be better explained in terms of the crossing of spiral arms.

Gilmore *et al.* (2002) presented also the first results of a study proposing that a satellite galaxy merged with the disk of the Milk Way 10 - 12 Ga ago. Navarro *et al.* (2004) propose that the Arcturus group is the solar neighborhood extension of such population.

Additionally, we might consider collisions with high-velocity clouds orbiting the Galaxy (see Alfaro *et al.* 1991, 1996). Four scenarios have been proposed to explain their origin: a) infalling gas from the galactic halo, b) the return branches of outbursts produced by SN explosions, c) tidal streams produced by tidal forces on satellite galaxies and d) capture by the Milky Way of cold intergalactic gas (see Wakker & Van Worden 1997 ; Wakker & Richter 2004).

7.4.4 Activity in the galactic centre

The central parts of galaxies are regions where there is a greater density of stars and also therefore of energetic events related to the later phases of stellar evolution, such as supernova explosions, gamma-rays bursts and similar events. However, in our Galaxy the dust absorbs visible radiation in the line of sight blocking much of our view of this region. Observations indicate that during the last 6 000 years, the Galactic centre has expelled 14 clouds of ionized gas (Lacy *et al.* 1980).

In fact, Clarke (1981) suggested that outbursts from galactic nuclei, happening with a periodicity of 10^8 years, could be a good explanation for the absence of extraterrestrial technological civilizations. Based on observations at sub-mm wavelengths Stark *et al.* (2004) have proposed that every 20 million years, on average, gas pours into the galactic centre creating new stars. The most massive explode as SNe completely sterilizing the surrounding space.

Based on these considerations, Gonzalez *et al.* (2001) have proposed the existence of a galactic habitable zone (GHZ), where the inner edge is determined by the proximity to the galactic centre, where more SN explosions occur¹⁴. Lineweaver *et al.* (2004) have modelled the evolution of the Milky Way to trace the distribution in space and time of the GHZ. To describe the GHZ these authors define a probability P_{GHZ} as the product of four terms:

$$P_{\text{GHZ}} = \text{SFR} \times P_{\text{metals}} \times P_{\text{evol}} \times P_{\text{SN}}$$

where P_{metals} is a metallicity-dependent probability of harboring terrestrial planets; P_{evol} is defined as the cumulative integral of a normal distribution of mean 4 Ga¹⁵ and dispersion 1 Ga and finally P_{SN} express the probability of SN explosions at a given galactocentric distance. They found that GHZ is an annular region located between 7 and 9 kpc from the Galactic centre that widens with time.

In summary, all these events could have affected the structure of the Milky Way, but their large spatial scale and age makes almost impossible to find their fingerprints in our Solar System. For this purpose we must zoom on our local environment, to look for the existence of transitory events, such as supernovae.

7.4.5 The Local Interstellar Medium

The Sun is at present located near the edge of a spiral arm of the Milky Way. The morphology of this region, the *Local Interstellar Medium*, was configured 4×10^7 years ago by the passage of an expanding shell (see Ferlet 1999). As star formation was triggered in the high-density gas ahead of the arc several OB stellar associations were formed, that now delineate the structure of what is known as Gould's Belt. Most stars in the solar neighbourhood younger than about 60 Ma are located in this flattened structure a few hundred parsecs in size, with the Sun inside it. It contains many young low-mass stars and interstellar gas (Stothers & Frogel 1974 ; Grenier 2000) and hosts 432 ± 15 SN progenitors with masses $> 8 M_\odot$ and its estimated lifetime implies a minimum of $40 \text{ SN events Ma}^{-1} \text{ kpc}^{-2}$ in

¹⁴The Earth itself lies about 25 000 light years away from the galactic centre.

¹⁵The assumed time necessary for complex life to be developed in a planet.

a few tens of Ma (Comeron *et al.* 1994 ; Grenier 2000). The Belt is evident in the night sky as a band of very bright stars inclined about 20 degrees relative to the Galactic plane. The map in Figure 7.7 shows the surrounding 1500 light years and the position of nearby high-density molecular clouds (Frisch 2000).

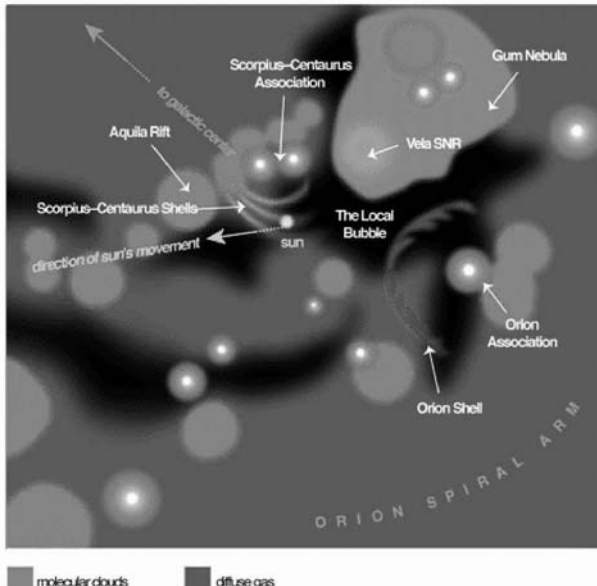


Figure 7.7: The Galactic environment within 1500 light-years of the Sun contains gas clouds of various densities and temperatures. The Sun has passed through a hot, very low-density region—the Local Bubble (black)—for several million years and it is now embedded in a shell of warm, partly ionized material flowing from the Scorpius–Centaurus star-forming region. Credit: Linda Huff (American Scientist) Priscilla Frisch (U. Chicago). Source: “Astronomy Picture of the Day”, 2002 Feb 17. Adapted from Frisch (2000), Fig.3

FUV radiation produced by short-lived massive stars is the main source of heating of the interstellar neutral gas giving rise to cold clouds ($T \sim 50\text{--}100\text{ K}$) or warm clouds ($T \sim 10^4$), depending on the flux (Parravano *et al.* 2003) .

The Local Bubble (Breitschwerdt *et al.* 1998; Maíz-Apellániz 2001) is a peanut-shaped structure about 300 light years long and almost completely empty. It is 1000 times less dense (0.001 atoms per cm^3 and 100 to 100 000 times hotter ($T \sim 10^6\text{ K}$) than ordinary interstellar material and flows through the Solar System with a relative Sun–cloud velocity of $\sim 26\text{ km/s}$ (Zank & Frisch 1999 ; Genova & Beckman 2003). The Local Interstellar Cloud, also known as the Local Fluff (Figure 7.8), is a region of higher density (~ 0.3 atoms per cubic centimetre) and lower temperatures ($T \sim 7000\text{ K}$) into which the Sun has (relatively) recently entered (2000–8000 years ago; see Frisch 1996). Using the UV instrumentation of the HST, Linsky *et al.* (2000) have produced detailed maps of this 20 light years long region.



Figure 7.8: The Local Bubble, in which the Sun is presently embedded (scale: 25 light years). Adapted from N. Henbest & H. Couper (1994) “The Guide to the Galaxy”, Cambridge University Press.

The Sun itself is not at rest in the local rest frame and has a proper motion of about 15 km/s in the direction of the constellation Hercules (approximately in the direction of the star Vega, see previous images), so that it will plow through the Local Fluff in less than 3000 years’s time, and eventually out through the left wall of the Local Bubble.

The Scorpius–Centaurus OB association is the closest star-forming region on the outskirts of the Local Bubble. Currently located at a distance of 450 light years, it is receding in a direction towards the above mentioned constellations. Maíz Apellániz (2001) has recently shown that this association has generated 20 SN explosions during the last 11 Ma, and that it was at its closest approach to the Earth, at a distance of 130 light years, 5 million of years ago (Figure 7.9). One of the supernovae, 2 Ma ago, exploded close enough to Earth to provoke or at least contribute to the Pliocene–Pleistocene boundary marine extinction, where the plankton and bivalve mollusks, all UV sensitive, were the species most affected¹⁶. The event seems to be confirmed by the finding of an excess of ^{60}Fe atoms in layers of the deep ocean (Knie *et al.* 1999).

Observations with the Extreme Ultraviolet Explorer have evidenced that the gas of the bubble surrounding the Sun is highly ionized in all directions. This has been interpreted (Barstow *et al.* 1997; Smith & Cox 2001) as having been produced by a nearby supernova explosion that occurred 4 million years ago.

¹⁶Conventional explanations for this event are based on the emergence of the Panama isthmus or climate cooling.

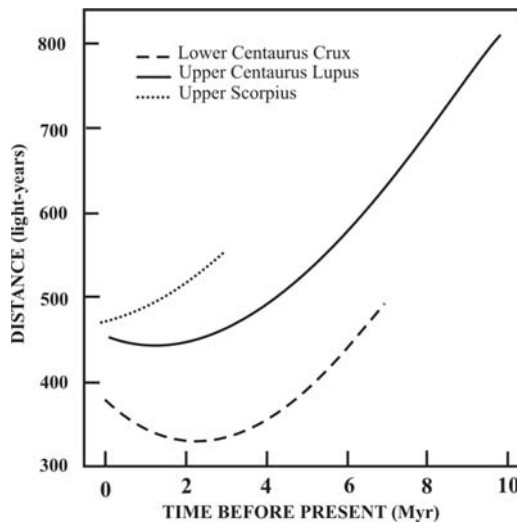


Figure 7.9: Varying distance between the Sun and the centres of the three Sco–Cen subgroups of hot young stars, calculated back to the time when each subgroup began to produce supernovae. The closest approach, by Lower Centaurus Crux, occurred about 2.5 million years ago. (Adapted from Maiz Apellániz, 2001 and Benítez et al. 2002). Courtesy: N. Benítez. Reprinted with permission of the American Physical Society.

7.4.6 Geomagnetic Field Reversals

Apart from the above mentioned variability of sources of ionizing radiation, we may expect changes in the ozone layer if our shield against the penetration of cosmic rays , the geomagnetic field, undergoes important changes. Such events probably occur at the time of field reversals. In 1835, C. F. Gauss (1777–1855) did the first reliable calculation of the strength of the terrestrial magnetic field. Bernard Brunhes (1867–1910) presented, in 1906, the first evidence of these changes. Measurements of such events in the past were possible through the discovery of S.K. Runcorn (1922–1995) that the inclination of the magnetic field is frozen in the ferric oxides of volcanic rocks, archaeological ceramics, lacustrine and marine sediments. Table 7.7 shows the main magnetic reversals, or *chrons*, occurring during the last 5 Ma. Between reversals, variations in the geomagnetic field show a typical saw-toothed pattern. The Earth's magnetic field has weakened by more than 50 per cent in the past 4 000 years, but this does not ensure that a reversal will occur in the near future (see Valet 2003 for a recent review of this subject).

In the Quaternary, two main events at low levels of the geomagnetic field have been detected: the Laschap event (39 kyr BP) and the Monolake (32 kyr BP) lasting 2500 and 1200 years, respectively. Apart from the above mentioned palaeomagnetic measurements, cosmogenic nuclides can be used to study the variation of the geomagnetic field in the Quaternary. Because of the long half-lives ^{10}Be (1.5×10^6 years) and ^{36}Cl (3.0×10^5 years) can be used, with the supplementary

Table 7.7: Main magnetic reversals during the last 5 Ma. Normal polarity means that the north of the magnet points towards geographical north

Chron	Polarity	Duration	Subchrons	Duration
Brunhes	Normal	0.690–0.000		
Matuyama	Reversed	2.430–0.690	Jaramillo	0.930–0.870
			Gilsa	1.630–1.610
			Olduvai	1.850–1.680
			Reunión	2.130–2.110
Gauss		3.320–2.470		
Gilbert		4.500–3.320		

advantage of being sensitive only to the global dipole field and being independent of local variations (Wagner *et al.* 2000; Christl *et al.* 2003).

Over longer time scales, a quiet magnetic period started 120 Ma ago lasting 35 Ma. At its end (\sim 65 Ma ago) the reversals began again, becoming more frequent up to the present.

Reid *et al.* (1976) and Raup (1985) have suggested the existence of a correlation between reversals and biological extinctions. In this context it is really tempting to combine all the above mentioned external causes for mass extinctions into a single mechanism.

Clube & Napier (1981) have proposed a model of this kind. Comets grow in nearby molecular clouds and are captured by the Sun as it passes through the spiral arms of the Galaxy. The impacts of comets on the Earth generate changes in the mantle and core, leading to episodes of magnetic field reversal and enhanced tectonic activity, while surface phenomena lead to ice-ages and mass extinctions. More recently, Muller (2002) has proposed that oblique extraterrestrial impacts could trigger instabilities in the core–mantle boundary, driving both hot spots or superplumes and magnetic reversals. During these events, the solar wind would be in contact with the ionosphere leading to additional ionization and heating of the upper atmosphere. The only exception to this relation between mass extinctions and magnetic reversals is given by the K/T event. To explain this discrepancy Muller has suggested that the Chicxulub crater was made by a vertical impact.

Pavlov *et al.* (2005) have simulated the impact of the passage through an interstellar cloud onto the ozone depletion. The period of 1 Ma is long enough for Earth to experience one magnetic reversal. In this case, the consequent increase in cosmic rays would decrease the ozone column globally by at least 40% and in polar regions up to 80%.

Birk *et al.* (2004) have simulated recently the interaction of the solar wind with the ionosphere in a completely unmagnetized Earth. They found that even in the case of a complete breakdown of the Earth's dynamo, the biosphere is still shielded against cosmic rays by the magnetic field induced by the solar wind.

7.5 Evidence of Nearby Supernovae

7.5.1 Frequency of External UV Events during the History of the Solar System

Sagan & Shklovskii (1966) first estimated that every 750 million of years a type II SN exploded at a distance less than 10 parsecs from the Sun, which means at least six times in the history of the Solar System.

Fields (2004) has estimated the rate, $\lambda(<r)$, of SNe within a distance r after a model of Shklovskii (1968), assuming a Galactic SN rate $R_{SN} \approx (30 \text{ yr})^{-1}$ and that star birth (and death) occur homogeneously in a disc of radius 15 kpc and scale height ~ 100 pc. The results are

$$\lambda(<r) = (10 \text{ Ma})^{-1} \left(\frac{r}{30 \text{ pc}} \right)^3 \text{ for } r < h$$

$$\lambda(<r) = (0.3 \text{ Ma})^{-1} \left(\frac{r}{100 \text{ pc}} \right)^2 \text{ for } r > h$$

Although the estimate is crude, we see that events within 100 pc are very common even within the history of Homo Sapiens.

Scalo *et al.* (2004) have estimated the recurrence rate, T , of energetic events giving a critical flux, F_{cr} (flux integrated over a given time interval), to produce biological effects on Earth or on Earth-like planets.

Assuming that these events occur at a rate per unit of volume, S , the frequency of these events at a distance D is

$$f = (4\pi/3)SD^3$$

with the mean time between events being $T = 1/f$.

Flux is related with distance as

$$F_{cr} = \frac{L}{4\pi D^2}$$

where L is the total energy (luminosity) of the source. If we take $S = 1.5 \times 10^{13}$ yr pc³ and $L = 10^{47}$ erg in the interval (200–300 nm), values for a type II SN, we have

$$T = (6\pi^{0.5}/S)(F_{cr}/L)^{3/2} = 0.067 F_{cr}^{3/2} \text{ years}$$

If we consider additionally the effects of density gradient perpendicular to the plane of the Galaxy and interstellar extinction, we reduce T by a factor of two.

Figure 7.10 shows the time between receptions of flux in the UV spectral region (200–300 nm) from type II SNe. The inset letters show where to read off the present day solar UV fluxes at the position of each of the planets indicated, using the top horizontal scale.

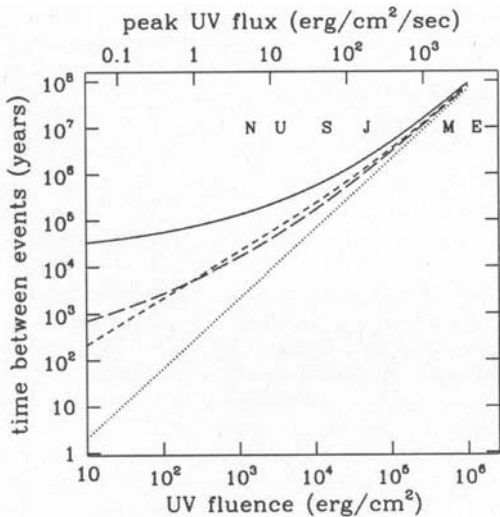


Figure 7.10: Time between receptions of a UV event due to a type II SN. Long-dashed line: effect of vertical galactic structure only included; short-dashed line: effect of galactic dust extinction only included; solid line; both vertical structure and extinction included; dotted line homogeneous no-extinction approximation. Courtesy: J. Scalo

7.5.2 Historical Supernovae

Clark & Stephenson (1976) , Stephenson (1976) and Stephenson & Green (2002) give a list of new stars considered as possible historical supernovae. At present we can see approximately 200 supernova remnants, six of which are from explosions as recent as 1000 years ago (Table 7.8). Current estimates of the frequency of supernova explosions give values between two or three per century. Most of them have escaped direct detection because the optical light was absorbed by the intervening gas and dust clouds of the interstellar medium. The portion of the Milky Way not obscured by dust is only of 15% of the Galactic plane.

One of the best examples is the Crab Nebula (Mitton 1979) , the remnant of SN 1054, first observed by John Bevis (1695–1771) in 1731 (Figure 7.11). The corresponding supernova, located in the constellation of Taurus, was seen from Earth in July or August of 1054 AD¹⁷ and described by Chinese astronomers as being six times brighter than Venus. It was visible in the daytime for almost a month and remained visible in the evening sky for one year.

SN 1006 was clearly observed by astronomers from Japan and China to Italy and Switzerland. According to the description of Ali bin Richwan, it reached a brightness between that of Venus and a waning crescent Moon, and was visible by day for months, by night for almost three years (Murdin 1985) , which indicates that the SN was probably of type II. The corresponding shell is now expanding at

¹⁷Two pictographs have been found in northern Arizona, both showing a crescent moon with a large star nearby. This happened in the morning of July 5, 1054.

Table 7.8: Characteristics of historical Supernovae

Date	Constellation	Distance (kpc)	Remnant
185	Centaurus	2.5	SN Remnant RCW 86
369	Cassiopeia	10	SN Remnant CTW 37 A/B
1006	Lupus	3.4	Radio source PKS 1459-41
1054	Taurus	2	Crab Nebula, Type II SN
1181	Cassiopeia		Radio Source 3C58, Type Ia or II
1572	Cassiopeia	5	RadioSource G120.1*1.4, type II
1604	Ophiuchus	4.8–6.4	Radio Source 3C 358, Type II
1987	Large Magellanic Cloud	50	

a speed of 2 900 km/s (Winkler *et al.* 2003).

Seen in the night for six months in the constellation Cassiopeia, SN 1181 was recorded only in China and Japan. Although the position of the SN was not very well defined, its remnant has been clearly identified (Fesen 1983).

The evolution of SN1572 was followed by Tycho Brahe (1546–1601) and his observations were published in 1573 in the book *De Nova Stella* and later in two volumes of his *Opera Omnia*. From the absence of parallax, he derived that the object was not sublunar. This was the end of the Aristotelian view of Nature, where the Earth was segregated from the heavens, which were perfect and unchanging. Ruiz-Lapuente (2004) has assembled historical records to recover the light curve of this supernova, finding that it was of type SNIa. Recently, Ruiz-Lapuente *et al.* (2004) discovered a type G0–G2 star, similar to our Sun, moving at more than three times the mean velocity of the stars at that distance, which appears to be the surviving companion of the supernova.

SN 1604 is related to a collaborator of Brahe, Johannes Kepler (1571–1630). The supernova was discovered on 1604 October 9 by several persons including Jan Brunowski in Prague, who notified Kepler, Altobelli in Verona, Cristoforo Clavius (1538 - 1612) in Rome, and Capra and Simon Marius (1573–1624) in Padua. Kepler first saw it on October 17, and started a systematic study of the phenomenon. At its peak, the magnitude was around –2.5, brighter than Jupiter. The distance to this SN is still poorly determined (Reynoso & Goss 1999).

Supernova remnants are clearly identified in the sky. They can be used to identify past nearby supernovae, whose explosion have passed unnoticed by terrestrial observers. The diameter $D(\text{pc})$ of the shock wave preceding the expanding shell of interstellar material is given by Sedov (1959) as

$$D = 4.3 \times 10^{-11} (E_0/n)^{1/5} t^{2/5}$$

where t (yr) is the time elapsed since the explosion, E_0 (ergs) is the energy released in the outburst, and n (cm^{-3}) is the number density of hydrogen atoms in the interstellar medium. The main historical supernovae seem to follow this law.

One young SN remnant is known as Cassiopeia A. From its present size and rate of expansion the explosion is calculated to have occurred in \sim 1680 a.C. However, no optical outbursts were reported, although was perhaps observed by John



Figure 7.11: The Crab Nebula. Photograph obtained at the 5 m Hale telescope. Malin/Pasachoff/Caltech/David Malin Images.

Flamsteed (1646–1719) on 1680 August 16. The suspicion is that the SN ejected a major part of its envelope before exploding.

The supernova remnant G266.2.1.2 in Vela may be only 700 years old and is near by, so that historical records might be expected. To look for this and other evidences we must search the terrestrial archive.

7.5.3 Terrestrial Fingerprints

Fields (2004) has summarized the radioisotopes that might give some information on the explosion of nearby supernova. We can divide them in two types: a) cosmogenic radionuclides (^{14}C , ^{10}Be , ^{36}Cl , ^{129}I), secondary products originated by reactions of the cosmic rays with the main components of the terrestrial atmosphere (the terrestrial surface density of the SN spike is set by the cosmic ray flux, $\Phi_{cr} \propto 1/r^2$) and b) direct deposition of SN ejecta, which includes ^{26}Al and ^{60}Fe and possibly r-process nuclides such as ^{182}Hf and ^{244}Pu .

Laster *et al.* (1968) and Ruderman (1974) first studied the possible biological consequences of a supernova explosion for our vicinity. Russell & Tucker (1971) proposed a supernova as the agent giving rise to the K/T event, which, in fact, was the first explanation investigated by the Alvarez team. However, the lack of plutonium 244, associated with iridium, constituted a clear negative test¹⁸. Detre *et al.* (1999) have proposed that the Permian mass extinction was produced by the passage of the Earth through a supernova remnant.

¹⁸Cited in Alvarez,W.,1997, T.Rex and the water of doom, Princeton University Press

Brakenridge (1981) was one of the first to propose a concrete supernova event as source of perturbations in the Solar System: the Vela supernova, 1600 light years and whose explosion took place 11000 BP (Figure 7.12). At the time, the expanding cloud was probably as bright as a crescent Moon (magnitude -8) in the constellation of Cygnus, visible for weeks. The author suggested that the formation of nitrogen compounds could contribute to an increase in organic materials, evidenced in some sediments dated between 10 800 and 9 500 years.



Figure 7.12: Image of the Veil Nebula obtained with the Isaac Newton Telescope at the Roque de los Muchachos Observatory (La Palma). Courtesy: C. Muñoz Tuñón (IAC)

Castagnoli *et al.* (1982) have obtained thermo-luminescence¹⁹ profiles for the last 1500 years. They find striking peaks during the years for which historical supernovae have been reported. Applied to the Crab SN, they estimate its energy at 4×10^{50} erg.

A correlation has been detected in Antarctica between concentrations of the NO₃ radical and the so-called historical supernovae dated at 1181, 1572 and 1604 years (Rood *et al.* 1979; Iyudin 2002), but this concentration is also influenced by solar activity (Zeller *et al.* 1986 ; Dreschhoff & Zeller 1998), geographical position and the season of the year.

We have previously mentioned the use of cosmogenic isotopes as indicators of the flux of cosmic rays on the Earth. Its changes can be produced by a combination of different factors, including supernova explosions. Anomalies in the concentrations of some isotopes could also indicate the possible existence of supernova events. The content of the radioisotope ⁶⁰Fe, with a half - life of 1.5 million of years, has recently been measured to a very high accuracy in ancient deep-sea

¹⁹Thermo-luminescence dating is used for rocks, minerals and pottery. Energy absorbed from ionizing radiation frees electrons, which move through the crystal lattice, and some are trapped at imperfections. Later heating releases the trapped electrons, producing light.

material (Knie *et al.* 1999). The surface density of ^{60}Fe deposited in a layer, $N(l)$, is expressed as (Fields & Ellis 1999)

$$N(\Delta l) = 4.1 \times 10^7 N_{\text{SN}} f \left(\frac{M_{^{60}\text{Fe}}}{10^{-5} M_s} \right) \left(\frac{100 \text{ pc}}{D} \right)^2 \text{ cm}^{-2}$$

where N_{SN} is the number of supernovae, assumed to occur to a distance D , f is the uptake factor ($\approx 1/150$) and $M_{^{60}\text{Fe}}$ the expected ^{60}Fe yield by a SN. These authors interpret these measurements in terms of a recent SN event, 5 million of years ago, exploding at a distance of 100 light years, in good agreement with the predictions of Benítez *et al.* (2002).

Wallner *et al.* (2004) have recently extended the search of SN fingerprints by using the radionuclide ^{244}Pu . The results are consistent with those suggested by ^{60}Fe signals.

The radioactive titanium, ^{44}Ti , is produced in the depths of a supernova and as it decays it emits gamma-rays, which can be detected more easily than optical light. However, the half-life of ^{44}Ti is only of 90 years so that its use is limited to young SNRs. Observations by using the COMPTEL telescope on the Compton gamma-ray Observatory, have detected X-ray emission from a supernova remnant at a distance of 650 light-years. The explosion took place 680 years ago (~ 1250 d.C), and could easily be seen by medieval astronomers, but no report exists of this event (Aschenbach 1998). One possible explanation is that the supernova exploded in the southern Vela constellation, but we cannot disregard other causes for the darkness linked to the intrinsic properties of the event itself. In fact optical subluminous SNe have been reported.

It has been suggested that binary systems with stars in the evolutionary late phases might be the most suitable sources of gamma rays bursts. Dar *et al.* (1998) have proposed that nearby mergers or the accretion induced collapse of neutron stars might be powerful sources of cosmic rays and could therefore can produce substantial ozone depletions, giving rise to the subsequent extinction of biological species. Fingerprints of these intense events can be found by measuring the content of radioactive nuclides such as ^{129}I , ^{146}Sm , ^{205}Pb and ^{244}Pu in lunar and terrestrial rock layers. The jet of relativistic particles with energies of about 1 TeV per nucleon at a distance of 1 kpc produces at sea level a flux of atmospheric muons of 10^{12} cm^{-2} . The lethal dose for human beings in 30 days is $300 \text{ rad} = 3 \times 10^4 \text{ erg g}^{-1}$, which could be reached with lower levels. The biological extinction pattern depends on the exposure and vulnerability of different species.

Radiosotope records with shorter lifetimes, such as ^{10}Be , can also give information about past SNe, because of its dependence on the flux of cosmic rays. Sonnet *et al.* (1987) have suggested that a peak around 35 kyr in ^{10}Be was produced by the explosion of a supernova at a distance closer than 100 parsecs. Florinski *et al.* (2003) used such records to suggest that the Solar System passed through a molecular cloud 35 000 to 60 000 years BP.

Another way is to look for climate changes associated with increases in cosmic rays. This is expected from a correlation between cosmic ray flux and low-lying clouds (Marsh & Svensmark 2000), giving rise to a cooling. However, this relation

must be clearly verified and the low time resolution of the terrestrial records and the influence of other factors make it difficult to verify this claim.

7.5.4 Future Supernova Candidates

Table 7.9 summarizes the nearby stars that might explode as SNe in the not too distant future. For most of these stars the distance determination could be affected by the Lutz–Kelker bias (Lutz & Kelker 1973) .

Table 7.9: Supernova candidates. Scheat and Mira are probably red giants and will therefore not explode as supernovae. The distances are in light years

Star	Constellation	Distance (l yr)	Type
Scheat	Pegasus	200	Red giant
Mira	Cetus	230	Red giant
Betelgeuse	Orion	1 400	Red supergiant
Antares	Scorpius	470	Red supergiant
Ras Algethi	Hercules	550	Red supergiant
Sher 25		25 000	Blue supergiant
Eta Carina		7 500	LBV

The best candidate is probably Eta Carinae, which might explode as a supernova within the next 10 000–20 000 years. It is classified as a Luminous Blue Variable (LBV)²⁰ and is a binary system located in the southern hemisphere with a small component containing 30 solar masses and a larger one 80 times more massive than the Sun. Discovered by Edmund Halley (1656–1742), it has suffered strong brightness variations, and between 1843 and 1856 it increased dramatically in brightness to become the brightest star in the sky except for Sirius. However, the star survived this dramatic release of energy. It is surrounded by a large nebula that blocks most of the UV radiation from the star. Figure 7.13 shows an X-ray image of the central part of the region.

Betelgeuse is a red supergiant²¹ located at the Orion constellation. Sher 25 shows a ring-shaped emission line nebula and a possible outflow (Brandner *et al.* 1997) , which was a previous signature of SN 1987a.

Antares (α Scorpii), the sixteenth brightest star in the sky, is the next star to become a SN in the Sco–Cen association. A fierce stellar wind blowing from its surface has resulted in a circumstellar gas cloud, illuminated by the light from a hot B-type companion star, which, at fifth magnitude, is hidden from view by the supergiant’s glare (separation 3”, period 900 years).

²⁰These are \sim 40–100 times as massive as the Sun and probably started out as early O-type stars.

²¹If placed at the location of the Sun, the optical surface of Betelgeuse would extend to the Asteroid Belt halfway between the orbits of Mars and Jupiter. Betelgeuse subtends the largest angular size of any star in the night sky visible from the northern hemisphere.

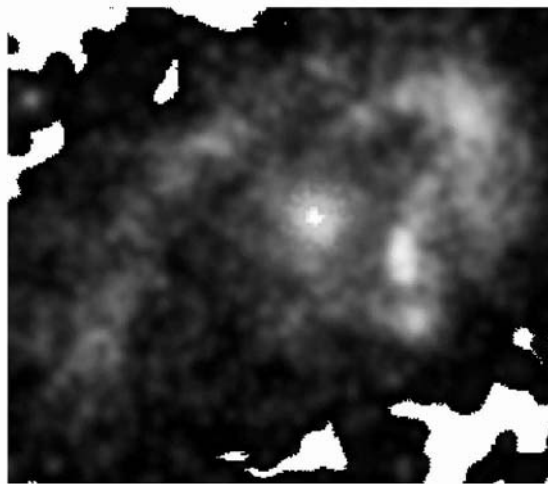


Figure 7.13: X-ray image of Eta Carinae. The binary system lies in the white area within the three-light-month-diameter central blue cloud inside a cooler, two-light-year-diameter "horse-shoe" of gas and dust blown off about a thousand years ago. Courtesy: Chandra Observatory

7.6 Beneficial Evolutionary Effects of UV Radiation

Previously, we considered catastrophic events producing hypermutations on living beings, leading in some cases to a sterilization process and perhaps to mass extinctions. We now consider the action of UV radiation from another point of view.

7.6.1 The Role of the Mutations

In previous chapters we have commented on some beneficial effects of UV radiation on human health. In fact, some biological extinctions could also be explained by a "lack" of UV radiation, mainly affecting the bones of vertebrates, following catastrophic events through absorption by NO_2 . Moreover, some animals, such as bees and other pollinators, have vision optimized in the UV-A range, the lack of which could affect their navigational capabilities when searching for food (Salcedo *et al.* 2003) .

Genetic diversity provided by mutations is an important mechanism for the evolution of living beings. Wallace (1951) had already observed changes in the chromosomes of *Drosophila melanogaster*, after irradiating specimens with ionizing radiation. He concluded than those that had been irradiated and that therefore had more mutations, were hardier than those that were not exposed. In contrast, H.J. Muller (1890–1967) concluded that mutations were deleterious and an accu-

mulation of them even more so²².

Scalo & Wheeler (2002) have suggested that the stochastic irradiation of ionizing radiation could be an accelerating factor in the evolution of life on a habitable planet through direct mutational enhancement or sterilization. In fact, as we commented in chapter 5, primitive bacteria evolved in a strong UV environment, probably developing a kind of “catastrophe kit” to survive. Laboratory experiments with *Pseudomonas fluorescens* seem to confirm this (Rainey & Travisano 1998). Exposure of E. Coli to large X-ray doses has produced mutant strains resistant to both X-ray and UV photons (Ewing 1997). Lethal fluxes for procarciots (E. coli; B. subtilis) are much larger than for mutagenesis.

For high-energy photons or particles greatest mutational lesions are also those leading to lethality, but the situation is different for UV mutagenesis. The mutation doubling dose (MDD) for microorganisms due to UV radiation may be smaller than the lethal dose. This is in contrast to the MDD for ionizing radiation, typically 0.1–0.3 times the lethal dose.

Wilke *et al.* (2001) have done numerical experiments to test the survival of organisms by looking at how they reproduce and utilize available resources. Organisms exposed to high mutation rates, develop over time a large tolerance to mutation; the authors therefore suggest that in a high-mutation environment these robust beings would beat the more prolific ones. This view clearly contradicts the traditional approach that the development of complex organisms primarily requires self-regulated stability of environment.

Experiments suggest that for mutagenesis the duration of the energetic event must be greater than a few hundred generation times of the organism (depending on population size) for fixation of mutation in population during the time of enhanced radiation environment. That means 1–2 weeks for E. coli (generation time 1 hour).

We should distinguish effects producing biological effects from those originating photochemical changes in the planetary atmosphere (e.g. ozone depletion). The duration of an event must be much longer than the relaxation time of atmosphere and the fixation time of organisms (for adaptive mutations to spread throughout population). The photochemistry of the outer planets and their satellites has probably been disturbed at least 50 000 times during the history of the Solar System (Scalo, Wheeler & Williams 2003).

For eukaryot organisms, biologically significant events damaging DNA occur at a rate of $\sim 100\text{--}500 \text{ Ga}^{-1}$. However, the contribution of such SN and γ burst events to mutagenesis is negligible, because of their short duration. According to this view, supernovae and γ -ray bursts can temporarily affect the photochemistry and biology of a planet. However, for a long-lasting and continuous process of mutagenesis we need another source.

²²See Carlson, E. A., 1981, Genes, Radiation and Society: The life and work of H. J. Muller, Cornell University Press.

7.6.2 Large Solar and Stellar Flares

Most of the stars in the Galaxy are low in mass ($M < 0.7$ solar masses), dim and red in colour (class-M). The youngest of this group are very efficient in producing flares and are called “flare stars”, “emission line stars” or “UV Ceti stars” (Gershberg *et al.* 1999). Above the atmosphere, X-ray fluxes and fluences of order 10^6 – 10^7 times larger than on Earth once per 100 hours are expected. Coronal soft X-rays 100 to 1000 stronger relative to L_{bol} than the Sun (Favata 2002). The habitable zone radii for stars between 0.6 and 0.2 solar masses is between 0.15 and 0.05 AU, but tidal locking is considered the main adverse effect for the habitability of planets orbiting such stars. Joshi *et al.* (1997) suggested that atmospheric retention will occur in synchronously rotating planets for atmospheres thicker than ≈ 30 mb. However, M-stars have long lifetimes and therefore enough time for developing life in planets.

The frequency distribution of flare energies from EUV to hard X-rays can be described by a fairly robust power law, ($f(E) \sim E^{-\alpha}$) scaling the flares observed on the Sun with the index α in the range 1.5–2.6 (Veronig *et al.* 2002; Güdel *et al.* 2003).

Figure 7.14 shows the UV habitable zone environment, which is relatively mild except during flares. These stars (see Table 7.10 for a list of the nearby ones) can produce chemically and biologically significant flares every ~ 100 hours (Me stars) to ~ 1000 years (an old G-star as the Sun). It has been suggested that light emitted may be too red in colour for the photosynthesis, a condition necessary only for complex organisms (see, however, Heath *et al.* 1999). This is sufficient to produce effects (atmospheric heating, ionization, chemistry and lethality) on many living beings every 10^6 years.

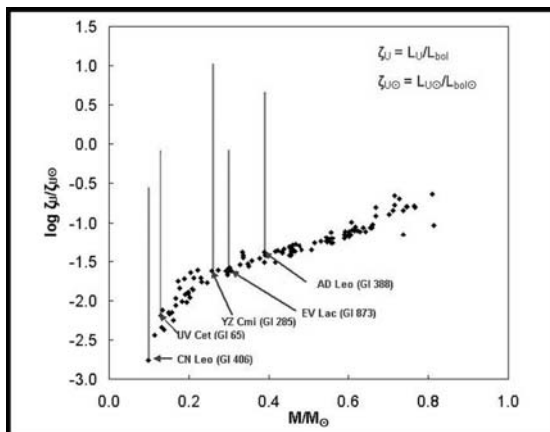


Figure 7.14: UV habitable zone environment. Courtesy: J. Scalo

Applying this concept to the Solar System, the flare activity of the Sun should have been intense enough during the Archaean era to result in sufficiently frequent

Table 7.10: Nearby Flare Stars

Star	Spectral type	Distance (light-years)
Lacaille 8760	M0-2Ve	7.4
Proxima Centauri	M5.5Ve	8.2
Epsilon Indi	K3-5Ve	8.9
70 Ophiuchi2	K0-1Ve	9.3
Lacaille 9352	M0-5Ve	9.6

blasts of UV radiation to produce effects on biological evolution, as well as on atmospheric chemistry (Smith *et al.* 2004) .

7.7 UV Resistance of Living Beings and the Panspermia Theory

The possible survival of bacteria inside comets, meteorites or asteroids is the basis of the panspermia theory, one of the hypotheses explaining the origin of life on our planet. Sales-Guyon de Montlivault first proposed, in 1821, that seeds from the Moon contributed to the origin of life on Earth. H. Richter (1824–1898), Lord Kelvin and H. von Helmholtz (1821–1894) preferred meteorites as the carrier of living beings and discussed the probabilities of surviving the entry into the terrestrial atmosphere. Svante Arrhenius (1859–1927) in the book “World in the Making” proposed the direct propagation of life between planets hurled into space by storms and then propelled by the stellar radiation pressure.

In numerous books and papers F. Hoyle (1915–2001) and C. Wickramasinghe have proposed that comets were the means of transport not only of our primitive ancestors but also in our time producing historical pandemics (Hoyle 1983; Hoyle & Wickramasinghe 1999). In this view, life originated inside dense molecular clouds (Hoyle & Wickramasinghe 1978). Features in the UV spectrum of meteorites (Nagy *et al.* 1963; Sakata *et al.* 1977) and in interstellar extinction curves (Hoyle & Wickramasinghe 1979, 1986) has been used as a proof of the presence of biological activity. However, these claims remain to be verified. Duley & Lazarev (2004) have recently suggested that the 217.5 nm feature is due to dehydrogenated PAH molecules, similar to molecular groups seen in amorphous carbon and Iglesias-Groth (2004) to the photoabsorption by fullerenes and buckyonions.

Independent of origin, and awaiting direct inspection of cometary samples from the Stardust mission ²³, the main issue concerning the reliability of the panspermia hypothesis is the survival of bacteria when subjected to the high level of ionizing and UV radiation in the interplanetary and interstellar medium. The sterility of surface material to tens or hundreds of centimetres of depth appears to be

²³On January 2, 2004 Stardust has collected particles of the comet Wild2. The spacecraft will return to Earth on 15 Jan. 2006 for a first direct analysis of cometary samples at a terrestrial laboratory.

inevitable, and to greater depths for bodies residing for long periods sunward of about 2 A.U (Clark *et al.* 1999) .

Sneath (1962) speculated that Ma survival might be possible “if suitable protected and maintained at temperatures close to absolute zero”. In this context L. Orgel has said²⁴: “You could take E. Coli and rapidly cool it to 10 K and leave it for 10 billion years and then put it back in glucose, and I suspect you would have 99 percent survival”. Endospores allow the organisms that create them to become dormant. Some can survive even in the vacuum of space, remaining for centuries and perhaps longer.

Real tests in space conditions are a good procedure for investigating the viability of meteorites or comets as vehicles for transporting microbes. The EXOBIOLOGIE experiment was run on the MIR station from 1999 April 16 to July 23 (Rettberg *et al.* 2002). Samples of *B. subtilis* were exposed to vacuum and the full UV extraterrestrial spectrum, receiving in total 48.7 mGy, compared to a reference sample in darkness that received only 36.8 mGy (see units in chapter 5). Results show that thin layers of anorganic material did not protect spores against the UV damage, a layer of inactivated spores being a much better shield. Similar experiments have been, and will be, carried out on the International Space Station (Panitz *et al.* 2001) .

Spores of *B. subtilis* were also exposed to space in the European BIOPAN facility on board the Russian FOTON satellite. Spores that were either unprotected or placed behind a quartz window were completely inactivated. Layers of clay, rock or meteorite are only successful in UV-shielding if they are in direct contact with the spores (Horneck *et al.* 2001) . A few centimetre in diameter could be sufficient, but micron-sized grains might not provide adequate protection for spores to survive (see also Napier 2004).

Ground-based laboratory experiments are a complementary tool to gain insight into the survival of microbes in extreme conditions. Weber & Greenberg (1985) placed *Bacillus subtilis* spores in vacuum under UV light. They found less damage at normal interstellar temperatures (10 K) than at higher temperatures, which suggest that inside molecular clouds survival time of Ma would be possible. Recently Peeters *et al.* (2003) have indicated that, if unprotected against UV radiation, the gas-phase adenine and uracil will be destroyed within hours in the Earth’s vicinity and only adenine could survive in DMC for a few million years (see Table 7.11). Some protection needs to be permanently provided (for example, comets)²⁵.

Delprato *et al.*(2001) have reported that, after suffering UV irradiation, colonies of *B. Subtilis* have migrate toward the edges of the exposed area, returning inward when the UV source was switched off.

Primitive lifeforms in different restricted habitats of the Earth can give us insight into the real limitations on the life. In Antarctica, where the UV levels are stronger than in other parts of the Earth, algae have been discovered that live inside solid rock. These are known as *endolithic lifeforms* and are located at depths

²⁴Quoted from “Here Be Dragons”, by David Koerner and Simon LeVay, Oxford University Press, 2000. p 32–33.

²⁵Another problem is survival during the ultimate deposition on a non-hostile host planet.

Table 7.11: Destruction Half-lives for nucleobases and glycine. DISM: Diffuse Interstellar Medium. DC: Dense Molecular Clouds. From Peeters *et al.* 2003.

Compound	Lab (sec)	DISM (yr)	DC (Ma)	1 AU (sec)
Adenine	518	82.7	8.27	8654
Uracil	127	20.3	2.03	2120
Glycine	115	18.4	1.84	1925

of 1–3 mm from the rock surface. On one hand, they are close enough to receive visible light for photosynthesis and on the other hand, they are protected from the damaging action of UV light. Bacteria collected from the interior of basalt rocks in the Sonora desert were subjected to different experiments to test the possibility of interplanetary transfer (Bernardini *et al.* 2003). *B. pumillus* was found to be resistant to 254 nm UV radiation and extreme acceleration shocks.

The possible discovery of Martian life in the meteorite ALH84001 (McKay *et al.* 1996) has brought the hypothesis of ballistic panspermia, meteorites ejected by impacts from a planet providing suitable transport for life between planets of the same planetary system. Experiments suggest a high probability of survival with initial populations of up to 10^{10} spores and interplanetary transfer times shorter than 400 years (Nicholson 2003).

Bacteria have been the only living beings on the Earth during most of its history. They have survived several crisis during the evolution of the Solar System, including those related to UV radiation (Cockell 2003) and they will also be the last habitants of our planet (see Ward & Brownlee 2002).

Bibliography

- Abbatt, J.P.D. and Molina, M. J. (1993). Status of the stratospheric ozone depletion. *Annual Review of Energy and Environment*, 18:1–29.
- Abbot, C. G., Fowle, F. E., and Aldrich, L. B. (1913). The Variation of the Sun. *Astrophysical Journal*, 38:181–186.
- Abbott, D. H. and Isley, A. E. (2002). Extraterrestrial influences on mantle plume activity. *Earth and Planetary Science Letters*, 205:53–62.
- Ackerman, M. (1972). Aeronomical Balloon Experiments. *Space Science Reviews*, 13:290–294.
- Ackerman, M., Frimout, D., and Pastiels, R. (1968). Mesure du rayonnement ultraviolet solaire par ballon stratosphérique. *Ciel et Terre*, 84:408.
- Agrawal, P. C. and Tueller, J. (2002). Scientific ballooning in the next centuries: Goals and Challenges. *Advances in Space Research*, 30:1065–1067.
- Aikin, A. C., Chandra, S., and Stecher, T. P. (1980). Supernovae effects on the terrestrial atmosphere. *Planetary and Space Sciences*, 28:639–644.
- Albert, M. R. and Ostheimer, K. G. (2002). The evolution of current medical and popular attitudes toward ultraviolet light exposure: Part 1. *Journal American Academy of Dermatology*, 47:930–937.
- Albert, M. R. and Ostheimer, K. G. (2003a). The evolution of current medical and popular attitudes toward ultraviolet light exposure: Part 2. *Journal American Acad. Dermatol.*, 48:909–918.
- Albert, M. R. and Ostheimer, K. G. (2003b). The evolution of current medical and popular attitudes toward ultraviolet light exposure: Part 3. *Journal American Acad. Dermatol.*, 49:1096–1106.
- Alfaro, E. J., Cabrera-Cano, J., and Delgado, A. J. (1991). Topography of the Galactic disk - Z-structure and large-scale star formation. *Astrophysical Journal*, 378:106–118.
- Alfaro, E. J. and Efremov, Y. N. (1996). On the Nature of the Vertical Structure of the Galactic Disk. In *Revista Mexicana de Astronomia y Astrofisica Conference Series*, volume 4, pages 1–6.

- Allen, D., Crisp, D., and Meadows, V. (1992). Variable oxygen airglow on Venus as a probe of atmospheric dynamics. *Nature*, 359:516–519.
- Allen, D. R. and Nakamura, N. (2002). Dynamical reconstruction of the record low column ozone over Europe on 30 November 1999. *Geophysical Research Letters*, 29:76–81.
- Allende Prieto, C., Lambert, D. L., Tull, R. G., and MacQueen, P. J. (2002). Convective Wavelength Shifts in the Spectra of Late-Type Stars. *Astrophysical Journal*, 566:L93–L96.
- Aller, L. H. (1963). *The Atmospheres of the Sun and Stars, 2nd edition*. The Ronald Press Co.
- Alvarez, L. W., Alvarez, W., Asaro, F., and Michel, H. V. (1980). Extraterrestrial Cause for the Cretaceous Tertiary Extinction. *Science*, 208:1095–1108.
- Anderson, J. G., Brune, W. H., and Proffitt, M.H. (1989). Ozone destruction by chlorine radicals within the Antarctic vortex: the spatial and temporal evolution of ClO/O₃ anticorrelation based on in situ ER-2 data. *Journal of Geophysical Research*, 94:11465–11479.
- Anderson, J. G., Toohey, D. W., and Brune, W. H. (1991). Free radicals within the Antarctic vortex: The role pf CFCs in Antarctic ozone loss. *Science*, 251:39–46.
- Angell, J. K. (1989). On the relation between atmospheric ozone and sunspot number. *Journal of Climate*, 2:1404–1416.
- Angell, J. K. (1997). Estimated impact of Agung, El Chichón, and Pinatubo volcanic eruptions on global and regional total ozone after adjustment for the quasi-biennial oscillation. *Geophysical Research Letters*, 24:647–650.
- Appleton, E. V. (1924). Geophysical influences on the transmission of wireless waves . *Proceedings of the Physical Society of London*, 37:D16–D22.
- Arnold, N. F. (2002). Solar variability, coupling between atmospheric layers and climate change. *Phil. Transaction Royal Society London, A*, 360:2787–2804.
- Arnold, N. F. and Robinson, T. R. (1998). Solar cycle changes to planetary wave propagation and their influence on the middle atmosphere circulation. *Annales Geophysicae*, 16:69–76.
- Arnold, N. F. and Robinson, T. R. (2000a). Amplification of the influence of solar flux variations on the winter stratosphere by planetary waves. *Space Science Reviews*, 94:279–286.
- Arnold, N. F. and Robinson, T. R. (2000b). Solar cycle changes to planetary wave propagation and their influences on the middle atmosphere circulation. *Annales Geophysicae*, 16:69–76.

- Arnold, N. F. and Robinson, T. R. (2003). Solar cycle modulation of the winter stratosphere: The role of atmospheric waves. *Advances in Space Research*, 31:2121–2126.
- Arribas, S. and Colina, L. (2002). INTEGRAL Field Spectroscopy of IRAS 15206+3342: Gas Inflows and Starbursts in an Advanced Merger. *Astrophysical Journal*, 573:576–583.
- Aschenbach, B. (1998). Discovery of a young nearby supernova remnant. *Nature*, 396:141–142.
- Aschenbach, B. (2001). Supernova Remnants - the past, the present and the future (Invited). In *ASP Conf. Ser. 251: New Century of X-ray Astronomy*, pages 32–+.
- Aschwanden, M. J., Tarbell, T. D., Nightingale, R. W., Schrijver, C. J., Title, A., Kankelborg, C. C., Martens, P., and Warren, H. P. (2000). Time Variability of the “Quiet” Sun Observed with TRACE. II. Physical Parameters, Temperature Evolution, and Energetics of Extreme-Ultraviolet Nanoflares. *Astrophysical Journal*, 535:1047–1065.
- Assman, R. (1902). Über die existenz eines wärmeren Luftstromes in der Höhe von 10 bis 15 km. *Proceedings Royal Prussian Academy of Sciences*, pages 1–10.
- Aversen, J. C., Griffen, R. N., and Pierson, B. D. (1969). Determination of extraterrestrial solar spectral irradiance from research aircraft. *Applied Optics*, 8:2215–2232.
- Avery, O. T., Mc Leod, C. M., and Mc Carty, M. (1944). Studies on the chemical nature of substances inducing transformation of Pneumococcal typoes. *Journal of Experimental Medicine*, 79:137–158.
- Ayres, T. R. (1997). Evolution of the solar ionizing flux. *Journal of Geophysical Research*, 102:1641–1652.
- Baade, W. and Zwicky, F. (1934). On Supernovae. *Proceedings of the National Academy of Sciences*, 20:254–259.
- Bachmann, K. T. and White, O. R. (1994). Observations of hysteresis in solar cycle variations among seven solar activity indicators. *Solar Physics*, 150:347–357.
- Balachandran, N. K., Rind, D., Lonergan, P., and Shindell, D. T. (1999). Effects of solar cycle variability on the lower stratosphere and the troposphere. *Journal of Geophysical Research*, 104:27321–27339.
- Baldwin, M. P. and Dunkerton, T. J. (1999). Propagation of the Arctic Oscillation from the stratosphere to the troposphere. *Journal of Geophysical Research*, 104:30937–30946.
- Baldwin, M. P. and et al. (2001). The Quasi-Biennial Oscillation. *Reviews of Geophysics*, 39:179–229.

- Baliunas, S.L. and Vaughan, A.H. (1985). Stellar Activity Cycles. *Annual Review of Astronomy and Astrophysics*, 23:379–412.
- Ballester et al., G. E. (1995). Far-UV emissions from the SL9 impacts with Jupiter. *Geophysical Research Letters*, 22:2425–2428.
- Band, D., Matteson, J., Ford, L., Schaefer, B., Palmer, D., Teegarden, B., Cline, T., Briggs, M., Paciesas, W., Pendleton, G., Fishman, G., Kouveliotou, C., Meegan, C., Wilson, R., and Lestrade, P. (1993). BATSE observations of gamma-ray burst spectra. I - Spectral diversity. *Astrophysical Journal*, 413:281–292.
- Banks, P. M. and Kockarts, G. (1973). *Aeronomy*. Academic Press.
- Baran, L. W., Ephishov, I. I., Shagimuratov, I. I., Ivanov, V. P., and Lagovsky, A. F. (2003). The response of the ionospheric total electron content to the solar eclipse on August 11, 1999. *Advances in Space Research*, 31:989–994.
- Barbier et al., L. M. (2005). NIGHTGLOW: an instrument to measure the Earth's nighttime ultraviolet glow: results from the first engineering flight. *Astroparticle Physics*, 22:439–449.
- Barnes, S. A. (2003). On the Rotational Evolution of Solar- and Late-Type Stars, Its Magnetic Origins, and the Possibility of Stellar Gyrochronology. *Astrophysical Journal*, 586:464–479.
- Barstow, M. A., Dobbie, P. D., Holberg, J. B., Hubeny, I., and Lanz, T. (1997). Interstellar and photospheric opacity from EUV spectroscopy of DA white dwarfs. *Monthly Notices Royal Astronomical Society*, 286:58–76.
- Barth, C. A., Stewart, A. I., Hord, C. W., and Lane, A. L. (1972). Mariner 9 Ultraviolet Spectrometer Experiment: Mars Airglow Spectroscopy and Variations in Lyman Alpha. *Icarus*, 17:457–468.
- Bartoe, J.-D. F., Brueckner, G. E., Purcell, J. D., and Tousey, R. (1977). Extreme ultraviolet spectrograph ATM experiment S082B. *Applied Optics*, 16:879–886.
- Barylak, M. and Ponz, J. D. (1998). The IUE Archive at Villafranca. In *ASP Conf. Ser. 145: Astronomical Data Analysis Software and Systems VII*, pages 404–407.
- Barylak, M., Talavera, A., Wamsteker, W., Ponz, J. D., and Driessen, C. (1995). The IUE Archives. In *ASSL Vol. 203: Information & On-Line Data in Astronomy*, pages 47–56.
- Bates, D. R. and Hays, P. B. (1967). Atmospheric nitrous oxide. *Planetary and Space Sciences*, 15:189–197.
- Bauer, S. J. (1973). *Physics of Planetary Ionospheres*. Springer.
- Bauer, S. J. (2002). Origin of planetary atmospheres and their role in the evolution of life. In *ESA SP-518: Exo-Astrobiology*, pages 21–24.

- Bauer, S. J. and Hantsch, M. H. (1989a). Solar cycle variation of the upper atmosphere temperature of Mars. *Geophysical Research Letters*, 16:373–376.
- Bauer, S. J. and Hantsch, M. H. (1989b). Solar cycle variation of the upper atmosphere temperature of Mars. *Geophysical Research Letters*, 16:373–376.
- Becker, L., Poreda, R. J., Basu, A. R., Pope, K. O., Harrison, T. M., Nicholson, C., and Iasky, R. (2004). Bedout: A Possible End-Permian Impact Crater Offshore of Northwestern Australia. *Science*, 304:1469–1476.
- Becker, L., Poreda, R. J., Hunt, A. G., Bunch, T. E., and Rampino, M. (2001). Impact Event at the Permian-Triassic Boundary: Evidence from Extraterrestrial Noble Gases in Fullerenes. *Science*, 291:1530–1534.
- Bedinger, J. F. and Manring, E. (1957). Emission from Sodium Vapor Ejected into the Earth's Atmosphere at Night. *Journal of Geophysical Research*, 62:162.
- Beer, J., Baumgartner, S. T., Dittrich-Hannen, B., Hauenstein, J., Kubik, P., Lukasczyk, C., Mende, W., Stellmacher, B., and Suter, M. (1994). Solar Variability Traced by Cosmogenic Isotopes. In *IAU Colloquium 143: The Sun as a Variable Star: Solar and Stellar Irradiance Variations*. Edited by J.M. Pap, C. Fröhlich, H.S. Hudson, and S. Solanki, (Cambridge Univ. Press), pages 291–300.
- Beer, J., Blinov, A., Finkel, R.C., Hofmann, H.J., Lehmann, B., Staffelbach, T., Stauffer, B., Suter, M., and Wölfle, W. (1990). Use of the ^{10}Be in polar ice to trace the 11 year cycle of solar activity. *Nature*, 347:164–166.
- Behring, W. E. (1970). A spectrometer for observations of the Solar Extreme Ultraviolet from the OSO-1 satellite. *Applied Optics*, 9:1006–1012.
- Behring, W. E., McAllister, H., and Rense, W. A. (1958). Ultraviolet Emission Lines in the Solar Spectrum. *Astrophysical Journal*, 127:676–679.
- Ben Jaffel, L., Leers, V., and Sandel, B. R. (1995). Dark Auroral Oval on Saturn Discovered in Hubble Space Telescope Ultraviolet Images. *Science*, 269:951–953.
- Benedick, R. A. (1998). *Ozone Diplomacy*. Harvard University Press.
- Benestad, R. E. (2002). *Solar Activity and Earth's Climate*. Springer Verlag.
- Benevolenskaya, E. E., Kosovichev, A. G., and Scherrer, P. H. (2001). Detection of High-Latitude Waves of Solar Coronal Activity in Extreme-Ultraviolet Data from the Solar and Heliospheric Observatory EUV Imaging Telescope. *Astrophysical Journal*, 554:L107–L110.
- Benítez, N., Maíz-Apellániz, J., and Canelles, M. (2002). Evidence for Nearby Supernova Explosions. *Physical Review Letters*, 88:81101(4).
- Benton, M. J. (1993). Late Triassic Extinctions and the Origin of Dinosaurs. *Science*, 260:769–770.

- Benton, M. J. (1995). Diversification and extinction in the History of Life. *Science*, 268:52–58.
- Benton, M. J. (2003). *When life nearly died*. Thames and Hudson, London.
- Berger, T. E., De Pontieu, B., Fletcher, L., Schrijver, C. J., Tarbell, T. D., and Title, A. M. (1999). What is Moss? *Solar Physics*, 190:409–418.
- Bernardini, J.N., Sawyer, J., Venkateswaran, K., and Nicholson, W. L. (2003). Spore UV and Acceleration Resistance of Endolithic Bacillus pumilus and Bacillus subtilis isolates obtained from Sonoran Desert Basalt: Implications for Lithopanspermia. *Astrobiology*, 3:709–717.
- Berner, R. A. (2002). Examination of hypotheses for the Permo-Triassic boundary extinction by carbon cycle modeling. *Proceedings National Academy of Sciences*, 99:4172–4173.
- Bernhard, G. and Seckmeyer, G. (1997). Measurements of spectral UV irradiance in tropical Australia. *Journal of Geophysical Research*, 102:8719–8730.
- Bernstein, M. P., Dworkin, J. P., Sandford, S. A., Cooper, G. W., and Allaman-dola, L. J. (2002). Astrobiology: seeds of life? *Nature*, 416:401–403.
- Bertaux, J., Widemann, T., Hauchecorne, A., Moroz, V. I., and Ekonomov, A. P. (1996). VEGA 1 and VEGA 2 entry probes: An investigation of local UV absorption (220–400 nm) in the atmosphere of Venus (SO₂, aerosols, cloud structure). *Journal of Geophysical Research*, 101:12709–12746.
- Bertaux, J. L., Blamont, J. E., and Festou, M. (1973). Interpretation of Hydrogen Lyman-Alpha Observations of Comets Bennett and Encke. *Astronomy and Astrophysics*, 25:415–430.
- Bertaux, J. L., Costa, J., Quémérais, E., Lallement, R., Berthé, M., Kyrölä, E., Schmidt, W., Summanen, T., Makinen, T., and Goukenleuke, C. (1998). Lyman-alpha observations of comet Hyakutake with SWAN on SOHO. *Planetary and Space Sciences*, 46:555–568.
- Bhardwaj, A. and Gladstone, G. R. (2000). Auroras on Saturn, Uranus, and Neptune. *Advances in Space Research*, 26:1551–1558.
- Bianciardi, G., Ranzini, G., and Venturoli, D. (2001). The biologic experiments on Mars by Viking landers and presumptive fossils on the Martian meteorite ALH84001. In *ESA SP-496: Exo-/Astro-Biology*, pages 303–304.
- Biermann, L. (1941). Der gegenwärtige Stand der Theorie konvektiver Sonnenmodelle. *Vierteljahrsschrift Astron. Gesellschaft*, 76:194–200.
- Biermann, L. (1946). *Naturwissenschaften*, 33:118–119.
- Biermann, L. (1948). Über die Ursache der chromosphärischen Turbulenz und des UV-Exzesses der Sonnenstrahlung. *Zeitschrift für Astrophysics*, 25:161–177.

- Bilstein, R. E. (1990). *Orders of magnitude. A history of NACA and NASA 1915–1990.* NASA SP-4406.
- Birk, G. T., Lesch, H., and Konz, C. (2004). Solar wind induced magnetic field around the unmagnetized Earth. *Astronomy and Astrophysics*, 420:L15–L18.
- Black, R. X. (2002). Stratospheric forcing of surface climate in the Arctic Oscillation. *Journal of Climate*, 15:268–277.
- Blake, R. L., Chubb, T. A., Friedman, H., and Unzicker, A. E. (1963). Interpretation of X-Ray Photograph of the Sun. *Astrophysical Journal*, 137:3–15.
- Blecker, J.A. M., Geiss, J., and (eds.), Huber, M.C.E (2002). *The Century of Space Science (2 Vols).* Kluwer Academic Publishers.
- Bocníček, J. and Hejda, P. (2002). Association between extraterrestrial phenomena and weather changes in the northern hemisphere in winter. *Surveys in Geophysics*, 23:303–333.
- Bodeker, G. E. and McKenzie, R. L. (1996). An Algorithm for Inferring Surface UV Irradiance Including Cloud Effects. *Journal of Applied Meteorology*, 35:1860–1877.
- Bodiwala, D., Luscombe, C. J., Liu, S., Saxby, M., French, M., Jones, P. W., Fryer, A. A., and Strange, R.C. (2003). Prostate cancer risk and exposure to ultraviolet radiation: further support for the protective effect of sunlight. *Cancer Letters*, 192:145–149.
- Bodiwala et al., D. (2004). Polymorphisms in the vitamin D receptor gene, ultraviolet radiation, and susceptibility to prostate cancer. *Environmental and Molecular Mutagenesis*, 43:121–127.
- Bojkow, R. D. (1986). Surface ozone during the second half of the nineteenth century. *Journal of Climate and Applied Meteorology*, 20:343–352.
- Boksenberg et al., A. (1973). The ultra-violet sky-survey telescope in the TD-IA satellite. *Monthly Notices Royal Astronomical Society*, 163:291–322.
- Bonnell, I. A. (2002). The Formation of Massive Stars through Stellar Collisions. In *Hot Star Workshop III: The Earliest Stages of Massive Star Birth. ASP Conference Proceedings, Vol. 267. Edited by Paul A. Crowther.*, pages 193–208.
- Bonnet, R. M., Decaudin, M., Bruner, E. C., Acton, L. W., and Brown, W. A. (1980). High-resolution Lyman-alpha filtergrams of the sun. *Astrophysical Journal*, 237:L47–L50.
- Borucki, J. G., Khare, B., and Cruikshank, D. P. (2002). A new energy source for organic synthesis in Europa's surface ice. *Journal of Geophysical Research (Planets)*, pages 24–1.

- Botta, O., Glavin, D. P., and Bada, J. L. (2002). Amino acid signatures in carbonaceous meteorites. In *Proc. SPIE Vol. 4495, Instruments, Methods, and Missions for Astrobiology IV*, Richard B. Hoover; Gilbert V. Levin; Roland R. Paepe; Alexei Y. Rozanov; Eds., pages 27–39.
- Bottema, M., Plummer, W., and Strong, J. (1965). A quantitative measurement of water vapour in the atmosphere of Venus. *Annales d'Astrophysique*, 28:225–228.
- Bougher, S. W., Engel, S., Roble, R. G., and Foster, B. (2000). Comparative terrestrial planet thermospheres 3. Solar cycle variation of global structure and winds at solstices. *Journal of Geophysical Research*, 105:17669–17692.
- Bougher, S. W., Gerard, J. C., Stewart, A. I. F., and Fessen, C. G. (1990). The Venus nitric oxide night airglow - Model calculations based on the Venus Thermospheric General Circulation Model. *Journal of Geophysical Research*, 95:6271–6284.
- Bouguess, A., Carr, F. A., Evans, D. C., Fischel, D., Freeman, H.R., Fuechsel, C. F., Kinglessmith, D. A., Kruger, V.L., Longanecker, G. W., and Moore, J. V. (1978). The IUE spacecraft and instrumentation. *Nature*, 275:372–377.
- Bowroski, N., Hönninger, G., Galle, B., and Platt, U. (2003). Detection of bromine monoxide in a volcanic plume. *Nature*, 423:273–276.
- Bowyer, A. and Malina, R. F. (1995). *Astrophysics in the Extreme Ultraviolet*. Kluwer Academic Press.
- Bowyer, S. (1991). The cosmic far ultraviolet background. *Annual Review of Astronomy and Astrophysics*, 29:59–88.
- Brakenridge, G. R. (1981). Terrestrial paleoenvironmental effects of a late quaternary-age supernova. *Icarus*, 46:81–93.
- Brandenburg, A., Saar, S. H., and Turpin, C. R. (1998). Time Evolution of the Magnetic Activity Cycle Period. *Astrophysical Journal*, 498:L51–L54.
- Brandner, W., Chu, Y., Eisenhauer, F., Grebel, E. K., and Points, S. D. (1997). The Hourglass Nebulae of Sher 25 and SN 1987A: Two of a Kind? 1. *Astrophysical Journal*, 489:L153–L156.
- Brasseur, G. and Solomom, S. (1994). *Aeronomy of the Middle Atmosphere*. D. Reidel, Dordrecht.
- Brasseur, G. P., Müller, J., and Granier, C. (1996). Atmospheric impact of NO_x emissions by subsonic aircraft: A three-dimensional model study. *Journal Geophysical Research*, 101:1423–1428.
- Breit, G. and Tuve, M. A. (1926). A Test of the Existence of the Conducting Layer. *Physical Review*, 28:554–575.
- Breitschwerdt, D., Freyberg, M. J., and Truemper, J. (1998). The Local Bubble and Beyond. *Lecture Notes in Physics*, Berlin Springer Verlag, 506.

- Brekke, P., Kjeldseth-Moe, O., Bartoe, J.-D. F., and Brueckner, G. E. (1991). An ultraviolet spectral atlas of a sunspot and an active region 1190-1730 A. *Astrophysical Journal Supplement*, 75:1337–1366.
- Brekke, P., Thompson, W. T., Woods, T. N., and Eparvier, F. G. (2000). The Extreme-Ultraviolet Solar Irradiance Spectrum Observed with the Coronal Diagnostic Spectrometer (CDS) on SOHO. *Astrophysical Journal*, 536:959–970.
- Brewer, A. W. (1949). Evidence for a world circulation provided by the measurement of helium and water vapor distribution in the stratosphere. *Quarterly Journal Meteorological Society*, 75:351–363.
- Brittnacher, M., Kang, J., Parks, G., Elsen, R., Germany, G., Spann, J., Fox, N., Puettner, R. C., and Yahil, A. (2001). Far-ultraviolet observations of the neutral comae of Comet Hale-Bopp (C/1995 01) near perihelion. *Geophysical Research Letters*, 28:2561–2564.
- Brković, A., Solanki, S. K., and Rüedi, I. (2002). Quiet-Sun variability observed with SUMER and CDS. *Astronomy and Astrophysics*, 385:257–263.
- Broadfoot, A. L., Atreya, S. K., Bertaux, J. L., Blamont, J. E., Dessler, A. J., and Linick, S. (1989). Ultraviolet spectrometer observations of Neptune and Triton. *Science*, 246:1459–1466.
- Broadfoot, A. L., Shemansky, D. E., and Kumar, S. (1976). Mariner 10 - Mercury atmosphere. *Geophysical Research Letters*, 3:577–580.
- Brosch, N. (1999). Ultraviolet sky surveys. Instruments, findings, and prospects. *Experimental Astronomy*, 9:119–187.
- Brosius, J. W., Davila, J. M., and Thomas, R. J. (1998). Solar Active Region and Quiet-Sun Extreme-Ultraviolet Spectra from SERTS-95. *Astrophysical Journal Supplement*, 119:255–276.
- Brown, T. M., Kimble, R. A., Ferguson, H. C., Gardner, J. P., Collins, N. R., and Hill, R. S. (2000). Measurements of the Diffuse Ultraviolet Background and the Terrestrial Airglow with the Space Telescope Imaging Spectrograph. *Astronomical Journal*, 120:1153–1159.
- Brückner, G. E., Edlow, K. L., Floyd, L. E., Lean, J. L., and Vanhoosier, M. E. (1993). The solar ultraviolet spectral irradiance monitor (SUSIM) experiment on board the Upper Atmosphere Research Satellite (UARS). *Journal of Geophysical Research*, 98:10695–10711.
- Bruns, A. V., Prokofiev, V. K., and Severny, A. B. (1970). On the Contribution of Solar Activity to the Ultra Violet Spectrum of the Sun. In *IAU Symp. 36: Ultraviolet Stellar Spectra and Related Ground-Based Observations*, pages 256–259.

- Bullock, M. A., Stocker, C. R., McKay, C. P., Zent, A. P., and Becker, J. F. (1989). The Oxidation and Degradation of Organic Compounds Under Simulated Martian Conditions. *Bulletin American Astronomical Society*, 21:956.
- Burge, W. E. (1916). The mode of action of ultra-violet radiation in injuring living cells with special reference to those constituting the eye. *American Journal of Physiology*, 131:1–22.
- Córdoba-Jabonero, C., Lara, L. M., Mancho, A. M., Márquez, A., and Rodrigo, R. (2003). Solar ultraviolet transfer in the Martian atmosphere: biological and geological implications. *Planetary and Space Science*, 51:399–410.
- Campbell, D. B., Black, G. J., Carter, L. M., and Ostro, S. J. (2003). Radar Evidence for Liquid Surfaces on Titan. *Science*, 302:431–434.
- Canuto, V. M., Levine, J. S., Augustsson, T. R., and Imhoff, C. L. (1982). UV radiation from the young sun and oxygen and ozone levels in the prebiological palaeoatmosphere. *Nature*, 296:816–820.
- Canuto, V. M., Levine, J. S., Augustsson, T. R., Imhoff, C. L., and Giampapa, M. S. (1983). The young sun and the atmosphere and photochemistry of the early earth. *Nature*, 305:281–286.
- Carlson, R. W. (2002). Radiolysis and Chemical Weathering on the Galilean Satellites. *AGU Fall Meeting Abstracts*, page C6.
- Carlson, R. W. and Judge, D. L. (1971). The extreme ultraviolet dayglow of Jupiter. *Planetary and Space Sciences*, 19:327–343.
- Carrington, R. C. (1858). On the Distribution of the Solar Spots in Latitudes since the Beginning of the Year 1854, with a Map. *Monthly Notices Royal Astronomical Society*, 19:1–3.
- Carrington, R. C. (1859). Description of a Singular Appearance seen in the Sun on September 1, 1859. *Monthly Notices Royal Astronomical Society*, 20:13–15.
- Carruthers, G. R., Opal, C. B., Page, T. L., Meier, R. R., and Prinz, D. K. (1974). Lyman-alpha imagery of Comet Kohoutek. *Icarus*, 23:526–537.
- Carson, R. (1962). *Silent Spring*. Houghton Mifflin, Boston.
- Castagnoli, G. C., Bonino, G., and Miono, S. (1982). Thermoluminescence in sediments and historical supernovae explosions. *Nuovo Cimento C Geophysics Space Physics C*, 5:488–494.
- Castanheira, J. M. and Graf, H.-F. (2003). North Pacific-North Atlantic relationships under stratospheric control? *Journal of Geophysical Research (Atmospheres)*, 108:11–+.
- Cebula, R. P. and Feldman, P. D. (1982). Ultraviolet spectroscopy of the zodiacal light. *Astrophysical Journal*, 263:987–992.

- Chakrabarti, S., Paresce, F., Bowyer, S., Kimble, R., and Kumar, S. (1983). The extreme ultraviolet day airglow. *Journal of Geophysical Research*, 88:4898–4904.
- Chakrabarty, D. K., Peshin, S. K., Srivastav, S. K., Shah, N. C., and Pandya, K. V. (2001). Further evidence of total ozone variation during the solar eclipse of 1995. *Journal of Geophysical Research*, 106:3213–3218.
- Chamberlain, J. W. (1955). The Ultraviolet Airglow Spectrum. *Astrophysical Journal*, 121:277–286.
- Chamberlain, J. W. (1961). *Physics of the Aurora and Airglow*. Academic Press.
- Chamberlain, J. W. (1995). *Physics of the Aurora and Airglow*. American Geophysical Union.
- Chandra, S. and McPeters, R. D. (1994). The solar cycle variation of ozone in the stratosphere inferred from Nimbus 7 and NOAA 11 satellites. *Journal of Geophysical Research*, 99:20665–20671.
- Chandra, S., Ziemke, J. R., and Stewart, R. W. (1999). An 11-year solar cycle in tropospheric ozone from TOMS measurements. *Geophysical Research Letters*, 26:185–.
- Chapman, G. A., Cookson, A. M., and Dobias, J. J. (1996). Variations in total solar irradiance during solar cycle 22. *Journal of Geophysical Research*, 101:13541–13548.
- Chapman, G. A., Herzog, A. D., and Lawrence, J. K. (1986). Time-integrated energy budget of a solar activity complex. *Nature*, 319:654–655.
- Chapman, G. A. and Meyer, A. D. (1986). Solar irradiance variations from photometry of active regions. *Solar Physics*, 103:21–31.
- Chapman, S. (1930). A theory of upper-atmosphere ozone. *Memoirs of the Royal Meteorological Society*, 3:103–125.
- Chapman, S. (1931). The absorption and dissociative or ionizing effect of monochromatic radiation in an atmosphere on a rotating earth . *Proceedings of the Physical Society*, 43:26–45.
- Charlson, R. J., Warren, S. G., Lovelock, J. E., and Andreae, M. O. (1987). Oceanic phytoplankton, atmospheric sulphur, cloud albedo and climate. *Nature*, 326:655–661.
- Chassefiere, E. (1996). Hydrodynamic Escape of Oxygen from Primitive Atmospheres: Applications to the Cases of Venus and Mars. *Icarus*, 124:537–552.
- Chen, R. H., Cravens, T. E., and Nagy, A. F. (1978). The Martian ionosphere in light of the Viking observations. *Journal of Geophysical Research*, 83:3871–3876.

- Chenoweth, M. (2001). Two major volcanic cooling episodes derived from global marine air temperature, AD 1807–1827. *Geophysical Research Letters*, 28:2963–2966.
- Chevalier, R. A. and Klein, R. I. (1979). Nonequilibrium processes in the evolution of type II supernovae. *Astrophysical Journal*, 234:597–608.
- Christensen et al., A. B. (2003). Initial observations with the Global Ultraviolet Imager (GUVI) in the NASA TIMED satellite mission. *Journal of Geophysical Research (Space Physics)*, 108:16–1.
- Christie, M. (2000). *The Ozone Layer*. Cambridge University Press.
- Christl, M., Strobl, C., and Mangini, A. (2003). Beryllium-10 in deep-sea sediments: a tracer for the Earth's magnetic field intensity during the last 200,000 years. *Quaternary Science Reviews*, 22:725–739.
- Chubachi, G. (1984). Preliminary result of ozone observation at Syowa Station from February 1982 to January 1983. *Memoirs of the National Institute Polar Research, Special Issue*, 13:1197–1198.
- Chubb, T. A., Friedman, H., Kreplin, R. W., Blake, R. L., and Unzicker, A. E. (1961). X-ray and ultraviolet measurements during the eclipse of October 12, 1958. *Memoires Soc. Royal Sciences Liege*, 4:228–240.
- Chyba, C. F. and Sagan, C. (1992). Endogenous production, exogenous delivery and impact-shock synthesis of organic molecules: an inventory for the origins of life. *Nature*, 355:125–132.
- Chyba, C. F. and Sagan, C. (1997). *Comets as a source of prebiotic organic molecules for the Early Earth*, pages 147–174. "Comets and the Origin and Evolution of Life", Springer Verlag.
- Ciaravella, A., Raymond, J. C., van Ballegooijen, A., Strachan, L., Vourlidas, A., Li, J., Chen, J., and Panasyuk, A. (2003). Physical Parameters of the 2000 February 11 Coronal Mass Ejection: Ultraviolet Spectra versus White-Light Images. *Astrophysical Journal*, 597:1118–1134.
- Cicerone, R. S., Elliot, S., and Turco, R. (1991). Reduced Antarctic Ozone depletions in a model with hydrocarbon injections. *Science*, 254:1191–1194.
- Clairemidi, J., Bréchignac, P., Moreels, G., and Pautet, D. (2004). Tentative identification of pyrene as a polycyclic aromatic molecule in UV spectra of comet P/Halley: An emission from 368 to 384nm. *Planetary and Space Sciences*, 52:761–772.
- Clancy, R. T., Wolff, M. J., James, P. B., Smith, E., Billawala, Y. N., Lee, S. W., and Callan, M. (1996). Mars ozone measurements near the 1995 aphelion: Hubble space telescope ultraviolet spectroscopy with the faint object spectrograph. *Journal of Geophysical Research*, 101:12777–12784.

- Clark, D. H. and Stephenson, F. R. (1976). Which historical new stars were supernovae. *Quarterly Journal Royal Astronomical Society*, 17:290–302.
- Clark et al., B. C. (1999). Survival of life on asteroids, comets and other small bodies. *Origins of Life and Evolution of the Biosphere*, 29:521–545.
- Clarke, J. N. (1981). Extraterrestrial Intelligence and Galactic Nuclear Activity. *Icarus*, 46:94–96.
- Clarke, J. T., Prange, R., Ballester, G. E., Trauger, J., Evans, R., Rego, D., Stapelfeldt, K., Ip, W., Gerard, J., Hammel, H., Ballav, M., Ben Jaffel, L., Bertaux, J., Crisp, D., Emerich, C., Harris, W., Horanyi, M., Miller, S., Storrs, A., and Weaver, H. (1995). HST Far-Ultraviolet Imaging of Jupiter During the Impacts of Comet Shoemaker-Levy 9. *Science*, 267:1302–1307.
- Clayton, H. H. (1930). The Atmosphere and the Sun. *Smithsonian Miscellaneous Collections*, 82:1–49.
- Clayton, R. N. and Thiemens, M.H. (1980). Lunar nitrogen: Evidence for secular change in the solar wind. In *The Ancient Sun: Fossil Record in the Earth, Moon and Meteorites*, pages 463–473.
- Close, R. M., Parnell, C. E., Longcope, D. W., and Priest, E. R. (2004). Recycling of the Solar Corona's Magnetic Field. *Astrophysical Journal*, 612:L81–L84.
- Clube, S. V. and Napier, W. M. (1981). Spiral arms, Comets and Terrestrial Catastrophism. *Quarterly Journal Royal Astronomical Society*, 23:45–.
- Cockell, C. S. (1998). Biological Effects of High Ultraviolet Radiation on Early Earth - a Theoretical Evaluation. *Journal Theoretical Biology*, 193:717–729.
- Cockell, C. S. (1999a). Carbon biochemistry and the ultraviolet environments of F, G and K main sequence stars. *Icarus*, 141:399–407.
- Cockell, C. S. (1999b). Crisis and extinction in the fossil record - a role for ultraviolet radiation? *Paleobiology*, 25:212–225.
- Cockell, C. S. (1999c). Life on Venus. *Planetary and Space Science*, 47:1487–1501.
- Cockell, C. S. (2001a). A Photobiological History of Earth. In *Ecosystems, Evolution, and Ultraviolet Radiation*, C.S. Cockell and A.R. Blaustein (eds.), pages 1–35. Springer Verlag.
- Cockell, C. S. (2001b). Ultraviolet Radiation and Exobiology. In *Ecosystems, Evolution, and Ultraviolet Radiation*, C.S. Cockell and A.R. Blaustein (eds.), pages 195–218. Springer Verlag.
- Cockell, C. S. (2002). *The ultraviolet radiation environment of Earth and Mars: past and present*, pages 219–232. Astrobiology. The quest for the conditions of life. Gerda Horneck, Christa Baumstark-Khan (eds.). Physics and astronomy online library. Berlin: Springer.

- Cockell, C. S. (2003). *Impossible Extinction*. Cambridge University Press.
- Cockell, C. S. and Airo, A. (2002). On the plausibility of a UV transparent biochemistry. *Origins of Life and Evolution of the Biosphere*, 32:255–274.
- Cockell, C. S. and Blaustein, A. R. (2000). “Ultraviolet spring” and the ecological consequences of catastrophic impacts. *Ecology Letters*, 3:77–81.
- Cockell, C. S., Catling, D. C., Davis, W. L., Snook, K., Kepner, R. L., Lee, P., and McKay, C. P. (2000). The Ultraviolet Environment of Mars: Biological Implications Past, Present, and Future. *Icarus*, 146:343–359.
- Cockell, C. S. and Raven, J. A. (2004). Zones of photosynthetic potential on Mars and the early Earth. *Icarus*, 169:300–310.
- Code, A. D., Houck, T. E., McNall, J. F., Bless, R. C., and Lillie, C. F. (1970). Ultraviolet Photometry from the Orbiting Astronomical Observatory. I. Instrumentation and Operation. *Astrophysical Journal*, 161:377–388.
- Cole, E. H., Smeins, L. G., Stechman, J. M., Becker, G., and Lorman, G. (1995). Space Telescope Imaging Spectrometer 1K by 1K MAMA detector charge amplifier and discriminator flight electronics performance. In *Proc. SPIE Vol. 2551, Photoelectronic Detectors, Cameras, and Systems*, C. Bruce Johnson; Ervin J. Fenyes; Eds., pages 239–247.
- Coll, P., Coscia, D., Gazeau, M., Guez, L., and Raulin, F. (1998). Review and Latest Results of Laboratory Investigations of Titan’s Aerosols. *Origins of Life and Evolution of the Biosphere*, 28:195–213.
- Combes, M., Vapillon, L., Gendron, E., Coustenis, A., Lai, O., Wittemberg, R., and Sirdey, R. (1997). Spatially Resolved Images of Titan by Means of Adaptive Optics. *Icarus*, 129:482–497.
- Combi, M. R., Brown, M. E., Feldman, P. D., Keller, H. U., Meier, R. R., and Smyth, W. H. (1998). Hubble Space Telescope Ultraviolet Imaging and High-Resolution Spectroscopy of Water Photodissociation Products in Comet Hyakutake (C/1996 B2). *Astrophysical Journal*, 494:816–821.
- Combi, M. R., Reinard, A. A., Bertaux, J.-L., Quemerais, E., and Mäkinen, T. (2000). SOHO/SWAN Observations of the Structure and Evolution of the Hydrogen Lyman- α Coma of Comet Hale-Bopp (1995 O1). *Icarus*, 144:191–202.
- Comeron, F., Torra, J., and Gomez, A. E. (1994). On the characteristics and origin of the expansion of the local system of young objects. *Astronomy and Astrophysics*, 286:789–798.
- Condie, K. C. (2001). *Mantle Plumes and Their Record in Earth History*. Cambridge University Press.
- Conway, R. R. (1981). Spectroscopy of the Cameron bands in the Mars airglow. *Journal of Geophysical Research*, 86:4767–4775.

- Coohill, T. P. (1989). Ultraviolet Action Spectra (280 to 380 nm) and solar effectiveness for higher plants. *Photochem. Photobiology*, 50:451–457.
- Coohill, T. P. (1996). Stratospheric ozone loss, ultraviolet effects and action spectroscopy. *Advances in Space Research*, 18:27–33.
- Cook, J. W., Brueckner, G. E., and Vanhoosier, M. E. (1980). Variability of the solar flux in the far ultraviolet 1175–2100 Å. *Journal of Geophysical Research*, 85:2257–2268.
- Cook, J. W. and Ewing, J. A. (1990). Relationship of magnetic field strength and brightness of fine-structure elements in the solar temperature minimum region. *Astrophysical Journal*, 355:719–725.
- Cornu, A. (1890). Sur la limite ultra-violette du spectre solaire, d'apres des clichés obtenus para M. le Dr. O. Simony au sommet du pic de Téneriffe. *Comptes Rendues*, 111:941–947.
- Coulson, K. L. (1975). *Solar and Terrestrial Radiation*. Academic Press.
- Courtillot, V. (1999). *Evolutionary Catastrophes*. Cambridge University Press.
- Cox, A. N. (2000). *Allen's Astrophysical Quantities*. Springer Verlag.
- Crane, P. C., Floyd, L. E., Cook, J. W., Herring, L. C., Avrett, E. H., and Prinz, D. K. (2004). The center-to-limb behavior of solar active regions at ultraviolet wavelengths. *Astronomy and Astrophysics*, 419:735–746.
- Craven, J. D., Nicholas, A. C., Frank, L. A., Strickland, D. J., and Immel, T. J. (1994). Variations in the FUV dayglow after intense auroral activity. *Geophysical Research Letters*, 21:2793–2796.
- Crisp, D., Meadows, V. S., Bézard, B., de Bergh, C., Maillard, J.-P., and Mills, F. P. (1996). Ground-based near-infrared observations of the Venus nightside: 1.27-μm $O_2(a\Delta_g)$ airglow from the upper atmosphere. *Journal of Geophysical Research*, 101:4577–4594.
- Cronin, J. R. and Pizzarello, S. (1983). Amino acids in meteorites. *Adv. Space Res.*, 3:5–18.
- Crouch, T. D. (1983). *The Eagle Aloft: Two centuries of the balloon in America*. Smithsonian Institution Press.
- Crutzen, P. (1970). The influence of nitrogen oxides on the atmospheric ozone content. *Quarterly Journal of the Royal Meteorological Society*, 96:320–325.
- Crutzen, P. and Bruhl, C. (1996). Mass extinctions and supernova explosions. *Proceedings National Academy of Sciences*, 93:1582–1584.
- Curdt, W., Brekke, P., Feldman, U., Wilhelm, K., Dwivedi, B. N., Schühle, U., and Lemaire, P. (2001). The SUMER spectral atlas of solar-disk features. *Astronomy and Astrophysics*, 375:591–613.

- Dar, A., Laor, A., and Shaviv, N. J. (1998). Life Extinctions by Cosmic Ray Jets. *Physical Review Letters*, 80:5813–5816.
- Dauvillier, A. (1947). *Nature et evolution des planètes*. Hermann, Paris.
- Davis, C. J., Clarke, E. M., Bamford, R. A., Lockwood, M., and Bell, S. A. (2001). Long term changes in EUV and X-ray emissions from the solar corona and chromosphere as measured by the response of the Earth's ionosphere during total solar eclipses from 1932 to 1999. *Annales Geophysicae*, 19:263–273.
- De Fabo, E. C. and Noonan, F. P. (1983). Mechanisms of immune suppression by ultraviolet radiation in vivo. I.- Evidence for the existence of an unique photoreceptor in skin and its role in photoimmunology. *Journal Exp. Medicine*, 158:84–98.
- de Jager, C. (1972). Solar Energy Sources. In *ASSL Vol. 29: The Sun. Part 1 of Solar-Terrestrial Physics/1970*, D. Reidel, pages 1–8.
- de La Fuente Marcos, R. and de La Fuente Marcos, C. (2004). On the recent star formation history of the Milky Way disk. *New Astronomy*, 9:475–502.
- de La Noë, J., Lezeaux, O., Guillemin, G., Lauqué, R., Baron, P., and Ricaud, P. (1998). A ground-based microwave radiometer dedicated to stratospheric ozone monitoring. *Journal of Geophysical Research*, 103:22147–22162.
- De Laubenfels, M. W. (1956). Dinosaur extinction: one more hypothesis. *Journal of Paleontology*, 30:207–.
- De Pontieu, B., Erdélyi, R., and James, S. P. (2004). Solar chromospheric spicules from the leakage of photospheric oscillations and flows. *Nature*, 430:536–539.
- De Vorkin, D. H. (1989). *Race to the Stratosphere: Manned scientific ballooning in America*. Springer Verlag.
- De Vorking, D. H. (1992). *Science with a Vengeance*. Springer Verlag.
- de Vries H. (1958). Variations in concentration of radiocarbon with time and location on earth. *Proc. K. Ned. Akad. Wet.*, B61:94–102.
- Degenstein, D. A., Lloyd, N. D., Bourassa, A. E., Gattinger, R. L., and Llewellyn, E. J. (2005). Observations of mesospheric ozone depletion during the October 28, 2003 solar proton event by OSIRIS. *Geophysical Research Letters*, 32.
- del Toro Iniesta, J. C. (1996). On the discovery of the Zeeman effect on the sun and in the laboratory. *Vistas in Astronomy*, 40:241–256.
- Deland, M. T. and Cebula, R. P. (1998). Solar UV Activity at Solar Cycle 21 and 22 Minimum from NOAA-9 SBUV/2 Data. *Solar Physics*, 177:105–116.
- Deland, M. T. and Cebula, R. P. (2001). Spectral solar UV irradiance data for cycle 21 . *Journal of Geophysical Research*, 106:21569–21584.

- Delprato, A. M., Samadani, A., Kudrolli, A., and Tsimring, L. S. (2001). Swarming Ring Patterns in Bacterial Colonies Exposed to Ultraviolet Radiation. *Physical Review Letters*, 87(15):158102(1–4).
- Dessler, A. E. (2000). *The Chemistry and Physics of Atmospheric Ozone*. Academic Press.
- Detre et al., C. H. (1999). The Permian-Triassic Supernova Impact. *Meteoritics & Planetary Science, Supplement*, 34:124.
- Diffey, B. L. (1991). Solar ultraviolet radiation effects on biological systems. *Physics in Medicine and Biology*, 36:299–328.
- Dillinger, J. H. (1935). A new radio transmission phenomenon. *Physical Review*, 48:705.
- Dobson, G.M.B. (1956). Origin and distribution of the polyatomic molecules in the atmosphere. *Philosophical Transactions Royal Soc. London, A*, 236:187–193.
- Dobson, G.M.B. (1968). Forty years research on atmospheric ozone at Oxford. *Applied Optics*, 7:387–345.
- Dollfus, A. (1964). Observations of Water Vapor on Mars and Venus. In *The Origin and Evolution of Atmospheres and Oceans*, pages 257–+.
- Dollfus, A., Cailleux, A., Cervelle, B., Hua, C. T., and Mandeville, J.-C. (1980). Reflectance spectrophotometry extended to U.V. for terrestrial, lunar and meteoritic samples. *gca*, 44:1293–1310.
- Donnelly, R. F. and Puga, L. C. (1990). Thirteen-day periodicity and the center-to-limb dependence of UV, EUV, and X-ray emission of solar activity. *Solar Physics*, 130:369–390.
- Doschek, G. A. and Feldman, U. (1977). High-resolution spectra of the solar Mg II h and k lines from SKYLAB. *Astrophysical Journal Supplement*, 35:471–482.
- Downes, A. and Blunt, P. (1877). Researches on the effect of light upon bacteria and other organisms. *Proceedings Royal Society*, 26:488–498.
- Dreschhoff, G. and Zeller, E. J. (1998). Ultra-High Resolution Nitrate in Polar Ice as Indicator of Past Solar Activity. *Solar Physics*, 177:365–374.
- Duley, W. W. and Lazarev, S. (2004). Ultraviolet Absorption in Amorphous Carbons: Polycyclic Aromatic Hydrocarbons and the 2175 Å Extinction Feature. *Astrophysical Journal*, 612:L33–L35.
- Durand, E., Oberly, J. J., and Tousey, R. (1949). Analysis of the First Rocket Ultraviolet Solar Spectra. *Astrophysical Journal*, 109:1–16.
- Durney, B. R., Mihalas, D., and Robinson, R. D. (1981). A preliminary interpretation of stellar chromospheric CA II emission variations within the framework of stellar dynamo theory. *Publications Astronomical Society of Pacific*, 93:537–543.

- Durrance, S. T., Barth, C. A., and Stewart, A. I. F. (1980). Pioneer Venus observations of the Venus dayglow spectrum 1250-1430 Å. *Geophysical Research Letters*, 7:222–224.
- Eddy, J. A. (1976). The Maunder Minimum. *Science*, 192:1189–1202.
- Edelsohn, D. J. and Elmegreen, B. G. (1997). Computer models of the Sagittarius dwarf interaction with the Milky Way. *Monthly Notices Royal Astronomical Society*, 290:7–14.
- Edlén, B. (1943). Die Deutung der Emissionslinien im Spektrum der Sonnenkorona. *Zeitschrift für Astrophysics*, 22:30–64.
- Edlén, B. (1945). The identification of the coronal lines. *Monthly Notices Royal Astronomical Society*, 105:323–333.
- Ehrenfreund, P., Irvine, W., Becker, L., Blank, J., Brucato, J. R., Colangeli, L., Derenne, S., Despois, D., Dutrey, A., Fraaije, H., Lazcano, A., Owen, T., Robert, F., and International Space Science Institute Issi-Team (2002). Astrophysical and astrochemical insights into the origin of life. In *ESA SP-518: Exo-Astrobiology*, pages 9–14.
- Einstein, A. (1905). Über einen dir Erzeugung und Verwandlung des Lichtes betreffenden heuristischen Gesichtspunkt. *Annalen der Physik*, 17:132–148.
- Eisenhohr, W. F. (1854). Über die wirkung des violetten und ultravioletten Lichts. *Annalen der Physik 2nd ser.*, 92:623–626.
- Ellis, J. and Schramm, D. N. (1995). Could a nearby supernova have caused a mass extinction. *Proc. National Academy Sciences*, 92:235–238.
- Encrenaz, T., Bézard, B., Greathouse, T. K., Richter, M. J., Lacy, J. H., Atreya, S. K., Wong, A. S., Lebonnois, S., Lefèvre, F., and Forget, F. (2004). Hydrogen peroxide on Mars: evidence for spatial and seasonal variations. *Icarus*, 170:424–429.
- Engelsen, O., Hansen, G. H., and Svenøe, T. (2004). Long-term (1936–2003) ultraviolet and photosynthetically active radiation doses at a north Norwegian location in spring on the basis of total ozone and cloud cover. *Geophysical Research Letters*, 31:12103–12107.
- Ensman, L. and Burrows, A. (1992). Shock breakout in SN 1987A. *Astrophysical Journal*, 393:742–755.
- Ervin, D. H. (1994). The Permo-Triassic extinction. *Nature*, 367:231–236.
- Evans, W. F. J. and Kerr, J. B. (1983). Estimates of the amount of sulphur dioxide injected into the stratosphere by the explosive volcanic eruptions - El Chichón, mystery volcano, Mt. St. Helens. *Geophysical Research Letters*, 10:1049–1051.

- Eviatar, A., Strobel, D. F., Wolven, B. C., Feldman, P. D., McGrath, M. A., and Williams, D. J. (2001). Excitation of the Ganymede Ultraviolet Aurora. *Astrophysical Journal*, 555:1013–1019.
- Ewing, D. (1997). Production of radiation-resistant E. Coli strains by daily X-Irradiation. *International Journal Radiative Biology*, 71:253–258.
- Fagan, B. (2000). *The Little Ice Age*. Basic Books.
- Falconer, P. D. and Holdeman, J. D. (1976). Measurements of atmospheric ozone made from a GASP-equipped 747 airliner Mid-March, 1975. *Geophysical Research Letters*, 3:101–104.
- Farges, T., Le Pichon, A., Blanc, E., Perez, S., and Alcoverro, B. (2003). Response of the lower atmosphere and the ionosphere to the eclipse of August 11, 1999. *Journal of Atmospheric and Terrestrial Physics*, 65:717–726.
- Farman, P. C., Gardiner, B.G., and Shanklin, J. D. (1985). Large losses of total ozone reveal seasonal ClO_x/NO_x interaction. *Nature*, 315:207–210.
- Favata, F. (2002). Large stellar flares: a review of recent novel results. In *ASP Conf. Ser. 277: Stellar Coronae in the Chandra and XMM-Newton Era*, pages 115–126.
- Feldman, P. D. (1977). Ultraviolet spectroscopy of the zodiacal light at 20-deg elongation. *Astronomy and Astrophysics*, 61:635–639.
- Feldman, P. D., A'Hearn, M. F., and Millis, R. L. (1984). Temporal and spatial behavior of the ultraviolet emissions of comet IRAS-Araki-Alcock 1983d. *Astrophysical Journal*, 282:799–802.
- Feldman, P. D., Burgh, E. B., Durrance, S. T., and Davidsen, A. F. (2000a). Far-Ultraviolet Spectroscopy of Venus and Mars at 4 Å Resolution with the Hopkins Ultraviolet Telescope on Astro-2. *Astrophysical Journal*, 538:395–400.
- Feldman, P. D., Davidsen, A. F., Blair, W. P., Bowers, C. W., Dixon, W. V., Durrance, S. T., Ferguson, H. C., Henry, R. C., Kimble, R. A., Kriss, G. A., Kruk, J. W., Long, K. S., Moos, H. W., Vancura, O., and Gull, T. R. (1991). Observations of Comet Levy (1990c) with the Hopkins Ultraviolet Telescope. *Astrophysical Journal*, 379:L37–L40.
- Feldman, P. D., Festou, M. C., Ahearn, M. F., Arpigny, C., Butterworth, P. S., Cosmovici, C. B., Danks, A. C., Gilmozzi, R., Jackson, W. M., McFadden, L. A., Patriarchi, P., Schleicher, D. G., Tozzi, G. P., Wallis, M. K., Weaver, H. A., and Woods, T. N. (1987). IUE Observations of Comet p/ Halley - Evolution of the Ultraviolet Spectrum Between 1985SEP and 1986JUL. *Astronomy and Astrophysics*, 187:325–328.
- Feldman, P. D., McGrath, M. A., Moos, H. W., Durrance, S. T., Strobel, D. F., and Davidsen, A. F. (1993). The spectrum of the Jovian dayglow observed at 3 Å resolution with the Hopkins ultraviolet telescope. *Astrophysical Journal*, 406:279–284.

- Feldman, P. D., McGrath, M. A., Strobel, D. F., Moos, H. W., Retherford, K. D., and Wolven, B. C. (2000b). HST/STIS Ultraviolet Imaging of Polar Aurora on Ganymede. *Astrophysical Journal*, 535:1085–1090.
- Feldman, P. D., Sahnow, D. J., Kruk, J. W., Murphy, E. M., and Moos, H. W. (2001). High-resolution FUV spectroscopy of the terrestrial day airglow with the Far Ultraviolet Spectroscopic Explorer. *Journal of Geophysical Research*, 106:8119–8130.
- Feldman, P. D., Takacs, P. Z., Fastie, W. G., and Donn, B. (1974). Rocket Ultraviolet Spectrophotometry of Comet Kohoutek (1973f). *Science*, 185:705–707.
- Feldman, P. D., Weaver, H. A., and Burgh, E. B. (2002). Far Ultraviolet Spectroscopic Explorer Observations of CO and H₂ Emission in Comet C/2001 A2 (LINEAR). *Astrophysical Journal*, 576:L91–L94.
- Feldman, P. D., Weaver, H. A., Festou, M., A'Hearn, M. F., Jackson, W. M., Donn, B., Rahe, J., Smith, A. M., and Benvenuti, P. (1980). IUE observations of the UV spectrum of Comet Bradfield. *Nature*, 286:132–135.
- Felling, W. E. and Witunski, M. (1960). Polarization Measurements from the 2 October 1959 Eclipse. *Astronomical Journal*, 65:488–489.
- Ferlet, R. (1999). The Local Interstellar Medium. *The Astronomy and Astrophysics Review*, 9:153–169.
- Fesen, R. A. (1983). Discovery of large radial velocities in the supernova remnant 3C 58. *Astrophysical Journal*, 270:L53–L57.
- Festou, M. C., Atreya, S. K., Donahue, T. M., Sandel, B. R., Shemansky, D. E., and Broadfoot, A. L. (1981). Composition and thermal profiles of the Jovian upper atmosphere determined by the Voyager ultraviolet stellar occultation experiment. *Journal of Geophysical Research*, 86:5715–5725.
- Fields, B. D. (2004). Live radioisotopes as signatures of nearby supernovae. *New Astronomy Review*, 48:119–123.
- Fields, B. D. and Ellis, J. (1999). On deep-ocean ⁶⁰Fe as a fossil of a near-earth supernova. *New Astronomy*, 4:419–430.
- Finlayson-Pitts, B. J. and Pitts, J. N. (2000). *Chemistry of the upper and lower atmosphere*. Academic Press.
- Firsoff, V. A. (1978). Ultraviolet radiation as a threat to life on Mars. *The Observatory*, 98:138–140.
- Fjeldbo, G., Fjeldbo, W. C., and Eshleman, V. R. (1966). Models for the Atmosphere of Mars Based on the Mariner 4 Occultation Experiment. *Journal of Geophysical Research*, 71:2307.

- Fleming, E. L., Chandra, S., Jackman, C. H., Considine, D. B., and Douglass, A. R. (1995). The middle atmospheric response to short and long term solar UV variations: analysis of observations and 2D model results. *Journal of Atmospheric and Terrestrial Physics*, 57:333–365.
- Fligge, M. and Solanki, S. K. (2000). The solar spectral irradiance since 1700. *Geophysical Research Letters*, 27:2157–2160.
- Fligge, M., Solanki, S. K., and Unruh, Y. C. (2000). Modelling irradiance variations from the surface distribution of the solar magnetic field. *Astronomy and Astrophysics*, 353:380–388.
- Florinski, V., Zank, G. P., and Axford, W. I. (2003). The Solar System in a dense interstellar cloud: Implications for cosmic-ray fluxes at Earth and ^{10}Be records. *Geophysical Research Letters*, 30:5–1.
- Floyd, L. and et al. (1997). Correlations of Solar Cycle 22 UV Irradiance. In *ESA SP-415: Correlated Phenomena at the Sun, in the Heliosphere and in Geospace*, pages 235–242.
- Floyd, L., Tobiska, W. K., and Cebula, R. P. (2002). Solar UV irradiance, its variation, and its relevance to the earth. *Advances in Space Research*, 29:1427–1440.
- Floyd, L. E., Cook, J. W., Herring, L. C., and Crane, P. C. (2003). SUSIM'S 11-year observational record of the solar UV irradiance. *Advances in Space Research*, 31:2111–2120.
- Formisano, V., Atreya, S., Encrenaz, T., Ignatiev, N., and Giuranna, M. (2004). Detection of Methane in the Atmosphere of Mars. *Science*, 306:1758–1761.
- Foukal, P. (1993). The Curious Case of the Greenwich Faculae. *Solar Physics*, 148:219–232.
- Foukal, P. (1996). The behavior of solar magnetic plages measured from Mt. Wilson observations between 1915–1984. *Geophysical Research Letters*, 23:2169–2172.
- Foukal, P. (2002). A comparison of variable solar total and ultraviolet irradiance outputs in the 20th century. *Geophysical Research Letters*, 29:4–1.
- Foukal, P., Fowler, L. A., and Livshits, M. (1983). A thermal model of sunspot influence on solar luminosity. *Astrophysical Journal*, 267:863–871.
- Foukal, P. and Milano, L. (2001). A measurement of the quiet network contribution to solar irradiance variation. *Geophysical Research Letters*, 28:883–886.
- Fowler, A. and Strutt, R. J. (1917). Absorption bands of atmospheric ozone in the spectra of Sun and Stars. *Proceedings Royal Society, A*, 93:577–586.
- Fröhlich, C. and Lean, J. (1998). The Sun's total irradiance: Cycles, trends and related climate change uncertainties since 1976. *Geophysical Research Letters*, 25:4377–4380.

- Franck, S., Block, A., Von Bloh, W., Bounama, C., Garrido, L., and Schellnhuber, H. J. (2001). Planetary Habitability: is Earth commonplace in the Milky Way? *Naturwissenschaften*, 88:416–426.
- Frey, A., Hofmann, W., and Lemke, D. (1977). Spectrum of the zodiacal light in the middle UV. *Astronomy and Astrophysics*, 54:853–855.
- Frisch, P. C. (1996). LISM Structure - Fragmented Superbubble Shell? *Space Science Reviews*, 78:213–222.
- Frisch, P. C. (2000). The Galactic Environment of the Sun. *American Scientist*, 88:52–59.
- Fusco, A. C. and Salby, M.L. (1999). Interannual variations of total ozone and their relationship to variations of planetary wave activity. *Journal of Climate*, 12:1619–1629.
- Génova, R. and Beckman, J. E. (2003). Kinematical Structure of the Local Interstellar Medium: The Galactic Anticenter Hemisphere. *Astrophysical Journal Supplement Series*, 145:355–412.
- Güdel, M., Audard, M., Kashyap, V. L., Drake, J. J., and Guinan, E. F. (2003). Are Coronae of Magnetically Active Stars Heated by Flares? II. Extreme Ultraviolet and X-Ray Flare Statistics and the Differential Emission Measure Distribution. *Astrophysical Journal*, 582:423–442.
- Galsgaard, K. and Nordlund, Å. (1996). Heating and activity of the solar corona 1. Boundary shearing of an initially homogeneous magnetic field. *Journal of Geophysical Research*, 101:13445–13460.
- García-Pichel, F. (1998). Solar ultraviolet and the evolutionary history of cyanobacteria. *Origins of Life and Evolution of the Biosphere*, 28:321–347.
- Garcia, R. R. and Solomon, S. (1994). A new numerical model of the middle atmosphere. 2. Ozone and related species. *Journal of Geophysical Research*, 99:12937–12952.
- García-Sánchez, J., Weissman, P. R., Preston, R. A., Jones, D. L., Lestrade, J.-F., Latham, D. W., Stefanik, R. P., and Paredes, J. M. (2001). Stellar encounters with the solar system. *Astronomy and Astrophysics*, 379:634–659.
- Garrison, W. M., Morrison, D. C., Hamilton, J. S., Benson, A. A., and Calvin, M. (1951). Reduction of carbon dioxide in aqueous solutions by ionizing radiation. *Science*, 114:416–418.
- Garssen, J. and Van Loveren, H. (2001). Effects of ultraviolet exposure on the immune system. *Crit. Rev. Immunology*, 21:359–397.
- Garzón, L. and Garzón, M. L. (2001). Radioactivity as a significant energy source in prebiotic synthesis. *Origins of Life and Evolution of the Biosphere*, 31:3–13.

- Gates, F. L. (1928). On nuclear derivatives and the lethal action of ultraviolet light. *Science*, 68:478–480.
- Gaustad, J. E. and Vogel, S. N. (1982). High-Energy Solar Radiation and the Origin of Life. *Origins of Life and Evolution of the Biosphere*, 12:3–8.
- Gehrels, N., Laird, C. M., Jackman, C. H., Cannizzo, J. K., Mattson, B. J., and Chen, W. (2003). Ozone Depletion from Nearby Supernovae. *Astrophysical Journal*, 585:1169–1176.
- Gehrels, T., Matthews, M. S., and Schumann, A. M., editors (1994). *Hazards due to comets and asteroids*.
- Geller, M. A. (1981). Middle atmosphere dynamics and composition. In *Exploration of the polar upper atmosphere; Proceedings of the Advanced Study Institute, Lillehammer, Norway*. Dordrecht, D. Reidel Publishing Co., pages 1–16.
- Gendron, E., Coustenis, A., Drossart, P., Combes, M., Hirtzig, M., Lacombe, F., Rouan, D., Collin, C., Pau, S., Lagrange, A.-M., Mouillet, D., Rabou, P., Fusco, T., and Zins, G. (2004). VLT/NACO adaptive optics imaging of Titan. *Astronomy and Astrophysics*, 417:L21–L24.
- Genzel, R., Lutz, D., and Tacconi, L. (1998). Star formation triggered by galaxy collisions. *Nature*, 395:859–862.
- Gershberg, R. E., Katsova, M. M., Lovkaya, M. N., Terebizh, A. V., and Shakhovskaya, N. I. (1999). Catalogue and bibliography of the UV Cet-type flare stars and related objects in the solar vicinity. *Astronomy and Astrophysics Supplement Series*, 139:555–558.
- Ghostl, S. N. (2002). *The Neutral Upper Atmosphere*. Kluwer Academic Publishers.
- Gil, M., Puentedura, O., Yela, M., and Cuevas, E. (2000). Behavior of NO₂ and O₃ columns during the eclipse of February 26, 1998, as measured by visible spectroscopy. *Journal of Geophysical Research*, 105:3583–3594.
- Giles, G., Marks, R., and Foley, P. (1988). Incidence of non-melanocytic skin cancer treated in Australia. *Br. Medical Journal*, 296:13–16.
- Gillet, N.P. and Thompson, D. W. (2003). Simulation of recent Southern Hemisphere Climate Change. *Science*, 302:273–275.
- Gilmore, G., Wyse, R. F. G., and Norris, J. E. (2002). Deciphering the Last Major Invasion of the Milky Way. *Astrophysical Journal*, 574:L39–L42.
- Giménez, A. and Sabau-Graziati, L. (1996). The Spanish MINISAT-01 mission. *Memorie della Societa Astronomica Italiana*, 67:563–568.
- Gladstone, G. R., Hall, D. T., and Waite, J. H. J. (1995). EUVE Observations of Jupiter During the Impact of Comet Shoemaker-Levy 9. *Science*, 268:1595–1597.
- Glaisher, J. (1871). *Travels in the Air*. Richard Bentley and Son, London.

- Gleason, D. F. and Wellington, G. M. (1993). Ultraviolet radiation and coral bleaching. *Nature*, 365:836–838.
- Godin, S., Bergeret, V., Bekki, S., David, C., and Mégie, G. (2001). Study of the interannual ozone loss and the permeability of the Antarctic polar vortex from aerosol and ozone lidar measurements in Dumont d'Urville (66.4 °S, 140 °E). *Journal of Geophysical Research*, 106:1311–1330.
- Goldberg, L. (1967). Ultraviolet and X Rays from the Sun. *Annual Review of Astronomy and Astrophysics*, 5:279–323.
- Goldberg, L. (1974). Research with Solar Satellites. *Astrophysical Journal*, 191:1–38.
- Goldblatt, H. and Soames, K. N. (1923). A study of rats on a normal diet irradiated daily by the mercury vapor quartz lamp or kept in darkness. *Biochemical Journal*, 17:294–297.
- Gonzalez, G., Brownlee, D., and Ward, P. (2001). The Galactic Habitable Zone: Galactic Chemical Evolution. *Icarus*, 152:185–200.
- Gopalswamy, N. (2003). Coronal mass ejections: Initiation and detection. *Advances in Space Research*, 31:869–881.
- Gotrian, W. (1939). Zur Deutung der Linien in Spektrum der Sonnenkorona. *Naturwissenschaften*, 27:214–214.
- Gough, D. O. (1981). Solar interior structure and luminosity variations. *Solar Physics*, 74:21–34.
- Graham, J. B., Dudley, R., Aguilar, N. M., and Gaub, C. (1995). Implications of the late Paleozoic oxygen pulse for physiology and evolution. *Nature*, 375:117–120.
- Grant, R. H., Heisler, G. M., and Gao, W. (1997). Clear sky radiance distributions in ultraviolet wavelength bands. *Journal of Theoretical and Applied Climatology*, 56:123–135.
- Grant, W. B., Browell, E. V., Fishman, J., Brackett, V. G., Veiga, R. E., Nganga, D., Minga, A., Cros, B., Butler, C. F., Fenn, M. A., Long, C. S., and Stowe, L. L. (1994). Aerosol-associated changes in tropical stratospheric ozone following the eruption of Mount Pinatubo. *Journal of Geophysical Research*, 99:8197–8212.
- Green, A.E., Sawada, T., and Shettle, E. P. (1974). The middle ultraviolet reaching the ground. *Photochem. Photobiology*, 19:251–259.
- Greenpeace (1997). *Report to the 9th Meeting of the Parties to the Montreal Protocol*. Greenpeace.
- Greer, R. G. H., Murtagh, D. P., McDade, I. C., Dickinson, P. H. G., and Thomas, L. (1986). ETON 1 - A data base pertinent to the study of energy transfer in the oxygen nightglow. *Planetary and Space Sciences*, 34:771–788.

- Gregg, J. W., Jones, C. G., and Dawson, T. E. (2003). Urbanization effects on tree growth in the vicinity of New York city. *Nature*, 424:183–187.
- Grenier, I. A. (2000). Gamma-ray sources as relics of recent supernovae in the nearby Gould Belt. *Astronomy and Astrophysics*, 364:L93–L96.
- Grotian, W. (1939). Zur Frage der Deutung der linien im Spektrum der Sonnenkorona. *Naturwissenschaften*, 22:20.
- Grunberg-Manago, M., Ortiz, P. J., and Ochoa, S. (1955). Enzymatic synthesis of nucleic acidlike polynucleotides. *Science*, 122:907–910.
- Gudiksen, B. V. and Nordlund, Å. (2002). Bulk Heating and Slender Magnetic Loops in the Solar Corona. *Astrophysical Journal*, 572:L113–L116.
- Guinan, E. F. and Ribas, I. (2002). Our Changing Sun: The Role of Solar Nuclear Evolution and Magnetic Activity on Earth's Atmosphere and Climate. In *ASP Conf. Ser. 269: The Evolving Sun and its Influence on Planetary Environments*, pages 85–106.
- Guinan, E. F., Ribas, I., and Harper, G. M. (2003). Far-Ultraviolet Emissions of the Sun in Time: Probing Solar Magnetic Activity and Effects on Evolution of Paleoplanetary Atmospheres. *Astrophysical Journal*, 594:561–572.
- Gulick, V. C., Tyler, D., McKay, C. P., and Haberle, R. M. (1997). Episodic Ocean-Induced CO₂ Greenhouse on Mars: Implications for Fluvial Valley Formation. *Icarus*, 130:68–86.
- Gurnett, D. A., Kurth, W. S., Hospodarsky, G. B., Persoon, A. M., Zarka, P., Lecacheux, A., Bolton, S. J., Desch, M. D., Farrell, W. M., Kaiser, M. L., Ladreiter, H.-P., Rucker, H. O., Galopeau, P., Louarn, P., Young, D. T., Pryor, W. R., and Dougherty, M. K. (2002). Control of Jupiter's radio emission and aurorae by the solar wind. *Nature*, 415:985–987.
- Guy, C., Diab, R., and Martincigh, B. (2003). Ultraviolet radiation exposure of children and adolescents in Durban, South Africa. *Photochemistry and Photobiology*, 77:265–270.
- Haagen-Smit, A. J. and Fox, M. M. (1954). Photochemical Ozone formation with hydrocarbons and automobile exhaust. *J. Air Pollut. Control Assoc.*, 4:105–108.
- Haigh, J. (1996). The impact of solar variability on climate. *Science*, 272:981–984.
- Haigh, J. D. (1999). Modelling the impact of solar variability on climate. *Journal of Atmospheric and Solar-Terrestrial Physics*, 61:63–72.
- Haldane, J.B. (1954). The origins of life. *New Biology*, 16:21–26.
- Hale, G. E. (1908). On the probable existence of a magnetic field in sunspots. *Astrophysical Journal*, 28:315–343.

- Hall, D. T., Feldman, P. D., McGrath, M. A., and Strobel, D. F. (1998). The Far-Ultraviolet Oxygen Airglow of Europa and Ganymede. *Astrophysical Journal*, 499:475–481.
- Hall, D. T., Strobel, D. F., Feldman, P. D., McGrath, M. A., and Weaver, H. A. (1995). Detection of an Oxygen Atmosphere on Jupiter’s Moon Europa. *Nature*, 373:677–681.
- Hall, J. C. and Lockwood, G. W. (2000). Evidence of a Pronounced Activity Cycle in the Solar Twin 18 Scorpii. *Astrophysical Journal*, 545:L43–L45.
- Hallan, A. and Wignall, P. B. (1997). *Mass extinctions and their aftermath*. Oxford University Press.
- Hamill, P., Toon, O. B., and Turco, R. P. (1986). Characteristics of polar stratospheric clouds during the formation of the Antarctic ozone hole. *Geophysical Research Letters*, 13:1288–1291.
- Hanser, F. A., Sellers, B., and Hunerwadel, J. L. (1978). Measurement of 200-400 NM solar UV fluxes on the STRATCOM 8A balloon flight. In *STRATCOM 8 Data Workshop and Suppl.*, pages 56–62.
- Hanslmeier, A. (2002). *The Sun and Space Weather*. Kluwer Academic Publishers.
- Hargreaves, J. K. (1979). *The upper atmosphere and Solar-terrestrial relations*. Van Nostrand Reinhold.
- Harm, W. (1980). *Biological effects of Ultraviolet radiation*. Cambridge University Press.
- Harris, N., Hudson, R., and Philips, C. (Eds.) (1998). *Assessment of Trends in the Vertical Distribution of Ozone*. SPARC Report No.1. WMO Ozone Research and Monitoring Project Report No. 43.
- Harrison, R. A. (2003). Soho observations relating to the association between flares and coronal mass ejections. *Advances in Space Research*, 32:2425–2437.
- Harrison, R. A. (2005). *EUV and UV Imaging and Spectroscopy from Space*, pages 131–193. XV IAC Winter School, “Payload and mission definition in Space Sciences”, Cambridge University Press.
- Harrison, R. A., Bryans, P., Simnett, G. M., and Lyons, M. (2003a). Coronal dimming and the coronal mass ejection onset. *Astronomy and Astrophysics*, 400:1071–1083.
- Harrison, R. A., Harra, L. K., Brković, A., and Parnell, C. E. (2003b). A study of the unification of quiet-Sun transient-event phenomena. *Astronomy and Astrophysics*, 409:755–764.
- Harrison, R. A., Lang, J., Brooks, D. H., and Innes, D. E. (1999). A study of extreme ultraviolet blinker activity. *Astronomy and Astrophysics*, 351:1115–1132.

- Hartley, D. E., Villarin, J., Black, R. X., and Davis, C. A. (1998). A new perspective on the dynamical link between the stratosphere and troposphere. *Nature*, 391:471–474.
- Hartley, W.N. (1880). On the absorption spectrum of ozone. *Chemical News*, 42:268.
- Harvey, J. (1999). Hale's Discovery of Sunspot Magnetic Fields. *Astrophysical Journal*, 525:35–60.
- Harvey, K. L. and White, O. R. (1999). Magnetic and Radiative Variability of Solar Surface Structures. I. Image Decomposition and Magnetic-Intensity Mapping. *Astrophysical Journal*, 515:812–831.
- Harwitt, M. (1973). *Astrophysical Concepts*. John Wiley Sons.
- Heagle, A.S. (1989). Ozone and crop yield. *Annual Review of Phytopathology*, 27:397–423.
- Heath, D. F., Krueger, A. J., and Crutzen, P. J. (1977). Solar proton event - Influence on stratospheric ozone. *Science*, 197:886–889.
- Heath, D. F. and Schlesinger, B. M. (1986). The Mg 280-nm doublet as a monitor of changes in solar ultraviolet irradiance. *Journal of Geophysical Research*, 91:8672–8682.
- Heath, M. J., Doyle, L. R., Joshi, M. M., and Haberle, R. M. (1999). Habitability of planets around red dwarf stars. *Origins of Life and Evolution of the Biosphere*, 29:405–424.
- Hedges, S. B., Blair, J. M., Venturi, M., and Shoe, J. L. (2004). A molecular timescale of eukaryote evolution and the rise of complex multicellular life. *BMC Evolutionary Biology*, 4.
- Hendrix, A. R., Domingue, D. L., and King, K. (2005). The icy Galilean satellites: ultraviolet phase curve analysis. *Icarus*, 173:29–49.
- Henry, R. C. (1991). Ultraviolet background radiation. *Annual Review of Astronomy and Astrophysics*, 29:89–127.
- Hentschel, K. (2002). *Mapping the Spectrum*. Oxford University Press.
- Heppner, J. P. and Meredith, L. H. (1958). Nightglow Emission Altitude From Rocket Measurements. *Journal of Geophysical Research*, 63:51–65.
- Herbert, F. and Sandel, B. R. (1999). Ultraviolet observations of Uranus and Neptune. *Planetary and Space Sciences*, 47:1119–1139.
- Hermite, G. (1893). L'exploration de la haute atmosphère. Expérience du 21 mars 1893. *Comptes Rendus acad. Sci. Paris*, 126:766–768.

- Herschel, W. (1800). Experimente on the refrangibility of the invisible rays of the Sun. *Philosophical Transactions Royal Society*, 90:284–292.
- Hershey, A. D. and Chasse, M. (1952). Independent functions of viral protein and nucleic acid in growth of baceriphage. *Journal of general Physiology*, 36:39–56.
- Herzberg, G. (1950). *Molecular spectra and Molecular structure*. Van Nostrand.
- Hess, A. (1922). Influence of light on the prevention of rickets. *Lancet*, 2:1222.
- Hess, V. F. (1912). Über Beobachtungen der durchdringenden Strahlung bei sieben Freiballonfahrten. *Physik Zeitschrift*, 13:1084–1091.
- Hey, J. S. (1946). Solar radiation in the 4-6 metre radio wave-length band. *Nature*, 157:47–48.
- Hillebrandt, A. R., Pemfield, G.T., Kring, D. A., Pilkington, M., Camargo, A., Jacobsen, S. B., and Boynton, W. V. (1991). Chicxulub crater: a possible Cretaceous/Tertiary boundary impact crater on the Yucatan peninsula, Mexico. *Geology*, 19:867–871.
- Hillebrandt, W. and Niemeyer, J. C. (2000). Type IA Supernova Explosion Models. *Annual Review Astronomy and Astrophysics*, 38:191–230.
- Hills, J. G. (1971). The Nature of the Far Ultraviolet Excess in the Nucleus of M 31. *Astronomy and Astrophysics*, 12:1–4.
- Hinson, D. P., Kliore, A. J., Flasar, F. M., Twicken, J. D., Schinder, P. J., and Herrera, R. G. (1998). Galileo radio occultation measurements of Io's ionosphere and plasma wake. *Journal of Geophysical Research*, 103:29343–29358.
- Hinteregger, H. E. (1977). EUV flux variation during end of solar cycle 20 and beginning cycle 21, observed from AE-C satellite. *Geophysical Research Letters*, 4:231–234.
- Hinteregger, H. E., Fukui, K., and Gilson, B. R. (1981). Observational, reference and model data on solar EUV, from measurements on AE-E. *Geophysical Research Letters*, 8:1147–1150.
- Hinteregger, H. E. and Hall, L. A. (1969). Solar Extreme Ultraviolet Emissions in the Range 260-1300 Å observed from OSO-III. *Solar Physics*, 6:175–182.
- Hjorth et al., J. (2003). A very energetic supernova associated with the γ -ray burst of 29 March 2003. *Nature*, 423:847–850.
- Ho, C. M., Strangeway, R. J., Russell, C. T., Luhmann, J. G., and Brace, L. H. (1993). The nightside ionosphere of Venus under varying levels of solar EUV flux. *Geophysical Research Letters*, 20:2727–2730.
- Hockberger, P. E. (2002). A history of Ultraviolet Photobiology for Humans, Animals and Microorganisms. *Photochemistry and Photobiology*, 76:561–569.

- Hoegh-Guldberg, O. (1999). Climate change, coral bleaching and the future of the world's coral reefs. *Marine and Freshwater Research*, 50:839–866.
- Hofmann, D. J., Harder, J. W., Rolf, S. R., and Rosen, J. M. (1986). Balloon-borne observations of the development and vertical structure of the Antarctic ozone hole in 1986. *Nature*, 326:59–62.
- Hojaev et al., A. S. (2003). EUV and X-Ray Bright Features in the Sun. In *IAU Symposium no. 219 "Stars as Suns: Activity, Evolution and Planets"*.
- Holick, M. F., Matsuoka, J., and Worstman, J. (1989). Age, vitamin D and solar ultraviolet. *Lancet*, 1:1104–1105.
- Holman, C. D.J., Armstrong, B. K., and Heenan, P. J. (1986). The cause of malignant melanoma: results from the West Australian Lions melanoma research project. *Recent Results Cancer Research*, 102:18–37.
- Hood, L. L. and McCormack, J. P. (1992). Components of interannual ozone change based on Nimbus 7 TOMS data. *Geophysical Research Letters*, 19:2309–2312.
- Hord, C. W., Barth, C. A., Esposito, L. W., McClintock, W. E., Pryor, W. R., Simmons, K. E., Stewart, A. I. F., Thomas, G. E., Ajello, J. M., and Lane, A. L. (1991). Galileo ultraviolet spectrometer experiment - Initial Venus and interplanetary cruise results. *Science*, 253:1548–1550.
- Hord, C. W., Pryor, W. R., Stewart, A. I. F., Simmons, K. E., Gebben, J. J., Barth, C. A., McClintock, W. E., Esposito, L. W., Tobiska, W. K., West, R. A., Edberg, S. J., Ajello, J. M., and Naviaux, K. L. (1995). Direct observations of the Comet Shoemaker-Levy 9 fragment G impact by Galileo UVS. *Geophysical Research Letters*, 22:1565–1568.
- Horneck et al., G. (2001). Protection of Bacterial Spores in Space, a Contribution to the Discussion on Panspermia. *Origins of Life and Evolution of the Biosphere*, 31:527–547.
- Horvath, J. E. (2003). On gamma-ray bursts and their biological effects :a case for an extrinsic trigger of the Cambrian explosion ? *ArXiv Astrophysics e-prints*.
- Houghton, H. G. (1985). *Physical Meteorology*. The MIT Press.
- Houghton, J. (1997). *Global Warming, 2nd edition*. Cambridge University Press.
- Houghton, J. (2002). *The Physics of Atmospheres, 3rd edition*. Cambridge University Press.
- Houghton, J. T., Ding, Y., Griggs, D. J., Noguer, M., Van der Linden, P. J., Dai, X., Maskell, K., and Johnson, C.A. (eds) (2002). *Climate Change 2001: The Scientific Basis*. Cambridge University Press.
- Hoyle, F. (1983). *The intelligent Universe*. Michael Joseph Limited, London.

- Hoyle, F. and Wickramasinghe, C. (1978a). Comets, ice ages, and ecological catastrophes. *Astrophysics and Space Science*, 53:523–526.
- Hoyle, F. and Wickramasinghe, C. (1979). Biochemical Chromophores and the Interstellar Extinction at Ultraviolet Wavelengths. *Astrophysics and Space Sciences*, 65:241–244.
- Hoyle, F. and Wickramasinghe, N. C. (1978b). *Lifecloud: The origin of Life in the Universe*. Harper and Row.
- Hoyle, F. and Wickramasinghe, N. C. (1986). On the nature of the particles causing the 2200 Å peak in the extinction of starlight. *Astrophysics and Space Sciences*, 122:181–184.
- Hoyle, F. and Wickramasinghe, N. C. (1999). Biological Evolution. *Astrophysics and Space Science*, 268:55–75.
- Hoyt, D. V. (1979a). Atmospheric transmission from the Smithsonian Astrophysical Observatory pyrheliometric measurements from 1923 to 1957. *Journal of Geophysical Research*, 84:5018–5028.
- Hoyt, D. V. (1979b). The Smithsonian Astrophysical Observatory Solar Constant Program. *Reviews of Geophysics and Space Physics*, 17:427–458.
- Hoyt, D. V. and Schatten, K. (1998). *The Role of the Sun in Climate Change*. Oxford University Press.
- Hoyt, D. V. and Schatten, K. H. (1993). A discussion of plausible solar irradiance variations, 1700–1992. *Journal of Geophysical Research*, 98:18895–18906.
- Hoyt, D. V., Schatten, K. H., and Nesmes-Ribes, E. (1994). The one hundredth year of Rudolf Wolf's death: Do we have the correct reconstruction of solar activity? *Geophysical Research Letters*, 21:2067–2070.
- Hudson, H. S., Silva, S., Woodard, M., and Willson, R. C. (1982). The effects of sunspots on solar irradiance. *Solar Physics*, 76:211–219.
- Hufbauer, K. (1991). *Exploring the Sun: Solar Science since Galileo*. Johns Hopkins University Press.
- Hufbauer, K. (1993). *Exploring the Sun*. The Johns Hopkins University Press.
- Huggins, W. (1889). On the Limit of Solar and Stellar Light in the Ultra-Violet Part of the Spectrum. *Royal Society of London Proceedings Series I*, 46:133–135.
- Hulbert, E. O. (1928). Ionization in the Upper Atmosphere of the Earth. *Physical Review*, 31:1018–1037.
- Hunhausen, A. J. (1996). A summary of SMM observations from 1980 and 1984–1989. In *The Many Faces of the Sun*. Springer Verlag.

- Hunsucker, R. D. and Hargreaves, J. K. (2002). *The High-latitude ionosphere and its Effects on Radio Propagation*. Cambridge University Press.
- Hunten, D. (1979). Possible oxidant sources in the atmosphere and surface of Mars. *Journal of Molecular Evolution*, 14:57.
- Hyde, J. N. (1906). On the influence of light in the production of cancer of the skin. *American Journal Med. Sci.*, 131:1–22.
- Ibata, R. A., Gilmore, G., and Irwin, M. J. (1994). A Dwarf Satellite Galaxy in Sagittarius. *Nature*, 370:194–196.
- Ichihashi et al., M. (2003). UV-induced skin damage. *Toxicology*, 189:21–39.
- Iglesias-Groth, S. (2004). Fullerenes and Buckyonions in the Interstellar Medium. *Astrophysical Journal*, 608:L37–L40.
- Iqbal, M. (1983). *An introduction to Solar Radiation*. Academic Press.
- Iyudin, A. F. (2002). Terrestrial impact of the galactic historical SNe. *Journal of Atmospheric and Terrestrial Physics*, 64:669–676.
- Jackman, C. H., McPeters, R. D., Labow, G. J., Fleming, E. L., Praderas, C. J., and Russell, J. M. (2001). Northern Hemisphere atmospheric effects due to the July 2000 solar proton event. *Geophysical Research Letters*, 28:2883–2886.
- Jacob, D. J. (1999). *Introduction to Atmospheric Chemistry*. Princeton University Press.
- Jakosky, B. M. and Lindner, B. L. (1984). Mars Atmospheric Photochemistry, Surface Reactions, and Climate Change. In *Lunar and Planetary Institute Conference Abstracts*, pages 399–400.
- Jamar, C., Macau-Hercot, D., Monfils, A., Thompson, G. I., Houziaux, L., and Wilson, R. (1976). *Ultraviolet Bright Star Spectrophotometric Catalogue*. ESA Special Report No. 27.
- Jansky, K. (1932). Directional studies of atmospherics at high frequencies. *Proceedings of the Institute of Radio Engineers*, 20:1920.
- Johannesson, A., Marquette, W. H., and Zirin, H. (1998). A 10-Year Set of CA II K-Line Filtergrams. *Solar Physics*, 177:265–278.
- Johnson, F. S., Malitson, H. H., Purcell, J. D., and Tousey, R. (1955). Emission lines in the solar ultraviolet spectrum. *Astronomical Journal*, 60:165–166.
- Johnson, F. S., Purcell, J. D., Tousey, R., and Watanabe, K. (1952). Direct Measurements of the Vertical Distribution of Atmospheric Ozone to 70 Kilometers Altitude. *Journal of Geophysical Research*, 57:157.
- Johnston, H. (1992). Atmospheric Ozone. *Annual Review of Physical Chemistry*, 43:1–31.

- Joshi, M. M., Haberle, R. M., and Reynolds, R. T. (1997). Simulations of the Atmospheres of Synchronously Rotating Terrestrial Planets Orbiting M Dwarfs: Conditions for Atmospheric Collapse and the Implications for Habitability. *Icarus*, 129:450–465.
- Kaneda, E., Ashihara, O., Shimizu, M., Takagi, M., and Hirao, K. (1986). Observation of comet Halley by the ultraviolet imager of Suisei. *Nature*, 321:297–299.
- Kano, R. and Tsuneta, S. (1995). Scaling Law of Solar Coronal Loops Obtained with YOHKOH. *Astrophysical Journal*, 454:934–944.
- Kasting, J. F. (1988). Runaway and moist greenhouse atmospheres and the evolution of earth and Venus. *Icarus*, 74:472–494.
- Kasting, J. F. (1991). CO₂ condensation and the climate of early Mars. *Icarus*, 94:1–13.
- Kasting, J. F. (1993). Earth's early atmosphere. *Science*, 259:920–926.
- Kasting, J. F. and Catling, D. (2003). Evolution of a Habitable Planet. *Annual Review of Astronomy and Astrophysics*, 41:429–463.
- Kasting, J. F. and Siefert, J. L. (2002). Life and the Evolution of Earth's Atmosphere. *Science*, 296:1066–1068.
- Kasting, J. F., Whitmire, D. P., and Raynolds, D. T. (1993). Habitable zones around main sequence stars. *Icarus*, 101:108–128.
- Kasting, J. F., Whittet, D.C.B., and Sheldon, W. R. (1997). Ultraviolet radiation from F and K stars and implications for planet habitability. *Origins of Life and Evolution of the Biosphere*, 27:413–420.
- Katsukawa, Y. and Tsuneta, S. (2001). Small Fluctuation of Coronal X-Ray Intensity and a Signature of Nanoflares. *Astrophysical Journal*, 557:343–350.
- Kaye, J. A. and Strobel, D. F. (1984). Phosphine photochemistry in the atmosphere of Saturn. *Icarus*, 59:314–335.
- Keil, S. L. and Worden, S. P. (1984). Variations in the solar calcium K line 1976–1982. *Astrophysical Journal*, 276:766–781.
- Kelley, M. C. (1989). *The Earth's Ionosphere: Plasma Physics and Electrodynamics*. Academic Press.
- Kerridge, J. F. (1993). Long-term compositional variation in solar corpuscular radiation: Evidence from nitrogen isotopes in the lunar regolith. *Reviews of Geophysics*, 31:423–438.
- Khalil, M. A.K., Rasmussen, R., and Gunawardena, R. (1993). Atmospheric methyl bromide: Trends and global mass balance. *Geophysical Research Letters*, 98:2887–.

- Khare, B. N., Sagan, C., Ogino, H., Nagy, B., Er, C., Schram, K. H., and Arakawa, E. T. (1986). Amino acids derived from Titan Tholins. *Icarus*, 68:176–184.
- Kiepenheuer, K.O. (1937). Über die Sonnenstrahlung zwischen 2000 und 3000 Å. *Zeitschrift für Astrophysik*, 14:348–356.
- Kiepenheuer, K.O. (1946). On the relations between ionosphere, sunspots and solar corona. *Monthly Notices Royal Astron. Soc.*, 106:515–524.
- Kinnison, D., Johnston, H., and Wuebbles, D. (1988). Ozone calculations with large nitrous oxide and chlorine changes. *Journal of Geophysical Research*, 93:14165–14175.
- Kirk-Davidoff, D. B., Hintsa, E. J., Anderson, J. G., and Keith, D. W. (1999). The effect of climate change in ozone depletion through changes in stratospheric water vapour. *Nature*, 402:399–401.
- Kirschner, E. J. (1985). *Balloons - From Montgolfiere to Space*. Aero Publishers Inc., Calif.
- Klebesadel, R. W., Strong, I. B., and Olson, R. A. (1973). Observations of Gamma-Ray Bursts of Cosmic Origin. *Astrophysical Journal*, 182:L85–L88.
- Klein, H. P. (1978). The Viking Biological Experiments on Mars. *Icarus*, 34:666–674.
- Klein, H. P. (1998). The search for life on Mars: What we learned from Viking. *Journal of Geophysical Research*, 103:28463–28466.
- Kneer, F. and von Uexküll, M. (1999). Diagnostics and Dynamics of the Solar Chromosphere. In *ASSL Vol. 239: Motions in the Solar Atmosphere*, pages 99–118.
- Knie, K., Korschinek, G., Faestermann, T., Wallner, C., Scholten, J., and Hillebrandt, W. (1999). Indication for Supernova Produced 60Fe Activity on Earth. *Physical Review Letters*, 83:18–21.
- Kniveton, D.R., Todd, M. C., Sciare, J., and Mihalopoulos, N. (2003). Variability of atmospheric dimethylsulphide over the southern Indian ocean due to changes in ultraviolet radiation. *Global Biochemical Cycles*, 17:1096.
- Kocharov, G. E., Ogurtsov, M. G., and Dreschhoff, G. A. M. (1999). On the Quasi-Five-Year Variation of Nitrate Abundance in Polar ice and Solar Flare Activity in the Past. *Solar Physics*, 188:187–190.
- Kodera, K. (1995). On the origin and nature of the interannual variability of the winter stratospheric circulation in the northern hemisphere. *Journal of Geophysical Research*, 100:14077–14088.
- Kodera, K., Koide, H., and Yoshimura, H. (1999). Northern hemisphere winter circulation associated with the North Atlantic Oscillation and stratospheric polar night jet. *Geophysical Research Letters*, 26:443.

- Kohl, J. L. and Parkinson, W. H. (1976). The MG II H and K lines. I - Absolute center and limb measurements of the solar profiles. *Astrophysical Journal*, 205:599–611.
- Koller, L. R. (1965). *Ultraviolet Radiation*. John Wiley and Sons.
- Kondo, Y., editor (1987). *Exploring the universe with the IUE satellite*. D. Reidel.
- Kondo, Y., de Jager, C., Hoekstra, R., van der Hucht, K. A., Kamperman, T. M., Lamers, H. J. G. L. M., Modisette, J. L., and Morgan, T. H. (1979). Balloon-borne ultraviolet stellar spectrograph. I - Instrumentation and observation. II - Highlights of first observational results. *Astrophysical Journal*, 230:526–539.
- Kondratyev, K. and Nikolsky, G. A. (1970). Solar Radiation and Solar Activity. *Quarterly Journal of the Royal Meteorological Society*, 96:509.
- Koomen, M. J., Scolnik, R., and Tousey, R. (1956). Measurements of the night airglow from a rocket. *Astronomical Journal*, 61:182–182.
- Korendyke, C. M., Vourlidas, A., Cook, J. W., Dere, K. P., Howard, R. A., Morrill, J. S., Moses, J. D., Moulton, N. E., and Socker, D. G. (2001). High-resolution Imaging of the Upper Solar Chromosphere: First Light Performance of the Very-high-Resolution Advanced Ultraviolet Telescope. *Solar Physics*, 200:63–73.
- Kornberg, A. (1950). Biological synthesis of deoxyribonucleic acid. *Science*, 131:1503–1508.
- Koscheev, A. P., Mukhin, L. M., Dikov, Y. P., Huth, J., and Wanke, H. (1994). Stability of martian salts under UV radiation and low energy impact. *Meteoritics*, 29:485–486.
- Koutchmy, S. (1975). Study of the white corona from Concorde 001 during the total solar eclipse of June 30, 1973. *L'Astronomie*, 89:149–157.
- Kraft, R. P. (1967). Studies of Stellar Rotation. V. The Dependence of Rotation on Age among Solar-Type Stars. *Astrophysical Journal*, 150:551–570.
- Krasnopolsky, V. A. (2001). Middle Ultraviolet Spectroscopy of Pluto and Charon. *Icarus*, 153:277–284.
- Krasnopolsky, V. A., Bjorkaker, G. L., Mumma, M. J., and Jennings, D. E. (1997). High-resolution spectroscopy of Mars at 3.7 and 8 μm : A sensitive search of H_2O_2 , H_2CO , HCl , and CH_4 , and detection of HDO . *Journal of Geophysical Research*, 102:6525–6534.
- Krasnopolsky, V. A. and Cruikshank, D. P. (1999). Photochemistry of Pluto's atmosphere and ionosphere near perihelion. *Journal of Geophysical Research*, 104:21979–21996.
- Krasnopolsky, V. A., Maillard, J. P., and Owen, T. C. (2004). Detection of methane in the martian atmosphere: evidence for life? *Icarus*, 172:537–547.

- Krivova, N. A. and Solanki, S. K. (2003). Solar total and spectral irradiance: modelling and a possible impact on climate. In *ESA SP-535: Solar Variability as an Input to the Earth's Environment*, pages 275–284.
- Krol et al., M. C. (2003). Continuing emissions of methyl chloroform from Europe. *Nature*, 421:131–135.
- Krucker, S. and Benz, A. O. (1998). Energy Distribution of Heating Processes in the Quiet Solar Corona. *Astrophysical Journal*, 501:L213–L216.
- Krüger, A. J. (1983). Sighting of El Chichon sulfur dioxide clouds with the Nimbus7 Total Ozone mapping spectrometer. *Science*, 220:1377–1379.
- Krzyscin, J. W., Eerme, K., and Janouch, M. (2004). Long-term variations of the UV-B radiation over Central Europe as derived from the reconstructed UV time series. *Annales Geophysicae*, 22:1473–1485.
- Kuiper, G. P. (1944). Titan: a Satellite with an Atmosphere. *Astrophysical Journal*, 100:378–383.
- Kulkarni, S. R., Djorgoski, S. G., Ramaprakash, A. N., Goodrich, R., Bloom, J. S., Adelberger, K. L., Kundic, T., Lubin, L., Frail, D. A., Frontera, F., Feroci, M., Nicastro, L., Barth, A. J., Davis, M., Filippenko, A. V., and Newman, J. (1998). Identification of a host galaxy at redshift $Z = 3.42$ for the gamma-ray burst of 14 December 1997. *Nature*, 393:35–39.
- Kumar, S. and Broadfoot, A. L. (1975). He 584 Å airglow emission from Venus - Mariner 10 observations. *Geophysical Research Letters*, 2:357–360.
- Kushmaro, A., Loya, Y., Fine, M., and Rosenberg, E. (1996). Bacterial infection and coral bleaching. *Nature*, 380:396–.
- Kyte, F. T. (1998). A meteorite from the Cretaceous/Tertiary boundary. *Nature*, 361:608–615.
- López-Moreno, J. J., Morales, C., Gómez, J. F., Trapero, J., Bowyer, S., Edelstein, J., Lampton, M., and Korpela, E. J. (1998). EURD observations of EUV nighttime airglow lines. *Geophysical Research Letters*, 25:2937–2940.
- Labitzke, K. (1987). Sunspots, the QBO, and the stratospheric temperature in the north polar region. *Geophysical Research Letters*, 14:535–537.
- Labitzke, K. (2001). The global signal of the 11-year sunspot cycle in the stratosphere: Differences between solar maxima and minima. *Meteorologische Zeitschrift*, 10:83–90.
- Labitzke, K. (2003). The global signal of the 11-year sunspot cycle in the atmosphere: When do we need the QBO? *Meteorologische Zeitschrift*, 12:209–216.

- Labitzke, K., Austin, J., Butchart, N., Knight, J., Takahashi, M., Nakamoto, M., Nagashima, T., Haigh, J., and Williams, V. (2002). The global signal of the 11-year solar cycle in the stratosphere: observations and models. *Journal of Atmospheric and Terrestrial Physics*, 64:203–210.
- Labitzke, K. and Van Loon, H. (1999). *The Stratosphere*. Springer Verlag.
- Labitzke, K. and van Loon, H. (2000). The QBO effect on the solar signal in the global stratosphere in the winter of the Northern Hemisphere. *Journal of Atmospheric and Terrestrial Physics*, 62:621–628.
- Labs, D. and Neckel, H. (1962). Die absolute Strahlungsintensität der Sonnenmitte im Spektralbereich $4010 < \lambda < 6569 \text{ \AA}$. *Zeitschrift für Astrophysik*, 55:269–289.
- Lacy, J. H., Townes, C. H., Geballe, T. R., and Hollenbach, D. J. (1980). Observations of the motion and distribution of the ionized gas in the central parsec of the Galaxy. II. *Astrophysical Journal*, 241:132–146.
- Laffont, C., Boice, D. C., Moreels, G., Clairemidi, J., Rousselot, P., and Andernach, H. (1998). Tentative identification of S₂ in the IUE spectra of Comet Hyakutake (C/1996 B2). *Geophysical Research Letters*, 25:2749–2752.
- LaFond, C. D. (1962). UK-1 Satellite Turns Up Surprises. *Missiles and Rockets*, 11:26–32.
- Laget, M. (1980). A survey of high-latitude regions at balloon ultraviolet wavelengths. *Astronomy and Astrophysics*, 81:37–42.
- Lammer, H., Selsis, F., Ribas, I., Guinan, E. F., Bauer, S. J., and Weiss, W. W. (2003a). Atmospheric Loss of Exoplanets Resulting from Stellar X-Ray and Extreme-Ultraviolet Heating. *Astrophysical Journal*, 598:L121–L124.
- Lammer, H., Selsis, F., Ribas, I., Guinan, E. F., Bauer, S. J., and Weiss, W. W. (2003b). Atmospheric Loss of Exoplanets Resulting from Stellar X-Ray and Extreme-Ultraviolet Heating. *Astrophysical Journal*, 598:L121–L124.
- Landini, M., Monsignori Fossi, B. C., Poletto, G., and Tagliaferri, G. L. (1972). Solar XUV fluxes of SOLRAD 10 satellite from July to December 1971 (Lettera alla Direzione). *Memorie della Società Astronomica Italiana*, 43:383.
- Lane, A. L. and Domingue, D. L. (1997). IUE's View of Callisto: Detection of an SO₂ Absorption Correlated to Possible Torus Neutral Wind Alterations. *Geophysical Research Letters*, 24:1143–1146.
- Lane, A. L., Nelson, R. M., and Matson, D. L. (1981). Evidence for sulphur implantation in Europa's UV absorption band. *Nature*, 292:38–39.
- Langematz, U., Kunze, M., Krüger, K., and Labitzke, K. (2003). Thermal and dynamical changes of the stratosphere since 1979 and their link to ozone and CO₂ changes. *Journal of Geophysical Research*, 108:4027–4040.

- Lara, L. M., Ip, W.-H., and Rodrigo, R. (1997). Photochemical Models of Pluto's Atmosphere. *Icarus*, 130:16–35.
- Lara, L.M., Lellouch, E., Lopez-Moreno, J.J., and Rodrigo, R. (1999). Vertical distribution of Titan's atmospheric neutral constituents. *Journal of Geophysical Research*, 101:23,262–23,283.
- Larkin, A., Haigh, J. D., and Djavidnia, S. (2000). The Effect of Solar UV Irradiance Variations on the Earth's Atmosphere. *Space Science Reviews*, 94:199–214.
- Lary, D. J. (1996). Gas phase Atmospheric Bromine Photochemistry. *Journal of Geophysical Research, Atmospheres*, 101:1505–1516.
- Lary et al., D. J. (1996). Heterogeneous Atmospheric Bromine Photochemistry. *Journal of Geophysical Research, Atmospheres*, 101:1489–1504.
- Laster, H., Tucker, W. H., and Terry, K. D. (1968). Cosmic Rays from Nearby Supernovae: Biological Effects. *Science*, 160:1138–1139.
- Laue, E. G. and Drummond, A. J. (1968). Solar constant: First direct measurements. *Science*, 161:888–891.
- Lawrence, G. M., Barth, C. A., and Argabright, V. (1977). Excitation of the Venus night airglow. *Science*, 195:573–574.
- Lean, J. (1989). Contribution of ultraviolet irradiance variations to changes in the sun's total irradiance. *Science*, 244:197–200.
- Lean, J. (1997). The Sun's Variable Radiation and Its Relevance For Earth. *Annual Review of Astronomy and Astrophysics*, 35:33–67.
- Lean, J. (2000). Evolution of the Sun's spectral irradiance since the Maunder Minimum. *Geophysical Research Letters*, 27:2425–2428.
- Lean, J. and Rind, D. (1998). Climate forcing by changing solar radiation. *Journal of Climate*, 11:3069–3094.
- Lean, J. L., Livingston, W. C., White, O. R., and Skumanich, A. (1984). Modelling solar spectral irradiance variations at ultraviolet wavelengths. In *Solar Irradiance Variations on Active Region Time Scales*, NASA, pages 253–288.
- Lean, J. L., Warren, H. P., Mariska, J. T., and Bishop, J. (2003). A new model of solar EUV irradiance variability 2. Comparisons with empirical models and observations and implications for space weather. *Journal of Geophysical Research (Space Physics)*, pages 2–1.
- Lean, J. L., White, O. R., Livingston, W. C., and Picone, J. M. (2001). Variability of a composite chromospheric irradiance index during the 11-year activity cycle and over longer time periods. *Journal of Geophysical Research*, pages 10645–10658.

- Lean, J. L., White, O. R., and Skumanich, A. (1995). On the solar ultraviolet spectral irradiance during the Maunder Minimum. *Global Biochemical Cycles*, 9:171–182.
- Leblanc, T. and McDermid, I. S. (2000). Stratospheric ozone climatology from lidar measurements at Table Mountain (34.4 °N, 117.7 °W) and Mauna Loa (19.5 °N, 155.6 °W). *Journal of Geophysical Research*, 105:14613–14624.
- Lee, J. A.H. (1989). The relationship between malignant melanoma of skin and exposure to sunlight. *Photochemistry and Photobiology*, 50:493–496.
- Leibundgut, B. (2000). Type Ia Supernovae. *The Astronomy and Astrophysics Review*, 10:179–209.
- Leinert, C., Bowyer, S., Haikala, L. K., Hanner, M. S., Hauser, M. G., Levasseur-Regourd, A.-C., Mann, I., Mattila, K., Reach, W. T., Schlosser, W., Staude, H. J., Toller, G. N., Weiland, J. L., Weinberg, J. L., and Witt, A. N. (1998). The 1997 reference of diffuse night sky brightness. *Astronomy and Astrophysics Supplement Series*, 127:1–99.
- Leitch, E.M. and Vasisht, G. (1998). Mass extinctions and the Sun's encounters with spiral arms. *New Astronomy*, 3:51–56.
- Lelieveld, J. and Dentener, F. J. (2000). What controls tropospheric ozone? *Journal Geophysical Research*, 105:3531–3552.
- Lemaire, P. and Blamont, J. E. (1967). Stigmatic Balloon Spectra of the Solar MG II Doublet. *Astrophysical Journal*, 150:L129–L131.
- Lena, P., Hall, D., Soufflot, A., and Viala, Y. (1974). The thermal emission of the dust corona, during the eclipse of June 30, 1973. II - Photometric and spectral observations. *Astronomy and Astrophysics*, 37:81–86.
- Lesser, M. P. and Shick, J.M. (1990). Effects of visible and ultraviolet radiation on the ultrastructure of zooxanthellae (*Symbiodinium* sp.) in culture and in situ. *Cell Tissue Research*, 261:501–508.
- Levin, G. and Straatt, P. (1981). Antarctic soil No. 726 and implications for the Viking Labelled Release Experiment. *Journal of Theoretical Biology*, 91:41–45.
- Levin, G. V. (2002). Oxides of Mars. In *Proc. SPIE Vol. 4495, Instruments, Methods, and Missions for Astrobiology IV*, Richard B. Hoover; Gilbert V. Levin; Roland R. Paepe; Alexei Y. Rozanov; Eds., pages 131–136.
- Lewis, B. R. and Carver, J. H. (1983). Temperature dependence of the carbon dioxide photoabsorption cross section between 1200 and 1970 Å. *Journal of Quantitative Spectroscopy and Radiative Transfer*, 30:297–309.
- Lewis, J. S. and Prinn, R. G. (1984). Planets and their atmospheres - Origin and evolution. *Orlando FL Academic Press Inc International Geophysics Series*, 33.

- Li, L. H. and Sofia, S. (2001). Measurements of Solar Irradiance and Effective Temperature as a Probe of Solar Interior Magnetic Fields. *Astrophysical Journal*, 549:1204–1211.
- Lindemann, F.A. and Dobson, G.M.B. (1922). A theory of Meteors, and the Density and Temperature of the Outer Atmosphere to which it Leads. *Proc. Roy. Soc. London*, pages 411–437.
- Lineweaver, C. H., Fenner, Y., and Gibson, B. K. (2004). The Galactic Habitable Zone and the Age Distribution of Complex Life in the Milky Way. *Science*, 303:59–62.
- Link, R., Gladstone, G. R., Chakrabarti, S., and McConnell, J. C. (1988). A reanalysis of rocket measurements of the ultraviolet dayglow. *Journal of Geophysical Research*, 93:14631–14648.
- Linker, J. A., Mikić, Z., Riley, P., Lionello, R., and Odstrcil, D. (2003). Models of Coronal Mass Ejections: A Review with A Look to The Future. In *AIP Conf. Proc. 679: Solar Wind Ten*, pages 703–710.
- Linsky, J. L., Pagano, I., Valenti, J., Gagne, M., and Duncan, D. K. (2003). The Sun as a Star: Comparing Alpha CEN a to UV Solar Spectra. In *IAU Symposium no. 219, Sydney, Australia, meeting abstract*.
- Linsky, J. L., Redfield, S., Wood, B. E., and Piskunov, N. (2000). The Three-dimensional Structure of the Warm Local Interstellar Medium. I. Methodology. *Astrophysical Journal*, 528:756–766.
- Liu, W. and Dalgarno, A. (1996). The Ultraviolet Spectra of the Jovian Aurora. *Astrophysical Journal*, 467:446–453.
- Livingston, W. and Harvey, J. (1969). Observational Evidence for Quantization in Photospheric Magnetic Flux. *Solar Physics*, 10:294–296.
- Livio, M. (1999). How Rare Are Extraterrestrial Civilizations, and When Did They Emerge? *Astrophysical Journal*, 511:429–431.
- Lockwood, M. (2003). Twenty-three cycles of changing open solar magnetic flux. *Journal of Geophysical Research (Space Physics)*, 108:1128–1143.
- Lockwood, M., Stamper, R., and Wild, M. N. (1999). A doubling of the sun's coronal magnetic field during the past 100 years. *Nature*, 399:437–439.
- Logan, J. A., Jones, D. B. A., Megretskaya, I. A., Oltmans, S. J., Johnson, B. J., Vömel, H., Randel, W. J., Kimani, W., and Schmidlin, F. J. (2003). Quasibiennial oscillation in tropical ozone as revealed by ozonesonde and satellite data. *Journal of Geophysical Research (Atmospheres D8)*, 108:6–1.
- Lovelock, J. E. (1971). Atmospheric fluorine compounds as indicators of air movements. *Nature*, 230:379.

- Lovelock, J. E. and Maggs, R. J. (1973). Halogenated Hydrocarbons in and over Atlantic. *Nature*, 241:194–196.
- Lowell, R. P. and Dubose, M. (2003). Hydrothermal Systems on Europa. *AGU Fall Meeting Abstracts*, page A1055.
- Luterbacher et al., J. (1999). Reconstruction of monthly NAO and EU indices back to A.D 1675. *Geophysical Research Letters*, 26:2745–2748.
- Lutz, T. E. and Kelker, D. H. (1973). On the Use of Trigonometric Parallaxes for the Calibration of Luminosity Systems: Theory. *Publications Astronomical Society of the Pacific*, 85:573–578.
- Lyman, T. (1908). The Absorption of Some Gases for Light of Very Short Wave-Length. *Astrophysical Journal*, 27:87–105.
- Lyman, T. (1916). The Extension of the Spectrum Beyond the Schumann Region. *Astrophysical Journal*, 43:89–102.
- Lyons, M. M., Aas, P., Pakulski, J.D., Van Waasbergen, L., Miller, R. V., Mitchell, D. L., and Jeffrey, W. H. (1998). DNA damage induced by ultraviolet radiation in coral-reef microbial communities. *Marine Biology*, 130:537–543.
- Mészáros, P. (2003). γ -ray bursts: The supernova connection. *Nature*, 423:809–810.
- MacMunn, C. A. (2003). On the pigments of certain corals, with a note on the pigment of an asteroid. In *The fauna and geography of the Maldives and Laccadive Archipelagoes*, Gardiner, J.S., ed. , Cambridge University Press, pages 184–190.
- Mahajan, K. K. and Dwivedi, A. K. (2004). Ionospheres of Venus and Mars: a comparative study. *Advances in Space Research*, 33:145–151.
- Maíz-Apellániz, J. (2001). The Origin of the Local Bubble. *Astrophysical Journal*, 560:L83–L86.
- Majeed, T. and McConnell, J. C. (1991). The upper ionospheres of Jupiter and Saturn. *Planetary and Space Sciences*, 39:1715–1732.
- Makarova, K. S., Wolf, Y.I., White, O., Minton, K., and Daly, M. J. (1999). Short repeats and IS elements in the extremely radiation-resistant bacterium *Deinococcus radiodurans* and comparison to other bacterial species. *Research in Microbiology*, 150:711–724.
- Malin, D. (2001). Detectors: Photography. In *Encyclopedia of Astronomy and Astrophysics*, ed. P. Murdin, volume 1, pages 599–602. Nature Publishing Group.
- Mancinelli, R. L. and Klovstad, M. (2000). Martian soil and UV radiation: microbial viability assessment on spacecraft surfaces. *Planetary and Space Sciences*, 48:1093–1097.

- Mankin, W. C. and Coffey, M. T. (1984). Increased stratospheric hydrogen chloride in the El Chichon cloud. *Science*, 226:170–172.
- Manney, G. L., Froidevaux, L., Santee, M. L., Livesey, N. J., Sabutis, J. L., and Waters, J. W. (2003). Variability of ozone loss during Arctic winter (1991–2000) estimated from UARS Microwave Limb Sounder measurements. *Journal of Geophysical Research (Atmospheres)*, 108:10.
- Marignac, C. and De la Rive, M. (1845). Sur la production et la nature de l' ozone. *Comptes Rendus Acad. Sci. Paris*, 20:808.
- Marochnik, L. S. (1983). On the origin of the solar system and the exceptional position of the sun in the galaxy. *Astrophysics and Space Science*, 89:61–75.
- Marsh, N. D. and Svensmark, H. (2000). Low Cloud Properties Influenced by Cosmic Rays. *Physical Review Letters*, 85:5004–5007.
- Marshall, H. T. (1928). Ultraviolet and extinction. *American Naturalist*, 62:165–187.
- Martínez-Delgado, D., Aparicio, A., Gómez-Flechoso, M. A., and Carrera, R. (2001). Tidal Streams in the Galactic Halo: Evidence for the Sagittarius Northern Stream or Traces of a New Nearby Dwarf Galaxy. *Astrophysical Journal*, 549:L199–L202.
- Matsuoka, L. Y., Worstman, J., Hanifan, N., and Holick, M. F. (1988). Chronic sunscreen use decreased circulating concentrations of 25-hydroxyvitamin D: A preliminary study. *Arch. Dermatology*, 12:1802–1804.
- Mattila, K., Vaeisaenen, P., and Appen-Schnur, G. F. O. V. (1996). Sky brightness at the ESO La Silla Observatory 1978 to 1988. *Astronomy and Astrophysics Supplements*, 119:153–170.
- Mattimore, V. and Battista, J. R. (1996). Radioresistance of *Deinococcus radiodurans* functions necessary to survive ionizing radiation are also necessary to survive prolonged desiccation. *Journal Bacteriology*, 178:633–637.
- Matzner, C. D. and McKee, C. F. (1999). The Expulsion of Stellar Envelopes in Core-Collapse Supernovae. *Astrophysical Journal*, 510:379–403.
- Maucherat-Joubert, M., Deharveng, J. M., and Cruvellier, P. (1979). Ultraviolet observation of the zodiacal light from the D2B-Aura satellite. *Astronomy and Astrophysics*, 74:218–224.
- Mauk, B. H., Mitchell, D. G., Krimigis, S. M., Roelof, E. C., and Paranicas, C. P. (2003). Energetic neutral atoms from a trans-Europa gas torus at Jupiter. *Nature*, 421:920–922.
- Maund, J. R., Smartt, S. J., Kudritzki, R. P., Podsiadlowski, P., and Gilmore, G. F. (2004). The massive binary companion star to the progenitor of supernova 1993J. *Nature*, 427:129–131.

- Maunder, E. W. (1894). A prolonged sunspot minimum. *Knowledge*, 17:173–176.
- Mc Culloch, A., Ashford, P., and Midgley, P. M. (2001). Historic Emissions of Fluorotrichloromethane (CFC-11) based on a market survey. *Atmospheric Environment*, 35:4387–4397.
- Mc Ghee, G. R. (1996). *The Late Devonian Mass Extinction*. Columbia University Press.
- Mc Kay, D. S., Gibson, E.K., Thomas-Kerpta, K. L., Vali, H., Romanek, C.S., Clemett, S. J., Chillier, X. D., Maechling, C.R., and Zare, R. N. (1996). Search for past life on Mars: Possible relic biogenic activity in Martian Meteorite ALH84001. *Science*, 273:924–930.
- Mc Lennan, J. C. and Shrum, G. M. (1925). On the origin of the auroral green line 5577 - and other associated with aurora borealis. *Proc. Royal Society London*, page 501.
- Mc Neill, J.R. (2000). *Something New Under the Sun: An Environmental History of the Twentieth-Century World*. W.W. Norton.
- McClements, K. G., Harrison, R. A., and Alexander, D. (1991). The detection of wave activity in the solar corona using UV line spectra. *Solar Physics*, 131:41–48.
- McConnell, J. C., Sandel, B. R., and Broadfoot, A. L. (1981). Voyager U.V. spectrometer observations of He 584 Å dayglow at Jupiter. *Planetary and Space Sciences*, 29:283–292.
- McCormack, B. M., editor (1971). *The radiating atmosphere*.
- McCoy, R. P., Carruthers, G. R., and Opal, C. B. (1986). Far-ultraviolet spectral images of comet Halley from sounding rockets. *Nature*, 324:439–441.
- McCrory, R. and Wang, Z., editors (1996). *Supernovae and supernova remnants*.
- McDonald, G. D., de Vanssay, E., and Buckley, J. R. (1998). Oxidation of Organic Macromolecules by Hydrogen Peroxide: Implications for Stability of Biomarkers on Mars. *Icarus*, 132:170–175.
- McDonald, G. D., Whited, L. J., Deruiter, C., Khare, B. N., Patnaik, A., and Sagan, C. (1996). Production and Chemical Analysis of Cometary Ice Tholins. *Icarus*, 122:107–117.
- McElroy, C. T. (1995). A spectroradiometer for the measurement of direct and scattered solar irradiance from on-board the NASA ER-2 high-altitude research aircraft. *Geophysical Research Letters*, 22:1361.
- McElroy, M. B., Salawitch, R. J., and Wofsy, S. C. (1986). Antarctic O₃ - Chemical mechanisms for the spring decrease. *Geophysical research Letters*, 13:1296–1299.

- McGrath, M. A., Feldman, P. D., Ballester, G. E., and Moos, H. W. (1989). IUE observations of the Jovian dayglow emission. *Geophysical Research Letters*, 16:583–586.
- McKenzie, R. and Elwood, J. M. (1990). Intensity of solar ultraviolet and its implications for skin cancer. *New Zealand Medical Journal*, 103:152.
- McKenzie, R., Smale, D., Bodeker, G., and Claude, H. (2003). Ozone profile differences between Europe and New Zealand: Effects on surface UV irradiance and its estimation from satellite sensors. *Journal of Geophysical Research (Atmospheres)*, 108:4179.
- McPhate, J. B., Feldman, P. D., McCandliss, S. R., and Burgh, E. B. (1999). Rocket-borne Long-Slit Ultraviolet Spectroscopy of Comet Hale-Bopp. *Astrophysical Journal*, 521:920–927.
- Meadows, A. J. (1970). *Early Solar Physics*. Pergamon.
- Meier, R. R., Warren, H. P., Nicholas, A. C., Bishop, J., Huba, J. D., Drob, D. P., Lean, J. L., Picone, J. M., Mariska, J. T., Joyce, G., Judge, D. L., Thonnard, S. E., Dymond, K. F., and Budzien, S. A. (2002). Ionospheric and dayglow responses to the radiative phase of the Bastille Day flare. *Geophysical Research Letters*, 29:99–10X.
- Mellanby, E. and Cantag, M. D. (1919). Experimental investigation on rickets. *Lancet*, 196:407–412.
- Melott et al., A. (2004). Did a Gamma-Ray Burst Initiate the Ordovician Extinction? *International Journal of Astrobiology*, 3:55–61.
- Mendel, G. (1866). Versuche über Pflanzenhybriden. *Verh. naturforsch. Ver. Brünn*, 4:3–47.
- Menzel, D. H., Coblenz, W. W., and Lampland, C. O. (1926). Planetary Temperatures Derived from Water-Cell Transmissions. *Astrophysical Journal*, 63:177–187.
- Messina, S. and Guinan, E. F. (2002). Magnetic activity of six young solar analogues I. Starspot cycles from long-term photometry. *Astronomy and Astrophysics*, 393:225–237.
- Meyer, E. (1903). Über die Absorption der ultravioletten Strahlung in Ozon. *Annalen der Physik*, 12:849–859.
- Micheletti, M. I. (2002). Solar UVB and Plant damage Irradiances for different Argentinian Regions. *Photochemistry and Photobiology*, 76:294–300.
- Middlebrook, A. M. and Tolbert, M. A. (1973). *Stratospheric Ozone Depletion*. University Science Books, Calif.
- Midgley, T. and Henne, A. L. (1930). Organic fluorides as refrigerants. *Industrial and Engineering Chemistry*, 22:542–545.

- Mie, G. (1908). Beiträge zur Optik trüber Medien, spezielle kolloidaler Metallösungen. *Annalen der Physik*, 25:377–445.
- Mihalas, D. (1978). *Theory of Stellar Atmospheres*. Freeman & Co., San Francisco.
- Mikhailov, A. V., Chernigovskaya, M. A., Beletsky, A. B., Kazimirovsky, E. S., and Pirog, O. M. (1999). Variations of the Ground-Measured Solar Ultraviolet Radiation During the Solar Eclipse on March 9, 1997. *Advances in Space Research*, 24:611–619.
- Miller, S. L. (1953). A production of aminoacids under possible primitive Earth conditions. *Science*, 117:528–529.
- Milliard, B., Donas, J., and Laget, M. (1991). A 40-cm UV (2000 Å) balloon-borne imaging telescope - Results and current work. *Advances in Space Research*, 11:135–138.
- Mitchel, J. M. (1973). An Overview of Climatic Variability and Its Causal Mechanisms. *Quaternary Research*, 6:481–493.
- Mitchell, W. E. and Livingston, W. C. (1991). Line-blanketing variations in the irradiance spectrum of the sun from maximum to minimum of the solar cycle. *Astrophysical Journal*, 372:336–348.
- Mitton, S. (1979). *The Crab Nebula*. Faber and Faber, London.
- Moffat, T. (1875). On the apparent connection between sunspots, atmosphere ozone and the force of wind. *Nature*, 12:374.
- Molina, M. J. and Rowland, F. S. (1974). Stratospheric sink for chlorofluoromethanes: chlorine atom catalysed destruction of ozone. *Nature*, 249:810–812.
- Molina-Cuberos, G. J., López-Moreno, J. J., Rodrigo, R., Lichtenegger, H., and Schwingenschuh, K. (2001a). A model of the martian ionosphere below 70 km. *Advances in Space Research*, 27:1801–1806.
- Molina-Cuberos, G. J., Stumptner, W., Lammer, H., Kömle, N. I., and O'Brien, K. (2001b). Cosmic Ray and UV Radiation Models on the Ancient Martian Surface. *Icarus*, 154:216–222.
- Montesinos, B. and Jordan, C. (1993). On Magnetic Fields Stellar Coronae and Dynamo Action in Late Type Dwarfs. *Monthly Notices Royal Astronomical Society*, 264:900–918.
- Moore, C. E. (1952). *An ultraviolet multiplet table*. NBS Circular, Washington: US Government Printing Office (USGPO).
- Morgan, T. H. and Killen, R. M. (1997). A non-stoichiometric model of the composition of the atmospheres of Mercury and the Moon. *Planetary and Space Sciences*, 45:81–94.

- Morris, R. V. (1981). Ultra-violet radiation as a weathering agent on Mars: How important is it? *LPI Contributions*, 441:163.
- Moses, J. (2000). Photochemistry in Giant-Planet Atmospheres. In *ASP Conf. Ser. 212: From Giant Planets to Cool Stars*, pages 196–206.
- Muhleman, D. O., Grossman, A. W., Butler, B. J., and Slade, M. A. (1990). Radar reflectivity of Titan. *Science*, 248:975–980.
- Mulkidjanian, A. Y., Cherepanov, D.A., and Galperin, M. Y. (2003). Survival of the fittest before the beginning of life: Selection of the first oligonucleotide-like polymers by UV light. *BMC Evolutionary Biology*, 3(12).
- Muller, G. (1912). Die Extinktion des Lichtes in der Erdatmosphaere und die Energieverteilung im Sonnenspektrum nach spektralphotometrischen Beobachtungen auf der Insel Teneriffa. *Publikationen des Astrophysikalischen Observatoriums zu Potsdam*, 64.
- Muller, R. (1999). The Solar Granulation. In *ASSL Vol. 239: Motions in the Solar Atmosphere*, Kluwer Academic Publishers, pages 35–70.
- Muller, R. A. (2002). Avalanches at the core-mantle boundary. *Geophysical Research Letters*, 29:411–414.
- Murdin, P. (1985). *Supernovae*. Cambridge University Press, 2nd. ed.
- Murthy, J., Henry, R. C., Feldman, P. D., and Tennyson, P. D. (1990). Observations of the diffuse near-UV radiation field. *Astronomy and Astrophysics*, 231:187–198.
- Nagy, A. F., Liu, Y., Hansen, K. C., Kabin, K., Gombosi, T. I., Combi, M. R., DeZeeuw, D. L., Powell, K. G., and Kliore, A. J. (2001). The interaction between the magnetosphere of Saturn and Titan's ionosphere. *Journal of Geophysical Research*, 106:6151–6160.
- Nagy, B., Fredrikson, K., Kudynowsky, J., and Carlson, L. (1963). Ultra-violet spectra of organized elements. *Nature*, 200:565–566.
- Nair, H., Gerstell, M. F., and Yung, Y. L. (1993). The young Sun and photochemistry of the primitive Martian atmosphere. In *Early Mars: How Warm and How Wet?*, page 19. Lunar and Planetary Institute Workshop.
- Nakamura, T. and Tajika, E. (2004). Drastic Climate Change of Mars Induced by H₂O Ice Caps. In *Lunar and Planetary Institute Conference Abstracts*, page 1672.
- Name, A. N. (2003). Impact eject layer from the mid-Devonian: possible connection to global mass extinctions. *Science*, 300:1734–1737.
- Napier, W. M. (2004). A mechanism for interstellar panspermia. *Monthly Notices Royal Astronomical Society*, 348:46–51.

- Naujokat, B. (1986). An update of the observed quasi-biennial oscillation of the stratospheric winds over the tropics. *Journal Atmospheric Sciences*, 43:1873–1877.
- Naujokat, B., Krüger, K., Matthes, K., Hoffmann, J., Kunze, M., and Labitzke, K. (2002). The early major warming in December 2001 - exceptional? *Geophysical Research Letters*, 29:19–1.
- Navach, C., Lehmann, M., and Huguenin, D. (1973). Feasibility of UV astronomy by balloon-borne observations 1 Stellar spectrophotometry. *Astronomy and Astrophysics*, 22:361–370.
- Navarro, J. F., Helmi, A., and Freeman, K. C. (2004). The Extragalactic Origin of the Arcturus Group. *Astrophysical Journal*, 601:L43–L46.
- Nelson, R. M. and Domingue, D.L. (1999). *The Solar System at Ultraviolet Wavelengths*, pages 697–713. Encyclopedia of the Solar System. P. Weissman (eds.). Academic Press.
- Ness, N. F., Acuña, M. H., Connerney, J. E. P., Kliore, A. J., Breus, T. K., Krymskii, A. M., Cloutier, P., and Bauer, S. J. (2000). Effects of magnetic anomalies discovered at Mars on the structure of the Martian ionosphere and solar wind interaction as follows from radio occultation experiments. *Journal of Geophysical Research*, pages 15991–16004.
- Neufeld, M.J. (1994). *The Rocket and the Reich: Peenemünde and the Coming of the ballistic Missile Era*. Simon Schuster.
- Newberg et al., H. J. (2002). The Ghost of Sagittarius and Lumps in the Halo of the Milky Way. *Astrophysical Journal*, 569:245–274.
- Newchurch et al., M. J. (2003). Evidence for slowdown in stratospheric ozone loss: first stage of ozone recovery. *Journal of Geophysical Research*, 108:12–.
- Newkirk, G. (1959). The airglow of Venus. *Planetary and Space Sciences*, 1:32–36.
- Newkirk, G. and Bohlin, J. D. (1965). Coronoscope II : observations of the white light corona from a stratospheric balloon. *Annales d'Astrophysique*, 28:234–238.
- Newkirk, G. J. and Eddy, J. A. (1962). Daytime sky radiance from forty to eighty thousand feet. *Nature*, 194:638–641.
- Newman, M. J. and Rood, R. T. (1977). Implications of solar evolution for the earth's early atmosphere. *Science*, 198:1035–1037.
- Newman, P. A., Nash, E. R., and Rosenfield, J. E. (2001). What controls the temperature of the Arctic stratosphere during the spring? *Journal of Geophysical Research*, 106:19999–20010.
- Nicholson, W. (2003). Using thermal inactivation kinetics to calculate the probability of extreme spore longevity: Implications for paleomicrobiology and lithopanspermia. *Origins of Life and Evolution of the Biosphere*, 33:621–631.

- Nishimura, J. (2002). Scientific ballooning in the 20th century; a historical perspective. *Advances in Space Research*, 30:1071–1085.
- Noll, K. S., Johnson, R. E., McGrath, M. A., and Caldwell, J. J. (1997). Detection of SO₂ on Callisto with the Hubble Space Telescope. *Geophysical Research Letters*, 24:1139–1142.
- Noll, K. S., McGrath, M. A., Trafton, L. M., Atreya, S. K., Caldwell, J. J., Weaver, H. A., Yelle, R. V., Barnet, C., and Edgington, S. (1995). HST Spectroscopic Observations of Jupiter After the Collision of Comet Shoemaker-Levy 9. *Science*, 267:1307–1313.
- O'Brien, K. (1979). Secular Variations in the production of cosmogenic isotopes in the Earth's atmosphere. *Journal of Geophysical Research*, 84:423–431.
- O'Connell, R. W. (1987). Ultraviolet detection of very low-surface-brightness objects. *Astronomical Journal*, 94:876–882.
- Ogden, J. M. (1999). Prospects for building a hydrogen energy infrastructure. *Annual Review Energy and Environment*, 24:227–279.
- Olsen et al., P. E. (296). Ascent of dinosaurs linked to iridium anomaly in the Triassic-Jurassic boundary. *Science*, 296:1305–1307.
- Omukai, K. (2001). Primordial Star Formation under Far-Ultraviolet Radiation. *Astrophysical Journal*, 546:635–651.
- Opal, C. B. and Carruthers, G. R. (1977). Lyman-alpha observations of Comet West /1975n/. *Icarus*, 31:503–509.
- Orsolini, Y. J. and Limpasuvan, V. (2001). The North Atlantic Oscillation and the occurrences of ozone miniholes. *Geophysical Research Letters*, 28:4099–4102.
- Orth, C. J., Gilmore, J. S., Knight, J. D., Pillmore, C.L., Tschudy, R.H., and Fasset, J. E. (1981). An iridium abundance anomaly at the paleontological Cretaceous-Tertiary boundary in northern New Mexico. *Science*, 214:1341–1343.
- Oyama, V. I. and Berdahl, B. J. (1977). The Viking gas exchange experiment results from Chryse and Utopia surface samples. *Journal of Geophysical Research*, 82:4669–4676.
- Pallavicini, R. (2003). Why solar astronomers should be interested in stars. *Advances in Space Research*, 32:885–894.
- Palmer, T. (1997). *Controversy: catastrophism and Evolution: The Ongoing Debate*. Kluwer Academic Publishers.
- Panitz, C., Rettberg, P., Rabbow, E., and Horneck, G. (2001). The ROSE experiments on the EXPOSE facility of the ISS. In *ESA SP-496: Exo-/Astro-Biology*, pages 383–388.

- Pap, J. M. (2003). Total Solar and Spectral Irradiance Variations from Near-UV to Infrared. *The Sun's Surface and Subsurface: Investigating Shape. Edited by J.-P. Rozelot. Lecture Notes in Physics, Springer Verlag*, 599:129–155.
- Pap, J. M., Turmon, M., Floyd, L., Fröhlich, C., and Wehrli, C. (2002). Total solar and spectral irradiance variations from solar cycles 21 to 23. *Advances in Space Research*, 29:1923–1932.
- Paresce, F. and Jakobsen, P. (1980). The diffuse UV background. *Nature*, 288:119–126.
- Park, D. (1997). *The fire within the eye*. Princeton University Press.
- Parker, B. (1990). *Colliding galaxies: The Universe in Turnmoil*. Plenum, New York.
- Parker, E. N. (1972). Topological Dissipation and the Small-Scale Fields in Turbulent Gases. *Astrophysical Journal*, 174:499–510.
- Parker, E. N. (1983). Magnetic neutral sheets in evolving fields. I - General theory. II - Formation of the solar corona. *Astrophysical Journal*, 264:635–647.
- Parker, E. N. (1988). Nanoflares and the solar X-ray corona. *Astrophysical Journal*, 330:474–479.
- Parnell, C. E. (2002). Nature of the magnetic carpet - I. Distribution of magnetic fluxes. *Monthly Notices Royal Astronomical Society*, 335:389–398.
- Parravano, A., Hollenbach, D. J., and McKee, C. F. (2003). Time Dependence of the Ultraviolet Radiation Field in the Local Interstellar Medium. *Astrophysical Journal*, 584:797–817.
- Parson, E. A. and Greene, O. (1995). The complex chemistry of the International Ozone Agreements. *Environment*, 37:17–43.
- Patel, M. R., Bérçes, A., Kerékgyárto, T., Rontó, Gy., Lammer, H., and Zarnecki, J. C. (2004). Annual solar UV exposure and biological effective dose rates on the Martian surface. *Advances in Space Research*, 33:1247–1252.
- Patel, M. R., Bérçes, A., Kolb, C., Lammer, H., Rettberg, P., Zarnecki, J. C., and Selsis, F. (2003). Seasonal and diurnal variations in Martian surface ultraviolet irradiation: biological and chemical implications for the Martian regolith. *International Journal of Astrobiology*, 2:21–34.
- Patel, M. R., Zarnecki, J. C., and Catling, D. C. (2002). Ultraviolet radiation on the surface of Mars and the Beagle 2 UV sensor. *Planetary and Space Science*, 50:915–927.
- Pauluhn, A. and Solanki, S. K. (2003). Dependence of UV radiance of the quiet Sun on the solar cycle: Surface magnetic fields as the cause. *Astronomy and Astrophysics*, 407:359–367.

- Pavlov, A. A., Pavlov, A. K., Mills, M. J., Ostryakov, V. M., Vasilyev, G. I., and Toon, O. B. (2005). Catastrophic ozone loss during passage of the Solar System through an interstellar cloud. *Geophysical Research Letters*, 32.
- Peeters, Z., Botta, O., Charnley, S. B., Ruiterkamp, R., and Ehrenfreud, P. (2003). The Astrobiology of Nucleobases. *Astrophysical Journal*, 593:L129–L132.
- Petit, E. and Nicholson, S. B. (1924). Measurements of the radiation from the planet Mars. *Pop. Astronomy*, 32:601.
- Pfotzer, G. (1972). History of the Use of Balloons in Scientific Experiments. *Space Science Reviews*, 13:199–242.
- Piccard, A. and Cosyns, M. (1932). Étude du rayonnement cosmique en grande altitude. *Comptes Rendus Acad. Sci. Paris*, 195:604–606.
- Picone, J. M., Lean, J. L., and Emmert, J. T. (2003). STARSHINE Studies of Thermospheric Response to Solar Forcing. *AGU Fall Meeting Abstracts*, page A494.
- Pinto, J. P., Toon, O. B., and Turco, R. P. (1989). Self-limiting physical and chemical effects in volcanic eruption clouds. *Journal of Geophysical Research*, 94:11165–11174.
- Piszkejewicz, D. (1995). *The Nazi Rocketeers*. Praeger Publishers.
- Pitz, E., Leinert, C., Schulz, A., and Link, H. (1978). Ultraviolet Zodiacal Light Observed by the Astro 7 Rocket Experiment. *Astronomy and Astrophysics*, 69:297–304.
- Ponamperuma, C., Mariner, S., and Sagan, C. (1963). Formation of adenosine by ultraviolet irradiation of a solution of adenine and ribose. *Nature* 198, 1199–1200.
- Ponz, J. D., Barylak, M., Ojero, E., and Yurrita, I. (1993). The Final IUE Archive. In *ESO Conf. Proc. 41: 5th ESO/ST-ECF Data Analysis Workshop Garching*, pages 141–145.
- Prather, M. J., García, M. M., Douglass, A. R., Jackman, C. H., Ko, M. K. W., and Sze, N. D. (1990). The space shuttle's impact on the stratosphere. *Journal of Geophysical Research*, 95:18583–18590.
- Preece, R. D., Briggs, M. S., Mallozzi, R. S., Pendleton, G. N., Paciesas, W. S., and Band, D. L. (2000). The BATSE Gamma-Ray Burst Spectral Catalog. I. High Time Resolution Spectroscopy of Bright Bursts Using High Energy Resolution Data. *Astrophysical Journal Supplement*, 126:19–36.
- Priest, E. R., Heyvaerts, J. F., and Title, A. M. (2002). A Flux-Tube Tectonics Model for Solar Coronal Heating Driven by the Magnetic Carpet. *Astrophysical Journal*, 576:533–551.

- Pryor, W. R. and et al. (2001). Cassini UVIS Observations of Jupiter's Auroral Variability. *AGU Fall Meeting Abstracts*, page A835.
- Pryor, W. R., Lasica, S. J., Stewart, A. I. F., Hall, D. T., Lineaweaver, S., Colwell, W. B., Ajello, J. M., White, O. R., and Kent Tobiska, W. (1998). Interplanetary Lyman α observations from Pioneer Venus over a solar cycle from 1978 to 1992. *Journal of Geophysical Research*, 103:26833–26850.
- Pun, C. S. J., Kirshner, R. P., Sonneborn, G., Challis, P., Nassiopoulos, G., Arquilla, R., Crenshaw, D. M., Shrader, C., Teays, T., Cassatella, A., Gilmozzi, R., Talavera, A., Wamsteker, W., Fransson, C., and Panagia, N. (1995). Ultra-violet Observations of SN 1987A with the IUE Satellite. *Astrophysical Journal Supplement*, 99:223–261.
- Purcell, J. D., Packer, D. M., and Tousey, R. R (1959a). Lyman- α photographs of the Sun. *Nature*, 184:8–10.
- Purcell, J. D. and Tousey, R. (1960). The Profile of Solar Hydrogen-Lyman- α . *Journal of Geophysical Research*, 65:370–372.
- Purcell, J. D., Tousey, R. R., Packer, D. M., and Hunter, W. R. (1959b). Solar disk photographs made with Lyman- α of hydrogen. *Astronomical Journal*, 64:131.
- Quillen, A. C., Trilling, D. E., and Blackman, E. G. (2004). The impact of a close stellar encounter on the Edgeworth-Kuiper Belt. *ArXiv Astrophysics e-prints*.
- Rainey, P. B. and Travisano, M. (1998). Adaptive radiation in a heterogeneous environment. *Nature*, 394:69–72.
- Ramachandran, S., Ramaswamy, V., Stenchikov, G. L., and Robock, A. (2000). Radiative impact of the Mount Pinatubo volcanic eruption: Lower stratospheric response. *Journal of Geophysical Research*, 105:24409–24430.
- Rampino, M. R. (2002). Supereruptions as a Threat to Civilizations on Earth-like Planets. *Icarus*, 156:562–569.
- Rampino, M. R. and Stothers, R. B. (1984). Terrestrial mass extinctions, cometary impacts and the sun's motion perpendicular to the galactic plane. *Nature*, 308:709–712.
- Randel, W. J., Wu, F., and Stolarski, R. (2002). Changes in column ozone correlated with the stratospheric EP flux. *Journal of Meteorological Society Japan*, 80:849–862.
- Raulin, F. and Bruston, P. (1996). Photochemical growing of complex organics in planetary atmospheres. *Advances in Space Research*, 18:41–49.
- Raulin, F. and Owen, T. (2002). Organic Chemistry and Exobiology on Titan. *Space Science Reviews*, 104:379–395.
- Raup, D. (1985). Magnetic reversals and mass extinctions. *Nature*, 314:341–343.

- Raup, D. and Sepkoski, J. J. (1984). Periodicity of extinction in the geological past. *Proceedings National Academy of Sciences*, 81:801–805.
- Raup, D. M. (1992). *Extinctions: Bad genes or bad luck*. W.W. Norton.
- Raymond, J. C., Uzzo, M., Ko, Y.-K., Mancuso, S., Wu, R., Gardner, L., Kohl, J. L., Marsden, B., and Smith, P. L. (2002). Far-Ultraviolet Observations of Comet 2P/Encke at Perihelion. *Astrophysical Journal*, 564:1054–1060.
- Reed, R. J., Campbell, W. J., Rasmussen, L. A., and Rogers, D. G. (1961). Evidence of a downward-propagating, annual wind reversal in the equatorial stratosphere. *Journal of Geophysical Research*, 66:813–818.
- Reedy, R. C., Arnold, J. R., and Lal, D. (1983). Cosmic-ray record in solar system matter. *Science*, 219:127–135.
- Reeves, E. M. and Parkinson, W. H. (1970). An Atlas of Extreme-Ultraviolet Spectroheliograms from OSO-IV. *Astrophysical Journal Supplement*, 21:1–30.
- Reeves, E. M., Timothy, J. G., and Huber, M. C. E. (1977). Extreme UV spectrophotometer on the Apollo Telescope Mount. *Applied Optics*, 16:837–848.
- Regener, E. and Regener, V. (1934). Aufnahme des ultravioletten Sonnen-spektrums in der Stratosphäre und vertikale Ozonverteilung. *Physikalische Zeitschrift*, 66:788–793.
- Reid, G. C., Isaksen, I.S., Helger, T. E., and Crutzen, P. J. (1976). Influence of ancient solar-proton events on the evolution of life. *Nature*, 259:177–179.
- Reid, S. J. (2000). *Ozone and Climate Change - A Beginners Guide* -. Gordon and Breach Science Publishers.
- Rettberg, P., Eschweiler, U., Strauch, K., Reitz, G., Horneck, G., Wänke, H., Brack, A., and Barbier, B. (2002). Survival of microorganisms in space protected by meteorite material: Results of the experiment ‘EXOBIOLOGIE’ of the PERSEUS mission. *Advances in Space Research*, 30:1539–1545.
- Rex, M., Salawitch, R. J., von der Gathen, P., Harris, N. R. P., Chipperfield, M. P., and Naujokat, B. (2004). Arctic ozone loss and climate change. *Geophysical Research Letters*, 31:4116.
- Reynoso, E. M. and Goss, W. M. (1999). A New Determination of the Distance to Kepler’s Supernova Remnant. *Astronomical Journal*, 118:926–929.
- Ribas, I., Guinan, E. F., Guedel, M., and Audard, M. (2004). Evolution of the Solar Activity over Time and Effects on Planetary Atmospheres: I. High-energy Irradiances (1–1700 Å). *ArXiv Astrophysics e-prints*.
- Richling, S. and Yorke, H. W. (2000). Photoevaporation of Protostellar Disks. V. Circumstellar Disks under the Influence of Both Extreme-Ultraviolet and Far-Ultraviolet Radiation. *Astrophysical Journal*, 539:258–272.

- Richling, S. and Yorke, H. W. (2003). The Influence of External UV Radiation on the Evolution of Protostellar Disks. *Communications of the Konkoly Observatory Hungary*, 103:103–108.
- Richmond, A. D. (1987). The Ionosphere. In *The Solar Wind and the Earth*, D. Reidel, pages 123–140.
- Ries, G., Puchta, H., Sandermann, H., Seidlitz, H. K., and Hohn, B. (2000). Elevated UV-B radiation reduces genome stability in plants. *Nature*, 406:98–101.
- Rind, D. and Balachandran, N. K. (1995). Modeling the Effects of UV Variability and the QBO on the Troposphere-Stratosphere System. Part II: The Troposphere. *Journal of Climate*, 8:2080–2096.
- Rind, D. and Overpeck, J. (1993). Hypothesized causes of decade-to-century climate variability: Climate model results. *Quaternary Science Reviews*, 12:357–374.
- Rind, D., Shindell, D., Perlwitz, J., and Lerner, J. (2004). The relative importance of solar and anthropogenic forcing of climate change between the Maunder Minimum and the present. *Journal of Climate*, 17:906–928.
- Rinsland et al., C. P. (2003). Long-term trends of inorganic chlorine from ground-based infrared solar spectra: Past increases and evidence for stabilization. *Journal of Geophysical Research (Atmospheres)*, 108:4252.
- Rishbeth, H. and Garriott, O. K. (1969). *Introduction to Ionospheric Physics*. Academic Press.
- Ritter, J. W. (1801). Auffindung nicht-sichbarer Sonnenstrahlen und der Seite des Violett. *Annalen der Physik*, 7:527.
- Ritter, J. W. (1803). Versuche über das Sonnenlicht. *Annalen der Physik*, 12:409–415.
- Roach, F. E. and Gordon, J. L. (1973). *The Light of the Night Sky*. D. Reidel.
- Robertson, M. P. and Miller, S. L. (1995). An efficient prebiotic synthesis of cytosine and uracil. *Nature*, 375:772–774.
- Roble, R. G. and Emergy, B. A. (1983). On the global mean temperature of the thermosphere. *Planetary and Space Sciences*, 31:597–614.
- Rocha-Pinto, H. J., Scalo, J., Maciel, W. J., and Flynn, C. (2000). Chemical enrichment and star formation in the Milky Way disk. II. Star formation history. *Astronomy and Astrophysics*, 358:869–885.
- Roelandts, R. (2002). The history of phototherapy: Something new under the Sun? *Journal American Academy of Dermatology*, 46:926–930.

- Roettger, E. E. and Buratti, B. J. (1994). Ultraviolet spectra and geometric albedos of 45 asteroids. *Icarus*, 112:496–512.
- Rolfe, E. and Heck, A., editors (1982). *Third European IUE Conference*.
- Rolfe, E. J., editor (1986). *Proceedings of an International Symposium on New Insights in Astrophysics. Eight Years of UV Astronomy with IUE*.
- Rollier, A. (1915). *La Cure de Soleil*. Baillire & fils, Paris.
- Rontó, G., Bércecs, A., Lammer, H., Cockell, C. S., Molina-Cuberos, G.J., Patel, M.R., and Selsis, F. (2003). Solar UV Irradiation Conditions on the Surface of Mars. *Photochemistry and Photobiology*, 77:1–7.
- Rosenberg, E. and Falkovitz, L. (2004). The Vibrio shiloi/Oculina patagonica model system of coral bleaching. *Annual Review of Microbiology*, 58:143–159.
- Ross, F. E. (1928). Photographs of Venus. *Astrophysical Journal*, 68:57–92.
- Rottman, G. (2003). Measurement of the Solar Spectral Irradiance and its Variability. *AGU Fall Meeting Abstracts*.
- Rottman, G. J., Woods, T. N., and Sparn, T. P. (1993). Solar-Stellar Irradiance Comparison Experiment 1. I - Instrument design and operation. *Journal of Geophysical Research*, 98:10667–10677.
- Rowlands, I.-H. (1993). The fourth meeting of the parties to the Montreal Protocol: Report and reflection. *Environment*, 35:25–34.
- Rozema, J., Bjorn, L. O., and Manetas, Y. (2002). *Responses of Plant to UV-B Radiation*. Kluwer Academic Publishers.
- Rubenstein, E. P. and Schaefer, B. E. (2000). Are Superflares on Solar Analogues Caused by Extrasolar Planets? *Astrophysical Journal*, 529:1031–1033.
- Rubey, W. W. (1974). Fifty Years of the Earth Sciences-A Renaissance. *Annual Review of Earth and Planetary Sciences*, 2:1–25.
- Ruderman, M. A. (1974). Possible consequences of nearby supernova explosions for atmospheric ozone and terrestrial life. *Science*, 184:1079–1081.
- Rudiman, W. F. (2001). *Earth's climate: Past and Future*. W.H.Freeman, New York.
- Rudwick, M.J. (1997). *Georges Cuvier, Fossil Bones, and Geological catastrophes*. The University of Chicago Press.
- Ruiz-Lapuente, P. (2004). Tycho Brahe's Supernova: Light from Centuries Past. *Astrophysical Journal*, 612:357–363.
- Ruiz-Lapuente, P., Comeron, F., Méndez, J., Canal, R., Smartt, S. J., Filippenko, A. V., Kurucz, R. L., Chornock, R., Foley, R. J., Stanishev, V., and Ibata,

- R. (2004). The binary progenitor of Tycho Brahe's 1572 supernova. *Nature*, 431:1069–1072.
- Russell, D. and Tucker, W. (1971). Supernovae and the extinction of the dinosaurs. *Nature*, 229:553–554.
- Rye, R. and Holland, H. D. (2000). Life associated with a 2.76 Ga ephemeral pond? Evidence from Mount Roe 2 paleosol. *Geology*, 28:483–486.
- Saar, S. H. and Brandenburg, A. (1999). Time Evolution of the Magnetic Activity Cycle Period. II. Results for an Expanded Stellar Sample. *Astrophysical Journal*, 524:295–310.
- Sackmann, I.-J. and Boothroyd, A. I. (2003). Our Sun. V. A Bright Young Sun Consistent with Helioseismology and Warm Temperatures on Ancient Earth and Mars. *Astrophysical Journal*, 583:1024–1039.
- Saffer, R. A., Sepinski, J. F., Demarchi, G., Livio, M., Paresce, F., Shara, M. M., and Zurek, D. (2002). Massive, Collisionally Produced Blue Stragglers in the Galactic Globular Cluster NGC 6397. In *ASP Conf. Ser. 263: Stellar Collisions, Mergers and their Consequences*, page 157.
- Sagan, C. (1973). Ultraviolet selection pressure on the earliest organisms. *Journal of Theoretical Biology*, 39:195–200.
- Sagan, C. and Chyba, C. (1997). The faint young Sun paradox: organic shielding of ultraviolet - labile greenhouse gases. *Science*, 276:1217–1221.
- Sagan, C. and Khare, B.N. (1971). Long-wavelength ultraviolet photoproduction of aminoacids on the primitive Earth. *Science*, 173:417–420.
- Sagan, C. and Shklovskii, I.S. (1966). *Intelligent Life in the Universe*. Holden-Day, San Francisco.
- Sagan, C., Thompson, W. R., and Kahre, B. N. (1992). Titan: a laboratory for prebiological organic chemistry. *Accounts of Chemical Research*, 25:286–292.
- Sakata, A., Nakagawa, N., Iguchi, T., Isobe, S., Morimoto, M., Hoyle, F., and Wickramasinghe, N. C. (1977). Spectroscopic evidence for interstellar grain clumps in meteoritic inclusions. *Nature*, 266:241.
- Salby, M. and Callaghan, P. (2000). Connection between the Solar Cycle and the QBO: The Missing Link. *Journal of Climate*, 13:328–338.
- Salcedo et al., E. (2003). Molecular basis for UV vision in invertebrates. *Journal of Neuroscience*, 23:10873–10878.
- Sandel, B. R., Shemansky, D. E., and Broadfoot, A. L. (1979). Observations of the diffuse interstellar EUV radiation field. *Astrophysical Journal*, 227:808–815.
- Sanford, S. A., Bernstein, M. P., Dworkin, J. P., Cooper, G. W., and Allamandola, L. J. (2002). The Production of Amino Acids in Interstellar Ices : Im-

- plications for Meteoritic Organics. *Meteoritics and Planetary Science*, vol. 37, Supplement, 37:125.
- Scalo, J. and Wheeler, J. C. (2002). Astrophysical and Astrobiological Implications of Gamma-Ray Burst Properties. *Astrophysical Journal*, 566:723–737.
- Scalo, J. M. (1987). The initial mass function, starbursts, and the Milky Way. In *Starbursts and Galaxy Evolution*, pages 445–465.
- Scalo, J. M., Wheeler, J. C., and Williams, P. (2004). Intermittent Jolts of Galactic UV Radiation: Mutagenetic Effects. In Celnikier, L.M., editor, *Frontiers of Life; 12 th Rencontres de Blois*.
- Schaefer, B. E., King, J. R., and Deliyannis, C. P. (2000). Superflares on Ordinary Solar-Type Stars. *Astrophysical Journal*, 529:1026–1030.
- Schafer, J. S., Saxena, V. K., Wenny, B. N., Barnard, W., and De Luisi, J. J. (1996). Observed influence of clouds on ultraviolet-B radiation. *Geophysical Research Letters*, 23:2625–2628.
- Schatzman, E. (1962). A theory of the role of magnetic activity during star formation. *Annales d'Astrophysique*, 25:18–29.
- Schauffler, S. M., Atlas, E. L., Flocke, F., Leub, R. A., Stroud, V., and Travnicek, W. (1998). Measurements of bromine-containing organic compounds at the tropical tropopause. *Geophysical Research Letters*, 25:317–320.
- Schein et al., D. O. (1995). Ocular and dermatological health effects of UV radiation exposure from the ozone hole in southern Chile. *American Journal of Public Health*, 85:546–550.
- Schmidtke, G. (2000). Solar Variability in Ionizing Radiation (UV, X-rays). In *ESA SP-463: The Solar Cycle and Terrestrial Climate, Solar and Space weather*, pages 61–68.
- Schoeberl, M. R., Lait, L. R., Newman, P. A., and Rosenfield, J. E. (1992). The Structure of the Polar Vortex. *Journal of Geophysical Research*, 97:7859–7882.
- Schönbein, C. F. (1845). Einige Bemerkungen über die anwesenheit des Ozones in der atmosphärischen Luft und die Rolle welcher dieser bei langsamem Oxydationen spielen durfte. *Annalen Phys. Chem. (Poggendorf Annalen)*, 65:161–172.
- Schönbein, C. F. (1850). Über das Ozon. *Journal Praktische Chemie*, 51:321.
- Schrijver, C. J. and Zwaan, C. (2000). *Solar and Stellar Magnetic Activity*. Cambridge University Press.
- Schrijver, C. J. (1990). Relations between the photospheric magnetic field and the emission from the outer atmospheres of cool stars. II - The C IV 1550 Å doublet. *Astronomy and Astrophysics*, 234:315–322.
- Schrijver, C. J. (1992). The basal and strong-field components of the solar atmosphere. *Astronomy and Astrophysics*, 258:507–520.

- Schrijver, C. J., Cote, J., Zwaan, C., and Saar, S. H. (1989). Relations between the photospheric magnetic field and the emission from the outer atmospheres of cool stars. I - The solar CA II K line core emission. *Astrophysical Journal*, 337:964–976.
- Schrijver, C. J., Title, A. M., Berger, T. E., Fletcher, L., Hurlburt, N. E., Nightingale, R. W., Shine, R. A., Tarbell, T. D., Wolfson, J., Golub, L., Bookbinder, J. A., Deluca, E. E., McMullen, R. A., Warren, H. P., Kankelborg, C. C., Handy, B. N., and de Pontieu, B. (1999). A new view of the solar outer atmosphere by the Transition Region and Coronal Explorer. *Solar Physics*, 187:261–302.
- Schrödinger, E. (1926). Quantisierung als Eigenwertproblem. *Annalen der Physik*, 79:361–376.
- Schumann, V. (1896). A New Method of Preparing Plates Sensitive to the Ultra-Violet Rays. *Astrophysical Journal*, 4:144–154.
- Schwartz, R. D. and James, P. B. (1984). Periodic mass extinctions and the sun's oscillation about the galactic plane. *Nature*, 308:712–713.
- Schwarzschild, M. (1948). On Noise Arising from the Solar Granulation. *Astrophysical Journal*, 107:1–5.
- Schwarzschild, M. (1959). Photographs of the Solar Granulation Taken from the Stratosphere. *Astrophysical Journal*, 130:345–363.
- Scott, A. F. (1984). The Invention of the Balloon and the Birth of Modern Chemistry. *Scientific American*, 250:102–111.
- Seckmeyer, G. and Mc Kenzie, R. L. (1992). Increased ultraviolet radiation in New Zealand (45 degrees-S) relative to Germany (45 degrees-N). *Nature*, 359:135–137.
- Sedov, L. I. (1959). *Similarity and Dimensional Methods in Mechanics*. Academic Press.
- Segura, A., Krelove, K., Kastings, J. F., Sommerlatt, D., Meadows, V., Crisp, D., Cohen, M., and Mlawer, E. (2004). Ozone concentration and ultraviolet fluxes on Earth-like planets around other stars. *Astrobiology*, 3:689–708.
- Sekine, Y., Sugita, S., Kadono, T., and Matsui, T. (2003). Methane production by large iron meteorite impacts on Early Earth. *Journal of Geophysical Research*, 108:5070–+.
- Self, S. and Rampino, M. R. (1981). The 1883 eruption of Krakatau. *Nature*, 294:699–704.
- Setlow, R. B. (1974). The wavelengths in sunlight effective in producing skin cancer: a theoretical analysis. *Proc. National Academy Sciences*, 71:3363–3366.

- Shaposhnikov, V. E., Zaitsev, V. V., Rucker, H. O., and Litvinenko, G. V. (2001). Origin of ultraviolet emission source in the Jovian ionosphere at the feet of the Io flux tube. *Journal of Geophysical Research*, 106:26049–26056.
- Shara, M. M., editor (2002). *Stellar Collisions, Mergers and their Consequences*. Astronomical Society of the Pacific Conference Series 263.
- Shaviv, N. J. (2003). The spiral structure of the Milky Way, cosmic rays, and ice age epochs on Earth. *New Astronomy*, 8:39–77.
- Shea, M. A. and Smart, D. F. (1995). A comparison of energetic solar proton events during the declining phase of four solar cycles (cycles 19-22). *Advances in Space Research*, 16:37–46.
- Sheehan, P. M. (2001). The late Ordovician mass extinction. *Annual Review Earth and Planetary Sciences*, 29:331–364.
- Sheeley, N. R. (1969). The Evolution of the Photospheric Network. *Solar Physics*, 9:347–357.
- Shindell, D. T. (2001). Climate and ozone response to increased stratospheric water vapor. *Geophysical Research Letters*, 28:1551–1554.
- Shindell, D. T. and Faluvegi, G. (2002). An exploration of ozone changes and their radiative forcing prior to the chlorofluorocarbon era. *Atmospheric Chemistry and Physics*, 2:363–374.
- Shindell, D. T., Rind, D., Balachandran, N., Lean, J., and Lonergan, P. (1999). Solar cycle variability, ozone and climate. *Science*, 284:305–308.
- Shindell, D. T., Rind, D., and Lonergan, P. (1998). Increased polar stratospheric ozone losses and delayed eventual recovery owing to increasing greenhouse-gas concentrations. *Nature*, 392:589–592.
- Shindell, D. T. and Schmidt, G. A. (2004). Southern Hemisphere climate response to ozone changes and greenhouse gas increases. *Geophysical Research Letters*, 31:18209(1–4).
- Shindell, D. T., Schmidt, G. A., Mann, M. E., Rind, D., and Waple, A. (2001a). Solar forcing of regional climate change during the Maunder Minimum. *Science*, 294:2149–2152.
- Shindell, D. T., Schmidt, G. A., Miller, R. L., and Rind, D. (2001b). Northern Hemisphere winter climate response to greenhouse gas, ozone, solar and volcanic forcing. *Journal of Geophysical Research*, 106:7193–7210.
- Shindell, D. T., Schmidt, G. A., Miller, R. L., and Mann, M. E. (2003). Volcanic and solar forcing of climate change during the Preindustrial Era. *Journal of Climate*, 16:4094–4107.

- Shindo, F., Benilan, Y., Guillemin, J.-C., Chaquin, P., Jolly, A., and Raulin, F. (2003). Ultraviolet and infrared spectrum of C₆H₂ revisited and vapor pressure curve in Titan's atmosphere. *Planetary and Space Science*, 51:9–17.
- Shoemaker, E. M. (1983). Asteroid and comet bombardment of the earth. *Annual Review of Earth and Planetary Sciences*, 11:461–494.
- Shumilov, O. I., Raspopov, O. M., Kasatkina, E. A., Kokin, G. A., and Chizhov, A. F. (1991). Decrease of total ozone content inside the polar cap after solar proton flares. *Akademii Nauk SSSR Doklady*, 318:576–580.
- Simon, G. W. and Leighton, R. B. (1964). Velocity Fields in the Solar Atmosphere. III. Large-Scale Motions, the Chromospheric Network, and Magnetic Fields. *Astrophysical Journal*, 140:1120–1147.
- Simon, T., Herbig, G., and Boesgaard, A. M. (1985). The evolution of chromospheric activity and the spin-down of solar-type stars. *Astrophysical Journal*, 293:551–570.
- Simony, O. (1889). *Anzeiger der K. Akademie der Wissenschaften, Wien - Mathem. naturwissenschaftliche Classe*, pages 37–41.
- Simony, O. (1890). Über eine naturwissenschaftlichen Reise nach der westlichen Gruppen der Canarischen Inseln. *M. th. der K.K. Geograph. Gesellschaft in Wien*, 33:145–152.
- Sinha, R. P. and Häder, D. P. (2002). UV-induced DNA damage and repair: a review. *Photochemical and Photobiological Sciences*, 1:225–236.
- Skumanich, A. (1972). Time Scales for CA II Emission Decay, Rotational Braking, and Lithium Depletion. *Astrophysical Journal*, 171:565–567.
- Skumanich, A., Lean, J. L., Livingston, W. C., and White, O. R. (1984). The sun as a star - Three-component analysis of chromospheric variability in the calcium K line. *Astrophysical Journal*, 282:776–783.
- Skumanich, A., Smythe, C., and Frazier, E. N. (1975). On the statistical description of inhomogeneities in the quiet solar atmosphere. I - Linear regression analysis and absolute calibration of multichannel observations of the Ca/+ emission network. *Astrophysical Journal*, 200:747–764.
- Slanger, T. G., Cosby, P. C., Huestis, D. L., and Bida, T. A. (2001). Discovery of the Atomic Oxygen Green Line in the Venus Night Airglow. *Science*, 291:463–465.
- Slanger, T. G. and Wolven, B. C. (2002). Airglow Processes in Planetary Atmospheres. In *Atmospheres in the Solar System: Comparative Aeronomy*, pages 77–.
- Slipher, V. M. (1908). The Spectrum of Mars. *Astrophysical Journal*, 28:397–404.

- Smith, D. S., Scalo, J., and Wheeler, J. C. (2004a). Redistribution of Incident Ionizing Radiation to Biologically Active Surface UV in Planetary Atmospheres. *Origins of Life and Evolution of the Biosphere*, 34:513–532.
- Smith, D. S., Scalo, J., and Wheeler, J. C. (2004b). Transport of ionizing radiation in Terrestrial-like Exoplanet Atmospheres. *Icarus*, 171:229–253.
- Smith, G. J., Miller, I. J., Clare, J. F., and Diffey, B.L. (2002). The effect of UV absorbing sunscreens on the reflectance and the consequent protection of skin. *Photochemistry and Photobiology*, 75:122–125.
- Smith, G. R., Strobel, D. F., Broadfoot, A. L., Sandel, B. R., Shemansky, D. E., and Holberg, J. B. (1982). Titan's upper atmosphere - Composition and temperature from the EUV solar occultation results. *Journal of Geophysical Research*, 87:1351–1359.
- Smith, P. H., Lemmon, M. T., Lorenz, R. D., Sromovsky, L. A., Caldwell, J. J., and Allison, M. D. (1996). Titan's Surface, Revealed by HST Imaging. *Icarus*, 119:336–349.
- Smith, R. K. and Cox, D. P. (2001). Multiple Supernova Remnant Models of the Local Bubble and the Soft X-Ray Background. *Astrophysical Journal Supplement Series*, 134:283–309.
- Smith et al., R. (1992). Ozone depletion: Ultraviolet radiation and phytoplankton biology in antarctic waters. *Science*, 255:952–955.
- Sneath, P. (1962). Longevity of microorganisms. *Nature*, 195:643.
- Sobotka, M. (1999). Fine Structures in Sunspots. In *ASSL Vol. 239: Motions in the Solar Atmosphere*, pages 71–97.
- Socas-Navarro, H. and Uitenbroek, H. (2004). On the Diagnostic Potential of H α for Chromospheric Magnetism. *Astrophysical Journal*, 603:L129–L132.
- Solanki, S. K., Lagg, A., Woch, J., Krupp, N., and Collados, M. (2003). Three-dimensional magnetic field topology in a region of solar coronal heating. *Nature*, 425:692–695.
- Solanki, S. K., Schüssler, M., and Fligge, M. (2002). Secular variation of the Sun's magnetic flux. *Astronomy and Astrophysics*, 383:706–712.
- Solanki, S. K. and Steiner, O. (1990). How magnetic is the solar chromosphere? *Astronomy and Astrophysics*, 234:519–529.
- Solanki, S. K., Usoskin, I. G., Kromer, B., Schüssler, M., and Beer, J. (2004). Unusual activity of the Sun during recent decades compared to the previous 11,000 years. *Nature*, 431:1084–1087.
- Solomon, S. and Albritton, D. L. (1992). Time-dependent ozone depletion potentials for short and long-term Forecasts. *Nature*, 357:33–37.

- Solomon, S., Garcia, R. R., Rowland, F. S., and Wuebbles, D. J. (1986). On the depletion of Antarctic ozone. *Nature*, 321:755–758.
- Somerville, R.C.J. (1996). *The Forgiving Air*. University of California Press.
- Sonett, C. P., Giampapa, M. S., and Matthews, M. S., editors (1991). *The Sun in Time*. University of Arizona Press.
- Sonnett, C. P., Morfill, G. E., and Jokipii, J. R. (1987). Interstellar shock waves and 10Be from ice cores. *Nature*, 330:458–460.
- Soon, W. and Yaskell, S. H. (2003). *The Maunder Minimum and the variable Sun-Earth Connection*. World Scientific.
- Soukharev, B. and Labitzke, K. (2001). The 11-year solar cycle, the Sun's rotation, and the middle stratosphere in winter. Part II: Response of planetary waves. *Journal of Atmospheric and Terrestrial Physics*, 63:1931–1939.
- Spindler, A. (1999). *Hot Air Balloons*. Todtri Prod. Limited.
- Spinrad, H., Münch, G., and Kaplan, L. D. (1963). The Detection of Water Vapor on Mars. *Astrophysical Journal*, 137:1319–1321.
- Spörer, G. (1885). Über die Periodicität der Sonnenflecken seit dem Jahre 1618 . *Nova Acta der ksl. Leop.-Carol Deutschen Akademie der Naturforscher*, 53:283–324.
- Spruit, H. C. and Zwaan, C. (1981). The size dependence of contrasts and numbers of small magnetic flux tubes in an active region. *Solar Physics*, 70:207–228.
- Staath, E. and Lemaire, P. (1995). High resolution profiles of the Mg II h and Mg II k lines. *Astronomy and Astrophysics*, 295:517–528.
- Staehelin, J., Kegel, R., and Harris, N. R. P. (1998). Trend analysis of the homogenized total ozone series of Arosa (Switzerland), 1926-1996. *Journal of Geophysical Research*, 103:8389–8400.
- Stair, R. and Ellis, H. T. (1968). The solar constant based on new spectral irradiance data from 310 to 530 nanometers. *Journal of Applied Meteorology*, 7:635–644.
- Stark, A. A., Martin, C. L., Walsh, W. M., Xiao, K., Lane, A. P., and Walker, C. K. (2004). Gas Density, Stability, and Starbursts near the Inner Lindblad Resonance of the Milky Way. *Astrophysical Journal*, 614:L41–L44.
- Steinegger, M., Vázquez, M., Bonet, J. A., and Brandt, P. N. (1996). On the Energy Balance of Solar Active Regions. *Astrophysical Journal*, 461:478–498.
- Stenchikov, G., Robock, A., Ramaswamy, V., Schwarzkopf, M. D., Hamilton, K., and Ramachandran, S. (2002). Arctic Oscillation response to the 1991 Mount Pinatubo eruption: Effects of volcanic aerosols and ozone depletion. *Journal of Geophysical Research (Atmospheres)*, 107:28–+.

- Stenflo, J. O. (1966). On the influence of the slit size on measurements with a solar magnetograph. *The Observatory*, 86:73–75.
- Stephenson, F. R. (1976). Revised Catalogue of Pre-Telescopic Galactic Novae and Supernovae. *Quarterly Journal Royal Astronomical Society*, 17:121–138.
- Stephenson, F. R. and Green, D.A. (2002). *Historical Supernova and their Remnants*. Oxford University Press.
- Stern, S. A., Brosch, N., Barker, E. S., and Gladstone, G. R. (1991). Rotationally resolved midultraviolet studies of Triton and the Pluto/Charon system. I - IUE results. *Icarus*, 92:332–341.
- Stern, S. A., Parker, J. W., Festou, M. C., A'Hearn, M. F., Feldman, P. D., Schwehm, G., Schulz, R., Bertaux, J., and Slater, D. C. (1998). HST mid-ultraviolet spectroscopy of comet 46P/Wirtanen during its approach to perihelion in 1996-1997. *Astronomy and Astrophysics*, 335:L30–L36.
- Stern, S. A., Skinner, T. E., Brosch, N., van Santvoort, J., and Trafton, L. M. (1989). The UV spectrum of Pluto-Charon - IUE observations from 2600 to 3100 Å. *Astrophysical Journal*, 342:533–538.
- Stevens, M. H. (2001). The EUV airglow of Titan: Production and loss of $N_2c'_4(0) - X$. *Journal of Geophysical Research*, pages 3685–3690.
- Stewart, A. I. and Barth, C. A. (1979). Ultraviolet night airglow of Venus. *Science*, 205:59–62.
- Stewart, B. (1886). On the Cause of the Solar-Diurnal Variations of Terrestrial Magnetism . *Proceedings of the Physical Society of London*, 8:38–49.
- Stolarski, R. S. and Cicerone, R. J. (1974). Stratospheric Chlorine: A possible sink for Ozone. *Canadian Journal of Chemistry*, 52:1610–1615.
- Störmer, C. (1929). Remarkable clouds at high altitudes. *Nature*, 123:260–261.
- Stothers, R. and Frogel, J. A. (1974). The local complex of O and B stars. I. Distribution of stars and interstellar dust. *Astronomical Journal*, 79:456–471.
- Stothers, R. B. (1984). The great Tambora eruption in 1815 and its aftermath. *Science*, 224:1191–1198.
- Stothers, R. B. (1996). The Great Dry Fog of 1783. *Climate Change*, 32:79–89.
- Stothers, R. B. (1998). Galactic disc dark matter, terrestrial impact cratering and the law of large numbers. *Monthly Notices Royal Astronomical Society*, 300:1098–1104.
- Strickland, D. J., Lean, J. L., Meier, R. R., Christensen, A. B., Paxton, L. J., Morrison, D., Craven, J. D., Walterscheid, R. L., Judge, D. L., and McMullin, D. R. (2004). Solar EUV irradiance variability derived from terrestrial far ultraviolet dayglow observations. *Geophysical Research Letters*, 31:3801–+.

- Strobel, D. F. (1969). Photochemistry of methane in the jovian atmosphere. *Journal of Atmospheric Sciences*, 26:906–911.
- Strobel, D. F. (1982). Chemistry and evolution of Titan's atmosphere. *Planetary and Space Sciences*, 30:839–848.
- Strobel, D. F. (2003). Comparative Planetary Atmospheres of the Galilean Satellites. *Recent Progress in Planetary Exploration, 25th meeting of the IAU, Special Session 1, 17-18 July, 2003 in Sydney, Australia*, 1.
- Strobel, D. F., Meier, R. R., Summers, M. E., and Strickland, D. J. (1991). Nitrogen airglow sources - Comparison of Triton, Titan, and earth. *Geophysical Research Letters*, 18:689–692.
- Strobel, D. F., Summers, M. E., Herbert, F., and Sandel, B. R. (1990). The photochemistry of methane in the atmosphere of Triton. *Geophysical Research Letters*, 17:1729–1732.
- Struck, C. (1999). Galaxy collisions. *Physics Reports*, 321:1–137.
- Strutt, J. W. (Lord Rayleigh) (1871). On the light from the sky, its polarization and colour. *Philosophical Magazine*, 41:107–120.
- Strutt, R. (1922). The aurora line in the spectrum of the nightsky. *Proc. Royal Society*, page 366.
- Stuiver, M. (1961). Carbon- 14 content of 18th and 19th century wood, variations correlated with sunspot activity. *Science*, 149:533–535.
- Summers, M. E. and Strobel, D. F. (1989). Photochemistry of the atmosphere of Uranus. *Astrophysical Journal*, 346:495–508.
- Szuromi, P. (1995). Saturn's Aurora. *Science*, 269:901–904.
- Talavera, A., González-Riestra, R., Solano, E., and Ines Team At Vilspa (2001). INES: The IUE archive in Spain. In *Highlights of Spanish astrophysics II*, pages 341–+.
- Tammann, G. A., Loeffler, W., and Schroeder, A. (1994). The Galactic supernova rate. *Astrophysical Journal Supplement*, 92:487–493.
- Taylor, F. W. (2003). The Stratosphere. *Philosophical Transactions Royal Society London*, 361:11–22.
- Teisserenc de Bort, L. P. (1902). Variations de la température de l'air libre dans la zone comprise entre 8 et 13 km altitude. *Comptes rendus du la Academie Sciences Paris*, 134:987–989.
- Terndrup, D. M., Stauffer, J. R., Pinsonneault, M. H., Sills, A., Yuan, Y., Jones, B. F., Fischer, D., and Krishnamurthi, A. (2001). Rotational Veloci-

- ties of Low-mass Stars in the Pleiades and Hyades (CD-ROM Directory: contribs/terndrup). In *ASP Conf. Ser. 223: 11th Cambridge Workshop on Cool Stars, Stellar Systems and the Sun*, pages 1502–1507.
- Tevini(ed.), M. (1993). *UV-B radiation and Ozone Depletion*. Lewis Publishers, Florida.
- Thekaekara, M. P., Kruger, R., and Duncan, C. H. (1969). Solar Irradiance Measurements from a Research Aircraft. *Applied Optics*, 8:1713–1732.
- Thiemens, M. H. (1986). Meteorite isotopic anomalies can be produced by ultraviolet light. *Lunar Planetary Institute Contributions*, 592:33–34.
- Thomas, B. C., Jackman, C. H., Melott, A. L., Laird, C. M., Stolarski, R. S., Gehrels, N., Cannizzo, J. K., and Hogan, D. P. (2004). Terrestrial Ozone Depletion Due to a Milky Way Gamma-Ray Burst. *ArXiv Astrophysics e-prints*.
- Thomas, J. H. and Weiss, N. O. (2004). Fine Structure in Sunspots. *Annual Review of Astronomy and Astrophysics*, 42:517–548.
- Thompson, G. I., Nandy, K., Jamar, C., Monfils, A., Houziaux, L., Carnochan, D. J., and Wilson, R. (1978). *Catalogue of stellar ultraviolet fluxes. A compilation of absolute stellar fluxes measured by the Sky Survey Telescope (S2/68) aboard the ESRO satellite TD-1*. Publisher Unknown.
- Thompson, W. J. and Wallace, J. W. (1998). The Arctic oscillation signature in the wintertime geopotential height and temperature fields. *Geophysical Research Letters*, 25:1297–1300.
- Thompson, W. R. and Sagan, C. (1992). Organic chemistry on Titan: Surface interactions. In *ESA SP-338: Symposium on Titan*, pages 167–176.
- Thordarson, T. and Self, S. (2003). Atmospheric and environmental effects of the 1783–1784 Laki eruption: A review and reassessment. In *Journal of Geophysical Research (Atmospheres), Volume 108, Issue D1*, pages 7–1.
- Thuillier, G. (2000). Absolute UV radiation, its variability and consequences for the Earth's climate. In *The Solar Cycle and Terrestrial Climate, ESA SP-463*, pages 69–78.
- Thuillier, G., Floyd, L., Woods, T. N., Cebula, R., Hilsenrath, E., Hersé, M., and Labs, D. (2004). Solar irradiance reference spectra for two solar active levels. *Advances in Space Research*, 34:256–261.
- Thuillier, G., Herse, M., Simon, P. C., Labs, D., Mandel, H., and Gillotay, D. (1997). Observation of the UV Solar Spectral Irradiance Between 200 and 350 NM during the Atlas i Mission by the SOLSPEC Spectrometer. *Solar Physics*, 171:283–302.
- Tinsley, B.A (1988). The solar cycle and the QBO influences on the latitude of storm tracks in the North Atlantic. *Geophysical Research Letters*, 15:409–412.

- Tobias, S. M. and Weiss, N. O. (2000). Resonance in a coupled solar-climate model. *Space Science Reviews*, 94:153–160.
- Tobiska, W. K. (1993). Recent solar extreme ultraviolet irradiance observations and modeling: A review. *Journal Geophysical Research*, 98:18879–+.
- Tobiska, W. K., Woods, T., Eparvier, F., Viereck, R., Floyd, L., Bouwer, D., Rottman, G., and White, O. R. (2000). The SOLAR2000 empirical solar irradiance model and forecast tool. *Journal of Atmospheric and Terrestrial Physics*, 62:1233–1250.
- Toon, O. B., Zahnle, K., Morrison, D., Turco, R. P., and Covey, C. (1997). Environmental perturbations caused by the impacts of asteroids and comets. *Reviews of Geophysics*, 35:41–78.
- Toublanc, D., Parisot, J. P., Brillet, J., Gautier, D., Raulin, F., and McKay, C. P. (1995). Photochemical modeling of Titan's atmosphere. *Icarus*, 113:2–26.
- Tousey, R. (1961). Solar spectroscopy in the far ultraviolet. *Journal of the Optical Society of America*, 51:384–395.
- Tousey, R., Strain, C. V., Johnson, F. S., and Oberly, J. J. (1947). The solar ultraviolet spectrum from a V-2 rocket. *Astronomical Journal*, 52:158.
- Tran, B. N., Joseph, J. C., Ferris, J. P., Persans, P. D., and Chera, J. J. (2003). Simulation of Titan haze formation using a photochemical flow reactorThe optical constants of the polymer. *Icarus*, 165:379–390.
- Tromp, T. K., Shia, R.L., Allen, M., Eiler, J. M., and Yung, Y.L. (2003). Potential environmental impact of a hydrogen economy on the stratosphere. *Science*, 300:1740–1742.
- Turco, R. P., Toon, O. B., Ackerman, T. P., Pollack, J. B., and Sagan, C. (1983). Nuclear winter: Global consequences of multiple nuclear explosions. *Science*, 222:1283–1292.
- Turco, R.P. (1997). *Earth under Siege*. Oxford University Press.
- Turnbull, D. J. and Parisi, A. V. (2003). Spectral UV in public shade settings. *Journal of Photochemistry and Photobiology*, 69:13–19.
- Twersky, V. (1964). Rayleigh scattering. *Applied Optics*, 3:1150–1162.
- UNEP (1994). *Environmental effects of ozone depletion*. United Nations Environment Programme, Nairobi.
- UNEP (1998). *Production and consumption of ozone-depleting substances 1986–1996*. United Nations Environment Programme, Nairobi.
- UNEP (2002). *Production and consumption of ozone-depleting substances 1986–2000*. United Nations Environment Programme, Secretariat to the Montreal Protocol.

- Unna, P. (1894). *Die Histopathologie der Hautkrankheiten*. A. Hirschwold, Berlin.
- Urbach, F. and Gauge, R. W. (1986). *The Biological effects of UV-A*. Praeger, New York.
- Urbach (ed.), F. (1992). *Biological responses to ultraviolet A radiation*. Valdenmar Publishing Company.
- Urey, H. C. (1973). Cometary collisions and geological periods. *Nature*, 242:32–33.
- Usoskin, I. G., Mursula, K., Solanki, S. K., Schüssler, M., and Kovaltsov, G. A. (2002). A physical reconstruction of cosmic ray intensity since 1610. *Journal of Geophysical Research (Space Physics)*, 107:13–1.
- Vázquez, M. (1999). Long-Term Changes in the Total Solar Irradiance. In *ASSL Vol. 239: Motions in the Solar Atmosphere*, pages 169–195. Kluwer Academic Publishers.
- Valet, J. (2003). Time variations in geomagnetic intensity. *Reviews of Geophysics*, 41:1–44.
- van Ballegooijen, A. A. (1986). Cascade of magnetic energy as a mechanism of coronal heating. *Astrophysical Journal*, 311:1001–1014.
- Van de Hulst, H. C. (1957). *Light scattering by small particles*. Wiley, New York.
- Van der Hoeve, J. (1920). Eye lesions produced by light rich in ultraviolet rays. Senile cataract, senile degeneration of macula. *American Journal of Ophthalmology*, 3:178–194.
- Van der Leun, J. C. and De Gruijl, F. R. (2002). Climate change and skin cancer. *Photochemical and Photobiological Sciences*, 1:324–326.
- van Loon, H. and Labitzke, K. (2000). The Influence of the 11-year Solar Cycle on the Stratosphere Below 30km: a Review. *Space Science Reviews*, 94:259–278.
- Vande Noord, E. L. (1970). Observations of the Zodiacial Light with a Balloon-Borne Telescope. *Astrophysical Journal*, 161:309–316.
- Vaughan, A. H. and Preston, G. W. (1980). A survey of chromospheric CA II H and K emission in field stars of the solar neighborhood. *Publications Astronomical Society of Pacific*, 92:385–391.
- Vázquez, M. and Wittmann, A. (2005). *Solar Research with Stratospheric Balloons*, in “Development of Solar Research”, Acta Historia Astronomiae Vol. 25, pp. 262–284, Verlag Harry Deutsch.
- Vekstein, G. and Katsukawa, Y. (2000). Scaling Laws for a Nanoflare-Heated Solar Corona. *Astrophysical Journal*, 541:1096–1103.
- Vernazza, J. E., Avrett, E. H., and Loeser, R. (1973). Structure of the Solar Chromosphere. Basic Computations and Summary of the Results. *Astrophysical journal*, 184:605–632.

- Vernazza, J. E., Avrett, E. H., and Loeser, R. (1981). Structure of the solar chromosphere. III - Models of the EUV brightness components of the quiet-sun. *Astrophysical Journal Supplement*, 45:635–725.
- Veronig, A., Temmer, M., Hanslmeier, A., Otruba, W., and Messerotti, M. (2002). Temporal aspects and frequency distributions of solar soft X-ray flares. *Astronomy and Astrophysics*, 382:1070–1080.
- Vervack, R. J., Sandel, B. R., and Strobel, D. F. (2004). New perspectives on Titan's upper atmosphere from a reanalysis of the Voyager 1 UVS solar occultations. *Icarus*, 170:91–112.
- Viereck, R. A. and Puga, L. C. (1999). The NOAA Mg II core-to-wing solar index: Construction of a 20-year time series of chromospheric variability from multiple satellites. *Journal of Geophysical Research*, 104:9995–10006.
- Visscher et al., H. (2004). Environmental mutagenesis during the end-Permian ecological crisis. *Proceedings National Academy of Sciences*, 101:12952–12956.
- Vogelmann, A. M., Ackerman, T. P., and Turco, R. P. (1992). Enhancements in biologically effective ultraviolet radiation following volcanic eruptions. *Nature*, 359:47–49.
- Volland, H. (1988). *Atmospheric Tidal and Planetary Waves*. Kluwer Academic Publishers.
- Volz, A. and Klein, D. (1988). Evaluation of the Montsounis series of ozone measurements made in the nineteenth century. *Nature*, 332:240–242.
- Volz, F. E. (1975). Distribution of turbidity after the 1912 Katmai eruption in Alaska. *Journal of Geophysical Research*, 80:2643–2648.
- Von Braun, W., Ordway, F., and Dooling, D. (1985). *Space Travel: A history*. Harper and Row.
- Vrsnak, B., Ruzdjak, V., and Placko, D. (1991). Calcium plage intensity and solar irradiance variations. *Solar Physics*, 133:205–213.
- Wagner, G., Beer, J., Laj, C., Kissel, C., Masarik, J., Muscheler, R., and Synal, H.-A. (2000). Chlorine-36 evidence for the Mono Lake event in the Summit GRIP ice core. *Earth and Planetary Science Letters*, 181:1–6.
- Wakker, B. P. and Richter, P. (2004). Our growing, breathing Galaxy. *Scientific American*, 290:28–37.
- Wakker, B. P. and van Woerden, H. (1997). High-Velocity Clouds. *Annual Review of Astronomy and Astrophysics*, 35:217–266.
- Wallace, B. (1951). Genetic changes in populations under irradiation. *The American Naturalist*, 85:209–222.

- Wallace, J. M. (2000). North Atlantic Oscillation/annular mode: Two paradigms - one phenomenon. *Quarterly Journal Royal Meteorological Society*, 126:791–806.
- Wallner, C., Faestermann, T., Gerstmann, U., Knie, K., Korschinek, G., Lierse, C., and Rugel, G. (2004). Supernova produced and anthropogenic ^{244}Pu in deep sea manganese encrustations. *New Astronomy Review*, 48:145–150.
- Walter, F. M. and Barry, D. C. (1991). Pre- and main-sequence evolution of solar activity. In *The Sun in Time*, pages 633–657.
- Walton, S. R., Preminger, D. G., and Chapman, G. A. (2003). The Contribution of Faculae and Network to Long-Term Changes in the Total Solar Irradiance. *Astrophysical Journal*, 590:1088–1094.
- Wamsley et al., P. R. (1998). Distribution of halon-1211 in the upper troposphere and lower stratosphere and the 1994 total bromine budget. *Journal of Geophysical Research*, 103:1513–1526.
- Wamsteker, W., Gonzalez Riestra, R., and Harris, B., editors (1998). *Ultraviolet astrophysics beyond the IUE final archive*.
- Wang, K., Orth, C. J., Attrep, M., Chatterton, B. D., Hou, H., and Geldsetzer, H. H. (1991). Geochemical evidence for a catastrophic biotic event at the Frasnian/Famennian boundary in South China. *Geology*, 19:776–779.
- Ward, P. D. and Brownlee, D. (2002). *The Life and Death of Planet Earth*. Times Books, New York.
- Ward et al., P. D. (2001). Sudden productivity collapse associated with the Triassic-Jurassic boundary mass extinction. *Science*, 292:1148–1151.
- Warren, H. P., Mariska, J. T., and Lean, J. (2001). A new model of solar EUV irradiance variability: 1. Model formulation. *Journal of Geophysical Research*, 106:15745–15758.
- Watson, J. and Crick, F. (1953). Molecular structure of nucleic acids. *Nature*, 171:737–738.
- Webb, A. R. and Holick, M. F. (1988). The role of sunlight in the cutaneous production of vitamin D3. *Annual Review of Nutrition*, 8:375–399.
- Webb, D. F. (1998). CMEs and Prominences and Their Evolution over the Solar Cycle. In *ASP Conf. Ser. 150: IAU Colloq. 167: New Perspectives on Solar Prominences*, pages 463–474.
- Weber, M., Burrows, J. P., and Cebula, R. P. (1998). Some Solar UV/VIS Irradiance Measurements between 1995 and 1997 - First Results on Proxy Solar Activity Studies. *Solar Physics*, 177:63–77.
- Weber, P. and Greenberg, J. (1985). Can Spores Survive in Interstellar Space? *Nature*, 316:403–407.

- Welsh, C. and Diffey, B. L. (1981). The protection against solar actinic radiation afforded by common clothing fabrics. *Clinic Exp. Dermatology*, 6:577–582.
- Wheeler, J. C. (2000). *Supernovae, gamma-ray bursts and adventures in Hyperspace*. Cambridge University Press.
- Whipple, F. (1932). The Propagation to great Distances of Airwaves from Gunfire. Progress of the Investigation during 1931. *Quarterly Journal Royal Meteorological Society*, 63:471–478.
- White, O. R., Fontenla, J., and Fox, P. A. (2000). Extreme solar cycle variability in strong lines between 200 and 400 NM. *Space Science Reviews*, 94:67–74.
- White et al., O. (1999). Genome sequence of the radioresistant bacterium *Deinococcus Radiodurans* R1. *Science*, 286:1571–1577.
- Whitten, R. C., Borucki, W. J., Wolfe, J. H., and Cuzzi, J. (1976). Effect of nearby supernova explosions on atmospheric ozone. *Nature*, 263:398–400.
- Wilde, S. A., Valley, J. W., Peck, W. H., and Graham, C.M. (2001). Evidence from detrital zircons for the existence of continental crust and oceans on the Earth 4.4 Gyr. ago. *Nature*, 409:175–178.
- Wildt, R. (1934). The Atmospheres of Giant Planets. *Nature*, 134:418.
- Wildt, R. (1937a). Photochemistry of Planetary Atmospheres. *Astrophysical Journal*, 86:321–336.
- Wildt, R. (1937b). Photochemistry of Planetary Atmospheres. *Astrophysical Journal*, 86:321–336.
- Wilhelm, K., Dwivedi, B. N., Marsch, E., and Feldman, U. (2004). Observations of the Sun at Vacuum- Ultraviolet Wavelengths from Space. Part I: Concepts and Instrumentation. *Space Science Reviews*, 111:415–480.
- Wilke, C., Wang, J.L., Ofria, C., Lenski, R., and Adami, C. (2001). Evolution of Digital Organisms at High Mutation Rate Leads To Survival of the Flattest. *Nature*, 412:331–333.
- Williams, V., Austin, J., and Haigh, J. D. (2001). Model simulations of the impact of the 27-day solar rotation period on stratospheric ozone and temperature. *Advances in Space Research*, 27:1933–1942.
- Willis, A. J., editor (1979). *The first year of IUE; Proceedings of the Symposium, University College, London, England*.
- Willson, R. C., Gulkis, S., Janssen, M., Hudson, H. S., and Chapman, G. A. (1981). Observations of solar irradiance variability. *Science*, 211:700–702.
- Willson, R. C. and Mordvinov, A. V. (2003). Secular total solar irradiance trend during solar cycles 21-23. *Geophysical Research Letters*, 30:1199–1202.

- Wilson, R. and Boksenberg, A. (1969). Ultraviolet Astronomy. *Annual Review of Astronomy and Astrophysics*, 7:421–472.
- Winkler, P. F., Gupta, G., and Long, K. S. (2003). The SN 1006 Remnant: Optical Proper Motions, Deep Imaging, Distance, and Brightness at Maximum. *Astrophysical Journal*, 585:324–335.
- Withbroe, G. L. and Noyes, R. W. (1977). Mass and energy flow in the solar chromosphere and corona. *Annual Review of Astronomy and Astrophysics*, 15:363–387.
- Wofsy, S., Mc Elroy, M., and Yung, Y. (1975). The chemistry of atmospheric bromine. *Geophysical Research Letters*, 2:215–218.
- Wolkoff, P. (1999). Photocopiers and Indoor Air Pollution. *Atmospheric Environment*, 33:2129–2130.
- Wood, B. E., Müller, H., Zank, G. P., and Linsky, J. L. (2002). Measured Mass-Loss Rates of Solar-like Stars as a Function of Age and Activity. *Astrophysical Journal*, 574:412–425.
- Wood, R. (1903). On screens transparent only to ultraviolet light and their use in spectrum photography. *Philosophical magazine*, 5:257–263.
- Wood, R. D., Skopet, T. R., and Hutchinson, F. (1984). Changes in DNA base sequence induced by targeted mutagenesis of lambda phage DNA by ultraviolet light. *Journal Molecular Biology*, 173:273–291.
- Woodgate, B. E., Brandt, J. C., Kalet, M. W., Kenny, P. J., Tandberg-Hanssen, E. A., Bruner, E. C., Beckers, J. M., Henze, W., Knox, E. D., and Hyder, C. L. (1980). The Ultraviolet Spectrometer and Polarimeter on the Solar Maximum Mission. *Solar Physics*, 65:73–90.
- Woods, T. N., Feldman, P. D., Dymond, K. F., and Sahnow, D. J. (1986). Rocket ultraviolet spectroscopy of comet Halley and abundance of carbon monoxide and carbon. *Nature*, 324:436–438.
- Woods, T. N., Tobiska, W. K., Rottman, G. J., and Worden, J. R. (2000). Improved solar Lyman α irradiance modeling from 1947 through 1999 based on UARS observations. *Journal of Geophysical Research*, 105:27195–27216.
- Woon, D. E. (2002). Pathways to Glycine and Other Amino Acids in Ultraviolet-irradiated Astrophysical Ices Determined via Quantum Chemical Modeling. *Astrophysical Journal*, 571:L177–L180.
- Worden, J. R., White, O. R., and Woods, T. N. (1998). Evolution of Chromospheric Structures Derived from Ca II K Spectroheliograms: Implications for Solar Ultraviolet Irradiance Variability. *Astrophysical Journal*, 496:998–1014.

- Worden, J. R., Woods, T. N., and Bowman, K. W. (2001). Far-Ultraviolet Intensities and Center-to-Limb Variations of Active Regions and Quiet Sun Using UARS SOLSTICE Irradiance Measurements and Ground-based Spectrohe liograms. *Astrophysical Journal*, 560:1020–1034.
- World Meteorological Organization (1995). *Scientific Assessment of Ozone Depletion: 1994*. WMO Global Ozone Research and Monitoring Project - Report No. 37, Geneva.
- World Meteorological Organization (1999). *Scientific Assessment of Ozone Depletion: 1998*. WMO Global Ozone Research and Monitoring Project - Report No. 44, Geneva.
- World Meteorological Organization (2002). *Scientific Assessment of Ozone Depletion: 2001*. WMO Global Ozone Research and Monitoring Project - Report No. 47, Geneva.
- Wuebbles, D. J., Wei, C.-F., and Patten, K. O. (1998). Effects on stratospheric ozone and temperature during the Maunder Minimum. *Geophysical Research Letters*, 25:523–526.
- Yanny, B., Newberg, H. J., Grebel, E. K., Kent, S., Odenkirchen, M., Rockosi, C. M., Schlegel, D., Subbarao, M., Brinkmann, J., Fukugita, M., Ivezić, Ž., Lamb, D. Q., Schneider, D. P., and York, D. G. (2003). A Low-Latitude Halo Stream around the Milky Way. *Astrophysical Journal*, 588:824–841.
- Yen, A. S., Kim, S. S., Hecht, M. H., Frant, M. S., and Murray, B. (2000). Evidence That the Reactivity of the Martian Soil Is Due to Superoxide Ions. *Science*, 289:1909–1912.
- Yoshikawa, I., Yamazaki, A., Murachi, T., Kameda, S., Sagawa, H., Okano, S., Okada, T., and Nakamura, M. (2004). Development of an extreme ultraviolet imaging spectrometer for the BepiColombo mission. *Advances in Space Research*, 33:2195–2199.
- Yung, Y. L., Allen, M., and Pinto, J. P. (1984). Photochemistry of the atmosphere of Titan - Comparison between model and observations. *Astrophysical Journal Supplement*, 55:465–506.
- Zahnle, K. J. and Walker, J. C. G. (1982). The evolution of solar ultraviolet luminosity. *Reviews of Geophysics and Space Physics*, 20:280–292.
- Zank, G. P. and Frisch, P. C. (1999). Consequences of a Change in the Galactic Environment of the Sun. *Astrophysical Journal*, 518:965–973.
- Zeller, E. J., Dreschhoff, G. A. M., and Laird, C. M. (1986). Nitrate flux on the Ross Ice Shelf, Antarctica and its relation to solar cosmic rays. *Geophysical Research Letters*, 13:1264–1267.

- Zerefos, C. S., Balis, D. S., Meleti, C., Bais, A. F., Tourpali, K., Kourtidis, K., Vanicek, K., Cappellani, F., Kaminski, U., Colombo, T., Stübi, R., Manea, L., Formenti, P., and Andreae, M. O. (2000). Changes in surface solar UV irradiances and total ozone during the solar eclipse of August 11, 1999. *Journal Geophysical Research*, 105:26463–26474.
- Zerefos, C. S., Tourpali, K., Bojkov, B. R., Balis, D. S., Rognerund, B., and Isaksen, I. S. A. (1997). Solar activity-total column ozone relationships: Observations and model studies with heterogeneous chemistry. *Journal of Geophysical Research*, 102:1561–1570.
- Zreda-Gostynska, G., Kyle, P. R., and Finnegan, D. L. (1993). Chlorine, fluorine, and sulfur emissions from Mount Erebus, Antarctica and estimated contributions to the Antarctic atmosphere. *Geophysical Research Letters*, 20:1959–1962.

Index

- Abbot,C., 44
Absorption coefficient, 159
Acoustic Heating, 64
Action Spectra, 170, 192, 193
Aeronauts
 Charles,J.A., 16
 Coxwell,H., 17
 Croce-Spinelli,J., 17
 Glaisher,J., 17
 Hess,V., 18
 Piccard A., 18
 Pilatre de Rozier,J.F., 15
Air Quality Index, 200
Albedo, 250
ALH84001, 301
Antarctic Treaty, 175
Appleton,E., 118
Arctic Oscillation, 153
Aristarchus, 36
Arrhenius,S., 299
Assman,R., 17
Asteroids, 248
- Bacteria
 B.pumillus, 301
 Bacillus Subtilis, 234, 297, 300
 Deinococcus radiodurans, 191
 E.Coli, 297, 300
 Pseudomonas fluorescens, 297
 Staphylococcus, 190
 Thermus Themophilus, 191
 Tubercular Bacillus, 190
 Vibrio shiloi, 192
- Balloons, 15
Balmer,J., 8
Becquerel,P., 190
- Betelgeuse, 295
Big Bang, 43
Black Body, 7
Black,J., 11
Bohr,N., 9
Brewer-Dobson circulation, 176
Bromine, 178
Bunsen,R., 2
- Carrington, 37
Cavendish,H., 12
Chapman,S., 112, 129
Chemoluminescence, 110
chlorine, 173
Chlorofluorocarbons, 171
Chromosphere, 51
 chromospheric network, 54
 Plages, 54
Comas Solà,J., 253
Comets
 Churyumov G., 246
 Hale-Bopp, 246
 Halley, 243
 Hyakutake, 245
 SL-9, 239, 246
- Continuity Equation
 Ionosphere, 120
 Ozone, 132
- Coodlidge,W.D., 191
Coral bleaching, 192
Cornu,A., 14
Corona
 Coronal Holes, 62
 Blinkers, 67
 Coronal loops, 58
 General Parameters, 39, 57

- helmet streamers, 61
- polar plumes, 62
- Waves, 75
- Coronal Mass Ejections, 74
- Cosmic Rays, 89, 287, 292
- Crab Nebula, 290
- Cuvier,G., 267
- Daguerre,L., 4
- Darwin,C., 267
- Davy,H., 3, 10
- Deep sea sediments, 90
- Deslandres,H., 37
- DNA, 157
 - Damage, 297
 - Repair, 278
- Dobson Unit, 128, 226
- Dobson,G., 127, 130
- Dollfus,A., 18
- Draper,J.W., 5
- Dynamics Activity Index, 149
- Dynamo, 224
- Early Earth, 94
- Eclipses, 35, 135
- Einstein,A., 8
- Equation
 - Appleton-Hartree, 124
 - Schwarzschild, 105
- Erythema, 193
- Eta Carinae, 295
- Exosphere, 213
- Extinction
 - Cretaceous, 269, 292
 - Ordovician, 276
 - Permian, 269, 292
- Fabricius, 36
- Fabry,C., 15, 127, 129
- Faint Sun Paradox, 94
- Finsen,N.R., 189
- Fizeau,L., 5
- Flare
 - Classification, 73
 - Definition, 71
- Flares, 271, 298
- Discovery, 38
- Stellar Flares, 96
- Fluorescence, 110, 114
- Fullerenes, 269, 299
- Galactic Centre, 284
- Galaxies
 - Andromeda, 281
 - Canis Majoris, 282
 - Sagittarius, 281
- Galilei,G., 37, 235
- Galle,J.G., 235
- Gamma Ray Bursts, 274
- Gauss,C., 287
- Gauss,C.F., 118
- Gay-Lussac,J., 17
- Gene, 158
- Genome, 158
- Geocorona, 113
- Geomagnetic field
 - Reversals, 90, 287
- Geostrophic wind, 138
- Glisson,F., 190
- Global Warming, 186, 194, 200
- Goddard,R.H., 26
- Golberg,L., 29
- Gould Belt, 284
- Gravity Waves, 140
- Great Red Spot, 236
- Greenhouse gases, 153
- Hale,G.E., 37
- Halley,E., 295
- Harriot,T., 36
- Hartley,W.N., 14
- Heaviside,O., 118
- Heliosphere, 88
- Heliotherapy, 189
- Helium, 37
- Herschel,J., 5
- Herschel,W., 2, 37, 48, 235
- Hertz,H., 3, 8
- HII regions, 41
- Hubble Space Telescope, 117, 154, 240, 241, 245, 250, 257, 263, 285

- Huggins,W., 15
Huygens,C., 252
Hydrogen peroxide, 162
- International Geophysical Year, 143, 198
International Space Station, 300
Interstellar medium, 41
Ionosonde, 124
Ionosphere
 Chapman layers, 121
 Ionosonde, 119
 Radio transmission, 118
- Isotopes
 ^{10}Be , 89, 288, 292
 ^{14}C , 89, 91, 292
 ^{36}Ar , 216
 ^{36}Cl , 288, 292
 $^{40}\text{Ar}/^{36}\text{Ar}$, 93
 ^{44}Ti , 92
 ^{56}Ni , 273
 ^{60}Fe , 294
 D/H, 90
- Janssen,P.J., 37
Jeans criterion, 41
Jeans,J., 6, 253
Jupiter, 234
- Kepler,J., 291
Kiepenheuer,K.O., 28, 125
Kirchhoff,G., 2, 6
Korolev,S., 31
Kyoto Protocol, 183
- Lacrustine sediments, 90
Langley,S.P., 21
Large Magellanic Cloud, 282
Lavoisier,A., 12
Levy,A., 13
Limb darkening, 45
Local Bubble, 285
Local Group, 280
Local Interstellar Cloud, 285
Lovelock,J., 171
Lyman,T., 9, 10
- Magnetic Carpet, 67
- Magnetic Heating, 96
Magnetic pressure, 40
Mangley,T., 171
Mars
 Dust absorption, 227
 Interior, 224
 Landings, 223
 Methane, 230, 234
 Orbit, 223
 Ultraviolet Environment, 225
 UV Hotspot, 227
 Viking, 231
- Mascart,M.E., 5
Maunder Minimum, 81, 86, 90, 135, 153
Maunder,E., 37
Melanin, 193
Mendel,G., 157
Mercury, 234
Mesosphere, 24
Meteorites, 92
Methyl Bromine, 178
Microflares, 73
Mie,G., 108
Miller,S., 216
Millikan,R.A., 11
Molecular clouds, 41
Montgolfier, E., 15
Montgolfier, J., 15
Montreal Treaty, 183
Moon, 4, 92
Moss, 56
Muller,H.J., 296
Mutations, 296
- Nanoflares, 67
NAO, 185
Newton,I., 2, 26, 36
Niepce,J., 4
Nitrates, 88
North Atlantic Oscillation, 148
Nuclear Winter, 270
- Oberth,H., 27
Oparin,A., 165
Optical Depth, 110
Ozone, 12
 Absorption bands, 15

- Discovery, 12
- Internacional Conferences, 130
- Ozonoscope, 13
- Ozone depletion
 - Bromine, 178
 - Iodine, 180
 - Nuclear explosions, 182
 - Stratospheric Flights, 181
 - Volcanoes, 178, 181
- Ozone hole, 171
- PAH, 248, 261, 299
- Panspermia, 299
- Pasteur,L., 164
- Phlogiston, 11
- Photoaging, 195
- Photography, 4
- Photolysis, 210
- Photosphere
 - Granulation, 48
 - Sunspots, 49
- Phytoplankton, 196
- Planck,M., 7
- Planetary Waves, 138, 185, 187
- Plasma β , 40
- Pluto, 263
- Polar ice, 90
- Polar Night Jet, 176
- Polar Stratospheric Clouds, 177
- Polar Vortex, 148, 176
- Potential temperature, 25
- Prominences, 54
- Quasi-Biannual Oscillation, 142
- Rayleigh, 6, 21, 107
- Regener,E., 18
- Reyn,A., 190
- Richter,H., 299
- Ritter,J.W., 4
- RNA, 157
- Rockets
 - Black Braut X, 33
 - Bumper-2, 30
 - V-2, 119
- Rollier,A., 189
- Rossby Number, 96
- Rossby Radius, 97
- Rossby,C.G., 138
- Rutherford,L., 5
- Sala,A., 3
- Satellite Drag, 154
- Scattering
 - Classical oscillator, 106
 - Compton, 107, 276
 - Rayleigh, 107, 226
 - Thompson, 107
- Schönbein,C., 12
- Scheele,K.W., 3
- Schumann,V., 10
- Schwabe,S., 37
- Sco-Cen Association, 286
- Sea spray, 182
- Secchi,A., 55
- SIDC, 76
- Skin Cancer, 193, 206
- Solar activity cycle, 37
- Solar Irradiance
 - Total, 77
 - Ultraviolet, 81
- Source function, 87
- Spörer's law, 37
- Spörer,G., 37
- Spacecrafts
 - Ariel I, 32
 - Aura, 128
 - BepiColombo, 234
 - Cassini, 240
 - Envisat, 204
 - ER-2, 128
 - EUE, 286
 - FOTON, 300
 - Galileo, 221, 241
 - IUE, 33, 241, 252, 264, 273
 - Magellan, 217
 - Mariner IV, 223
 - Mariner IX, 223, 228
 - Mariner VI, 44
 - Mariner VII, 226
 - Mariner X, 234
 - Mars Express, 223
 - Mars Pathfinder, 223

- Minisat, 116
Nimbus 7, 81, 82, 128, 175
OAO, 32
OSO, 32
OSO-8, 64
Rosetta, 246
Skylab, 53
SOHO, 61, 67, 75, 83, 87
Solar Maximum Mission, 63
Sputnik, 31
TD-1, 32
TRACE, 59, 75
UARS, 82
Vega, 217
Venera, 217
Voyager, 117, 241, 252, 258
YOHKOH, 59, 75
Spectroheliograph, 37
Spicules, 55
Spiral Arms, 288
Star Formation Rate, 281
Stellar Collisions, 279
Stokes,G.G., 10
Stratosphere
 cooling, 187
 Discovery, 17
Strutt,R.J.J., 112
Sun
 Birth, 41
 Chromosphere, 39
 Convection zone, 39
 Core, 39
 Dynamo, 96
 Energy generation, 42
 Evolution, 41
 Mass, 36
 Mass Loss, 94
 Photosphere, 39, 48
 Physical parameters, 38
 Radiative zone, 39
 Rotation, 37
 Rotation axis, 36
 Solar Wind, 288
 Transition region, 39
 UV variation, 42
 X-rays, 31
 Sun Protection Factor, 206
 Sunscreens, 206
 Sunspot number, 37, 76, 88, 92
 Sunspots, 77
 Supergranulation, 48, 54
 Supernova
 Classification, 272
 Historical, 290
 Tachocline, 39
 Tanning, 193
 Thermosphere, 24, 143
 Tidal stream, 281
 Titan, 253
 Airglow, 256
 Escape velocity, 215
 Ionosphere, 255
 Tholins, 261
 Toftoy,H.T., 29
 Tousey,R., 29
 Triton, 252
 Tycho Brahe, 291
Ultraviolet
 Age decay, 101
 Catastrophe, 7
 Climate, 143
 Diffuse background, 116
 Discovery, 4
 Erythema Dose, 202
 Human damage, 193
 Interstellar Medium, 285, 299
 Meteorites, 299
 Photography, 6
 Plant damage, 192
 Solar Cycle, 81
 Solar-like Stars, 101
 Spring, 230, 270
 Star Formation, 100
 Vitamin D, 190
 UV Index, 201
Valier,M., 27
Venus
 Airglow, 221
 Early Water, 218
 Ionosphere, 221

- Villard,P., 6
Vitamin D, 190
Vogel,H., 5
Volcanoes, 135, 181
Von Braun,W., 27
Von Helmont,J.B., 11
Von Karman,T., 27
Wallace,A., 268
Warburg,E., 127
Wedgwood,T., 3
Weissmann,A., 158
Wien,W., 6
Winkler,J., 27
Wolf number, 76
Wolf,R., 37
Wollaston,W., 2
Young Sun, 229
Young,C., 28
Zeeman effect, 38
Zodiacal Light, 117